Theory of cortical plasticity in vision

by

George J. Kalarickal

A dissertation submitted to the faculty of the University of North Carolina at Chapel Hill in partial fulfillment of the requirements for the degree of Doctor of Philosophy in the Department of Computer Science.

Chapel Hill

1998

Approved by:

Prof. Jonathan A. Marshall, Advisor

Dr. William D. Ross, Reader

Prof. Oleg V. Favorov, Reader

Prof. David Fitzpatrick

Prof. Stephen M. Pizer

To Wg. Cdr. and Mrs. K.J. Joseph and Fr. Sebastian Kalarickal, S.J.

GEORGE J. KALARICKAL. Theory of cortical plasticity in vision
(Under the direction of Professor Jonathan A. Marshall.)

ABSTRACT

A theory of postnatal activity-dependent neural plasticity based on synaptic weight modification is presented. Synaptic weight modifications are governed by simple variants of a Hebbian rule for excitatory pathways and an anti-Hebbian rule for inhibitory pathways. The dissertation focuses on modeling the following cortical phenomena: long-term potentiation and depression (LTP and LTD); dynamic receptive field changes during artificial scotoma conditioning in adult animals; adult cortical plasticity induced by bilateral retinal lesions, intracortical microstimulation (ICMS), and repetitive peripheral stimulation; changes in ocular dominance during "classical" rearing conditioning; and the effect of neuropharmacological manipulations on plasticity. Novel experiments are proposed to test the predictions of the proposed models, and the models are compared with other models of cortical properties.

The models presented in the dissertation provide insights into the neural basis of *perceptual learning*. In perceptual learning, persistent changes in cortical neuronal receptive fields are produced by conditioning procedures that manipulate the activation of cortical neurons by repeated activation of localized cortical regions. Thus, the analysis of synaptic plasticity rules for receptive field changes produced by conditioning procedures that activate small groups of neurons can also elucidate the neural basis of perceptual learning.

Previous experimental and theoretical work on cortical plasticity focused mainly on afferent excitatory synaptic plasticity. The novel and unifying theme in this work is self-organization and the use of the lateral inhibitory synaptic plasticity rule. Many cortical properties, e.g., orientation selectivity, motion selectivity, spatial frequency selectivity, etc. are produced or strongly influenced by inhibitory interactions. Thus, changes in these properties could be produced by lateral inhibitory synaptic plasticity.

Acknowledgements

I thank Dr. Jonathan Marshall for his guidance, advice, and support during my five years at UNC-Chapel Hill. I immensely enjoyed working with Dr. Marshall. I am grateful to him for imparting to me his good taste for relevant and important research work and for teaching me the art of identifying important research questions. I appreciate his help in improving my writing and public speaking skills.

I am grateful for the encouragement and the support from Dr. Stephen Pizer, Dr. David Fitzpatrick, Dr. Oleg Favorov, and Dr. William Ross. I appreciate their advice and critical review of my work. I am thankful to Dr. Nestor Schmajuk for initially serving on my dissertation committee. I was very lucky to have Dr. Oleg Favorov join the committee at very short notice. I thank Dr. Favorov and Dr. Ross for reading my dissertation.

I thank Richard Alley, Vinay Gupta, Charles Schmitt, and Viswanath Srikanth for their help, advice, and support. I am grateful to all in the Department of Computer Science for making it a fun and happy place to work.

This work was supported in part by the Office of Naval Research (Cognitive and Neural Sciences) and by the Whitaker Foundation (Special Opportunity Grant).

Contents

List of Figures

List of Tables

Chapter 1

Introduction: Motivation and overview

1.1 Introduction

The visual system, even in adult animals, is highly plastic, i.e., easily modifiable. The perception of a visual feature depends on the surrounding (contextual) visual features in space (simultaneously presented neighboring stimuli) and in time (e.g., previously presented stimuli).

For example, adaptation (from continuous viewing of a stimulus for few minutes) to a stimulus produces a contextual, orientation specific contrast threshold elevation for test stimuli (Blakemore & Nachmias, 1971). Adaptation effects are not persistent; they wear off within a few minutes in the absence of visual stimulation. Adaptation to orientation stimuli can distort perception of test stimuli. In the *tilt aftereffect*, after viewing a grating of a particular orientation (e.g., vertical), an observer perceives off-vertical gratings to be more tilted away from the vertical than the actual test grating (Mayo et al., 1968). The response properties of neurons in the primary visual cortex, the first visual cortical processing stage, fatigue/adapt after the conditioning phase (Maffei & Fiorentini, 1973; Movshon & Lennie, 1979), and the neural adaptation is consistent with the tilt aftereffect (see Sekuler & Blake, 1994, pp. 135).

Prior viewing of stimuli over a longer period can also produce persistent changes in visual perception. For example, in *perceptual learning*, human observers improve their performance in perceptual tasks such as orientation perception (Fiorentini & Berardi, 1980), vernier acuity (Fahle & Edelman, 1993), and discrimination of texture (Karni & Sagi, 1991) after training. Perceptual learning is stable, as it does not wear off after periods without visual stimulation, unlike the adaptation effects. The effects of perceptual learning are very specific; the improvement may be restricted to the orientation (Fahle et al., 1995; Poggio et al., 1992) and visual field position (Fahle et al., 1995; Karni & Sagi, 1991; Poggio et al., 1992) of the training stimuli. The effects of perceptual learning can be masked by adaptation/fatigue. Improvement in perceptual performance may not be apparent during training, but may manifest itself following a rest period during which the effects of adaptation/fatigue dissipate (Fahle, 1997; Karni & Sagi, 1991).

It has been proposed that the long-range lateral pathways in the primary visual cortex may subserve the effects of contextual stimuli and visual plasticity. The lateral long-range pathways in the primary visual cortex connect neurons with non-overlapping "classical" receptive fields, but with similar stimulus feature preferences, e.g., orientation (Gilbert & Wiesel, 1989; Weliky et al., 1995). Thus, neural representations of distant visual stimuli may interact via the long-range pathways to produce the contextual effects. The receptive field properties of primary visual cortical neurons are affected by simultaneously presented contextual stimuli (Gilbert & Wiesel, 1990; Sengpiel et al., 1997; Toth et al., 1996). Repeated presentation of stimuli used to characterize the effects of neighboring stimuli on orientation preference of a neuron produced persistent changes in its orientation tuning (Gilbert & Wiesel, 1990). Karni and Sagi (1991) suggested that perceptual learning occurs even at the monocular stage of visual cortical processing. Herzog and Fahle (1995) suggested that perceptual learning may involve reciprocal interactions among several visual cortical processing stages.

Perceptual learning occurs in other sensory modalities too. For example, monkeys gradually improved their performance of a tactile frequency discrimination task during several weeks of training (Recanzone et al., 1992a). The training also produced changes in the receptive field properties of neurons in the somatosensory cortex

(Recanzone et al., 1992acde).

From an information theoretic viewpoint, animal brains adapt during long-term development and during short-term conditionings to maximize the information content of neural signals (Atick & Redlich, 1990). Following changes in living environment, loss of sensory organs (e.g., damage to retina, loss of limbs, etc.), or brain damage (e.g., from stroke) the brain adapts to maximize the information content of its remaining capacities with respect to the new condition.

An information-theoretic analysis of brain adaptation does not reveal the brain processes or the rules by which the brain adapts, although it constrains plausible rules for plasticity. Knowledge of the substrate(s) and the rules for brain adaptation is useful for clinical applications, e.g., treatment of brain damage, or recovery from loss of sense organs, as well as for design of artificial systems capable of mimicking animal brain functions, e.g., face recognition systems. The information theoretic approach does not elucidate the mechanistic processes of the brain.

Current psychophysical and neurobiological data suggest that cortical plasticity can be produced by changes in efficacy of individual synapses (synaptic plasticity) (Kirkwood et al., 1993), by habituation of individual synapses (synaptic habituation/adaptation) or in individual neurons (neuronal habituation/adaptation) (Movshon & Lennie, 1979; Varela et al., 1997), and by changes in axonal arborization and synaptogenesis (Darian-Smith & Gilbert, 1994). Changes in these sites differ in their persistence/stability and in the time scales at which they occur. Synaptic and neuronal habituation are short-term changes; they are induced within a few seconds by synaptic activity and neuronal activity, respectively, and last for a few seconds after removal of the activation. Synaptic plasticity depends on activation in pre- and postsynaptic elements; it is produced in several minutes and lasts for several tens of minutes. Changes in axonal arborization and synaptogenesis take several months and last for several months.

In this dissertation, simple synaptic plasticity rules are used to model persistent changes in receptive field properties of cortical neurons that are produced by conditioning procedures that selectively activate afferent pathways to cortical neurons, manipulate the activation of cortical neurons, and produce activation in localized cortical regions. In

perceptual learning, a stimulus configuration is repeatedly presented. It is assumed that the neurons selective for the features of the training stimuli become repeatedly activated. Thus, the analysis of synaptic plasticity rules for receptive field changes produced by conditioning procedures that activate small groups of neurons can shed light on the neural basis of perceptual learning.

The synaptic plasticity rules are compared with experimental data on synaptic plasticity in the cortex and the hippocampus, and the rules are used to model several phenomena of cortical plasticity in early postnatal and adult animals. Several cortical plasticity phenomenona are characterized as the emergent properties of a small set of synaptic plasticity rules. In particular, the EXIN rules (Marshall, 1995a; Marshall & Gupta, 1998), which comprise a Hebbian afferent excitatory synaptic plasticity rule and an anti-Hebbian lateral inhibitory synaptic plasticity rule, are used to model

- long-term potentiation (LTP) and long-term depression (LTD);
- changes in ocular dominance during "classical" rearing conditioning;
- changes in ocular dominance during visual deprivation with cortical infusion of pharmacological agents;
- dynamic receptive field (RF) changes during artificial scotoma conditioning and retinal lesions;
- changes in RF topography and RF properties after intracortical microstimulation; and
- changes in RF topography and stimulus discrimination following repeated local peripheral stimulation.

The novel and unifying theme in this work is self-organization and the use of the lateral inhibitory synaptic plasticity rule. Many experiments (Benevento et al., 1972; Rose & Blakemore, 1974; Sillito, 1975, 1977, 1979; Sillito et al., 1980; Sillito & Versiani, 1977) have shown that many cortical properties are produced or strongly influenced by inhibitory interactions. A biologically plausible neural model of primary visual cortex has reproduced several neurobiological results on the effects of simultaneously presented contextual stimuli

and adaptation effects (Somers et al., 1996, 1998; Todorov et al, 1997). In the model, lateral inhibitory interactions are responsible for producing the effects of high-contrast contextual stimuli. The lateral excitatory interactions were responsible for the facilitatory effects produced by subthreshold contextual stimuli. In spite of the experimental data on the role of lateral inhibition in producing cortical feature selectivity, there is little experimental information on lateral inhibitory synaptic plasticity and its role in the development and maintenance of cortical properties. Thus, the analysis of the role of lateral inhibitory synaptic plasticity in the development of cortical receptive field properties and changes in receptive field properties in adult animals advances our understanding of the possible neural mechanisms of cortical plasticity. Several novel and testable experiments are also suggested to probe the predictions of the models.

The following section (Section 1.2) describes a simplified neural circuit used in the simulations in this dissertation. The conditioning procedures that produce synaptic plasticity and cortical plasticity that are modeled in this dissertation are briefly described in Section 1.3. The synaptic plasticity rules used in this dissertation are briefly described in Section 1.4. Section 1.5 relates this work to previous self-organization based theories of cortical development and cortical plasticity. The absence of lateral excitatory pathways in the EXIN model simulations is justified in Section 1.6. A summarizing thesis statement is presented in Section 1.7, and the overall contributions and significance of this work are stated in Section 1.8. Finally, Section 1.9 outlines the organization of this dissertation.

1.2 Simplified neural circuit

Most of the data modeled in this dissertation are from experiments on primary visual cortical plasticity. Some persistent plasticity in the somatosensory cortex and the hippocampus is also modeled. In this section, the pathway connections within the primary visual cortex are briefly described. Although, the cortical areas differ in their cytoarchitecture, corticocortical and subcortical connectivity, neural response properties, and behavioral role, they share several anatomical and functional properties (Sur et al., 1990). In fact, re-routing the retinal afferents to medial geniculate nucleus

causes primary auditory cortical neurons to become visually responsive, and some of these neurons even become orientation selective (Sur et al., 1990).

The visual cortical connectivity has a hierarchical organization (Felleman & Van Essen, 1991) – information from the sensors flows through several stages of processing; at each successive stage, the information undergoes more complex transformations. The cortical areas interact via reciprocal excitatory pathways. The pathways from an early/lower processing stage to a later/higher processing stage are called *feedforward* pathways, and the reciprocal pathways from a higher to a lower processing stage are called *feedback* pathways. The pathways conveying inputs to neurons are called *afferent* pathways, and the pathways channeling outputs to other neurons are called *efferent* pathways. The cortical areas also perform parallel information processing; the efferent pathways from a cortical area can provide inputs to two or more cortical areas (Felleman & Van Essen, 1991). The cortical areas receiving inputs from a common cortical area may also have reciprocal excitatory pathways between them. In this situation, feedforward and feedback pathways cannot truly be defined based on sequential processing stages. Maunsell and Van Essen (1983) defined feedforward and feedback pathways in cortex in terms of the cortical lamina in which the pathways originate and terminate. Feedforward pathways originate mainly from superficial layers and terminate mainly in layer 4, and feedback pathways originate from superficial and deep layers and terminate mainly outside layer 4 (Maunsell & Van Essen, 1983).

The cortex in cross-section has a layered structure. Figure 1.1 shows a simplified cross-section of the primary visual cortex. The primary visual cortex receives feedforward excitatory afferents from the lateral geniculate nucleus (LGN) in layer 4C (Hubel & Wiesel, 1972). There are reciprocal excitatory pathways between the layers (Blasdel et al., 1985; Fitzpatrick et al., 1985). The cortex contains excitatory and inhibitory neurons, but the proportion of inhibitory neurons is about 20 percent (Somogyi & Martin, 1985). The excitatory and inhibitory neurons receive afferent excitatory inputs (Somogyi, 1989). In addition, there are lateral/horizontal pathways within the layers (Blasdel et al., 1985; Gilbert & Wiesel, 1983, 1989; Rockland & Lund, 1983). The lateral excitatory (inhibitory) pathways originate from excitatory (inhibitory) neurons and terminate on excitatory and inhibitory neurons (McGuire et al., 1991; Somogyi et al., 1983;

Somogyi & Martin, 1985).

A simplified neural circuit is shown in Figure 1.2. The neural circuit shows the major input pathways to a cortical neuron. For ease of computer simulations, the neural circuit of Figure 1.2 is abstracted to the circuit shown in Figure 1.3. In Figure 1.3, it is assumed that there is a inhibitory neuron for every excitatory neuron and that they receive similar excitatory and inhibitory pathways. This simplification is reasonable because the models are designed to produce the qualitative changes in cortical properties following various conditioning procedures. A working hypothesis is that the persistent/long-term cortical plasticity in early postnatal development and in adulthood are produced by changes in inputs to the neurons because of synaptic plasticity in the excitatory and the inhibitory pathways. The emphasis is on the rules of synaptic plasticity that can qualitatively model the different cortical plasticity phenomena. Although the proportion of inhibitory neurons in the cortex is small, response properties of cortical neurons are heavily influenced by inhibition.

Neural circuits in the hippocampus are similar to those in the cortex. Excitatory and inhibitory neurons receive afferent excitatory pathways, and there are lateral excitatory and inhibitory pathways within hippocampal layers (McMahon & Kauer, 1997; Miles & Wong, 1987; Sik et al., 1995).

1.3 Plasticity in early postnatal and adult cortex

In this section, the synaptic and cortical plasticity phenomena that are modeled in this dissertation are described. The experiments on long-term synaptic plasticity provide information on changes in neural circuits at the level of synapses and individual pathways.

The "classical" rearing experiments were conducted on young animals in their critical periods. In these experiments, the *ocular dominance* of cortical neurons was modified by varying the correlation in the visual stimulation to the two eyes. Ocular dominance describes the relative responsiveness of primary visual cortical neurons to stimulation in the two eyes. Some neurons respond exclusively to one of the eyes, and are called *monocular neurons*. *Binocular neurons* respond equally to both eyes, and other

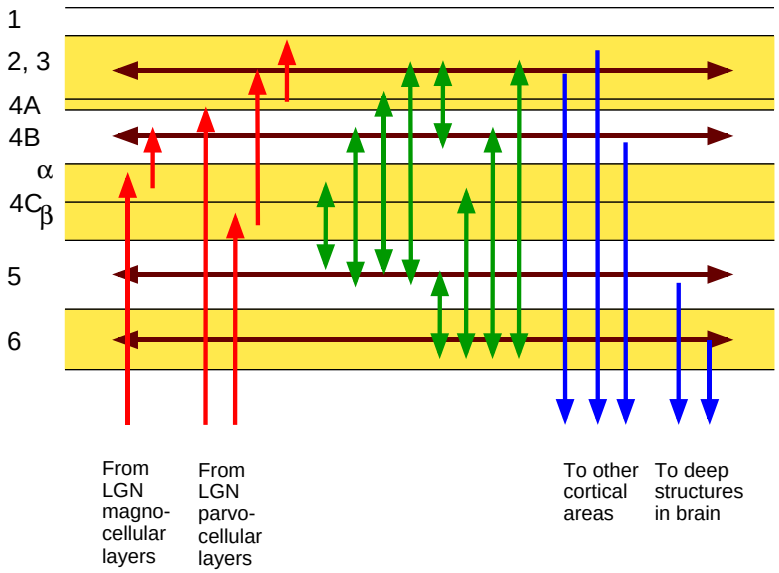

Figure 1.1: **Pathway connection pattern in the primary visual cortex.** The pathways from the parvocellular layers in the LGN terminate mainly in layers 4Cβ and 4A, and the pathways from the magnocellular layers in the LGN terminate in layer 4Cα. Layers 3B and 4A receive afferent pathways from the parvocellular layers in the LGN and from neurons in layer 4Cβ. Neurons in layers 3B/4A project mainly to layers 2/3A and 5A and sparsely to layer 6. The neurons in layer 4B receive major afferents from neurons in layer 4Cα, and they project pathways to layers 2/3A, 5, and 6 (these projections are sparse). Layer 4B neurons also send efferent pathways to other cortical areas, e.g., area MT. Neurons in layer 2/3A receive major afferents from layer 3B/4A and from layer 4B and send pathways to layers 4B, 5, and 6. Layer 2/3A sends corticocortical pathways, e.g., to area V2. The layer 5A receives major input pathways from layers 4Cα, 4Cβ, 3B/4A, and 2/3A, and some sparse input pathways from layer 6. Layer 5A sends pathways to layers 2/3A, 3B/4A, and 4C. The layer 5B neurons receive major inputs from layer 2/3A and project pathways to layers 2/3A and 6. Layer 5B also projects to subcortical areas, e.g., the superior colliculus. Layer 6 neurons receive prominent input from layer 5. Layer 6 also receives afferents from other cortical layers, i.e., 2/3A, 3B/4A, 4B, 4Cα, and 4Cβ and some input from the LGN. Layer 6 sends pathways to layer 4C, 4A, and 5A and to the LGN. There are also long-range lateral pathways within layers 2/3A, 4B, 5, and 6. The primary cortical pathway connectivity is summarized from Blasdel et al. (1985). The shading in the layers represents the density of neurons. Layers 4C and 6 are the most dense. The density of neurons in layers 1, 4B, and 5 is small. Layer 1 mainly contains axons, dendrites, and synapses.

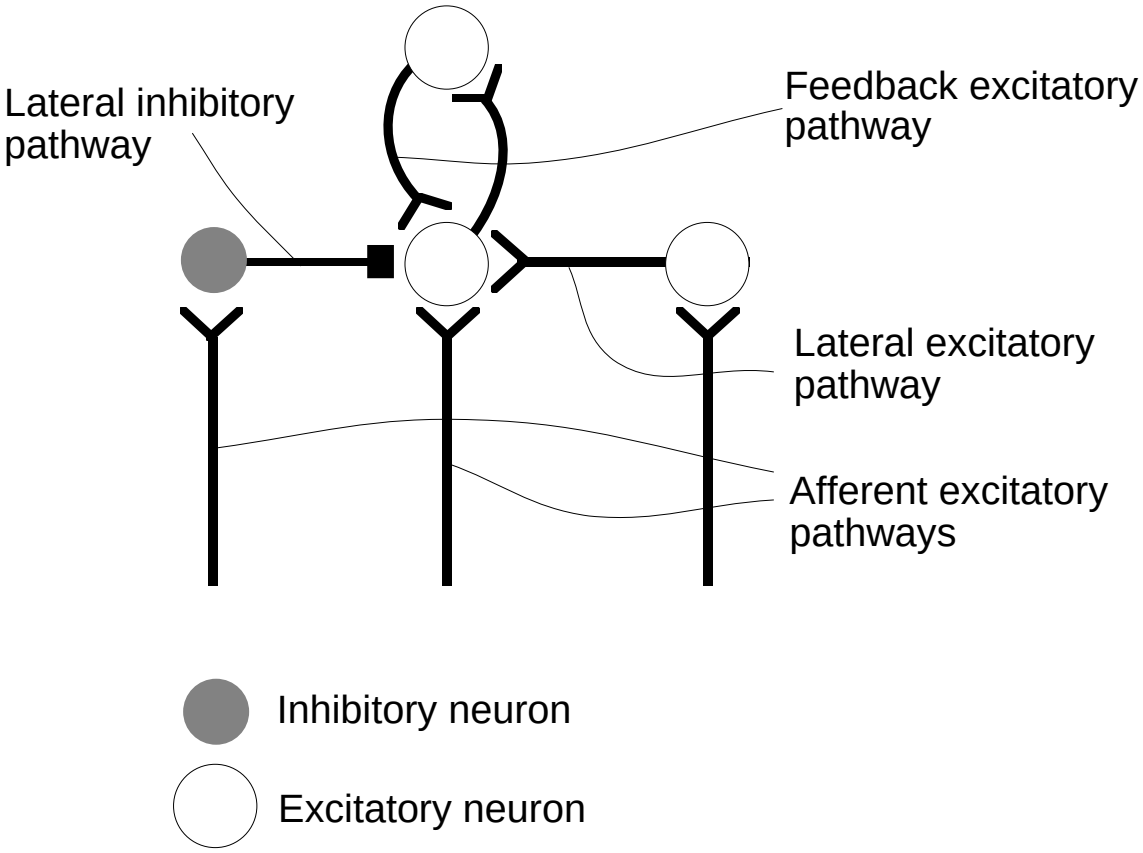

Figure 1.2: **Simplified neural circuit.**

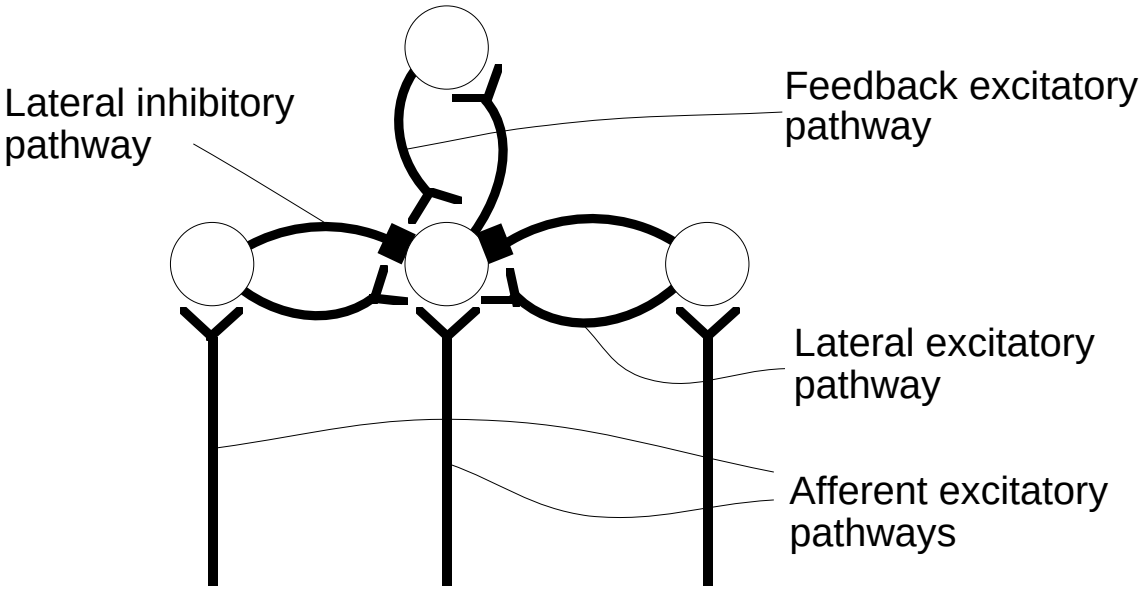

Figure 1.3: **Abstract neural circuit.**

neurons show preferential responsiveness to one of the eyes. Data from "classical" rearing experiments elucidate the development of afferent excitatory pathways and lateral excitatory and lateral inhibitory pathways and their role in the development of cortical properties.

Experiments involving visual deprivation of animals in their critical periods along with cortical infusion of pharmacological agents that block specific neural sites were designed to identify the site(s) of ocular dominance plasticity.

Artificial scotoma conditioning, localized peripheral stimulation, retinal lesions, and intracortical microstimulation in adult animals selectively activate small groups of cortical neurons. In these experiments, persistent changes in receptive field properties were studied. These experimental data provide insights into the neural basis of adult cortical plasticity.

1.3.1 Long-term synaptic plasticity

Plasticity has been induced experimentally in synapses between isolated test pathways and individual target neurons (Figure 1.4). The stimulation strength of the test pathway is the *pre*synaptic activation, and the activation of the target neuron is

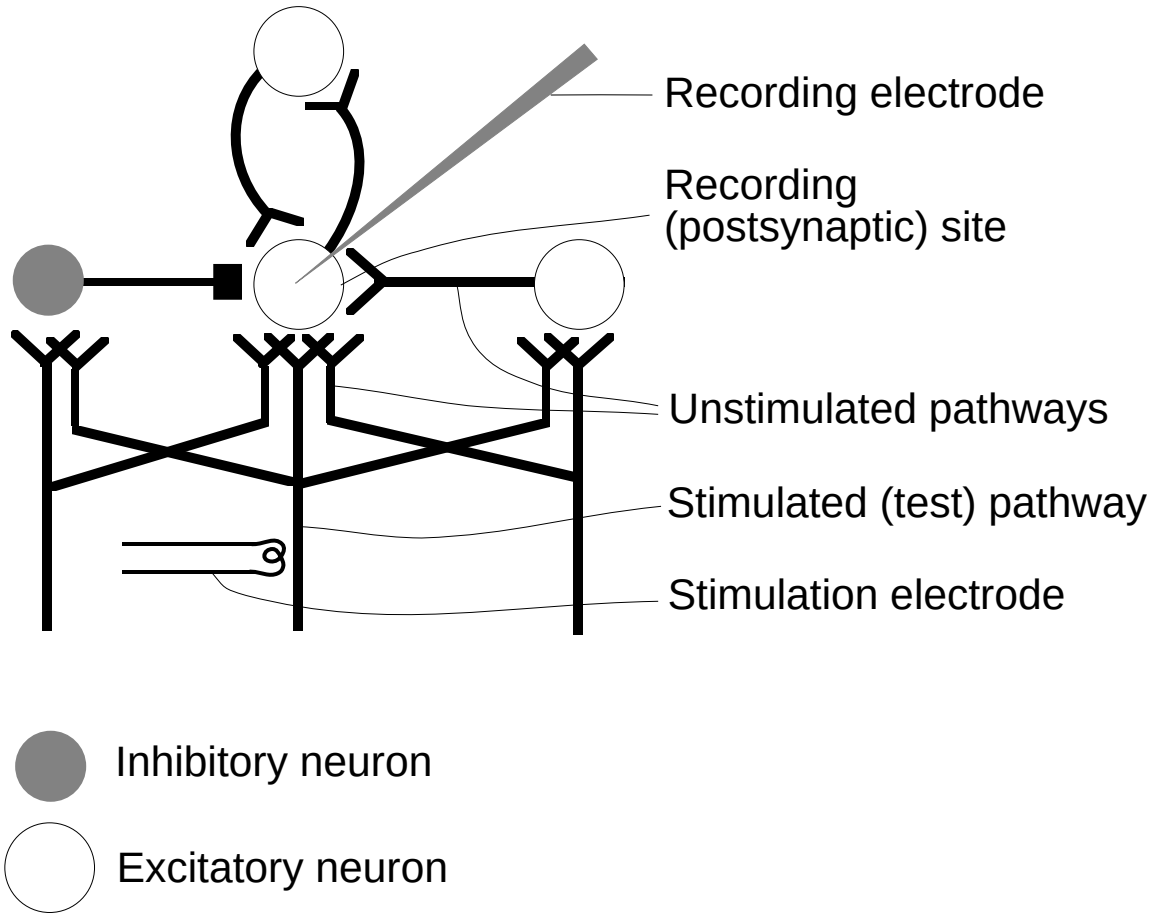

Figure 1.4: **Experimental configuration for experiments on long-term synaptic plasticity.**

the *post*synaptic activation. In these experiments, plasticity in the synapses is produced by artificially controlling the activations of the test pathway and the postsynaptic neuron. The test pathways can be stimulated by stimulation electrodes. The activation of the postsynaptic neuron can be controlled independently of the presynaptic activation by depolarizing or hyperpolarizing the postsynaptic neuron using current injections or pharmacological agents (Artola et al., 1990; Frégnac et al., 1994).

The efficacy of synapses between a pathway and a postsynaptic neuron is determined in terms of the activation subsequently evoked in the postsynaptic neuron in response to a test stimulation of the pathway.

During the conditioning phase, the correlation in the pre- and postsynaptic activation is maintained at some fixed level. Change in the efficacy of the synapses between the test pathway and the postsynaptic neuron is called *homosynaptic plasticity*. Synaptic plasticity in unstimulated pathways to the postsynaptic neuron is called *heterosynaptic plasticity*. An increase in synaptic efficacy is called synaptic *potentiation*, and a decrease in synaptic efficacy is synaptic *depression*.

Synaptic plasticity has been induced *in vitro* in brain slices from several different areas (e.g., cortex, hippocampus, cerebellum) and *in vivo* in young and adult animals. Induction of synaptic plasticity takes minutes and lasts for tens of minutes (Dudek & Bear, 1992; Frégnac et al., 1994; Kirkwood et al., 1993; Miles & Wong, 1987). Persistent synaptic plasticity is called long-term synaptic plasticity.

1.3.2 Cortical plasticity in early postnatal development

Changes in cortical neuronal properties such as orientation selectivity and ocular dominance in young animals are produced by manipulations of the visual input distribution.

For example, primary visual cortical neurons in cats have orientation selectivity from very early postnatal stages, but a normal visual environment is needed to maintain and develop orientation selectivity (Frégnac & Imbert, 1978). Optical recording of the developing primary visual cortex in very young ferrets showed that the structure of orientation maps is stable during development, but the orientation tuning of primary cortical neurons sharpens during normal development (Chapman et al., 1996). Weliky and Katz (1997) produced weakening of orientation selectivity of primary visual cortical neurons in ferret kittens by artificially correlated activation of optic nerve fibers, although the overall organization of orientation column maps was unaltered.

Dramatic changes in ocular dominance of primary cortical neurons are produced during a critical period (Hubel & Wiesel, 1970). The ocular dominance of primary cortical neurons is modified by the "classical" rearing paradigms, which include monocular deprivation, reverse suture, strabismus, binocular deprivation, and normal stimulation following monocular and binocular deprivation.

In monocular deprivation, one eye is deprived of visual stimulation while the other

eye receives normal visual stimulation (Hubel & Wiesel, 1970). Changes in ocular dominance can be induced within a few hours of monocular deprivation (Freeman & Olson, 1982). In reverse suture conditioning (Blakemore & Van Sluyters, 1974), after a period of monocular deprivation the previously closed eye is opened and the previously open eye is closed. In strabismus conditioning (Hubel & Wiesel, 1965), uncorrelated input to the eyes is surgically induced (e.g., by cutting muscles controlling eye movements in one eye). Uncorrelated input to the two eyes can also be produced by alternating occlusion of the eyes, rotating the image in one eye relative to the other, or simultaneously producing different patterns of stimulation on corresponding regions of the two eyes. Binocular deprivation is produced by deprivation of normal stimulation in both eyes for a period comparable to that of monocular deprivation (Wiesel & Hubel, 1965). In recovery experiments, normal binocular vision after weeks of monocular deprivation or binocular deprivation restores the ocular dominance distribution (Buisseret et al., 1982; Freeman & Olson, 1982).

1.3.3 Cortical plasticity during pharmacological infusions

The following experiments were designed to study the sites of ocular dominance plasticity. The basic idea was to block specific neural sites that are hypothesized to be involved in cortical plasticity. For example, based on theoretical and experimental considerations (Bear et al., 1987; Fox & Daw, 1993; Goda & Stevens, 1996), it has been hypothesized that NMDA receptors may be the site of synaptic plasticity and that postsynaptic activations are necessary to enable excitatory synaptic plasticity.

To test these predictions, the following experiments were performed. Reiter and Stryker (1988) locally infused muscimol, a GABA agonist selective for $GABA_A$ receptors, into the primary visual cortex of kittens during monocular deprivation. Muscimol at strong concentrations blocked postsynaptic action potentials without affecting presynaptic activity. Bear et al. (1990) treated kitten primary visual cortex with D,L-2-amino-5-phosphonovaleric acid (APV) during monocular deprivation. APV is an NMDA receptor antagonist. Visually evoked responses could be evoked during APV infusion at concentrations sufficient to block NMDA receptors (Bear et al., 1990).

Ocular dominance, responsiveness, and orientation selectivity of primary visual

cortical neurons are also affected by about 10 hours of infusion of an NMDA receptor antagonist in adult cats (Kasamatsu et al., 1997, 1998a) without any visual deprivation. Normal cortical properties are restored by 68 hours after cessation of APV infusion (Kasamatsu et al., 1997, 1998a).

1.3.4 Cortical plasticity induced by peripheral conditioning

Several experimental procedures (artificial scotoma conditioning, retinal lesions, localized repetitive peripheral stimulation) have been used to produce cortical plasticity in adult animals. In these experiments, the distribution of the peripheral input stimulation is such that a region of the cortex is stimulated while a neighboring region is unstimulated. In some of these experiments, the cortical plasticity has been studied in conjuction with behavioral changes produced by the conditioning.

The cortical plasticity observed in these experiments may be related to the phenomenon of perceptual learning. Because neurons in the cortex are selective for specific stimulus features, repeated presentation of training stimuli repeatedly activates a small group of neurons. Thus, perceptual learning may be realized by cortical plasticity that depends on repeated activation of a group of neurons, as in the following conditioning procedures.

In artificial scotoma conditioning (Pettet & Gilbert, 1992), a pattern of moving lines is presented in the visual field while masking out an artificial "scotoma" region covering the original receptive field of the recorded neuron. Cortical plasticity occurs after 10–15 minutes of conditioning and can last for as long as 20 minutes in the absence of any patterned visual stimulation. Cortical plasticity following artificial scotoma conditioning can be restored by presentation of moving lines in the entire visual field for about 10–15 minutes. Artificial scotoma conditioning can also produce short-term changes in neuronal properties (DeAngelis et al., 1995). A few seconds of artificial scotoma conditioning in human observers produces distortions in position judgments (Kapadia et al., 1994)

A permanent retinal scotoma can be produced by localized retinal lesions (Chino et al., 1992; Darian-Smith & Gilbert, 1995). Retinal lesions allow study of cortical plasticity over a long time range, e.g., a few minutes to hours of retinal lesions, to over

several months to a year after the lesions.

Repetitive stimulation of a restricted skin region for several weeks (Jenkins et al., 1990; Recanzone et al., 1992acde) produces extensive changes in cortical properties in primary somatosensory cortex. Recanzone et al. (1992acde) determined changes in behavior and somatosensory cortical receptive field properties following three to twenty weeks of training adult owl monkeys on a tactile frequency discrimination task.

1.3.5 Cortical plasticity induced by intracortical microstimulation

In experiments employing intracortical microstimulation, specific cortical sites are directly stimulated without any peripheral stimulation. Intracortical microstimulation involves stimulating a single cortical site by delivering current pulses using a microelectrode. Intracortical microstimulation almost simultaneously excites nearly all excitatory and inhibitory terminals and excitatory and inhibitory cortical neurons within a few microns of the stimulating electrode. The strength of excitation of cortical neurons, the afferent excitatory pathways, and the lateral inhibitory pathways is maximum at the intracortical microstimulation site and decreases with distance from the intracortical microstimulation site (Recanzone et al., 1992b). In addition, some of the excitatory and inhibitory terminals receive secondary, ortho- and antidromic excitation. However, not all ortho- and antidromically excited excitatory afferents succeed in driving their target neurons above threshold (Recanzone et al., 1992b). Two to six hours of intracortical microstimulation of a single site in layers 3–4 of primary somatosensory cortex of rats and monkeys produced extensive reorganization of receptive field topography (Recanzone et al., 1992b).

1.4 The rules of long-term synaptic plasticity

In this section, the synaptic plasticity rules used to model long-term synaptic plasticity and cortical plasticity are briefly described.

Response properties of neurons can change because of synaptic plasticity in the various pathways to the neurons (Figure 1.2). Thus, long-term synaptic plasticity in

afferent, feedback, and lateral excitatory pathways and in lateral inhibitory pathways may be responsible for cortical plasticity.

Previous models of cortical development and cortical plasticity were based on synaptic plasticity in afferent excitatory pathways (Bienenstock et al., 1982; Clothiaux et al., 1991; Kohonen, 1987; Linsker, 1986abc; von der Malsburg, 1973; Miller et al., 1989). Grossberg (1976abc, 1980, 1982) used synaptic plasticity in afferent excitatory and feedback excitatory pathways to model development of feature detectors and neural codes. Lateral excitatory synaptic plasticity has been used in models of the development of cortical properties and cortical plasticity (Grajski & Merzenich, 1990; von der Malsburg & Singer, 1988).

Many models (e.g., Douglas & Martin, 1991; von der Malsburg & Singer, 1988; Marshall, 1989, 1990abcd; Marshall & Alley, 1993; Marshall et al., 1996ab; Martin & Marshall, 1993; Sirosh et al., 1996; Sirosh & Miikkulainen, 1997; Somers et al., 1995, 1998; Xing & Gerstein, 1994) have emphasized lateral intracortical interactions to model several cortical and perceptual properties. In fact, geniculocortical afferent synapses comprise only 4% to 24% of all synapses received by layer 4 neurons (Ahmed et al., 1994; Einstein et al., 1987; Peters & Payne, 1993). Furthermore, recent anatomical, electrophysiological, and optical recording based studies have shown that the interlayer and lateral pathways within the primary visual cortex are highly specific and that their connectivity is related to the stimulus feature selectivities of the neurons. Long-range intracortical horizontal pathways (Gilbert & Wiesel, 1979) develop during the early postnatal stages during which ocular dominance and orientation selectivity develop and are refined (Dalva & Katz, 1994; Katz & Callaway, 1992; Löwel & Singer, 1992). The long-range pathways connect non-adjacent cortical neurons having similar input feature selectivity, e.g., orientation selectivity (Gilbert & Wiesel, 1989). Thus, it is possible that lateral intracortical interactions may contribute to cortical development and adult cortical plasticity. However, the development of lateral pathways during early postnatal stages and its effects on cortical properties have not been fully explored.

XX

Synaptic and cortical plasticity produced by the conditioning procedures described

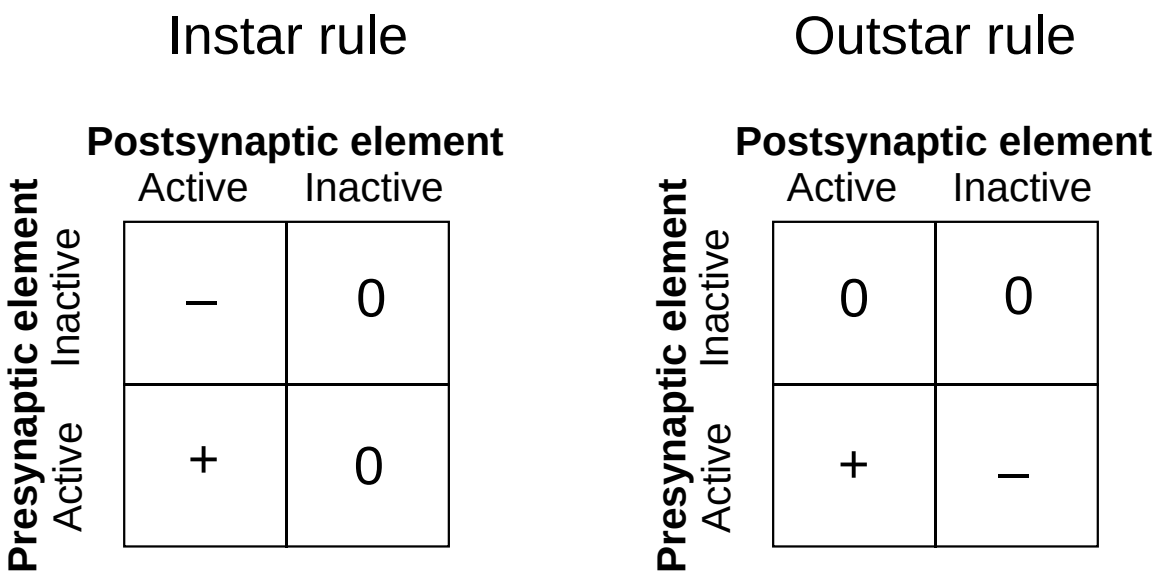

Figure 1.5: **Comparison of instar and outstar plasticity rules.** The symbol '+' represents synaptic potentiation, '–' represents synaptic depression, and '0' represents no synaptic plasticity. In an instar rule, when the *post*synaptic neuron is inactive synaptic plasticity is disabled, and when the *post*synaptic neuron is active, synaptic potentiation occurs when the presynaptic activation is strong and synaptic depression occurs when the presynaptic activation is very weak or absent. In an outstar rule, when the *pre*synaptic neuron is inactive synaptic plasticity is disabled, and when the *pre*synaptic neuron is active, synaptic potentiation occurs when the postsynaptic activation is strong and synaptic depression occurs when the postsynaptic activation is very weak or absent.

in Section 1.3 are modeled using the EXIN rules (Marshall, 1995a), which consist of an *instar* afferent excitatory synaptic plasticity rule and an *outstar* lateral inhibitory synaptic plasticity rule. In an instar rule, plasticity is enabled when the *post*synaptic neuron is active, and the weights of pathways *in*to the postsynaptic neuron are adjusted according to the *pre*synaptic signals on the pathways. (Grossberg, 1976ab). In an outstar rule, plasticity is enabled when the *pre*synaptic neuron is active, and the weights of pathways *out* of the presynaptic neuron are adjusted according to the *post*synaptic activations of the pathway targets (Grossberg, 1976c). Some experimental data on excitatory synaptic plasticity are modeled using an outstar feedback excitatory synaptic plasticity rule (Grossberg, 1976c).

XX

The instar excitatory and the outstar excitatory synaptic plasticity rules are part of the adaptive resonance theory (ART) network (Carpenter & Grossberg, 1987). The instar excitatory and the outstar *inhibitory* synaptic plasticity rules form the EXIN model (Marshall, 1995a). Thus, the synaptic plasticity rules used in the models in this dissertation have been previously used to model some cortical properties. However, the work presented in this dissertation is original in applying these rules (especially the lateral inhibitory plasticity rule), to some classical problems – classical "rearing" conditioning, long-term potentiation, and long-term depression – and to some recently discovered phenomena – ocular dominance changes during visual deprivation with cortical infusion of pharmacological agents in animals in their critical period, dynamic receptive field changes in adult animals after artificial scotoma conditioning, and changes in receptive field topography after intracortical microstimulation and local peripheral stimulation in adult animals. Novel explanations are proposed for receptive field changes in adults, long-term potentiation and long-term depression, and ocular dominance plasticity during visual deprivation with cortical infusion of pharmacological agents. Furthermore, novel experiments are suggested based on the modeling.

1.5 Relation to previous theories

Neural networks that self-organize using unsupervised learning rules can model how cortical circuitry and receptive field properties form during biological development and how they change in adults in response to the input environment (Grossberg, 1982; von der Malsburg & Singer, 1988; Willshaw & von der Malsburg, 1976). Thus, self-organization provides a unified framework for discussing and understanding synaptic plasticity, cortical circuits, receptive field properties, and behavior.

A unifying theory based on self-organization has succeeded in modeling several cortical properties and functions – disparity selectivity (Marshall, 1990c), motion selectivity and grouping (Marshall, 1990a, 1995b; Schmitt & Marshall, 1995, 1996), visual inertia (Hubbard & Marshall, 1994), the aperture problem (Marshall, 1990a), length selectivity and end-stopping (Marshall, 1990b), visibility/invisibility and depth from occlusion

events (Marshall & Alley, 1993; Marshall et al., 1996a), depth from motion parallax (Marshall, 1989), motion smearing (Martin & Marshall, 1993), orientation selectivity (Marshall, 1990d), and stereomatching (Marshall & Kalarickal, 1995; Marshall et al., 1996b). The proposed research provides further support for a unified theory of cortical processing based on self-organization.

Recent neural network models (Marshall, 1995a; Marshall & Gupta, 1998) have demonstrated that the outstar lateral inhibitory synaptic plasticity rule leads to the development of neurons with high stimulus feature selectivity and high stimulus discrimination. Lateral inhibitory synaptic plasticity also reduces redundancy in neural coding and produces sparse, distributed codes for input stimuli (Marshall & Gupta, 1998; Sirosh et al., 1996). Marshall (1995a) has shown that neural networks using the instar afferent excitatory synaptic plasticity rule in concert with the outstar inhibitory synaptic plasticity rule can self-organize to represent multiple simultaneously presented input stimuli, represent transparency, perform scale and context sensitive processing, and maintain high discrimination in the presence of noise.

XX

1.6 Emphasis on lateral inhibitory interactions

In this dissertation, the role of lateral inhibitory plasticity in producing cortical plasticity is emphasized. In the cortex, there are lateral excitatory and lateral inhibitory pathways (Gilbert & Wiesel, 1989; McGuire et al., 1991; Somogyi et al., 1983; Somogyi & Martin, 1985). The lateral excitatory and inhibitory pathways terminate on excitatory and inhibitory neurons. Stimulation of thalamocortical pathways produces a monosynaptic excitatory postsynaptic potential (EPSP) and disynaptic inhibitory postsynaptic potential (IPSP) in primary visual cortical neurons, and disynaptic EPSPs are occasionally produced (Gil & Amitai, 1996; Ferster, 1989). Direct stimulation of lateral excitatory pathways have an excitatory effect at low stimulation strength and have an inhibitory effect at high stimulation strength (Gil & Amitai, 1996; Weliky et al., 1995). In addition, cortical neurons receive feedback excitatory inputs from other cortical layers.

Thus, the response properties of cortical neurons depends on a combination of the various pathways onto the neurons.

The EXIN model, however, does not have lateral excitatory connections. But, lateral excitatory connections with signal transmission latencies have been used in conjunction with the EXIN rules to model several aspects of visual motion perception (Hubbard & Marshall, 1994; Marshall, 1989, 1990a, 1991, 1995b; Marshall & Alley, 1993; Martin & Marshall, 1993). Plasticity in lateral excitatory pathways has been used in development of topologically ordered RFs (Sirosh & Miikkulainen, 1994b).

In the EXIN simulations presented in the dissertation, lateral excitatory pathways were not incorporated. This simplified the simulations. The use of lateral inhibitory pathways alone is justified by the observation that in the cortex, suprathreshold stimulation produces overall inhibitory lateral interaction (Ferster, 1989; Gil & Amitai, 1996; Toth et al., 1996; Weliky et al., 1995). The overall lateral interaction is facilitatory when the input stimulus is subthreshold (Toth et al., 1996). Combined measurement of spiking point-spread using extracellular recording and optical point-spread in cat primary visual cortex showed that the spiking point-spread accounts for only 5% of the optical point-spread; the remainder of the optical point-spread was largely caused by inhibition (Das & Gilbert, 1995a). Thus, the EXIN model can be viewed is a functional model that describes the overall effect of lateral interactions in the cortex.

Furthermore, lateral inhibition strongly influences most cortical properties. Several stimulus feature specificities of cortical neurons such as orientation selectivity and spatial frequency selectivity are abolished by cortical infusion of a $GABA_A$ antagonist (Sillito, 1975, 1977, 1979). Blocking intracortical inhibition also reveals new peripheral regions capable of evoking neuronal responses (Lane et al., 1997; Sillito et al., 1981). Thus, changes in overall lateral inhibitory strength can contribute to cortical plasticity.

Neurophysiologically, the EXIN lateral inhibitory synaptic plasticity rule could be realized in a disynaptic circuit containing a lateral excitatory horizontal connection (either short- or long-range) and an inhibitory interneuron, either by modifying the excitatory weights from the excitatory neuron or by changing the inhibitory weight from the inhibitory neuron (Darian-Smith & Gilbert, 1994, 1995; Das & Gilbert, 1995ab; Gilbert et al., 1996;

Hirsch & Gilbert, 1993).

XX

1.7 Thesis statement

Lateral inhibitory plasticity is crucial in modeling a diverse set of cortical and behavioral properties and functions. Together with excitatory plasticity, it allows the self-organization of neural network models that exhibit many fundamental properties found in neurobiological experiments: the cortical, synaptic, and behavioral reorganization that follows classical rearing conditioning, artificial scotoma conditioning, retinal lesions, intracortical microstimulation, repetitive peripheral stimulation, and neuropharmacological manipulations. These reorganization properties can be seen as manifestations of the more general properties of high selectivity, high discrimination, and efficient representation that emerge from lateral inhibitory synaptic plasticity.

1.8 Overall contributions and significance

Experimental data from different conditioning paradigms – stimulation of individual pathways and isolated postsynaptic neurons, classical rearing, artificial scotoma conditioning, retinal lesions, local peripheral stimulation, intracortical microstimulation, and pharmacological treatments – are modeled using a small set of simple synaptic plasticity rules. This work

1. models the phenomena of long-term potentiation and depression;
2. models ocular dominance plasticity in during classical rearing procedures and during visual deprivation with pharmacological infusions in the cortex;
3. provides a complete model for dynamic receptive field changes produced by artificial scotoma conditioning;
4. models changes in receptive field properties after retinal lesions;
5. models changes in receptive field topography after intracortical microstimulation;

6. models changes in receptive field properties and improvement in stimulus discrimination after repeated localized peripheral stimulation;
7. compares the EXIN model with other models for synaptic and cortical plasticity;
8. demonstrates the dramatic effects that are produced by the subtle distinctions between instar, outstar, and covariance rules;
9. analyzes the role of lateral inhibitory synaptic plasticity in neuronal feature selectivity and stimulus discrimination during development and adult cortical plasticity; and
10. suggests novel and feasible experiments to test predictions of the models.

Overall, the dissertation provides further support for a unified theory of cortical processing based on self-organization and highlights the possible role of lateral inhibitory synaptic plasticity in cortical development and adult cortical plasticity. Novel experiments and the predictions of the models are provided to facilitate further experimental investigations of cortical development and adult cortical plasticity. Furthermore, the simulations demonstrate that the outstar lateral inhibitory synaptic plasticity rule is sufficient to model the receptive field changes produced by artificial scotoma conditioning and localized peripheral stimulation in adult animals. Because artificial scotoma conditioning and localized peripheral stimulation are similar to the conditioning procedures used in perceptual learning, lateral inhibitory synaptic plasticity may also be involved in perceptual learning.

1.9 Outline of the dissertation

The dissertation is organized as follows. The main chapters (Chapters 2–6) are each self-contained and can be read independently of one another. In these chapters, specific cortical plasticity phenomena are modeled, and novel experiments are proposed based on the predictions of the models.

In Chapter 2, the phenomena of long-term potentiation (LTP) and long-term depression (LTD) are modeled using the instar and the outstar excitatory synaptic plasticity

rules. The experiments on synaptic plasticity provide direct evidence for the relationship between correlation in pre- and postsynaptic activation and synaptic plasticity. The working hypothesis is that long-term synaptic plasticity is responsible for the development and refinement of cortical properties and functions during early postnatal stages and for cortical plasticity in adults. Thus, the rules for synaptic plasticity used for modeling cortical development and adult cortical plasticity must be consistent with data on long-term synaptic plasticity. This chapter shows that the instar and the outstar excitatory synaptic plasticity rules model data on LTP and LTD more accurately than a popular excitatory synaptic plasticity rule, the BCM rule (Bienenstock, Cooper, & Munro, 1982). Furthermore, the properties of the outstar lateral inhibitory synaptic plasticity rule are characterized and compared with the few available experimental data on inhibitory synaptic plasticity. The functional roles of the instar and outstar excitatory and the outstar lateral inhibitory synaptic plasticity rules in development of cortical properties are discussed.

Chapter 3 presents computer simulations of the effects of afferent excitatory and lateral inhibitory synaptic plasticity rules on ocular dominance, responsiveness, and receptive field width of model cortical neurons during classical rearing conditioning. The model is based on the EXIN synaptic plasticity rules (Marshall, 1995a), which consist of the instar afferent excitatory and the outstar lateral inhibitory synaptic plasticity rules. In the model, the afferent excitatory synaptic plasticity plays the primary role in ocular dominance plasticity during the classical rearing paradigms, and lateral inhibitory interactions produce secondary ocular dominance changes. The relationship between the strength of lateral inhibitory pathway weights and the ocular dominance distribution after normal rearing is demonstrated.

In Chapter 4, the effects of cortical infusion of an NMDA antagonist (Bear et al., 1990) and a GABA agonist (Reiter & Stryker, 1988) during monocular deprivation and effects of cortical infusion of an NMDA antagonist on ocular dominance in adult animals (Kasamatsu et al., 1997, 1998a) are modeled. The salient effects produced by the model are caused by lateral inhibitory interactions, and the model is consistent with experimental data on excitatory synaptic plasticity in the presence of NMDA receptor antagonists and postsynaptic hyperpolarization.

In Chapter 5, the dynamic changes in the size, shape, and position of neuronal receptive fields in response to artificial scotoma conditioning (Pettet & Gilbert, 1992; DeAngelis et al., 1995) and retinal lesions (Darian-Smith & Gilbert, 1995) are modeled using the EXIN synaptic plasticity rules. The effects produced by the EXIN rules are compared with those produced by models based on neuronal adaptation (Xing & Gerstein, 1994) and on the LISSOM learning rules (Sirosh et al., 1996). The comparison of the effects produced by the models and the neurophysiological data show that the outstar lateral inhibitory synaptic rule and the LISSOM lateral excitatory rule provide the best fit for the experimental data. A novel *complementary scotoma* conditioning experiment, in which stimulation of scotoma and non-scotoma regions are alternated repeatedly, is proposed to differentiate the outstar lateral inhibitory synaptic rule and the LISSOM lateral excitatory synaptic plasticity rule.

A model for the dynamic changes in the size and position of neuronal receptive fields in response to intracortical microstimulation (Recanzone et al., 1992b) based on the EXIN synaptic plasticity rules is presented in Chapter 6. Changes in cortical topography, receptive field properties, and stimulus discrimination following local repetitive peripheral stimulation (Jenkins et al., 1990; Recanzone et al., 1992acde) are also modeled. The effects of the outstar lateral inhibitory synaptic plasticity rule during ICMS and peripheral stimulation on the relationship between receptive field size and cortical magnification is also analyzed.

The final chapter, Chapter 7, summarizes the main results of the dissertation and presents several research questions related to the issues addressed in this dissertation.

Chapter 2

Comparison of generalized Hebbian rules for long-term synaptic plasticity

Abstract

A large variety of synaptic plasticity rules have been used in models of excitatory synaptic plasticity (Brown et al., 1990). These rules are generalizations of the Hebbian rule and have some properties consistent with experimental data on long-term excitatory synaptic plasticity, but they also have some properties inconsistent with experimental data. For example, the BCM rule (Bear et al., 1987; Bienenstock et al., 1982) produces homosynaptic potentiation and depression, which has been observed experimentally (Artola et al., 1990; Dudek & Bear, 1992; Kirkwood et al., 1993; Frégnac et al., 1994; Yang & Faber, 1991). But the BCM rule is also inconsistent with some experimental results; e.g., the BCM rule cannot produce heterosynaptic depression (Abraham & Goddard, 1983; Lynch et al., 1977). In addition, long-term synaptic plasticity in inhibitory pathways has been emphasized in some models of cortical function (Marshall, 1990abc, 1995a; Sirosh et al., 1996), but experimental data on inhibitory synaptic plasticity is

sparse. This paper compares three popular excitatory synaptic plasticity rules – the BCM rule, the instar rule (Grossberg, 1972, 1976ab; Kohonen, 1988; Levy & Burger, 1987; Levy & Desmond, 1985; Marshall, 1995a), and the outstar excitatory rule (Grossberg, 1976c; Rescorla & Wagner, 1972) – and presents and characterizes the outstar inhibitory synaptic plasticity rule (Marshall, 1995a). These rules are evaluated by comparing their predictions with neurobiological data.

2.1 Introduction

There is a large number of synaptic plasticity rules that have been proposed to model developmental, structural, functional, cognitive, and behavioral properties of animal brains (Bienenstock et al., 1982; Grossberg, 1972, 1976abc, 1980, 1982; Kohonen, 1987, 1988; Linsker, 1986abc, 1988; von der Malsburg, 1973; Marshall, 1995a; Miller et al, 1989; Rescorla & Wagner, 1972; Rumelhart & McClelland, 1986; Sejnowski, 1977ab; Sirosh & Miikkulainen, 1994b). Experimentally, synaptic plasticity in excitatory synapses has been extensively studied in hippocampus (Brown et al., 1990), sensory neocortex (Kirkwood et al., 1993), and cerebellum (Crepel et al., 1995). But there have been very few studies comparing abstract synaptic plasticity rules with experimental data (e.g., Bear et al., 1987; Dudek & Bear, 1992). In addition, only a few models use and emphasize the role of inhibitory synaptic plasticity (e.g., Marshall, 1990abc, 1995a; Marshall & Gupta, 1998; Sirosh & Miikkulainen, 1996) in development of important computational and neurobiological properties.

In this paper, a widely studied (both theoretically and experimentally) synaptic plasticity rule – the BCM rule (Bear et al., 1987; Bienenstock et al., 1982; Clothiaux et al., 1991) – is compared with two generalized Hebbian (Brown et al., 1990) excitatory synaptic plasticity rules – an instar excitatory synaptic plasticity rule (Grossberg, 1972, 1976ab; Kohonen, 1988; Levy & Desmond, 1985; Levy & Burger, 1987; Marshall, 1995a) and an outstar excitatory synaptic plasticity rule (Grossberg, 1976c; Rescorla & Wagner, 1972) – and with the experimental data on excitatory synaptic plasticity. The plasticity governed by an instar rule is enabled when the *post*synaptic

neuron is activated, and excitatory pathways *in*to the neuron undergo synaptic plasticity (Grossberg, 1972, 1976ab). In contrast, the plasticity governed by an outstar rule is enabled when the *pre*synaptic neuron or presynaptic element is activated, and excitatory pathways *out* of the neuron undergo synaptic plasticity (Grossberg, 1976c). This paper furthermore describes an outstar *inhibitory* synaptic plasticity rule and elucidates and compares the rule's properties with the currently sparse experimental database on inhibitory synaptic plasticity.

Many experimental results on excitatory synaptic plasticity have been attributed to the covariance rule (Sejnowski, 1977ab; Stanton & Sejnowski, 1990) or the BCM rule (Bear et al., 1987; Dudek & Bear, 1992). This paper shows that many of the experimental data are also consistent with the instar and outstar excitatory synaptic plasticity rules. Only a few experiments are available today to illuminate the subtleties of the different rules. Thus, novel experiments are proposed, and explicit predictions of the synaptic plasticity rules are made. The plausible functional capabilities of the rules are also discussed.

The instar excitatory synaptic plasticity rule alone can be used to self-organize a neural network that categorizes arbitrary input patterns (Carpenter & Grossberg, 1987; Grossberg, 1976ab, 1980, 1982; Marshall, 1995a; Nigrin, 1993). The instar excitatory synaptic plasticity rule moves the synaptic input weight vector of an active neuron closer to the presynaptic activation vector.

The outstar excitatory synaptic plasticity rule has been used to govern synaptic efficacy of feedback pathways roles (Baloch & Grossberg, 1997; Carpenter & Grossberg, 1987; Grunewald & Grossberg, 1997; Grossberg et al., 1997a; Schmitt & Marshall, 1995; Nigrin, 1993) and to make predictions in classical conditioning protocols (Pavlov, 1927; Rescorla & Wagner, 1972; Schmajuk, 1997). The outstar excitatory synaptic plasticity rule moves the synaptic output weight vector of an active neuron closer to the postsynaptic activation vector.

The outstar lateral inhibitory synaptic plasticity rule produces strong lateral inhibitory pathways between neurons that are consistently coactivated (Marshall, 1995a). Neurons are consistently coactivated if they are selective for similar patterns, and the strong lateral inhibition between such neurons improves stimulus discriminability. According

to the outstar lateral inhibitory synaptic plasticity rule, lateral inhibitory pathways between neurons that are not consistently coactivated become weak. Neurons are not consistently coactivated if they are selective for very different input patterns. This selective development of lateral inhibitory pathways between neurons leads to exclusive allocation and simultaneous representation of separate multiple patterns, e.g., transparently overlaid surfaces (Marshall, 1995a; Marshall et al., 1996b).

The instar excitatory and the outstar inhibitory synaptic plasticity rules have been used together within a single model, and they are together referred to as the EXIN synaptic plasticity rules (Marshall, 1995a). The EXIN rules develop an efficient representation of input patterns according to their distribution in an input environment. The EXIN rules self-organize networks capable of representing multiple superimposed patterns, ambiguous patterns, overlapping patterns at different scales, and contextually constrained patterns starting from completely nonspecific afferent excitatory and lateral inhibitory pathway weights (Marshall, 1995a). In EXIN networks, the instar excitatory synaptic plasticity rule modifies weights so that the active neurons become more responsive to the currently presented input pattern. The development of weights of lateral inhibitory pathways according to the outstar lateral inhibitory synaptic plasticity rule ensures that different neurons become selective to different input patterns. Yet if the input environment contains several similar patterns, the outstar lateral inhibitory synaptic plasticity rule develops strong lateral inhibitory pathways between neurons selective for the similar input patterns, thereby producing high discrimination. In EXIN networks, lateral inhibitory pathways from often activated neurons to unresponsive neurons weaken, thereby making the unresponsive neurons more likely to respond to some input. This feature of the EXIN lateral inhibitory synaptic plasticity rule is comparable to that of "conscience" rules (DeSieno, 1988).

EXIN synaptic plasticity rules have been used to model the development of visual motion selectivity and grouping (Marshall, 1990a), visual inertia (Hubbard & Marshall, 1994), motion integration in the aperture problem (Marshall, 1990a), length selectivity and end-stopping (Marshall, 1990b), depth perception from occlusion events (Marshall & Alley, 1993; Marshall et al., 1996a), depth from motion parallax (Marshall, 1989), motion smearing (Martin & Marshall, 1993), orientation selectivity

(Marshall, 1990d), stereomatching (Marshall et al., 1996b), dynamic receptive field changes produced by artificial scotoma conditioning (Kalarickal & Marshall, 1997b; Marshall & Kalarickal, 1997), and changes in somatosensory cortical RF structure after intracortical microstimulation (Kalarickal & Marshall, 1998b).

The BCM synaptic plasticity rule (Bienenstock et al., 1982) has been used to model the results of "classical" rearing conditions (Bienenstock et al., 1982; Clothiaux et al., 1991). The important feature of the BCM rule is its adaptable synaptic modification threshold. The adaptable synaptic modification threshold is nonlinearly related to the activation history of the postsynaptic neuron and contributes to the development of selectivity and stability of the system in the absence of lateral inhibition (Bienenstock et al., 1982; Intrator & Cooper, 1992; Shouval et al., 1996). The synaptic modification function proposed by the BCM rule has been shown to be in partial agreement with studies on synaptic plasticity (Bear et al., 1987; Dudek & Bear, 1992; Kirkwood et al., 1993). These properties cannot be produced by some other synaptic plasticity rules, such as the covariance rule (Sejnowski & Stanton, 1990; Brown & Chattarji, 1995).

In the cortex, interactions via lateral pathways may influence cortical neuronal properties (Gilbert et al., 1990). In fact, geniculocortical synapses comprise only 4% to 24% of all synapses received by layer 4 neurons (Ahmed et al., 1994; Einstein et al., 1987; Peters & Payne, 1993). Recent models (e.g., Kalarickal & Marshall, 1997b, 1998b; Marshall, 1989, 1990abc; Marshall & Alley, 1993; Marshall et al., 1996ab; Marshall & Kalarickal, 1997; Martin & Marshall, 1993; Sirosh et al., 1996; Somers et al., 1995) have emphasized lateral intracortical interactions to model several cortical and perceptual properties. In the simulations the synaptic plasticity rules are applied in a small, simple model neural network to demonstrate the properties that can be produced by the rules because of network interactions.

2.2 Methods

In the simulations, a simple two layered network was used. Layer 1 may correspond to part of the lateral geniculate nucleus (LGN), and Layer 2 may correspond to part of the

primary visual cortex. In Section 2.2.1, the activation equation used in the simulations is described. Section 2.2.2 describes the BCM, the instar, and the outstar excitatory synaptic plasticity rules and the outstar inhibitory synaptic plasticity rule.

2.2.1 The activation equation

In order to analyze the influence of lateral interactions on the various synaptic plasticity rules, a non-linear activation equation was used. The activation equation expresses the activation of neurons in terms of the total excitation and inhibition received by the neurons. Let i refer to Layer 1 neurons and j to Layer 2 neurons. The activation level x_j of a neuron j was governed by a shunting equation (Grossberg, 1972) based on the Hodgkin (1964) model:

$$\frac{d}{dt}x_j \;=\; -Ax_j \;+\; \beta(B - x_j)E_j \;-\; \gamma(C + x_j)I_j, \tag{2.1}$$

where A, B, C, β, and γ are constants, and E_j and I_j represent respectively the neuron's total afferent excitatory and lateral inhibitory input signals. Because Equation 2.1 is a shunting equation, if $x_j(0) \in [-C, B]$ then $x_j(t) \in [-C, B]$ for all time $t \geq 0$ (Cohen & Grossberg, 1983). Thus, activation levels remain within a bounded range, between $-C$ and B. The total input excitation E_j was defined as

$$E_j = \left(\sum_i [x_i] W_{ij}^{+} \right), \tag{2.2}$$

and the total input inhibition I_j was given by

$$I_j = \sum_k [x_k] W_{kj}^{-}, \tag{2.3}$$

where $[a] \equiv \max(a, 0)$, $W_{ij}^{+} \geq 0$ represents the weight of the afferent excitatory pathway from presynaptic neuron i to postsynaptic neuron j, and $W_{kj}^{-} \geq 0$ represents the weight of the lateral inhibitory pathway from presynaptic neuron k to postsynaptic neuron j. Parameters β and γ govern the effectiveness of the excitation and inhibition, respectively, received by a neuron.

The shunting equation (Equation 2.1) with $W_{jk}^{-} = W_{kj}^{-} \geq 0$, belongs to a class of competitive dynamical systems that are absolutely stable; i.e., the system has fixed points

(stable equilibrium states) for any choice of parameters (Cohen & Grossberg, 1983). The neuronal activations in such a system are guaranteed to reach stable equilibrium values for all synaptic weight values, with the restriction that $W_{jk}^{-} = W_{kj}^{-} \geq 0$ for all pairs of neurons.

However, it is not known whether the shunting equation remains absolutely stable when $W_{jk}^{-} \neq W_{kj}^{-}$ for some pairs of neurons. Nevertheless, empirically the shunting equation reaches an equilibrium state even when reciprocal pairs of lateral inhibitory weights are not equal.

2.2.2 Synaptic plasticity rules

This section briefly describes the BCM rule, the instar excitatory synaptic plasticity rule, the outstar excitatory synaptic plasticity rule, and the outstar inhibitory synaptic plasticity rule.

The BCM excitatory synaptic plasticity rule

According to the theory presented by Bienenstock, Cooper, & Munro (1982), synaptic weights change over time as a function of local and global variables. Bienenstock et al. (1982) proposed a synaptic plasticity rule, now known as the BCM rule, to model ocular dominance plasticity in animals during a critical period. The focus of the BCM synaptic plasticity rule is a variable threshold, which depends on the postsynaptic activation history, and which controls whether the synaptic weights undergo potentiation or depression (Bienenstock et al., 1982; Clothiaux et al., 1991; Intrator & Cooper, 1992). According to a recent formulation of the BCM synaptic plasticity rule (Clothiaux et al., 1991; Intrator & Cooper, 1992; Shouval et al., 1996),

$$\frac{d}{dt} W_{ij}^{+}(t) \;=\; \eta\, \phi\left(x_j(t), \theta_j(t)\right)\; x_i(t)\,, \tag{2.4}$$

where x_i is the presynaptic activation, x_j is the postsynaptic activation, and η is a small positive constant that determines the magnitude of the synaptic modification. The function ϕ is

$$\phi\left(x_j(t), \theta_j(t)\right) \;=\; x_j(t)\;\left(x_j(t) \;-\; \theta_j(t)\right) \tag{2.5}$$

(Shouval et al., 1996), and $\theta_j(t)$ is a nonlinear time-averaged function of the postsynaptic activation given by

$$\theta_j(t) \;=\; \frac{1}{\tau}\int_{-\infty}^{t}\left(\frac{x_j(t')}{c_0}\right)^p \exp\left(-\frac{t-t'}{\tau}\right) dt' \tag{2.6}$$

(Clothiaux et al., 1991; Intrator & Cooper, 1992), where c_0 and τ are positive constants. The parameter p is chosen to be greater than 1. The usual choice is $p = 2$ (Clothiaux et al., 1991). Choosing $p > 1$ causes the BCM rule to give neurons high selectivity for input features (Bienenstock et al., 1982; Intrator & Cooper, 1992). The constant c_0 is a normalizing constant. The parameter τ controls the rate of change of θ_j; as τ increases, θ_j changes more slowly in response to changes in the neuronal activation.

According to the shunting equation (Equation 2.1),the activation level of neurons can go below zero. No output signals or spikes are given below the zero level. Therefore, in the simulations $x_j(t)$ and $x_i(t)$ are replaced by $[x_j(t)]$ and $[x_i(t)]$, respectively, in Equations 2.4, 2.5, and 2.6. In the simulations using the BCM synaptic plasticity rule (Section 2.3.3), the plasticity is disabled when either the presynaptic activation or the postsynaptic activation is less than or equal to zero, i.e., when one or both neurons are hyperpolarized.

In the simulations, changes in the BCM LTP threshold was approximated by

$$\theta_j(t+1) \;=\; \theta_j(t)\exp\left(\frac{-1}{\tau}\right) \;+\; \left(\frac{[x_j(t+1)]}{c_0}\right)^p \left(1-\exp\left(\frac{-1}{\tau}\right)\right), \tag{2.7}$$

by assuming that $x_j(t') \approx x(t+1)$ for $t' \in (t, t+1]$.

The instar excitatory synaptic plasticity rule

The instar excitatory synaptic plasticity rule (Grossberg, 1972, 1982) is a variant of a Hebbian rule. In an instar plasticity rule, *post*synaptic activity enables the plasticity; when the plasticity is enabled, the weight tends to become proportional to the *pre*synaptic activity. The rule can be expressed (Grossberg, 1982) as

$$\frac{d}{dt}W_{ij}^{+}(t) \;=\; \epsilon\,\mathcal{F}\left(x_j(t)\right)\left(-W_{ij}^{+}(t) \;+\; \mathcal{P}(x_i(t))\right), \tag{2.8}$$

where $\epsilon > 0$ is a small learning rate constant, and $\mathcal{F}$ and $\mathcal{P}$ are half-rectified non-decreasing functions. Thus, *whenever a neuron is active, its input excitatory connections from*

active neurons tend to become slightly stronger, while its input excitatory connections from inactive neurons tend to become slightly weaker. Neuron activations remain within $[-C, B]$ according to the shunting equation (Section 2.2.1); this causes the excitatory weight values to be bounded, because according to Equation 2.8, $W_{ij}^{+}(t) \in [0, \mathcal{P}(B)]$ for $t \geq 0$, if $W_{ij}^{+}(0) \in [0, \mathcal{P}(B)]$ and $x_i(t) \leq B$ (Grossberg, 1982).

The outstar excitatory synaptic plasticity rule

In an outstar plasticity rule (Grossberg, 1972, 1982), *pre*synaptic activity enables the plasticity at a synapse; when the plasticity is enabled, the weight tends to become proportional to the *post*synaptic activity. The rule can be expressed (Grossberg, 1982) as

$$\frac{d}{dt} W_{ij}^{+}(t) \;=\; \xi \; \mathcal{G}(x_i(t)) \left(-W_{ij}^{+}(t) \;+\; \mathcal{Q}(x_j(t)) \right), \tag{2.9}$$

where $\xi > 0$ is a small learning rate constant, and $\mathcal{G}$ and $\mathcal{Q}$ are half-rectified non-decreasing functions. The positions of x_i and x_j are reversed, compared with the instar rule. Thus, *whenever a neuron is active, its output excitatory connections to active neurons tend to become slightly stronger, while its output excitatory connections to inactive neurons tend to become slightly weaker.* Neuron activations remain within $[-C, B]$ according to the shunting equation (Section 2.2.1); this in turn causes the excitatory weight values to be bounded between 0 and $\mathcal{Q}(B)$ (Grossberg, 1982).

The outstar lateral inhibitory synaptic plasticity rule

The lateral inhibitory weights, W_{jk}^{-}, are modified according to the anti-Hebbian rule

$$\frac{d}{dt} W_{jk}^{-} \;=\; \delta \; \mathcal{H}(x_j) \left(-W_{jk}^{-} \;+\; \mathcal{R}(x_k) \right) \tag{2.10}$$

(Marshall, 1995a; Marshall & Gupta, 1998) where $\delta > 0$ is a small learning rate constant, and $\mathcal{H}$ and $\mathcal{R}$ are half-rectified non-decreasing functions.

Thus, *whenever a neuron is active, its output inhibitory connections to other active neurons tend to become slightly stronger (i.e., more inhibitory), while its output inhibitory connections to inactive neurons tend to become slightly weaker*. Neuron activations remain

within $[-C, B]$ according to the shunting equation (Equation 2.1); this causes the inhibitory weight values to remain bounded as well, between 0 and $\mathcal{R}(B)$ (Grossberg, 1982).

2.3 Results

In order to evaluate the BCM rule, the instar and outstar excitatory synaptic plasticity rules, and the outstar lateral inhibitory synaptic plasticity rule in comparison to experimental data, the properties of the rules are studied by analysis and computer simulations.

In Section 2.3.1, synaptic plasticity in pathways to a postsynaptic neuron is expressed analytically as a function of input excitation according to the BCM, the instar, and the outstar excitatory synaptic plasticity rules, by making simplifying assumptions about the postsynaptic activation. Lateral inhibitory synaptic plasticity, according to the outstar lateral inhibitory synaptic plasticity rule, is expressed analytically as a function of input excitation in Section 2.3.2.

In Section 2.3.3, the subtle properties of the BCM, the instar, and the outstar excitatory synaptic plasticity rules are studied as a function of pre- and postsynaptic activation, initial synaptic weight, and simultaneous stimulation of different pathways. The effects of lateral inhibitory interactions are also explored.

In some experiments (Artola et al., 1990; Frégnac et al., 1994; Kirkwood et al., 1993), the conditioning stimulation was applied at the white matter–layer 6 border. Stimulation at the white matter–layer 6 border can activate geniculocortical and corticocortical feedback pathways (Kirkwood et al., 1993). Many models (e.g., Carpenter & Grossberg, 1987; Grossberg, 1980; Grossberg et al., 1997a; Grossberg & Merrill, 1997; Grunewald & Grossberg, 1997; Nigrin, 1993) use both the instar and the outstar excitatory synaptic plasticity rules. In these models, the instar rule governs synaptic plasticity in afferent excitatory pathways, and the outstar rule governs synaptic plasticity in feedback excitatory pathways. Thus, the effects of a combination of the instar and the outstar excitatory synaptic plasticity rules are studied in Section 2.3.4.

Finally, Section 2.3.5 presents the properties of the outstar lateral inhibitory

synaptic plasticity rule as a function of the input excitation to model neurons, pre- and postsynaptic activation, and initial inhibitory synaptic weight.

Computer simulations were used to study synaptic plasticity in Sections 2.3.3–2.3.5 because, with lateral interactions, the activation equation does not have a closed-form formula in the model neural network.

2.3.1 Analyses of excitatory synaptic plasticity rules

In this section, the postsynaptic activation of a neuron is first expressed as a function of presynaptic stimulation by supposing that the neuron does not receive any inhibitory input and that postsynaptic activation is linearly related to input excitation. These simplifying assumptions are helpful in deriving analytical expressions that elucidate the important properties of the synaptic plasticity rules.

Let $x > 0$ represent the strength of presynaptic stimulation applied to excitatory pathways to postsynaptic neuron j. Let x_j represent the activation level of the postsynaptic neuron j. Let W_{ij}^{+} be the weight of the excitatory synapse from the afferent i and to neuron j. The presynaptic activation of unstimulated pathways to neuron j is zero.

Neuronal activation as a function of input stimulation.

The excitation received by neuron j is

$$E_j = \sum_{i \in \text{ active presynaptic input}} [x_i] W_{ij}^{+}, \tag{2.11}$$

where $[x_i]$ is defined to mean $\max(0, x_i)$. For each stimulated excitatory pathway i to neuron j, the presynaptic activation $x_i = x$ in this test simulation. Thus

$$E_j = E\, x \tag{2.12}$$

where $E = \sum_{i \in \text{ active presynaptic input}} W_{ij}^{+}$. From Equation 2.1, the activation level of neuron j, at equilibrium, is

$$x_j \;=\; \frac{\beta B E_j - \gamma C I_j}{A + \beta E_j + \gamma I_j} \;=\; \frac{\beta B E\, x - \gamma C I_j}{A + \beta E\, x + \gamma I_j} \tag{2.13}$$

In general, the relationship between x_j and x is difficult to determine because of lateral inhibition. It is possible that with increasing x, x_j decreases because of increasing I_j (Figure 2.12). If j is the only active neuron in a winner-take-all (WTA) network, x_j can increase with increasing x (Figure 2.8). However, the activation of a neuron can increase monotonically with presynaptic activation even if there are other active neurons sending inhibition to it (Figure 2.13).

To facilitate analytical expressions for synaptic plasticity, the following simplifying assumptions are made: (1) the Layer 2 neuronal responses are linearly related to the input excitation, i.e. $x_j \propto E_j$, and (2) the network behaves in a WTA fashion (the winner neuron does not receive any lateral inhibition).

Assuming that the activation of layer 2 neurons is in their linear region, $x_j = \Phi E_j = \Phi E x$. Under the WTA assumption, the winner neuron j does not receive any inhibition; i.e., $I_j = 0$, and therefore, the equilibrium activation of neuron j, is

$$x_j \;=\; \frac{\beta B E_j}{A + \beta E_j} \;=\; \frac{\beta B E\, x}{A + \beta E\, x}. \tag{2.14}$$

In this case, the activation of the winner neuron monotonically increases with input excitation.

Analysis of the BCM excitatory synaptic plasticity rule

Assuming that the activation of neuron j is in its linear region, let $x_j = \Phi E_j = \Phi E x$. Substituting for x_j in Equation 2.4, and because $x > 0$, the BCM excitatory synaptic plasticity rule becomes

$$\frac{d}{dt} W_{ij}^{+} = \eta \Phi E x \left(\Phi E x - \theta_j\right) x. \tag{2.15}$$

The synaptic weight change as a function of the presynaptic stimulation strength x, controlled by Equation 2.15, is shown in Figure 2.1.

Under a WTA assumption, the equilibrium activation level of the winner neuron, j, is given by Equation 2.14. Substituting the value of x_j in the BCM rule (Equation 2.4), and because $x > 0$, Equation 2.4 becomes

$$\frac{d}{dt} W_{ij}^{+} \;=\; \eta \frac{\beta B E\, x}{A + \beta E\, x} \left(\frac{\beta B E\, x}{A + \beta E\, x} - \theta_j \right) x. \tag{2.16}$$

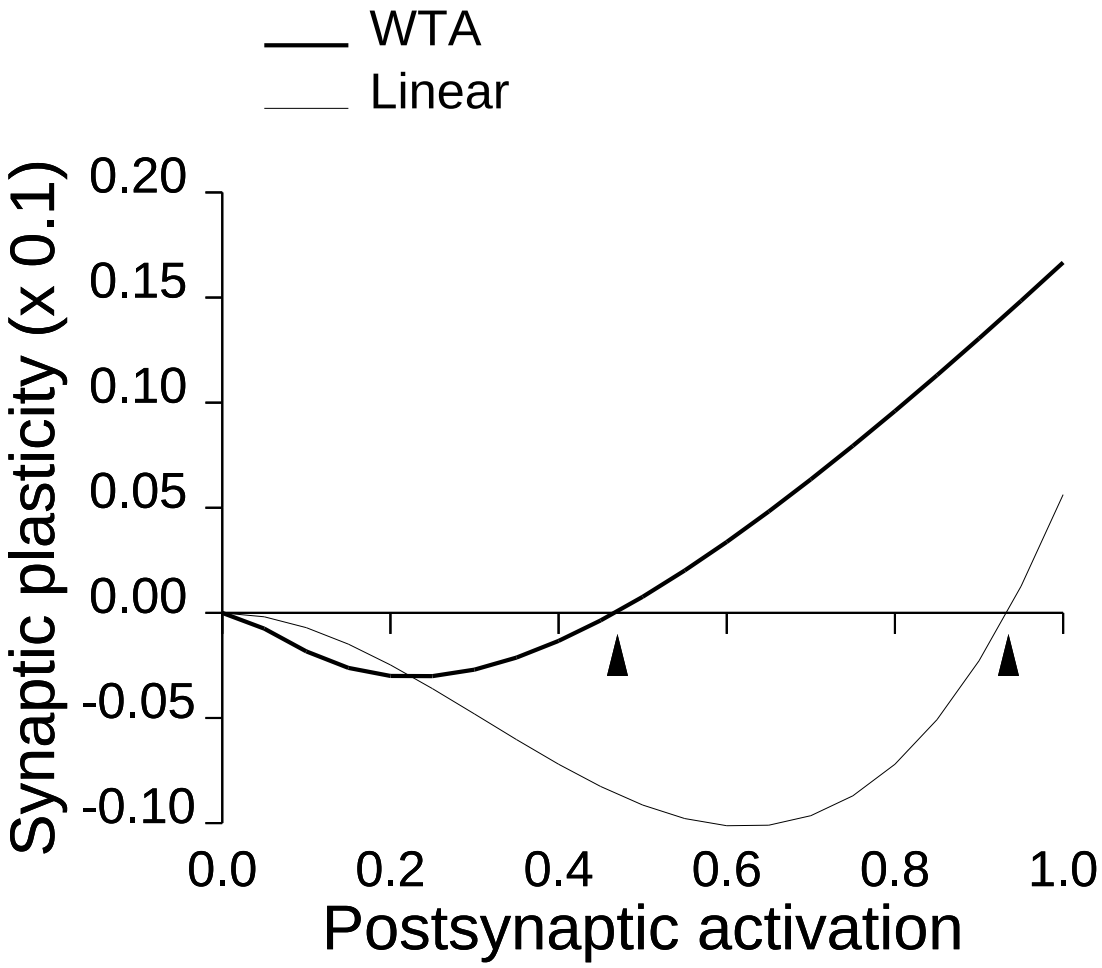

Figure 2.1: **The BCM excitatory synaptic plasticity rule.**
The change in synaptic weight as a function of the presynaptic activity proposed by the BCM excitatory synaptic plasticity rule. The rule induces LTP when the postsynaptic activation level is above the LTP threshold (indicated by arrow-head) and induces LTD when the postsynaptic activation level is below the LTP threshold. In both curves, $\eta = 0.05$, $E = 0.5$, $\theta_j = 0.7$, and $W_{ij} = 0.5$. In the WTA case, the synaptic plasticity curve is governed by Equation 2.14 with $\beta = 1.0$, $A = 0.1$, and $B = 1.0$. In the linear case, synaptic plasticity is governed by Equation 2.15 with $\Phi = 1.5$.

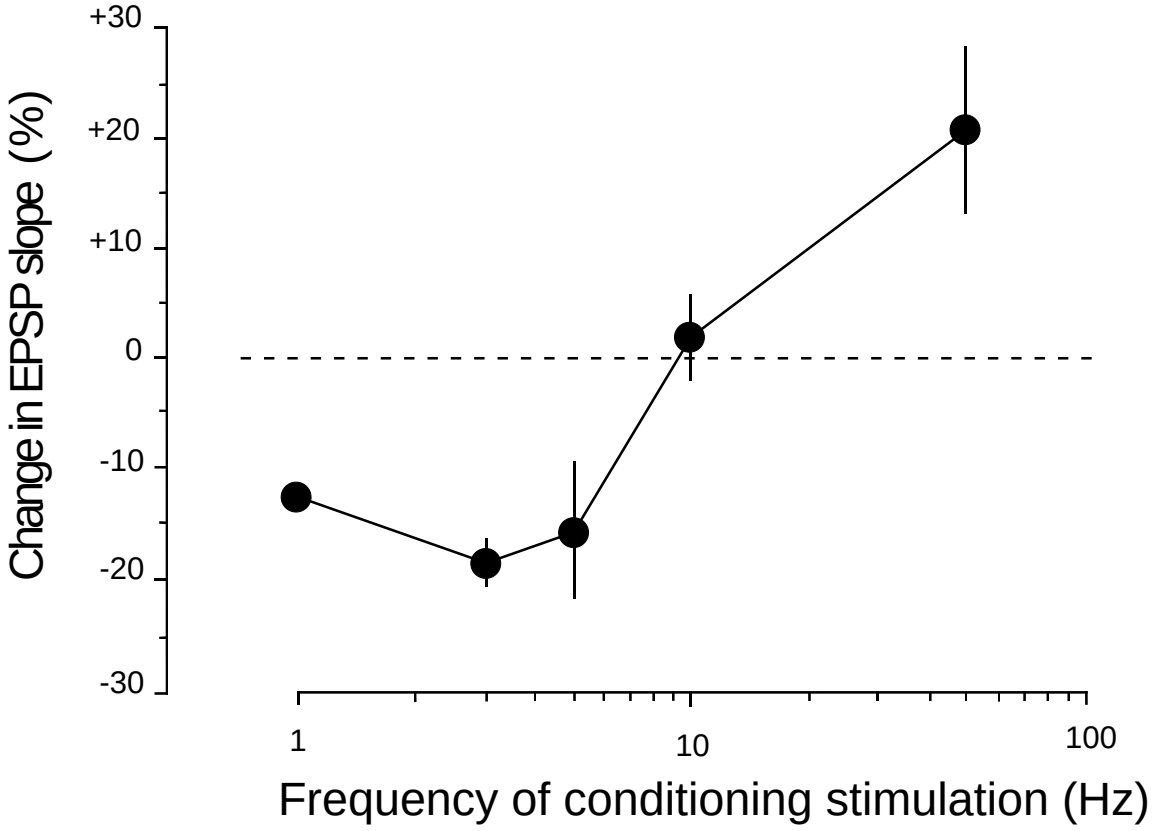

Figure 2.2: **The BCM excitatory synaptic plasticity rule.**
The change in synaptic weight as a function of the presynaptic stimulation strength observed experimentally by Dudek & Bear (1992). The presynaptic stimulation strength was varied by changing the frequency of conditioning stimulation, and synaptic weight was estimated by measuring the slope of excitatory postsynaptic potential evoked by a test stimulation of the pathway. LTP is observed at higher presynaptic stimulation frequencies, and LTD is observed at lower frequencies. Redrawn with permission, from Dudek and Bear (1992).

The synaptic weight change as a function of presynaptic stimulation strength $x > 0$, according to Equation 2.16 is plotted in Figure 2.1.

The graphs in Figure 2.1 are similar to the experimental data on synaptic weight modification as a function of presynaptic stimulation strength shown in Figure 2.2.

In the general case, where inhibition is present, the weight change is obtained by substituting x_j given by Equation 2.13 in Equation 2.4. Assuming that synaptic plasticity is blocked when the postsynaptic neuron is hyperpolarized and that $x > 0$,

$$\frac{d}{dt}W_{ij}^{+} = \eta \left[\frac{\beta BE\ x - \gamma CI_j}{A + \beta E\ x + \gamma I_j}\right] \left(\left[\frac{\beta BE\ x - \gamma CI_j}{A + \beta E\ x + \gamma I_j}\right] - \theta_j\right) x. \tag{2.17}$$

The term $\left(\left[\frac{\beta BE\ x - \gamma CI_j}{A + \beta E\ x + \gamma I_j}\right] - \theta_j\right)$ in Equation 2.17 captures the property of change in sign of synaptic modification. The multiplicative term $\eta \left[\frac{\beta BE\ x - \gamma CI_j}{A + \beta E\ x + \gamma I_j}\right] x$ modulates the rate of change.

In the BCM synaptic plasticity rule, the weight change is zero when the postsynaptic or the presynaptic activity is zero. The LTP threshold θ_j determines the sign of weight change in *all* stimulated pathways to an active postsynaptic neuron. The shape of the function ϕ is shown in Figure 2.3 for two different values of the threshold $\theta_j(t)$. The two important features of the function ϕ are that it changes sign at the modification threshold $\theta_j(t)$ and that it is zero when $x_j(t)$ is zero.

The BCM synaptic plasticity rule exhibits homosynaptic depression when the postsynaptic activation is less than the LTP threshold and homosynaptic potentiation when the postsynaptic activation is greater than the LTP threshold. Heterosynaptic depression of the synaptic weight of inactive pathways to active neurons does not occur, because the BCM rule disables synaptic plasticity in unstimulated pathways.

Analysis of the instar excitatory synaptic plasticity rule

Assuming that the activation of neuron j is in its linear region, let $x_j = \Phi E_j = \Phi E x$. Substituting for x_j in Equation 2.8 with $\mathcal{F}(x) = [x]$, $\mathcal{P}(x) = [x]$, and $x > 0$, the instar excitatory synaptic plasticity rule becomes

$$\frac{d}{dt}W_{ij}^{+} = \epsilon \Phi E x \left(-W_{ij}^{+} + x\right). \tag{2.18}$$

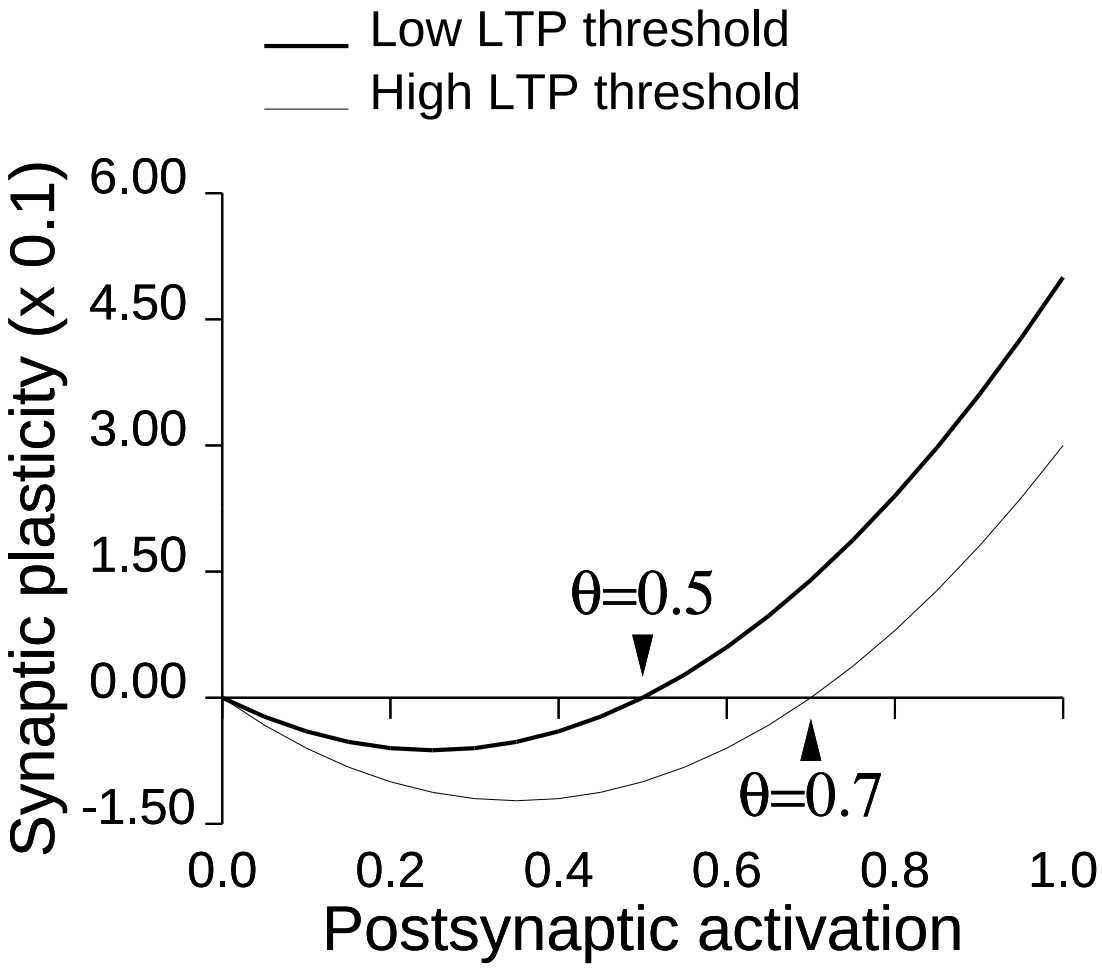

Figure 2.3: **Change in synaptic weight as a function of the postsynaptic activity using the BCM rule.**
The BCM rule induces LTP (positive synaptic weight change) when the postsynaptic activation is above the variable synaptic modification threshold θ and induces LTD (negative synaptic weight change) when it is below θ.

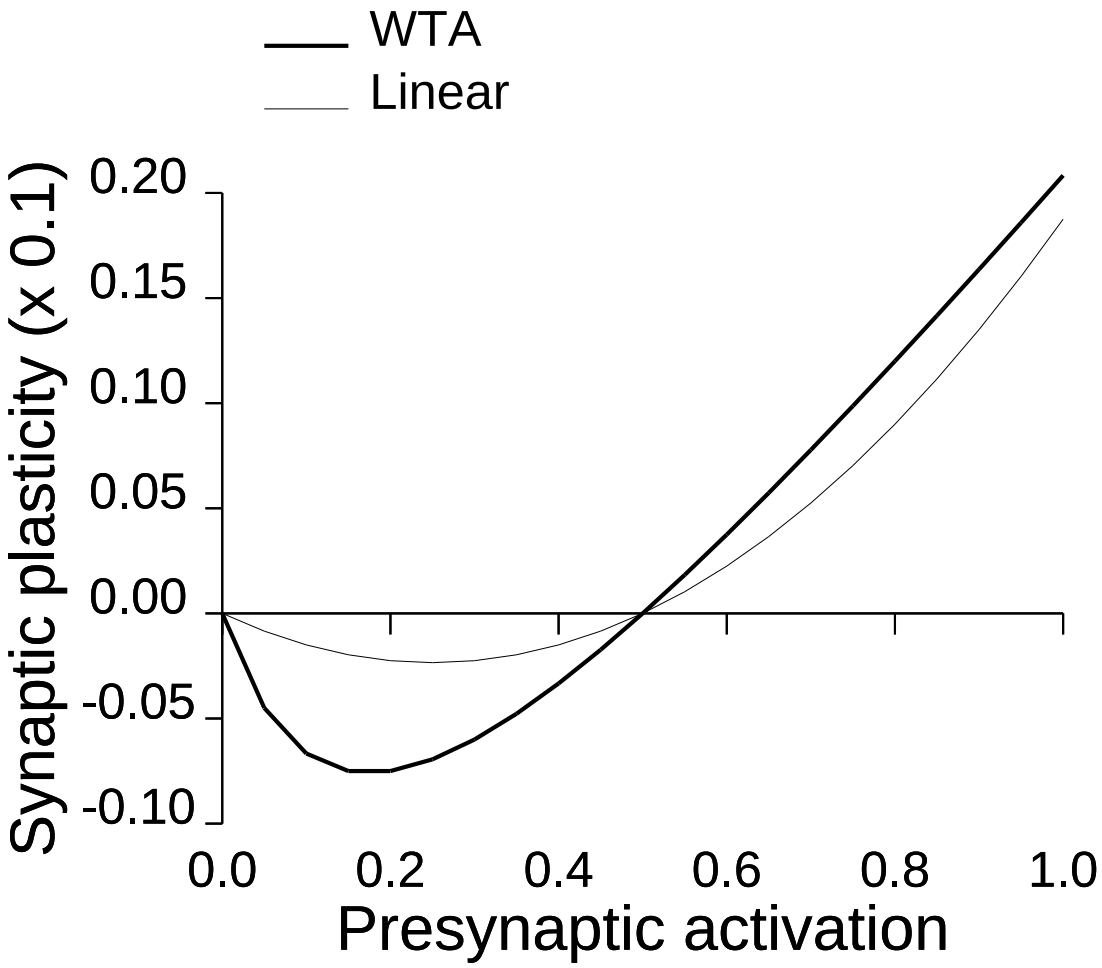

Figure 2.4: **Change in synaptic weight as a function of the presynaptic activity using the instar excitatory synaptic plasticity rule.**
The rule induces LTP when the presynaptic activation level is above the current synaptic weight (which acts like the LTP threshold) and induces LTD when it is below the weight. In the WTA case, the synaptic plasticity curve is governed by Equation 2.17 with $\epsilon = 0.05$, $\beta = 1.0$, $E = 0.5$, $A = 0.1$, $B = 1.0$, and $W_{ij}^{+} = 0.5$. In the linear case, synaptic plasticity is governed by Equation 2.18 with $\epsilon = 0.05$, $\Phi = 1.5$, $E = 0.5$, and $W_{ij}^{+} = 0.5$.

The synaptic weight change as a function of presynaptic stimulation strength x, controlled by Equation 2.18, is shown in

Under a WTA assumption, the equilibrium activation level of the winner neuron j is given by Equation 2.14. Substituting the value of x_j in the instar excitatory synaptic plasticity rule (Equation 2.8), and assuming $\mathcal{F}(x) = [x]$, $\mathcal{P}(x) = [x]$, and $x > 0$, Equation 2.8 becomes

$$\frac{d}{dt}W_{ij}^{+} = \epsilon \frac{\beta B E\, x}{A + \beta E\, x}\left(-W_{ij}^{+} + x\right). \tag{2.19}$$

The synaptic weight change as a function of presynaptic stimulation strength x, according to Equation 2.19, is plotted in Figure 2.4. Figure 2.4. The graphs in Figure 2.4 are similar to the experimental data in Figure 2.2.

In the general case, when inhibition is present, the weight change is obtained by substituting x_j from Equation 2.13 in Equation 2.8 and assuming that $\mathcal{F}(x) = [x]$ and $\mathcal{P}(x) = [x]$. When $x > 0$,

$$\frac{d}{dt}W_{ij}^{+} = \epsilon \left[\frac{\beta B E\, x - \gamma C I_j}{A + \beta E\, x + \gamma I_j}\right]\left(-W_{ij}^{+} + x\right). \tag{2.20}$$

The term $(-W_{ij}^{+} + x)$ in Equation 2.20 captures the property of change in sign of synaptic modification. The multiplicative term $\epsilon \left[\frac{\beta B E\, x - \gamma C I_j}{A + \beta E\, x + \gamma I_j}\right]$ modulates the rate of change.

In the instar excitatory synaptic plasticity rule, the weight change is zero when the postsynaptic activity less than or equal to zero. When a postsynaptic neuron is active, all unstimulated pathways to the active neuron weaken: $\mathcal{P}(x_i) = 0$ in Equation 2.8, and thus the right-hand side of Equation 2.8 is negative.

The weight W_{ij}^{+} in Equation 2.8 behaves like a variable synaptic weight modification threshold, because W_{ij}^{+} is variable. In addition, W_{ij}^{+} is *independent* for every synaptic connection.

The instar excitatory synaptic plasticity rule exhibits homosynaptic depression when the function $\mathcal{P}$ of presynaptic activation is less than the synaptic weight, and it exhibits homosynaptic potentiation when the the function $\mathcal{P}$ of presynaptic activation is greater than the synaptic weight. Heterosynaptic depression of the synaptic weight of inactive pathways occurs during postsynaptic activation.

Analysis of outstar excitatory synaptic plasticity rule

Assuming that the activation of neuron j is in its linear region, let $x_j = \Phi E_j = \Phi E x$. Substituting for x_j in Equation 2.9 with $\mathcal{G}(x) = [x]$, $\mathcal{Q}(x) = [x]$, and $x > 0$, the outstar excitatory synaptic plasticity rule becomes

$$\frac{d}{dt} W_{ij}^{+} = \xi x \left(-W_{ij}^{+} + \Phi E x \right). \tag{2.21}$$

The synaptic weight change as a function of presynaptic stimulation strength x, controlled by Equation 2.21, is shown in Figure 2.5.

Under a WTA assumption, the equilibrium activation level of the winner neuron j, is given by Equation 2.14. Substituting the value of x_j in the outstar excitatory synaptic plasticity rule (Equation 2.9) with $\mathcal{G}(x) = [x]$, $\mathcal{Q}(x) = [x]$, and $x > 0$, Equation 2.9 becomes

$$\frac{d}{dt} W_{ij}^{+} = \xi x \left(-W_{ij}^{+} + \frac{\beta B E\, x}{A + \beta E\, x} \right). \tag{2.22}$$

The synaptic weight change as a function of presynaptic stimulation strength x, according to Equation 2.22, is plotted in Figure 2.5. The graphs in Figure 2.5 are similar to the experimental data on synaptic weight modification as a function of presynaptic stimulation strength shown in Figure 2.2.

In the general case, the weight change is obtained by substituting x_j from Equation 2.13 in Equation 2.9 and assuming $\mathcal{G}(x) = [x]$ and $\mathcal{Q}(x) = [x]$. Since $x > 0$,

$$\frac{d}{dt} W_{ij}^{+} = \xi x \left(-W_{ij}^{+} + \left[\frac{\beta B E\, x - \gamma C I_j}{A + \beta E\, x + \gamma I_j} \right] \right). \tag{2.23}$$

The term $(-W_{ij}^{+} + \left[\frac{\beta B E\, x - \gamma C I_j}{A + \beta E\, x + \gamma I_j}\right])$ in Equation 2.23 captures the property of change in sign of synaptic modification, and the multiplicative term ξx modulates the rate of change.

In the outstar excitatory synaptic plasticity rule, the weight change is zero when the presynaptic activity is less than or equal to zero; thus in the outstar rule, synaptic plasticity is *specific* to stimulated pathways into a postsynaptic neuron. W_{ij}^{+} in Equation 2.9 behaves like a variable synaptic weight modification threshold, because W_{ij}^{+} is variable. In addition, W_{ij}^{+} is *independent* for every synaptic connection.

The outstar excitatory synaptic plasticity rule exhibits homosynaptic depression when $\mathcal{Q}$ of the postsynaptic activation is less than the synaptic weight, and homosynaptic potentiation when $\mathcal{Q}$ of the postsynaptic activation is greater.

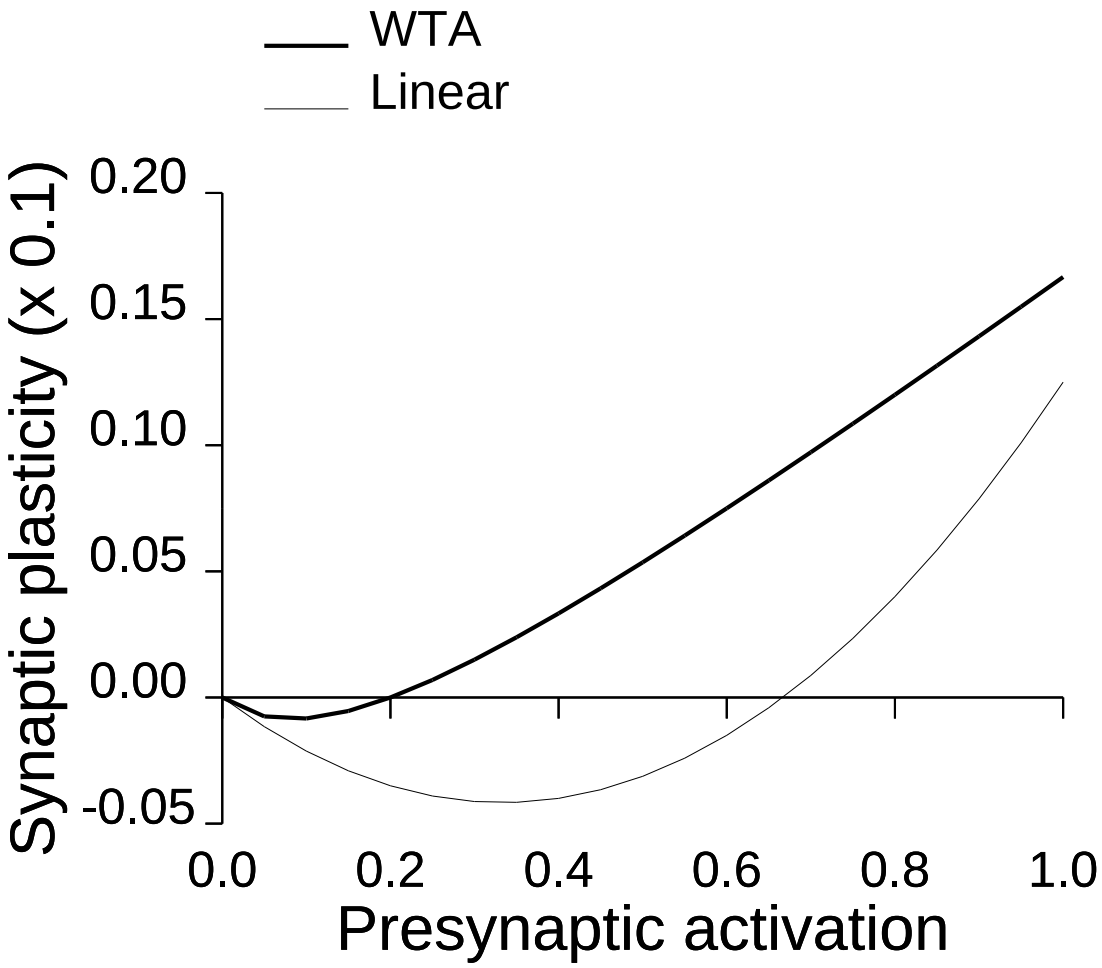

Figure 2.5: **Change in synaptic weight as a function of the presynaptic activity using the outstar excitatory synaptic plasticity rule.**
The rule induces LTP when the postsynaptic activation level is above the current synaptic weight (which acts like the LTP threshold) and induces LTD when it is below the weight. In the WTA case, the synaptic plasticity is governed by Equation 2.20 with $\xi = 0.05$, $\beta = 1.0$, $E = 0.5$, $A = 0.1$, $B = 1.0$, and $W_{ij}^{+} = 0.5$. In the linear case, the synaptic plasticity is governed by Equation 2.21 with $\xi = 0.05$, $\Phi = 1.5$, $E = 0.5$, and $W_{ij}^{+} = 0.5$.

2.3.2 Analysis of the outstar lateral inhibitory synaptic plasticity rule

In this section, changes in lateral inhibitory synaptic weights between two neurons are expressed in terms of excitatory inputs to the two neurons. To derive an analytical expression for the weight changes, it is assumed that the activation of the neurons are linearly related to input excitation.

Let j and k be two Layer 2 neurons, and let W_{jk}^{-} and W_{kj}^{-} be the weights of lateral inhibitory pathways between them. The outstar lateral inhibitory synaptic plasticity rule (Equation 2.10) depends on the activation levels of the Layer 2 neurons, and the weight of inhibitory pathways between them. The changes in inhibitory weights between Layer 2 neurons can be studied either by activating Layer 1 neurons or by activating just the Layer 2 neurons by other means.

Let presynaptic input neurons to neurons j and k be stimulated with stimulation strength $x > 0$. The presynaptic activation of unstimulated excitatory pathways is zero. The excitation received by neurons j and k, E_j and E_k, respectively is

$$E_j = \sum_{\text{i } \in \text{ active Layer 1 neurons}} W_{ij}^{+} x = Jx \tag{2.24}$$

and

$$E_k = \sum_{\text{i } \in \text{ active Layer 1 neurons}} W_{ik}^{+} x = Kx \tag{2.25}$$

According to the shunting equation (Equation 2.1), at equilibrium

$$x_j = \frac{\beta B E_j - \gamma C I_j}{A + \beta E_j + \gamma I_j} = \frac{\beta B J x - \gamma C I_j}{A + \beta J x + \gamma I_j} \tag{2.26}$$

and

$$x_k = \frac{\beta B E_k - \gamma C I_k}{A + \beta E_k + \gamma I_k} = \frac{\beta B K x - \gamma C I_k}{A + \beta K x + \gamma I_k}. \tag{2.27}$$

Substituting for x_j and x_k in Equation 2.10, and assuming $\mathcal{H}(x) = [x]$ and $\mathcal{R}(x) = [x]$,

$$\frac{d}{dt} W_{kj}^{-} = \delta \left[\frac{\beta B K x - \gamma C I_k}{A + \beta K x + \gamma I_k} \right] \left(-W_{kj}^{-} + \left[\frac{\beta B J x - \gamma C I_j}{A + \beta J x + \gamma I_j} \right] \right) \tag{2.28}$$

and

$$\frac{d}{dt} W_{jk}^{-} = \delta \left[\frac{\beta B J x - \gamma C I_j}{A + \beta J x + \gamma I_j} \right] \left(-W_{jk}^{-} + \left[\frac{\beta B K x - \gamma C I_k}{A + \beta K x + \gamma I_k} \right] \right). \tag{2.29}$$

For simplicity, assume that the activations of Layer 2 neurons are in their linear regions. Then, $x_j = \Gamma E_j = \Gamma J x$, $x_k = \Delta E_k = \Delta K x$, and with $\mathcal{H}(x) = [x]$, $\mathcal{R}(x) = [x]$, and $x > 0$,

$$\frac{d}{dt} W_{kj}^- = \delta \Delta K x \left(-W_{kj}^- + \Gamma J x \right) \tag{2.30}$$

and

$$\frac{d}{dt} W_{jk}^- = \delta \Gamma J x \left(-W_{jk}^- + \Delta K x \right). \tag{2.31}$$

The lateral inhibitory synaptic weight modification as a function of the Layer 1 stimulation strength x, governed by the outstar lateral inhibitory synaptic plasticity rule, is shown in Figure 2.6. Qualitatively similar relation between inhibitory weight change and input excitation exists when the postsynaptic activation is half-rectified and increases monotonically with $x > 0$.

Consider the situation when neuron k is active and neuron j is not. This can occur, for example, if the Layer 1 stimulation activates strong excitatory pathways to k, but activates only weak excitatory pathways to j (see Figure 2.8), or if k is stimulated externally. In these cases $x_j \leq 0$ and $x_k > 0$. Thus,

$$\frac{d}{dt} W_{kj}^- = \delta x_k \left(-\theta W_{kj}^- \right) \tag{2.32}$$

and

$$\frac{d}{dt} W_{jk}^- = 0, \tag{2.33}$$

i.e., W_{kj}^- decreases, and W_{jk}^- does not change. This shows that the outstar rule is asymmetric. Lateral inhibitory weights of pathways from active neurons to inactive neurons weaken, but lateral inhibitory weights of pathways from the inactive neurons do not change.

2.3.3 Characteristics of the excitatory synaptic plasticity rules

In Section 2.3.1, excitatory synaptic weight changes according to the BCM, the instar, and the outstar rules were analytically expressed by making simplifying assumptions about postsynaptic activation. The effect of lateral inhibition on postsynaptic activation was ignored. In this section, the properties of the instar, outstar, and the BCM excitatory synaptic plasticity rules are studied using a simple neural network with lateral inhibitory

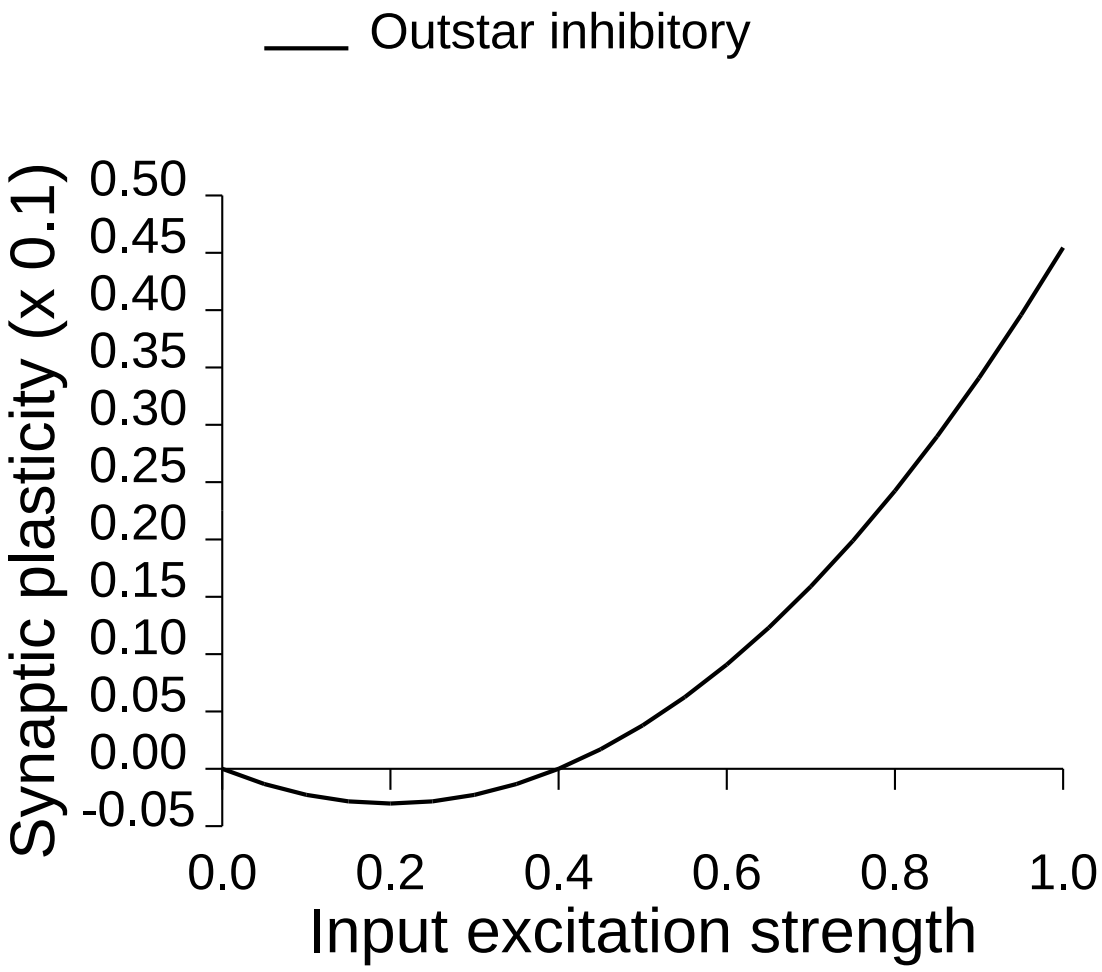

Figure 2.6: **The outstar inhibitory synaptic plasticity rule under the linearity assumption.**
The change in synaptic weight as a function of the presynaptic activity according to the outstar lateral inhibitory synaptic plasticity rule. The rule produces LTP when postsynaptic activation exceeds a variable inhibitory synaptic LTP threshold (a function of the current synaptic weight) and LTD when postsynaptic activation is below the variable threshold. The inhibitory synaptic plasticity under the linearity assumption is governed by Equation 2.29 with $\delta = 0.10$, $\Delta = 1.5$, $\Gamma = 4.0$, $J = 0.25$, $K = 0.5$, and $W_{kj}^{-} = 0.4$.

pathways. Because the activation of model neurons in the network with lateral inhibition cannot be expressed analytically, the activation equation was solved numerically.

If pre- and postsynaptic activations can be controlled independently, the three excitatory synaptic plasticity rules give different results. In the following subsections, the properties of the three rules are studied as a function of presynaptic stimulation strength, and the role of postsynaptic activation in the three rules is explored. Synaptic plasticity in stimulated (homosynaptic) and unstimulated (heterosynaptic) pathways is studied.

Some experiments have shown dependence of synaptic plasticity on the initial excitatory synaptic weight. Therefore, the effects of the initial synaptic weight on synaptic plasticity according to the instar, the outstar, and the BCM excitatory synaptic plasticity rules are analyzed.

Finally, associative synaptic plasticity (Brown et al., 1990; Levy & Steward, 1979; Barrionuevo & Brown, 1983; Kelso & Brown, 1986) is modeled using the instar, the outstar, and the BCM excitatory synaptic plasticity rules in the last subsection.

The simple neural network used in the simulations is shown in Figure 2.7. The postsynaptic neurons a and b receive excitatory inputs from the presynaptic neurons c, d, and e. The postsynaptic neurons a and b inhibit each other via lateral inhibitory pathways. The activation of the postsynaptic neurons a and b in response to activation of the presynaptic neurons c, d, and e is governed by the shunting equation (Equation 2.1). In Appendix A, the behavior of the shunting equation as a function of the various parameters is presented.

Synaptic plasticity in excitatory synapses as a function of presynaptic stimulation strength

This section explores excitatory synaptic plasticity as a function of presynaptic stimulation to excitatory pathways. First, excitatory synaptic plasticity in the conditioned pathways (homosynaptic plasticity) and in the unconditioned pathways (heterosynaptic plasticity) to active postsynaptic neurons are studied based on the three rules. Second, homosynaptic and heterosynaptic plasticity according to the three rules are studied in excitatory pathways to inactive neurons. Then, the equilibrium weights of conditioned

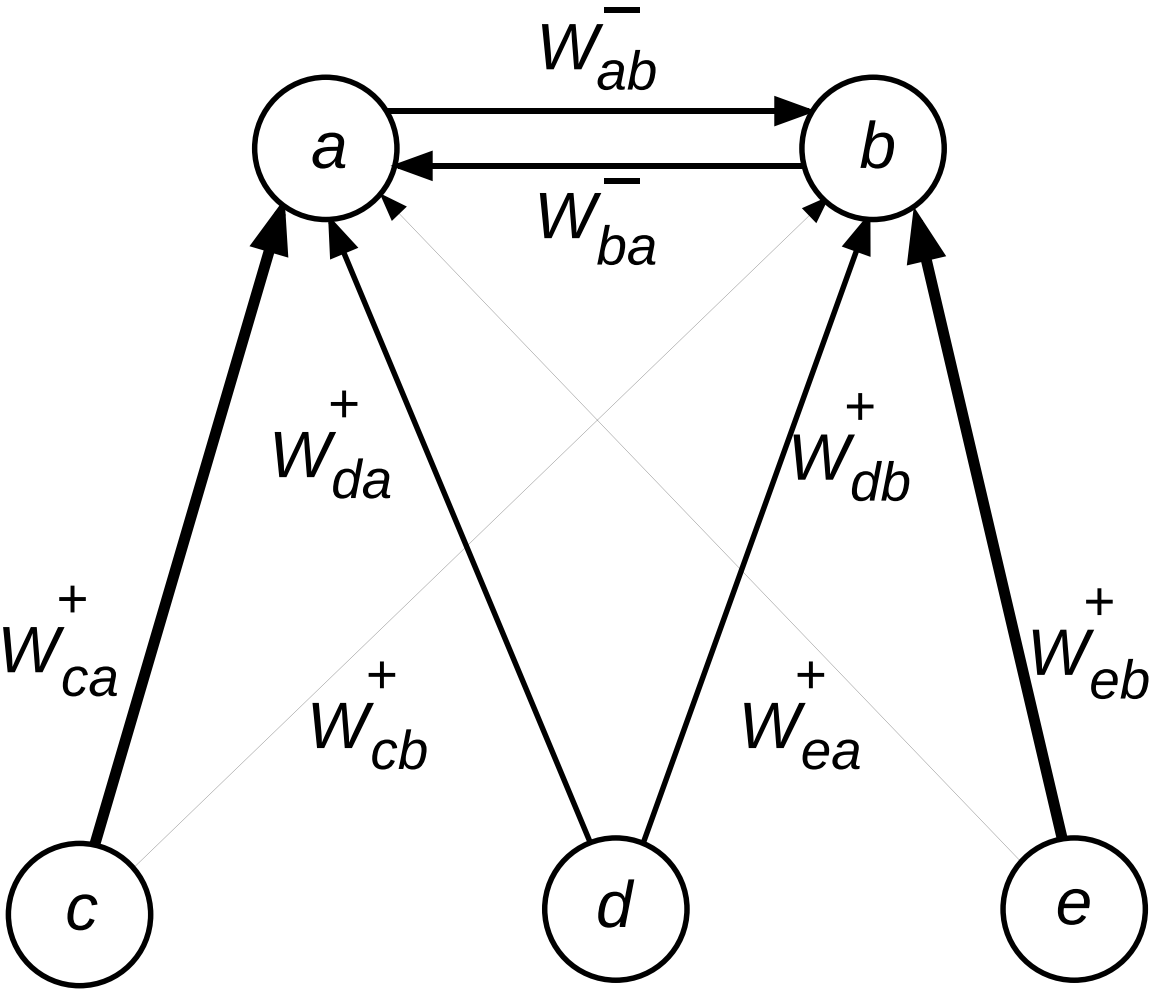

Figure 2.7: **Model network.**
The figure shows the simple network used in the simulations. W_{ij}^{+} represents the efficacy of the excitatory pathway from neuron i to neuron j, and W_{ij}^{-} represents the efficacy of the inhibitory pathway from neuron i to neuron j.

and unconditioned pathways after repeated conditioning stimulations, according to the three rules, are presented. Finally, some of the effects of network interactions on synaptic plasticity, according to the three rules, are considered.

Synaptic plasticity in pathways to an active neuron. In Figure 2.8, the presynaptic neuron c was stimulated. The stimulation of neuron c is presented by x_c. Figures 2.8a and 2.8b show the activation level of postsynaptic neurons a and b, respectively, as x_c was varied from 0 to 1.

Synaptic plasticity in the stimulated pathways (homosynaptic plasticity) based on the three rules as a function of presynaptic stimulation strength is shown in Figure 2.8. Synaptic plasticity in the unstimulated pathways (heterosynaptic plasticity) is also shown in Figure 2.8.

In the stimulated pathway from neuron c to active neuron a in Figure 2.8, the three rules weakened the excitatory synaptic weight W_{ca}^{+} when presynaptic stimulation x_c was weak and strengthened W_{ca}^{+} when x_c was strong (Figure 2.8c). In the absence of any presynaptic stimulation, W_{ca}^{+} did not change according to the three rules (Figure 2.8c). Thus, the instar, the outstar, and the BCM excitatory synaptic plasticity rules can produce homosynaptic LTP and LTD.

In the unstimulated excitatory pathways to neuron a, e.g., from neuron d, only LTD was produced by the instar excitatory synaptic plasticity rule, because the synaptic weight W_{da}^{+} was greater than the activation level of neuron d, x_d, which was zero (Figure 2.8e). As x_c was increased, W_{da}^{+} decreased more (Figure 2.8e). This happened because in the instar rule the magnitude of change in excitatory synaptic weight is proportional to the postsynaptic activation, and x_a increased with x_c (Figure 2.8a). According to the outstar and the BCM excitatory synaptic plasticity rules, presynaptic activation is required for the learning rules to be enabled (Equations 2.4 and 2.9). Thus, in the unstimulated pathways no synaptic plasticity occurred (Figure 2.8e).

In Figure 2.8c, the amount of LTD produced by the outstar and the BCM rules was small, because of the simulation parameters. For comparison, a simulation with a different set of parameters was run, to produce larger LTD (Figure 2.9c). In Figure 2.9, the initial weight of the stimulated pathway ca was increased, and the learning rate parameters ϵ and

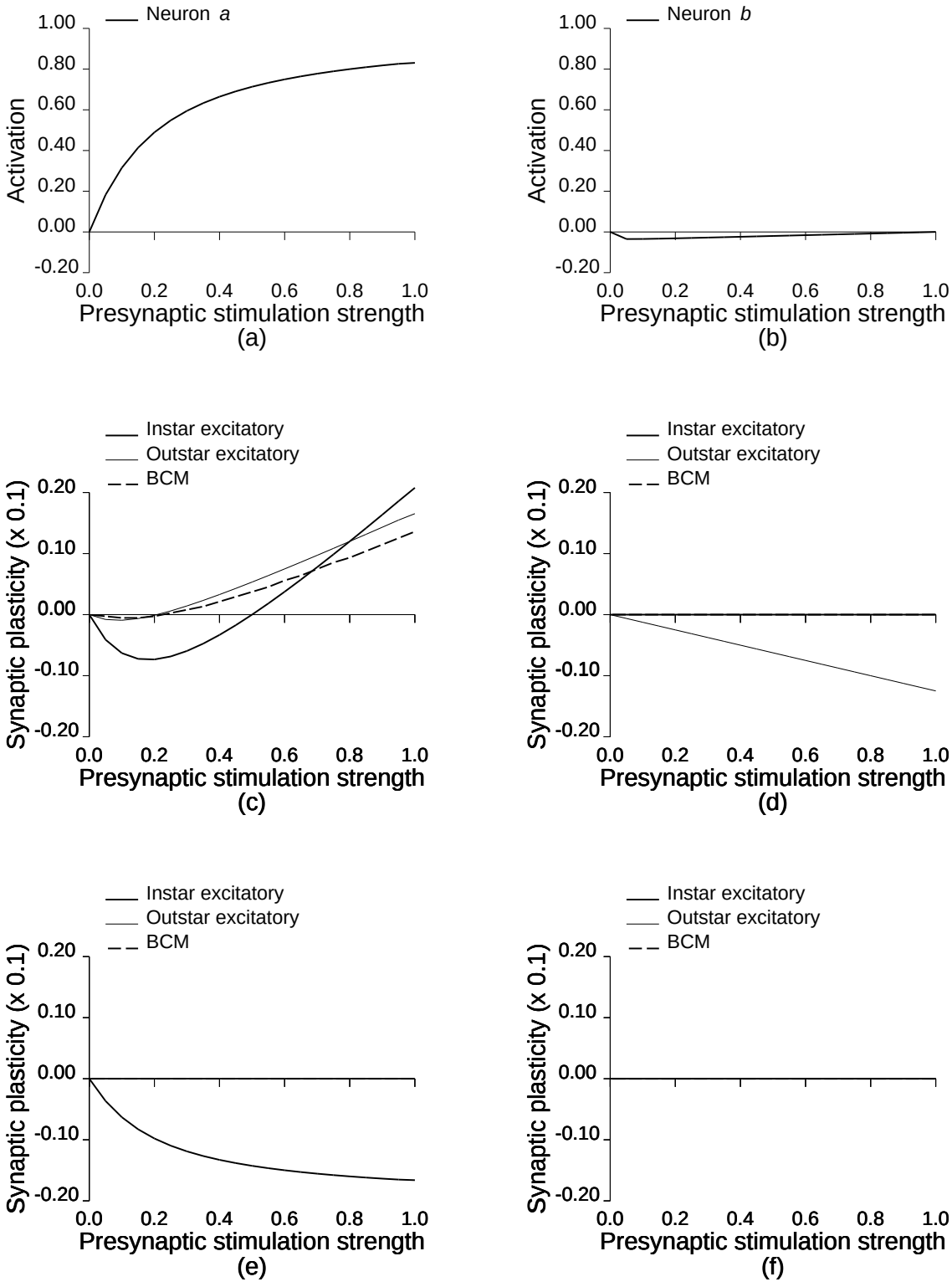

Figure 2.8: Legend on next page.

Figure 2.8: **Simulation results: Changes in excitatory synaptic efficacy of stimulated and unstimulated pathways as a function of presynaptic stimulation strength.**
Figure on previous page. The synaptic weight changes are shown according to the three rules after activating neuron c; the activation level of neuron c of Figure 2.7, x_c, was varied from 0 to 1. Panels (a) and (b) show the activation of neurons a and b, respectively, as x_c was varied, (c) and (d) show plasticity in the stimulated pathways from neuron c to neuron a and from neuron c to neuron b, respectively, as x_c was varied, and (e) and (f) show plasticity in the unstimulated pathways from neuron d to neuron a and from neuron d to neuron b, respectively, as x_c was varied. The rate of weight change in the instar rule became zero when postsynaptic activation was suppressed (d), (f). The rate of weight change in the outstar rule became zero when presynaptic activation was suppressed (e), (f). The rate of weight change in the BCM rule became zero when either pre- or postsynaptic activation was suppressed (d), (e), (f). In this simulation the initial synaptic pathway weights in the network shown in Figure 2.4 were assigned as follows: $W_{ca}^{+} = 0.5$, $W_{cb}^{+} = 0.25$, $W_{da}^{+} = 0.4$, $W_{db}^{+} = 0.4$, $W_{ea}^{+} = 0.25$, $W_{eb}^{+} = 0.5$, $W_{ab}^{-} = W_{ba}^{-} = 0.4$. The parameters for the activation equation (Equation 2.1) were $A = 0.1$, $B = 1$, $C = 0.05$, $\beta = 1$, and $\gamma = 15$. The activation level was computed using the Euler method with a time step of 0.04 until $t = 40$. The initial activation level of neurons a and b was set to zero. The parameters for the instar excitatory synaptic plasticity rule were $\epsilon = 0.05$, $\mathcal{F}(x) = [x]$, and $\mathcal{P}(x) = [x]$, for the outstar excitatory synaptic plasticity rule were $\xi = 0.05$, $\mathcal{G}(x) = [x]$, and $\mathcal{Q}(x) = [x]$, and for the BCM rule were $\eta = 0.05$, and $\theta_a = \theta_b = 0.5$.

η for the outstar and the BCM rules, respectively, were increased. For the BCM rule, the initial LTP threshold for neuron a was also increased. The magnitude of weight change increased with increase in the learning rate parameters. In addition, increasing the initial weight increased the magnitude of the difference between the postsynaptic activation and the initial weight and therefore increased the magnitude of weight change according to the outstar rule. Increasing the LTP threshold increased the magnitude of the difference between the postsynaptic activation and the LTP threshold and therefore increased the magnitude of weight change according to the BCM rule.

Synaptic plasticity in pathways to an inactive neuron. In Figure 2.8bd, the stimulated excitatory pathway from neuron c to inactive neuron b did not undergo synaptic plasticity under the instar excitatory synaptic plasticity rule because neuron b was inactive. The outstar excitatory synaptic plasticity rule produced LTD in the excitatory pathway from neuron c to neuron b because neuron b was inactive. Under the BCM excitatory

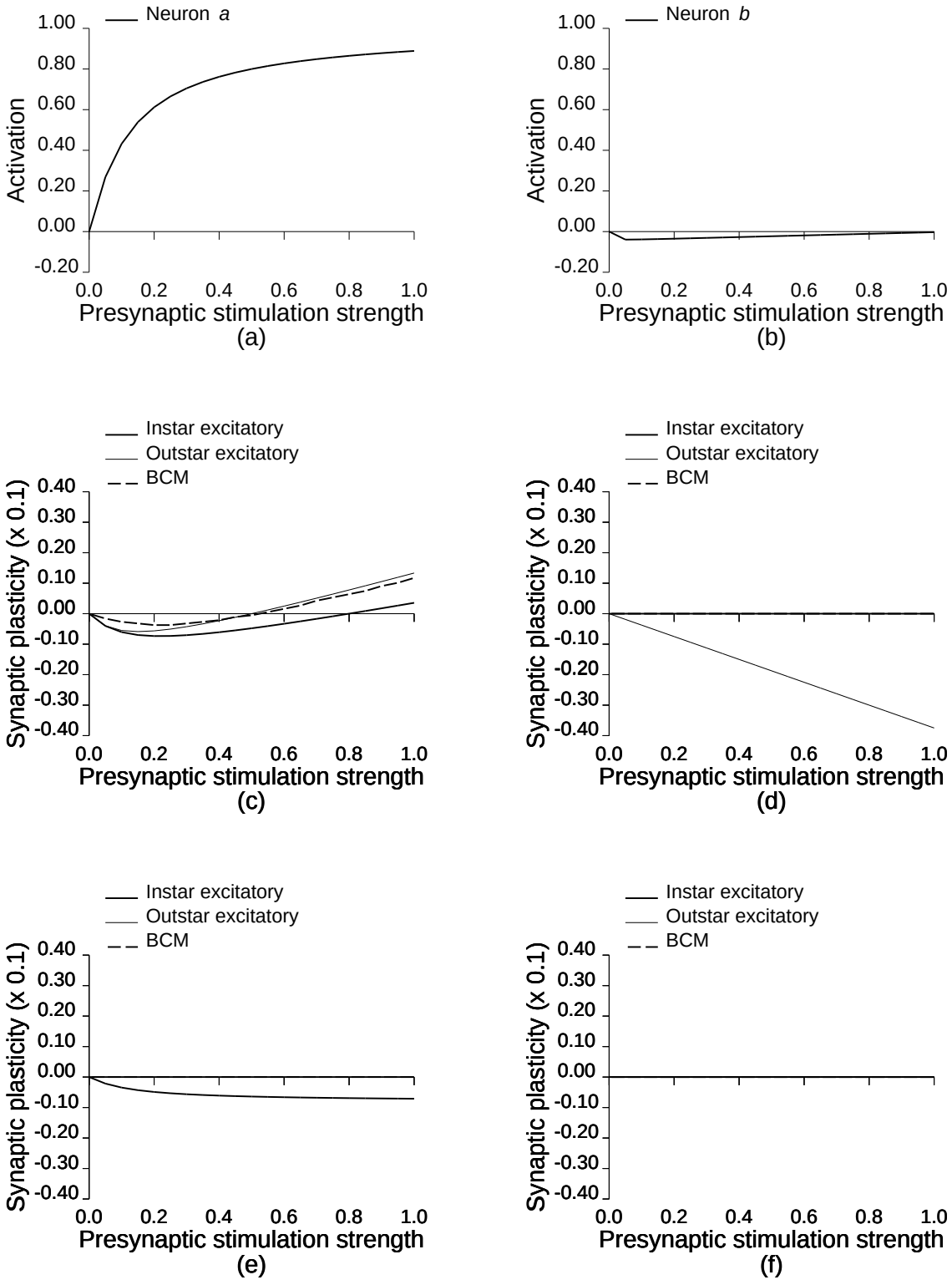

Figure 2.9: Legend on next page.

Figure 2.9: **Simulation results: Changes in excitatory synaptic efficacy of stimulated and unstimulated pathways under faster learning parameters.** Figure on previous page. See Figure 2.8 for conventions. There was no synaptic weight change under the instar rule in (d,f), under the outstar rule (e,f), and under the BCM rule (d,e,f). In this simulation the initial synaptic pathway weights in the network shown in Figure 2.4 were assigned as follows: $W_{ca}^{+} = \mathbf{0.8}$, $W_{cb}^{+} = 0.25$, $W_{da}^{+} = 0.4$, $W_{db}^{+} = 0.4$, $W_{ea}^{+} = 0.25$, $W_{eb}^{+} = \mathbf{0.8}$, $W_{ab}^{-} = W_{ba}^{-} = 0.4$. The parameters for the activation equation (Equation 2.1) were $A = 0.1$, $B = 1$, $C = 0.05$, $\beta = 1$, and $\gamma = 15$. The activation level was computed using the Euler method with a time step of 0.04 until $t = 40$. The initial activation of neurons a and b was set to zero. The parameters for the instar excitatory synaptic plasticity rule were $\epsilon = \mathbf{0.02}$, $\mathcal{F}(x) = [x]$, and $\mathcal{P}(x) = [x]$, for the outstar excitatory synaptic plasticity rule were $\xi = 0.15$, $\mathcal{G}(x) = [x]$, and $\mathcal{Q}(x) = [x]$, and for the BCM rule were $\eta = \mathbf{0.15}$, and $\theta_a = \theta_b = \mathbf{0.8}$. The parameter values in boldface differ from the values used in the simulations for Figure 2.8.

synaptic plasticity rule, no plasticity was observed because neuron b was inactive.

In the unstimulated excitatory pathways to the inactive neuron b, e.g., from neuron d, no plasticity was produced in W_{db}^{+} because $x_b \leq 0$ (Figure 2.8f). Under the outstar excitatory and the BCM synaptic plasticity rules, presynaptic activation is required for the plasticity to be enabled (Equations 2.4 and 2.9). Thus, in the unstimulated pathways no synaptic plasticity occurred.

Under the instar excitatory synaptic plasticity rule, the stimulated pathway can be potentiated or depressed; however, the unstimulated pathways can only weaken, or at best, remain constant. Under the outstar excitatory synaptic plasticity rule, the stimulated pathways may be potentiated or depressed, and unstimulated pathways do not undergo synaptic plasticity. The BCM rule also potentiates or depresses the stimulated pathways onto a postsynaptic neuron and does not modify synaptic weight of unstimulated pathways.

Equilibrium values of synaptic weights. In this section, changes in the weights of excitatory pathways according to the three excitatory synaptic plasticity rules are studied when an excitatory pathway is continuously stimulated.

According to the instar excitatory synaptic plasticity rule, the synaptic weight W_{ca}^{+} equilibrates to a value proportional to a function, $\mathcal{P}()$, of the presynaptic stimulation strength x_c (Grossberg, 1982; see Figure 2.10ce). The weight change in W_{ca}^{+} approaches zero as W_{ca}^{+} approaches $\mathcal{P}(x_a)$, and for $\mathcal{P}(x_d(t)) = 0$ weight change in W_{da}^{+} approaches zero

as W_{da}^{+} approaches zero.

The outstar excitatory synaptic plasticity rule causes the synaptic weight W_{ca}^{+} to equilibrate at a value proportional to a function, $\mathcal{Q}()$, of the postsynaptic activation x_a (see Figure 2.10ce); the weight change of W_{ca}^{+} approaches zero as W_{ca}^{+} approaches $\mathcal{Q}(x_a)$, and for $\mathcal{Q}(x_b) = 0$ the weight change of W_{cb}^{+} approaches zero as W_{cb}^{+} approaches zero.

On the other hand, the synaptic weight W_{ca}^{+} may not equilibrate when synaptic plasticity is governed by the BCM rule (Figures 2.10 and 2.11). In Figure 2.10, stimulating neuron c with $x_c = 1$ activates neuron a, which suppresses neuron b. In this WTA case, $x_a = \frac{\beta B W_{ca}^{+} x_c}{A + \beta W_{ca}^{+} x_c}$ at equilibrium in response to x_c according to Equation 2.1 because $x_b \leq 0$. In the simulation in Figure 2.10, $\theta_a(t) < x_a(t)$ for $t \geq 0$ (Figure 2.10a), and W_{ca}^{+} increases under the BCM rule. According to the BCM rule, W_{ca}^{+} equilibrates at some time t', if $\theta_a(t') = [x_a(t')]$, and $\theta_a(t) = \theta_a(t+1)$ for $t \geq t'$. With $p = 2$ and $c_0 = 1$, $\theta_a(t) = \theta_a(t+1)$ implies that $\theta_a(t) = [x_a(t)]^2$ according to the approximation for the BCM LTP threshold modification (Equation 2.7), and $\theta_a(t) = [x_a(t)]^2$, when $\theta_a(t) = [x_a(t)] = 1$, or when $\theta_a(t) = [x_a(t)] = 0$. But, $x_a = \frac{\beta B W_{ca}^{+} x_c}{A + \beta W_{ca}^{+} x_c} < B = 1$ (for the parameters in Figure 2.10), and x_a approaches 1 as W_{ca}^{+} approaches ∞. Thus, for the parameters used in Figure 2.10, the BCM rule caused W_{ca}^{+} to increase without bound. Since neuron b remained inactive, W_{cb}^{+}, the weight of the stimulated pathway from neuron c to neuron b did not change, and θ_b decayed to 0 according to the BCM rule (Figure 2.10d).

Figure 2.11 shows changes in weights of stimulated excitatory pathways according to the BCM rule using several different parameters. The curves labeled "Initial LTP threshold = 1" show weight changes when the initial LTP thresholds of neurons a and b were 1 and were greater than $x_a(0)$ and $x_b(0)$, respectively. Since the activation of neuron a was less than 1, W_{ca}^{+} increased without bound (Figure 2.11e).

When x_a was allowed to become equal to 1, for example, when the decay parameter in the activation equation was set to 0, the BCM rule with $p = 2$ and $c_0 = 1$ caused W_{ca}^{+} to reach an equilibrium value (curves labeled "A = 0" in Figure 2.11eg). When the parameter A in Equation 2.1 is set to zero, under WTA conditions $x_a = B = 1$ (Figure 2.11a), and θ_a equilibrated at 1 (Figure 2.11c).

The BCM rule causes the weights to reach stable values if p is set to 1. According

to the BCM rule, W_{ca}^{+} equilibrates at some time t', if $\theta_a(t') = [x_a(t')]$, and $\theta_a(t) = \theta_a(t+1)$ for $t \geq t'$. With $p = 1$, $\theta_a(t) = \theta_a(t+1)$ implies that $\theta_a(t) = [x_a(t)]/c_0$ according to the approximation for the BCM LTP threshold modification (Equation 2.7). In the simulations, when $\theta_a(0) = 1 > x_a(0)$, W_{ca}^{+} equilibrated at 0 because $x_a(t) < \theta_a(t)$ for $t \geq 0$ (Figure 2.11eg). When W_{ca}^{+} decreased, neuron b became activated (Figure 2.11b), and W_{cb}^{+} increased to its equilibrium value (Figure 2.11fh). When $\theta_a(0) = 0.5 < x_a(0)$, W_{ca}^{+} increased and eventually reached astable value (Figure 2.11eg).

Effects of network interactions. This section shows some of the effects of network interactions on the shape of the synaptic plasticity curves under the three excitatory synaptic plasticity rules.

In Figure 2.12, the weight of the lateral inhibitory pathways between neurons a and b was decreased. Therefore, as the strength of stimulation applied to neuron c was increased, neuron b became activated. When neuron b became activated, the activation of neuron a began to decrease. When the postsynaptic neuron b was actived, W_{cb}^{+} changed according to the instar and the BCM rules (Figure 2.12d). When the postsynaptic neuron b was active, the unstimulated pathway from neuron d began to weaken (Figure 2.12f).

In Figure 2.13, the neuron d was stimulated. In this case, neurons a and b were equally activated because they received the same amounts of excitation and inhibition. The postsynaptic activation of neurons a and b remained less than W_{da}^{+} and W_{bd}^{+}, respectively, and therefore, only LTD was produced in W_{da}^{+} and W_{bd}^{+} according to the outstar rule. The postsynaptic activation of neurons a and b was less than θ_a and θ_a, respectively, and therefore, W_{da}^{+} and W_{bd}^{+} underwent LTD according to the BCM rule. According to the instar rule, changes in W_{da}^{+} and W_{bd}^{+} switched from LTD to LTP when the function $\mathcal{P}$ of the presynaptic stimulation strength exceeded the initial values of W_{da}^{+} and W_{bd}^{+} (Figure 2.13cd).

Synaptic plasticity in excitatory synapses as a function of postsynaptic activation level

These simulations are based on experiments in which the role of postsynaptic activation in producing synaptic plasticity was studied by depolarizing and hyperpolarizing the postsynaptic neuron (Brown et al., 1990; Frégnac et al., 1994; Sejnowski et al., 1990;

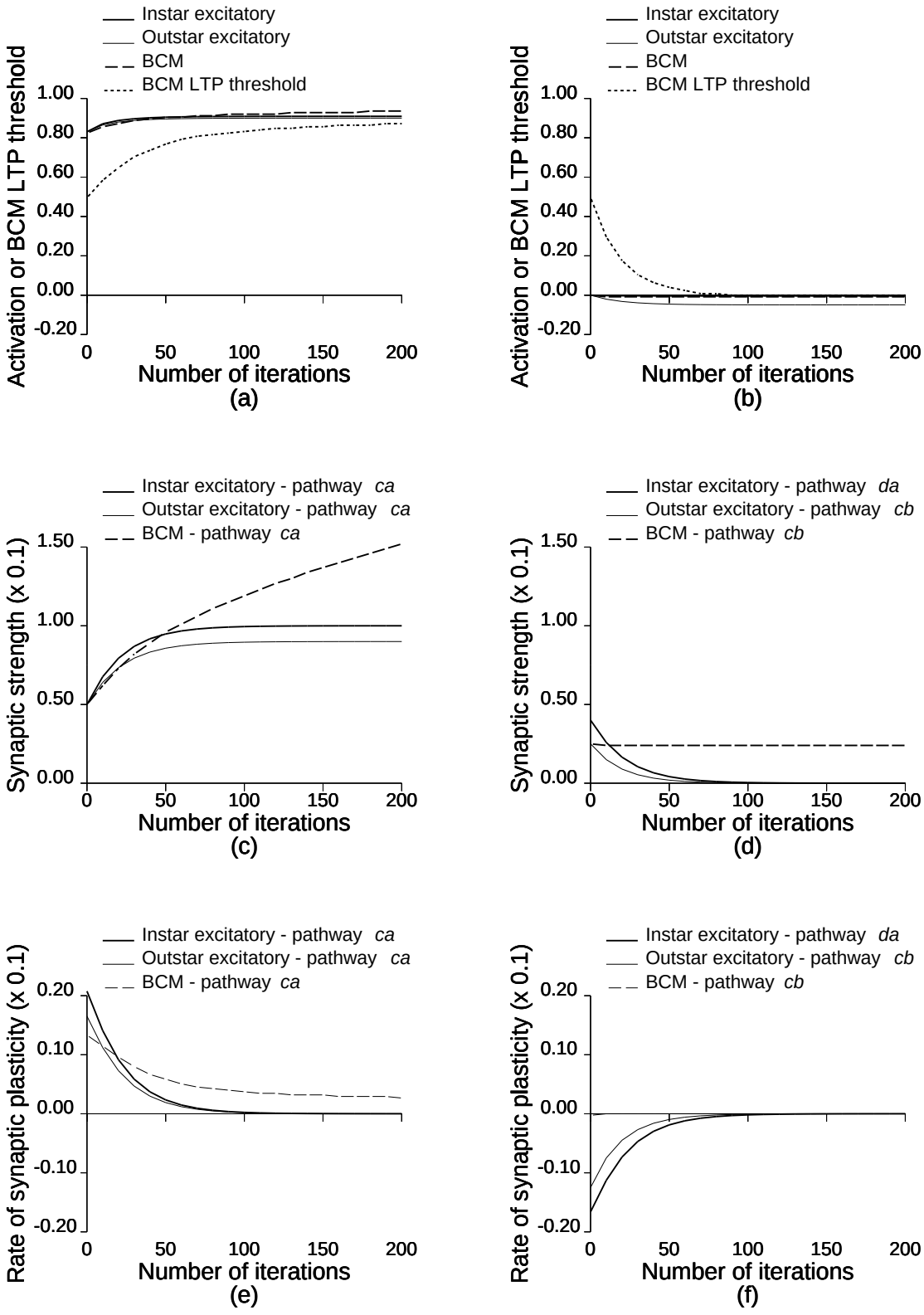

Figure 2.10: Legend on next page.

Figure 2.10: **Simulation results: Equilibrium values of excitatory synaptic efficacy of stimulated and unstimulated pathways.**
Figure on previous page. The simulation parameters were the same as those in Figure 2.8. In this simulation, presynaptic stimulation was applied by keeping x_c fixed at 1 for 200 iterations. The synaptic weights were changed every iteration. Panels (a) and (b) show the activation level of neurons a and b, respectively, over a period of 200 iterations as the excitatory synaptic weights change. In the case of the BCM rule, panels (a) and (b) also show the LTP threshold of neurons a and b, respectively. The LTP threshold for the instar and the outstar excitatory synaptic plasticity rules are the excitatory synaptic weight itself. Panels (c) and (d) show the excitatory synaptic weight of different excitatory pathways, and panels (e) and (f) show the rate of excitatory synaptic weight change in the different excitatory pathways. The pathway from neuron i to neuron j is labeled pathway ij. In the simulations, $p = 2$, $\tau = 20$, and $c_0 = 1$. In the simulations, activation of neuron b was suppressed (b), and therefore the weight of the excitatory pathway from neuron c to neuron b did not change under the BCM rule (d,f).

Stanton & Sejnowski, 1989).

In the simulations, a presynaptic element was stimulated at a fixed level, e.g., neuron c was stimulated at $x_c > 0$, and the activation level of a postsynaptic neuron, e.g., that of neuron a, x_a, was varied independently.

The instar excitatory synaptic plasticity rule increased the magnitude of change in W_{ca}^+ as x_a was increased (Figure 2.14a); however, the sign of change in W_{ca}^+ remained the same because it depends on the sign of $(-W_{ca}^+ + \mathcal{P}(x_c))$ (Figure 2.14a), which was fixed for fixed initial W_{ca}^+ and $\mathcal{P}(x_c)$. Furthermore, synaptic plasticity was disabled when postsynaptic activation was zero (Figure 2.14a). When the postsynaptic activation of neuron a, x_a, was kept fixed and presynaptic activation of neuron c, x_c, was varied from 0 to 1 in Figure 2.14b, the synaptic plasticity in W_{ca}^+ went from LTD to LTP; for higher values of x_a the rate of plasticity increased. Thus, according to the instar excitatory synaptic plasticity rule, postsynaptic activation is required to enable plasticity, postsynaptic activation affects the rate of plasticity, and postsynaptic activation does not affect the sign of plasticity (the sign of plasticity depends on presynaptic activation and the weight).

According to the outstar excitatory synaptic plasticity rule, the sign of change in W_{ca}^+ depended on the postsynaptic activation; as x_a was increased when $x_c > 0$ was kept fixed, the change in W_{ca}^+ went from depression to potentiation (Figure 2.14c). In the outstar

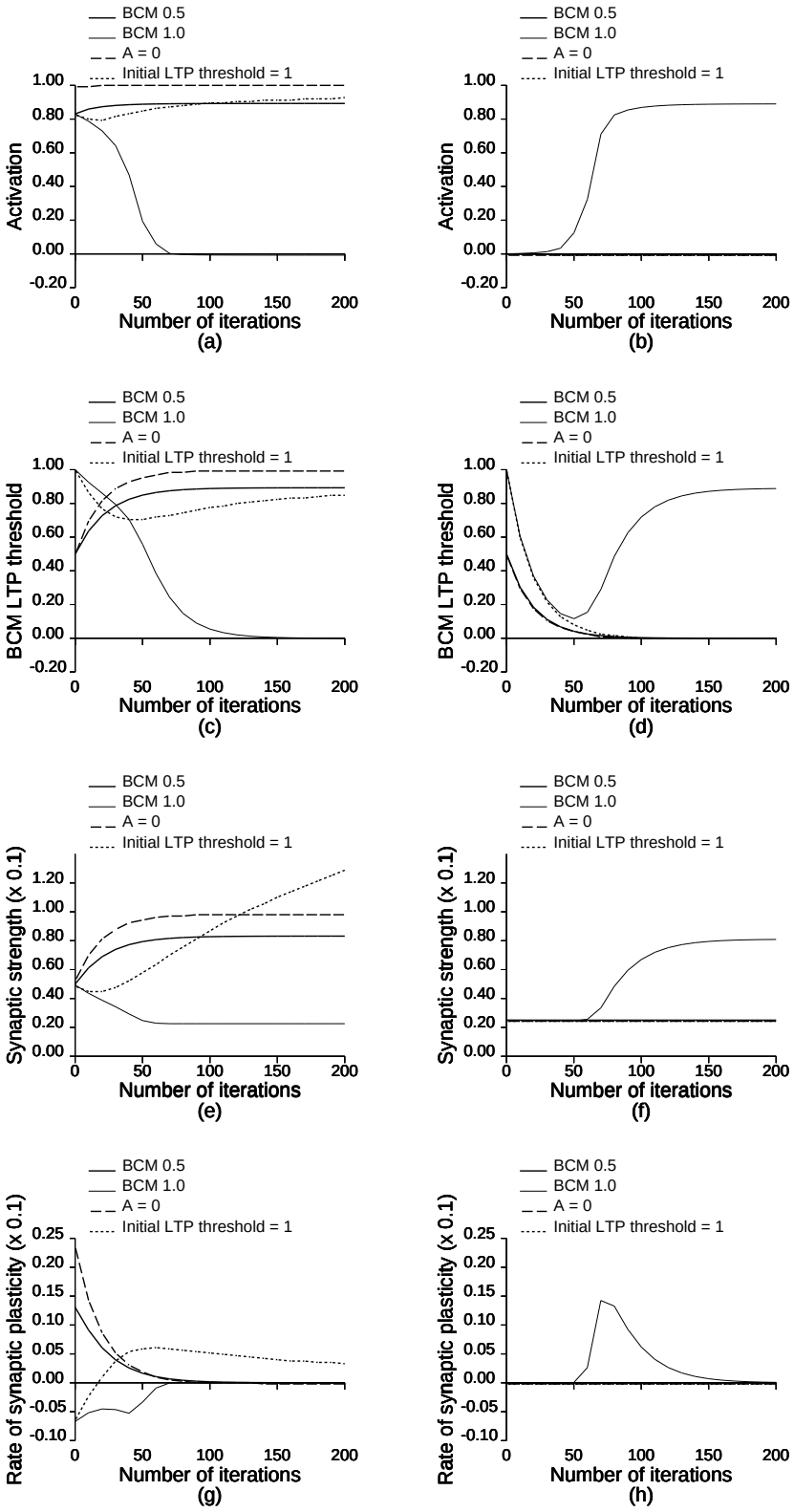

Figure 2.11: Legend on next page.

Figure 2.11: **Simulation results: Equilibrium values of excitatory synaptic efficacy of stimulated and unstimulated pathways according to the BCM rule.**
Figure on previous page. The relationship between θ_j and x_j and their effect on synaptic plasticity are shown. The initial network weights and the BCM excitatory synaptic plasticity rule parameters are given in Figure 2.8. As in Figure 2.12, neuron c is activated at a fixed level of 1 for 200 iterations. Panels (a) and (b) show the activation level of neurons a and b, respectively. In the curves labeled "BCM 0.5," the BCM LTP threshold modification function parameters were $p = 1$, $c_0 = 1$, and $\tau = 20$, the activation equation parameters were the same as in Figure 2.8, and the initial LTP thresholds for neurons a and b were $\theta_a = \theta_b = 0.5$. In the curves labeled "BCM 1.0," the parameters were the same, except that $\theta_a = \theta_b = 1.0$. In the curves labeled "A = 0," the decay parameter A in the activation equation was set to 0, and the other activation equation parameters were the same as in Figure 2.8, $\theta_a(0) = \theta_b(0) = 0.5$, and the LTP threshold was varied as in Figure 2.12. In the curves labeled "Initial LTP threshold = 1," the initial LTP thresholds for neurons a and b were set to 1, the activation equation parameters were the same as in Figure 2.8, and the LTP threshold was varied as in Figure 2.12. Panels (c) and (d) show the LTP threshold of neurons a and b, respectively. Panel (e) shows W_{ca}^+, and panel (g) shows the rate of change in W_{ca}^+. Panel (f) shows W_{cb}^+, and panel (h) shows the rate of change in W_{cb}^+. In the curves labeled "BCM 0.5," "A = 0," and "Initial LTP threshold = 1," the activation of neuron b was suppressed (b), and therefore W_{cb}^+ did not change under the BCM rule (f,h). The curves labeled "BCM 0.5," "A = 0," and "Initial LTP threshold = 1," are overlapping in (f,h). In (d), the curves labeled "BCM 0.5" and "A = 0," are overlapping.

rule, the sign of weight change depends on the sign of $(-W_{ca}^+ + \mathcal{Q}(x_a))$, and the magnitude of weight change in W_{ca}^+ is affected by the magnitude of $(-W_{ca}^+ + \mathcal{Q}(x_a))$. The magnitude of weight change also depended on the presynaptic activation level (Figure 2.14cd); as the presynaptic activation x_c was increased, the magnitude of synaptic weight change increased. When the postsynaptic activation x_a was fixed and presynaptic activation x_c was varied, the magnitude of weight change in W_{ca} increased, but the sign of weight change was fixed (Figure 2.14d). According to the outstar rule, synaptic weight change did not occur when the presynaptic activation was zero (Figure 2.14d). According to the outstar excitatory synaptic plasticity rule, postsynaptic activation affects both the sign of plasticity and the magnitude of weight change.

In the BCM excitatory synaptic plasticity rule, the sign of change in W_{ca}^+ depended on the postsynaptic activation level. As x_a was increased with fixed $x_c > 0$, the change in W_{ca}^+ was zero when $x_a = 0$, W_{ca}^+ underwent depression when $0 < x_a < \theta_a$

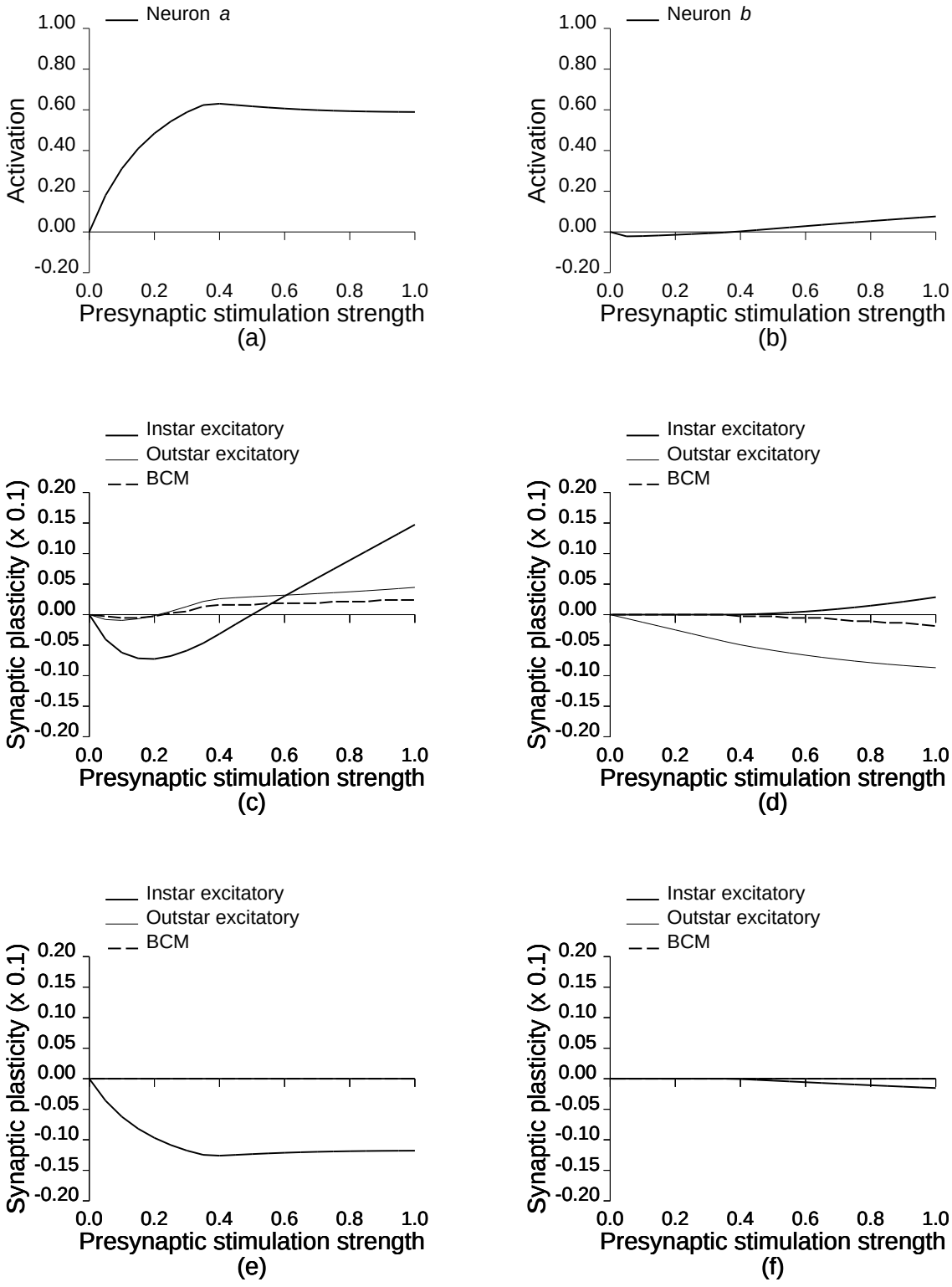

Figure 2.12: Legend on next page.

Figure 2.12: **Simulation results: The effects of lateral inhibitory weight on excitatory synaptic plasticity.**
Figure on previous page. In these simulations, all the parameters are the same as in Figure 2.8 except that $W^-_{ab} = W^-_{ba} = 0.2$, i.e., the lateral inhibitory weights are weakened. Weakening the lateral inhibitory weights causes neuron b to be activated when input excitation was strong (b). See Figure 2.8 for conventions. There was no synaptic weight change under the instar rule (d,f) when neuron b was inactive. There was no synaptic weight change under the outstar rule (e,f) and under the BCM rule (d,e,f) in the unstimulated pathway.

(the LTP threshold), and W^+_{ca} underwent potentiation when $x_a > \theta_a$ (Figure 2.14ef). The magnitude of weight change in W^+_{ca} also depended on x_a, although it was non-monotonic (Figure 2.14e). According to the BCM excitatory synaptic plasticity rule, the magnitude of change increased with the presynaptic stimulation strength (Figure 2.14ef).

Synaptic plasticity in excitatory synapses as a function of initial synaptic weight

Yang and Faber (1991) reported that LTD was more easily achieved after prior induction of LTP in the pathway. Based on this result, they suggested that synaptic plasticity in excitatory pathways may depend on their initial synaptic weights. In this section, the effects of varying the initial weight of the conditioned pathway in the instar, outstar, and the BCM excitatory synaptic plasticity rules are presented.

In the simulations in this section, an excitatory pathway, e.g., from neuron c to neuron a, was stimulated at a fixed strength. The initial synaptic weight of the stimulated excitatory pathway was varied. The initial synaptic weight may be varied by prior induction of LTP or LTD in the pathway. A variation is to apply a fixed presynaptic stimulation to different excitatory pathways to the same postsynaptic neuron and to plot the weight changes in the pathways as a function of the initial synaptic weight of the excitatory pathways to the postsynaptic neuron.

Figures 2.15a and b show the activation of neurons a and b caused by stimulation of neuron c at a fixed level as the weight W^+_{ca} was varied. When W^+_{ca} was small, the activation of neuron a was suppressed, and when W^+_{ca} was large the activation of neuron b was suppressed.

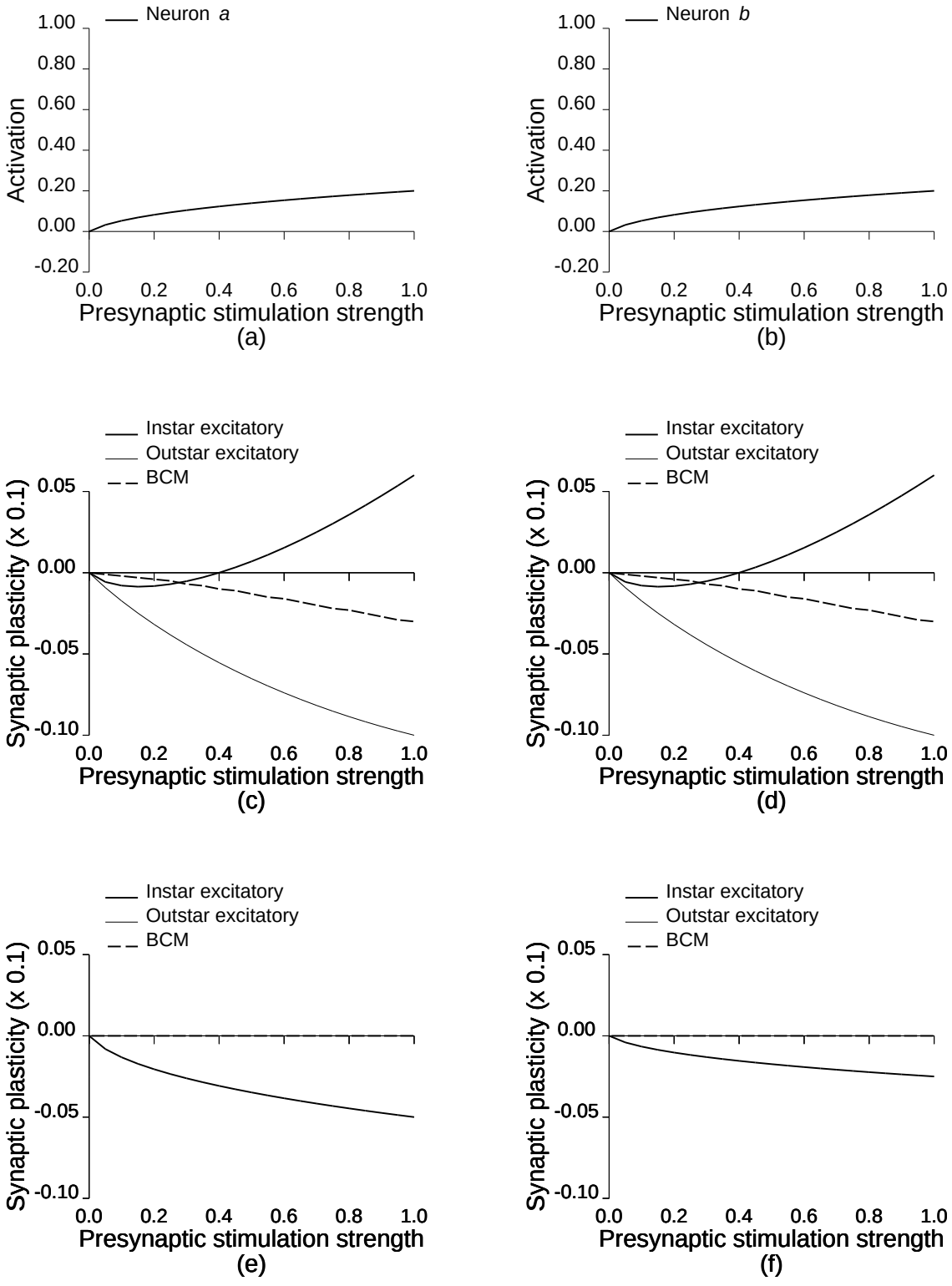

Figure 2.13: Legend on next page.

Figure 2.13: **Simulation results: Excitatory synaptic plasticity produced by stimulation of equally strong pathways to different neurons.**
Figure on previous page. In these simulations, all the parameters were the same as in Figure 2.8. The figure shows the synaptic weight changes under the three rules after activating neuron d; the activation of neuron d, x_d, was varied from 0 to 1. Panels (a) and (b) show the activation level of neurons a and b, respectively, as x_d was varied, panels (c) and (d) show synaptic plasticity in the stimulated pathways from neuron d to neuron a and from neuron d to neuron b, respectively, as x_d was varied, and panels (e) and (f) show synaptic plasticity in the unstimulated pathways from neuron c to neuron a and from neuron c to neuron b, respectively. There was no synaptic weight change under the outstar rule and the BCM rule in panels (e) and (f) since there was no presynaptic stimulation.

Under the instar excitatory synaptic plasticity rule with neuron c stimulated at a fixed level, W_{ca}^+ increased when the initial value of W_{ca}^+ was small and decreased when the initial value of W_{ca}^+ was large (Figure 2.15c). When W_{ca}^+ was very small, no change occurred in W_{ca}^+ because $x_a \leq 0$ (Figure 2.15ac). The weight W_{cb}^+ increased when $x_b > 0$ (Figure 2.15d) because, in the simulation, $W_{cb}^+ < \mathcal{P}(x_c)$. Weights of unstimulated pathways to neurons a and b, e.g., W_{da}^+ and W_{db}^+, respectively, decreased when the corresponding postsynaptic neuron was activated (Figure 2.15ef).

The outstar excitatory synaptic plasticity rule weakened W_{ca}^+ when the initial value of W_{ca}^+ was small (Figure 2.15c). When the initial value of W_{ca}^+ was small, activation of neuron a produced very weak or no response in neuron a (Figure 2.15a), and $W_{ca}^+ > \mathcal{Q}(x_a)$. As the initial value of W_{ca}^+ was increased, activation level of neuron a increased, and W_{ca}^+ underwent LTP when $W_{ca}^+ < \mathcal{Q}(x_a)$. For larger values of W_{ca}^+, $\mathcal{Q}(x_a)$ was less than the initial value of W_{ca}^+, and therefore, W_{ca}^+ weakened (Figure 2.15c). Thus, for a fixed activation level of neuron c, the outstar excitatory rule can produce LTD at very low and very high initial values of W_{ca}^+, and LTP at intermediate initial values of W_{ca}^+. The weight W_{cb}^+ increased for small values of W_{ca}^+ (Figure 2.15d) because, in the simulation, $W_{cb}^+ < \mathcal{Q}(x_b)$, and W_{cb}^+ decreased for large values of W_{ca}^+ (Figure 2.15d) because $W_{cb}^+ > \mathcal{Q}(x_b)$. Weights of unstimulated pathways to neurons a and b, e.g., W_{da}^+ and W_{db}^+, respectively, did not change (Figure 2.15ef).

The sign of synaptic weight change according to the BCM rule depends on the postsynaptic activation and the BCM LTP threshold (Equations 2.4 and 2.5), and the

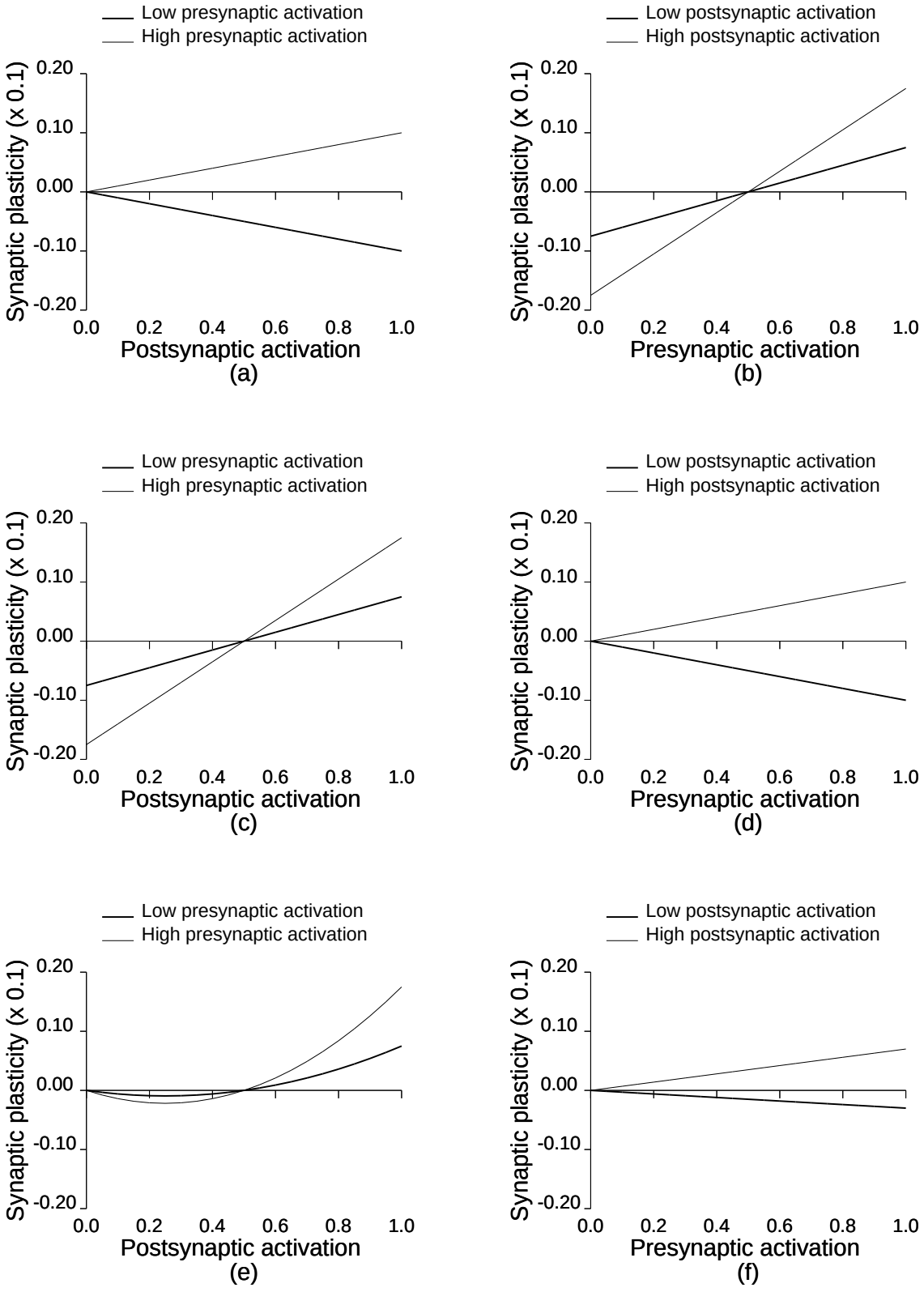

Figure 2.14: Legend on next page.

Figure 2.14: **Simulation results: Changes in excitatory synaptic efficacy of the stimulated pathway as a function of postsynaptic activation.**
Figure on previous page. The dependence of the changes in W_{ca}^+ on postsynaptic activation level x_a is shown under the instar excitatory rule (a), (b), under the outstar excitatory rule (c), (d), and under the BCM rule (e), (f). The initial value of W_{ca}^+ was 0.5. In the panels in the left column, x_c was kept fixed at a low presynaptic activation level ($x_c = 0.3$) and at a high presynaptic activation level ($x_c = 0.7$), and the postsynaptic activation x_a was varied from 0 to 1. In the panels in the right column, x_a was kept fixed at a low postsynaptic activation level ($x_a = 0.3$) and at a high postsynaptic activation level ($x_a = 0.7$), and the presynaptic activation x_c was varied from 0 to 1. The parameters for the plasticity rules were the same as in Figure 2.8.

BCM LTP threshold depends on the postsynaptic activation history (Equation 2.6). When synaptic weight is varied to test the dependence of the initial weight on synaptic plasticity as in Yang and Faber (1991), by prior induction of synaptic plasticity, the BCM rule affects the BCM threshold in addition to the synaptic weight. Thus, two cases were considered in the simulations: one in which the BCM LTP threshold was held constant as the excitatory synaptic weight was varied, and another in which the initial weight and the BCM LTP threshold were changed by prior conditioning.

When a fixed value for θ_a was used as the initial value of W_{ca}^+ was varied, the BCM synaptic plasticity rule weakened W_{ca}^+ for low initial values of W_{ca}^+ and strengthened W_{ca}^+ for high initial values of W_{ca}^+ (Figure 2.15c). When W_{ca}^+ was very small, no change occurred in W_{ca}^+ because $x_a \leq 0$ (Figure 2.15ac). The weight W_{cb}^+ decreased when $x_b > 0$ (Figure 2.15d) because $\theta_b > x_b$ in the simulation. Weights of unstimulated pathways to neurons a and b, e.g., W_{da}^+ and W_{db}^+, respectively, did not change (Figure 2.15ef).

Suppose the initial weight W_{ca}^+ was varied using the BCM rule by activating neuron c to different levels. Figure 2.16a shows the change in W_{ca}^+, and Figure 2.16b shows θ_a after activating neuron c to different levels for a fixed duration. Subsequent activation of neuron c with a fixed activation level increased W_{ca}^+ when a weak activation level was used in the prior conditioning and decreased W_{ca}^+ when a strong activation level was used in the prior conditioning (Figure 2.16c). Thus, the BCM rule can produce LTP when the weight of the conditioned pathway was previously decreased by LTD-inducing stimulation, and LTD when the initial weight of the conditioned pathway was previously increased by

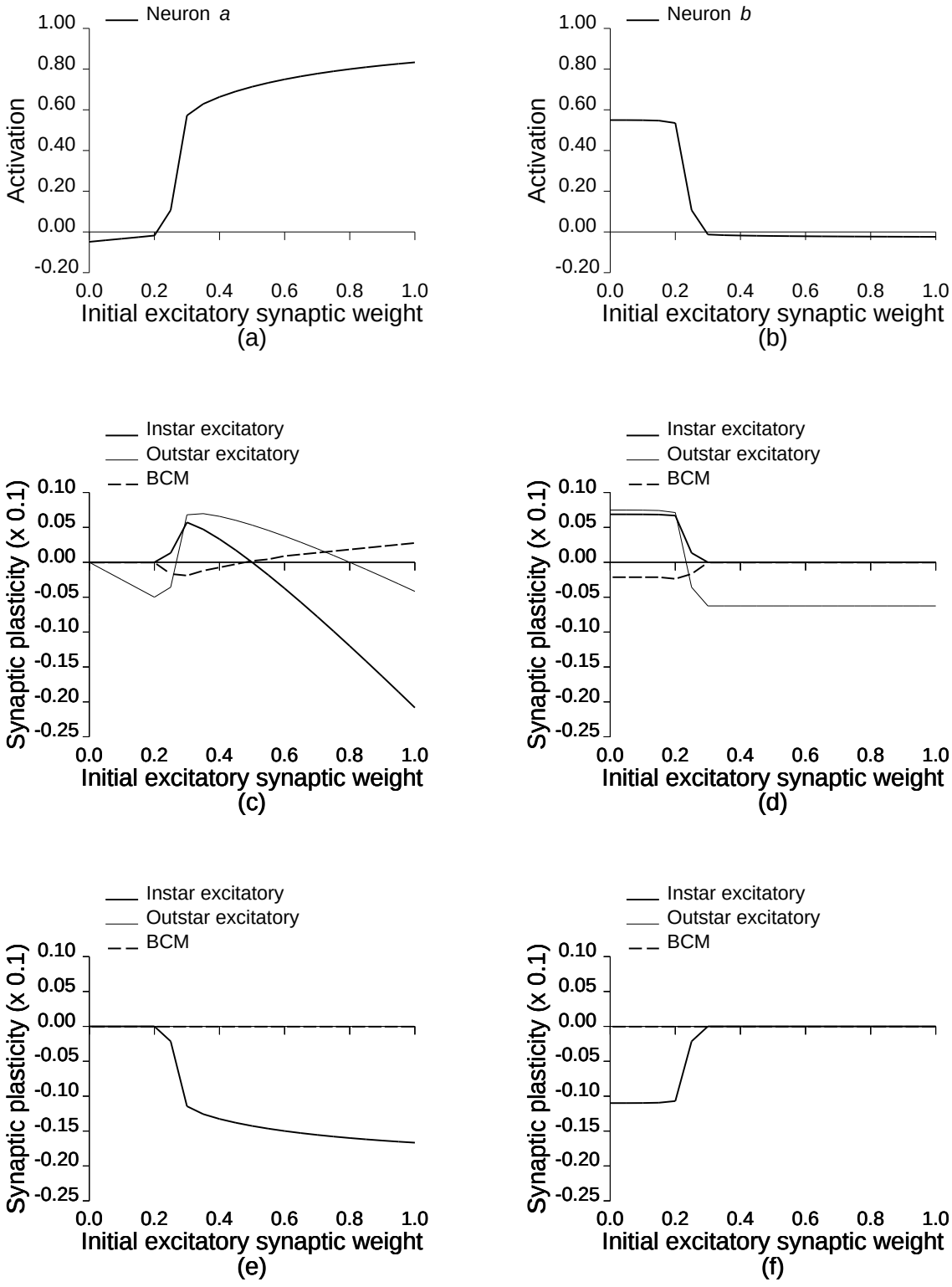

Figure 2.15: Legend on next page.

Figure 2.15: **Simulation results: Changes in excitatory synaptic efficacy of the stimulated pathway as a function of initial synaptic efficacy.**
Figure on previous page. The parameters for the plasticity rules and the activation equation were the same as in Figure 2.8. The initial network synaptic weights were the same except that W_{ca}^{+} was varied from 0 to 1, and neuron c was activated at a fixed level of 0.5. (a,b) Activation level of neurons a and b, respectively, as W_{ca}^{+} was varied. (c,d) Synaptic plasticity in the stimulated pathways from neuron c to neuron a and from neuron c to neuron b, respectively. (e,f) Synaptic plasticity in the unstimulated pathways from neuron d to neuron a and from neuron d to neuron b, as W_{ca}^{+} was varied. For the BCM rule the initial LTP threshold of neurons a and b was fixed at 0.7 as W_{ca}^{+} was varied. There was no synaptic weight change according to the instar rule when postsynaptic activation was suppressed (c,d,e,f). Synaptic plasticity was blocked according to the BCM rule when postsynaptic activation was suppressed (c), (d) and when presynaptic stimulation was absent (e), (f). Absence of presynaptic stimulation blocked synaptic plasticity in (e), (f) according to the outstar rule.

LTP-inducing stimulation.

Associative synaptic plasticity

Associative LTP (Brown et al., 1990; Levy & Steward, 1979; Barrionuevo & Brown, 1983; Kelso & Brown, 1986) refers to LTP produced in a weak excitatory pathway to a neuron by simultaneous stimulation of the weak excitatory pathway and a strong excitatory pathway to the neuron; but LTP is not induced in the weak excitatory pathway to the neuron by exclusive stimulation of the weak or the strong excitatory pathway. Figures 2.18 and 2.20 show changes in the synaptic efficacy governed by the three rules in response to stimulation of independent excitatory pathways to neuron a. In the simulations, the excitatory pathway from neuron e to neuron a in Figure 2.7 was weak, and the excitatory pathway from neuron c to neuron a in Figure 2.7 was strong.

In the simulations in Figures 2.17 and 2.18, when the weak excitatory pathway from neuron e to neuron a was stimulated, neuron a was inactive (Figure 2.17a). Therefore, W_{ea}^{+} and W_{ca}^{+} did not change according to the instar and the BCM excitatory synaptic plasticity rules (Figure 2.18ab) because postsynaptic activation was below zero. The outstar excitatory synaptic plasticity rules weakened W_{ea}^{+} because W_{ea}^{+} was greater than $\mathcal{Q}(x_a) = 0$ (Figure 2.18a); W_{ca}^{+} did not change because the pathway from neuron c to neuron a was not

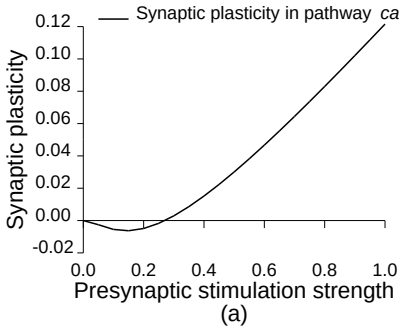

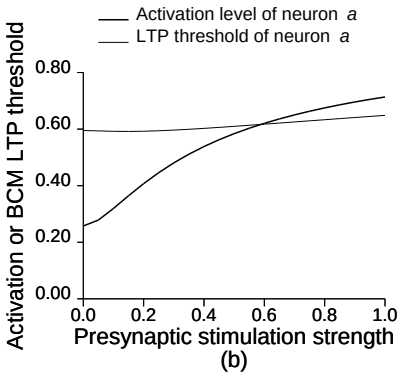

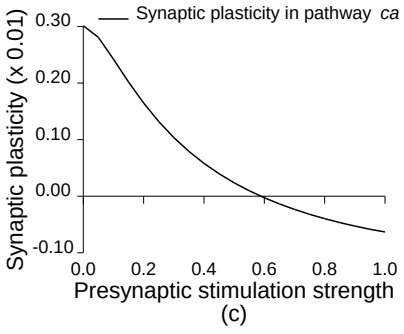

Figure 2.16: Legend on next page.

Figure 2.16: **Simulation results: Changes in excitatory synaptic efficacy of the stimulated pathway according to the BCM rule as a function of prior presynaptic stimulation.**
Figure on previous page. The initial network synaptic weights, the BCM rule parameters, and the activation equation parameters are the same as in Figure 2.8. The initial LTP threshold of neurons a and b was 0.7. (a) The change in W_{ca}^{+} after stimulating neuron c at different activation levels for 20 iterations. The LTP threshold was changed according to the equation in Figure 2.12. The LTP threshold of neuron a and the activation level of neuron a in response to activation of neuron c at $x_c = 0.3$ are shown following the stimulation of neuron c for 20 iterations (b). The changes in W_{ca}^{+} when neuron c was activated at $x_c = 0.3$ are also shown in (c).

stimulated. Thus, according to the three excitatory synaptic plasticity rules, stimulation of a weak excitatory pathway to a neuron may not induce LTP in the weak pathway, because network interaction may render the neuron inactive.

When the strong excitatory pathway from neuron c to neuron a was stimulated, neuron a became strongly activated (Figure 2.17a). The instar excitatory synaptic plasticity rule weakened W_{ea}^{+} because $x_e = 0$ (Figure 2.18c). The outstar and the BCM excitatory synaptic plasticity rules did not modify W_{ea}^{+} because $x_e = 0$ (Figure 2.18c). All three rules produced LTP in the stimulated strong excitatory pathway from neuron c to neuron a when x_c was large (Figure 2.18d). Thus, stimulation of the strong excitatory pathway alone did not produce LTP in the weak pathway.

When neurons c and e were simultaneously activated at the same level, x_a was smaller than when x_c was stimulated alone (Figure 2.17a); the strong lateral inhibitory interactions between neurons a and b reduced their activation levels. In this particular network, when neurons c and e were simultaneously stimulated with the same strength, the instar excitatory synaptic plasticity rule produced LTP in W_{ea}^{+} and W_{ca}^{+} at high stimulation strengths (Figure 2.18ef). Thus, in this network the instar excitatory synaptic plasticity rule exhibited associative LTP when the presynaptic stimulation strength was high. When neurons c and e were simultaneously stimulated with the same stimulation strength, they had different LTP thresholds under the instar rule (Figure 2.18ef). When the outstar rule was used during simultaneous stimulation of neurons c and e, LTP was produced in W_{ea}^{+} at high stimulation strengths (Figure 2.18e), but W_{ca}^{+} underwent LTD even at high

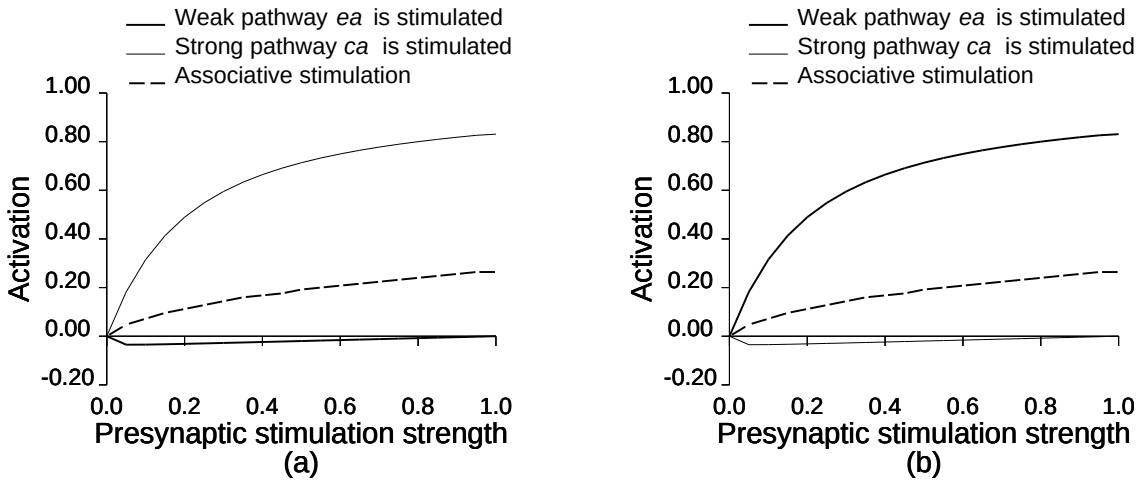

Figure 2.17: **Simulation results: Postsynaptic activation caused by stimulation of independent excitatory pathways.**
The activation level of neuron a (panel (a)) and of neuron b (panel (b)) is shown when neuron e was stimulated alone, when neuron c was stimulated alone, and when neurons e and c were simultaneously stimulated using the same stimulation strength. The initial network synaptic weights, the activation equation parameters, the synaptic plasticity rule parameters, and the initial BCM LTP thresholds were the same as in Figure 2.8.

stimulation strengths (Figure 2.18f). Thus, it is possible to induce associative LTP in a weak excitatory pathway to a postsynaptic neuron under the outstar rule. Furthermore, the LTP threshold in independent pathways can be different according to the outstar excitatory synaptic plasticity rule (Figure 2.18ef). In this network, the BCM rule did not produce LTP when neurons c and e were simultaneously stimulated with the same stimulation strength because θ_a was greater than x_a (Figure 2.18ef). If the initial value of θ_a were chosen to be less than the activation level of x_a when $x_c = x_e = 0.5$, then the BCM rule would produce LTP in W_{ea}^+ and W_{ca}^+ when $x_c = x_e > 0.5$. Thus, the BCM rule too can produce associative LTP in W_{ea}^+. The changes in W_{ea}^+ and W_{ca}^+ produced by the BCM rule were identical because $x_c = x_e$, and the independent pathways had a single LTP threshold θ_a.

Figure 2.20 demonstrates associative LTP in W_{ea}^+ under the outstar and the BCM excitatory synaptic plasticity rules, but not under the instar excitatory synaptic plasticity rule. The BCM rule has a single LTP threshold for independent pathways, whereas the instar and the outstar synaptic plasticity rules have independent LTP thresholds for

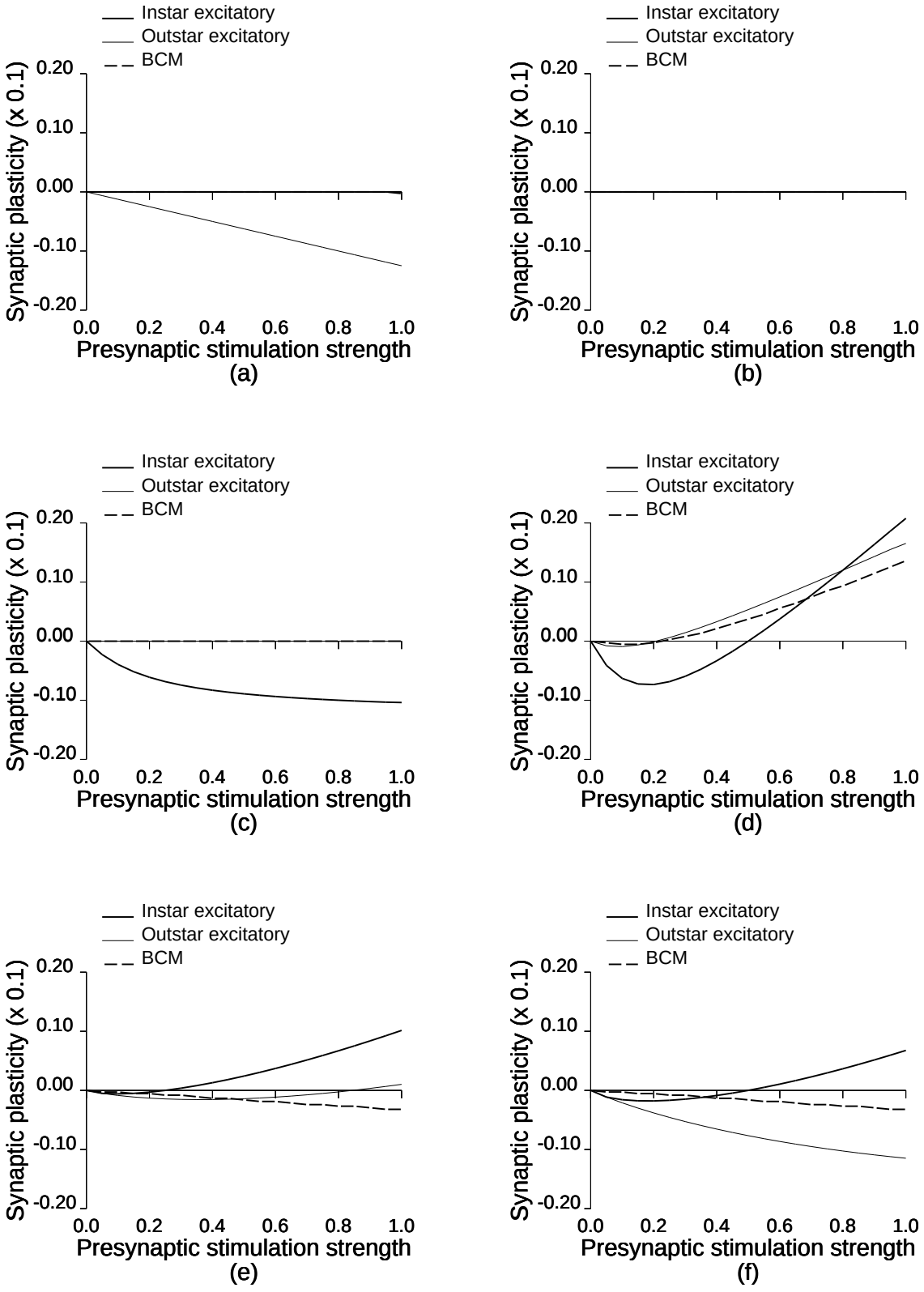

Figure 2.18: Legend on next page.

Figure 2.18: **Simulation results: Associative synaptic plasticity.**
Figure on previous page. The simulation parameters are given in Figure 2.17. The panels in the left column show changes in the weak pathway from neuron e to neuron a, and the panels in the right column show changes in the strong pathway from neuron c to neuron a, when the weak pathway alone was stimulated (top row), the strong pathway alone was stimulated (middle row), and the weak and the strong pathways were simultaneously stimulated using the same stimulation strength (bottom row). Activation of neuron a was suppressed when the pathway ea was stimulated, and therefore the weight of pathway ea and pathway ca was not changed under the instar rule and the BCM rule (a), (b). The weight of pathway ca was not changed under the outstar rule (b), since the pathway was not stimulated. (c) Synaptic plasticity in pathway ea was blocked according to the outstar rule and the BCM rule because pathway ea was not stimulated.

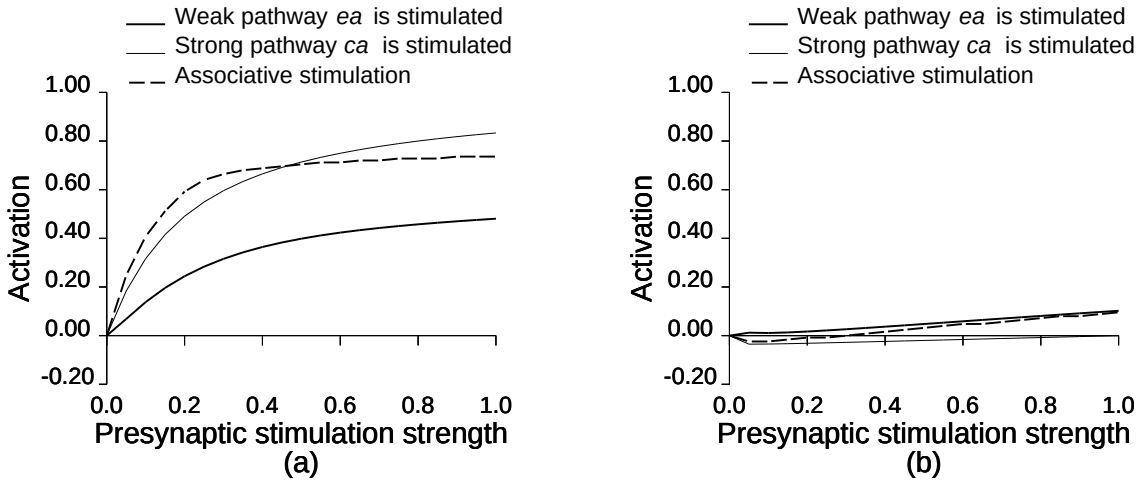

Figure 2.19: **Simulation results: Postsynaptic activation caused by stimulation of independent excitatory pathways in a network with asymmetric lateral inhibitory weights.**
The activation of neuron a (panel (a)) and of neuron b (panel (b)) is shown when neuron e was stimulated alone, when neuron c was stimulated alone, and when neurons e and c were simultaneously stimulated using the same stimulation strength. The activation equation parameters, the synaptic plasticity rule parameters, and the initial BCM LTP thresholds were the same as in Figure 2.8. The initial network synaptic weights were the same as in Figure 2.8 except that $W_{ab}^{-} = 0.4$ and $W_{ba}^{-} = 0.1$.

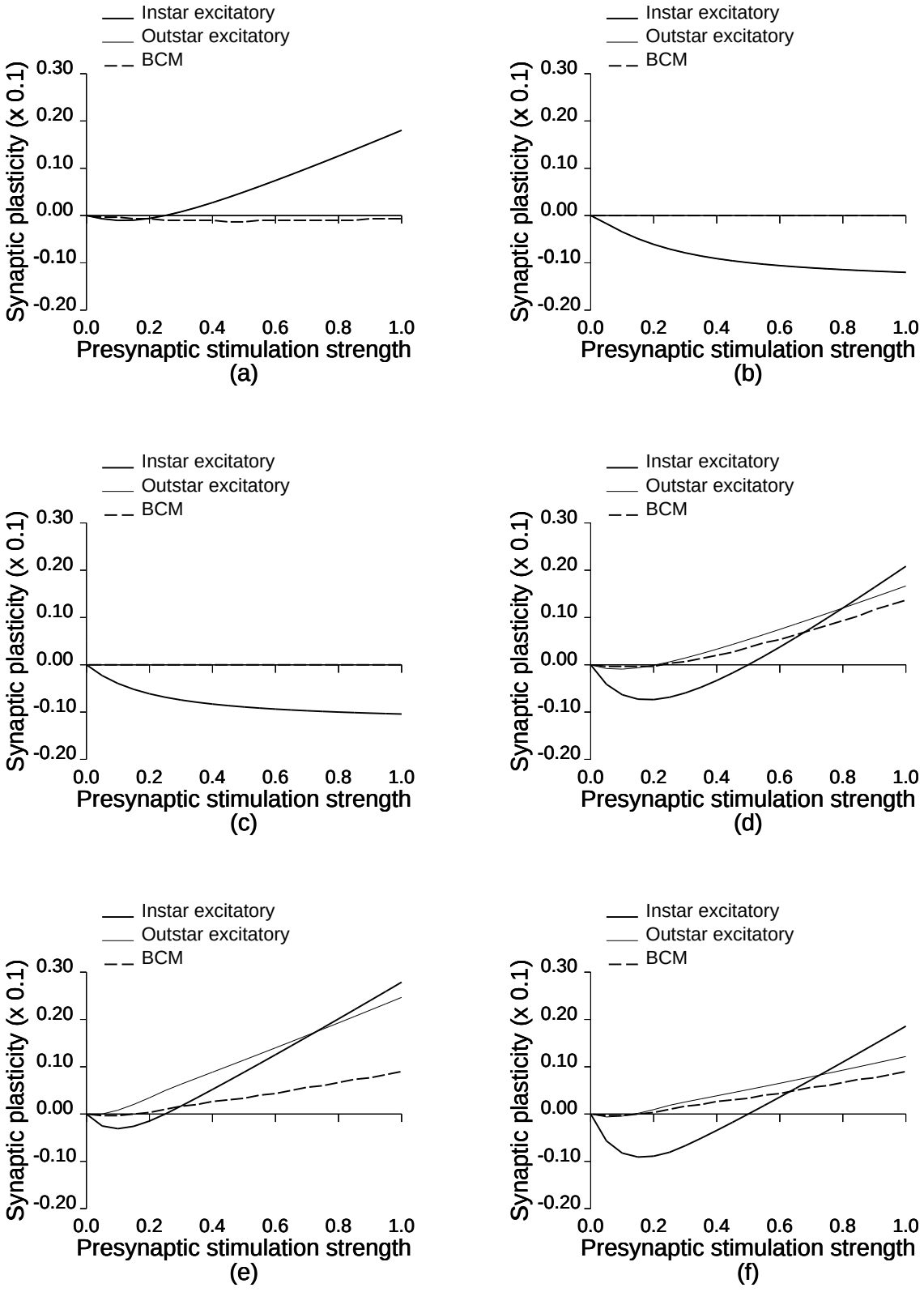

Figure 2.20: Legend on next page.

Figure 2.20: **Simulation results: Associative synaptic plasticity in a network with asymmetric lateral inhibitory weights.**
Figure on previous page. The simulation parameters are given in Figure 2.19. See Figure 2.18 for conventions. The weights of pathways ca and ea were not changed under the outstar rule and the BCM rule (b), (c) because the pathways were not stimulated.

independent pathways (Figure 2.20ef).

In the case of the outstar and the BCM excitatory synaptic plasticity rules, to demonstrate associative plasticity the postsynaptic activation level should be below the LTP threshold of the weak pathway when the weak pathway is stimulated alone. However, when the weak and a strong pathway are simultaneously stimulated, the postsynaptic activation should exceed the LTP threshold of the weak pathway. Under the outstar and the BCM excitatory synaptic plasticity rules, no synaptic plasticity occurs in the unstimulated weak pathway when the strong pathway alone is stimulated. In the case of the instar excitatory synaptic plasticity rule, to produce associative plasticity the postsynaptic activation should be suppressed when the weak pathway is stimulated alone, but when the weak and the strong pathway are simultaneously stimulated the postsynaptic neuron should be activated.

If stimulation of the weak pathway activates the postsynaptic neuron, then associative LTP cannot be produced according to the instar rule alone. When the postsynaptic neuron is active, then the sign of weight change depends only on the presynaptic stimulation strength to the weak pathway and the synaptic strength of the weak pathway. Any stimulation that produces LTP (LTD) in the weak pathway when the weak pathway alone is stimulated will produce LTP (LTD) in the weak pathway when the weak pathway and the strong pathway are simultaneously stimulated with the same stimulation strength.

2.3.4 Combined effects of instar and outstar excitatory synaptic plasticity rules

Artola et al. (1990) found that for a fixed presynaptic stimulation at the white matter–layer 6 border, synaptic plasticity in the excitatory pathways to layers 2–4 neurons depended on the postsynaptic activation level. Plasticity was blocked,

or very little LTD was produced, when the postsynaptic activation was suppressed below a threshold. Increasing postsynaptic activation above the threshold produced larger LTD; and further increase in postsynaptic activation above a second higher threshold produced LTP. In this section, it is shown that a combination of the instar and the outstar rules models the results of Artola et al. (1990).

Stimulation at the white matter–layer 6 border can activate geniculocortical pathways and corticocortical pathways to neurons in layers 2–4 (Kirkwood et al., 1993). In the absence of any pharmacological treatment, white matter stimulation produces complex postsynaptic potentials involving monosynaptic and polysynaptic EPSP and IPSP sequences (Frégnac et al., 1994). A measure of synaptic efficacy such as the amplitude of the early peak of the postsynaptic potential may involve interactions of a variety of membrane currents, and therefore, this measure of synaptic efficacy of the pathway from white matter is an estimate of the "effective weight" of the pathway (Frégnac et al., 1994).

In the simulations presented in this section, it was assumed that plasticity in afferent feedforward (Felleman & Van Essen, 1991; Maunsell & Van Essen, 1983) excitatory pathways from lateral geniculate nucleus to neurons in layers 2–4 is governed by the instar excitatory rule and that plasticity in feedback (Felleman & Van Essen, 1991; Maunsell & Van Essen, 1983) excitatory corticocortical pathways to neurons in layers 2–4 is governed by the outstar excitatory rule. In Sections 2.4.3 and 2.4.4, a plausible computational basis for the above assumptions is discussed.

Figure 2.21 shows the effects of combining the weights of feedforward and feedback pathways. In Figure 2.21, a postsynaptic neuron k was innervated by a feedforward pathway ik with synaptic weight W_{ik}^{+}, and by a feedback pathway jk with synaptic weight W_{jk}^{+}. The feedforward pathway synaptic plasticity was governed by the instar excitatory rule, and the feedback pathway synaptic plasticity was governed by the outstar excitatory rule. In the simulation, both the pathways were stimulated using the same stimulation. Because the total excitation to the postsynaptic neuron was given by Equation 2.2, which is linear in the synaptic weights, and because the presynaptic stimulation strength to the two pathways was the same, the effective weight of the two pathways was computed by adding their synaptic weights.

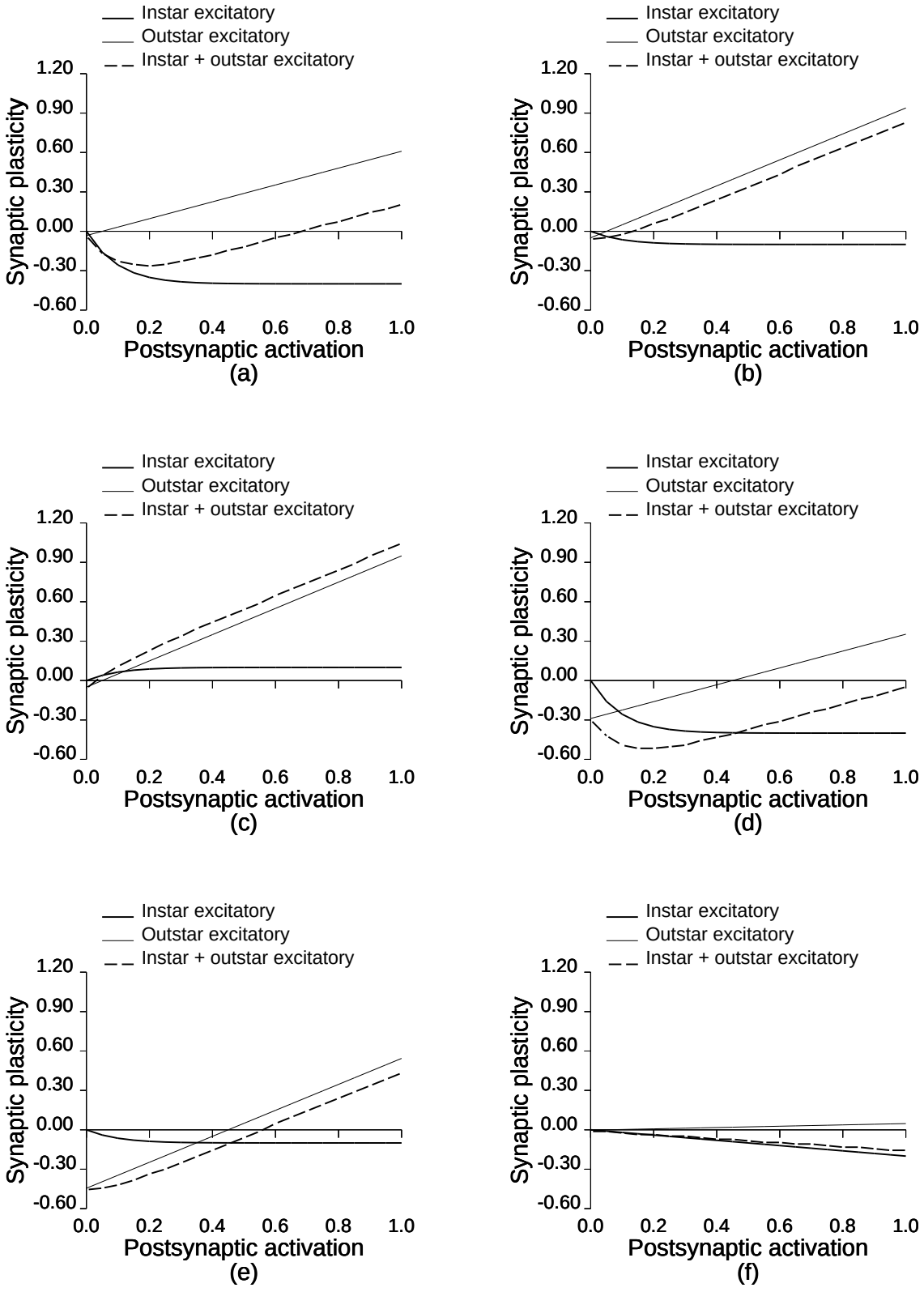

Figure 2.21: Legend on next page.

Figure 2.21: **Simulation results: Synaptic plasticity with fixed presynaptic stimulation and variable postsynaptic activation level under the instar and the outstar excitatory synaptic plasticity rules.**
Figure on previous page. In this simulation, a postsynaptic neuron received feedforward and feedback pathways. The feedforward pathway synaptic plasticity was governed by the instar excitatory rule, and the feedback pathway synaptic plasticity was governed by the outstar excitatory rule. The two pathways were stimulated by the same stimulation strength, and the effective synaptic weight of the two pathways was obtained by adding the synaptic weights of the two pathways. The presynaptic stimulation strength of the two pathways was held constant, and the postsynaptic activation was varied. (a)–(e) The synaptic weight changes were computed after pairing the pre- and postsynaptic activation for 20 iteration. (f) The synaptic weight changes were computed after a single pairing of the pre- and postsynaptic activation. The initial synaptic weight of the feedforward pathway was 0.5, and the initial synaptic weight of the feedback pathway was 0.05. The presynaptic stimulation strength was 0.1 in panels (a) and (f), 0.4 in panel (b), and 0.6 in panel (c). In panels (d) and (e), the initial synaptic weight of the feedforward pathway was 0.5, and the initial synaptic weight of the feedback pathway was 0.45. The presynaptic stimulation strength was 0.1 in panel (d) and 0.4 in panel (e). The parameters for the instar and the outstar rules were the same as in Figure 2.8.

The changes in the combined synaptic weight according to the instar and the outstar excitatory synaptic plasticity rules in Figure 2.21a are similar to those experimentally observed by Artola et al. (1990). However, the changes in the combined weight of the feedforward and the feedback pathways produced by the instar and the outstar excitatory synaptic plasticity rules were parameter dependent.

The following paragraphs analyze the parameter dependence of the combined weight changes based on the combination of the instar and the outstar excitatory synaptic plasticity rules. The shape of the curve relating the combined weight changes and postsynaptic activation level depends on the duration of stimulation, the presynaptic stimulation strength, and the initial synaptic weights.

In Figure 2.21a the presynaptic stimulation was presented for 20 time steps. Under the instar excitatory rule, the feedforward weight change reached an asymptote because presynaptic stimulation was fixed while postsynaptic activation was varied. The outstar excitatory rule caused the feedforward pathway weight to approach the postsynaptic activation level, and the weight change in the feedback pathway did not reach an asymptote

as the postsynaptic activation was increased. Thus, as the postsynaptic activation level was increased, the feedforward pathway weight change equilibrated, but the feedback pathway weight change increased, and the change in combined weight of the two pathways went from LTD to LTP (Figure 2.21a). When the postsynaptic activation was less than or equal to zero, the plasticity under the instar rule was disabled, but the plasticity in the outstar rule, which is enabled by presynaptic stimulation alone, caused a small LTD in the feedback pathway because the initial weight of the feedback pathway was small.

In Figures 2.21b and 2.21c, the presynaptic stimulation strength was varied. When the presynaptic stimulation strength was close to but less than the feedforward pathway synaptic weight (Figure 2.21b), the maximal decrease in the feedforward pathway according to the instar rule was small, and therefore the LTP threshold for the combined synaptic weight decreased. When the presynaptic stimulation strength was close to but greater than the feedforward pathway synaptic weight (Figure 2.21c), the feedforward pathway underwent LTP according to the instar rule, and the LTP threshold for the combined synaptic weight decreased even further. When the initial synaptic weight of the feedback pathway was large, large LTD was produced in the combined synaptic weight when the postsynaptic neuron was inactive (Figures 2.21de). In Figure 2.21f, the synaptic weight changes are shown after only one iteration when the weights were far from their equilibrium values. In this case, the combined weight decreased.

The instar and the outstar rules alone can not reproduce the experimental results; in fact, the instar and the outstar rules alone cannot produce the results for any parameter values. If the instar rule alone were used for a fixed presynaptic activation, the sign of the synaptic weight change would be fixed as the postsynaptic activation was changed (Figure 2.14). If the outstar rule alone were used for a fixed presynaptic activation, the maximal LTD would be produced when the postsynaptic neuron was hyperpolarized or inactive (Figure 2.14).

2.3.5 Characteristics of the outstar inhibitory synaptic plasticity rule

There have been only a few experiments on lateral inhibitory synaptic plasticity (e.g., Levy & Desmond, 1985; Miles & Wong, 1987; Rutherford et al., 1997).

Levy and Desmond (1985) suggested several inhibitory synaptic plasticity rules, including the outstar inhibitory rule, to model some aspects of classical conditioning. To motivate further experimentation on lateral inhibitory synaptic plasticity, predictions of the outstar lateral inhibitory synaptic plasticity rule (Marshall, 1990a, 1995a; Marshall & Gupta, 1998) are presented. As in the case of the excitatory synaptic plasticity rules, changes in the lateral inhibitory synaptic weights under the outstar lateral inhibitory synaptic plasticity rule are studied as a function of input excitation to model neurons, pre- and postsynaptic activation, and initial lateral inhibitory weights.

The properties of the outstar lateral inhibitory synaptic plasticity rule are illustrated using the simple neural network described in Section 2.3.3 (Figure 2.7). In the simulations in this section, only the lateral inhibitory pathway weights were plastic; the excitatory pathway weights were held constant.

Synaptic plasticity in lateral inhibitory synapses as a function of input excitation

Figure 2.22 shows the activation of neurons a and b as x_d was varied from 0 to 1. The activations x_a and x_b increased as x_d was increased (Figure 2.22ab), and x_a and x_b remained equal, because of the symmetry of the initial weights.

Synaptic plasticity in the lateral inhibitory pathways between neurons a and b as a function of input stimulation strength is shown in Figure 2.22cd. When the excitatory input to neurons a and b was low, both neurons were weakly activated (Figure 2.22ab), and according to the outstar lateral inhibitory plasticity rule pathway the lateral inhibitory pathways between the two neurons underwent LTD, because $\mathcal{R}(x_a)$ and $\mathcal{R}(x_b)$ were less than W_{ba}^- and W_{ab}^-, respectively. As x_d increased, x_a and x_b increased (Figure 2.22ab), and W_{ba}^- and W_{ab}^- were potentiated (Figure 2.22cd).

In Figure 2.23, neuron c was stimulated. Figure 2.23ab shows the activation of neurons a and b as x_c was varied from 0 to 1. When x_b was below zero, according to the outstar lateral inhibitory synaptic plasticity rule W_{ba}^- did not undergo any change, and W_{ab}^- decreased (Figure 2.23cd). At high values of x_c, when x_a and x_b are greater than zero, changes in the lateral inhibitory pathway weights depended on the initial value of the inhibitory weights and on the postsynaptic activation level (Figure 2.23cd); the inhibitory

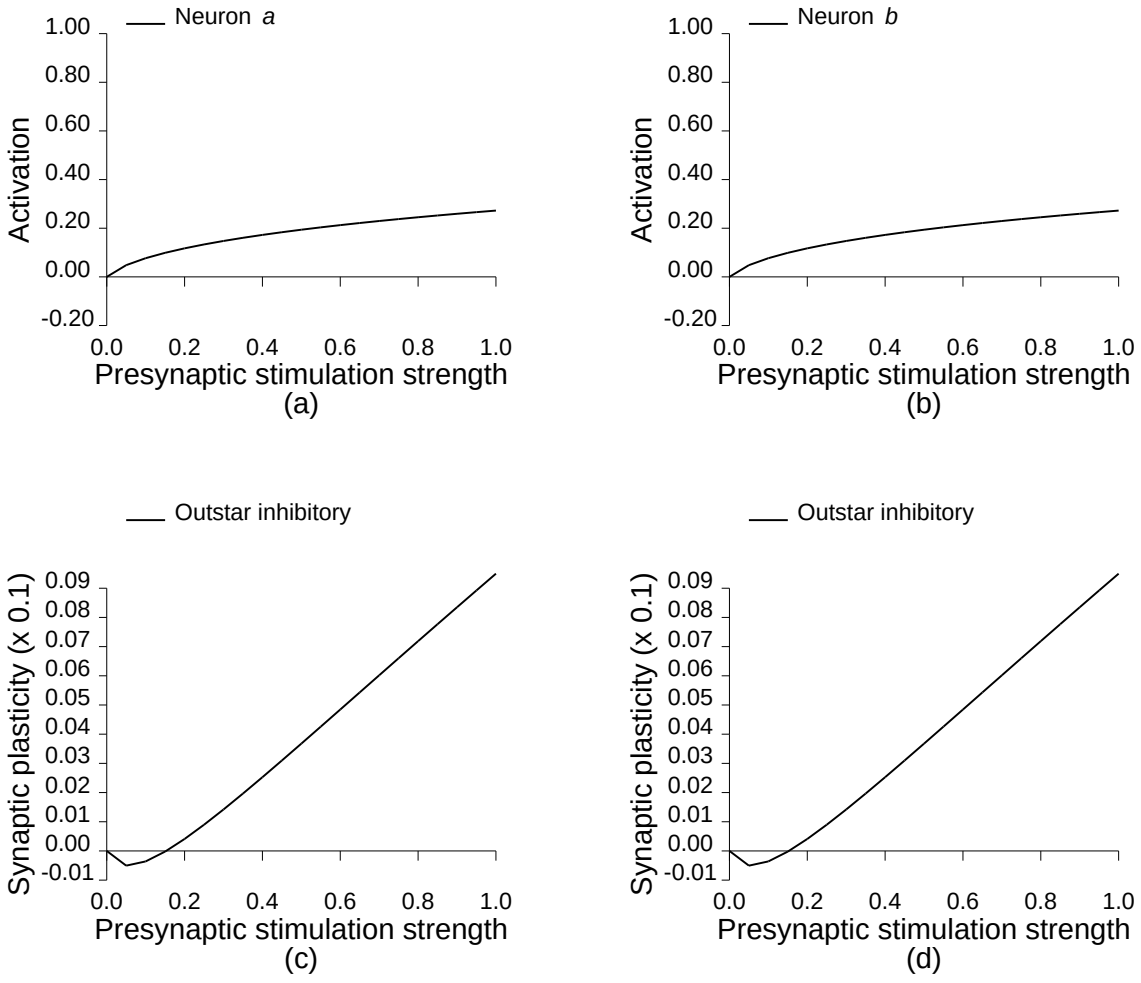

Figure 2.22: **Simulation results: Changes in inhibitory synaptic efficacy under the outstar inhibitory synaptic plasticity rule as a function of input excitation.** Figure on previous page. In this simulation, the initial pathway synaptic weights in the network shown in Figure 2.4 were assigned as follows: $W_{ca}^{+} = 0.5$, $W_{cb}^{+} = 0.25$, $W_{da}^{+} = 0.4$, $W_{db}^{+} = 0.4$, $W_{ea}^{+} = 0.25$, $W_{eb}^{+} = 0.5$, $W_{ab}^{-} = W_{ba}^{-} = 0.2$. The parameters for the activation equation (Equation 2.1) were $A = 0.1$, $B = 1$, $C = 0.05$, $\beta = 1$, and $\gamma = 15$. The activation level was computed using the Euler method with a time step of 0.04 until $t = 40$. The initial activation level of neurons a and b was set to zero. The parameters for the outstar lateral inhibitory synaptic plasticity rule were assigned the following values: $\delta = 0.1$, $\mathcal{H}(x) = [x]$, and $\mathcal{R}(x) = 2[x]$. The figure shows the synaptic weight changes according to the outstar lateral inhibitory synaptic plasticity rule after activating neuron d. The activation level of neuron d, x_d, was varied from 0 to 1. Panels (a) and (b) show the activation level of neurons a and b, respectively, as x_d was varied, and panels (c) and (d) show changes in W_{ab}^{-} and W_{ba}^{-}, respectively, as x_d was varied.

pathway from the strongly active neuron a to the weakly active neuron b weakened (became less inhibitory), while the inhibitory pathway from the weakly active neuron b to the strongly active neuron a strengthened.

Figure 2.24 shows the changes in the lateral inhibitory pathways when a fixed stimulation was continuously applied to neuron c. The lateral inhibitory weights equilibrated to a value proportional to the postsynaptic activation level (Figure 2.24cd), and the rate of change approached zero as the lateral inhibitory weights approached their equilibrium values (Figure 2.24ef).

Synaptic plasticity in lateral inhibitory synapses as a function of activation level of the pre- and postsynaptic neurons

In Figure 2.25a, activation level of postsynaptic neuron b was varied for fixed values of activation level of presynaptic neuron a. As x_b was increased, the change in W_{ab}^- went from LTD to LTP. As x_a was increased, the magnitude of change in W_{ab}^- increased. In Figure 2.25b, activation level of presynaptic neuron a was varied for fixed values of the activation level of postsynaptic neuron b. As x_a was increased the sign of change in W_{ab}^- was fixed, but the magnitude of change increased. As x_b was increased, the change in W_{ab}^- went from LTD to LTP.

Synaptic plasticity in lateral inhibitory synapses as a function of initial inhibitory synaptic efficacy

The simulations in this section illustrate that under the outstar lateral inhibitory synaptic plasticity rule, in general, the lateral inhibitory pathway weights increase if the initial weights are low, and the lateral inhibitory pathway weights decrease if the initial weights are high. Figure 2.26 shows changes in W_{ab}^- and W_{ba}^-, as only W_{ab}^- was varied for a fixed value of x_d. At low values of W_{ab}^-, neuron a was inactive, and at high values of W_{ab}^-, neuron b was inactive. Figure 2.26 shows that plasticity in a lateral inhibitory pathway was blocked when the presynaptic neuron was inactive.

Figure 2.27 shows the changes in W_{ab}^- and W_{ba}^-, as W_{ab}^- and W_{ba}^- were varied for a fixed value of x_a. W_{ab}^- underwent potentiation when the initial value of W_{ab}^- was low and

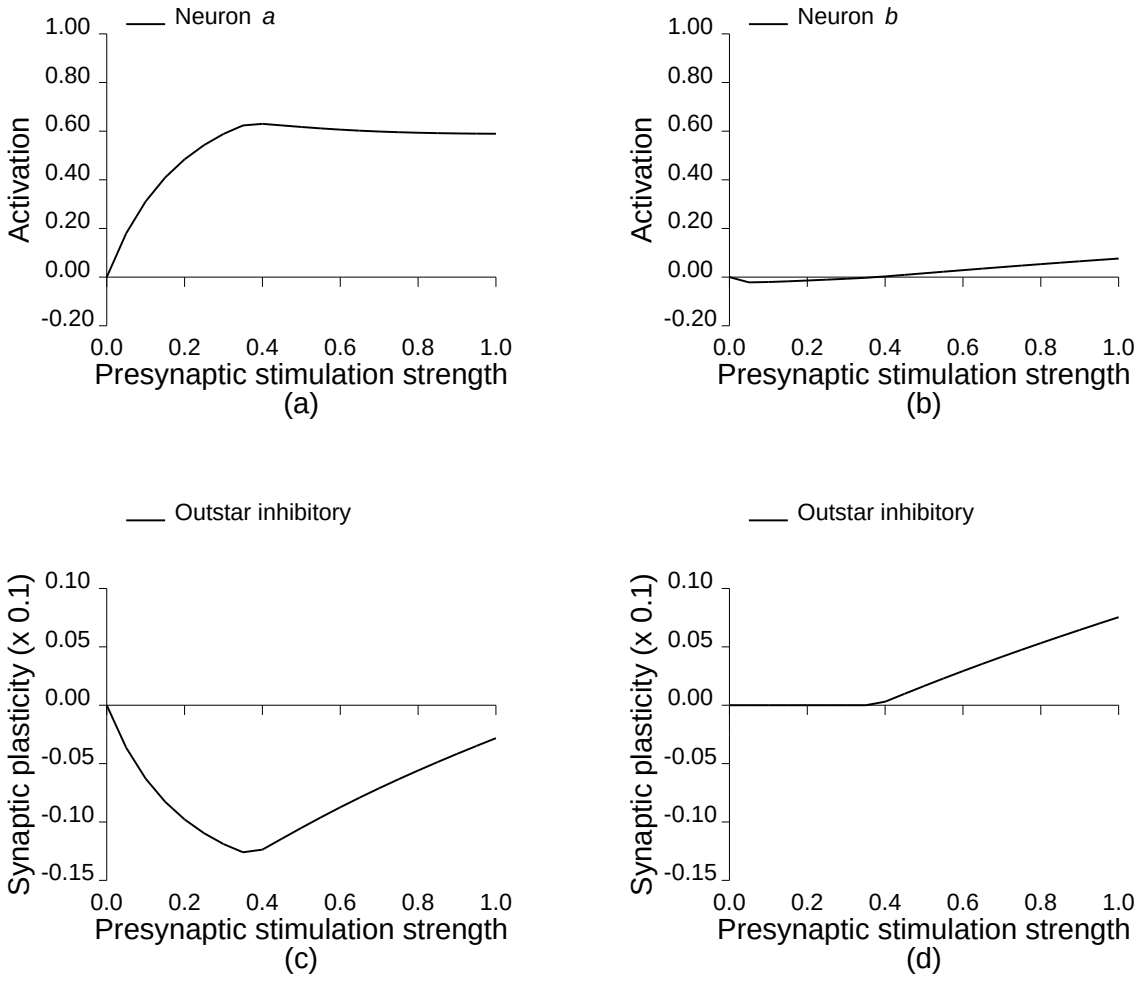

Figure 2.23: **Simulation results: Changes in inhibitory synaptic efficacy under the outstar inhibitory synaptic plasticity rule produced by unequal activation of neurons.**

The synaptic weight changes under the outstar lateral inhibitory synaptic plasticity rule are shown after activating neuron c. The activation x_c was varied from 0 to 1. Panels (a) and (b) show the activation level of neurons a and b, respectively, as x_c was varied, and panels (c) and (d) show changes in W_{ab}^{-} and W_{ba}^{-}, respectively, as x_c was varied. The initial synaptic weights, the parameters for the activation equation, and the parameters for the outstar lateral inhibitory synaptic plasticity rule are given in Figure 2.22. (d) There was no weight change in the inhibitory pathway from neuron b to neuron a when activity in neuron b was suppressed.

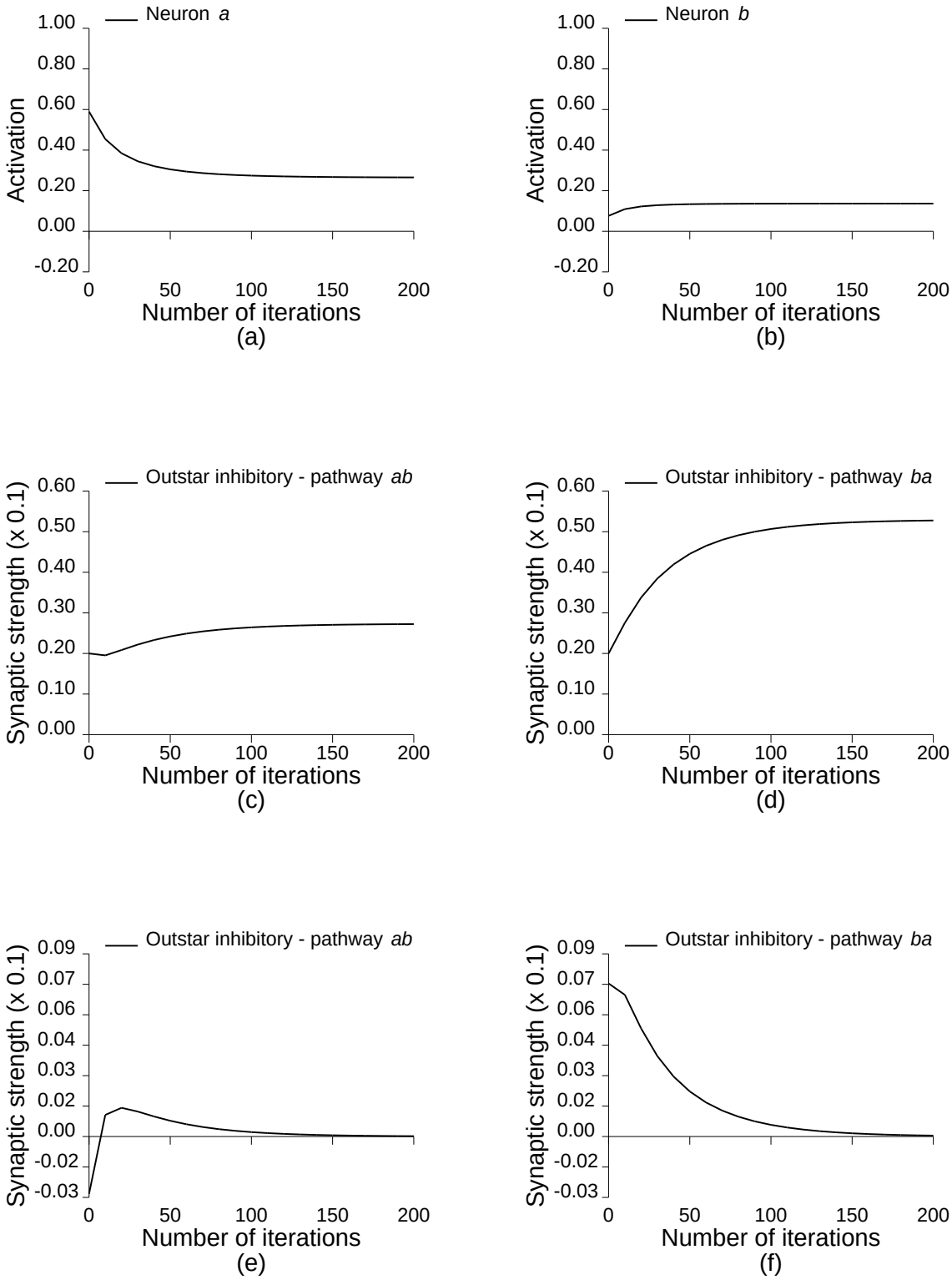

Figure 2.24: Legend on next page.

Figure 2.24: **Simulation results: Equilibrium value of inhibitory synaptic efficacy under the outstar inhibitory synaptic plasticity rule.**
Figure on previous page. The simulation parameters were the same as those given in Figure 2.23. In this simulation, presynaptic stimulation was applied by keeping x_c fixed at 1 for 200 iterations. The synaptic weights were changed every iteration. Panels (a) and (b) show the activation level of neurons a and b, respectively, over a period of 200 iterations as the lateral inhibitory synaptic weights change. The LTP threshold for the outstar lateral inhibitory synaptic plasticity rule was proportional to the lateral inhibitory synaptic weight. Panels (c) and (d) show the synaptic weight of the inhibitory pathways, and panels (e) and (f) show the rate of inhibitory synaptic weight change in the inhibitory pathways.

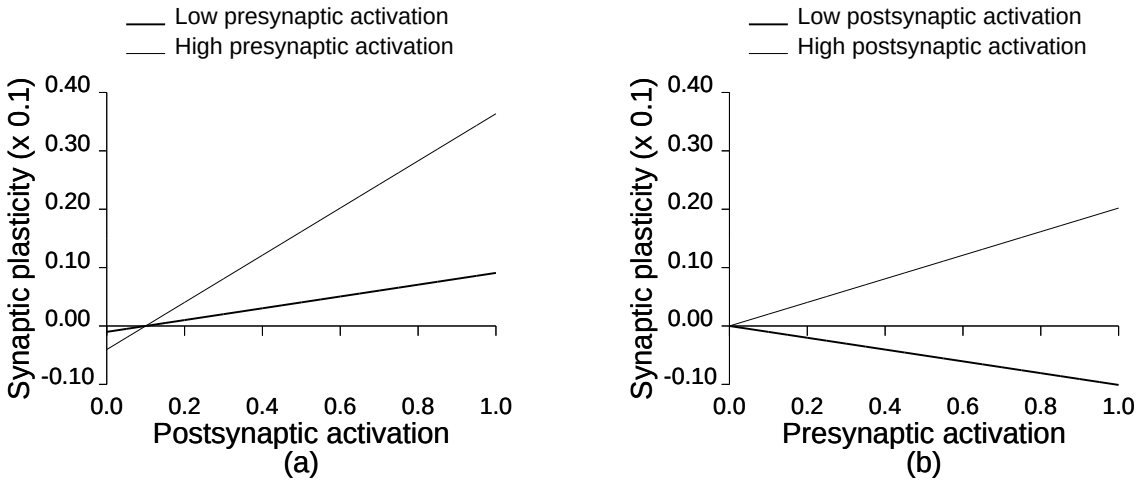

Figure 2.25: **Simulation results: Changes in inhibitory synaptic efficacy under the outstar inhibitory synaptic plasticity rule as a function of pre- and postsynaptic activation.**
The dependence of synaptic plasticity in W_{ab}^{-} on presynaptic activation level x_a and on postsynaptic activation level x_b under the outstar inhibitory synaptic plasticity rule is shown. The initial value of W_{ab}^{-} was 0.2. (a) The presynaptic activation x_a was kept fixed at a low level ($x_a = 0.05$) and at a high level ($x_a = 0.2$), and the postsynaptic activation x_b was varied from 0 to 1. (b) The postsynaptic activation x_b was kept fixed at a low level ($x_b = 0.05$) and at a high level ($x_b = 0.2$), and the presynaptic activation x_a was varied from 0 to 1. The parameters for the inhibitory synaptic plasticity rule were the same as in Figure 2.22.

x_b was high and underwent depression when the initial value of W_{ab}^- was high and x_b was low. Figure 2.28 shows the changes in W_{ab}^- and W_{ba}^-, as W_{ab}^- and W_{ba}^- were varied for a fixed value of x_d; because of the equal excitation and inhibition received by the Layer 2 neurons, neurons a and b were equally activated as W_{ab}^- and W_{ba}^- were varied and kept equal. In Figure 2.28, W_{ab}^- and W_{ba}^- underwent potentiation when their initial values of were low and x_a and x_b were high, and they underwent depression when their initial values were high and x_a and x_b were low.

Although several factors affected the activation of neurons a and b as input excitation and inhibition were varied, the most important factors determining the sign of plasticity in the lateral inhibitory pathway weights, were the initial inhibitory synaptic weight and the postsynaptic activation level. The rate of change was determined by the presynaptic activation level.

2.4 Discussion

Three generalized Hebbian excitatory synaptic plasticity rules – the BCM (Bear et al., 1987; Bienenstock et al., 1982; Clothiaux et al., 1991), the instar (Grossberg, 1972, 76ab; Kohonen, 1988; Levy & Desmond, 1985; Levy & Burger, 1987; Marshall, 1995a), and the outstar (Grossberg, 1976c; Rescorla & Wagner, 1972) – have been compared. In addition, an outstar inhibitory synaptic plasticity rule (Marshall, 1990a, 1995a; Marshall & Gupta, 1998) has been analyzed.

The important distinctions between the BCM, and the instar and the outstar excitatory synaptic plasticity rules are the following:

1. the BCM rule has only one LTP threshold for all the pathways converging onto a neuron; the instar and the outstar excitatory synaptic plasticity rules have independent LTP thresholds for different pathways onto the same neuron;

2. under the BCM rule, all pathways to the same postsynaptic neuron undergo simultaneous LTD or simultaneous LTP; under the instar and the outstar excitatory synaptic plasticity rules, pathways to the same postsynaptic neuron may undergo LTP or LTD independent of one another; and

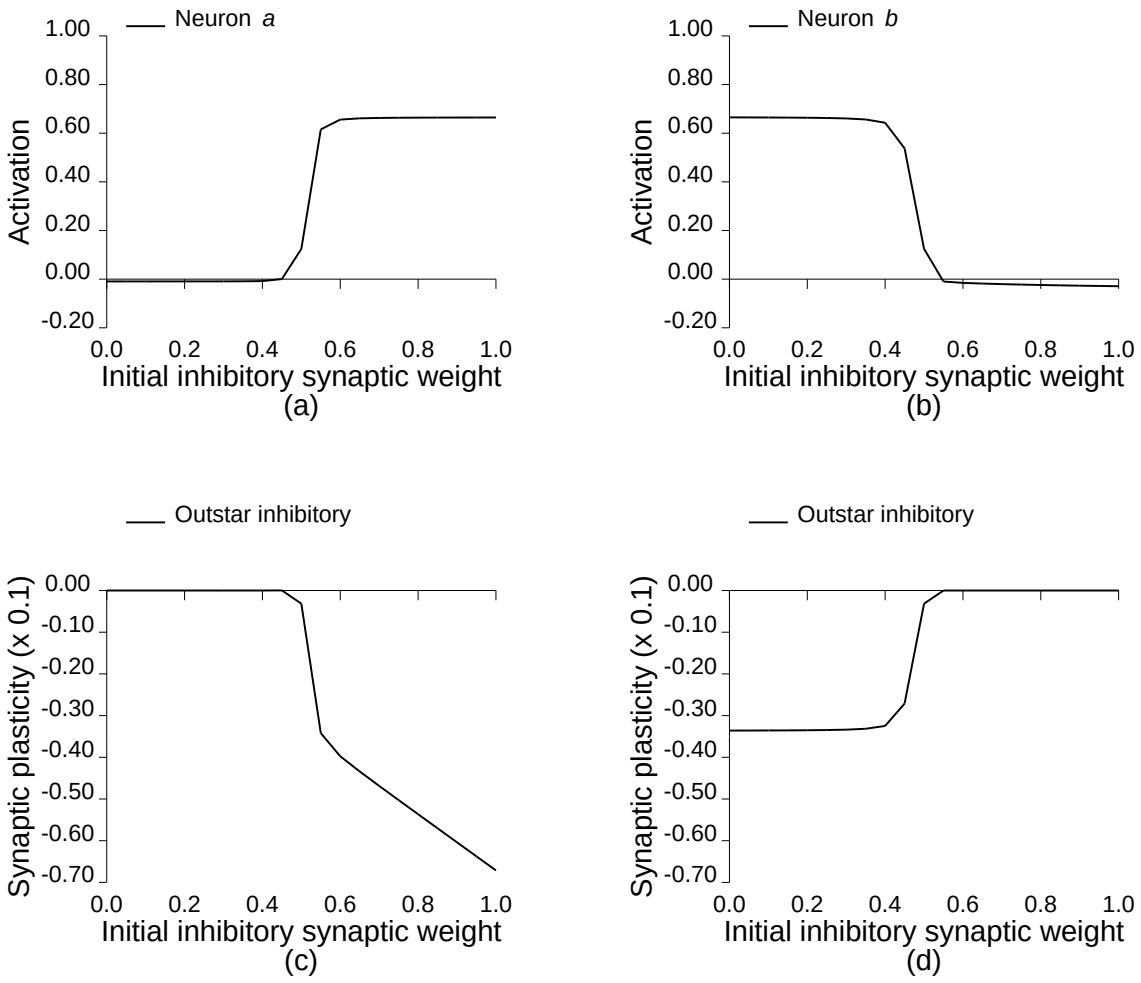

Figure 2.26: **Simulation results: Changes in inhibitory synaptic efficacy under the outstar inhibitory synaptic plasticity rule as a function of initial inhibitory weight.**

The parameters for the outstar inhibitory synaptic plasticity rule and the activation equation were the same as in Figure 2.22. The initial network synaptic weights were the same except that W_{ab}^{-} was varied from 0 to 1, $W_{ba}^{-} = 0.5$, and neuron d was activated at a fixed activation level of 0.5. Panels (a) and (b) show the activation level of neurons a and b, respectively, and panels (c) and (d) show synaptic plasticity in the inhibitory pathways from neuron a to neuron b and from neuron b to neuron a, respectively, as W_{ab}^{-} was varied.

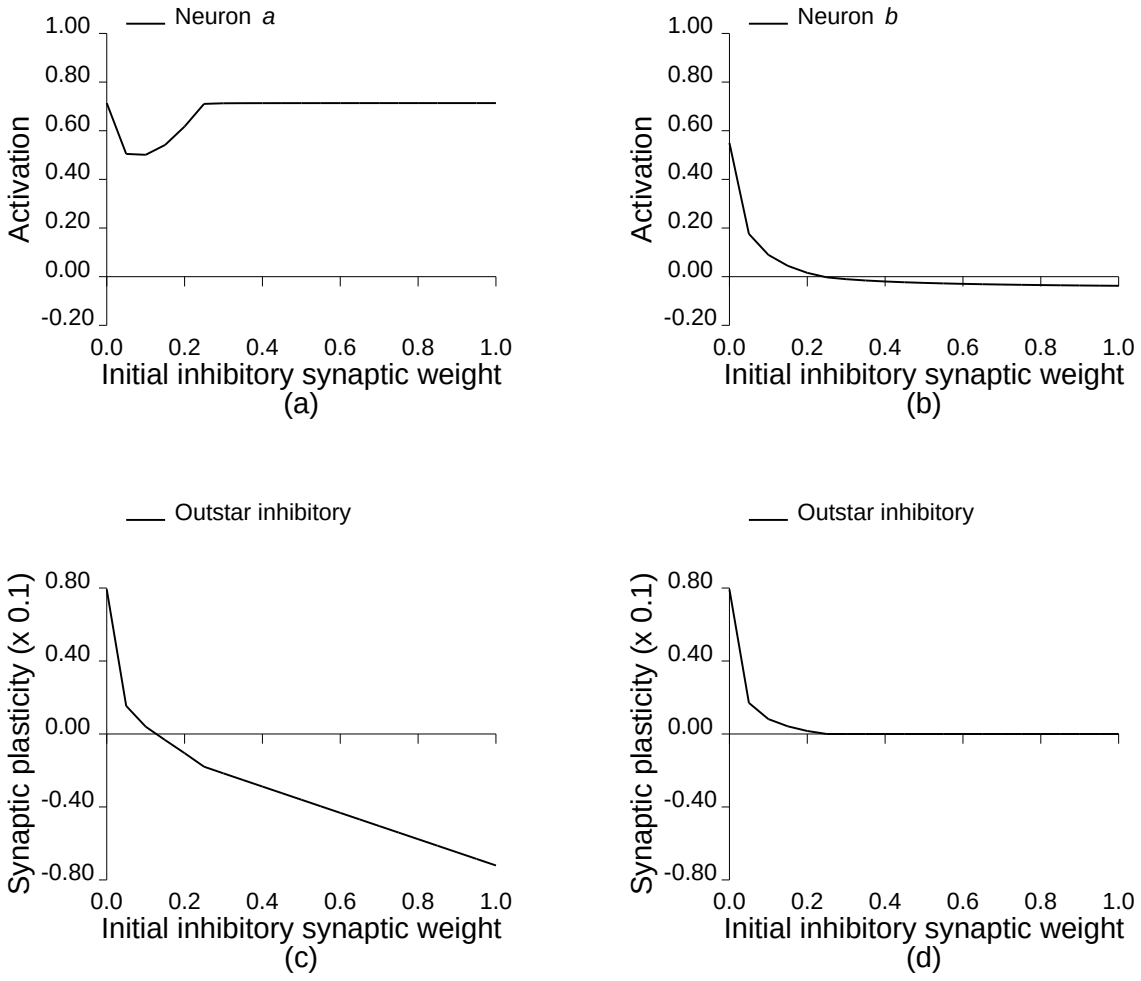

Figure 2.27: **Simulation results: Changes in inhibitory synaptic efficacy under the outstar inhibitory synaptic plasticity rule as reciprocal inhibitory weights were varied.**

The parameters for the outstar inhibitory synaptic plasticity rule and the activation equation were the same as in Figure 2.22. The initial network synaptic weights were the same except that W_{ab}^{-} and W_{ba}^{-} were varied from 0 to 1 and $W_{ab}^{-} = W_{ba}^{-}$, and neuron c was activated at a fixed activation level of 0.5. Panels (a) and (b) show the activation level of neurons a and b, respectively, and panels (c) and (d) show synaptic plasticity in the inhibitory pathways from neuron a to neuron b and from neuron b to neuron a, respectively, as W_{ab}^{-} and W_{ba}^{-} were varied.

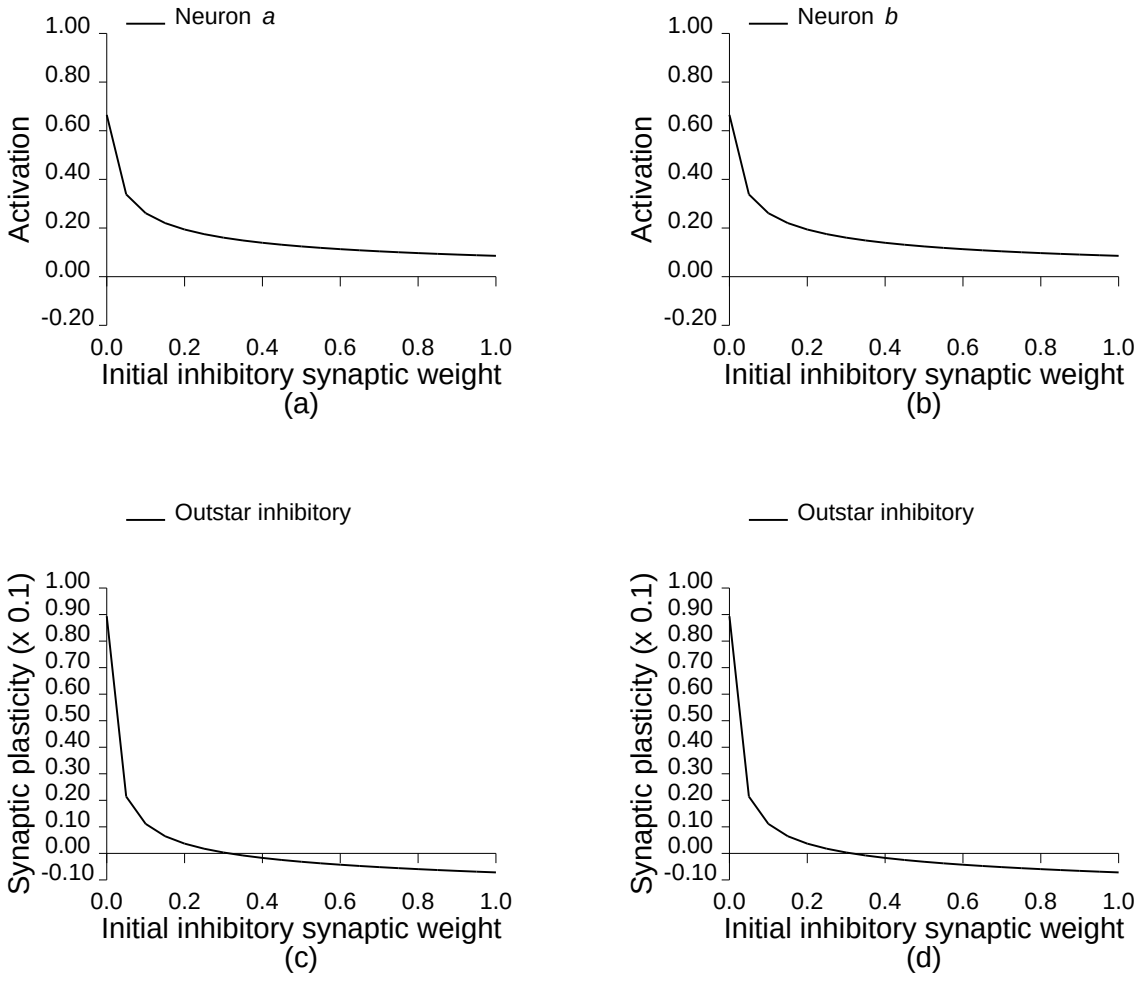

Figure 2.28: **Simulation results: Changes in inhibitory synaptic efficacy under the outstar inhibitory synaptic plasticity rule as reciprocal weights were varied and the neurons received equal input excitations.**
The parameters for the outstar inhibitory synaptic plasticity rule and the activation equation were the same as in Figure 2.22. The initial network synaptic weights were the same except that W_{ab}^{-} and W_{ba}^{-} were varied from 0 to 1 and $W_{ab}^{-} = W_{ba}^{-}$, and neuron d was activated at a fixed activation level of 0.5. Panels (a) and (b) show the activation level of neurons a and b, respectively, and panels (c) and (d) show synaptic plasticity in the inhibitory pathways from neuron a to neuron b and from neuron b to neuron a, respectively, as W_{ab}^{-} and W_{ba}^{-} were varied.

3. the LTP threshold in the BCM rule depends only on the postsynaptic activation history; the LTP thresholds in the instar and the outstar excitatory synaptic plasticity rules are a function of the synaptic efficacy of the pathways and depend on both pre- and postsynaptic activation levels.

The BCM and the outstar excitatory synaptic plasticity rules cannot produce heterosynaptic LTD; according to these rules, unstimulated pathways do not undergo synaptic plasticity. The instar excitatory synaptic plasticity rule, on the other hand, produces heterosynaptic LTD.

The characteristic features of the outstar lateral inhibitory synaptic plasticity rule are:

1. presynaptic activation is necessary to enable synaptic plasticity;
2. the rate of weight change is proportional to presynaptic activation; and
3. the sign of weight change depends on the difference between the initial weight and the postsynaptic activation level.

The three excitatory synaptic plasticity rules are compared with experimental data in Section 2.4.1. The experimental data supporting the three rules are summarized in Table 2.1, and experimental data inconsistent with the three rules are tabulated in Table 2.2. Table 2.3 summarizes the characteristics of the rules, the experimental support for the rules, and the predictions of the rules. The symbol ΓΤ in Table 2.3 indicates the absence of experimental data on some features of the rules. Experimental evidence for the outstar lateral inhibitory synaptic plasticity rule is presented in Section 2.4.2. Finally, plausible functional roles for the rules are discussed in Sections 2.4.3 and 2.4.4.

2.4.1 Experimental evidence for the excitatory synaptic plasticity rules

This section presents experimental data that provide some support for the instar, the outstar, and the BCM excitatory synaptic plasticity rules. The experimental data that have not been be explained by the three excitatory synaptic plasticity rules are also discussed. In many experiments, synaptic plasticity was induced in the conditioned pathway

by stimulating the pathway using pulses at different frequencies. In the simulations, presynaptic stimulation frequency was abstracted as presynaptic activation level; the presynaptic activation level in the model was proportional to the presynaptic stimulation frequency (Brown et al., 1990).

The results of many experiments can be explained by the instar, the outstar, or the BCM excitatory synaptic plasticity rule; these experiments are referred to as ambiguous experiments. Some of the ambiguous experimental results are explained by a combination of the instar and the outstar excitatory synaptic plasticity rules. Novel experiments are suggested to determine the rules underlying synaptic plasticity in the ambiguous experiments.

Experimental evidence for the instar excitatory synaptic plasticity rule

In this section, experimental evidence supporting the properties of the instar excitatory synaptic plasticity rules are presented. Some of these experimental results are inconsistent with the outstar and the BCM excitatory synaptic plasticity rules.

The instar rule requires postsynaptic activation to enable synaptic plasticity (Section 2.3.3, *Synaptic plasticity in excitatory synapses as a function of postsynaptic activation level*). Experimentally, homosynaptic LTD in hippocampal culture (Goda & Stevens, 1996) and in hippocampal slices (Mulkey & Malenka, 1992) was produced when low frequency stimulation of presynaptic sites was paired with postsynaptic depolarization, but was blocked when low stimulation of presynaptic sites was paired with postsynaptic hyperpolarization. In some experiments, it has been observed that pharmacological treatments that increase postsynaptic activation, e.g., pharmacological disinhibition, aid induction of synaptic plasticity (Artola & Singer, 1987; Bear et al., 1992; see subsections *Experimental evidence for the outstar excitatory synaptic plasticity rule* and *Ambiguous experimental results*).

The instar excitatory synaptic plasticity rule produces heterosynaptic depression (Section 2.3.3, *Synaptic plasticity in excitatory synapses as a function of presynaptic stimulation strength*). Furthermore, the instar rule can produce simultaneous LTP and LTD in different pathways. There are several experiments consistent with these properties of the

Plasticity rule	Characteristic properties		Experimental data
Instar excitatory	postsynaptic neuron is inactive	plasticity is disabled	Goda & Stevens (1996); Mulkey & Malenka (1992)
	postsynaptic neuron is active	stimulated pathway may undergo LTP or LTD	Abraham & Goddard (1983); Dudek & Bear (1992); Kirkwood & Bear. (1994); Kirkwood et al. (1993) Lynch et al. (1977)
		unstimulated pathways undergo LTD	Abraham & Goddard (1983); Levy (1985); Levy & Burger (1987); Levy & Desmond (1985); Levy & Steward (1979, 1983); Lynch et al. (1977)
Outstar excitatory	presynaptic neuron is inactive	plasticity is disabled	Andersen et al (1977); Dudek & Bear (1992); Hess & Donoghue (1994); Heynen et al. (1996); Hirsch & Gilbert (1993); Kirkwood & Bear (1994); Kirkwood et al. (1993); Kobayashi et al. (1996); Malinow & Tsien (1990); Sejnowski et al. (1990); Stanton & Sejnowski (1989); Yang et al. (1994); Yang & Faber (1991)
	presynaptic neuron is active	pathway undergoes LTD when postsynaptic neuron is inactive or weakly active	Hess & Donoghue (1994); Malinow & Tsien (1990); Sejnowski et al. (1990); Stanton & Sejnowski (1989); Yang et al. (1994); Yang & Faber (1991)
		pathway undergoes LTP when postsynaptic neuron is strongly active	Hess & Donoghue (1994); Malinow & Tsien (1990); Sejnowski et al. (1990); Stanton & Sejnowski (1989); Wigström & Gustafsson (1983)
BCM excitatory	presynaptic neuron is inactive	plasticity is disabled	Andersen et al (1977); Dudek & Bear (1992); Hess & Donoghue (1994); Heynen et al. (1996); Hirsch & Gilbert (1993); Kirkwood & Bear (1994); Kirkwood et al. (1993); Kobayashi et al. (1996); Malinow & Tsien (1990); Sejnowski et al. (1990); Stanton & Sejnowski (1989); Yang et al. (1994); Yang & Faber (1991)
	presynaptic neuron is active	pathway undergoes no plasticity or weak LTD when postsynaptic neuron is inactive or weakly active	Artola et al. (1990); Goda & Stevens (1996); Mulkey & Malenka (1992);
		pathway undergoes LTD when postsynaptic neuron is moderately active	Artola et al. (1990); Hess & Donoghue (1994); Yang et al. (1994); Yang & Faber (1991)
		pathway undergoes LTP when postsynaptic neuron is strongly active	Artola et al. (1990); Hess & Donoghue (1994); Malinow & Tsien (1990); Sejnowski et al. (1990); Stanton & Sejnowski (1989); Wigström & Gustafsson (1983)

Table 2.1: **Properties of the excitatory synaptic plasticity rules that are consistent with experimental data.**

Plasticity rule	Cannot model	Experimental data
Instar excitatory	absence of synaptic plasticity in unstimulated pathways	Andersen et al (1977); Dudek & Bear (1992); Hess & Donoghue (1994); Heynen et al. (1996); Hirsch & Gilbert (1993); Kirkwood & Bear (1994); Kirkwood et al. (1993); Kobayashi et al. (1996); Malinow & Tsien (1990); Sejnowski et al. (1990); Stanton & Sejnowski (1989); Yang et al. (1994); Yang & Faber (1991)
	LTD and LTP as postsynaptic is varied for a fixed presynaptic stimulation	Artola et al. (1990); Hess & Donoghue (1994); Yang et al. (1994); Yang & Faber (1991)
Outstar excitatory	heterosynaptic LTD	Abraham & Goddard (1983); Levy (1985); Levy & Burger (1987); Levy & Desmond (1985); Levy & Steward (1979, 1983); Lynch et al. (1977)
	absence of synaptic plasticity when postsynaptic neuron is inactive	Artola et al. (1990); Goda & Stevens (1996); Mulkey & Malenka (1992);
BCM excitatory	heterosynaptic LTD	Abraham & Goddard (1983); Levy (1985); Levy & Burger (1987); Levy & Desmond (1985); Levy & Steward (1979, 1983); Lynch et al. (1977)
	homosynaptic LTD when postsynaptic neuron is hyperpolarized or very weakly active	Malinow & Tsien (1990); Sejnowski et al. (1990); Stanton & Sejnowski (1989);

Table 2.2: **Properties of the excitatory synaptic plasticity rules that are inconsistent with experimental data.**

instar rule. Abraham and Goddard (1983) produced heterosynaptic LTD in the perforant pathways to the dendate gyrus of rat hippocampus. They showed that tetanization of either the lateral or the medial components of the perforant pathways to the dendate gyrus produced LTD in the other, regardless of whether LTP was produced in the tetanized pathway. In addition, associative LTP and heterosynaptic depression has been observed in the synapses of the perforant pathways to the dendate gyrus (Levy, 1985; Levy & Desmond, 1985; Levy & Steward, 1979, 1983). Lynch et al. (1977) showed that LTD in unstimulated pathways to a CA1 pyramidal neuron in rat hippocampus can be produced with concomitant LTP in a tetanized pathway to the same neuron; when a previously unstimulated pathway was conditioned using tetanic stimulation it underwent LTP, and the previously tetanized pathway underwent LTD.

According to the instar excitatory synaptic plasticity rule, LTD is produced in an excitatory pathway when presynaptic activation is low, and LTP is produced when the presynaptic activation is high (Section 2.3.3, *Synaptic plasticity in excitatory synapses as a*

	Measurement		Exp'tal Data	Instar Excitatory	Outstar Excitatory	BCM Excitatory
1	synaptic plasticity at zero postsynaptic activation		Yes/No	No	Yes	No
2	Homosynaptic LTP with strong presynaptic stimulation		Yes	Yes	Yes	Yes
3	Homosynaptic LTD with weak presynaptic stimulation		Yes	Yes	Yes	Yes
4	Heterosynaptic LTD along inactive/spontaneously active excitatory pathways		Yes/No	Yes	No	No
5	Synaptic plasticity in unstimulated excitatory pathways even with postsynaptic activation		Yes/No	Yes	No	No
6	LTD more likely with large initial weight		Yes	Yes	Yes	Yes
7	LTP more likely with small initial weight		Yes	Yes	Yes	Yes
8	LTD with presynaptic stimulation and postsynaptic hyperpolarization		Yes/No	No	Yes	No
9	Associative LTP		Yes	Yes	Yes	Yes
10	LTP and LTD in different pathways are independent of each other		Yes	Yes	Yes	No
11	For fixed presynaptic stimulation strength	magnitude of weight change depends on postsynaptic activation	??	Yes	Yes	Yes
		sign of weight change depends on postsynaptic activation level	??	No	Yes	Yes
12	For fixed postsynaptic activation level	magnitude of weight change depends on presynaptic stimulation	??	Yes	Yes	Yes
		sign of weight change depends on presynaptic stimulation strength	??	Yes	No	No
13	Different LTP thresholds for different pathways		??	Yes	Yes	No

Table 2.3: **Comparison of the excitatory synaptic plasticity rules.**

function of presynaptic stimulation strength). This is consistent with experiments showing that stimulated pathways undergo LTD when they are stimulated with low frequency stimuli and undergo LTP with high frequency stimuli (Dudek & Bear, 1992; Kirkwood & Bear, 1994; Kirkwood et al., 1993; see subsections *Experimental evidence for the outstar excitatory synaptic plasticity rule*, *Experimental evidence for the BCM excitatory synaptic plasticity rule*, and *Ambiguous experimental results*).

The instar excitatory synaptic plasticity rule also produces associative LTP (Section 2.3.3, *Associative synaptic plasticity*). Levy and Burger (1987) also used an instar excitatory synaptic plasticity rule to model associative LTP and heterosynaptic depression.

Heterosynaptic LTD (Abraham & Goddard, 1983; Levy, 1985; Levy & Burger, 1987; Levy & Desmond, 1985; Levy & Steward, 1979, 1983; Lynch et al., 1977) cannot be produced by the outstar and the BCM excitatory synaptic plasticity rules because they require presynaptic activation to enable synaptic weight changes (Section 2.3.3, *Synaptic plasticity in excitatory synapses as a function of presynaptic stimulation strength*). The BCM rule is consistent with blockade of LTD in a stimulated pathway when the postsynaptic neuron is hyperpolarized (Goda & Stevens, 1996; Mulkey & Malenka, 1992), but the outstar excitatory rule predicts weakening of the stimulated pathway to a hyperpolarized or weakly active postsynaptic neuron (Figures 2.8d and 2.12d).

Experimental evidence for the outstar excitatory synaptic plasticity rule

The defining characteristics of the outstar excitatory synaptic plasticity rule are (1) the plasticity is enabled by presynaptic stimulation, and (2) the pathway synaptic weight moves closer to a direct function of the postsynaptic activation.

In several experiments, the postsynaptic activation was varied for a fixed presynaptic stimulation, and synaptic plasticity in stimulated and unstimulated pathways was measured. LTD was produced in pathways to CA1 pyramidal neurons in hippocampal slices by stimulating presynaptic terminals while the postsynaptic neuron was hyperpolarized, and LTP was produced in pathways to CA1 neurons by stimulating presynaptic terminals while the postsynaptic neuron was depolarized (Malinow & Tsien, 1990; Sejnowski et al., 1990; Stanton & Sejnowski, 1989). Control excitatory

pathways to the postsynaptic neurons, which were unstimulated during induction of LTP or LTD in the stimulated pathways, did not undergo synaptic plasticity (Malinow & Tsien, 1990; Sejnowski et al., 1990; Stanton & Sejnowski, 1989). No long-term synaptic plasticity was observed in pathways to CA1 neurons after the neuron was depolarized or hyperpolarized, and low-frequency stimulation of pathways to CA1 neurons alone did not produce long-term synaptic plasticity (Malinow & Tsien, 1990; Sejnowski et al., 1990; Stanton & Sejnowski, 1989). These results are consistent with the outstar excitatory rule because the rule produces plasticity only in stimulated pathways, and the rule weakens stimulated pathways to inactive neurons and strengthens stimulated pathways to strongly active neurons (Section 2.3.3, *Synaptic plasticity in excitatory synapses as a function of postsynaptic activation level*). The instar excitatory and the BCM synaptic plasticity rules are inconsistent with the above results because they block synaptic plasticity or produce very little synaptic plasticity in pathways to inactive or very weakly active postsynaptic neurons (Section 2.3.3, *Synaptic plasticity in excitatory synapses as a function of postsynaptic activation level*). Furthermore, the instar excitatory synaptic plasticity rule weakens all unstimulated or weakly stimulated pathways to a highly active neuron (Section 2.3.3, *Synaptic plasticity in excitatory synapses as a function of postsynaptic activation level*), inconsistent with the observation of Malinow and Tsien (1990), Sejnowski et al. (1990), and Stanton and Sejnowski (1989) that unstimulated pathways depolarized or hyperpolarized neurons did not undergo synaptic plasticity.

According to the outstar excitatory synaptic plasticity rule, LTP is more likely to occur in a stimulated pathway to a highly active postsynaptic neuron than in a stimulated pathway to a weakly active or inactive postsynaptic neuron (Section 2.3.3, *Synaptic plasticity in excitatory synapses as a function of postsynaptic activation level*); thus, the rule exhibits a LTP intensity threshold. In some experiments, increasing the stimulation intensity increased the postsynaptic activation and increased the effectiveness of the tetanic stimulation in inducing LTP (Brown et al., 1990).

In some experiments, the postsynaptic activation was varied by pharmacological means, simultaneous stimulation of several excitatory pathways to the postsynaptic neuron, or stimulation of inhibitory pathways to the postsynaptic neuron. When

postsynaptic activation of layer 2/3 neurons in rat motor cortex was increased by pharmacological disinhibition or by simultaneous tetanization of two layer 2/3 horizontal pathways terminating on a neuron, the stimulated pathways were strengthened (Hess & Donoghue, 1994). In three out of eight cases the LTP was specific to the tetanized pathway, and in the remaining cases a small strengthening of the untetanized layer 2/3 horizontal pathways was observed. The LTP in the untetanized layer 2/3 horizontal pathways may occur because the pathways were not completely independent (Hess & Donoghue, 1994). A weak depression was produced in the tetanized pathway without the pharmacological disinhibition when the postsynaptic activation level was low. Thus, the same presynaptic tetanization caused LTP when the postsynaptic activation level was raised by pharmacological disinhibition and caused LTD when the postsynaptic activation was low in the absence of pharmacological disinhibition, just as predicted by the outstar excitatory synaptic plasticity rule (Section 2.3.3, *Synaptic plasticity in excitatory synapses as a function of postsynaptic activation level*).

Yang et al. (1994) produced LTD in Schaffer collaterals to rat hippocampal CA1 neurons by weak presynaptic stimulation and inhibition of the postsynaptic neuron by repeated brief exposure to the inhibitory transmitter GABA or GABA receptor agonists. Yang et al. (1994) suggested that the LTD could be caused by weakening of the pre- and postsynaptic activation by GABA infusion. But presynaptic stimulation with the $GABA_A$ receptor agonist muscimol also produced LTD in the stimulated pathway, and muscimol affected only the postsynaptic activation (Reiter & Stryker, 1988). Hippocampal LTP was easily obtained by presynaptic stimulation in slices disinhibited by GABA blockers (Wigström & Gustafsson, 1983). This suggests that it may the postsynaptic activation level that determines whether the stimulated pathway undergoes LTP or LTD. The LTD was reversed by strong presynaptic stimulation (Yang et al., 1994).

Yang and Faber (1991) reported that LTD is induced at mixed synapses between eighth nerve fibers and the goldfish Mauther (M) neuron *in vivo*, by pairing weak presynaptic stimuli with postsynaptic inhibition. The weak stimulation alone produced LTP. Postsynaptic inhibition was applied by stimulating inhibitory interneurons that synapse on M neuron dendrites and soma. The LTP and LTD was specific to the stimulated

pathway and depended on the postsynaptic activation level.

The results of Hess and Donoghue (1994), Wigström and Gustafsson (1983), Yang and Faber (1991), and Yang et al. (1994) cannot be modeled by the instar excitatory synaptic plasticity rule because the rule cannot produce LTP and LTD in the conditioned pathway with fixed stimulation as the postsynaptic activation alone is varied (Section 2.3.3, *Synaptic plasticity in excitatory synapses as a function of postsynaptic activation level*).

Yang and Faber (1991) also found that LTD was more easily produced in a pathway whose synaptic efficacy was previously raised than in a naive pathway. Section 2.3.3, *Synaptic plasticity in excitatory synapses as a function of initial synaptic weight*, shows that the outstar excitatory synaptic rule produces LTD when the initial synaptic weight is very high.

As discussed in Section 2.3.3, the outstar excitatory synaptic plasticity rule produces conditioned pathway-specific LTD and LTP as a function of presynaptic stimulation strength. The synaptic plasticity in Schaffer collateral pathway to CA1 pyramidal neurons in adult rat hippocampus goes from LTD to LTP as the stimulation frequency is increased, and the synaptic plasticity is specific to the tetanized pathway (Dudek & Bear, 1992). Conditioned pathway-specific presynaptic stimulation frequency dependent LTD and LTP have also been observed in pathways from layer 4 or white matter to layer 3 neurons in the primary visual cortex of adult rats and kittens *in vitro* (Kirkwood & Bear, 1994; Kirkwood et al., 1993), in Schaffer collaterals to hippocampal CA1 pyramidal neurons in adult rats *in vivo* (Heynen et al., 1996), and in hippocampal mossy fiber CA3 synapses (Kobayashi et al., 1996). Andersen et al. (1977) observed tetanized pathway specific LTP in pathways to CA1 neurons in guinea pig hippocampal slices. Horizontal excitatory pathways in layer 3 of cat primary visual cortex could be strengthened by pairing presynaptic stimulation and postsynaptic depolarization, and the LTP produced was conditioned pathway specific (Hirsch & Gilbert, 1993).

Section 2.3.3, *Associative synaptic plasticity*, shows that the outstar rule can produce associative LTP (Levy & Steward, 1979; Barrionuevo & Brown, 1983; Kelso & Brown, 1986). Associative LTP was produced in a test excitatory pathway to hippocampal CA1 pyramidal neurons when the test pathway was stimulated with low-frequency

stimulation in phase with high-frequency stimulation of an independent excitatory pathway to the same postsynaptic neuron (Sejnowski et al., 1990; Stanton & Sejnowski, 1989). High-frequency stimulation of the other excitatory pathway alone induced LTP in it, and no synaptic plasticity was observed in the unstimulated test pathway (Sejnowski et al., 1990; Stanton & Sejnowski, 1989). When the test pathway stimulation was out of phase with the high-frequency stimulation of the other excitatory pathway, the test pathway was weakened (Sejnowski et al., 1990; Stanton & Sejnowski, 1989). When the low-frequency stimulation in the test pathway was in phase with the high-frequency stimulation in another pathway to the same neuron, the postsynaptic neuron was highly depolarized when presynaptic terminals in the test pathway were activated. However, when the test stimulation was out of phase with the high-frequency stimulation, the postsynaptic neuron was hyperpolarized when presynaptic terminals in the test pathway were activated (Sejnowski et al., 1990; Stanton & Sejnowski, 1989). The outstar rule can produce LTD in a test pathway when the stimulation of the test pathway is out of phase with stimulation in an independent pathway to a common postsynaptic neuron because presynaptic activity in the test pathway is correlated with postsynaptic hyperpolarization.

Experimental evidence for the BCM excitatory synaptic plasticity rule

The BCM excitatory synaptic plasticity rule states that presynaptic stimulation of excitatory pathways to a postsynaptic neuron activated above a LTP threshold potentiates the pathways, and presynaptic stimulation of excitatory pathways to a postsynaptic neuron activated below the threshold depresses the pathways. Thus, the BCM rule exhibits a LTP intensity threshold; increasing the stimulation intensity increases the effectiveness of the tetanic stimulation to induce LTP (Brown et al., 1990). According to the BCM rule, the LTP threshold is a function of the activation history of the postsynaptic neuron. In addition, the rule does not produce synaptic plasticity if either presynaptic or postsynaptic activation is absent.

The following experimental results are consistent with the role of postsynaptic activation in producing synaptic plasticity according to the BCM rule.

Section 2.3.1 shows that the BCM rule produces LTD at low presynaptic

stimulation strength and LTP at high stimulation strength as shown experimentally by Dudek & Bear (1992). In addition, the BCM rule produces stimulated pathway-specific LTP and LTD consistent with several experiments (Dudek & Bear, 1992; Heynen et al., 1996; Kirkwood & Bear, 1994; Kirkwood et al., 1993; Kobayashi et al., 1996). The stimulated pathway specificity of the BCM rule is also consistent with stimulated pathway-specific LTP in reported by Andersen et al. (1977) and Hirsch and Gilbert (1993).

According to the BCM rule, as postsynaptic activation level is raised, the chances of inducing LTP with the same presynaptic stimulation protocol increases. This is consistent with experiments in which LTP was produced when the activation level was raised by pharmacological disinhibition (Hess & Donoghue, 1994; Wigström & Gustafsson, 1983) and LTD was produced in the absence of any pharmacological disinhibition (Hess & Donoghue, 1994) or in the presence of strong inhibition (Yang et al., 1994; Yang & Faber, 1991).

When the postsynaptic activation level was varied, a pathway that is stimulated by the same stimulation protocol did not undergo any significant change in pathway weight when the postsynaptic activation level was very small; the pathway underwent significant depression as the postsynaptic activation level was raised, and the pathway underwent significant potentiation when the activation level was raised very high (Artola et al., 1990). This behavior can be modeled by the BCM rule (Figure 2.14e).

Prior strong postsynaptic activation raises the LTP threshold in the BCM rule (Section 2.2.2, *The BCM excitatory synaptic plasticity rule*). Thus, a presynaptic stimulation that induces little LTP induces LTD when the presynaptic stimulation is preceded by strong postsynaptic activation because of strong presynaptic stimulation in another independent pathway. Yang and Faber (1991) reported such a phenomenon.

Section 2.3.3, *Associative synaptic plasticity*, shows that the BCM rule produces associative LTP (Levy & Steward, 1979; Barrionuevo & Brown, 1983; Kelso & Brown, 1986). The BCM rule is also consistent with associative plasticity based on correlation between stimulation applied to two pathways (Sejnowski et al., 1990; Stanton & Sejnowski, 1989). When low-frequency stimulation of a test pathway is in phase with high-frequency stimulation in another pathway to the same neuron, the postsynaptic neuron is highly

active (Sejnowski et al., 1990; Stanton & Sejnowski, 1989); according to the BCM rule if the high postsynaptic activation level is greater than the LTP threshold, LTP is induced in all stimulated pathways. When low-frequency stimulation in the test pathway is out of phase with high frequency stimulation in the other pathway, the postsynaptic neuron is hyperpolarized when the presynaptic terminals in the test pathway are activated (Sejnowski et al., 1990; Stanton & Sejnowski, 1989). Thus, according to the BCM rule, plasticity in the test pathway cannot occur because the postsynaptic neuron is inactive. But if the postsynaptic neurons were only very weakly activated when the presynaptic terminals in the test pathway are activated, the BCM rule induces weak LTD in the test pathway (Equations 2.4 and 2.5).The high-frequency stimulation of the other pathway alone can induce LTP in the stimulated pathway because the strong presynaptic stimulation can raise the postsynaptic activation above the LTP threshold, and the pathway weights of unstimulated pathways do not change. When the low-frequency stimulation is applied to the test pathway, the test pathway may undergo a small depression if the postsynaptic activation level is below the LTP threshold.

Ambiguous experimental results

In this section, experimental results that can be modeled by any one of the three rules are considered. Some experimental results that can be modeled by a combination of the instar and the outstar excitatory synaptic plasticity rules are also discussed.

In some experiments the stimulated pathway and the unstimulated control pathways are of different types, e.g., intracortical horizontal excitatory pathways and pathways from white matter to primary visual cortical layers. Pathways from white matter to primary visual cortical layers may include feedforward geniculocortical pathways and corticocortical feedback pathways (Felleman & Van Essen, 1991; Maunsell & Van Essen, 1983). It is hypothesized that synaptic plasticity in feedforward, feedback, and intracortical horizontal excitatory pathways may be governed by different synaptic plasticity rules. The assumption that the instar excitatory synaptic plasticity rule governs synaptic plasticity in feedforward pathways and the outstar excitatory synaptic plasticity rule governs synaptic plasticity in lateral and feedback pathways models many experimental

results. Some novel experiments are suggested to test the hypothesis.

Cortical plasticity based on temporal covariance in pre- and postsynaptic activation. Frégnac et al. (1988) obtained ocular dominance (OD) shifts and changes in orientation selectivity in neurons in the primary visual cortex of kittens and cats. They used iontophoresis to increase the visual response to a given stimulus and to decrease or block the neural response to a second stimulus which differed in ocularity or orientation. The neural selectivity shifted toward the stimulus paired with reinforced the visual response.

The observations of Frégnac et al. (1988) can be modeled by any of the three rules. According to the instar excitatory synaptic plasticity rule, increase in response to the stimulus that was paired with postsynaptic depolarization occurred because the pairing strengthens the stimulated excitatory pathways to the neuron and weakens the unstimulated/weakly active excitatory pathways to the neuron. Pairing the second stimulus with postsynaptic hyperpolarization does not change the synaptic weight of the excitatory pathways to the neuron because the postsynaptic activation was suppressed. Thus, according to the instar rule the excitatory pathways that were strongly activated by the second stimulus but not by the first stimulus are weakened, and the neuron loses responsiveness to the second stimulus. The excitatory pathways that were strongly activated by the first stimulus are strengthened, and the neuron becomes more responsive to the first stimulus.

In the case of the outstar excitatory synaptic plasticity rule, inactive presynaptic pathway weights do not change. The pathways activated by the first stimulus, which are paired with postsynaptic depolarization, are strengthened because of high postsynaptic activation level, and the pathways activated by the second stimulus, which are paired with postsynaptic hyperpolarization, are weakened because of low postsynaptic activation level. Thus, the postsynaptic neuron strengthens excitatory pathways that are strongly activated by the first stimulus and weakens excitatory pathways that are strongly activated by the second stimulus, and therefore, the neurons become more responsive to the first stimulus and become less responsive to the second stimulus.

In the case of the BCM excitatory synaptic plasticity rule, inactive presynaptic pathway weights do not change. The pathways activated by the first stimulus, which are

paired with postsynaptic depolarization, are strengthened because the high postsynaptic activation is greater than the LTP threshold. The pathways activated by the second stimulus, which are paired with postsynaptic hyperpolarization, are weakened because the low postsynaptic activation is less than the LTP threshold. Thus, the postsynaptic neuron strengthens excitatory pathways that are strongly activated by the first stimulus and weakens excitatory pathways that are strongly by the second stimulus. Therefore, the neurons become more responsive to the first stimulus and lose responsiveness to the second stimulus.

Synaptic plasticity based on temporal covariance in pre- and postsynaptic activation. Debanne et al. (1997) produced bidirectional associative plasticity in CA3 to CA1 pathways in rat hippocampus *in vitro*. To obtain LTP, presynaptic stimulation was repeatedly paired with synchronous postsynaptic depolarizing pulses. To induce LTD, asynchronous pairing of postsynaptic depolarization with a single delayed presynaptic stimulus was repeated. As shown in Section 2.3.3, the three rules can produce LTP during synchronous pairing, when the presynaptic and postsynaptic activations are strong. During asynchronous pairing, the instar rule can weaken the pathway when the postsynaptic neuron is activated by the depolarizing pulses and there is no presynaptic stimulation. The single delayed presynaptic pulse may not be strong enough to overcome the LTD produced during the preceding strong postsynaptic depolarization; during asynchronous pairing, the delayed single pulse stimulation of the presynaptic pathway after strong postsynaptic depolarization may only very weakly activate the postsynaptic neuron (Sejnowski et al., 1990; Stanton & Sejnowski, 1989). According to the outstar and the BCM excitatory synaptic plasticity rules, very weak postsynaptic activation paired with weak presynaptic stimulation weakens the pathway, and strong postsynaptic depolarization without any presynaptic stimulation of the excitatory pathways to the neuron does not change the pathway synaptic weight. Thus, asynchronous pairing weakens excitatory pathways according to the outstar and the BCM excitatory synaptic plasticity rules. Debanne et al. (1997) did not ascertain whether the LTP/LTD was specific to the stimulated pathway, and thus the results are consistent with all the three rules. As discussed in the preceding subsections, the instar rule can produce depression in unconditioned pathways, but the outstar and the BCM rules produce

plasticity only in conditioned pathways.

Bear et al. (1992) induced LTP in pathways from the white matter–layer 6 border to layer 3 neurons in kitten primary visual cortex *in vitro* by high-frequency stimulation of the pathway and local pharmacological disinhibition. As shown in Section 2.3.3, *Synaptic plasticity in excitatory synapses as a function of postsynaptic activation level*, all the three rules can produce larger LTP as the postsynaptic activation level is raised. Bear et al. (1992) did not verify the specificity of synaptic plasticity or the dependence of synaptic plasticity on postsynaptic activation level, and therefore, the evidence is insufficient to discard any of the three rules.

Synaptic plasticity in feedforward, feedback, and lateral excitatory pathways. Synaptic plasticity in pathways from white matter–layer 6 border to neurons in layers 2–4 in the primary visual cortex and in intracortical horizontal excitatory pathways in layers 2/3 of cats and guinea pigs (Frégnac et al., 1994) were studied (Frégnac et al., 1994) by varying the postsynaptic activation level and the temporal covariance of pre- and postsynaptic activity. In the following paragraphs, it is argued that the various details of synaptic plasticity in pathways to primary visual cortex neurons can be modeled by a combination of the instar and the outstar rules for excitatory synaptic plasticity, or by the BCM excitatory synaptic plasticity rule.

Frégnac et al. (1994) used intracellular techniques to vary postsynaptic activation level independent of activation of presynaptic elements. They found that pairing white matter stimulation with postsynaptic hyperpolarizing current injections weakened the pathway, and pairing white matter stimulation with postsynaptic depolarizing current injections strengthened the pathway. The potentiation and depression of the pathway synaptic weight was reversible. Successive pairing of white matter stimulation and postsynaptic depolarizing current pulses resulted in a significant but decreasing amount of potentiation.

In Section 2.3.3, *Synaptic plasticity in excitatory synapses as a function of postsynaptic activation level*, it was shown that plasticity under the instar rule is disabled when the postsynaptic neuron is inactive, and that weight changes under the instar rule in pathways to a weakly active postsynaptic neuron are small. On the other hand, the

outstar rule weakens stimulated excitatory pathways to inactive or very weakly active neurons. Based on the assumptions that synaptic plasticity in geniculocortical feedforward pathways is governed by the instar excitatory synaptic plasticity rule and that synaptic plasticity in corticocortical feedback pathways is governed by the outstar excitatory synaptic plasticity rule, the effective/combined weight of feedforward geniculocortical and feedback corticocortical pathways from white matter to layers 2–4 neurons can weaken when white matter stimulation is paired with hyperpolarizing current injections to the postsynaptic neuron. The BCM rule can weaken the stimulated white matter pathways because the hyperpolarizing current pulses can decrease the activation level of the postsynaptic neuron below the LTP threshold while the pathway is stimulated.

In Section 2.3.3, *Synaptic plasticity in excitatory synapses as a function of postsynaptic activation level*, it was shown that stimulation of an excitatory pathway to strongly active postsynaptic neurons can be strengthened under the outstar excitatory synaptic plasticity rule, if the initial synaptic weight of the pathway is less than a function of postsynaptic activation. Thus, when presynaptic stimulation is paired with postsynaptic depolarizing current injections, it is possible that the feedback corticocortical pathways to layers 2–4 neurons are strengthened according to the outstar rule. The feedforward geniculocortical pathways, which are assumed to undergo synaptic plasticity according to the instar excitatory synaptic plasticity rule, are strengthened if the initial weight of the geniculocortical pathway is less than a function of the presynaptic stimulation strength, and weakened otherwise. As the postsynaptic activation level is increased the magnitude of synaptic change increases, but the sign of synaptic weight change remains the same. If white matter stimulation activates both geniculocortical and corticocortical pathways, the effective weight of the pathways from white matter to layers 2–4 neurons is increased when both geniculocortical and corticocortical pathways are strengthened, or when the potentiation in the corticocortical pathways dominates the possible depression in the geniculocortical pathways or vice-versa. The BCM rule can strengthen the stimulated white matter pathways because the depolarizing current pulses can increase the activation level of the postsynaptic neuron above the LTP threshold, while the pathway is stimulated.

When white matter stimulation was paired with postsynaptic hyperpolarizing

current injections, the amount of decrease in the pathway weight was greater when the initial effective weight of the pathway was larger. When white matter stimulation was paired with postsynaptic depolarizing current injections, the amount of increase in the pathway weight was greater when the initial effective weight of the pathway was smaller (Frégnac et al., 1994). This result is consistent with the combination of instar and outstar rules and with the BCM rule. In Figures 2.10 and 2.11, it was shown that a presynaptic stimulation applied for sufficiently long duration, when postsynaptic activation level is below the LTP threshold, can cause the pathway weight to decrease to an equilibrium value under the outstar and the BCM rules, and that the rate of change in the pathway weight decreases as the pathway weight approaches the equilibrium value. When the postsynaptic activation level is very low, synaptic plasticity according to the instar rule is very small; thus, changes in effective weight of the white matter pathway will be dominated by changes under the outstar rule. Also, when the same presynaptic stimulation is applied for a sufficiently long duration and postsynaptic activation is above the LTP threshold, the pathway weight increases to an equilibrium value under the outstar or the BCM rules, and the rate of change in the pathway weight can decrease as the pathway weight approaches the equilibrium value (Figures 2.10 and 2.11). With a high postsynaptic activation, the sign of the synaptic changes under the instar rule depends on whether the initial weight was greater or smaller than a function of the presynaptic activation, and the rate of synaptic weight change decreases as the pathway weight approaches the equilibrium value (Figure 2.10).

In order to verify the assumptions that feedforward pathway plasticity is governed by the instar excitatory synaptic plasticity rule and that feedback and lateral excitatory pathway plasticities are governed by the outstar excitatory synaptic plasticity rule, the following experiments are suggested.

1. Depolarize a neuron in layers 2–4 above its spiking threshold without any presynaptic stimulation. The predictions based on the assumption are that the feedforward geniculocortical pathways to the active postsynaptic neuron weaken, under the instar rule, and that the feedback corticocortical pathways and the intracortical horizontal pathways to the active postsynaptic neuron do not undergo synaptic plasticity, under the outstar rule. Thus, the effective weight of pathways from white matter should

weaken, and the weight of intracortical horizontal excitatory pathways do not change.

2. When white matter stimulation at a site is paired with postsynaptic depolarizing current injections, the independent pathway from another white matter site to the postsynaptic neuron weakens. The instar excitatory synaptic plasticity rule weakens unstimulated feedforward geniculocortical pathways to active postsynaptic neurons, and the outstar excitatory synaptic plasticity rule does not modify unstimulated feedback corticocortical pathways to active postsynaptic neurons.

3. When white matter stimulation at a site is paired with strong postsynaptic hyperpolarizing current injections, the independent pathway from another white matter site to the postsynaptic neuron may not undergo synaptic plasticity; the instar excitatory synaptic plasticity rule does not modify the synaptic weight of feedforward geniculocortical pathways to inactive postsynaptic neurons, and the outstar excitatory synaptic plasticity rule does not modify unstimulated feedback corticocortical pathways.

In all the above cases, according to the BCM rule, the weight of unstimulated pathways to postsynaptic neuron at any level of activation will not change.

Synaptic plasticity produced by a dual stimulating electrode protocol. Frégnac et al. (1994) used a dual stimulating electrode protocol in which presynaptic stimulation of one pathway (white matter or intracortical horizontal) was paired with postsynaptic depolarizing or hyperpolarizing current pulses; this pathway is termed the paired pathway. Another pathway (the unpaired pathway) was stimulated in the absence of postsynaptic current injection in an alternating fashion. When the white matter pathway to neurons in layers 2–4 was the paired pathway, an intracortical horizontal pathway served as the unpaired pathway, and vice-versa. The same total number of stimuli was delivered to both pathways, and interstimulus intervals between the activation of the paired and the unpaired pathway were varied depending on the neuron.

In 41% (13 of 32) of the cases, pairing presynaptic stimulation with synchronous postsynaptic hyperpolarizing pulses resulted in significant weakening of the paired pathway efficacy. In 36% (8 of 22) of the cases, pairing presynaptic stimulation with synchronous

postsynaptic depolarizing pulses resulted in significant strengthening of the paired pathway. These statistics include both the white matter and the intracortical horizontal excitatory pathways to neurons in layers 2–4. In 68% (17 of 25) of the cases using the dual stimulation electrode protocol, the unpaired pathway weight was unaffected. In 32% (8 of 25) remaining cases, when the unpaired pathway was affected, the change in the unpaired pathway weight was opposite to that produced in the paired pathway.

As mentioned before, it was assumed that plasticity in feedforward geniculocortical pathways from white matter to neurons in layers 2–4 is governed by the instar excitatory rule and that plasticity in feedback corticocortical pathways from white matter to neurons in layers 2–4 and intracortical horizontal excitatory pathways to neurons in layers 2–4 is governed by the outstar excitatory rule. With this assumption, it is shown below that the model produces depression in the paired pathway when presynaptic stimulation is paired with synchronous postsynaptic hyperpolarizing pulses and produces potentiation in the paired pathway when presynaptic stimulation is paired with synchronous postsynaptic depolarizing pulses. The cases under which the unpaired pathway can be affected are discussed.

When white matter stimulation is paired with postsynaptic depolarizing current pulses, the instar and the outstar rules can strengthen the effective weight of the pathways from white matter; the initial weight can be less than a function of the presynaptic weight (for LTP under the instar rule) and less than a function of the postsynaptic weight (for LTP under the outstar rule). The unpaired intracortical horizontal excitatory pathway weight may not change if the postsynaptic activation remains the same as during the prior control stimulations. Any change in postsynaptic activation caused by test stimulation after the conditioning stimulation can affect the equilibrium weight of the intracortical horizontal excitatory pathway, under the outstar rule. If the interstimulus interval between the stimulation of the paired and the unpaired pathways is small, it is possible that because of the pairing protocol the neuron is in an adapted or fatigued state, and thus, stimulation of the unpaired pathway can evoke a smaller postsynaptic activation. This would cause a small depression of the unpaired intracortical pathway under the outstar rule. This hypothesis can be tested by stimulating the unpaired pathway with a stronger presynaptic stimulation

or by varying the interstimulus interval between the stimulation of the paired and unpaired pathway. The prediction of the outstar rule is that the stronger presynaptic stimulation will evoke a larger postsynaptic activation and therefore would strengthen the unpaired intracortical pathway. When the interstimulus interval between the paired pathway (white matter pathway) and the unpaired pathway (intracortical pathway) is increased, the amount of depression in the unpaired pathway would decrease. Assuming that the depression was caused by neuronal adaptation/fatigue, the postsynaptic neuron would recover from adaptation in the absence of postsynaptic activation (Movshon et al., 1978).

When intracortical horizontal excitatory pathway stimulation is paired with postsynaptic depolarizing current pulses, the outstar excitatory rule can strengthen the paired pathway. During stimulation of the intracortical horizontal excitatory pathway and synchronous postsynaptic depolarizing current injections, the postsynaptic neuron is strongly active, and therefore, under the instar excitatory synaptic plasticity rule, the feedforward geniculocortical pathways to the active neurons weaken. When the unpaired white matter pathway is stimulated during testing, the feedback corticocortical pathways may remain unchanged or weaken according to the outstar rule (similar to the situation when an intracortical horizontal pathway was the unpaired pathway). Thus, the effective weight of white matter pathways may decrease.

When the white matter pathways or intracortical horizontal excitatory pathways to neurons in layers 2–4 are paired with synchronous postsynaptic hyperpolarizing current pulses, the paired pathway is weakened (Frégnac et al., 1994). Interestingly, in some cases the unpaired pathway in the dual stimulating electrode protocol was potentiated. During pairing of presynaptic stimulation and postsynaptic hyperpolarizing current injections, the postsynaptic activation level is very small. Therefore, the synaptic weight changes in the feedforward geniculocortical pathways under the instar rule are very small. It is possible that because of the low activation during the pairing phase, the adaptation/fatigue level of the postsynaptic neuron decreases. Consequently, the postsynaptic neuron response to stimulation of the unpaired pathway during testing could be higher than during the prior control conditions. The higher activation in response to presynaptic stimulation of the unpaired pathway during testing can strengthen the unpaired pathway under the outstar

rule. It is also possible that during pairing of presynaptic stimulation with postsynaptic hyperpolarizing current injections, lateral inhibitory pathways to the postsynaptic neuron from other cortical neurons are weakened (see Section 2.2.2, *The outstar lateral inhibitory synaptic plasticity rule*), thereby leading to an apparent strengthening of the unpaired pathway.

The effects of the dual stimulating electrode protocol can be also explained by the BCM rule. When the paired pathway is stimulated with postsynaptic depolarizing current injections, the postsynaptic activation level is raised above the LTP threshold, and therefore under the BCM rule the paired pathway is potentiated. The strong postsynaptic activation during the pairing procedure also raises the LTP threshold. When the unpaired pathway is stimulated during testing, the postsynaptic activation level can be less than the raised LTP threshold, and hence the unpaired pathway can be depressed. When the paired pathway is stimulated with postsynaptic hyperpolarizing current injections, the postsynaptic activation level is below the LTP threshold, and therefore, under the BCM rule, the paired pathway is depressed. The weak postsynaptic activation during pairing procedure decreases the LTP threshold. When the unpaired pathway is stimulated during testing, the postsynaptic activation level can be greater than the lowered LTP threshold, and hence, the unpaired pathway can be potentiated. If the LTP threshold does not change much during the pairing procedures, the synaptic weight of the unpaired pathway may not change at all.

Postsynaptic voltage dependence of LTP and LTD. In Section 2.4.1, *Experimental evidence for the BCM excitatory synaptic plasticity rule*, it was shown that the BCM excitatory synaptic plasticity rule can explain the presence of different voltage-dependent thresholds for inducing LTP and LTD in visual cortical slices (Artola et al., 1990). For a fixed presynaptic stimulation strength, the stimulated pathway undergoes no synaptic plasticity or very small LTD when the postsynaptic neuron is hyperpolarized or is inactive; as the postsynaptic activation level increases, the stimulated pathway undergoes significant LTD; and when the postsynaptic activation level increases further, the stimulated pathway undergoes LTP.

The results of Artola et al. (1990) can be modeled by a combination of the instar and the outstar excitatory synaptic plasticity rules. Artola et al. (1990) stimulated a site

in the white matter–layer 6 border, through which feedforward geniculocortical pathways (whose synaptic plasticity is assumed to be governed by the instar rule) and corticocortical pathways (whose synaptic plasticity is assumed to be governed by the outstar rule) pass. Section 2.3.4 shows the result of combining the synaptic weight of feedforward and feedback pathways, which are similar to the results reported in Artola et al. (1990).

Independent LTP thresholds for different pathways. Huang et al. (1992) showed that LTP in a pathway to hippocampal CA1 neurons was inhibited by prior presynaptic stimulation with weak low-frequency stimulation or with single strong presynaptic shocks. LTP induction was attempted by using high-frequency stimulation. The inhibition of LTP was pathway specific; an independent control pathway to the same postsynaptic neuron easily underwent LTP. When the test and the control pathways were stimulated using the identical presynaptic stimulation to induce LTP at the same time, LTP in the test pathway (which was previously stimulated by low-frequency stimulation) was less than the LTP in the control pathway. Huang et al. (1992) suggested that the LTP thresholds in the different pathways could be different and pathway specific. Both the instar and the outstar excitatory synaptic plasticity rules have pathway specific LTP thresholds, which are dependent on the pathway synaptic weight. The BCM rule has only one postsynaptic activation history dependent LTP threshold for all pathways onto a postsynaptic neuron.

2.4.2 Experimental evidence for the outstar lateral inhibitory synaptic plasticity rule

Plasticity in inhibitory synapses has not received the extensive attention of the experimental and theoretical community, compared with that received by plasticity in excitatory synapses. This section presents experimental results on inhibitory synaptic plasticity and compares these results with the outstar inhibitory rule.

According to the outstar lateral inhibitory synaptic plasticity rule, presynaptic activation is necessary for plasticity, but when presynaptic stimulation is present, the sign of weight change depends on the postsynaptic activation. LTD is produced when the synaptic weight is greater than a function of the postsynaptic activation, and LTP is produced when the synaptic weight is less. There are several experimental results consistent with the

properties of the outstar lateral inhibitory synaptic plasticity rule.

In *Aplysia*, pairing stimulation of an excitatory pathway and postsynaptic hyperpolarization by an intracellular microelectrode increased the responsiveness of the postsynaptic neuron to stimulation of the excitatory pathway (Carew et al., 1984). Generalized Hebbian excitatory synaptic plasticity rules, including the BCM rule, the instar and outstar excitatory synaptic rules, and other rules (Brown et al. 1990) predict no plasticity or LTD in the stimulated excitatory pathway to the hyperpolarized neuron. Stimulation of a presynaptic input to a hyperpolarized neuron can activate another postsynaptic neuron, and under the outstar inhibitory rule, inhibitory pathways from active neurons to the inactive neuron weaken, and inhibitory pathways from the inactive neuron do not undergo synaptic plasticity. Thus, test stimulation of the input neuron will activate both neurons, but the previously hyperpolarized neuron receives less inhibition from the other active neuron, and hence its activation increases.

Responsiveness of a goldfish Mauther neuron to an unstimulated control pathway increased slightly after pairing presynaptic stimulation in another independent test pathway with postsynaptic inhibition (Yang & Faber, 1991). After a dual stimulating electrode protocol in rat and guinea pig visual cortex, the responsiveness of the unpaired pathway increased in some cases when the stimulation in the paired pathway was temporally associated with postsynaptic hyperpolarizing current injections (Frégnac et al., 1994). These results can be modeled by weakening of lateral inhibitory pathways to the weakly active neurons according to the outstar inhibitory rule.

Miles and Wong (1987) reported a weakening of lateral inhibitory pathways between CA3 pyramidal neurons in guinea pig hippocampal slices, several (approximately 15) minutes after tetanic stimulation of mossy fibers or longitudinal association pathways. The outstar lateral inhibitory synaptic plasticity rule can produce such an effect (see Figure 2.23c) when the initial lateral inhibitory pathway weight is less than a function of the postsynaptic activation.

In cerebellar Purkinje neurons, low-frequency stimulation of excitatory climbing fiber resulted in a long-term potentiation of $GABA_A$ receptor-mediated inhibitory postsynaptic currents (Kano et al., 1992). Kano et al. (1992) showed that intracellular

calcium ion concentration determines potentiation and depression of the inhibitory postsynaptic currents. When the postsynaptic calcium ion concentration was raised by climbing fiber stimulation or by direct activation of the voltage-gated calcium ion channels with a strong depolarizing pulse, long-lasting potentiation of inhibitory postsynaptic currents was observed. When the postsynaptic calcium ion concentration was low, during stimulation of climbing fibers with intracellular injection of a calcium ion chelator or during antidromic stimulation of Purkinje neuron axons in the granule neuron layer, a long-lasting depression of inhibitory postsynaptic currents was found. The outstar lateral inhibitory synaptic plasticity rule produces potentiation of stimulated lateral inhibitory pathways to strongly active neurons and produces depression of stimulated lateral inhibitory pathways to weakly active or inactive neurons. *In vivo*, high postsynaptic calcium ion concentration can be produced when the postsynaptic neuron is highly depolarized, since calcium ion channels are voltage-gated (Kano et al., 1992). Thus, the results in Kano et al. (1992) are consistent with the outstar lateral synaptic plasticity rule, if it is further assumed that depolarization of a Purkinje neuron or antidromic stimulation of Purkinje neuron axons in the granule neuron layer activates lateral inhibitory pathways to the Purkinje neuron via neural circuit interactions.

Hendry et al. (1990) reported a decrease in the density of $GABA_A$ receptors in ocular dominance columns corresponding to the closed eye in layer 4Cβ of adult monkey primary visual cortex after five or ten days of monocular deprivation. After monocular deprivation in adult cats, visual stimulation revealed a lack of lateral inhibitory interactions, which are seen in normal cortex, in the monocularly deprived cortex (Kasamatsu et al., 1998b). The outstar lateral inhibitory synaptic plasticity rule proposes weakening of inhibition to the inactive neurons. In neocortical cultures, blockade of spontaneous activity reversibly decreased the number of GABA-positive neurons, decreased GABA-mediated inhibition onto pyramidal neurons, and raised the firing rates of pyramidal neurons (Rutherford et al., 1997).

2.4.3 Functional significance of the synaptic plasticity rules

The excitatory synaptic plasticity rules – the instar, the outstar, and the BCM rules – and the outstar lateral inhibitory synaptic plasticity rule have been used in models of cortical properties and functions. In this section, the roles of the individual synaptic plasticity rules in the proposed models of cortical properties and functions are discussed. The unique functional properties of the rules are also discussed.

In Section 2.4.1, *Ambiguous experimental results*, it was assumed that the instar excitatory synaptic plasticity rule governs plasticity in feedforward pathways and that the outstar excitatory synaptic plasticity rule governs plasticity in lateral excitatory and feedback pathways. In this section, the functional bases for the assumption are discussed.

The instar excitatory synaptic plasticity rule

The instar excitatory synaptic plasticity rule modifies the synaptic efficacy of excitatory pathways to active postsynaptic neurons so that the postsynaptic neurons become more responsive to the input pattern; in fact, the synaptic weights move closer to a function of the presynaptic activation level (Grossberg, 1976ab; Kohonen, 1988; Marshall, 1995a; Nigrin, 1993). The instar excitatory synaptic plasticity rule has been used to self-organize neural network circuits in response to arbitrary input patterns (Carpenter & Grossberg, 1987; Grossberg, 1976ab, 1980, 1982; Marshall, 1995a; Nigrin, 1993).

Because the instar excitatory synaptic plasticity rule causes the weight vector of the excitatory pathways to active postsynaptic neurons to move closer to the input pattern vector, the instar rule can be used to model "fast" and "slow" learning (Carpenter & Grossberg, 1987; Grossberg, 1976ab, 1980, 1982; Marshall, 1995a; Nigrin, 1993). In fast learning, a network codes an input pattern in a small number of presentations, e.g., rapidly learning a person's face and name; whereas in slow learning, a network gradually establishes neural codes for an input pattern over a large number of input presentations, e.g., development of low-level feature selective neurons in primary visual cortex. Grossberg (1976a) showed that the instar excitatory synaptic plasticity rule is stable if the input patterns are sparse relative to the number of neurons coding the patterns,

and that no stable pathway weights exist in the simplest networks using instar excitatory plasticity if the number of patterns to be represented is large compared to the number of neurons used to represent the input environment or if the input patterns are densely distributed. Several sophisticated mechanisms to ensure stability in networks that use the instar excitatory synaptic plasticity rule have been proposed (Carpenter & Grossberg, 1987; Grossberg, 1976ab, 1980, 1982; Nigrin, 1993). Marshall (1995a) demonstrated the development of a stable representation of input patterns in a dense stationary input environment using a combination of the instar excitatory synaptic plasticity rule and the outstar lateral inhibitory synaptic plasticity rule under a slow learning paradigm.

The outstar excitatory synaptic plasticity rule

The outstar excitatory synaptic plasticity rule modifies the synaptic efficacy of excitatory pathways from active presynaptic neurons so that the synaptic weights of stimulated excitatory pathways move closer to a function of the postsynaptic activation level (Carpenter & Grossberg, 1981; Grossberg, 1976b, 1980, 1982; Nigrin, 1993).

Reciprocal geniculocortical and corticocortical excitatory pathways exist throughout the brain (Felleman & Van Essen, 1991; Maunsell & Van Essen, 1983). The firing pattern of neurons in the LGN can be modulated by corticogeniculate pathways (Sillito et al., 1994; Varela & Singer, 1987; Vidyasagar & Urbas, 1982). In addition, intracortical horizontal excitatory pathways exert subthreshold modulatory influences on cortical neurons (Gilbert & Wiesel, 1983, 1989, 1990; Gilbert et al., 1996; Kapadia et al., 1995; Toth et al, 1996; Ts'o et al., 1986). Feedback pathways or intracortical excitatory pathways may be involved in synchronized firing of cortical neurons (Engel et al., 1991; Gray et al., 1989; Gray & Singer, 1989; König et al, 1995). Somers et al. (1995) employed intracortical horizontal excitatory pathways between model cortical neurons with similar orientation preferences to enhance orientation selectivity. Thus, feedback pathways and intracortical horizontal excitatory pathways may modify the the activation of cortical neurons activated by feedforward pathways.

Feedback signals have been used to bias expected features in a temporal sequence or in spatial patterns (Nigrin, 1993), to resolve local ambiguities using global information

(Baloch & Grossberg, 1997; Grossberg & Rudd, 1992; Marshall et al., 1996b; Schmitt & Marshall, 1995), to bind elements of a group (Marshall et al., 1998), to perform line completions, formation of illusory boundaries, and texture processing (Gove et al., 1995; Grossberg & Mingolla, 1985ab; Grossberg et al., 1997b), to model spatial attention (Grossberg et al., 1994), to categorize of temporal input sequences (Grossberg et al, 1997a; Grossberg & Merrill, 1996; Nigrin, 1993), and to learn a stable representation of input patterns without supervision (Carpenter & Grossberg, 1987; Nigrin, 1993).

The outstar excitatory synaptic plasticity rule has been used to modify synaptic efficacy of feedback pathways in the aforementioned roles (Baloch & Grossberg, 1997; Carpenter & Grossberg, 1987; Grunewald & Grossberg, 1997; Grossberg et al., 1997a; Schmitt & Marshall, 1995; Nigrin, 1993). The outstar excitatory synaptic plasticity rule has also been used to model a large number of classical conditioning protocols (Pavlov, 1927; Rescorla & Wagner, 1972; Schmajuk, 1997).

The BCM synaptic plasticity rule

The BCM synaptic plasticity rule has been used to model development of a stable neural network having neurons with high selectivity in the absence of lateral inhibition (Bienenstock et al., 1982; Intrator & Cooper, 1992; Shouval et al., 1996). The BCM rule has been used to model visual cortical plasticity (Clothiaux et al., 1991; Law & Cooper, 1994; Shouval et al., 1996) and to extract features from very high dimensional vector spaces (Intrator, 1992).

The occurrence of negative and positive regions for the function ϕ the BCM rule (Equation 2.4) results in neurons becoming selective to subsets of stimuli in the visual environment. This happens because the response of the neuron is diminished to those patterns for which the postsynaptic activation is below the LTP threshold, while the response is enhanced to those patterns for which it is above (Bienenstock et al., 1982; Clothiaux et al., 1991).

As opposed to the instar rule, the BCM rule cannot be used for fast learning. If an input pattern activates a postsynaptic neuron above its LTP threshold, all active pathways to the postsynaptic neuron are strengthened. The pathway weights reach an

equilibrium level if the postsynaptic activation level and the LTP threshold become equal. Thus, during fast learning the BCM rule cannot keep the synaptic efficacy of pathways to the active postsynaptic neuron proportional to the input pattern.

However, even during slow learning the BCM rule can lead to loss of selectivity. For example, if only one input pattern is repeatedly presented, all excitatory pathways to the postsynaptic neuron most responsive to the input pattern will strengthen toward a maximum saturation level. If we assume that unstimulated pathways can be activated because of noise, then all pathways to the highly active neuron will strengthen (Clothiaux et al., 1991), and the neuron loses selectivity.

The outstar inhibitory synaptic plasticity rule

The outstar lateral inhibitory synaptic plasticity rule along with the instar excitatory synaptic plasticity rule (the EXIN rules) leads to development of neurons with high stimulus discrimination, sparse distributed coding, and exclusive allocation (Marshall, 1995a; Marshall & Gupta, 1998). The EXIN rules have been used to model the development of disparity selectivity (Marshall, 1990c), motion selectivity and grouping (Marshall, 1990a, 1995b; Schmitt & Marshall, 1995), orientation selectivity (Marshall, 1990d), and length selectivity and end-stopping (Marshall, 1990b).

Under the outstar lateral inhibitory synaptic plasticity rule, strong lateral inhibitory pathways develop between neurons that are consistently coactivated. Neurons can be consistently coactivated if they receive excitatory afferents from many common input neurons. Thus, in the EXIN network, model cortical neurons that share inputs tend to develop strong lateral inhibitory pathways between them (Marshall, 1995a). This is consistent with experimental results suggesting that a neuron receives the strongest inhibition when stimulated with the preferred stimuli of the neuron or when the stimuli is presented within the neuron's receptive field (Blakemore et al., 1970; Blakemore & Tobin, 1972; DeAngelis et al., 1992; Ferster, 1989; Sengpiel et al., 1997).

The outstar lateral inhibitory plasticity rule (Equation 2.10) is an asymmetric rule; lateral inhibitory pathways from active neurons to inactive neurons weaken; however, lateral inhibitory pathways from inactive neurons to other neurons *do not* change. The

outstar lateral inhibitory synaptic plasticity rule thus directly reduces inhibition to neurons inactivated by peripheral scotomas or lesions, thus making the inactive neurons more likely to respond to some visual stimuli (with reduced selectivity). The outstar lateral inhibitory synaptic plasticity rule enhances the efficiency of a neural network's representation of perceptual patterns by recruiting unused and under-used neurons to represent input data (Marshall, 1995a; Marshall & Gupta, 1998).

The lateral inhibitory synaptic plasticity rule is a *functional* rule that describes the modifications in the *effective* inhibition through synaptic weight changes. *In vivo*, intracortical inhibition to excitatory neurons is mediated by inhibitory neurons, which receive lateral excitation from excitatory neurons in addition to afferent input (McGuire et al., 1991; Somogyi, 1989; Somogyi & Martin, 1985). In addition, inhibitory neurons have inhibitory synapses with other inhibitory neurons (Somogyi, 1989; Somogyi & Martin, 1985). Neurophysiologically, the outstar lateral inhibitory synaptic plasticity rule could be realized directly by plasticity in the GABAergic synapses onto excitatory neurons – using the outstar lateral inhibitory synaptic plasticity rule – or indirectly by plasticity in lateral excitatory horizontal pathways (both short- and long-range) terminating on inhibitory neurons – using the outstar excitatory synaptic plasticity rule (Darian-Smith & Gilbert, 1995; Das & Gilbert, 1995ab; Gilbert et al., 1996; Hirsch & Gilbert, 1993). The axonal arbors of many inhibitory neurons (e.g., clutch, basket, chandelier) terminate mainly on excitatory neurons (Somogyi, 1989; Somogyi & Martin, 1985), and axonal arbors of most excitatory neurons terminate on other excitatory neurons (McGuire et al., 1991; Somogyi, 1989; Somogyi & Martin, 1985). Stimulation of the long-range horizontal excitatory pathways produce excitatory and inhibitory effects on excitatory neurons (Gil & Amitai, 1996; Weliky et al., 1995). Thus, changing the efficacy of either the lateral inhibitory pathways or the lateral excitatory pathways to inhibitory neurons will change effective inhibition to cortical neurons.

2.4.4 Comparison of the functional roles of the instar and outstar excitatory rules

The instar excitatory rule has been used to govern synaptic plasticity in feedforward pathways (Grossberg, 1976ab; Kohonen, 1988; Marshall, 1995a; Nigrin, 1993) and the outstar excitatory rule has been used to modify weights in feedback pathways (Carpenter & Grossberg, 1981; Grossberg, 1976b, 1980, 1982; Nigrin, 1993). In this section, the above choices are justified.

The appropriateness of using the instar excitatory synaptic plasticity rule in governing synaptic plasticity in feedforward excitatory pathways (e.g., the geniculocortical pathways), instead of the outstar synaptic plasticity rule, is shown using the following example.

In the developing primary visual cortex, neurons show some selectivity for specific input features, e.g., oriented line segments, from a quite early stage of development (Blasdel et al., 1995; Chapman et al., 1996; Frégnac & Imbert, 1978, 1984; Hubel & Wiesel, 1963; Wiesel & Hubel, 1974). An input pattern is composed of a small number of basic elements; e.g., a line segment at a particular position, length, width, and orientation is made up of a spatially linear sequence of adjacent stimulus positions. The basic elements that comprise an input pattern may belong to an extremely large number of different input patterns, e.g., a particular stimulus position may be an element of any line segment passing through that position. Because of the high selectivity in the developing cortex, only a small number of cortical neurons are activated in response to an input pattern; most cortical neurons are inactive or very weakly active, even though the input pattern that is presented contains elements that belong to input patterns that evoke strong response in the inactive/weakly active neurons. Under the instar excitatory synaptic plasticity rule, only active neurons can modify the synaptic efficacy of convergent excitatory pathways. Because of the high selectivity and the instar excitatory synaptic plasticity rule, only excitatory pathways to a small number of active neurons undergo plasticity in response to a input presentation. This contributes to the maintenance of stability of the pathway weights; only the excitatory pathways to strongly activated neurons are modified, and the weight changes

under the instar rule make the strongly active neurons even more responsive to the currently presented input patterns.

If the outstar excitatory synaptic plasticity rule were used to modify the synaptic efficacy of feedforward excitatory pathways, it would be difficult to maintain stable and strong feedforward pathway weights. Because of the high selectivity in the cortex, only a few cortical neurons are strongly activated. The plasticity in the outstar excitatory rule is enabled when the excitatory pathway is stimulated. Thus, stimulated excitatory pathways to a small number of strongly active cortical neurons are strengthened, and stimulated excitatory pathways to a large number of inactive or weakly active cortical neurons are weakened. Thus, excitatory feedforward pathways to cortical neurons are strengthened during presentation of a small number of input patterns, but are weakened during presentation of a large number of input patterns. This can cause all the excitatory feedforward pathways to become very weak. This conclusion is based on the observation that an input feature is composed of a small number of basic elements, but each element belongs to a large number of input patterns.

To clarify the above point, consider a worst-case scenario. During the early stages of cortical development, let the input environment be changed so that the animal is shown lines of only one orientation, e.g., vertical, over the entire visual field. Since only a small number of cortical neurons selective to the vertical line will be strongly active, while most cortical neurons are inactive or very weakly active, the outstar excitatory synaptic plasticity rule would weaken stimulated feedforward excitatory pathways to inactive neurons. Thus, presentation of one stimulus over the entire visual space leads to weakening of feedforward pathways to neurons selective to other stimuli, and eventual loss of responsiveness to visual stimulation in neurons selective to stimuli other than the presented stimulus.

Another problem with using the outstar excitatory synaptic plasticity rule for plasticity in feedforward excitatory pathways is that the rule causes all stimulated pathways to a common postsynaptic neuron to approach the same equilibrium value, which is a function of the postsynaptic activation level. Thus, the outstar rule is incapable of presenting input patterns that differ in activation level of the components of the input pattern, e.g., in representation of temporal patterns (Grossberg, 1978, 1985;

Grossberg et al., 1997a; Nigrin, 1993).

The instar excitatory synaptic plasticity rule on the other hand, allows plasticity in pathways to active neurons only, and cortical neurons previously less responsive to the vertical lines become more responsive to the vertical lines. Cortical neurons selective to other stimuli will retain their selectivity and responsiveness.

The outstar excitatory rule is well-suited for governing synaptic plasticity in feedback pathways, while the instar excitatory rule is not. In a hierarchical processing system, a higher stage neuron should send a feedback signal proportional to the activation pattern in the lower stage that strongly activates the higher level neuron to bias neurons in the lower stage (Nigrin, 1993). When the feedback signal is used to stabilize the pathway weights in an unsupervised learning network, the feedback signal is an expectation signal which allows the expected signal and the activation pattern in the lower stage to be locally compared. In this case too, the feedback signal should be proportional to the lower stage activation pattern that most strongly activates the higher stage neuron (Carpenter & Grossberg, 1987; Nigrin, 1993). The outstar rule is activated when the presynaptic neuron (a higher stage neuron in case of feedback pathways) is activated; the pathway weights then move closer to values proportional to the activation of the postsynaptic neurons (lower stage neurons in case of feedback pathways). Thus, the feedback pathway weights become proportional to the expected activation pattern in the lower stage, and feedback pathway weights change only when a higher stage neuron is activated. Thus, synaptic plasticity in feedback pathways governed by the outstar rule produces feedback pathways appropriate in generating biasing signals and stabilizing signals.

The instar excitatory synaptic plasticity rule is not appropriate for producing synaptic plasticity in feedback pathways. Because of the high input pattern selectivity in cortex, and because the constituent elements of an input pattern can belong to a large number of different input patterns, using the instar excitatory synaptic plasticity rule on feedback pathways would cause feedback pathways from a large number of higher stage neurons to an active lower stage neuron to weaken during the presentation of input patterns. Feedback pathways to a lower stage neuron would increase only when a higher stage neuron and the lower stage neuron are both active; this would happen during presentation of only

a small number of input patterns. Thus, if the instar rule were used to govern plasticity in feedback pathways, the feedback pathways would become very weak. Therefore the instar rule is not appropriate to govern plasticity in feedback pathways.

The outstar excitatory synaptic plasticity rule is also appropriate in producing synaptic plasticity in lateral excitatory pathways. A neuron in a given stage of processing may not be very predictive of the activation level of other neurons within the same stage; e.g., in a textured visual scene, the orientations of neighboring lines could be very different. The neurons selective to different simple input features in a lower stage can be combined to represent a more complex input feature or entity in a higher stage. When a neuron in a particular processing stage is active, lateral excitatory pathways from strongly active neurons within the same layer may strengthen under the instar excitatory rule, but lateral excitatory pathways from inactive or weakly active neurons weaken, and lateral excitatory pathways to inactive neurons do not change. On the other hand, when the outstar excitatory synaptic plasticity rule is used in lateral excitatory pathways, lateral excitatory pathways from an active neuron to a strongly active neuron may strengthen, but lateral excitatory pathways from the active neuron to inactive or weakly active neurons weaken. Thus, the instar and the outstar rules establish weights in lateral excitatory pathways between neurons within a processing stage proportional to the likelihood of coactivation of the neurons. In Section 2.4.1, *Ambiguous experimental results*, the outstar rule was assumed to govern plasticity in the intracortical lateral excitatory pathways because experimental evidence on synaptic plasticity in intracortical lateral pathways is consistent with the outstar rule but inconsistent with the instar rule.

2.4.5 Conclusions

This paper showed that the instar and the outstar excitatory rules modeled many experimental results on long-term potentiation and long-term depression. The main points of the paper are:

1. in the instar and the outstar rules, each synapse has a LTP threshold, whereas in the BCM rule, all synapses onto a neuron have a common LTP threshold;

2. in the instar and the outstar rules, independent pathways onto a neuron undergo synaptic plasticity independent of plasticity in other pathways, whereas in the BCM rule, the sign of weight changes in active pathways to a neuron is the same;

3. lateral inhibitory synapses can undergo LTP and LTD similar to excitatory synapses; and

4. lateral inhibitory synaptic plasticity improves models of experimentally observed synaptic plasticity.

Chapter 3

The role of afferent excitatory and lateral inhibitory synaptic plasticity in visual cortical ocular dominance plasticity

Abstract

Previous models of visual cortical ocular dominance (OD) plasticity (e.g., Clothiaux et al., 1991; Miller et al., 1989) are based on afferent excitatory synaptic plasticity alone; these models do not consider the role of lateral interactions and synaptic plasticity in lateral pathways in OD plasticity. Recent models of other cortical properties and functions have emphasized lateral intracortical interactions, however, and long-range lateral pathways develop during the early postnatal stages (Callaway & Katz, 1990). Thus, a biologically plausible model of OD plasticity should consider the development of intracortical pathways and its effects on OD and other cortical properties during early postnatal stages. In this paper, the EXIN model (Marshall, 1995a), which consists of afferent excitatory and lateral inhibitory synaptic plasticity, is used to model OD plasticity during

the "classical" rearing paradigms such as normal rearing, monocular deprivation, reverse suture, strabismus, binocular deprivation, and recovery from monocular and binocular deprivation, and to study the role of afferent excitatory and lateral inhibitory synaptic plasticity in the OD changes. Computer simulations using the EXIN model show that normal rearing produces model cortical neurons with high input feature selectivity and with a range of OD. The OD of model cortical neurons after normal rearing depends on the correlation between the patterns of stimulation in the two eyes. A novel result based on the EXIN model is that the weight of lateral inhibitory pathways has a strong effect on the OD distribution after normal rearing; as the strength of lateral inhibitory pathways is decreased, model cortical neurons become less selective and more monocular. In the model, the afferent excitatory synaptic plasticity plays the primary role in OD plasticity under the classical rearing paradigms, and lateral inhibitory interactions cause secondary OD changes. The EXIN model shows how afferent excitatory and lateral inhibitory pathways develop during normal rearing and undergo changes under the classical rearing paradigms. Novel experiments are suggested based on comparison of the EXIN model with previous models.

3.1 Introduction

The development of orientation selectivity and binocularity in primary visual cortex depends on the type of visual environment experienced during a critical period of development (Blakemore & Van Sluyters, 1975; Freeman et al., 1981; Frégnac & Imbert, 1978; Hubel & Wiesel, 1963, 1965, 1970; Wiesel & Hubel, 1963, 1965).

Primary visual cortical neurons in cats have orientation selectivity from very early postnatal stages, but a normal visual environment is needed to maintain and develop orientation selectivity (Frégnac & Imbert, 1978). Optical recording of the developing primary visual cortex in very young ferrets showed that the structure of orientation maps is stable during development, but the orientation tuning of primary cortical neurons is sharpened during normal development (Chapman et al., 1996). Weliky and Katz (1997) produced weakening of orientation selectivity of primary visual cortical neurons in ferret kittens by artificially correlated activation of optic nerve fibers, although the overall

organization of orientation column maps was unaltered.

The distribution of ocular dominance (OD) of primary cortical neurons is highly plastic during a critical period (Hubel & Wiesel, 1970). The OD of primary cortical neurons changes after "classical" rearing paradigms, which include monocular deprivation (MD), reverse suture (RS), strabismus (ST), binocular deprivation (BD), and recovery (RE) under normal stimulation following MD and BD. The classical rearing paradigms and their effects on cortical properties are reviewed below.

Brief periods of MD, in which one eye is deprived of visual stimulation, changes the OD of cortical neurons so that most become responsive exclusively to the open eye (Hubel & Wiesel, 1970). Changes in OD can be induced within a few hours of monocular experience (Freeman & Olson, 1982).

In RS conditioning (Blakemore & Van Sluyters, 1974), after a period of MD the previously closed eye is opened and the previously open eye is closed. RS shifts the OD of cortical neurons toward the newly opened eye (Blakemore & Van Sluyters, 1974). Cortical neurons lose responsiveness to the newly closed eye before becoming responsive to the newly opened eye (Mioche & Singer, 1989). Neurons may acquire an orientation tuning different from their original orientation tuning (Blakemore & Van Sluyters, 1974).

ST causes cortical neurons to become monocular (Hubel & Wiesel, 1965). In strabismic animals, stimulation of corresponding retinal positions is uncorrelated. Lack of correlated input to the eyes produced by alternating occlusion of the eyes, rotating the image in one eye relative to the other, or simultaneously producing different patterns of stimulation on corresponding regions of the two eyes, also causes loss of binocularity in cortical neurons.

In contrast to MD, most neurons remain equally responsive to both eyes after BD, in which animals are deprived of patterned stimulation in both eyes for a period comparable to that of MD (Wiesel & Hubel, 1965). Brief periods ($\leq$ 1 week) of BD produce about a 50% drop in peak responsiveness to the preferred orientation and a slight broadening of orientation tuning. Longer periods of BD lead to further reduction in responsiveness and orientation selectivity (Freeman et al., 1981).

Normal binocular vision after weeks of MD or BD restores normal binocularity of

cortical neurons (Buisseret et al., 1982; Freeman & Olson, 1982). However, binocularity may not be recovered after prolonged dark-rearing and MD followed by normal binocular vision (Cynader, 1983; Hubel & Wiesel, 1970; Freeman & Olson, 1982). Long periods of MD and BD can cause eye misalignment resulting in ST, and thereby preventing recovery of the binocularity of cortical neurons (Cynader, 1983; Olson & Freeman, 1978).

Several rules for excitatory synaptic plasticity have been proposed (e.g., Bienenstock et al., 1982; Clothiaux et al., 1991; Miller et al., 1989) to model OD changes during classical rearing experiments. These models rely only on afferent excitatory synaptic plasticity to produce OD changes.

Geniculocortical synapses comprise only 4% to 24% of all synapses received by layer 4 neurons (Ahmed et al., 1994; Einstein et al., 1987; Peters & Payne, 1993). Binocularity of cortical neurons is increased when intracortical inhibition is blocked by cortical infusion of GABA antagonists in animals conditioned by MD, suggesting that reduction of inhibition uncovers responsiveness to the eye that was closed during MD (Sillito et al., 1981). Thus, lateral intracortical interactions may contribute to cortical ocular dominance plasticity. Recent models (e.g., Douglas & Martin, 1991; Kalarickal & Marshall, 1997ab, 1998b; Marshall, 1989, 1990abcd; Marshall & Alley, 1993; Marshall et al., 1996ab; Marshall & Kalarickal, 1997; Martin & Marshall, 1993; Sirosh et al., 1996; Somers et al., 1995; Xing & Gerstein, 1994) have emphasized lateral intracortical interactions to model several cortical and perceptual properties.

Long-range intracortical horizontal pathways (Gilbert & Wiesel, 1979) develop during the early postnatal stages (Callaway & Katz, 1990). The long-range pathways connect non-adjacent cortical patches having similar input feature selectivity, e.g., orientation selectivity (Gilbert & Wiesel, 1989). The long-range pathways can have both facilitatory and suppressive effects on cortical neurons (Weliky et al., 1995). The effects of lateral intracortical interactions on cortical properties is under active investigation (Gilbert et al., 1996; Nelson et al., 1994; Sengpiel et al., 1997; Toth et al., 1996, 1997). The development of lateral pathways during early postnatal stages and its effects on cortical properties have not been fully explored.

This paper presents computer simulations of the effects of afferent excitatory and

lateral inhibitory synaptic plasticity rules on OD, responsiveness, and receptive field width of model cortical neurons under the classical rearing paradigms. The model is based on the EXIN synaptic plasticity rules (Marshall, 1995a), which consist of an afferent excitatory and a lateral inhibitory synaptic plasticity rule. In the model, afferent excitatory synaptic plasticity plays the primary role in OD plasticity under the classical rearing paradigms, and lateral inhibitory interactions produce secondary OD changes. The EXIN lateral inhibitory synaptic plasticity rule controls the development of lateral inhibitory pathway weights as a function of neuronal activation and contributes to the development of input feature selectivity and high discriminability of model cortical neurons and to sparse neuronal coding of input features (Marshall, 1995a; Marshall & Gupta, 1998).

3.2 Methods

3.2.1 EXIN model of ocular dominance shifts

We have formulated and tested a neural network model that exhibits OD changes similar to those observed experimentally. The model uses the EXIN (excitatory+inhibitory) plasticity rules (Marshall, 1995a). The EXIN rules consist of a Hebbian afferent excitatory plasticity rule (Grossberg, 1982) combined with an anti-Hebbian lateral inhibitory plasticity rule (Marshall, 1995a).

The EXIN lateral inhibitory plasticity rule

The EXIN lateral inhibitory plasticity rule (Marshall, 1995a) is an anti-Hebbian plasticity rule. Changes of the weight Z_{ij}^{-} of the lateral inhibitory pathway from neuron i to neuron j are governed by

$$\frac{d}{dt} Z_{ij}^{-} \;=\; \delta \; \mathcal{G}(x_i) \left(-Z_{ij}^{-} + \mathcal{Q}(x_j) \right), \tag{3.1}$$

where $\delta > 0$ is a small learning rate constant, x_i and x_j are the activations of neurons i and j, respectively, and $\mathcal{G}$ and $\mathcal{Q}$ are half-rectified non-decreasing functions with some noise (see Appendix B, Section B.6). Thus, *whenever a neuron is active, its output inhibitory connections to other active neurons tend to become gradually stronger (i.e., more*

inhibitory), while its output inhibitory connections to inactive neurons tend to become gradually weaker. In this rule, the *pre*synaptic activation (x_i) controls the *rate* of plasticity, and the *post*synaptic activation (x_j) determines the target value for the weight.

According to this rule, the weight of the lateral inhibitory pathways between two neurons is a direct function of the coactivation of the neurons. This leads to improved discrimination and sparse coding (Marshall, 1995a).

The EXIN afferent excitatory plasticity rule

The afferent excitatory pathway weight changes are governed by the EXIN excitatory plasticity rule. The rule can be expressed (Grossberg, 1982; Marshall, 1995a) as

$$\frac{d}{dt}Z_{ij}^{+} \;=\; \epsilon\, \mathcal{F}(x_j)\left(-Z_{ij}^{+} + \mathcal{H}(x_i)\right), \tag{3.2}$$

where Z_{ij}^{+} is the afferent excitatory weight from neuron i to neuron j, $\epsilon > 0$ is a small learning rate constant, and $\mathcal{F}$ and $\mathcal{H}$ are half-rectified non-decreasing functions with some noise (see Appendix B, Section B.6). Thus, *whenever a neuron is active, its input excitatory connections from active neurons become tend to become gradually stronger, while its input excitatory connections from inactive neurons tend to become gradually weaker*. In this rule, the *pre*synaptic activation (x_i) determines the *target value* for the weight, and the *post*synaptic activation (x_j) controls the rate of plasticity.

The EXIN excitatory plasticity rule operates as a competitive learning rule. It allows each modeled cortical neuron to become selective for a specific pattern of input activations.

The activation rule

The activation level x_j of each modeled cortical neuron is governed by a shunting equation (Grossberg, 1972) based on the Hodgkin model (Hodgkin, 1964):

$$\frac{d}{dt}x_j \;=\; -Ax_j \;+\; \beta(B - x_j)E_j \;-\; \gamma(C + x_j)I_j, \tag{3.3}$$

where A, B, C, β, and γ are positive constants. E_j represents the neuron's total excitatory signal

$$E_j = \left(\sum_{i \in \text{ Model input layer}} [x_i] Z_{ij}^{+} \right)^2, \tag{3.4}$$

and I_j represents the neuron's total inhibitory signal

$$I_j = \sum_{k \in \text{ Model cortical layer}} [x_k] Z_{kj}^{-}, \tag{3.5}$$

where $[a] \equiv \max(a, 0)$.

Because Equation 3.3 is a shunting equation, $x_j(t) \in [-C, B]$ if $x_j(0) \in [-C, B]$, for $t \geq 0$ (Cohen & Grossberg, 1983). Thus, B is the maximum activation level and $-C$ is the minimum activation level of Layer 2 neurons. Parameter A determines the passive decay rate. Parameters β and γ control the amount of excitation and inhibition, respectively, received by a model cortical neuron. The parameters of the activation equation were chosen so that the network would give a distributed activation response to an input, instead of a winner-take-all response. Also, the strength of inhibitory interaction was chosen so that weak afferent excitatory pathways to model cortical neurons would be ineffective in activating neurons. Thus, receptive field changes can occur when lateral inhibitory pathway weights change. The squaring in Equation 3.4 causes the maximal activation of model cortical neurons in response to binocular inputs to be more than twice the maximal activation level of the neurons in response to monocular inputs (Figure 3.1). Because of the squaring in Equation 3.4, the maximal excitation received by model cortical neurons during binocular stimulation is about four times that during monocular stimulation.

The shunting equation (Equation 3.3) with $Z_{jk}^{-} = Z_{kj}^{-} \geq 0$, belongs to a class of competitive dynamical systems that are absolutely stable; i.e., the system has fixed points for any choice of parameters (Cohen & Grossberg, 1983). The neuronal activations in such a system are guaranteed to reach stable equilibrium values for all synaptic weight values if $Z_{jk}^{-} = Z_{kj}^{-} \geq 0$ for all pairs of neurons.

However, it is not known whether the shunting equation remains absolutely stable when $Z_{jk}^{-} \neq Z_{kj}^{-} \geq 0$ for some pairs of neurons. Nevertheless, simulations demonstrate stability of the shunting equation when reciprocal pairs of lateral inhibitory weights are

not equal. In the simulations, the activation equations were solved numerically using the Euler method. The stability of the system was established empirically by observing the model's behavior under different Euler time step sizes. The step size and the number of steps were chosen so that the model cortical neuronal activations would reach a stable state without oscillations. The parameters used in the simulations are presented in Appendix B, Section B.6.

3.2.2 Initial network structure

We simulated a 1-dimensional patch of 42 model primary visual cortical neurons, receiving inputs from corresponding epipolar lines in the two eyes. The simulated input layer contained 14 monocular neurons, 7 each for the two eyes. The neurons in the input layer of the model were selective for different, overlapping positions along the epipolar lines and were topographically arranged. Topographic neighborhood relationships were arranged in a ring to eliminate boundary effects from the simulations. Orientation selectivity *per se* was not modeled in this 1-D network.

A network with initially nonspecific connection weights was trained on stimuli with a range of disparities and with a small amount of pre- and postsynaptic activation noise. The pre- and postsynaptic noise modeled spontaneous activity in the neurons. This training phase modeled a period of NR dependent development of the visual cortex during the early postnatal days. This network developed neurons with a normal ocular dominance distribution. The simulation details are in Appendix B, Sections B.1–B.6.

3.2.3 Measures of cortical properties

OD histograms were plotted according to the seven-point scale of Hubel and Wiesel (1962). The model cortical neurons were assigned to an OD group as follows. Let $x_{i,l}$ and $x_{i,r}$, respectively, be the maximal response of neuron i to stimulation of left and right eye selective model input layers, and

$$D = \frac{x_{i,l} - x_{i,r}}{x_{i,l} + x_{i,r}}. \tag{3.6}$$

Then the neuron is assigned to group 1 if $1 \geq D > 0.80$, group 2 if $0.80 \geq D > 0.45$, group 3 if $0.45 \geq D > 0.10$, group 4 if $0.10 \geq D > -0.10$, group 5 if $-0.10 \geq D > -0.45$, group 6 if $-0.45 \geq D > -0.80$, and group 7 if $-0.80 \geq D \geq -1$. Non-uniform bin sizes with smaller bins for groups 1, 4, and 7 than for groups 2, 3, 5, and 6 were chosen rather than uniform bin sizes, because the former provides a stricter condition to be a member of group 1 (neurons respond to only to the left eye), group 4 (neurons respond equally to both eyes), and group 7 (neurons respond to only to the right eye).

Changes in OD were expressed by a contralateral bias index (CBI)

$$\text{CBI} \;=\; 100 \times \frac{(N_1 \;-\; N_7) + (2/3)\,(N_2 \;-\; N_6) + (1/3)\,(N_3 \;-\; N_5) + N}{2N}, \tag{3.7}$$

where N_i represents the number of neurons in OD group i, and N is the total number of visually responsive neurons (Reiter & Stryker, 1988). The fraction of binocular neurons was measured by the binocularity index (BI)

$$\text{BI} \;=\; \frac{N_3 + N_4 + N_5}{N} \tag{3.8}$$

(Bear et al., 1990).

The receptive field width of left- and right-eye RFs of model cortical neurons were measured by width at half-height. Positional selectivity is the reciprocal of RF width.

3.3 Results

The EXIN rules modeled the effects of classical rearing paradigms. An explanation based on synaptic modifications governed by the EXIN rules is provided for normal binocular vision, monocular deprivation, binocular deprivation, reverse suture, strabimus, and restoration of normal binocular vision after various kinds of deprivation.

3.3.1 Normal rearing

Figure 3.1 shows the OD distribution of model cortical neurons after normal rearing. The figure also shows the average maximal responsiveness to monocular stimulation over all the neurons and the average left- and right eye RF width over all the neurons. The

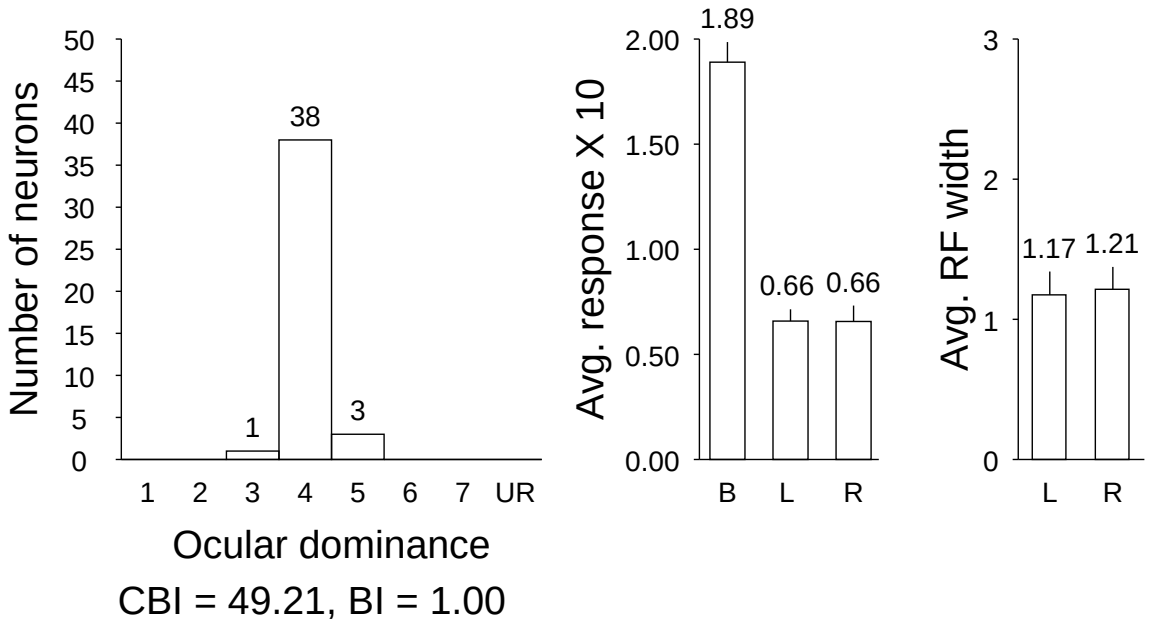

Figure 3.1: **Normal rearing.**
B represents binocular inputs, and L and R represent left and right eye monocular inputs. Average responsiveness is the average maximal responses over all the model cortical neurons neurons. UR represents the unresponsive neurons. The vertical lines on the bars represent the standard deviation, and the numbers above the bars represent the mean values. The simulation parameters are described in Section 3.2.4.

RF of model cortical neurons and the network pathway weights were stable after 1,500,000 presentations of binocular inputs during NR (see Appendix B, Section B.4). Figure 3.2 shows the development of left- and right eye RFs of two different model cortical neurons during NR. In the model, cortical neurons may become selective for non-corresponding left- and right eye positions (Figure 3.2a), and therefore, to a particular disparity, because of disparity in the training inputs.

Factors affecting binocularity, responsiveness, and RF width during NR

The binocularity of model cortical neurons decreased as the range of disparity in the binocular inputs for NR was increased (Figure 3.3). As the range of disparity in the NR inputs is increased, the maximal correlation in the activation of model left and right

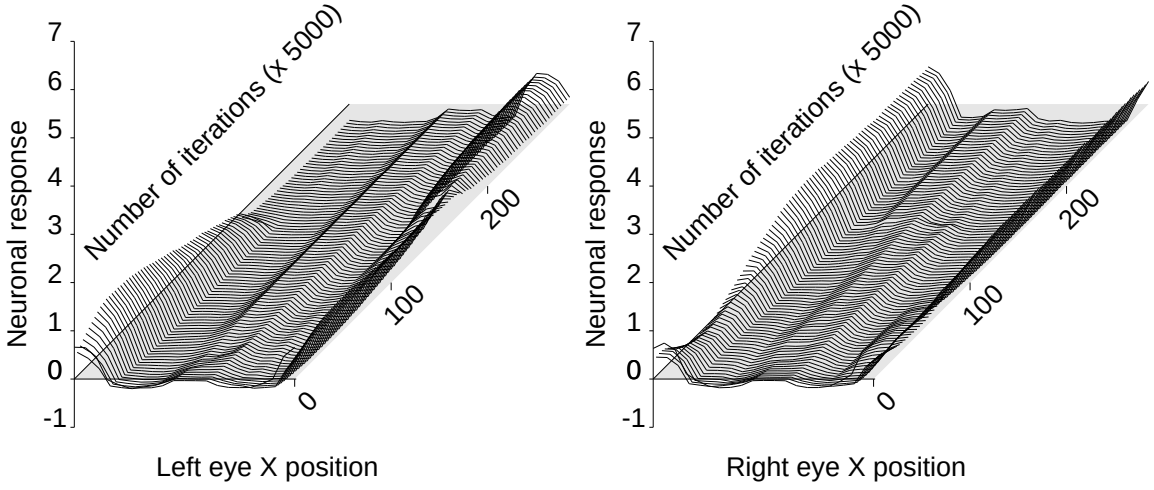

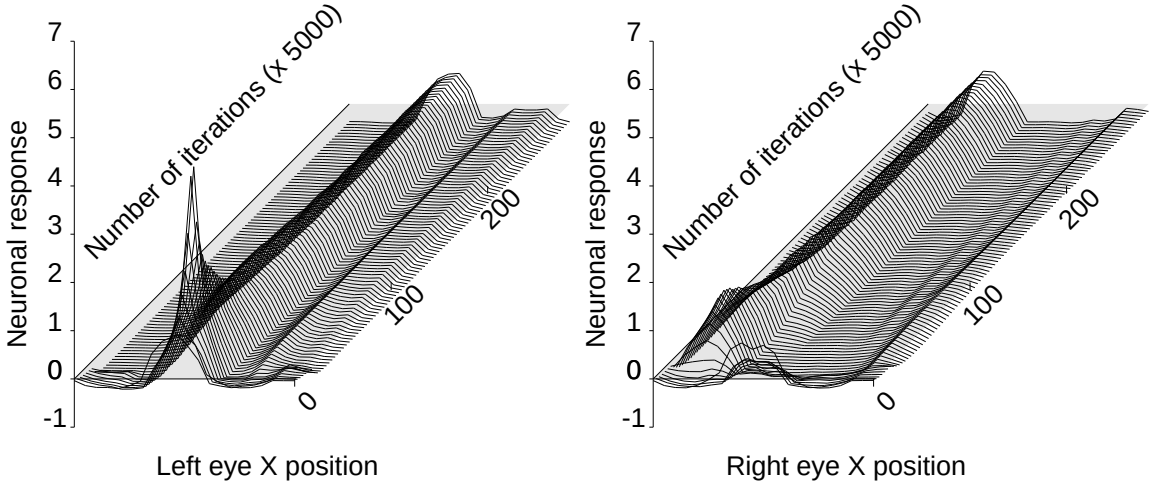

Figure 3.2: **Development of monocular RFs during NR.**
The figure shows the development of the left and right RFs of two model cortical neurons. The network was trained with 1,500,000 binocular inputs. The simulation parameters used are given in Section 3.2.4.

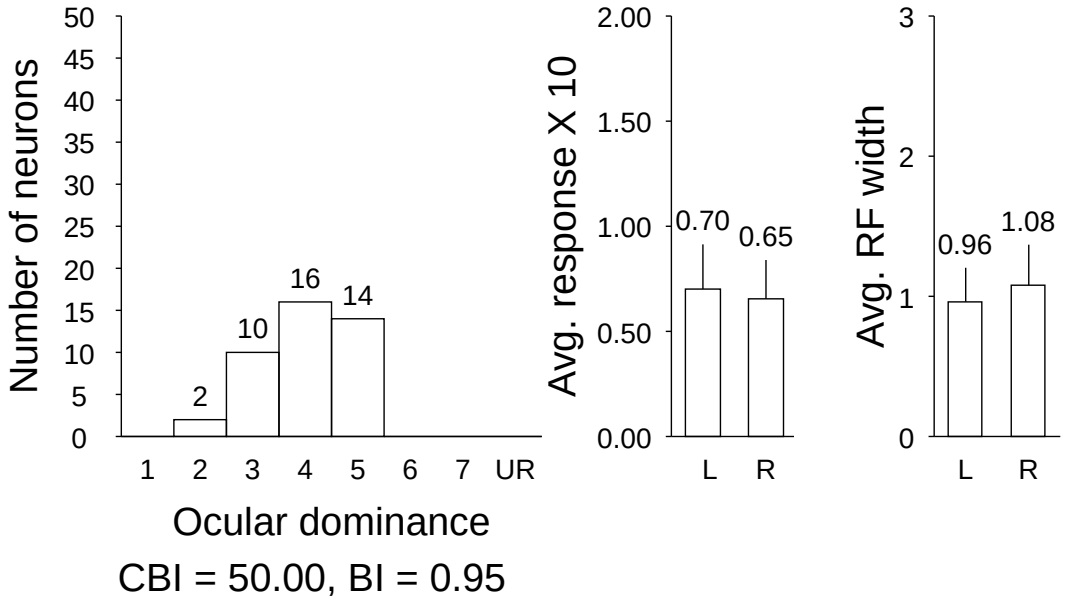

Figure 3.3: **NR with binocular inputs over a larger disparity range.** Binocular inputs with disparity in $\{-4, -10/3, -8/3, -2, -4/3, -2/3, 0, 2/3, 4/3, 2, 8/3, 10/3, 4\}$ were used in this simulation. Other simulation parameters were the same as those used for the simulation in Figure 3.1. The conventions are the same as in Figure 3.1.

eye selective input neurons decreases. If only zero disparity were allowed, the activation of corresponding positions in the left and right eye would be fully correlated. For non-zero disparity ranges, a position in one eye can be coactivated with any position in the other eye allowed by the disparity range. Assuming that all the disparities within the range are equally probable, as the disparity range increases the maximal correlation between the activation of input positions in the two eyes decreases. Furthermore, the correlation in the activation of model cortical neurons and monocular input neurons decreases.

When the correlation between the activation of a model cortical neuron and a binocular pattern of activation of input neurons is high, the model cortical neuron becomes binocular; the model cortical neuron is activated by a small range of binocular inputs close to its preferred stimuli and is unresponsive to other inputs. Thus, when a model cortical neuron is active, the correlation in the activation of left and right eye selective input neurons is high. According to the EXIN afferent excitatory synaptic plasticity rule,

plasticity occurs only when model cortical neurons are active. Thus, the model cortical neuron remains binocular.

As the number of binocular input patterns activating the neuron increases, the model cortical neuron can be activated by input stimulation in one RF (e.g., left eye RF) and input stimulation over a range of positions in the other eye. In this case, when a model cortical neuron is active, the correlation in the activation of monocular input neurons is low. According to the EXIN afferent excitatory synaptic plasticity rule, unstimulated afferent excitatory pathways to active model cortical neurons weaken, and strongly stimulated afferent excitatory pathways to active model cortical neurons strengthen. Thus, afferent excitatory pathways from one eye may weaken in competition with afferent pathways from the other eye, and model cortical neurons become less binocular. Because model cortical neurons became biased toward one of the eyes, the variance in the average maximal responsiveness to monocular inputs and in the average left and right eye RFs increased (Figure 3.3).

The binocularity, responsiveness, and RF width are also dependent on the strength of lateral inhibitory weights. In the simulations, the function $\mathcal{Q}(x) = \min(0.2, V[x])$ in Equation 3.1 was manipulated by varying V. As V was decreased, the maximal inhibitory weight in the network decreased. Parameter V was set to 3 in Figure 3.1, 0.3 in Figure 3.4a, and 0.03 in Figure 3.4b. As V was decreased, maximal responsiveness to monocular inputs and monocular RF width of the model cortical neuron increased (Figure 3.4). At very low values of V the model cortical neurons were less likely to be strongly monocular (compare Figures 3.4a and 3.4b) because the lateral inhibitory pathways were very weak. This phenomenon is analogous to the decrease in the number of neurons responsive exclusively to the eye that was open during MD, after a reduction in intracortical inhibition induced by cortical infusion of a GABA antagonist in kittens that were previously deprived of vision in one eye (Sillito et al., 1981).

As V was decreased, lateral inhibitory pathways weakened, thereby decreasing positional selectivity of model cortical neurons, i.e., their RF width increased. Because of low selectivity, model cortical neurons were actived by a larger number of binocular inputs, and as in the case of increasing disparity range in the training inputs, the model cortical

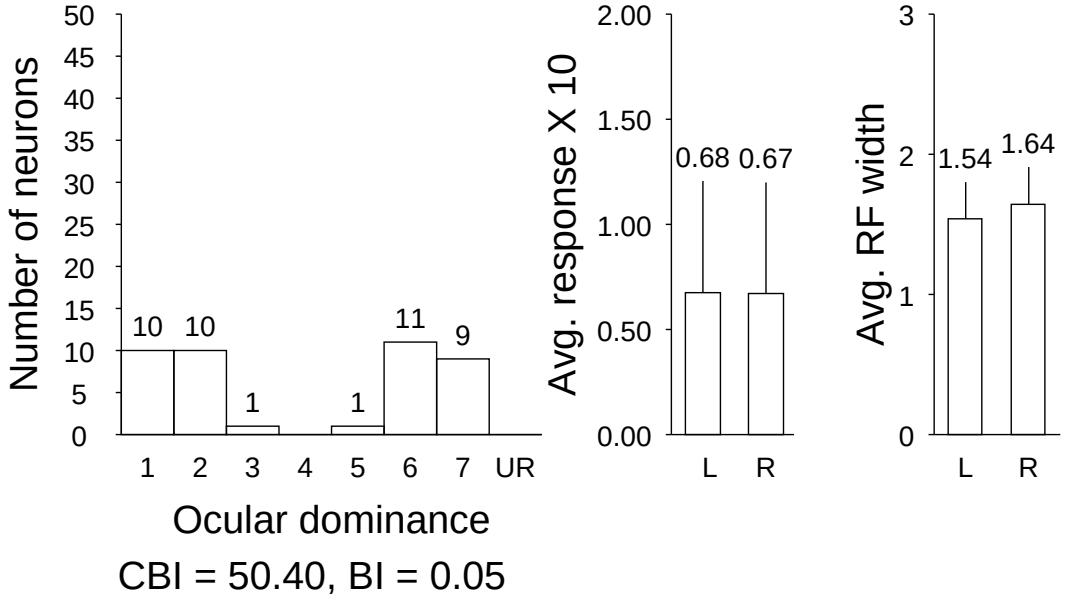

(a)

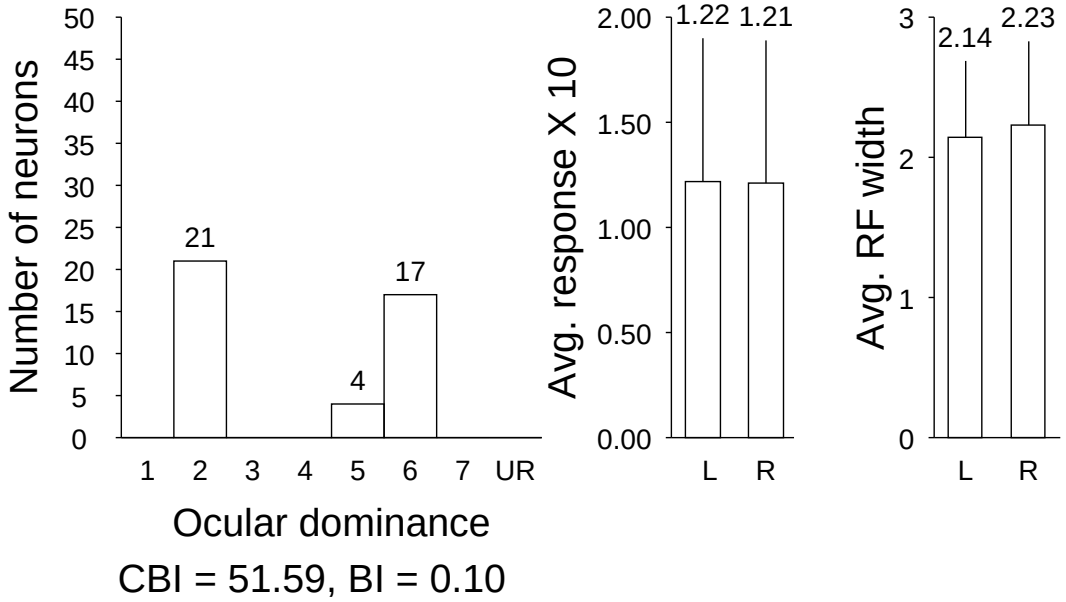

(b)

Figure 3.4: **The effects of varying the inhibitory weights during NR.** The simulation parameters are the same as for the simulation in Figure 3.1, except that $\mathcal{Q}(x) = \min(0.2, 0.3[x])$ in (a), and $\mathcal{Q}(x) = \min(0.2, 0.03[x])$ in (b). The conventions are given in Figure 3.1.

neurons became less binocular. Because model cortical neurons became biased toward one of the eyes, the variance in the average maximal responsiveness to monocular inputs and in the average left and right eye RFs increased (Figure 3.4).

In the simulations, model cortical neurons were biased to become tuned to binocular inputs because of the square non-linearity in the excitation equation (Equation 3.4), and in the EXIN afferent excitatory plasticity rule (Equation 3.2). The squaring in Equation 3.4 caused model cortical neurons to be more responsive when they received preferred binocular inputs, and the squaring in Equation 3.2 caused the more active neurons to learn faster. Since preferred binocular inputs activate model cortical neurons more strongly than other inputs, the excitatory plasticity rule caused the active neurons to learn the preferred stimuli faster than the less preferred inputs. Thus, the unlearning that occurs when less preferred stimuli active model cortical neurons is offset by the faster learning that occurs when the preferred stimuli is presented.

3.3.2 Monocular deprivation

In the model, MD resulted in OD shift toward the open eye (the left eye in Figure 3.5). Figure 3.6 shows the changes in the left and right RFs of two model cortical neurons during MD.

Stimulation of the open eye activates model cortical neurons. According to the excitatory synaptic plasticity rule, the synaptic weights of afferent excitatory pathways from the open eye selective active monocular input neurons increase, and the synaptic weights of afferent excitatory pathways from the inactive closed eye selective monocular input neurons decrease. Thus, the afferent excitatory pathway weights from the closed eye selective monocular input neurons to model cortical neurons eventually decay to low random values.

In the simulations, the average maximal responsiveness of model cortical neurons to the open eye stimulation increased, and the average maximal responsiveness of model cortical neurons to the closed eye stimulation decreased (Figures 3.5 and 3.6). Increase in responsiveness to the open eye has been observed in MD experiments (Mioche & Singer, 1989). The average width of the closed eye RFs of model cortical neurons

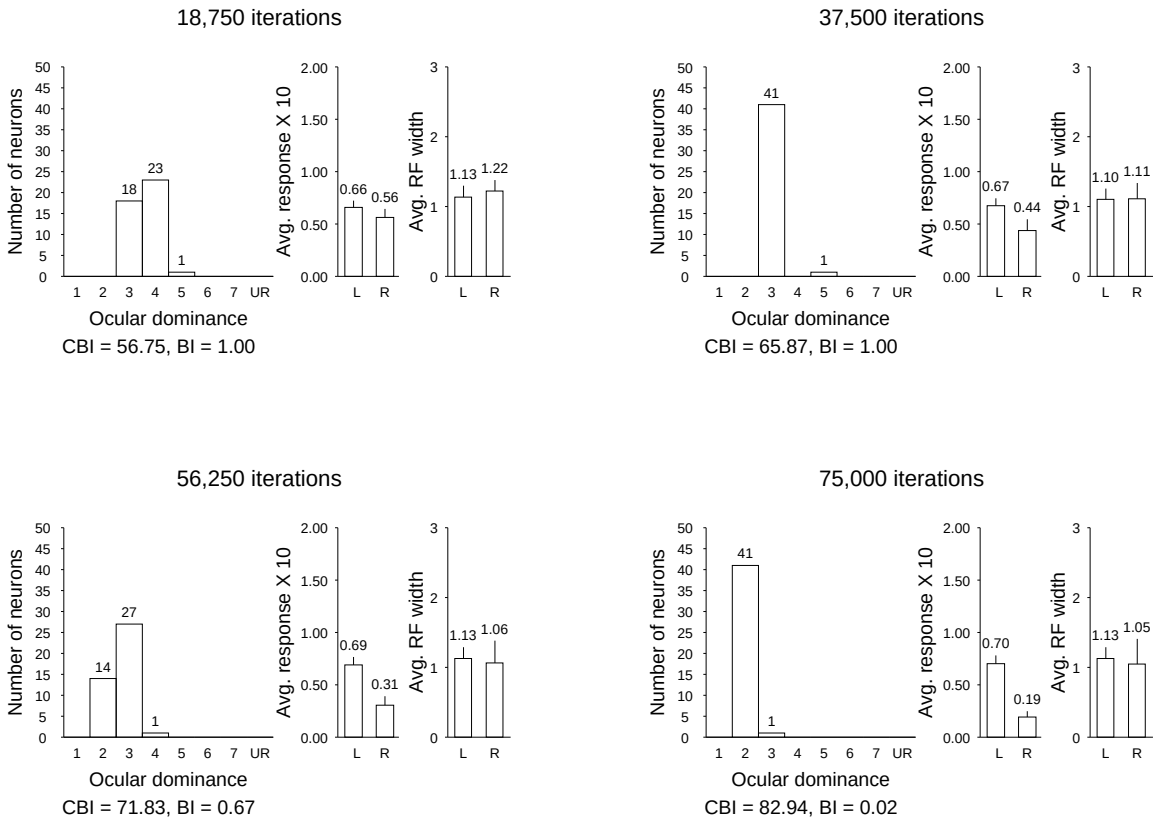

Figure 3.5: **OD changes during MD.**
The parameters are given in Section 3.2.4, and the conventions are in Figure 3.1. The left eye was the open eye and the right eye was closed.

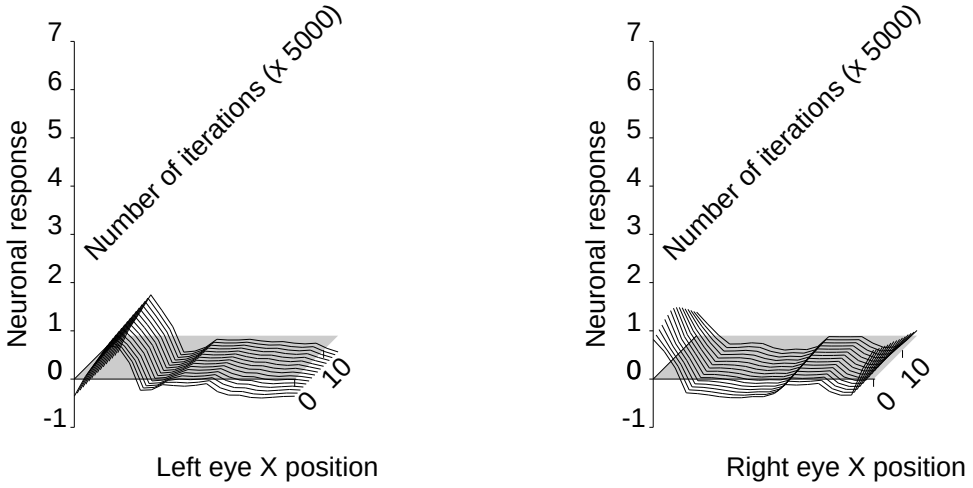

Figure 3.6: **Monocular RF changes during MD.**
The parameters are given in Section 3.2.4. The left eye was the open eye and the right eye was closed.

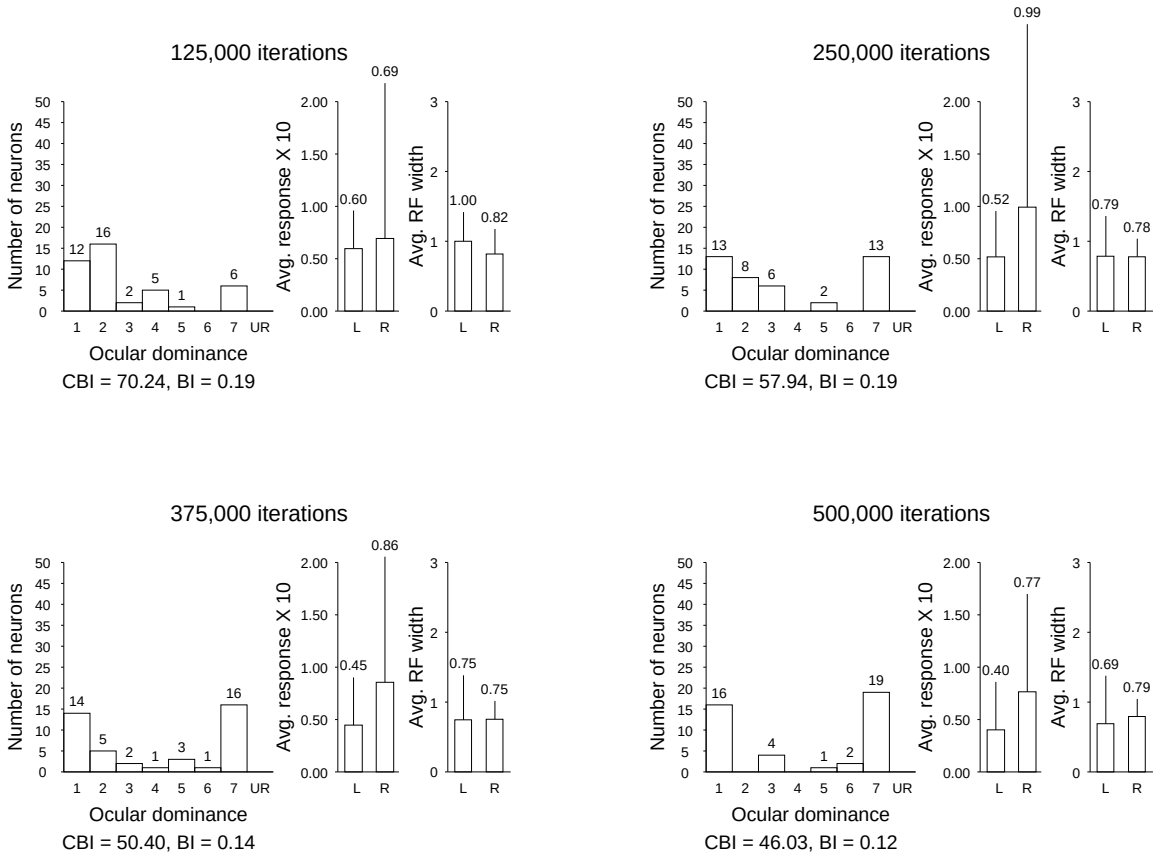

Figure 3.7: **OD changes during RS.**
The parameters are given in Section 3.2.4, and the conventions are in Figure 3.1. The right eye was the open eye and the left eye was closed.

decreased, and the variance in the average width increased (Figure 3.5).

3.3.3 Reverse suture

In RS, the stimulation of the eyes was reversed following MD in Section 3.3.2; i.e., the left eye received low, random inputs, and the right eye received monocular stimulation. During RS, OD of model cortical neurons shifted toward the newly opened eye (Figures 3.7 and 3.8).

Immediately after the reversal of the input presentation to the two eyes, model cortical neurons are weakly activated because the afferent excitatory pathways with strong weights receive low, random inputs, and the input patterns are presented to the monocular

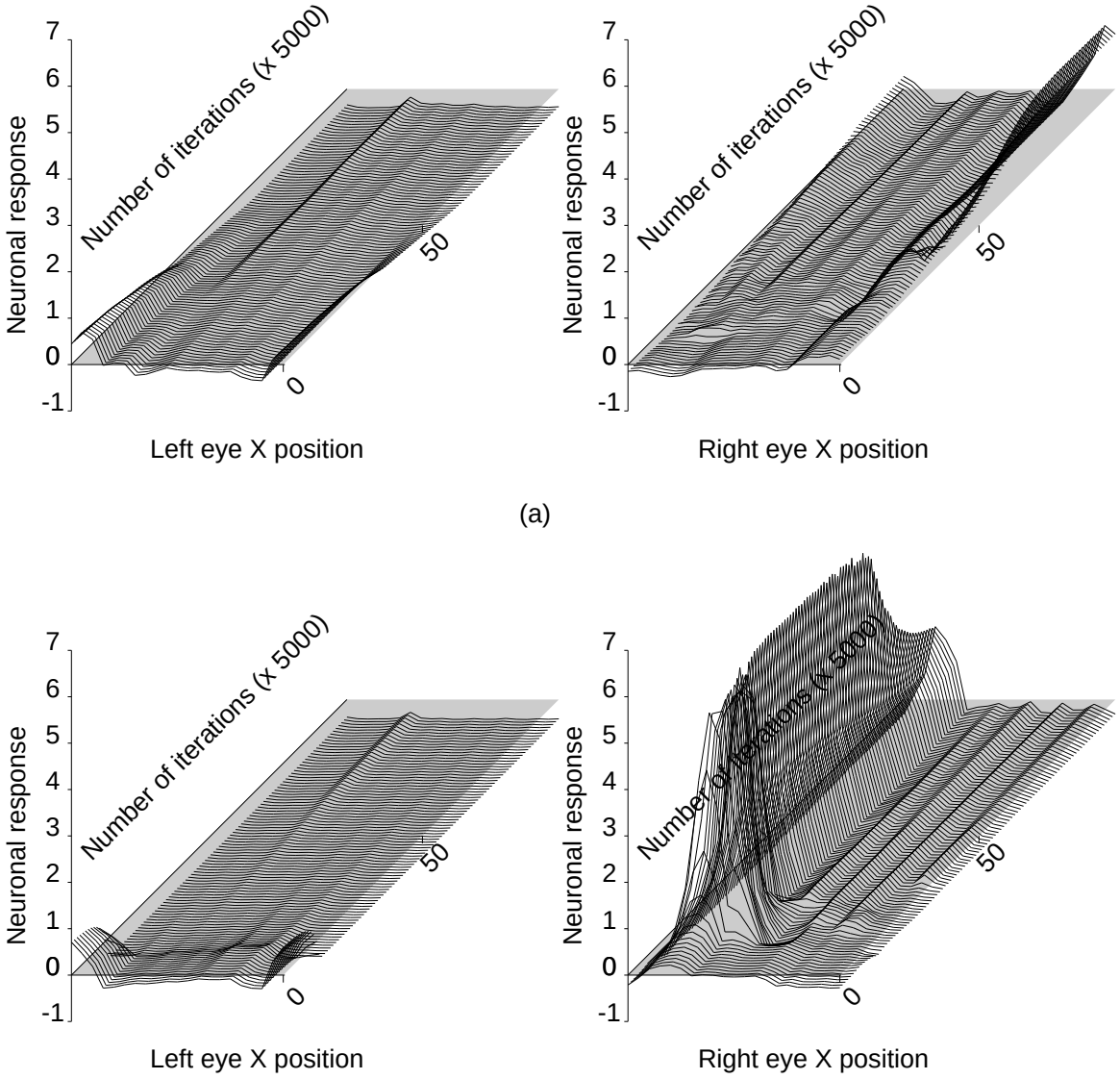

Figure 3.8: **Monocular RF changes during RS.**
The parameters are given in Section 3.2.4. The right eye was the open eye and the left eye was closed.

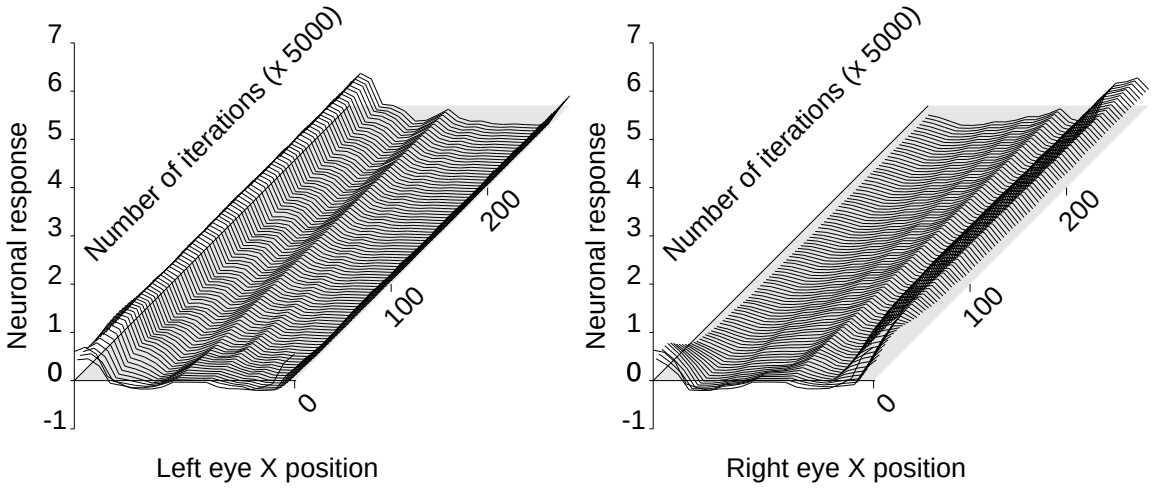

(a)

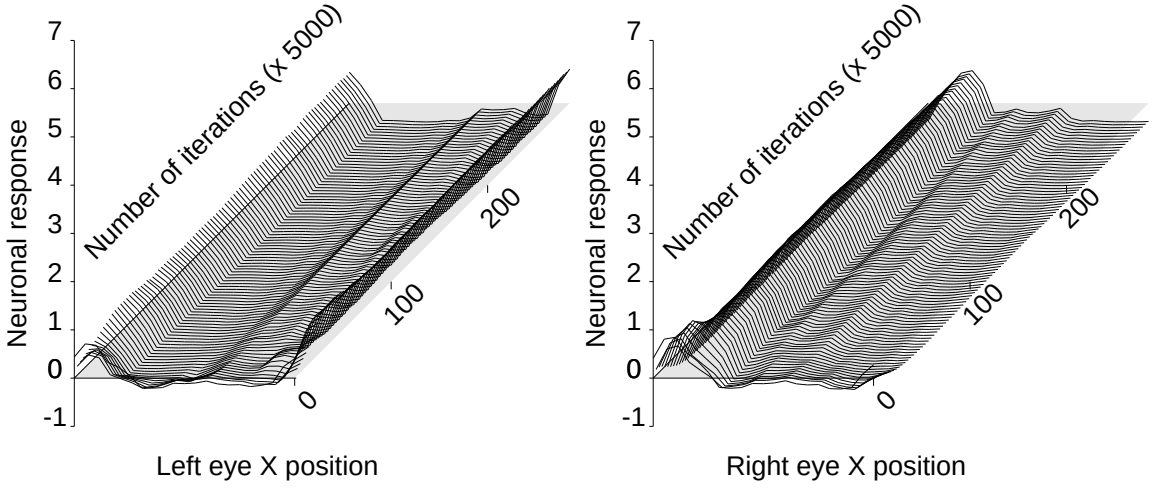

(b)

Figure 3.9: **Monocular RF changes during NR for the neurons in Figure 3.8.** Figures (a) and (b) show the monocular RFs of the neurons whose monocular RFs are shown in Figures 3.8a and 3.8b, respectively, during NR. The parameters are given in Section 3.2.4.

input layer with weak afferent pathways to model cortical neurons. Low activation of model cortical neurons causes slow changes in the afferent excitatory pathways. The initial large afferent pathway weights from the left eye selective input layer to the model cortical neurons are decreased every time model cortical neurons are actived. Simultaneously, model cortical neurons strengthen afferent excitatory pathways from the right eye selective input layer. The temporal competition among the various input patterns slows the development of strong afferent excitatory pathways from the right eye selective input neurons compared to the decay of afferent excitatory pathway weights between the left eye selective input neurons and model cortical neurons. Thus, in the simulations, model cortical neurons lost responsiveness to the newly closed eye before becoming responsive to the newly opened eye (Figure 3.8).

During RS, some neurons became highly responsive to the newly opened eye (Figure 3.8b). Because of the lateral inhibitory interactions, high responsiveness of some neurons to the newly opened eye caused complete suppression of responsiveness of other model cortical neurons to the newly opened eye, thereby increasing the number of neurons responsive only to the previously closed eye (Figure 3.7). A low activation level of model cortical neurons weakens the lateral inhibitory weights to the neurons according to the EXIN lateral inhibitory synaptic plasticity rule. In the simulation, the decrease in inhibitory weights increased the responsiveness of inactive neurons to the newly opened eye and eventually caused the neurons to become responsive exclusively to the newly opened eye (Figure 3.8a).

During RS, the average maximal responsiveness of model cortical neurons to the newly opened eye increased (Figure 3.7), and the average maximal responsiveness of model cortical neurons to the newly closed eye decreased (Figure 3.7). The variance in the maximal responsiveness of model cortical neurons to the newly opened eye was large; some neurons became highly responsive to the newly opened eye (Figure 3.8b) because of weakening of the lateral inhibitory pathways. In addition, most neurons responded to the left or the right eye; therefore, the maximal responsiveness of model cortical neurons to monocular stimulation varied widely.

In the MD simulation described in Section 3.3.2, model cortical neurons did not

completely lose their responsiveness to the closed eye (Figures 3.5 and 3.6). Therefore, during the subsequent RS conditioning, the RF tuning of the model cortical neurons for the newly opened eye was close to the neurons' original RF tuning in the same eye after NR (compare the right-eye RFs in Figures 3.8 and 3.9).

3.3.4 Strabismus

During ST, the left and right inputs were uncorrelated, and the model cortical neurons became selective for correlated patterns of activation in the monocular input layers. Thus, the model cortical neurons became monocular (Figures 3.10 and 3.11). The model cortical neurons became selective for positions in the left or right eye (Figure 3.11).

After ST, model cortical neurons responded to the left or the right eye. Thus, the monocular RF width and the maximal responsiveness of model cortical neurons to monocular stimulation varied widely, and the variance in the maximal responsiveness to monocular inputs, and in the monocular RF widths was high (Figure 3.10). During ST, some neurons became highly responsive (Figure 3.11b).

3.3.5 Binocular deprivation

After prolonged BD, the average maximal responsiveness to monocular inputs decreased, the average monocular RF width increased, and model cortical neurons remained binocular (Figure 3.12). During BD, the input neurons received very weak noisy activation, and according to the excitatory synaptic plasticity rule, unstimulated and weakly stimulated afferent excitatory pathways to active neurons weaken. The noise in the input activates model cortical neurons very weakly. To speed up the rate of weakening of the afferent excitatory pathways, a random-noise term was included in the excitatory synaptic plasticity rule (Appendix B, Section B.6).

The EXIN lateral inhibitory synaptic plasticity rule is instrumental in widening the monocular RFs. Since model cortical neurons are very weakly activated during BD, the lateral inhibitory pathways are weakened. Weakened lateral inhibitory pathways increased the RF width (decreased position selectivity) of model cortical neurons (Figure 3.12). When lateral inhibitory synaptic plasticity was disabled during BD, the average maximal

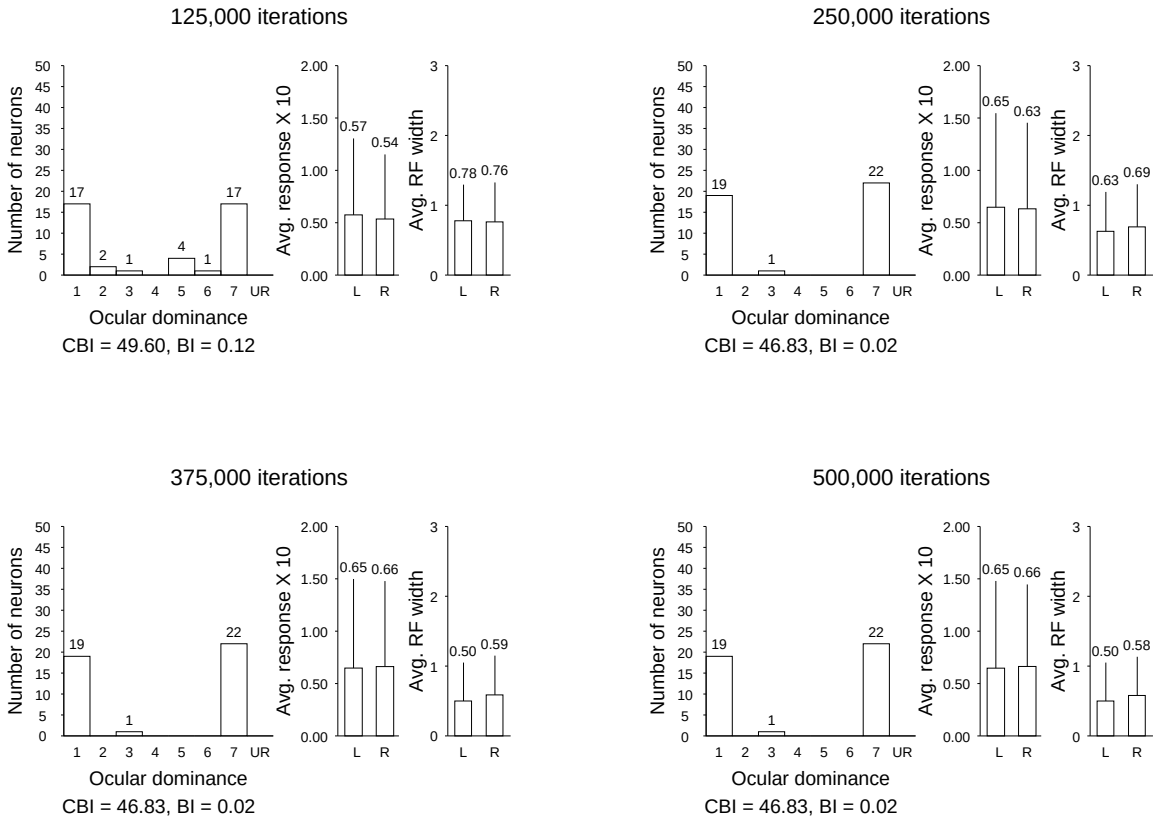

Figure 3.10: **OD changes during ST.**
The parameters are given in Section 3.2.4, and the conventions are in Figure 3.1.

responsiveness of model cortical neurons to monocular stimulation decreased, but the monocular RF widths of model cortical neurons also decreased (Figure 3.14).

3.3.6 Recovery

In the EXIN model, presentation of normal, binocular inputs following MD (Figures 3.15 and 3.16), ST (Figures 3.17 and 3.18), and BD (Figures 3.20 and 3.21) restored the OD distribution, the average maximal responsiveness of neurons to monocular inputs, and the average monocular RF widths.

During the prolonged BD in Section 3.3.5, the model cortical neurons became very weakly responsive to both eyes and lost their positional selectivity (Figures 3.12 and 3.13). During the subsequent normal training, model cortical neurons became selective for different

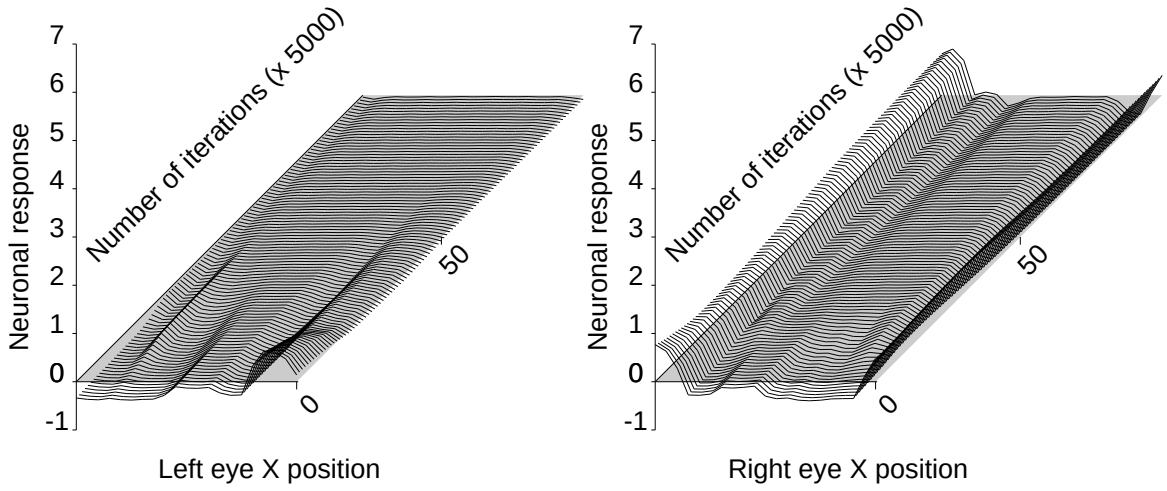

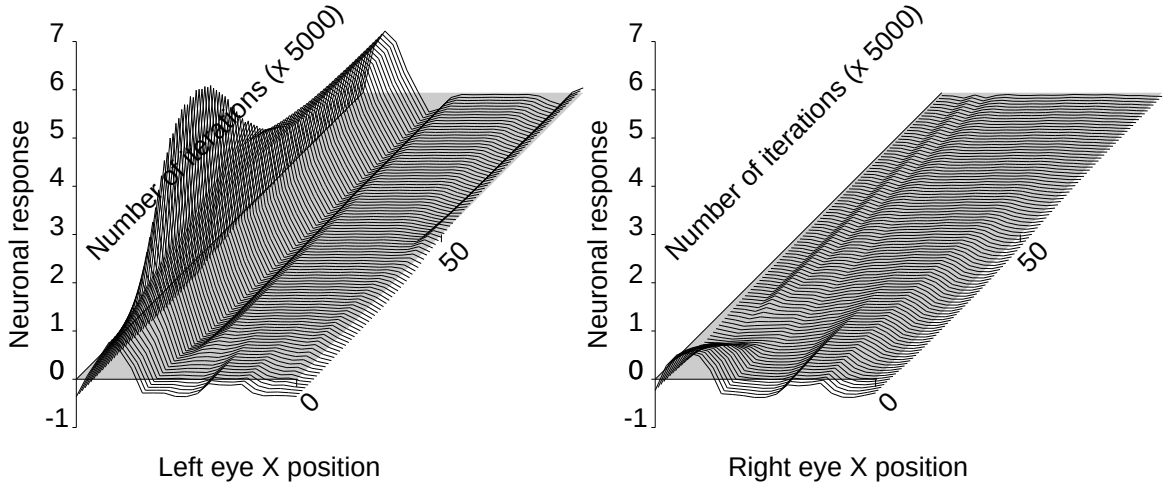

Figure 3.11: **Monocular RF changes during ST.**
The parameters are given in Section 3.2.4.

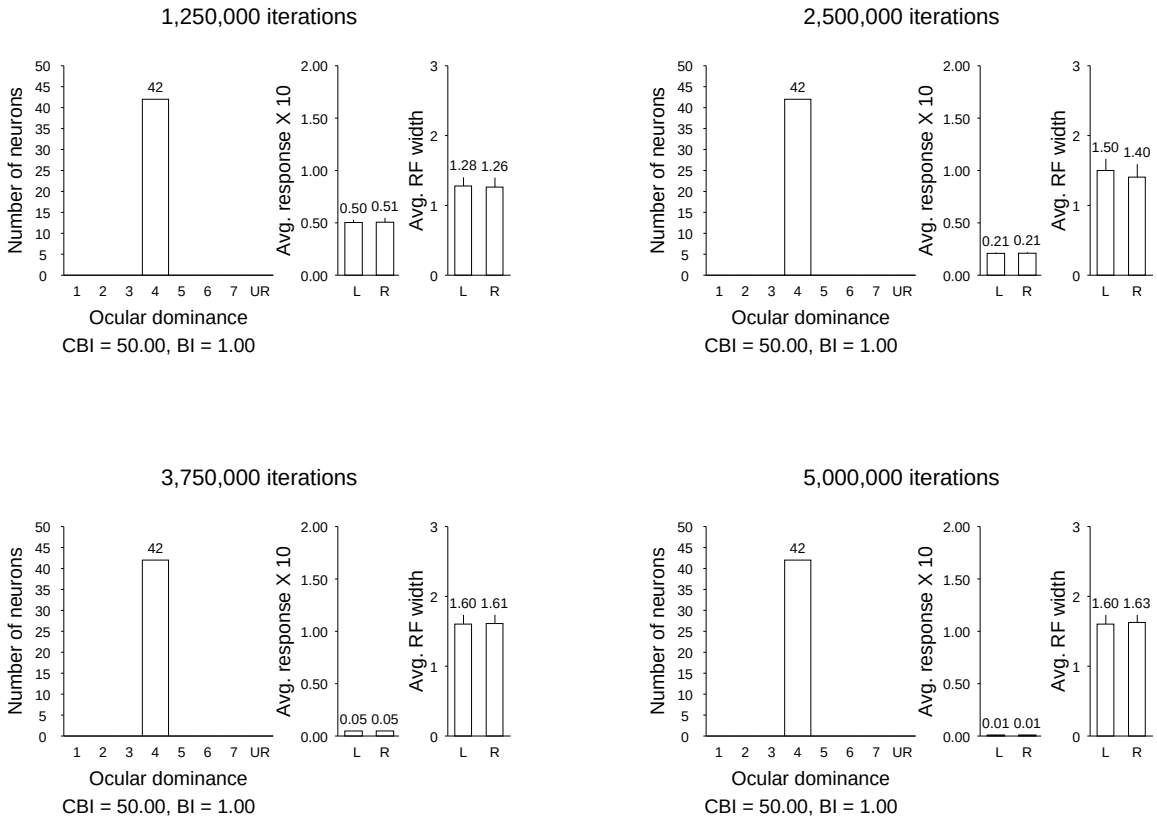

Figure 3.12: **OD changes during BD.**
The parameters are given in Section 3.2.4, and the conventions are in Figure 3.1.

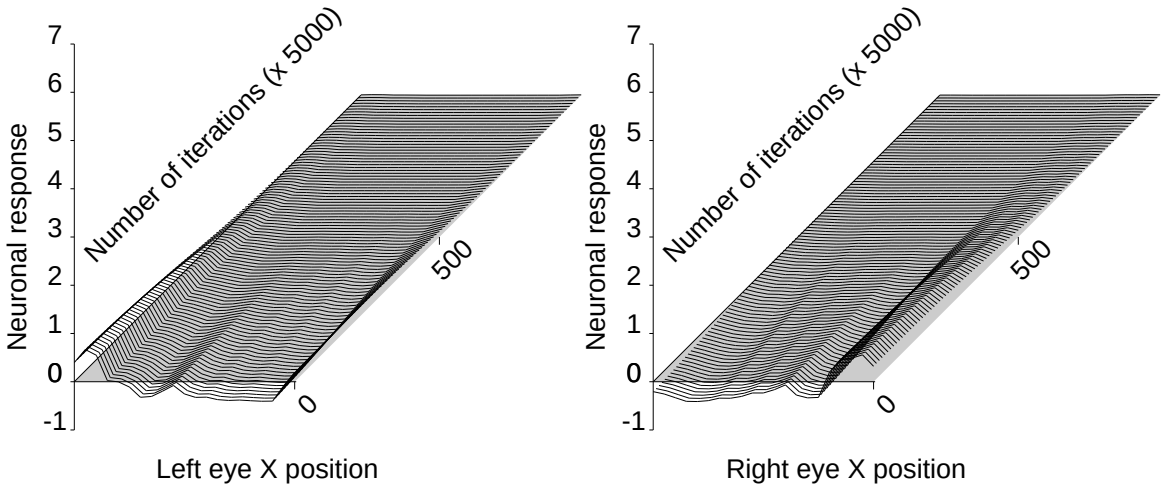

(a)

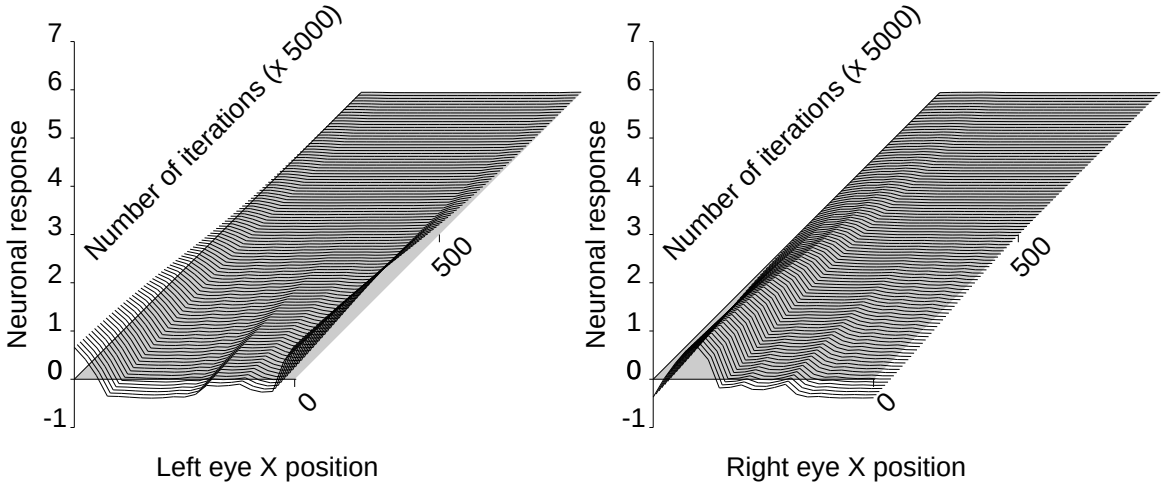

(b)

Figure 3.13: **Monocular RF changes during BD.**
The parameters are given in Section 3.2.4.

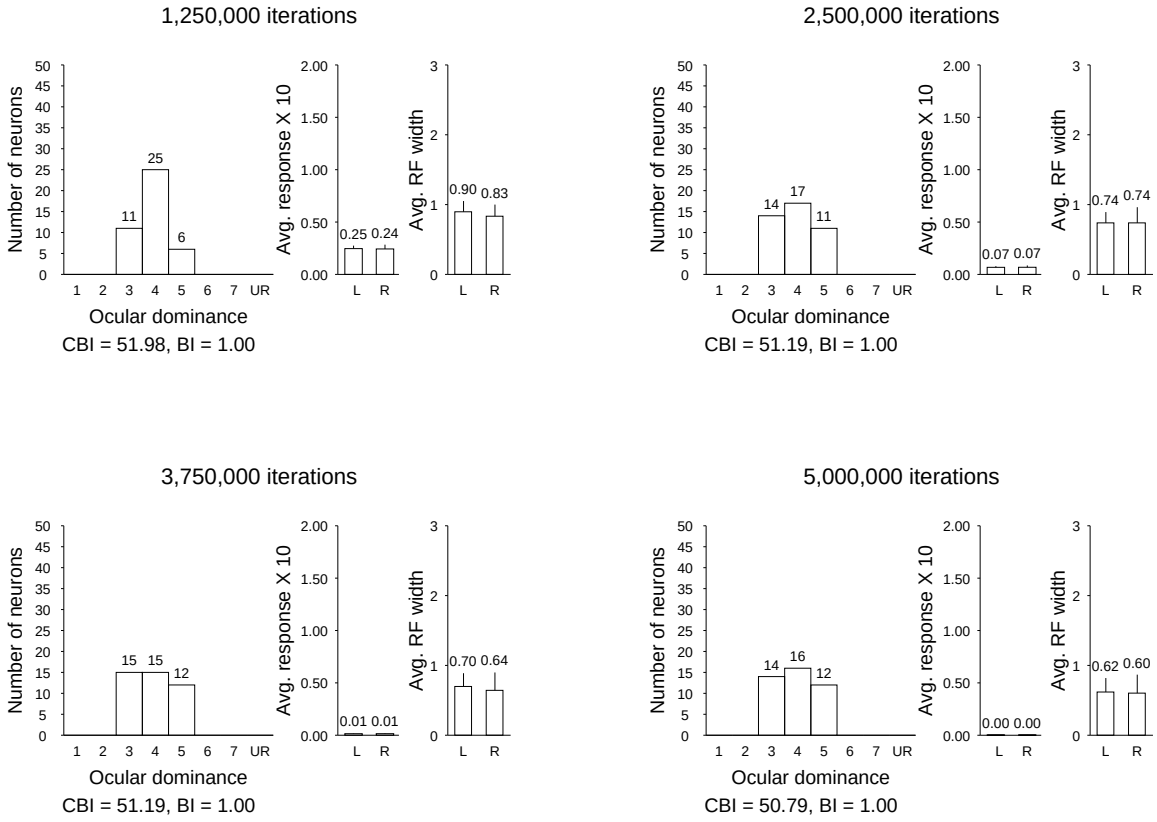

Figure 3.14: **Monocular RF changes during BD without lateral inhibitory synaptic plasticity.**
The parameters are the same as those in the simulation in Figure 3.11 except that the lateral inhibitory synaptic plasticity was blocked.

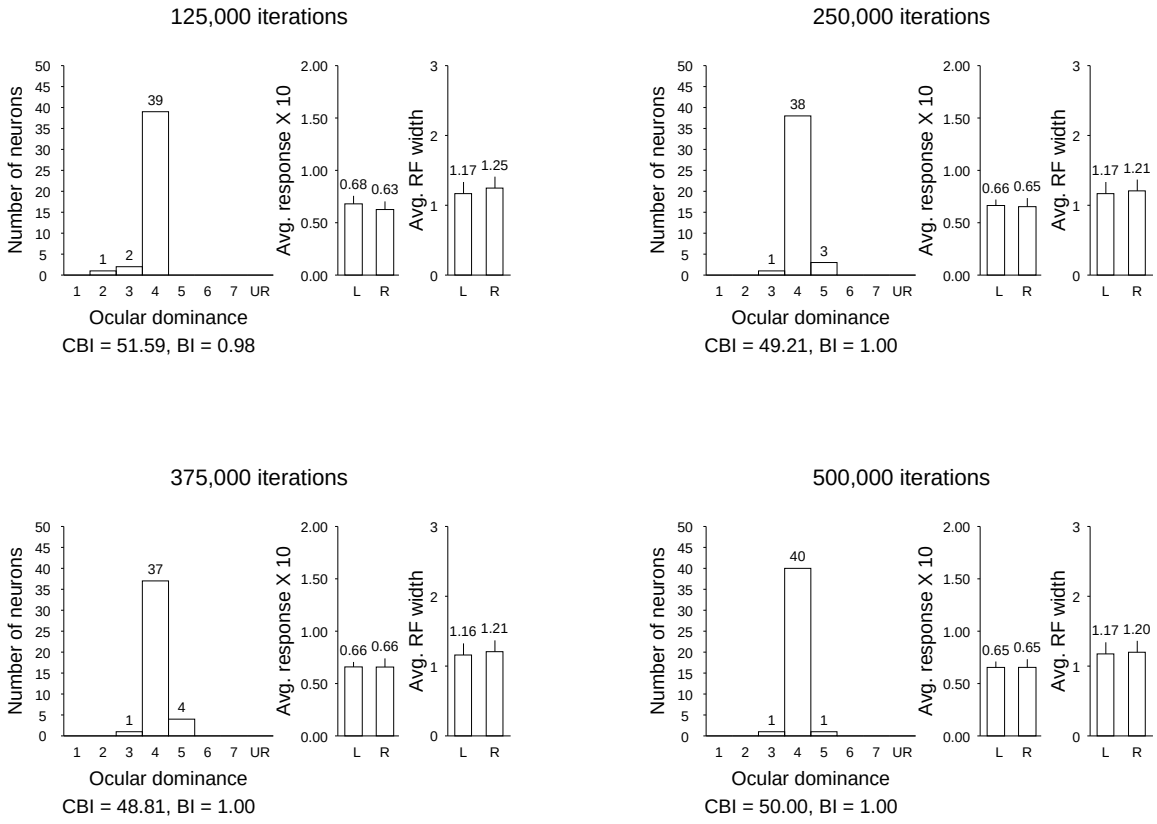

Figure 3.15: **OD during RE following MD.**
The parameters are given in Section 3.2.4, and the conventions are in Figure 3.1.

positions (Figure 3.19).

3.4 Discussion

The EXIN (excitatory + inhibitory) rules qualitatively model cortical ocular dominance plasticity during early postnatal stages produced by the classical rearing paradigms. During NR, the EXIN rules produced model cortical neurons with stable position and disparity tunings (Section 3.3.1). The EXIN rules have been used to model the development of motion selectivity (Marshall, 1990a, 1995b; Schmitt & Marshall, 1995), orientation selectivity (Marshall, 1990d), length-selectivity (Marshall, 1990b), and abstract pattern categorization (Marshall, 1995a).

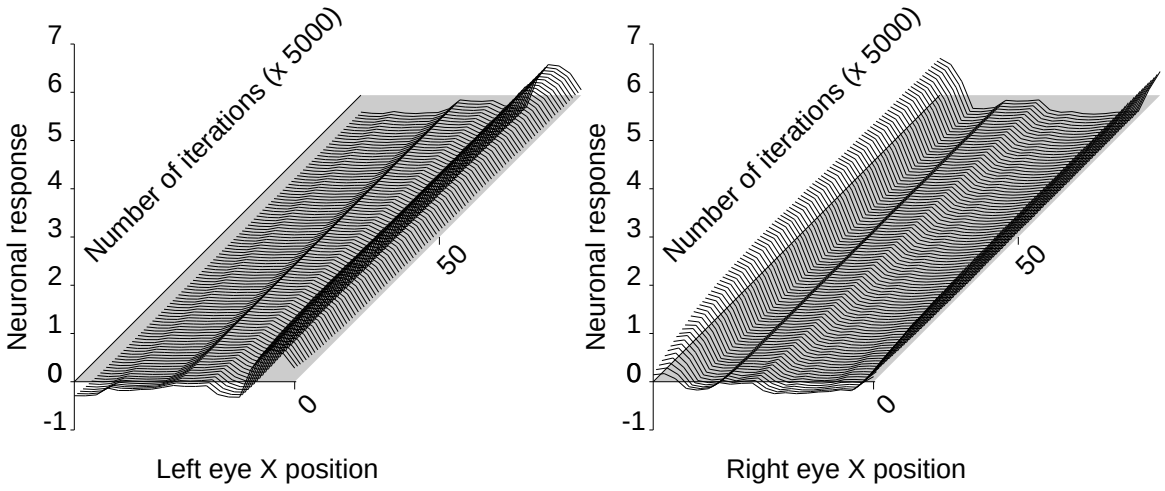

(a)

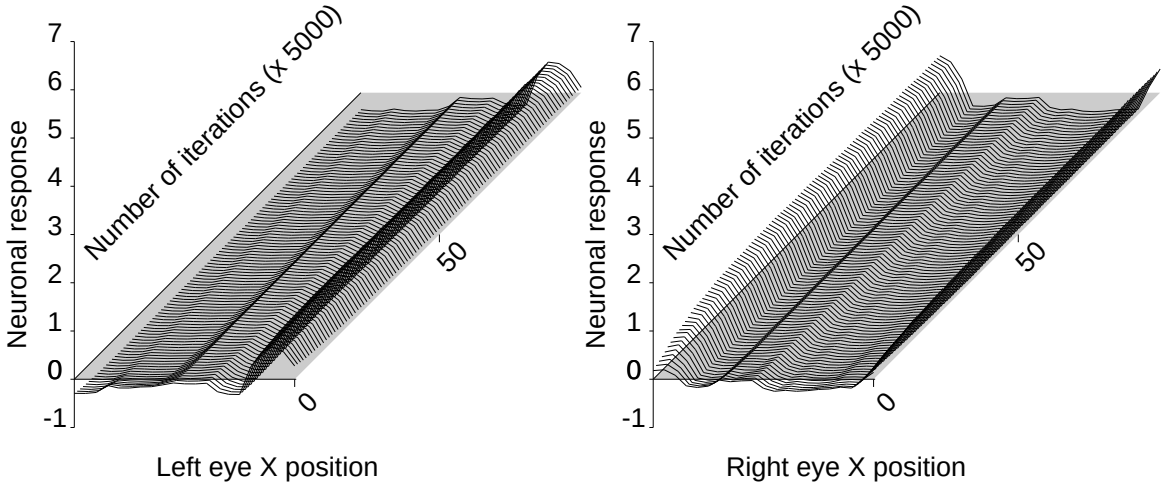

(b)

Figure 3.16: **Monocular RF changes during RE following MD.** The parameters are given in Section 3.2.4.

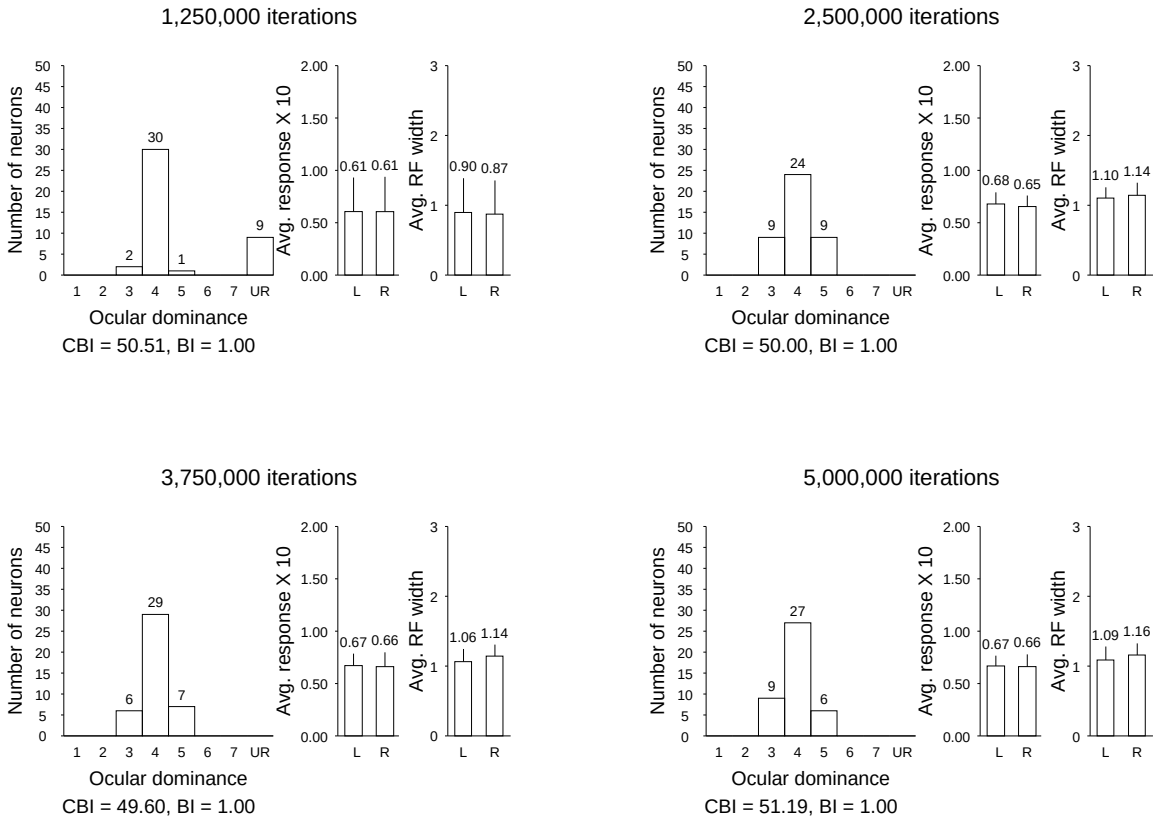

Figure 3.17: **OD during RE following BD.**
The parameters are given in Section 3.2.4, and the conventions are in Figure 3.1.

The EXIN rules also produced the following salient features of OD plasticity after MD, RS, ST, BD, and RE consistent with the experimental results reviewed in Section 3.1.

- OD shift toward the open eye after MD; model cortical neurons lost responsiveness to the closed eye and gained responsiveness to the open eye.
- OD shift toward the newly opened eye after RS; model cortical neurons lost responsiveness to the newly closed eye before gaining responsiveness to the newly opened eye.
- Loss of binocularity after ST; model cortical neurons became responsive exclusively to one of the eyes.
- Loss of responsiveness to both eyes without loss of binocularity, and loss of position

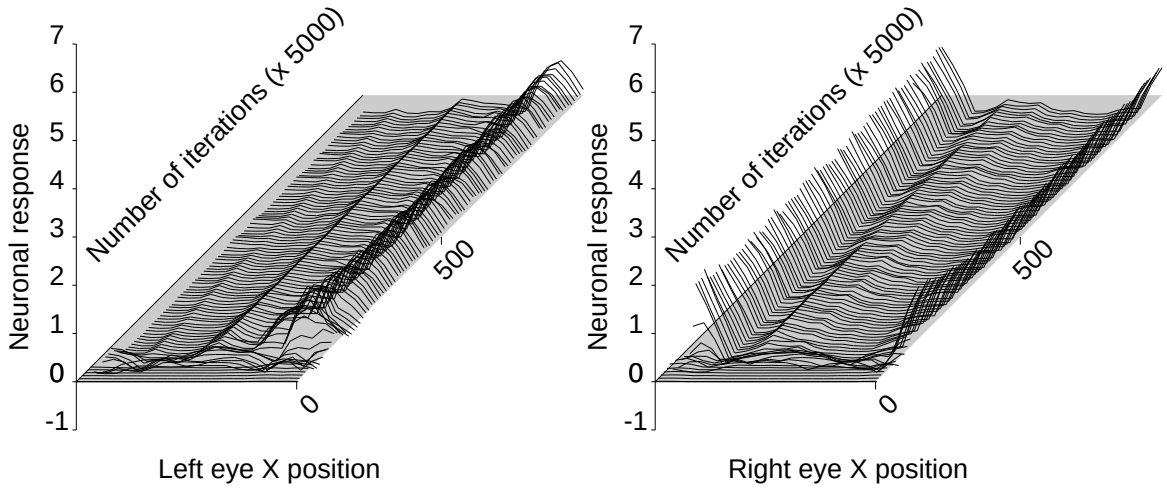

(a)

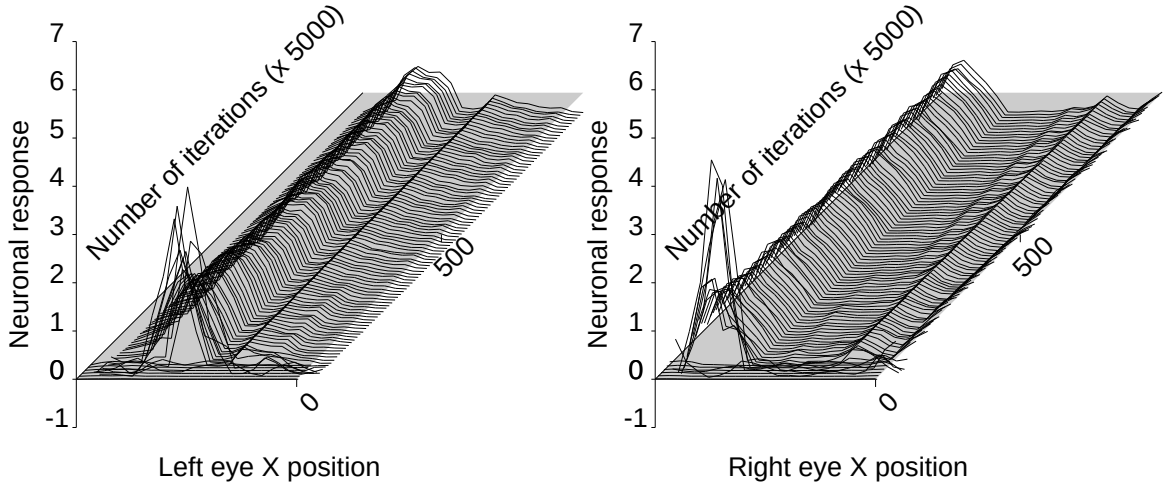

(b)

Figure 3.18: **Monocular RF changes during RE following BD.** The parameters are given in Section 3.2.4.

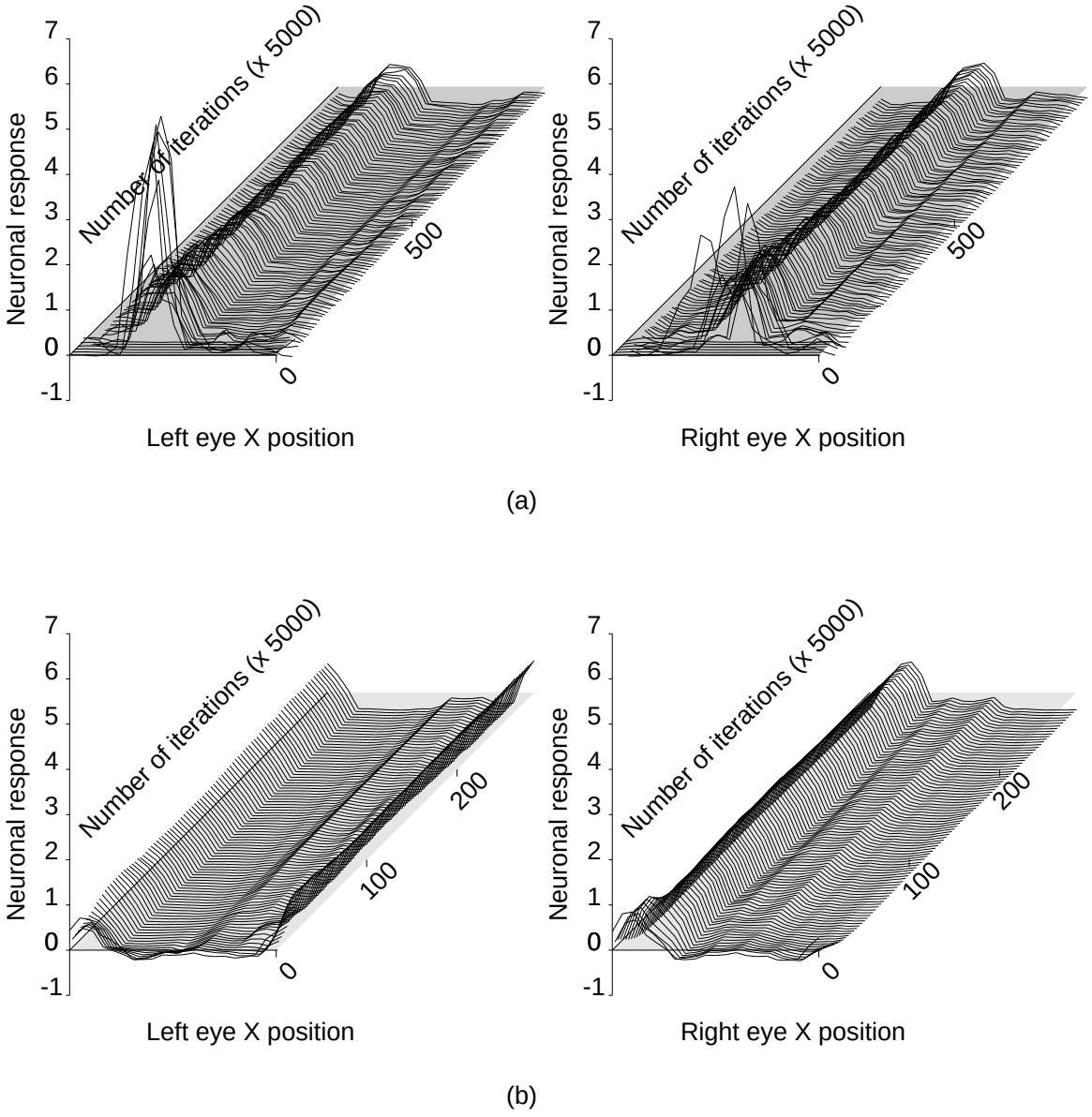

Figure 3.19: **Monocular RF changes during RE following prolonged BD and during NR.**
The figure shows the RF tuning of a model cortical neuron during RE following prolonged BD (a) and during NR (b). The neuron did not recover its original position selectivity after normal training following prolonged BD. The parameters are given in Section 3.2.4.

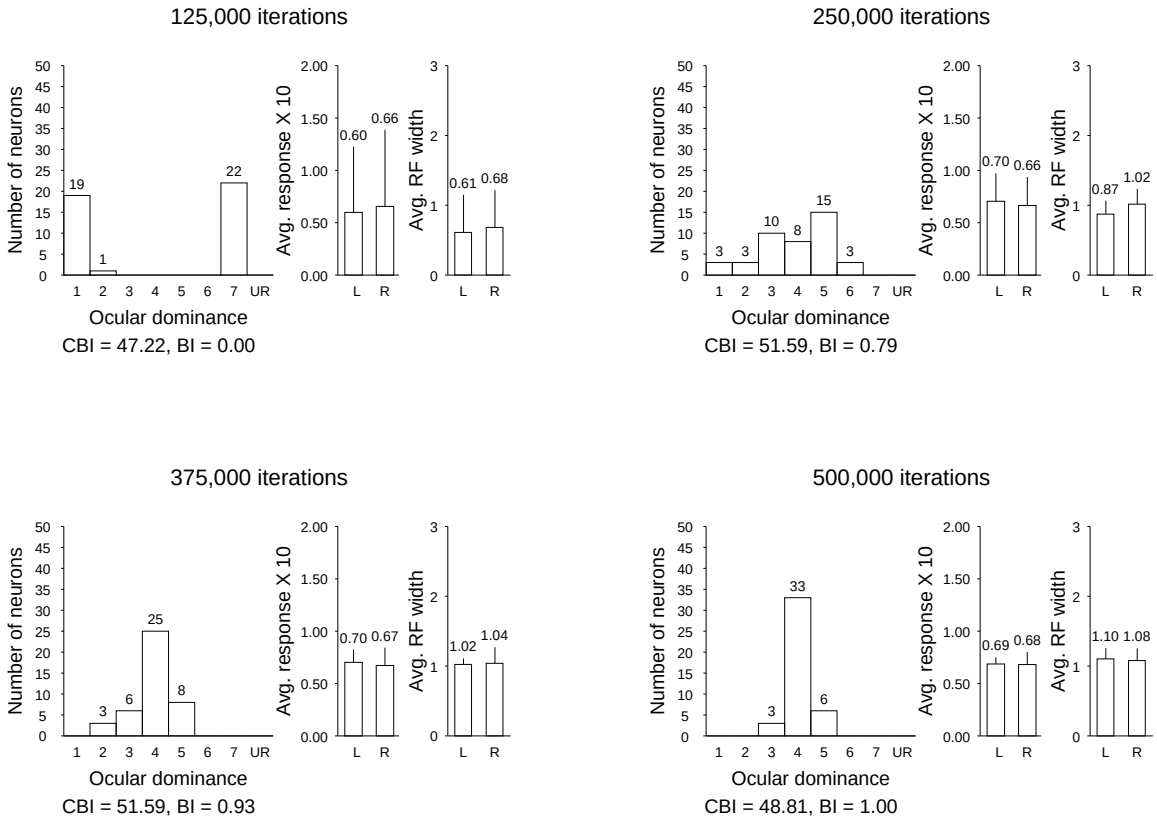

Figure 3.20: **OD during RE following ST.**
The parameters are given in Section 3.2.4, and the conventions are in Figure 3.1.

selectivity (i.e., increase in RF width) after prolonged BD.

- Restoration of OD distribution, responsiveness, and RF width after normal binocular stimulation following MD and BD. Model cortical neurons became selective to different positions after RE following prolonged BD.

In the EXIN model, OD changes during the classical rearing paradigms depend mainly on the afferent excitatory synaptic plasticity; the lateral inhibitory synaptic plasticity, however, is critical for the development of high input feature selectivity. As shown in Section 3.3.1, weak lateral inhibition produces model cortical neurons with low input feature selectivity, which in turn makes the model cortical neurons monocular. Furthermore, lateral inhibitory interactions produce secondary OD changes; when some model cortical

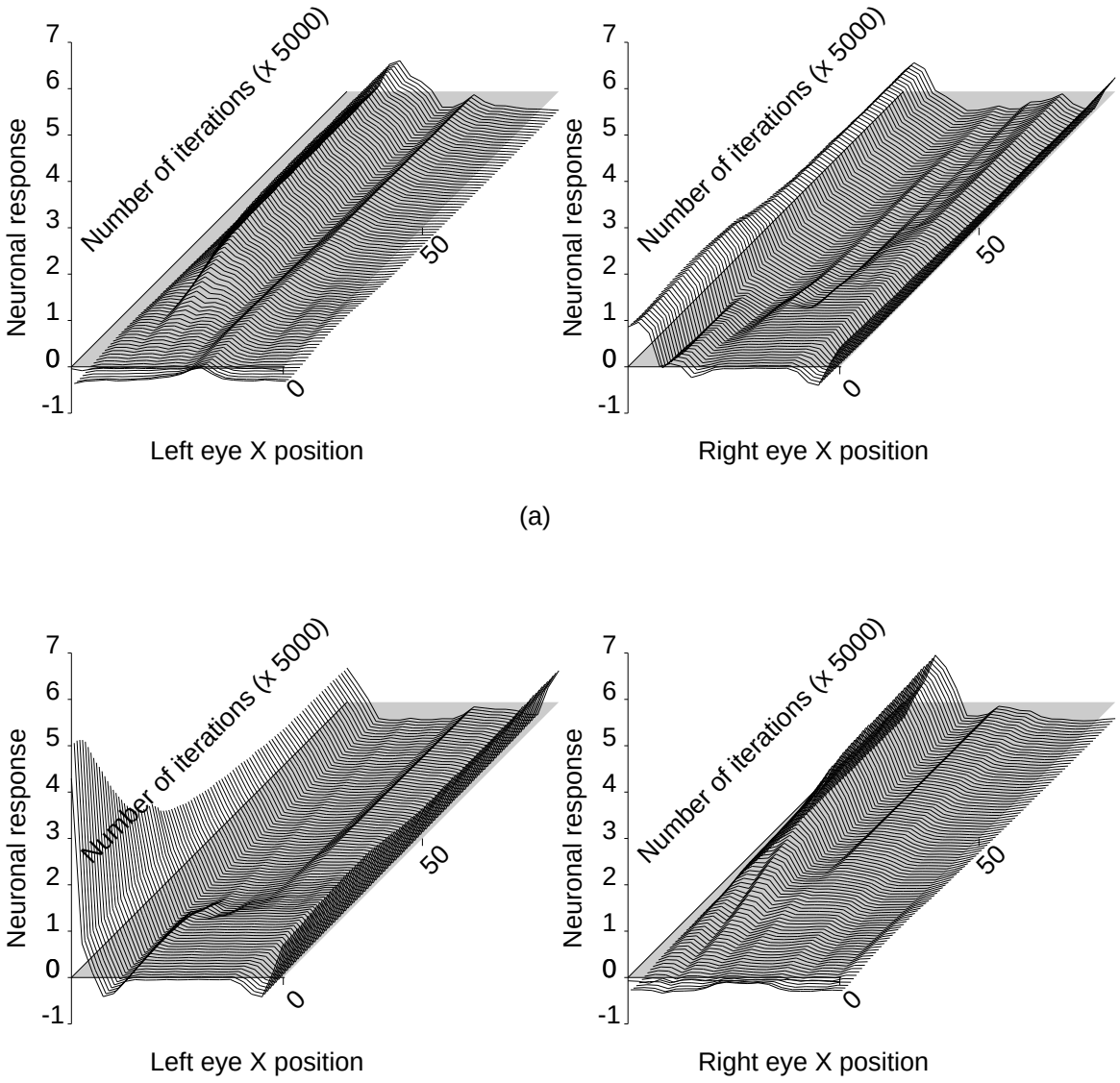

Figure 3.21: **Monocular RF changes during RE following ST.** The parameters are given in Section 3.2.4.

neurons become more responsive to one eye, the inhibitory interaction causes other neurons to become less responsive to that eye.

During NR, the correlation in the stimulation of corresponding locations in the two eyes affects the OD distribution. In the simulation, as the range of disparity in the left and right eye stimulation during binocular stimulation was increased, the correlation in the corresponding locations in the two eyes decreased, and model cortical neurons became less binocular. During MD, the OD shifted toward the open eye because of weakening of the afferent excitatory pathways from the closed eye to the model cortical neurons. In RS, OD shifted toward the newly opened eye because of weakening of afferent excitatory pathways from the newly closed eye to model cortical neurons and because of strengthening of afferent excitatory pathways from the newly opened eye to model cortical neurons. Lateral inhibitory interactions caused the OD of some model cortical neurons to shift toward the newly closed eye during RS, when some model cortical neurons became highly responsive to the newly opened eye. In ST, the stimulation patterns of corresponding positions in the two eyes were uncorrelated, and model cortical neurons became monocular because of the competitive afferent excitatory synaptic plasticity rule. During BD, the afferent excitatory synaptic plasticity rule was responsible for a reduction of responsiveness of model cortical neurons to both eyes, but the lateral inhibitory synaptic rule was responsible for weakening of position selectivity of the model cortical neurons. The afferent excitatory synaptic plasticity rule alone during BD reduced responsiveness and increased the position selectivity of model cortical neurons. Binocular stimulation following MD, BD, and ST restored the OD distribution, responsiveness, and receptive field width of model cortical neurons. The afferent excitatory synaptic plasticity rule restored the afferent excitatory pathway weights, and lateral inhibitory synaptic plasticity rule ensured high selectivity of the model cortical neurons.

3.4.1 Role of lateral inhibitory synaptic plasticity on neuronal feature selectivity

It has been proposed that several input feature selectivities depend on intracortical inhibition (Bonds & DeBruyn, 1985; Sillito, 1975, 1997, 1979; Somers et al., 1995;

Somogyi & Martin, 1985). The EXIN rules produce neurons with high selectivity and sparse distributed coding (Marshall, 1995a; Marshall & Gupta, 1998). In the EXIN model, strong lateral inhibitory pathways develop between neurons with overlapping receptive fields (Marshall, 1995a), consistent with experimental results suggesting that a neuron receives the strongest inhibition when the orientation of the input stimulus is the same as the neuron's preferred orientation (Blakemore & Tobin, 1972; Ferster, 1989), or when the position of the input stimulus is in the neuron's receptive field (DeAngelis et al., 1992).

In the EXIN model, position tuning and orientation tuning can change because of changes in either afferent excitatory pathway or lateral inhibitory pathway weight values. Weakening lateral inhibitory pathways in the model makes neurons more responsive to weak excitation; neurons can become more responsive to some of the less-preferred orientations or positions, leading to reduced orientation selectivity and position selectivity.

Hendry et al. (1990) reported a decrease in the density of $GABA_A$ receptors in ocular dominance columns corresponding to the closed eye in layer 4Cβ of adult monkey primary visual cortex after five or ten days of monocular deprivation. After monocular deprivation of adult cats, visual stimulation revealed a lack of lateral inhibitory interactions, which are seen in normal cortex, in the monocularly deprived cortex (Kasamatsu et al., 1998b). In neocortical cultures, blockade of spontaneous activity reversibly decreased the number of GABA-positive neurons, decreased GABA-mediated inhibition onto pyramidal neurons, and raised the firing rates of pyramidal neurons (Rutherford et al., 1997). The EXIN lateral inhibitory synaptic plasticity rule proposes weakening of inhibition to the inactive neurons, and it is therefore consistent with the above experimental results.

If prolonged BD also causes a decrease in GABA receptors and GABA-positive neurons during prolonged BD, the EXIN model provides an alternate explanation of the lack of recovery of binocularity of cortical neurons during normal binocular vision following prolonged BD (Cynader, 1983). Previously, it has been thought that long periods of BD produces eye misalignment and subsequent loss of correlated inputs to the two eyes when normal binocular vision is restored, leading to loss of binocularity (Cynader, 19983). If lateral inhibitory pathways remain weak during binocular vision after prolonged BD, cortical

neurons can become responsive to one of the eyes, as in the EXIN model with low inhibitory pathway weights (Figure 3.4).

3.4.2 Site of cortical OD plasticity

In this paper, cortical OD plasticity is modeled by plasticity in afferent excitatory and lateral inhibitory synapses. Changes in cortical OD can be induced by anatomical changes in the geniculocortical pathways (LeVay et al., 1980). However, there is also evidence that OD changes can be induced without a corresponding anatomical change in the geniculocortical projections, if MD is initiated late in the critical period (Wiesel, 1982). Furthermore, cortical OD plasticity can occur within four to eight hours (Freeman et al., 1981); the rapid OD plasticity suggests that OD plasticity may involve changes in the efficacy of individual cortical synapses. Responsiveness of cortical neurons to the deprived eye during MD can be restored by abolishing intracortical inhibition, thereby suggesting the involvement of lateral inhibitory interactions in OD plasticity (Sillito et al., 1981).

3.4.3 Comparison with other models of cortical OD plasticity

Previous models of OD plasticity (Clothiaux et al., 1991; Miller et al., 1989) are based on excitatory synaptic plasticity in geniculocortical pathways. Shouval et al. (1996) used the BCM afferent synaptic plasticity rule to show that misalignment of the two eyes causes model cortical neurons to become monocular. Sirosh and Miikkulainen (1997) used a self-organizing model with afferent excitatory, lateral excitatory, and lateral inhibitory synaptic plasticity rules, to model the development of ocular dominance columns and to study the relationship between the distribution of lateral excitatory and lateral inhibitory pathways and the ocular dominance and orientation selectivity of model cortical neurons. Sirosh and Miikkulainen (1997) showed that in their model, lateral pathways develop between cortical neurons with similar properties (e.g., orientation selectivity and ocular dominance).

The EXIN afferent excitatory synaptic plasticity rule differs from the rules used by Clothiaux et al. (1991) and Miller et al. (1989).

Clothiaux et al. (1991) used the BCM (Bienenstock et al., 1982) rule. According to the BCM rule, the synaptic weight of afferent pathways to cortical neurons varies as a product of input activity and a function (ϕ) of the postsynaptic response. For all postsynaptic responses greater than the spontaneous activation level but less than a modification threshold (θ), ϕ is negative; ϕ is positive when the postsynaptic activation exceeds θ. According to the BCM rule, an excitatory pathway synaptic weight is weakened only when the pathway receives input stimulation and the postsynaptic activation is less than θ and is strengthened only when the pathway receives input stimulation and the postsynaptic activation is greater than θ. The modification threshold θ varies as a non-linear function of the average postsynaptic activation (Bienenstock et al., 1982; Clothiaux et al., 1991).

An interesting feature of the BCM rule is that weakening of afferent excitatory pathways from the closed eye to a model cortical neuron during MD depends on the ratio of preferred to non-preferred open-eye patterns for the model cortical neuron (Clothiaux et al., 1991). According to the model in Clothiaux et al. (1991), if a single pattern is repeatedly presented to one eye with the other eye closed, the afferent excitatory pathways from both eyes will be strengthened; i.e., model cortical neurons will not lose responsiveness to the closed eye. In the EXIN model, however, model cortical neurons activated by the repeatedly presented pattern to the open eye weaken excitatory pathways from the closed eye because unstimulated/weakly stimulated pathways to active neurons weaken; thus, model cortical neurons lose responsiveness to the closed eye.

Miller et al. (1989) used an afferent excitatory synaptic plasticity rule that depends on the covariance in the presynaptic and postsynaptic activation. According to the rule, afferent excitatory pathways weaken if strong presynaptic activation is coincident with low postsynaptic activation, or if weak presynaptic activation is coincident with strong postsynaptic activation. An experiment in which the covariance-based rule used by Miller et al. (1989) and the EXIN rules produce different predictions is as follows. Suppress cortical activation without affecting presynaptic activation during normal binocular visual experience; cortical infusion of the $GABA_A$ agonist muscimol accomplishes this (Reiter & Stryker, 1988). According to the covariance-based rule, afferent excitatory

pathways from both the eyes would weaken, and therefore cortical neurons would lose responsiveness to both eyes. According to the EXIN model, afferent excitatory and lateral inhibitory synaptic plasticity is blocked by suppression of cortical activation, and therefore cortical neurons would remain responsive to both eyes.

The EXIN afferent excitatory and lateral inhibitory plasticity rules differ from those used by Sirosh and Miikkulainen (1997). Sirosh and Miikkulainen (1997) used a normalization based rule for afferent excitatory, lateral excitatory, and lateral inhibitory pathway synaptic plasticity. According to the normalization rule, when a postsynaptic neuron is active, active pathways to the neuron are strengthened, and inactive pathways to the neuron are weakened. However, if a postsynaptic neuron is active and all pathways of one kind (e.g., afferent excitatory, lateral inhibitory, or lateral excitatory) are inactive, the pathways do not undergo plasticity. In contrast, under the EXIN rules, inactive afferent pathways to active neurons weaken, while inactive lateral inhibitory pathways to inactive or active neurons do not undergo plasticity. According to Sirosh and Miikkulainen's normalization rule, active lateral inhibitory pathways to inactive neurons do not change, but according to the EXIN lateral inhibitory synaptic plasticity rule, active lateral inhibitory pathways to inactive neurons weaken.

During MD, the EXIN lateral inhibitory synaptic plasticity rule predicts weakening of lateral inhibitory pathways from active neurons, whose OD shifted toward the open eye, to neurons unresponsive during MD, i.e., monocular neurons responsive exclusively to the closed eye. In contrast, the lateral inhibitory synaptic plasticity rule in Sirosh and Miikkulainen (1997) predicts that lateral inhibitory pathways from the neurons unresponsive during MD to neurons whose OD shifted toward the open eye weaken.

Chapter 4

Plasticity in cortical neuron properties: Modeling the effects of an NMDA antagonist and a GABA agonist during visual deprivation

Abstract

Infusion of a GABA agonist (Reiter & Stryker, 1988) and infusion of an NMDA receptor antagonist (Bear et al., 1990), in the primary visual cortex of kittens during monocular deprivation, shifts ocular dominance toward the *closed* eye, in the cortical region near the infusion site. This *reverse* ocular dominance shift has been previously modeled by variants of a covariance synaptic plasticity rule (Bear et al., 1990; Clothiaux et al., 1991; Miller et al., 1989; Reiter & Stryker, 1988). Kasamatsu et al. (1997, 1998a) showed that infusion of an NMDA receptor antagonist in adult cat primary visual cortex changes ocular dominance distribution, reduces binocularity, and reduces orientation and direction selectivity. This chapter presents a novel account of the effects of these pharmacological treatments, based on the EXIN synaptic plasticity rules (Marshall, 1995), which include

both an instar afferent excitatory and an outstar lateral inhibitory rule. Functionally, the EXIN plasticity rules enhance the efficiency, discrimination, and context-sensitivity of a neural network's representation of perceptual patterns (Marshall, 1995; Marshall & Gupta, 1998). The EXIN model decreases lateral inhibition from neurons outside the infusion site (control regions) to neurons inside the infusion region, during monocular deprivation. In the model, plasticity in afferent pathways to neurons affected by the pharmacological treatments is assumed to be *blocked*, as opposed to previous models (Bear et al., 1990; Miller et al., 1989; Reiter & Stryker, 1988), in which afferent pathways from the open eye to neurons in the infusion region are *weakened*. The proposed model is consistent with results suggesting that long-term plasticity can be blocked by NMDA antagonists or by postsynaptic hyperpolarization (Bear et al., 1990; Dudek & Bear, 1992; Goda & Stevens, 1996; Kirkwood et al., 1993). Since the role of plasticity in lateral inhibitory pathways in producing cortical plasticity has not received much attention, several predictions are made based on the EXIN lateral inhibitory plasticity rule.

4.1 Introduction

Ocular dominance (OD) of primary visual cortical neurons in young animals is modified by visual deprivation within a critical period (Blakemore & Van Sluyters, 1974; Hubel & Wiesel, 1965, 1970; Hubel et al., 1977). Several models of afferent excitatory plasticity (e.g., Clothiaux et al., 1991; Miller et al., 1989) based on pre- and postsynaptic correlation and competition between left and right eye afferents have been proposed to account for these results. It has been hypothesized that NMDA receptors may serve to measure correlation in pre- and postsynaptic activity (Bear et al., 1987; Fox & Daw, 1993).

The primary visual cortex of kittens has been locally infused with an NMDA receptor antagonist (Bear et al., 1990) and a $GABA_A$ agonist (Reiter & Stryker, 1988) during monocular deprivation (MD), to determine the role of NMDA receptors and postsynaptic activation, respectively, in producing OD changes after MD. Some of the results of these experiments have been modeled by plasticity in afferent excitatory pathways (Bear et al., 1990; Reiter & Stryker, 1988).

In contrast to the models based on synaptic plasticity, Kasamatsu et al. (1997, 1998a) have proposed that changes in ocular dominance, binocularity, and orientation selectivity during MD with infusion of an NMDA receptor antagonist may be caused by aspecific action of the antagonist.

This chapter presents a novel account for the effects on OD of these pharmacological treatments during MD, based on the EXIN synaptic plasticity rules (Marshall, 1995) and suggests an account for changes in orientation selectivity during chronic dark rearing and the two pharmacological experiments. The EXIN rules consist of a Hebbian instar afferent excitatory synaptic plasticity rule (Grossberg, 1972), and an anti-Hebbian outstar lateral inhibitory synaptic plasticity rule (Marshall, 1995). Comparison of the predictions of the EXIN model and the previous rules can be used to design experiments to further elucidate the rules of cortical plasticity in developing cortex. Some experimental ideas are suggested in Section 4.5.2. It is hypothesized that the EXIN rules, which were developed from computational considerations (Marshall, 1990a, 1995; Marshall & Gupta, 1998), have a neurophysiological realization in the synaptic microcircuitry of cortical tissue and in the neuropharmacology of cortical plasticity.

4.1.1 Disruption of MD by pharmacological infusion

Reiter and Stryker (1988) locally infused muscimol, a GABA agonist selective for $GABA_A$ receptors, into the primary visual cortex of kittens during MD. Muscimol at strong concentrations blocked postsynaptic action potentials without affecting presynaptic activity. Bear et al. (1990) treated kitten primary visual cortex with D,L-2-amino-5-phosphonovaleric acid (APV) during MD. APV is an NMDA receptor antagonist. Visually evoked responses could be evoked during APV infusion at concentrations sufficient to block NMDA receptors (Bear et al., 1990). The salient results of these two experiments are: (1) in the untreated control regions and regions weakly affected by the pharmacological treatments, the OD distribution shifted toward the *open* eye; and (2) in regions in which neurons were completely inhibited by muscimol and in regions close to the APV infusion cannula where NMDA receptors are completely disabled, the OD distribution shifted toward the *closed* eye.

Bear et al. (1990) also reported a large increase in the number of neurons with reduced or eliminated orientation selectivity and reduced visual responsiveness close to the APV infusion site. Reiter and Stryker (1988) noted a small increase in the number of neurons with little or no orientation selectivity and reduced responsiveness. No specific rules have previously been proposed to model this loss of orientation selectivity. Bear et al. (1990) observed that the loss of orientation selectivity in their experiments was similar to that during chronic dark rearing (Frégnac & Imbert, 1984).

4.1.2 Aspecific effects of infusion of APV and muscimol

Kasamatsu et al. (1998a) measured ocular dominance during 33–48 hours of infusion of APV in primary visual cortex of adult cats. They found that APV infusion reduced responsiveness, orientation selectivity, and binocularity. After 10 hours of APV infusion in adult cats, the ocular dominance distribution was W-shaped, and average binocularity was low (Kasamatsu et al., 1998a). Normal ocular dominance distribution, binocularity, and responsiveness were restored within 68 hours after cessation of APV infusion (Kasamatsu et al., 1998a). Bear et al. (1990) reported reduced responsiveness in cortical neurons affected by APV.

Reiter and Stryker (1988) reported that cortical infusion of muscimol in kittens selectively blocked postsynaptic activity. It is not known whether muscimol infusion at low concentrations, at which postsynaptic activity is not completely blocked, changes ocular dominance distribution.

4.1.3 Previous models

Previous models of the effects of these pharmacological treatments during MD are based on several covariance rules (Bear et al., 1990; Clothiaux et al., 1991; Miller et al., 1989; Reiter & Stryker, 1988; Stanton & Sejnowski, 1989). These models propose homosynaptic LTD in the active afferent excitatory pathways from the open eye to the weakly active or inactive cortical neurons affected by the pharmacological treatments. The inactive afferent excitatory pathways from the closed eye to the weakly active or inactive cortical neurons are unaffected. These changes in the afferent excitatory pathways cause a

shift in ocular dominance to the closed eye after MD in the cortical region affected by the pharmacological infusions (Figure 4.1a).

Homosynaptic LTD has been observed in conditioned excitatory pathways to hyperpolarized neurons in hippocampus (Stanton & Sejnowski, 1989) and in visual cortex (Frégnac et al., 1994), although in some other preparations homosynaptic LTD could not be induced in the conditioned pathways to hyperpolarized neurons (Goda & Stevens, 1996). Several experiments have shown that homosynaptic LTD cannot be induced when NMDA receptors are antagonized (Bear et al., 1987, 1990; Dudek & Bear, 1992; Goda & Stevens, 1996; Kirkwood et al., 1993).

Kasamatsu et al. (1997, 1998a) suggested that aspecific action of APV on cortical neurons may contribute to changes in cortical properties. The loss of orientation selectivity in a large number of APV-affected neurons after MD with APV infusion (Bear et al., 1990) may be caused by the aspecific effects of some residual APV during orientation tuning measurement rather than by any specific synaptic plasticity (Kasamatsu et al., 1998a).

4.1.4 Significance and contributions of the chapter

In the EXIN model, in contrast to the previous models, homosynaptic LTD is assumed to be *blocked* by NMDA receptor antagonists and by postsynaptic hyperpolarization. OD shifts in the model cortical neurons affected by the pharmacological treatments occur because of lateral inhibitory interactions (Figure 4.1b). The proposed model uses plasticity in lateral inhibitory pathways in the development of cortical properties during normal rearing. A functional feature of the EXIN lateral inhibitory plasticity rule is that it enhances efficiency of representation by recruiting unused or under-used neurons (Marshall, 1995) in the presence of peripheral scotomas or lesions to represent some input information (Kalarickal & Marshall, 1997). The EXIN rules also produce neurons with high selectivity and sparse distribution coding (Marshall, 1995; Marshall & Gupta, 1998). It is hypothesized that anti-Hebbian outstar lateral inhibitory plasticity may be a general part of cortical development, and specific experiments to test the model's predictions are proposed.

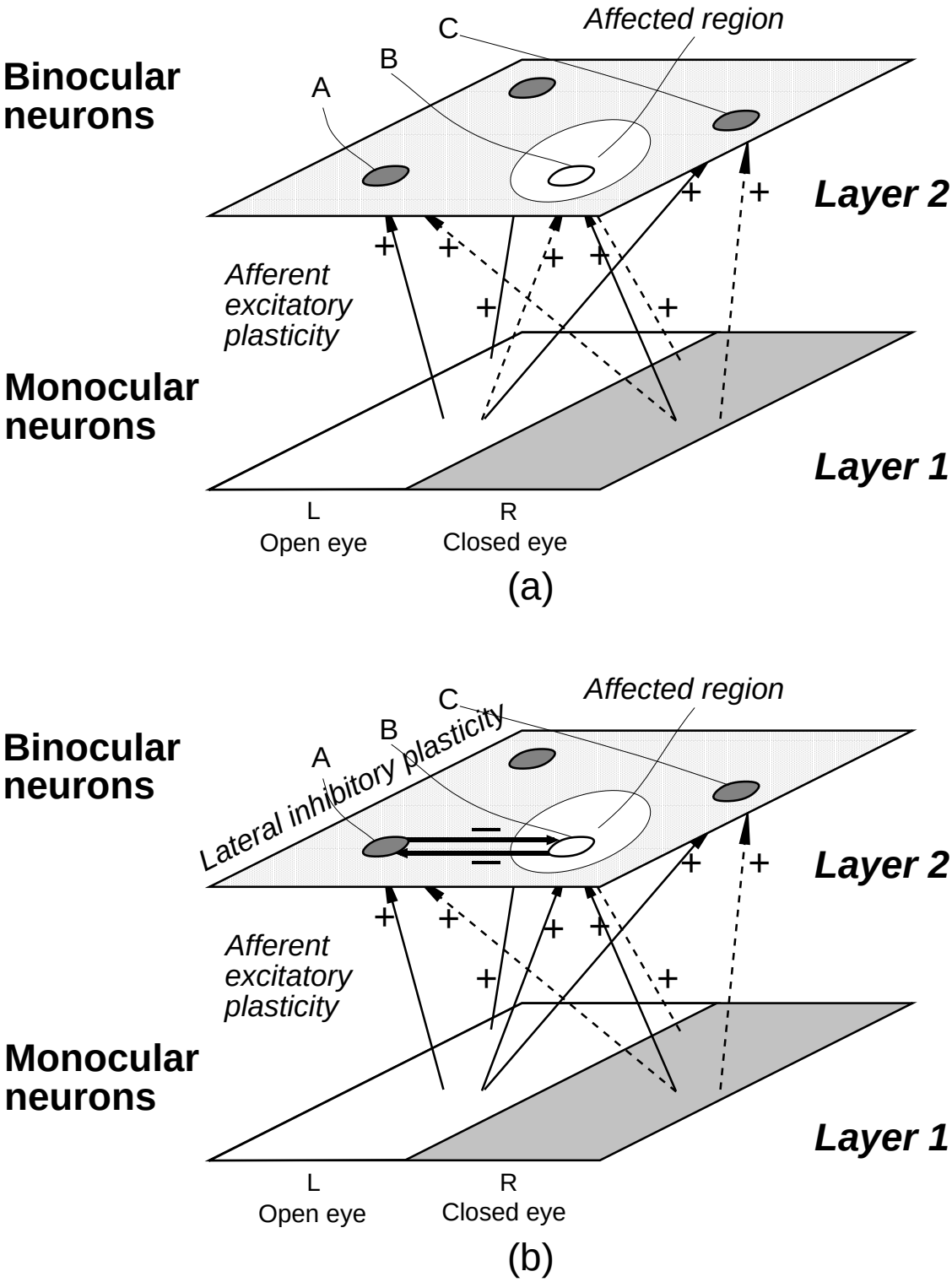

Figure 4.1: Legend on next page.

Figure 4.1: **Models OD changes.**
Figure on previous page. Layer 1 contains retinotopically arranged input neurons with monocular receptive fields. The monocular neurons project afferent excitatory pathways to layer 2 neurons, so that layer 2 neurons receive afferent pathways from both eyes. In the figure, the right eye is closed during MD with cortical infusion of muscimol or APV in the layer 2 region labeled "affected region;" the rest of the layer 2 is the "control region'." Neurons in the control region respond to stimulation in the left eye, and the activity of neurons in the affected region is blocked or is very weak. The dashed lines represent weakened afferent excitatory pathways. Panel (a) shows the basis for OD changes based on a covariance based afferent excitatory synaptic plasticity rule: afferent excitatory pathways from the unstimulated right eye to active neurons in the control region (e.g., neurons A and C) weaken, and afferent excitatory pathways from the stimulated left eye to inactive neurons in the affected region (e.g., neuron B) also weaken. Afferent excitatory pathways with correlated pre- and postsynaptic activity (e.g., stimulated afferent excitatory pathways from the open eye to active neurons in the control region and unstimulated afferent excitatory pathways from the closed eye to inactive neurons in the affected region) do not undergo synaptic plasticity. Thus, the OD of neurons in the control region shifts towards the open eye, and the OD of neurons in the affected region shifts towards the closed eye. Panel (b) shows the basis for OD changes based on the EXIN model. In the EXIN model, lateral inhibitory pathways develop most strongly between neurons receiving afferent excitation from common input neurons (e.g., between neurons A and B, but not between neurons A and C). In the EXIN model, plasticity in afferent excitatory pathways to neurons in the affected region is assumed to be blocked. The EXIN afferent excitatory plasticity rule weakens afferent excitatory pathways from the closed right eye to active neurons in the control region. Thus, neurons in the control region (neurons A and C) lose responsiveness to the closed eye, and their OD shifts towards the open eye. The afferent excitatory pathways to neurons in the affected region (e.g., neuron B) do not change. Because the response of neurons in the control region to open eye stimulation is much greater than their response to the closed eye, neuron B in the affected region receives greater inhibition during open eye stimulation than during closed eye stimulation. Thus, neuron B responds more strongly to closed eye stimulation than to open eye stimulation, and its OD shifts towards the closed eye.

4.2 EXIN model of changes in cortical properties

We have formulated and tested a neural network model that exhibits changes in cortical properties (OD, neuronal responsiveness, positional selectivity) similar to those observed experimentally. The model uses the EXIN (excitatory+inhibitory) plasticity rules (Marshall, 1995).

It has been proposed that several input feature selectivities depend on intracortical inhibition (Bonds & DeBruyn, 1985; Sillito, 1979; Somers et al., 1995; Somogyi & Martin, 1985). In the EXIN model, position tuning and orientation tuning can change because of changes in either afferent excitatory or lateral inhibitory weights. Weakening of lateral inhibitory pathways in the model makes neurons more responsive to weak excitation; neurons can become more responsive to some of the less-preferred orientations or positions, leading to reduced orientation selectivity or position selectivity. It is hypothesized that changes in lateral inhibition that underlie position selectivity in the simulations also underlie changes in orientation selectivity observed experimentally (Bear et al., 1990; Kasamatsu et al., 1998a; Reiter & Stryker, 1988).

4.2.1 The EXIN plasticity rules

The EXIN lateral inhibitory plasticity rule

The EXIN lateral inhibitory synaptic plasticity rule (Marshall, 1995) is an anti-Hebbian outstar synaptic plasticity rule. Changes of the weight Z_{ij}^{-} of the lateral inhibitory pathway from neuron i to neuron j are governed by

$$\frac{d}{dt} Z_{ij}^{-} \;=\; \delta \mathcal{G}(x_i) \left(-Z_{ij}^{-} + \mathcal{Q}(x_j) \right), \tag{4.1}$$

where $\delta > 0$ is a small plasticity rate constant, x_i and x_j are the activations of neurons i and j, respectively, and $\mathcal{G}$ and $\mathcal{Q}$ are half-rectified non-decreasing functions with some noise (Appendix B, Section B.6). Thus, *whenever a neuron is active, its output inhibitory connections to other active neurons tend to become slightly stronger (i.e., more inhibitory), while its output inhibitory connections to inactive neurons tend to become slightly weaker*. This rule is called an outstar rule (Grossberg, 1972) because the *pre*synaptic activation (x_i)

controls the *rate* of synaptic plasticity, and the *post*synaptic activation (x_j) determines the target value for the weight. In an instar rule (Grossberg, 1972) the subscripts of x_i and x_j would be interchanged.

According to this rule, the weight of the lateral inhibitory pathways between two neurons is a function of the coactivation of the neurons (Marshall, 1995). Thus, neurons with overlapping and similar receptive fields acquire strong reciprocal lateral inhibitory pathways, consistent with experimental results based on intracellular recordings of inhibitory postsynaptic potentials (Ferster, 1989; Gil & Amitai, 1996). This leads to improved discrimination and to sparse distributed coding (Marshall, 1995; Sirosh et al., 1996).

The EXIN afferent excitatory plasticity rule

The afferent excitatory pathway weight changes in the EXIN model are governed by an instar excitatory synaptic plasticity rule. The rule can be expressed (Grossberg, 1982; Marshall, 1995) as

$$\frac{d}{dt}Z_{ij}^{+} = \epsilon \mathcal{F}(x_j)\left(-Z_{ij}^{+} + \mathcal{H}(x_i)\right), \tag{4.2}$$

where Z_{ij}^{+} is the afferent excitatory weight from neuron i to neuron j, $\epsilon > 0$ is a small synaptic plasticity rate constant, $\mathcal{F}$ and $\mathcal{H}$ are half-rectified non-decreasing functions with some noise (Appendix B, Section B.6). Thus, *whenever a neuron is active, its input excitatory connections from active neurons tend to become slightly stronger, while its input excitatory connections from other inactive neurons tend to become slightly weaker.* This rule is called an instar rule (Grossberg, 1972) because the *pre*synaptic activation (x_i) determines the *target value* for the weight, and the *post*synaptic activation (x_j) controls the synaptic plasticity rate.

The afferent excitatory synaptic weight becomes stronger or weaker depending on whether $\mathcal{H}(x_i)$ is currently greater than or less than the synaptic weight Z_{ij}^{+} (see Equation 4.2). This behavior of Equation 4.2 is consistent with homosynaptic potentiation and depression (Dudek & Bear, 1992; Kalarickal & Marshall, 1996c).

The EXIN excitatory synaptic plasticity rule is a competitive learning rule. It causes each modeled cortical neuron to become selective for a specific pattern of input

activations (Grossberg, 1982; Marshall, 1995). Like other competitive learning rules, the EXIN rules do not produce absolutely stable fixed points. The stability of the network depends on the input environment and the rate of synaptic plasticity (Marshall, 1995). If the input distribution changes for a sufficiently long time, the weights change to encode the new statistics. Empirically, the EXIN synaptic plasticity rules are very stable in a stationary input environment (Marshall, 1995).

Applications of the EXIN rules

The EXIN rules have previously been used to model motion selectivity and grouping (Marshall, 1990a), visual inertia (Hubbard & Marshall, 1994), motion integration in the aperture problem (Marshall, 1990a), length selectivity and end-stopping (Marshall, 1990b), depth perception from occlusion events (Marshall & Alley, 1993; Marshall et al., 1996a), depth from motion parallax (Marshall, 1989), motion unsmearing (Martin & Marshall, 1993), orientation selectivity (Marshall, 1990d), stereomatching (Marshall et al., 1996b), long-term potentiation and long-term depression (Kalarickal & Marshall, 1996c), dynamic receptive field changes produced by artificial scotoma conditioning (Kalarickal & Marshall, 1997; Marshall & Kalarickal, 1997), and changes in somatosensory cortical RF topography after intracortical microstimulation (Kalarickal & Marshall, 1998b). The explanation for the effects of the pharmacological treatments during MD based on the EXIN rules is presented in Section 4.2.3.

4.2.2 The activation rule

The activation level x_j of each modeled cortical neuron is governed by a shunting equation (Grossberg, 1972) based on the Hodgkin model (Hodgkin, 1964):

$$\frac{d}{dt}x_j \;=\; -Ax_j \;+\; \beta(B - x_j)E_j \;-\; \gamma(C + x_j)I_j, \tag{4.3}$$

where A, B, C, β, and γ are positive constants. E_j represents the neuron's total excitatory signal

$$E_j = \left(\sum_{i \,\in\, \text{Model input layer}} [x_i] Z_{ij}^{+} \right)^2, \tag{4.4}$$

and I_j represents the neuron's total inhibitory signal

$$I_j = \sum_{k \in \text{ Model cortical layer}} [x_k] Z^-_{kj}, \tag{4.5}$$

where $[a] \equiv \max(a, 0)$. Because Equation 4.3 is a shunting equation, $x_j(t) \in [-C, B]$ for all $t \geq 0$ if $x_j(0) \in [-C, B]$ (Cohen & Grossberg, 1983). Thus, B is the maximum activation level and $-C$ is the minimum activation level of Layer 2 neurons. The constant A determines the passive decay rate. Parameters β and γ control the amount of excitation and inhibition, respectively, received by a model cortical neuron. The squaring in Equation 4.4 helps to contrast-enhance the input signal. The parameters of the activation equation were chosen so that the network would give a distributed activation response to an input, instead of a winner-take-all response. Also, the strength of inhibitory interaction was chosen so that weak afferent excitatory pathways to model cortical neurons would be ineffective in activating neurons. Thus, receptive field changes occur when lateral inhibitory pathway weights change.

The activation equation was computed using the Euler method. The stability of the activation equation was established empirically by observing the model's behavior under different Euler time step sizes. The step size and the number of steps were chosen so that the model cortical neuronal activations would be close to a stable state and there would be no oscillations. The parameters used in the simulations are presented in the Appendix B.

4.2.3 Explanation based on the EXIN plasticity rules

During MD in the presence of modeled muscimol or APV, the following synaptic modifications occurred in the EXIN model:

1. The synaptic weight of afferent pathways to neurons strongly affected by muscimol and APV was almost unaffected: model APV blocked model excitatory synaptic modifications ($\epsilon = 0$ in Equation 4.2), and muscimol prevented postsynaptic activation ($x_j \leq 0$). The only excitatory synaptic modifications were caused by noise and were small (see f and g in the Appendix B).

2. The weight of afferent pathways from the *closed* eye to neurons in the control regions was substantially *weakened* ($h(x_i) \approx 0$ for the closed eye), and the weight of afferent pathways from the *open* eye to neurons in the control regions were slightly *strengthened* (because of increased correlation between presynaptic activation from the open eye and the postsynaptic cortical neuron activations).

3. Lateral inhibitory weights between neurons in the control regions weakened (Equation 4.1), because neuronal responses to monocular stimulation during MD are less than neuronal responses to binocular stimulation during normal rearing (NR).

4. Because muscimol prevents postsynaptic activation ($x_j \leq 0$), lateral inhibitory pathways from neurons in the control regions ($x_i > 0$) to those inactivated by muscimol weakened ($q(x_j) = 0$ and $g(x_i) > 0$ in Equation 4.1). However, lateral inhibitory pathways from neurons inactivated ($x_i \leq 0$) by muscimol to other neurons changed very little.

5. Although APV does not block postsynaptic activity, it decreases activation levels. Thus, the weight of lateral inhibitory pathways to and from neurons affected by APV decreased.

After MD with muscimol and APV, the model cortical neurons in the control regions responded very weakly to closed eye stimulation compared to open eye stimulation. Thus, the OD of neurons in the control regions shifted toward the open eye. In addition, the control region neurons inhibited the neurons in the infusion site less strongly during closed eye stimulation than during the open eye stimulation. Therefore, neurons in the infusion site showed greater responsiveness to the closed eye than to the open eye, and the OD distribution shifted toward the closed eye (Figure 4.1b). A mechanism based on decrease in inhibition via weakening in afferent excitatory pathways has been proposed by Sirosh et al. (1996) to model receptive field shifts and expansions after artificial scotoma conditioning in adult cats (Pettet & Gilbert, 1992).

4.3 Methods

4.3.1 Initial network structure

We simulated a 1-D patch of 42 model primary visual cortical neurons, receiving inputs from corresponding epipolar lines in the two eyes. The simulated input layer contained 7 monocular neurons each for the two eyes. The neurons in the input layer of the model were selective for different positions along the epipolar lines and were topographically arranged. Topographic neighborhood relationships were arranged in a ring to eliminate boundary effects from the simulations. Orientation selectivity was not modeled in this 1-D network.

A network with initially nonspecific connection weights was trained with stimuli containing a range of disparities and with a small amount of pre- and postsynaptic activation noise to develop neurons with a normal ocular dominance distribution. The pre- and postsynaptic noise modeled spontaneous activity in the neurons. This training phase modeled a period of normal rearing (NR) of the visual cortex during the early postnatal days. The simulation details are in the Appendix B.

4.3.2 Pharmacological manipulations

APV application was simulated by multiplicatively weakening the afferent excitatory input signal to a neighborhood of 21 model cortical neurons. These affected neurons were surrounded by the remaining unaffected 21 neurons. Furthermore, the afferent excitatory synaptic plasticity rate, ϵ in Equation 4.2, was varied to model blocking of cortical LTP and LTD by APV (Kirkwood et al., 1993). The excitatory input to the affected neurons was computed by

$$E_j \;=\; \omega \times \left(\sum_{i \,\in\, \text{Model input layer}} [x_i] Z_{ij}^{+} \right)^2 , \tag{4.6}$$

where $\omega \in [0, 1]$ weakens afferent excitation, as caused by model APV. In the simulation, ω was inversely related to the APV concentration. APV concentration was characterized by the afferent excitation blocking strength of APV, which was $(1 - \omega)$. The excitatory input to neurons in the control region was computed by Equation 4.4.

Infusion of muscimol was modeled by applying strong inhibition to a neighborhood of 21 model cortical neurons surrounded by the other 21 neurons, which were unaffected. The neurons affected by muscimol received an additional amount $\Im > 0$ of inhibition. Thus, inhibition to the affected neurons was

$$I_j = \sum_{k \in \text{ Model cortical layer}} [x_k] Z^-_{kj} + \Im. \tag{4.7}$$

In the pharmacological experiments, APV or muscimol was continuously infused during MD to achieve a steady concentration of APV or muscimol, and cortical properties were assayed after allowing APV or muscimol to dissipate (Bear et al., 1990; Reiter & Stryker, 1988). Therefore, in the simulations ω and $\Im$ were kept fixed during MD, and model cortical properties were determined at a reduced concentration of model APV and muscimol.

4.3.3 Simulation procedure

During NR, 1,500,000 presentations of binocular stimuli containing a range of disparities and containing small amounts of pre- and postsynaptic noise were made. To simulate MD, 75,000 presentations of monocular stimuli with small amounts of pre- and postsynaptic noise were made. The simulation details are presented in the Appendix B.

4.3.4 Measures of cortical properties

OD histograms were plotted according to the seven-point scale of Hubel and Wiesel (1962). The model cortical neurons were assigned to an OD group as follows. Let $x_{i,l}$ and $x_{i,r}$, respectively, be the maximal response of neuron i to stimulation of left and right eye selective model input layers, and

$$D = \frac{x_{i,l} - x_{i,r}}{x_{i,l} + x_{i,r}}. \tag{4.8}$$

Then the neuron is assigned to group 1 if $1 \geq D > 0.80$, group 2 if $0.80 \geq D > 0.35$, group 3 if $0.35 \geq D > 0.05$, group 4 if $0.05 \geq D > -0.05$, group 5 if $-0.05 \geq D > -0.35$, group 6 if $-0.35 \geq D > -0.80$, and group 7 if $-0.80 \geq D \geq -1$.

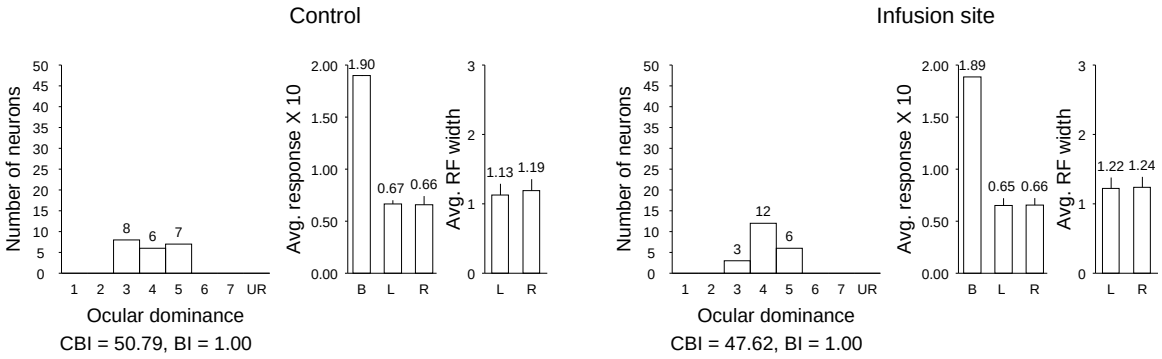

Figure 4.2: **Model OD distribution before MD.**
B represents binocular inputs, and L and R represent left and right eye monocular inputs. Average response is the average maximal responsiveness over all neurons in a region. UR represents the number of unresponsive neurons. The vertical lines on the bars represent the standard deviation. The control region represents neurons unaffected by APV or muscimol in the simulation of MD with APV or muscimol, and the infusion site represents neurons affected by APV or muscimol.

Changes in OD were expressed by a contralateral bias index (CBI)

$$\text{CBI} = \frac{100\left((N_1 - N_7) + (2/3)(N_2 - N_6) + (1/3)(N_3 - N_5) + N\right)}{2N}, \tag{4.9}$$

where N_i represents the number of neurons in OD group i, and N is the total number of visually responsive neurons (Reiter & Stryker, 1988). The fraction of binocular neurons was measured by the binocularity index (BI)

$$\text{BI} = \frac{N_3 + N_4 + N_5}{N} \tag{4.10}$$

(Bear et al., 1990).

The receptive field width of left and right eye RFs of model cortical neurons were measured by width at half-height. Positional selectivity is the reciprocal of RF width.

4.4 Results

Simulated changes in cortical properties caused by various pharmacological manipulations are presented in this section. Figure 4.2 shows some properties of the model

cortical neurons after the initial normal rearing.

4.4.1 Aspecific effects of pharmacological treatments

This subsection shows that the EXIN model produces changes in cortical properties under the aspecific action of APV or muscimol. A neighborhood of 21 neurons was affected by model APV or muscimol.

Aspecific effects of APV

Figure 4.3 shows the effects of the model APV infusion on ocular dominance, binocularity, responsiveness, and RF width without any synaptic plasticity. In the APV-affected model cortical region, increasing model APV concentration reduces responsiveness of the neurons because afferent excitation is reduced. Increasing model APV concentration also reduces binocularity. The OD distribution changes from the initial $\cap$-shape to W-shape, and then to U-shape, with a progressive reduction in binocularity and an increase in the number of unresponsive neurons.

OD is caused by the combined action of afferent excitation and lateral inhibition. In the model, a neuron can be binocular, although the left and right eye afferent pathways to the neuron may not be equally strong. Increasing model APV concentration eventually renders the weaker afferent pathways from one of the eyes ineffective, thus making the neuron strongly monocular.

In the model, the average RF width of the APV-treated model neurons decreases with increase in model APV concentration (Figure 4.3). The stronger APV makes the weak afferents ineffective, thereby reducing RF width.

Properties of model cortical neurons not treated by APV also changed. There is a decrease in the number of neurons in OD group 4, and their average responsiveness increases. As neurons affected by model APV become less responsive, they exert less inhibition on neurons in the control region. When $\omega = 0.2$, six (out of 21) control neurons showed an increase in their left eye RF width. The initial average width changed from 1.0 to 1.33, and one (out of 21) control neuron showed an increase in its left eye RF width. The initial average width changed from 1.0 to 1.67. This shows that decreased

responsiveness of APV-affected neurons increases RF width (reduces position selectivity) of some neurons unaffected by APV. The loss of orientation selectivity in some neurons observed by Kasamatsu et al. (1998a) could be caused by reduced inhibition to neurons less affected by APV from neurons rendered unresponsive by APV.

When lateral inhibitory plasticity was enabled during infusion of APV during NR, the responsiveness, RF width, and BI of APV-affected model neurons increased (Figure 4.4a). These effects were caused by weakening of lateral inhibitory inhibitory pathways to the APV-affected neurons. Figure 4.4b shows the model cortical properties when measured without any residual APV. The average responsiveness and RF width of the APV-treated neurons increased by a small amount.

Aspecific effects of muscimol

In the model, infusion of muscimol was modeled by increasing inhibition to the affected neurons without any synaptic plasticity, thereby reducing their responsiveness, and eventually completely blocking model cortical activity (Figure 4.5). As the concentration of model muscimol infusion was increased, responsiveness, binocularity, and RF width of the affected model neurons became reduced (Figure 4.5). Model neurons in the control region showed effects similar to those during model APV infusion.

With both afferent excitatory and lateral inhibitory plasticity during model muscimol infusion, the network showed effects (Figure 4.6) similar to those during model APV infusion with only lateral inhibitory plasticity.

4.4.2 Effects of pharmacological treatments during MD

The effects of model pharmacological treatments during model MD were assessed at different residual concentrations of model APV and muscimol. This revealed the contributions of synaptic plasticity and of the aspecific effects of model APV and muscimol to changes in cortical properties. In the model, presence of APV or muscimol enhanced shifts in the OD distribution.

Cortical infusion of muscimol blocks postsynaptic activation without affecting presynaptic activation (Reiter & Stryker, 1988). Some experimental data suggest that

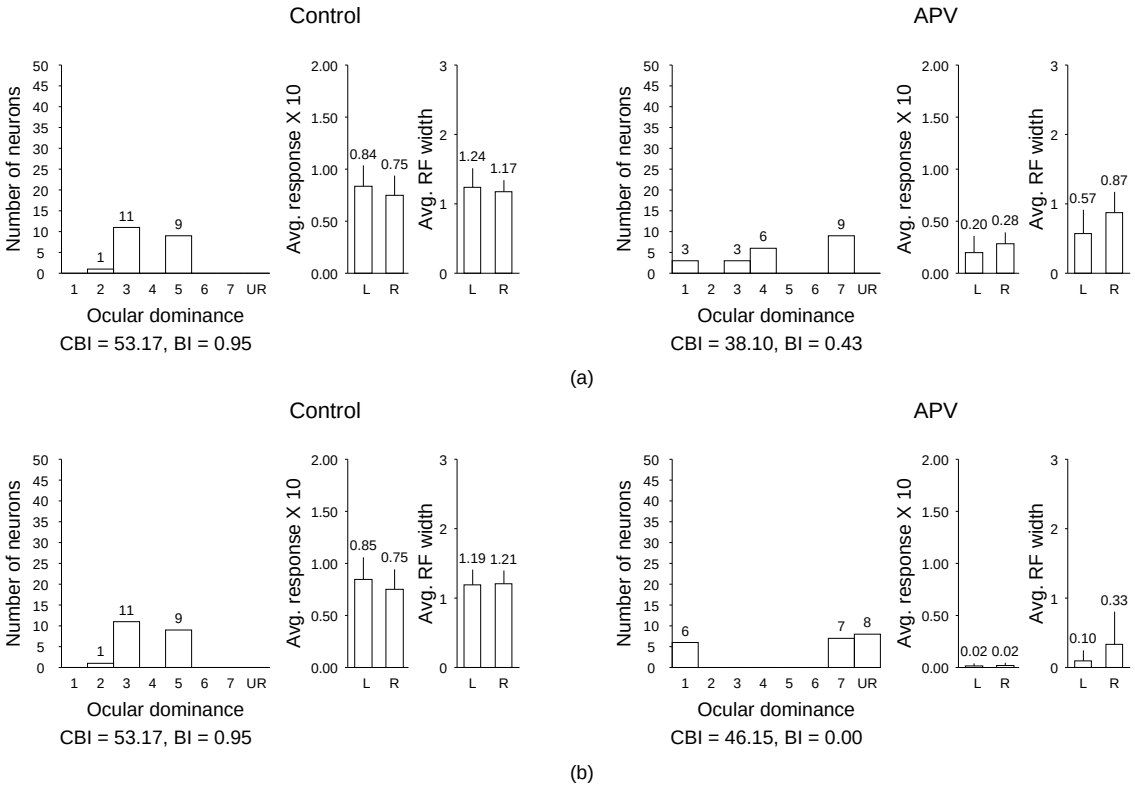

Figure 4.3: **Aspecific effects of APV.**
In these simulations, synaptic plasticity rules were not enabled. The strength of APV in the model was inversely proportional to ω. In (a) $\omega = 0.6$, and in (b) $\omega = 0.2$. As ω was decreased, i.e., afferent excitation was weakened, model cortical layer binocularity, responsiveness, and RF width decreased. See Figure 4.2 for conventions.

postsynaptic activation is necessary for excitatory synaptic plasticity and OD plasticity (Goda & Stevens, 1996; Rauschecker & Singer, 1979). On the other hand, APV blocks NMDA receptors without necessarily blocking neuronal responsiveness to visual stimulation (Bear et al., 1990). It has been hypothesized that NMDA receptors subserve long-term plasticity in excitatory synapses (Bear et al., 1987; Dudek & Bear, 1992; Kirkwood et al., 1993) and may be involved in visual cortical plasticity (Fox & Daw, 1993). In the model, strong muscimol concentration blocks postsynaptic activity and therefore disables plasticity in afferent excitatory pathways to the muscimol-affected neurons and in lateral inhibitory pathways from the muscimol-affected neurons. On the other hand,

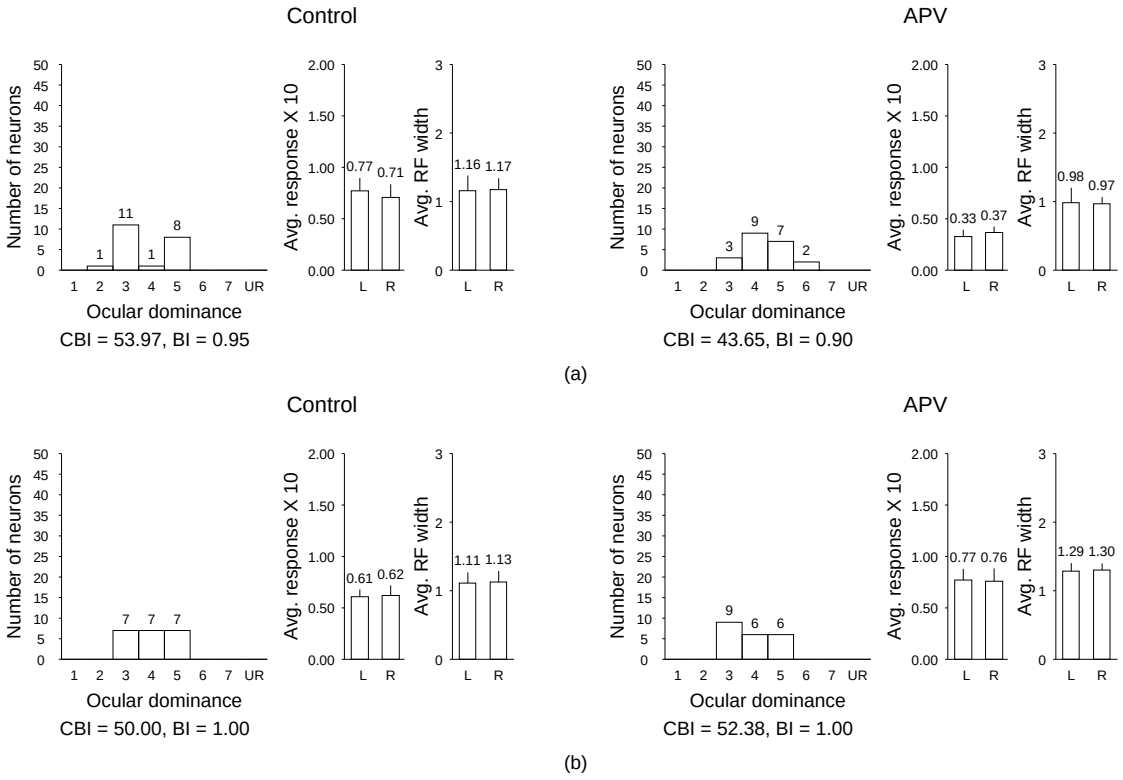

Figure 4.4: **Aspecific effects of APV with lateral inhibitory plasticity.** OD was measured after 500,000 presentations of binocular inputs (NR) with $\omega = 0.6$ and with only lateral inhibitory plasticity. APV is assumed to have blocked afferent excitatory plasticity. RF properties were measured with $\omega = 0.6$ in (a) and with $\omega = 1$ (i.e., zero residual APV) in (b). See Figure 4.2 for conventions.

in the model, APV is assumed to block plasticity in afferent excitatory pathways to the APV-affected neurons with reduced afferent excitation. Since APV-treated neurons are activated during MD in the model, plastic changes in lateral inhibitory pathways from the APV-treated neurons can occur.

In the simulations, MD with APV or muscimol were similar in that afferent excitatory pathways to the affected neurons were blocked and reverse OD shift in APV- or muscimol-affected neurons was observed (Section 4.4.2, *Changes in ocular dominance*). However, plasticity in lateral inhibitory pathways from muscimol-treated neurons was blocked, and plasticity in lateral inhibitory pathways from APV-treated

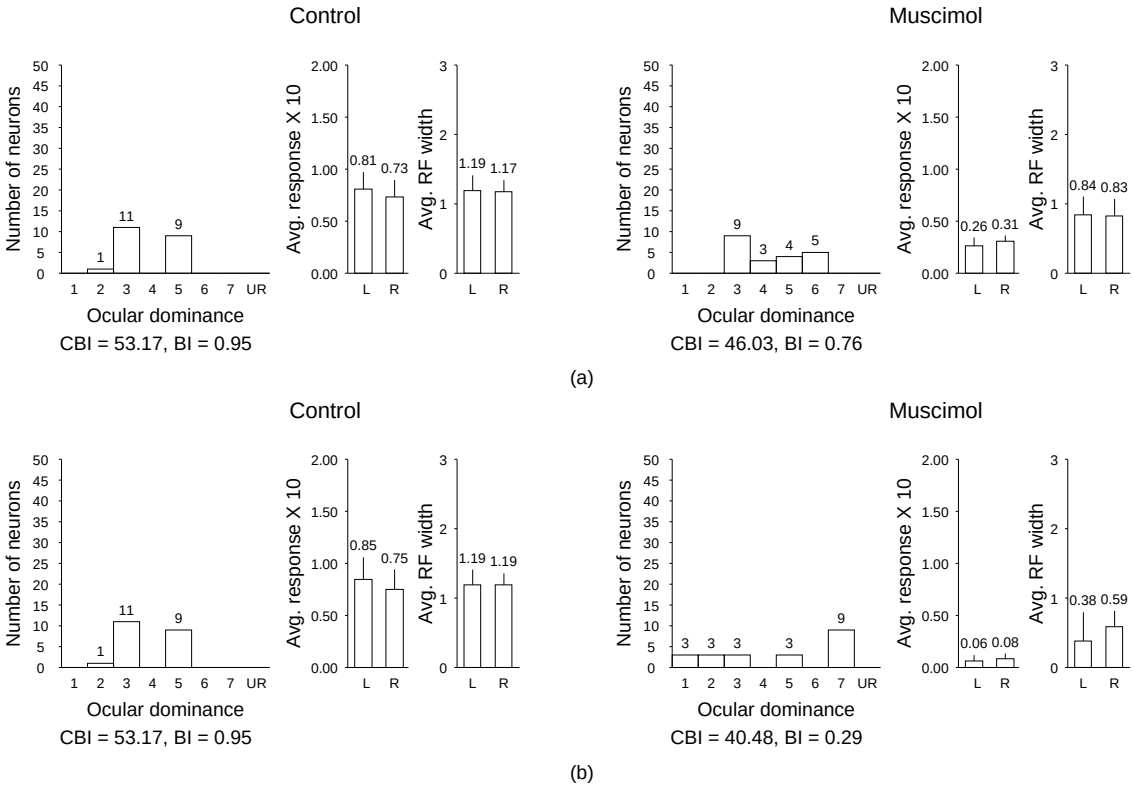

Figure 4.5: **Aspecific effects of muscimol.**
In these simulations, EXIN plasticity rules were not enabled. The strength of muscimol is directly proportional to $\Im$. In (a) $\Im = 0.05$, and in (b) $\Im = 0.1$. As $\Im$ was increased model cortical layer binocularity, responsiveness, and RF width decreased. See Figure 4.2 for conventions.

neurons was not blocked. This difference resulted in almost no loss of position selectivity in muscimol-treated neurons and a significant loss of position selectivity in APV-treated neurons (Section 4.4.2, *Changes in RF width*).

Changes in ocular dominance

Figures 4.7a and 4.9a present the modeled changes in OD after MD with APV and muscimol, respectively. In these figures, the residual concentration of APV and muscimol was half the concentration of APV and muscimol during model MD. In both these simulations, the OD of the control region shifted toward the open eye, and the OD of

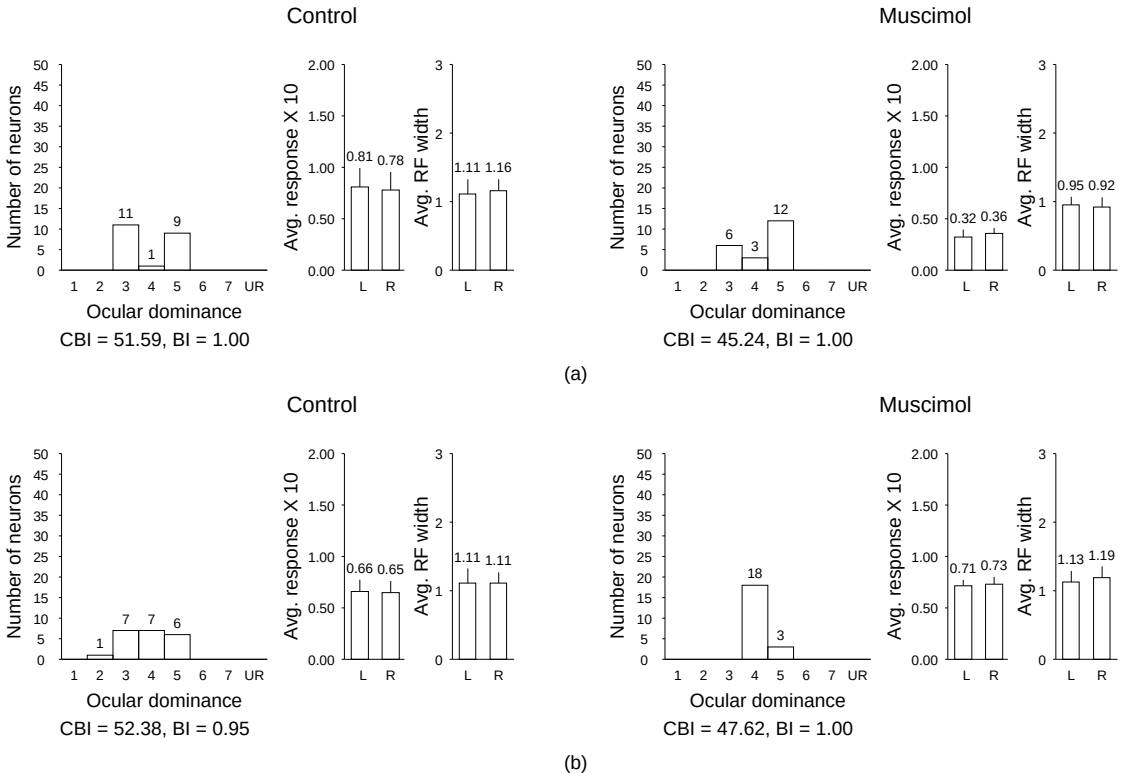

Figure 4.6: **Aspecific effects of muscimol with afferent excitatory and lateral inhibitory synaptic plasticity.**
OD was measured after 500,000 steps of NR with $\Im = 0.05$. At $\Im = 0.05$, the model cortical neuronal activation was not completely blocked (see Figure 4.5). After training, model cortical properties were measured with a residual muscimol concentration of $\Im = 0.05$ in (a) and $\Im = 0$ in (b). See Figure 4.2 for conventions.

the treated region shifted toward the closed eye.

Figures 4.7b and 4.9b present the modeled changes in OD after MD with no residual APV and muscimol, respectively. In this case, reverse OD shift in the affected regions was slightly reduced. Thus, the model produces reverse OD shifts in neurons affected by APV or muscimol after MD, as observed experimentally (Bear et al., 1990; Reiter & Stryker, 1988). In addition, the model predicts a decrease in the amount of reverse OD shift with increasing dissipation of APV or muscimol.

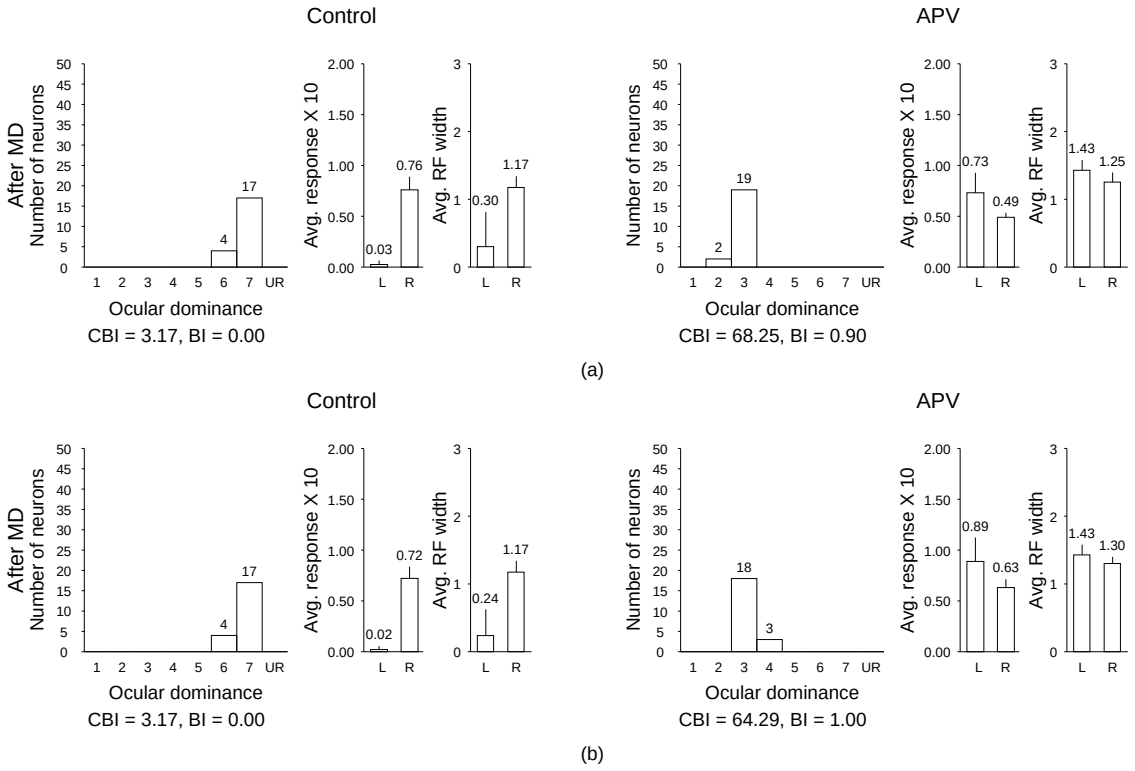

Figure 4.7: **Changes in RF properties after MD with APV infusion.** In this simulation, synaptic plasticity in afferent excitatory pathways to neurons in the infusion site was blocked. APV during MD reduced afferent excitation by a factor of 0.3; i.e., $\omega = 0.7$. The left eye was closed and the right eye was open during MD. OD was measured with $\omega = 0.85$ in (a) and $\omega = 1.0$ in (b). See Figure 4.2 for conventions.

Changes in responsiveness

As the residual concentration of APV and muscimol was reduced, neuronal responsiveness in the affected region increased (Figures 4.7 and 4.9). The maximal responsiveness in the affected region was greater than the maximal responsiveness in the control region after complete removal of APV and muscimol.

Bear et al. (1990) showed that neuronal responsiveness increased after stoppage of APV infusion and that the neuronal responsiveness was greater than control responsiveness three days after cessation of APV infusion. Reiter and Stryker (1988) noted that neuronal responsiveness of neurons affected by muscimol increased after stopping muscimol infusion.

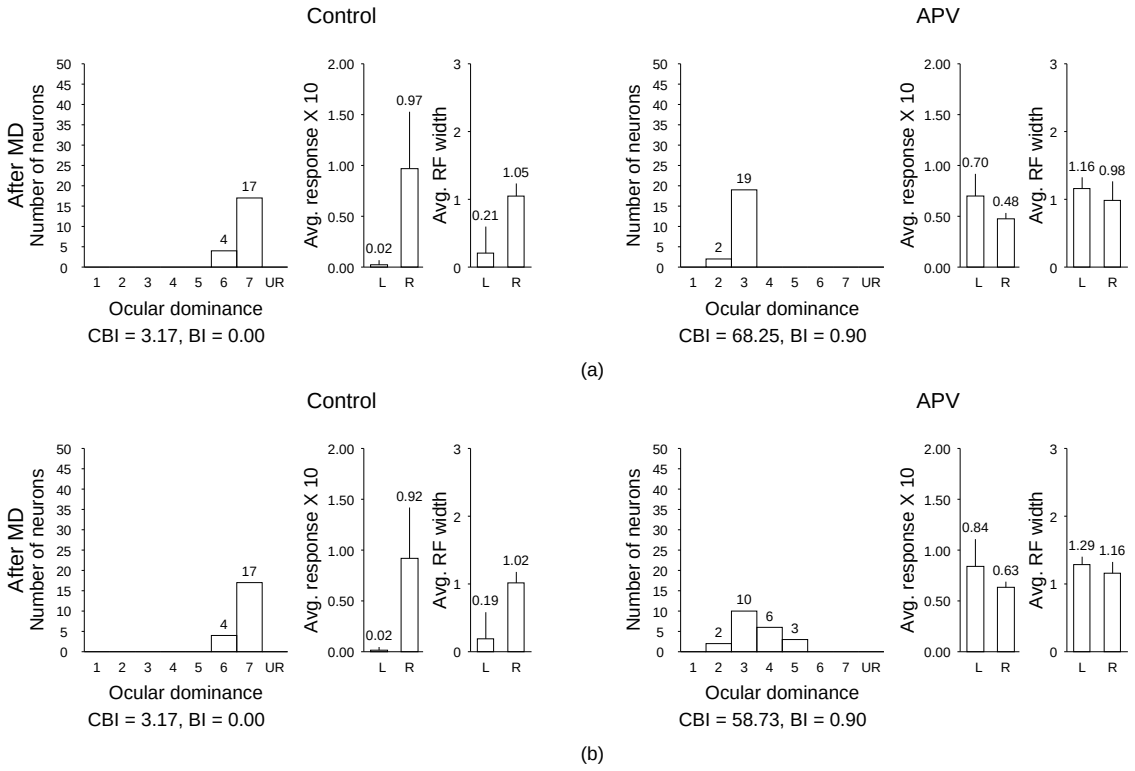

Figure 4.8: **Changes in RF properties after MD with APV infusion with lateral inhibitory pathway synaptic plasticity disabled.**
In this simulation, synaptic plasticity in afferent excitatory pathways to neurons in the infusion site was blocked, and lateral inhibitory learning was disabled in the model cortical layer. APV during MD reduced afferent excitation by a factor of 0.3; i.e., $\omega = 0.7$. The left eye was closed and the right eye was open during MD. OD was measured with $\omega = 0.85$ in (a) and $\omega = 1.0$ in (b). See Figure 4.2 for conventions.

Changes in RF width

At $\omega = 0.85$ and $\omega = 0$ (residual strength of APV), the average RF width of affected neurons was significantly greater than that in the control region and the initial average RF width before MD with APV (Figure 4.2), especially the closed eye RF width (Figures 4.7ab). The increase in RF width was caused by weakening of lateral inhibitory pathways between the APV-affected neurons, which were weakly responsive during MD. Figure 4.8 shows changes in average RF width in the model, when MD with APV infusion was simulated with lateral inhibitory learning in the model cortical layer disabled; the

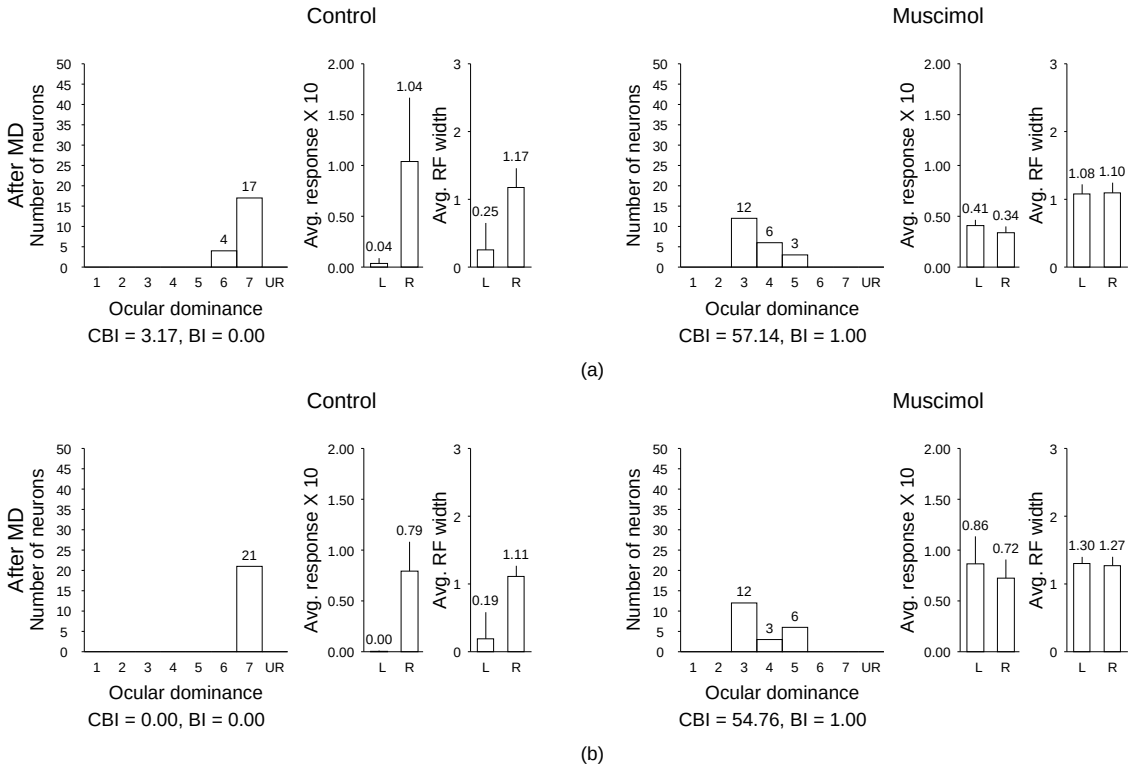

Figure 4.9: **Model OD distribution after MD with muscimol infusion.** In this simulation, afferent excitatory and lateral inhibitory plasticity were enabled. The left eye was closed, and the right eye was open during MD. The concentration of muscimol during MD was $\Im = 0.1$, and OD was measured with $\Im = 0.05$ in (a) and $\Im = 0.0$ in (b). See Figure 4.2 for conventions.

APV affected neurons show RF contraction when RF size was measured with $\omega = 0.85$. Bear et al. (1990) observed loss of orientation tuning in a significant number of APV-affected neurons after MD. The model predicts that the loss of orientation tuning in APV-affected neurons after MD with APV infusion (Bear et al., 1990) may be caused by weakening of the lateral inhibitory pathways. Based on the simulations, it is predicted that a significant number of APV-affected cortical neurons after MD with APV infusion will also show RF expansion. See Section 4.5.1 for further discussion.

At $\Im = 0.05$ (residual strength of muscimol), the average RF width in the affected region was slightly smaller than that in the control region (Figure 4.9a). At the zero residual

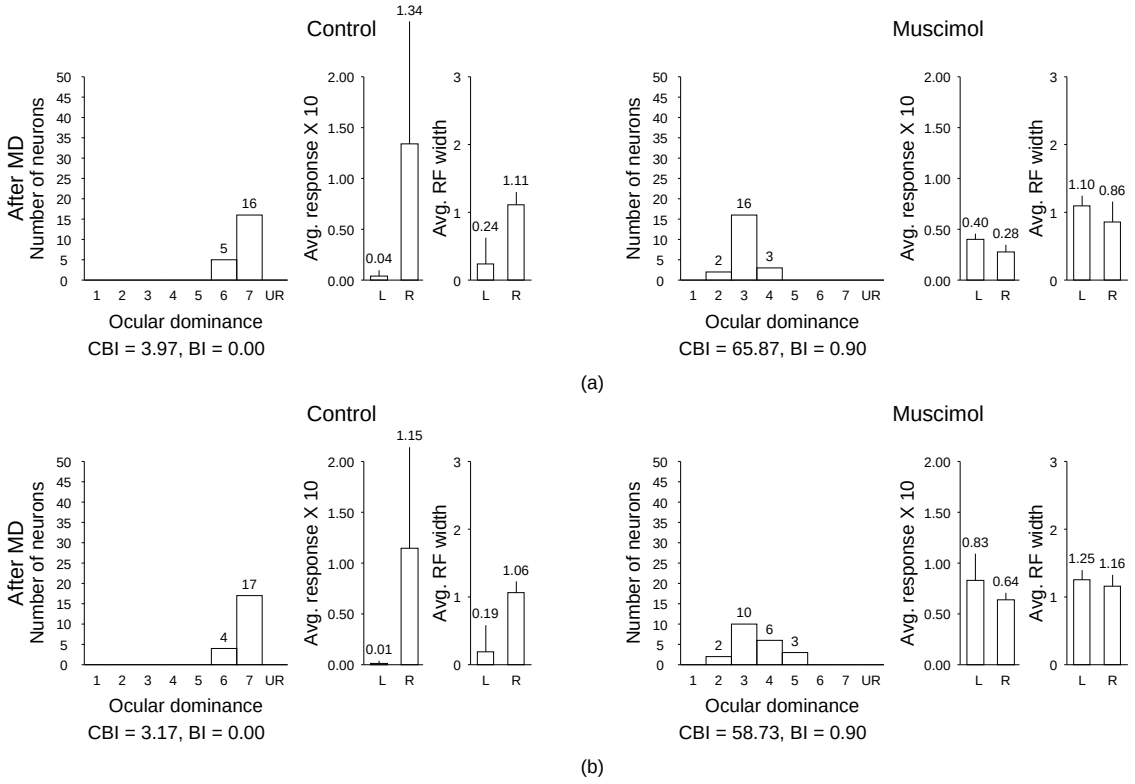

Figure 4.10: **Model OD distribution after MD with muscimol infusion with lateral inhibitory pathway synaptic plasticity disabled.**
In this simulation, only afferent excitatory plasticity was enabled. The left eye was closed, and the right eye was open during MD. The concentration of muscimol during MD was $\Im = 0.1$, and OD was measured with $\Im = 0.05$ in (a) and $\Im = 0.0$ in (b). See Figure 4.2 for conventions.

level of muscimol, the average RF width of model neurons in the affected region showed only a small increase (Figure 4.9b). At non-zero muscimol levels, increased inhibition due to muscimol reduced RF width. In addition, during MD with muscimol the neurons in the muscimol-treated region were very weakly active. Thus, lateral inhibitory pathways from these inactive neurons changed very little. However, lateral inhibitory pathways from active neurons to the inactive neurons weakened, according to the lateral inhibitory plasticity rule, thereby increasing the RF width of some neurons in the affected region. Compare Figure 4.9 with the changes in RF width when lateral inhibitory plasticity in the model cortical layer was blocked during MD with muscimol infusion in Figure 4.10. Reiter and Stryker (1988)

observed a reduction of orientation selectivity in only a small number of muscimol-treated neurons after MD with muscimol infusion. Most muscimol-treated neurons after MD with muscimol infusion may retain high orientation selectivity because (1) some residual muscimol enhances orientation selectivity, and (2) lateral inhibitory pathways between muscimol-affected neurons do not change, as their activation is fully suppressed by muscimol during MD.

4.4.3 Important model parameters

The most important factors influencing OD shifts and changes in receptive field width are the amount of change in the afferent excitatory and lateral inhibitory pathways. The model requires weakening of afferent excitatory pathways from the closed eye selective input layer neurons to the control model cortical neurons. Apart from this, the amount of plasticity in afferent excitatory and lateral inhibitory pathways to the affected neurons is important. These factors are discussed below.

Plasticity in afferent excitatory pathways to affected neurons

The amount of reverse OD shift in the region affected by APV or muscimol is highly dependent on the amount of plasticity in the afferent pathways to the affected neurons. With APV infusion, the greatest reverse OD shift occurred when afferent excitatory synaptic plasticity in pathways to APV treated neurons is assumed to be completely blocked (Figure 4.11), even though these neurons are active during MD. At low muscimol concentrations, reverse OD shift did not occur (Figure 4.12). When muscimol concentration was increased, postsynaptic activation decreased, afferent excitatory synaptic plasticity decreased, and OD shifted toward the closed eye in the muscimol treated region (Equation 4.2). In Figure 4.12, the amount of reverse OD shift is not a monotonic function of muscimol concentration when lateral inhibitory plasticity was enabled (see Section 4.4.3, *Plasticity in lateral inhibitory pathways to affected neurons*).

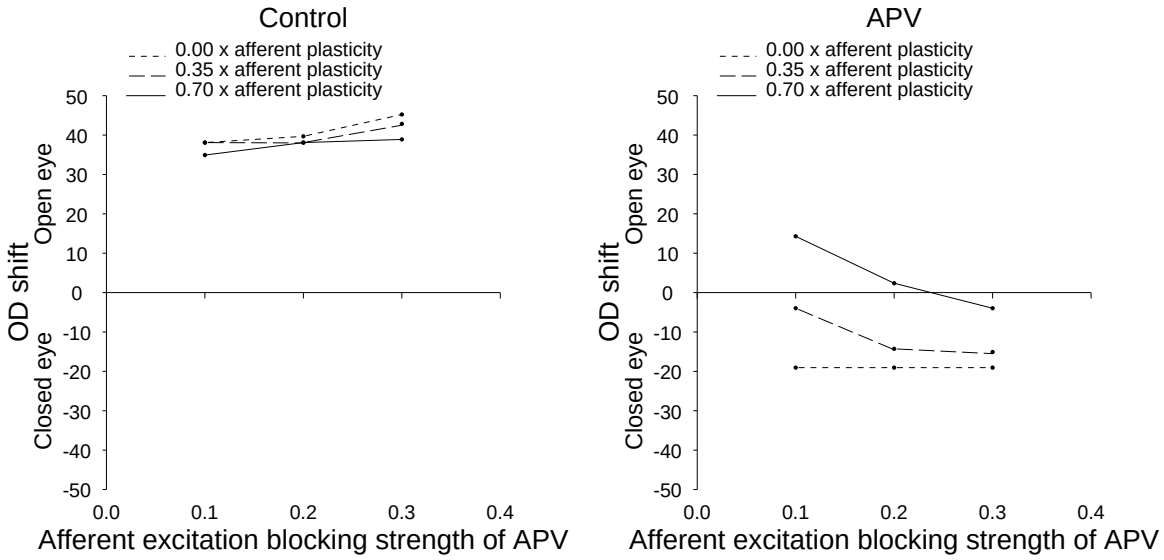

Figure 4.11: **Dependence of OD shifts on APV concentration.**
In these simulations, OD after MD was measured at APV concentrations that reduced afferent excitation by a factor that was half of the factor by which afferent excitation was reduced during MD. Model OD shifts are plotted as a function of afferent excitation blocking strength of APV $(1-\omega)$ at different synaptic plasticity rates in afferent excitatory pathways to neurons affected by APV.

Residual levels of APV and muscimol

The reverse OD shift was further enhanced by aspecific effects of residual APV and muscimol. Increasing APV or muscimol strength reduced neuronal responsiveness and hence slowed down afferent excitatory synaptic plasticity in pathways to the affected neurons. In addition, residual APV or muscimol reduced the effectiveness of afferent pathways to the affected neurons. Afferent pathways from the open eye to the affected neurons were less effective because the affected neurons received more inhibition during open eye stimulation. And hence, residual APV or muscimol made the afferent pathways from the open eye even less effective. Removing residual APV or muscimol reduced the reverse OD shift (Figures 4.7b and 4.9b).

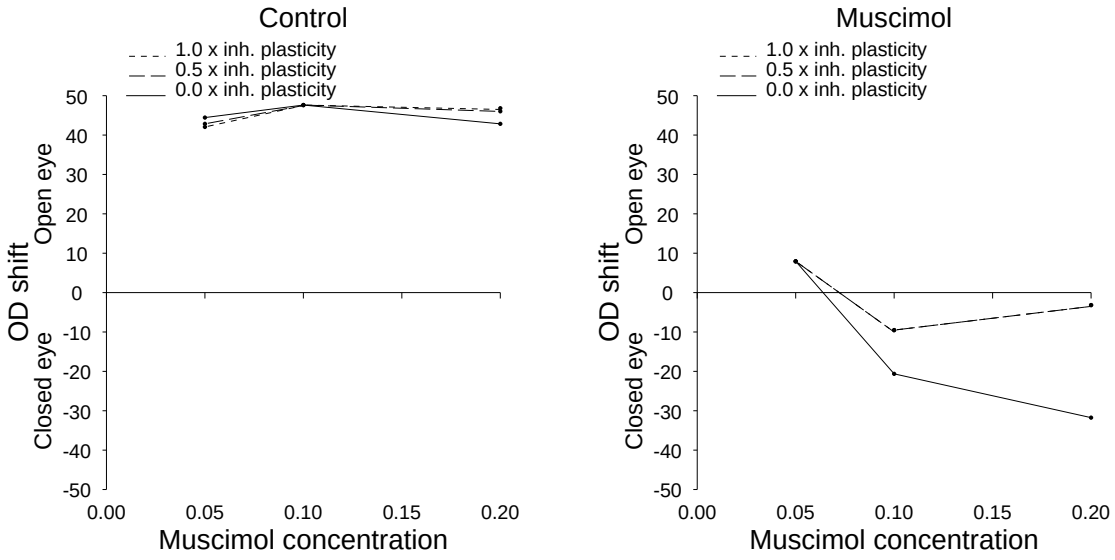

Figure 4.12: **Dependence of OD shifts on muscimol concentration.** In these simulations, OD after MD was measured at muscimol concentrations equal to half of the muscimol concentration during MD. Model OD shifts are plotted as a function of muscimol concentration ($\Im$) at different synaptic plasticity rates in lateral inhibitory pathways to neurons affected by muscimol.

Plasticity in lateral inhibitory pathways to affected neurons

The amount of change in the weight of the lateral inhibitory pathways from the control region to the treated region also determined the amount of reverse OD shift, especially in the case of model muscimol infusion. If muscimol completely blocks postsynaptic activation, lateral inhibitory pathway weights from active neurons to these inactive neurons can go to zero with sufficient conditioning (see Equation 4.1). When this happens, the neurons in the control region exert no inhibitory influence when either eye is stimulated. And therefore, the OD of the affected neurons may not shift toward the closed eye, although residual muscimol may reduce binocularity (see Section 4.4.1). The weakened inhibitory pathways produced non-monotonicity in the amount of reverse OD shift as model muscimol concentration increased, when lateral inhibitory plasticity was enabled (Figure 4.12). In Figure 4.12, as the rate of lateral inhibitory plasticity in pathways to the affected neurons was decreased with fixed muscimol concentration, the reverse OD

shift increased. In the case of model APV infusion, this issue is not crucial because the APV-affected neurons remained responsive to input stimulation.

In the model, increase in RF width is highly dependent on weakening of lateral inhibitory pathways to the affected neurons. The amount of change with fixed NR training depends on the activity of the source neuron and the target neuron (see Equation 4.1). Thus, during NR with APV infusion, if postsynaptic activation is blocked (using APV), lateral inhibitory pathways between affected neurons change very little (the only changes are caused by noise), and neurons show very little RF expansion. At near-normal postsynaptic activation, APV-affected neurons do not show much RF expansion because lateral inhibitory pathway strengths remain close to normal levels. At some intermediate, weak postsynaptic activation levels, APV-affected neurons show RF expansion (Figure 4.13). The RF width of neurons affected by muscimol during NR is also an inverted-U function of the strength of muscimol (Figure 4.13). In Figure 4.13 the RF properties were measured with zero residual APV or muscimol. Figure 4.13 shows responsiveness and RF width in the presence of APV or muscimol. During APV infusion, the afferent excitatory plasticity was blocked. Afferent excitatory plasticity was unchanged during model muscimol infusion.

In the EXIN lateral inhibitory plasticity rule (Equation 4.1), the postsynaptic activation determines the stable-state weight of the inhibitory pathways, and the presynaptic activation determines the rate of weight change. Thus, if the network is trained for a sufficiently long time, RF widths will increase as a function of the concentration of APV (instead of being an inverted-U curve).

During NR with very strong muscimol infusion, noise in the EXIN plasticity rules dominates neuronal activation. When this happens, neurons have no selectivity, and weight changes occur because of noise, resulting in weakening of afferent excitatory and lateral inhibitory pathways. When $\Im = 0.8$, model cortical neuronal activations were completely suppressed. After 1,500,000 presentations of binocular inputs, the average maximal responsiveness to monocular input was 0.073 (mean) ± 0.003 (standard deviation), and the average monocular RF width was 1.615 ± 0.121 (RF width increased).

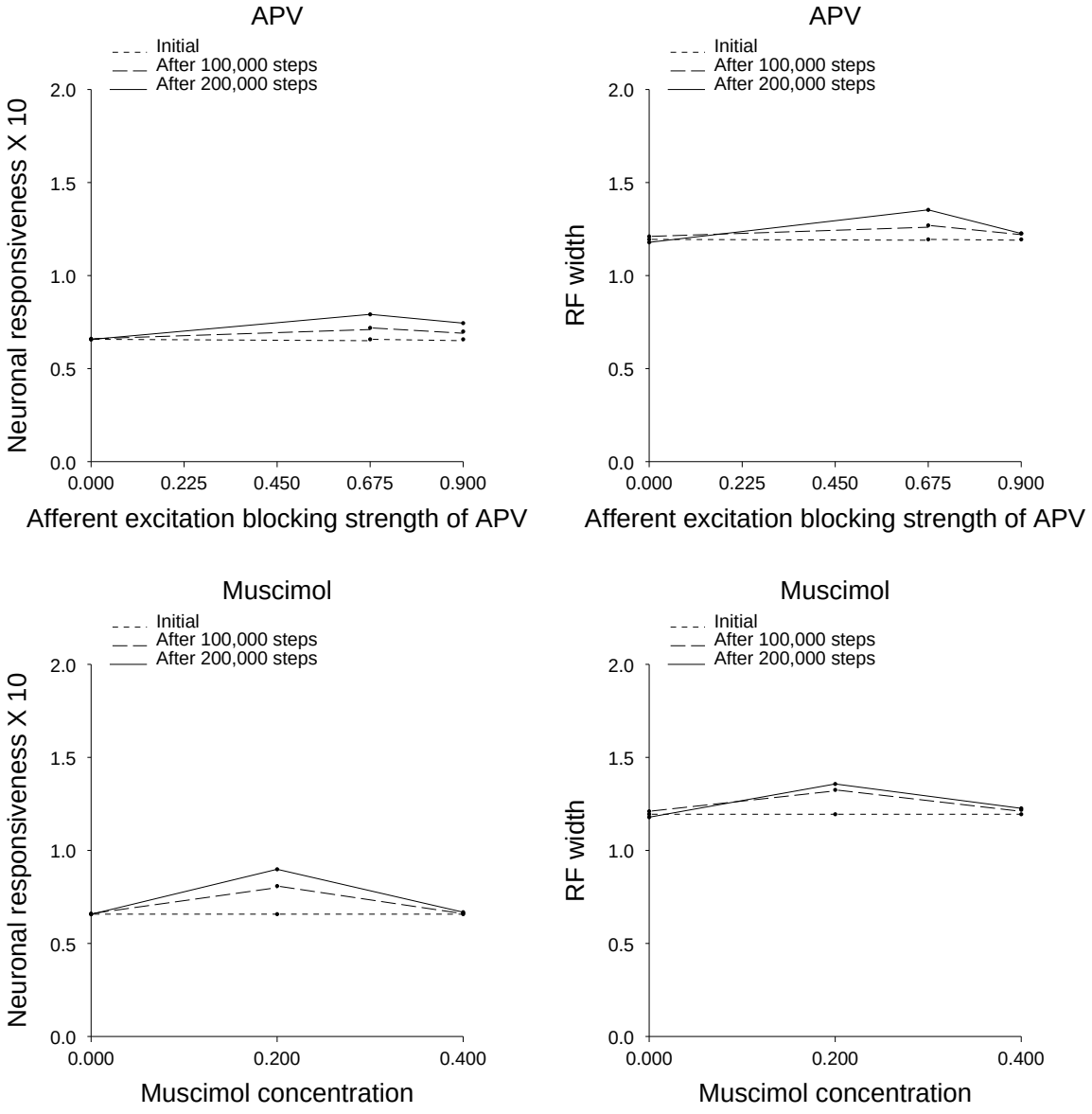

Figure 4.13: **Dependence of RF width and responsiveness on cortical activation.** The model cortical neuronal responsiveness to monocular inputs (left) and monocular RF width (right) was measured after NR with infusion of APV (top) and muscimol (bottom) with no residual APV or muscimol. With APV infusion, $\omega < 1$, the learning rate ϵ in Equation 2 was set to zero; i.e., afferent excitatory plasticity was blocked. APV afferent excitation blocking strength was $1 - \omega$. During muscimol infusion, ϵ was unchanged.

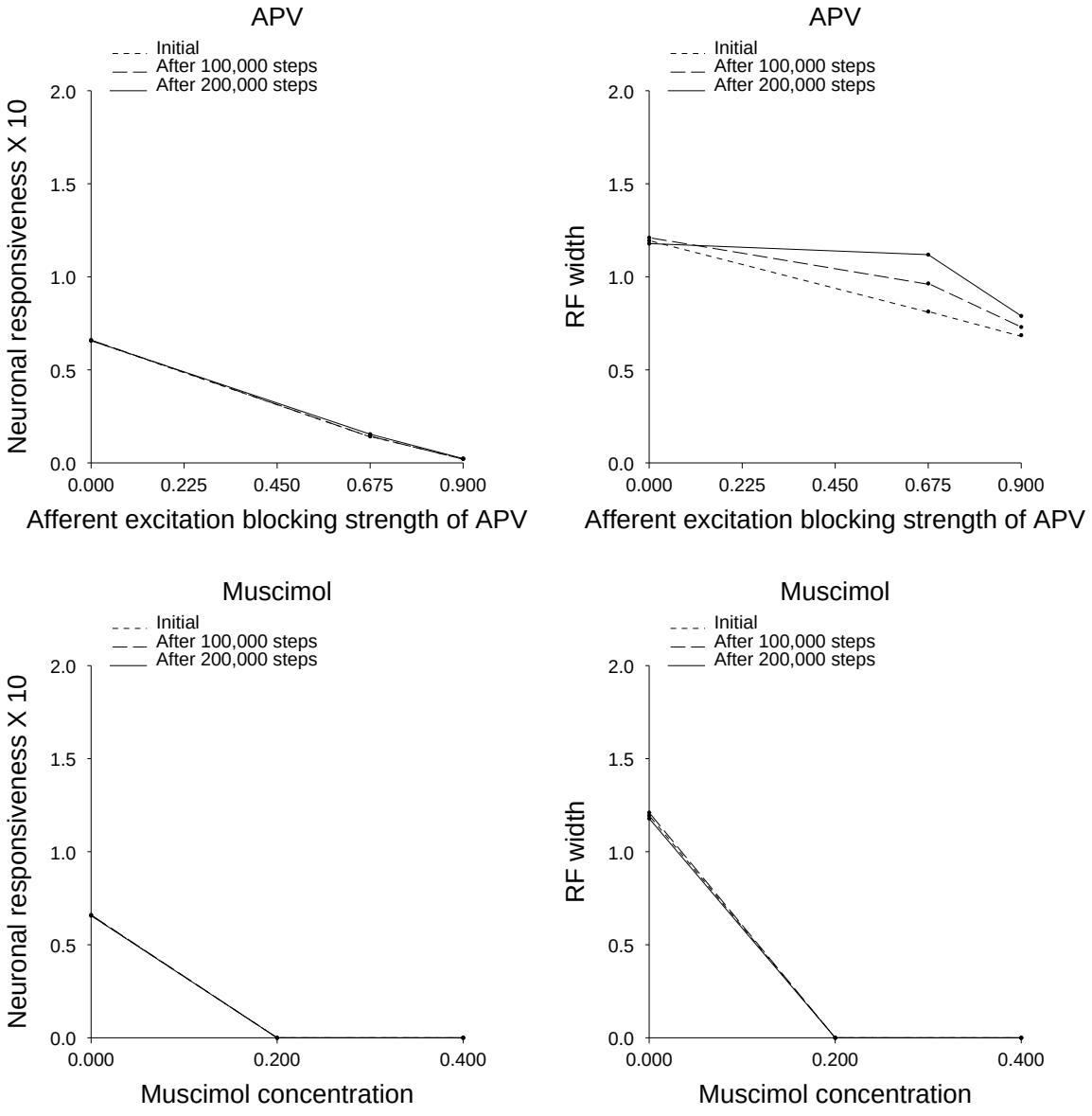

Figure 4.14: Legend on next page.

Figure 4.14: **RF width and responsiveness in the presence of APV or muscimol.** Figure on previous page. The model cortical neuronal responsiveness to monocular inputs (left) and monocular RF width (right) was measured after NR with infusion of APV (top) and muscimol (bottom). The measurements were made in the presence of APV or muscimol. With APV infusion, as ω was decreased, the learning rate ϵ in Equation 2 also was decreased by the same factor. APV afferent excitation blocking strength is $1 - \omega$. During muscimol infusion, ϵ was not changed. The average maximal responsiveness of the model cortical neurons to binocular inputs used during NR in the presence of APV or muscimol was 6.546×10^{-2} (mean) $\pm\, 2.280 \times 10^{-2}$ (standard deviation) with $\omega = 0.325$, $1.025 \times 10^{-2} \pm 1.467 \times 10^{-3}$ with $\omega = 0.1$, $6.157 \times 10^{-2} \pm 2.055 \times 10^{-3}$ with $\Im = 0.2$, and $1.283 \times 10^{-1} \pm 9.790 \times 10^{-4}$ with $\Im = 0.4$. The normal average maximal responsiveness of the model cortical neurons to binocular inputs was $1.893 \times 10^{-1} \pm 9.145 \times 10^{-4}$.

4.5 Discussion

The salient effects of the infusion of muscimol or APV during MD are an OD shift toward the open eye in the control region and a reverse OD shift toward the closed eye. These effects have been modeled using the EXIN synaptic plasticity rules (Marshall, 1995). The model is based on the observation that neurons in the control regions become less responsive to closed eye stimulation and hence exert less inhibition to neurons in the infusion region, where afferent synapses do not change. In addition, the aspecific action of APV and muscimol contributes to changes in cortical properties.

In two experiments (Bear et al., 1990; Reiter & Stryker, 1988), OD was measured within 48 hrs of stoppage of infusion, and responsiveness of neurons in the infusion site continued to increase. Bear et al. (1990) showed that responsiveness of neurons in the APV infusion site three days after stoppage of infusion was greater than the control responsiveness. This suggests a relatively long residual effect of muscimol and APV. Therefore, a small residual amount of APV or muscimol was assumed during measurement of model cortical properties in the present model.

Lateral inhibitory interactions can also play a role in producing reverse OD shifts even if a covariance rule (Miller et al., 1989; Stanton & Sejnowski, 1989) were used for afferent excitatory synaptic plasticity, instead of the EXIN afferent excitatory plasticity rule. The covariance rule would weaken afferent excitatory pathways from the open eye

to muscimol or APV treated neurons, thereby producing OD shift toward the closed eye. Furthermore, weakening of afferent pathways from the closed eye to control neurons according to the covariance rule would cause an additional OD shift toward the closed eye because of lateral inhibitory interactions, as in the EXIN model.

4.5.1 Loss of cortical neuronal stimulus feature selectivity

Several cortical properties – orientation selectivity, disparity selectivity, length selectivity, spatial frequency selectivity, motion direction selectivity, etc. – may depend on lateral inhibition (Bonds & DeBruyn, 1985; Sillito, 1979; Somers et al., 1995; Somogyi & Martin, 1985). Specificity of cortical neurons for several stimulus features is abolished by cortical infusion of a $GABA_A$ antagonist (Sillito, 1975, 1977, 1979). Blocking intracortical inhibition also reveals new peripheral regions capable of evoking neuronal responses (Lane et al., 1997; Sillito et al., 1981).

Kasamatsu et al. (1998a) observed loss of orientation selectivity and direction selectivity after APV infusion in adult cat primary visual cortex. Bear et al. (1990) reported loss of orientation selectivity in a region affected by APV after MD with APV infusion. Prolonged binocular deprivation reduces neuronal responsiveness and orientation selectivity (Frégnac & Imbert, 1984). In these experiments, cortical activation was much lower than during normal rearing.

According to the EXIN lateral inhibitory plasticity rule, weak neuronal activation is sufficient for weakening lateral inhibitory pathways between these neurons (albeit relatively slowly) and may lead to reduction of neuronal stimulus feature specificity. During chronic binocular deprivation, the afferent pathways may weaken, thereby weakening neuronal responsiveness. In the model, loss of position selectivity (increase in RF width) occurred after APV infusion and after MD with APV infusion.

Biologically, the EXIN inhibitory rule could be realized either by modifying the weights of inhibitory synapses onto excitatory neurons or by modifying the weights of excitatory synapses onto inhibitory interneurons. In the developing cortex, lateral excitatory pathways too may undergo synaptic plasticity. If changes in the lateral inhibitory pathways dominate changes in lateral excitatory pathways, the effects predicted by the EXIN model

would arise.

The loss of orientation selectivity during APV infusion observed by Kasamatsu et al. (1998a) could also be caused by weakening of afferent excitatory inputs to inhibitory neurons, thus reducing intracortical inhibition. Kasamatsu et al. (1998a) observed reduced orientation selectivity and binocularity during APV infusion. In the EXIN model, model APV infusion in a group of neurons caused RF expansion in some control neurons. When lateral inhibitory plasticity was enabled, APV-affected neurons recovered binocularity. Thus, the model suggests both an immediate and a prolonged effect of APV on neuronal selectivity. The model suggests that APV-affected neurons will have weak orientation selectivity after complete removal of APV because of weakened lateral inhibitory pathways.

The loss of stimulus feature specificity of cortical neurons based on the EXIN rule is valid even if lateral excitatory pathways contribute to feature selectivity (Somers et al., 1995). Somers et al. (1995) assume that lateral excitation from neighboring neurons is orientation selective, and weakened lateral inhibition will render all neurons less selective.

4.5.2 Model predictions

In the model, it was assumed that plasticity in lateral inhibitory pathways is not affected by muscimol or APV. However, in the cortex it is possible that APV blocks plasticity in lateral excitatory pathways to inhibitory neurons; and if the biological realization of the EXIN lateral inhibitory rule requires plasticity in lateral excitatory pathways to inhibitory neurons, then APV can affect plasticity in lateral inhibitory pathways in the cortex. There are very few reports of possible plasticity in lateral inhibitory pathways (e.g., Miles & Wong, 1987). The effect of muscimol on plasticity in lateral inhibitory pathways is not known. Thus, the effects produced by the lateral inhibitory rule in the simulations are predictive.

Intracellular measurement of excitatory and inhibitory postsynaptic potentials

Thalamocortical stimulation produces monosynaptic excitatory postsynaptic potentials (EPSPs) and disynaptic inhibitory postsynaptic potentials (IPSPs) (Gil & Amitai, 1996; Ferster, 1989). The EXIN model makes the following predictions, for young animals during their critical period after MD with strong concentrations of APV or muscimol.

1. Monosynaptic EPSPs evoked in APV or muscimol treated neurons by left or right eye selective thalamocortical afferent stimulation remain unchanged. (It should be ensured that there is no residual APV or muscimol.)

2. Monosynaptic EPSPs evoked in control neurons by closed eye selective thalamocortical afferent stimulation decrease substantially, and monosynaptic EPSPs evoked in control neurons by open eye selective thalamocortical afferent stimulation may increase slightly (see Section 4.2.3).

3. Disynaptic IPSPs in neurons treated with muscimol or APV by stimulation of thalamocortical afferents selective to the closed eye decreases, because neurons in the control region become weakly responsive to closed eye stimulation and hence send weaker inhibition to neurons affected by muscimol or APV.

4. Disynaptic IPSPs in control neurons caused by stimulation of thalamocortical afferents selective to either eye may change by a small amount (the afferent excitatory pathways to these neurons strengthen slightly because of increased correlation with monocular inputs, and lateral inhibitory pathways to these neurons weaken by a small amount because the neurons are weakly active).

In contrast, models based on depression in the afferent excitatory pathways from the open eye to neurons affected by APV or muscimol (Bear et al., 1990; Miller et al., 1989; Reiter & Stryker, 1988) predict decrease in monosynaptic EPSPs in APV or muscimol treated neurons by stimulation of open eye selective thalamocortical afferents.

Changes in RF width and stimulus feature selectivity as a function of cortical activity

During binocular rearing of young animals for a fixed duration within their critical period, neuronal activation of a small region of the cortex can be varied, e.g., by infusion of muscimol or APV, or by controlling the input stimulation strength. The EXIN model suggests the following predictions.

1. With muscimol or APV infusion, the amount of increase in RF size and neuronal responsiveness and the amount of decrease in stimulus feature selectivity (e.g., orientation selectivity) as a function of cortical activation level (concentration of muscimol or APV) will be an inverted-U shaped curve (see Section 4.4.3, *Plasticity in lateral inhibitory pathways to affected neurons*). Because of normal input stimulation, the afferent excitatory pathways may not change during muscimol infusion.

2. As the strength of input stimulation is decreased (cortical activation also decreases), the magnitude of change in RF size, responsiveness, and stimulus feature selectivity will be inverted-U shaped. When input stimulation strength is decreased, the afferent excitatory pathways may weaken; therefore, the change in RF width, neuronal responsiveness, and stimulus feature selectivity will depend on whether decrease in excitation or decrease in inhibition dominates. During prolonged binocular deprivation, neuronal responsiveness and orientation selectivity decrease (Frégnac & Imbert, 1984).

3. APV can be infused to block afferent excitatory plasticity when the strength of input stimulation is decreased. The amount of increase in RF size and neuronal responsiveness and the amount of decrease in stimulus feature selectivity will be inverted-U shaped as a function of the input stimulation strength.

Artificial scotoma conditioning with pharmacological treatments

Pettet and Gilbert (1992) showed RF expansion in primary visual cortical neurons whose RF was occluded with just 15 minutes of artificial scotoma conditioning in one

eye with the other eye closed. This RF expansion has been modeled by weakening lateral inhibitory pathways from active neurons to inactive neurons, without requiring any plasticity in the afferent excitatory pathways (Kalarickal & Marshall, 1997; Marshall & Kalarickal, 1997). The reduced weights of inhibitory pathways to neurons whose RF is inside the scotoma from neurons whose RF is outside then allows greater and wider responses by the neurons whose RF is inside. In contrast, Sirosh et al. (1996) modeled the RF expansion using afferent excitatory plasticity. During artificial scotoma conditioning, neurons whose RF straddles the scotoma boundary have active afferent excitatory pathways from positions outside the scotoma and inactive afferent excitatory pathways from positions inside the scotoma. Thus, active afferent excitatory pathways to the neuron can be competitively weakened. Since afferent excitatory plasticity in animals during the critical period is easily induced (Hubel & Wiesel, 1965, 1970; Hubel et al., 1977), artificial scotoma conditioning with cortical infusion of APV can be used to assess (1) the efficiency of APV in blocking afferent plasticity and (2) the contribution of afferent excitatory and lateral inhibitory plasticity in producing the effects of artificial scotoma conditioning.

We propose the following experiments:

1. Perform artificial scotoma conditioning in animals during the critical period. With both afferent and lateral inhibitory synaptic plasticity, the EXIN model predicts

   (a) RF expansion in neurons whose RF is in the scotoma region during artificial scotoma conditioning; and

   (b) RF contraction in neurons whose RF straddles the artificial scotoma boundary. These neurons will be active during conditioning, and hence the afferent excitatory pathways from parts of the scotoma region will weaken (Kalarickal & Marshall, 1997; Sirosh et al., 1996).

2. Perform artificial scotoma conditioning with a large cortical infusion of APV. If APV blocks afferent excitatory plasticity, the EXIN model predicts

   (a) RF expansion in neurons whose RF is in the scotoma region (because of lateral inhibitory plasticity); and

(b) no RF contraction in neurons whose RF straddles the scotoma boundary.

Temporary cortical scotoma conditioning with normal input stimulation

To determine the role of lateral inhibitory plasticity, a temporary local cortical scotoma can be produced by infusion of muscimol, during normal stimulation in animals during their critical period. The EXIN model predicts RF expansion in neurons affected by muscimol (after sufficient time to allow dissipation of the effects of muscimol) because of weakening of lateral inhibitory pathways from the active neurons to the muscimol-treated inactive neurons. The lateral inhibitory pathways from the muscimol-treated inactive neurons to other neurons and the afferent excitatory pathways to the muscimol-treated neurons may change by a very small amount because of noise. In contrast, if the active afferent excitatory pathways to the cortical neurons whose activation is suppressed by muscimol were weakened as proposed by Reiter and Stryker (1988) and Miller et al. (1989), then the RF size of the muscimol-treated neurons would shrink.

4.5.3 Conclusions

In the EXIN model, plasticity in lateral inhibitory pathways develops as a function of overlap in the RF of neurons. Previously, it was shown that lateral inhibitory plasticity produces neurons with high selectivity and sparse distributed coding (Marshall, 1995; Marshall & Gupta, 1998). Therefore, the role of the lateral inhibitory plasticity rule in producing RF changes was studied in detail in the context of MD with infusion of APV and muscimol. The predictions made based on the EXIN plasticity rules can be used to design experiments to reveal the rules of afferent excitatory and lateral inhibitory plasticity and their role in cortical plasticity.

Chapter 5

Models of receptive field dynamics in visual cortex

Abstract

The position, size, and shape of the receptive field (RF) of some cortical neurons change dynamically, in response to artificial scotoma conditioning (Pettet & Gilbert, 1992) and to retinal lesions (Chino et al., 1992; Darian-Smith & Gilbert, 1995) in adult animals. The RF dynamics are of interest because they show how visual systems may adaptively overcome damage (from lesions, scotomas, or other failures), may enhance processing efficiency by altering RF coverage in response to visual demand, and may perform perceptual learning.

This chapter presents an afferent excitatory synaptic plasticity rule and a lateral inhibitory synaptic plasticity rule – the EXIN rules (Marshall, 1995a) – to model persistent RF changes after artificial scotoma conditioning and retinal lesions. The EXIN model is compared to the LISSOM model (Sirosh et al., 1996) and to a neuronal adaptation model (Xing & Gerstein, 1994). The rules within each model are isolated and are analyzed independently, to elucidate their roles in adult cortical RF dynamics. Based on computer simulations, the EXIN lateral inhibitory synaptic plasticity rule and the

LISSOM lateral excitatory synaptic plasticity rule produced the best fit with current neurophysiological data on visual cortical plasticity in adult animals (Chino et al., 1992; Darian-Smith & Gilbert, 1995; Pettet & Gilbert, 1992) including (1) the retinal position of the expanding RFs, (2) the amount of change in spontaneous activation in the absence of any visual stimulation, (3) the corticotopic direction in which responsiveness returns to lesioned cortex, (4) the direction of RF shifts, (5) the amount of change in response to blank stimuli, and (6) the lack of dynamic RF changes during conditioning with a retinal lesion in one eye and the unlesioned eye kept open, in adult animals. The effects of the LISSOM lateral inhibitory synaptic plasticity rule during artificial scotoma conditioning are in conflict with those of the other two LISSOM synaptic plasticity rules. A novel "complementary scotoma" conditioning experiment, in which stimulation of two complementary regions of visual space alternates repeatedly, is proposed to differentiate the predictions of the EXIN and LISSOM rules.

5.1 Introduction

In experiments using artificial scotoma conditioning (Pettet & Gilbert, 1992) and retinal lesions (Chino et al., 1992; Darian-Smith & Gilbert, 1995), neurons in primary visual cortex corresponding to a particular region of visual space were deprived of visual stimulation, while neurons corresponding to a surrounding region received visual stimulation. In response to these manipulations, a variety of dynamic changes occurred in the position, size, and shape of the receptive field (RF) of some of the neurons. For example, after 15 minutes of artificial scotoma conditioning, the RF area of some cortical neurons whose RF was located inside the scotoma expanded by a factor of five; after 15 minutes of subsequent normal stimulation, the RF returned to its original size (Pettet & Gilbert, 1992). The dynamic RF expansion following artificial scotoma conditioning in one eye also transfers to the other eye (Volchan & Gilbert, 1994).

Pettet and Gilbert (1992) simulated a retinal lesion experiment by presenting a pattern of moving lines in the visual field while masking out an artificial "scotoma" region covering the original RF of the recorded neuron. After 10–15 minutes of stimulation, a

five-fold average expansion in RF area was found. In the second phase of the experiment, the scotoma region was unmasked, and moving lines were presented in the whole field. After several minutes of stimulation, the RF shrank back to its original extent. The RF expansion and contraction was repeatable. A key observation was that stimulation exclusively in the surrounding region was necessary for the RF expansion to occur. Exposure to a blank screen for as long as 20 minutes had little effect on the RF size.

Pettet and Gilbert (1992) tested the effect of orientation of the conditioning stimuli on RF expansion, during artificial scotoma conditioning. For a few neurons (3 out of 15), they found an expansion with iso-orientation conditioning stimuli and did not find an expansion with the orthogonal pattern. In these cases, the orthogonal pattern actually reduced the RF size and responsiveness of the neuron.

Darian-Smith and Gilbert (1995) studied topographic reorganization in the striate cortex of the adult cat and monkey after binocular retinal lesions, using physiological and anatomical techniques. They found that immediately (between 5 minutes and up to 1 hour) after making corresponding retinal lesions of 3.5°–14° in diameter, there was a cortical scotoma region containing neurons whose RF was located more than 0.5–1.0 mm inside the initial scotoma boundary. However, cortical neurons located close to or just inside the cortical scotoma boundary showed an increase in RF size. The greatest expansion occurred for neurons whose RF was located closest to the scotoma boundary. In addition, the expanded RFs shifted centrifugally toward the outside of the scotoma. Neurons that acquired responsiveness to locations outside the scotoma, i.e., neurons in the recovered region of the original cortical scotoma, were less responsive, more sluggish in their response, and more easily fatigued compared to those in normal cortex or in cortex located more than 1 mm outside the cortical scotoma boundary. In spite of the changes in their RF size and position, these neurons retained some of their original RF properties, such as directionality, orientation specificity, and binocularity.

Measurements within the same cortex 2–12 months after the lesions showed that cortical neurons located several millimeters inside the original boundary of the cortical scotoma became responsive to stimulation of perilesion retina (Darian-Smith & Gilbert, 1995). Over time, function returned to the cortex in a roughly concentric inward

direction. The cortical reorganization was accompanied by RF shifts. In spite of distortions in representation, topographic order was maintained.

In contrast to the cortical reorganization, the LGN scotoma and thalamocortical afferents did not undergo any change, as reflected in electrophysiological recordings and anatomical studies. This led Darian-Smith and Gilbert to conclude that the reorganization of cortical topography following retinal lesions originates in the cortex and is likely to be mediated, at least in part, by the long-range collaterals of cortical neurons rather than by thalamocortical afferents.

5.1.1 Significance of RF dynamics

The dynamics of RFs are of interest for several reasons. They reveal some of the ways in which visual systems may adaptively overcome damage from lesions or scotomas. In addition, they reveal some of the functional organization of visual cortex (Das, 1997; Gilbert, 1998). Dynamic visual RFs might also be related to the dynamic response properties found in other cortical areas (Das, 1997), such as the tactile RF expansion/contraction found in adult somatosensory cortex in response to intracortical microstimulation (Recanzone et al., 1992b) and localized peripheral stimulation (Recanzone et al., 1992d).

Artificial scotoma conditioning can elucidate the neural basis of *perceptual learning*. In perceptual learning, human observers improve their performance in perceptual tasks such as orientation perception (Fiorentini & Berardi, 1980), vernier acuity (Fahle & Edelman, 1993), and discrimination of texture (Karni & Sagi, 1991) after training (repeated performance of a perceptual task). Perceptual learning is stable: it does not wear off after periods without visual stimulation. Furthermore, in these studies perceptual learning was not simply a matter of becoming accustomed to the perceptual task. Perceptual learning was specific for features of the training stimuli (Crist et al., 1997; Fahle, 1997); it was usually confined to the portion of the retina that was stimulated during training, or the improvement was restricted to the orientation of the training stimuli. Since neurons in the visual cortex are selective for specific stimulus features, repeated presentation of training stimuli repeatedly activates a small group of neurons. Thus, perceptual learning may be

realized by cortical plasticity that depends on repeated activation of a group of neurons. In artificial scotoma conditioning, visual cortical neurons selective for a particular region of visual space are deprived of visual stimulation while neurons selective for surrounding visual space receive stimulation. Thus, artificial scotoma conditioning provides a systematic procedure to control the activation of specific groups of neurons and to study the neural basis of perceptual learning.

5.1.2 Modeling of RF dynamics

Figure 5.1 shows the input pathways to primary visual cortical neurons. The RF of a cortical neuron can be affected by changes in the inputs to the neuron. The long-range horizontal excitatory or inhibitory pathways in visual cortex have been regarded as the substrate for RF dynamics (Darian-Smith & Gilbert, 1995; Das & Gilbert, 1995ab; Gilbert et al., 1996; Pettet & Gilbert, 1992; Somogyi & Martin, 1985; Volchan & Gilbert, 1994). It has been shown that dynamic RF changes result from changes in the amount of excitation and/or inhibition received by the neurons (Chapman & Stone, 1996; Petersen & Taylor, 1997). Changes in the amount of excitation and/or inhibition to neurons can result from neuronal adaptation (DeAngelis et al., 1995; Xing & Gerstein, 1994), short-term inhibitory synaptic adaptation (Todorov et al., 1997), long-term synaptic modifications in long-range horizontal pathways (Darian-Smith & Gilbert, 1994, 1995; Das & Gilbert, 1995ab; Gilbert et al., 1996; Pettet & Gilbert, 1992), long-term synaptic plasticity in lateral inhibitory pathways (Marshall & Kalarickal, 1997), or long-term synaptic plasticity in afferent excitatory pathways (Marshall, 1995a; Sirosh et al., 1996). Reafferent feedback pathways between cortical layers may also be involved in producing cortical plasticity (Gilbert, 1996).

A drawback of adaptation-based models (Todorov et al., 1997; Xing & Gerstein, 1994) is that they cannot sustain the RF expansions during periods with no visual stimulation in artificial scotoma conditioning as reported by Pettet and Gilbert (1992). Sirosh et al. (1996) attributed RF expansion after artificial scotoma conditioning to afferent excitatory plasticity in their LISSOM model. Their model also had plasticity in lateral excitatory and lateral inhibitory pathways, but the role of these forms of plasticity in

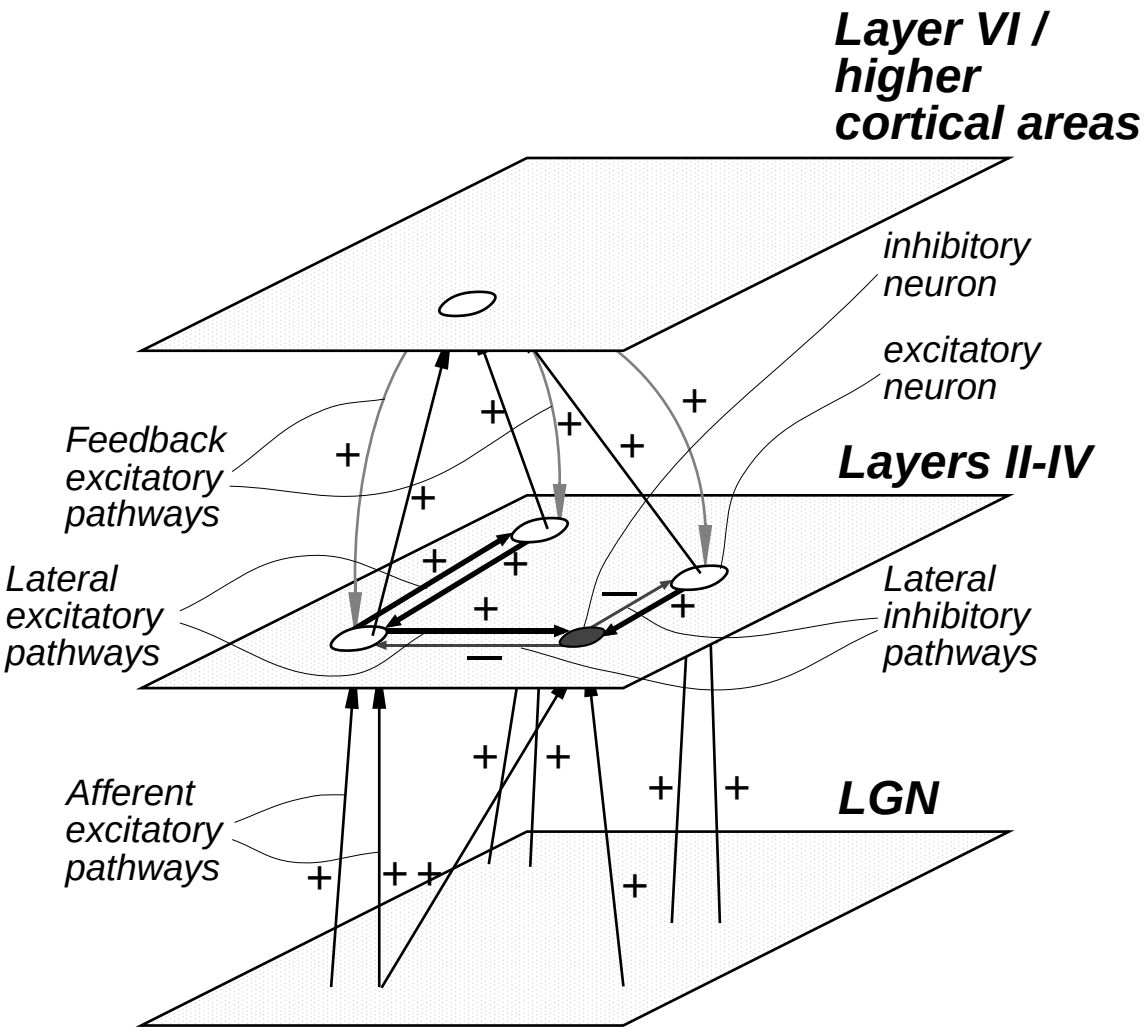

Figure 5.1: **Site of RF changes.**
The RF of cortical neurons changes when input excitation and inhibition to the neurons change. Cortical neurons receive afferent, lateral, and feedback excitation. Cortical neurons receive lateral inhibition from inhibitory neurons (shown by the shaded ellipse in layer 2). The excitatory cortical neurons (represented by the unfilled ellipses) send lateral excitation to excitatory and inhibitory neurons. Changes in input excitation and inhibition can occur because of synaptic plasticity in excitatory and inhibitory synapses, respectively, or because of adaptation cortical neurons.

RF changes after artificial scotoma conditioning was not analyzed.

This chapter compares the properties of RF changes produced by several models of cortical plasticity to the neurobiological data on RF changes after artificial scotoma conditioning and after retinal lesions in adult animals. In particular, RF changes after artificial scotoma conditioning and retinal lesions produced by the EXIN rules (Marshall, 1990a, 1995a), the LISSOM rules (Sirosh & Miikkulainen, 1994ab, 1995, 1997; Sirosh et al., 1996), and an adaptation rule (Xing & Gerstein, 1994) are analyzed.

EXIN plasticity rules

The EXIN model uses an an instar Hebbian afferent excitatory synaptic plasticity rule and an outstar anti-Hebbian lateral inhibitory synaptic plasticity rule (Marshall, 1990a, 1995a). An instar rule is enabled when the postsynaptic neuron is activated, and excitatory pathways *in*to the neuron undergo synaptic plasticity (Grossberg, 1972, 1976ab), whereas an outstar rule is enabled when the presynaptic neuron or presynaptic element is activated, and excitatory pathways *out* of the neuron or the presynaptic element undergo synaptic plasticity (Grossberg, 1976c). This subtle distinction makes dramatic difference in the plasticity and behavior of the neural circuits (Grossberg, 1976abc; Marshall, 1995a).

In EXIN networks, the instar excitatory synaptic plasticity rule modifies the weights of afferent excitatory pathways to active neurons so that the active neurons become more responsive to the currently presented input pattern. The instar excitatory synaptic plasticity rule is responsible for the development of the broad excitatory RF of the neurons. The development of weights of lateral inhibitory pathways according to the outstar lateral inhibitory synaptic plasticity rule ensures that different neurons become selective to different input patterns. Yet, if the input environment contains several similar patterns, the outstar lateral inhibitory synaptic plasticity rule causes strong lateral inhibitory pathways to develop between neurons selective for the similar input patterns, thereby producing high discrimination. In EXIN networks, lateral inhibitory pathways from often-activated neurons to unresponsive neurons weaken, thereby making the unresponsive neurons more likely to respond to some input. The outstar lateral inhibitory synaptic plasticity rule is responsible for dispersion of neuronal selectivity and sharpening of the RF of the neurons. The EXIN

rules develop efficient representation of input patterns according to their distribution in an input environment. The EXIN rules self-organize networks capable of representing multiple superimposed patterns, ambiguous patterns, overlapping patterns at different scales, and contextually constrained patterns starting from completely nonspecific afferent excitatory and lateral inhibitory pathway weights (Marshall, 1995a).

LISSOM plasticity rules

The LISSOM model (Sirosh & Miikkulainen, 1994b) uses instar Hebbian afferent excitatory and lateral excitatory synaptic plasticity rules, and an instar anti-Hebbian lateral inhibitory synaptic plasticity rule. Unlike the EXIN model, the LISSOM model has modifiable lateral excitatory pathways and uses an instar lateral inhibitory synaptic plasticity rule. However, like the EXIN rules, the LISSOM rules produce a sparse, distributed coding that reduces redundancies (Marshall, 1995a; Marshall & Gupta, 1998; Sirosh et al., 1996). Lateral excitatory pathways in the LISSOM model help the development of a topographic RF arrangement. The LISSOM lateral excitatory and inhibitory synaptic plasticity rules cause highly specific lateral pathway connectivity to develop between neurons that have similar RF properties (Sirosh & Miikkulainen, 1997).

Adaptation rules

In adaptation models (Xing & Gerstein, 1994), the RF changes occur as a result of adaptive modifications in the sensitivity of *single* neurons, rather than as a result of modifications in the synaptic weights between *pairs* of neurons.

5.1.3 Significance and contributions of this chapter

This chapter analyzes the role of each rule individually. The EXIN rules and the LISSOM rules have been used to model development of cortical properties and functions in young animals. Studies on young animals in their critical periods show that the afferent and lateral pathway connectivity in the primary visual cortex are modified by changes in the visual environment (Hubel & Wiesel, 1965, 1970; Hubel et al., 1977; Katz & Callaway, 1992). However, the neural basis of adult cortical plasticity, e.g., RF changes after artificial scotoma

conditioning and retinal lesions in adult animals, is not known. Thus, the rules in the EXIN model, the LISSOM model, and the adaptation models are studied individually to determine whether they produce effects consistent with the experimentally observed RF changes after artificial scotoma conditioning and retinal lesions in adult animals. The possible effects of the full EXIN and the full LISSOM model are also discussed. The simulation results based on individual rules serve as predictions for the effects of artificial scotoma conditioning and retinal lesions in adult animals in the presence of pharmacological agents that block plasticity in specific pathways, e.g., NMDA receptor antagonists which block plasticity in excitatory pathways (Kirkwood et al., 1993). The simulations show differences in two plausible rules for plasticity in lateral inhibitory pathways (the outstar EXIN lateral inhibitory rule and the instar LISSOM lateral inhibitory rule) in the context of artificial scotoma conditioning and retinal lesions. A novel experiment is suggested to further differentiate between the rules.

In this chapter, experimental data on cortical effects of artificial scotoma conditioning and retinal lesions are used to constrain plausible rules for dynamic RF changes. In particular,

1. the chapter analyzes the effects of an *instar* and an *outstar* lateral inhibitory synaptic plasticity rule during scotoma conditioning;

2. the effects of different plausible ways of modifying *effective* inhibition to neurons during scotoma conditioning, e.g. due to changes in lateral excitatory or afferent excitatory pathway strength, or neuronal adaptation, are studied;

3. some of the possible rules that *could* produce dynamic RF changes are eliminated based on comparison with experimental data;

4. the chapter shows that the EXIN outstar lateral inhibitory synaptic plasticity rule and the LISSOM instar lateral excitatory synaptic plasticity rule are sufficient to account for most of the data on artificial scotoma conditioning and on the short-term effects of retinal lesions (the effects of orientation selectivity on RF dynamics during artificial scotoma were not simulated);

5. the sufficiency of the EXIN lateral inhibitory synaptic plasticity rule in producing RF changes after artificial scotoma conditioning and after retinal lesions in adult animals provides indirect evidence for the existence of plasticity in lateral inhibitory pathways and predicts characteristics of inhibitory synaptic plasticity in cortex; and

6. a novel experiment, *complementary scotoma conditioning*, is proposed to distinguish the effects caused by neuronal adaptation from those caused by synaptic plasticity.

5.2 Methods

5.2.1 Network simulation organization

The architecture used for the simulations is a two-layered neural network with afferent and lateral connections, corresponding to parts of subcortex and primary visual cortex. A patch of neurons in the primary visual cortex, arranged in a 30×30 grid of spatial positions, was simulated. The position of each neuron's RF corresponded to the neuron's position in the grid. Adjacent RFs initially had more than 50% spatial overlap.

In the computer simulations, Layer 1 (corresponding to LGN processing) and Layer 2 (corresponding to early laminae of primary visual cortex) each had a 30×30 array of neurons. For ease of simulation, the initial afferent pathway weight and lateral pathway weight distributions in the simulations are chosen to be spatially isotropic. Furthermore, the input feature to these networks is an isotropic Gaussian blob (see Section 5.2.2), which when used to train the networks produces spatially isotropic receptive fields. However, isotropic RFs are not essential for these networks to produce changes in RF properties during the various forms of input conditioning. The EXIN and LISSOM learning rules are competitive learning rules and produce orientation selective neurons if the input features are oriented (Marshall, 1990d; Sirosh et al., 1996); scotoma conditioning using oriented features would affect the networks as described in Sections 5.2.5 and 5.2.6. The adaptation networks are based on neuronal adaptation, without synaptic plasticity. The weights in the adaptation networks can be assigned to produce orientation selective neurons. The adaptation of the orientation selective neurons during artificial scotoma conditioning

will produce RF expansions because of differences in adaptation levels as explained in Section 5.2.7.

Following Xing and Gerstein (1994), orientation selectivity is not built into the simulations. This is a gross simplification, as it discounts the effects of neurons selective to other orientations on dynamic RF changes. The simplification of representing only iso-orientation selective neurons in Layer 2 is partially justified by observing that the RF expansion was more pronounced and robust during conditioning with iso-orientation patterns than during conditioning with ortho-orientation patterns (Pettet & Gilbert, 1992). In the discussion section, a mechanism for orientation selectivity is described which may model the influence of neurons with other orientation selectivity on dynamic RF properties.

The following symbols are used to refer to the various entities of the network. The indices (i,j) and (k,l) are used to refer to Layer 1 neurons, and (p,q), (r,s), and (u,v) refer to Layer 2 neurons, where $i,j,k,l,p,q,r,s,u,v \in \{-15,\ldots,14\}$. These indices also represent the retinotopic coordinates of the neurons' RF. The weight of the afferent excitatory connection pathway from a Layer 1 neuron (i,j) to a Layer 2 neuron (p,q) is denoted by $Z^{+}_{ij,pq}(t)$. The weight of the lateral inhibitory connection pathway and the weight of the lateral excitatory connection pathway from Layer 2 neuron (p,q) to Layer 2 neuron (r,s) are represented by $Z^{-}_{pq,rs}(t)$ and $Z^{+}_{pq,rs}(t)$, respectively. These pathway weight values may represent the effect of a monosynaptic connection, the total effect of a polysynaptic chain of connections (see Section 5.5.7), or the population effect of multiple direct synapses. The activation levels (mean spike rate) over time of Layer 1 neuron (i,j) and Layer 2 neuron (p,q) are represented by $x_{ij}(t)$ and $x_{pq}(t)$, respectively.

5.2.2 The inputs

The inputs to Layer 1 were obtained as follows. First, two-dimensional 30×30 images were convolved with a Gaussian kernel, K, with toroidal wraparound. The input stimulus at each position in the images could be 0 or 1. The input at each position took value 1 with probability Φ during a given simulation step. After convolution, the resultant image was normalized by the maximum intensity value in the image. In the simulations, the mean of the normalization factor was 1.68, with a standard deviation of 0.34, over 10,000

inputs. The resultant images from the normalization stage were the inputs to Layer 1. These inputs to Layer 1 are called normal stimuli.

In artificial scotoma conditioning, random stimulation in the whole visual field except in a masked region was followed by whole-field random stimulation. To simulate inputs with a scotoma, images with a scotoma were convolved with the kernel K and then normalized. Input stimuli at positions outside the scotoma region had probability Φ of being assigned value 1, and input stimuli inside the scotoma region had value 0. These inputs are called scotoma stimuli. The term "cortical scotoma" refers to the silenced region in Layer 2 as a result of using retinal scotoma stimuli (Xing & Gerstein, 1994; Darian-Smith & Gilbert, 1995).

5.2.3 Simulation procedure

In the simulations, the experimental paradigm of Pettet and Gilbert (1992) was followed. The original RF was determined after a period of random whole-field stimulation. In all the simulations, the initial whole-field stimulation was continued until the sum of the magnitude of individual weight changes after 100 training steps had reached an asymptote. Then the RF was again measured after conditioning with the artificial scotoma. To determine reversibility of RF changes, the RF was measured again after whole-field stimulation.

5.2.4 RF measurements

The RF was mapped using single-point stimulation, blurred with the Gaussian kernel K, at all input positions (i, j). The RF of a Layer 2 neuron (p, q) is defined as the collection of positions (i, j) at which the test input causes the activation level x_{pq} to exceed a threshold Θ.

5.2.5 The EXIN model

The EXIN model (Figure 5.2) combines an instar afferent EXcitatory synaptic plasticity rule and an outstar lateral INhibitory synaptic plasticity rule. The EXIN synaptic

plasticity rules change the weights as a function of the input stimuli so that different neurons become selective for different input patterns and every input pattern is represented by a sparse output pattern (Marshall, 1995a). In scotoma conditioning, a subset of the visual input is removed, and therefore neurons previously selective for these inputs are not stimulated. The EXIN rules change the weights so that the unstimulated neurons become responsive to different input patterns, resulting in changes in their RFs.

The EXIN lateral inhibitory synaptic plasticity rule

The lateral inhibitory weights, $Z^-_{pq,rs}$, are modified according to the anti-Hebbian rule

$$\frac{d}{dt}Z^-_{pq,rs} \;=\; \delta\; \mathcal{G}(x_{pq})\left(-Z^-_{pq,rs} \;+\; \mathcal{Q}(x_{rs})\right) \tag{5.1}$$

(Marshall, 1995a), where $\delta > 0$ is a small learning rate constant and $\mathcal{G}$ and $\mathcal{Q}$ are half-rectified non-decreasing functions. Thus, *whenever a neuron is active, its output inhibitory connections to other active neurons tend to become slightly stronger (i.e., more inhibitory), while its output inhibitory connections to inactive neurons tend to become slightly weaker*. Neuron activations remain within $[-C, B]$ according to a shunting equation (Equation 5.3) based on the Hodgkin model (Hodgkin, 1964); this causes the weight values to remain bounded as well, because according to Equation 5.1, $Z^-_{pq,rs}(t) \in [0, \mathcal{Q}(B)]$ for $t \geq 0$, if $Z^-_{pq,rs}(0) \in [0, \mathcal{Q}(B)]$ (Grossberg, 1982). The weight change in Equation 5.1 approaches zero as $Z^-_{pq,rs}$ approaches $\mathcal{Q}(x_{rs})$, the weight change is positive when $Z^-_{pq,rs} < \mathcal{Q}(x_{rs})$, and the weight change is negative when $Z^-_{pq,rs} > \mathcal{Q}(x_{rs})$. The weight change approaches zero as $Z_{pq,rs}$ approaches $\mathcal{Q}(x_{rs})$.

In an outstar synaptic plasticity rule (Grossberg, 1972), *pre*synaptic activity "enables" the plasticity at a synapse; when the plasticity is enabled, the weight tends to become proportional to the postsynaptic activity. In an instar synaptic plasticity rule, *post*synaptic activity enables the plasticity; when the plasticity is enabled, the weight tends to become proportional to the presynaptic activity. Thus, to make Equation 5.1 into an instar rule, x_{pq} and x_{rs} would be interchanged.

An effect of the EXIN inhibitory synaptic plasticity rule is that if two neurons are frequently coactivated, then the lateral inhibitory weights between them become strong.

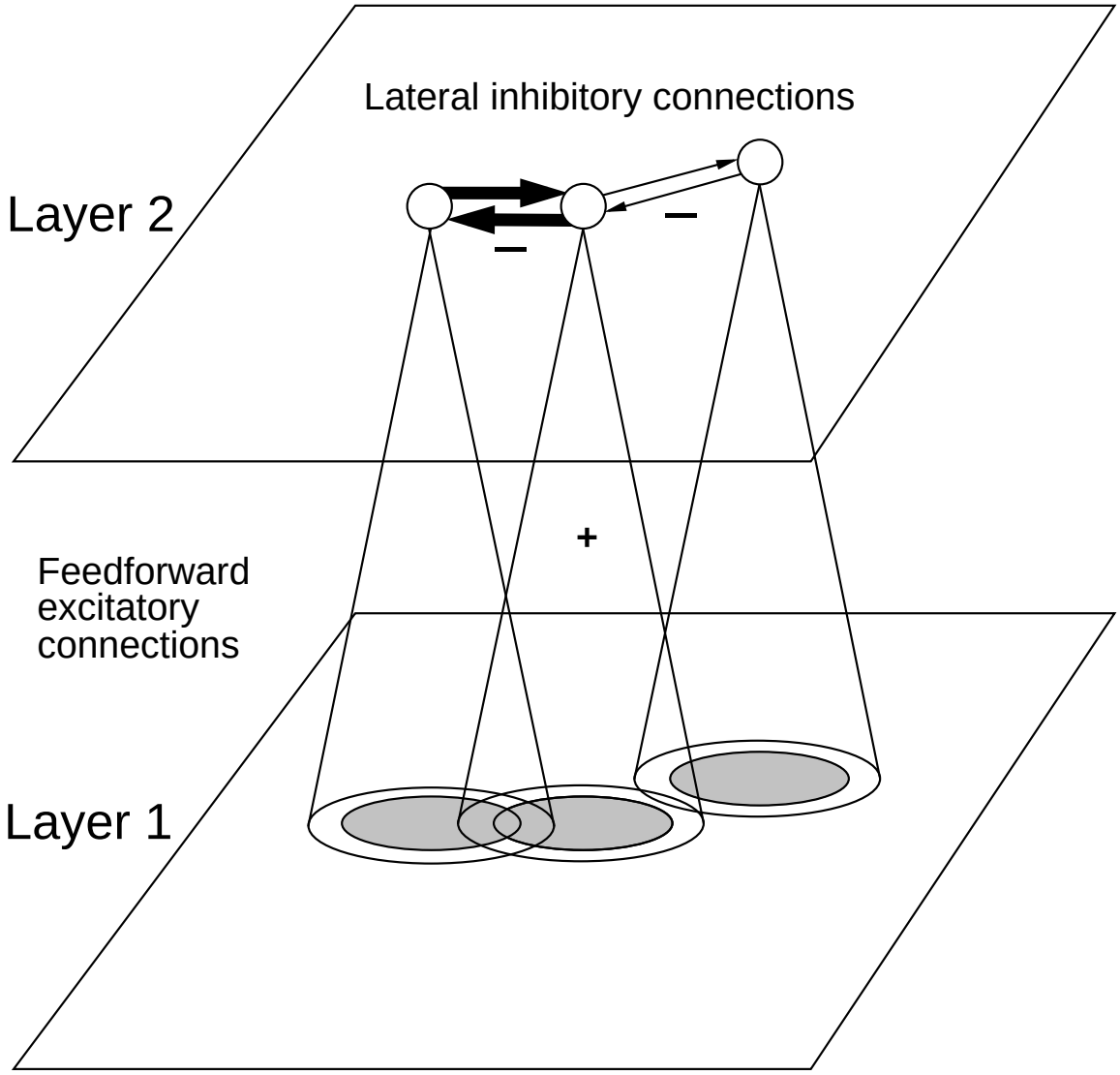

Figure 5.2: **Network architecture for the EXIN model.**
The afferent pathways from Layer 1 to Layer 2 are excitatory. The lateral pathways within Layer 2 are inhibitory. The unfilled ellipses represent the afferent connectivity pattern from Layer 1 to Layer 2 neurons. The shaded ellipses represent the RFs of Layer 2 neurons. The strength of lateral inhibitory pathways is a function of the amount of overlap in the afferent connectivity patterns to the Layer 2 neurons. The strength of lateral inhibitory pathways is indicated by the thickness of the arrows.

If two neurons are only rarely coactivated then their reciprocal lateral inhibitory weights become weak. Strong lateral inhibition between two neurons tends to make them less likely to be coactivated, causing the two to become selective to different inputs according to the excitatory synaptic plasticity rule (Equation 5.2). Thus, when the network is exposed to normal stimuli, the lateral inhibitory weights and the excitatory afferent weights are modified so that each neuron becomes selective to different inputs and the RFs of all Layer 2 neurons cover the input space (Marshall, 1995a; Marshall & Gupta, 1998). This leads to improved discrimination and sparse coding (Marshall, 1995a).

The EXIN afferent excitatory synaptic plasticity rule

The afferent excitatory weight changes are governed by a variant of a Hebbian learning rule. The rule can be expressed (Grossberg, 1982; Marshall, 1995a) as

$$\frac{d}{dt} Z^{+}_{ij,pq} \;=\; \epsilon \; \mathcal{F}(x_{pq}) \left(-Z^{+}_{ij,pq} \;+\; \mathcal{H}(x_{ij}) \right), \tag{5.2}$$

where $\epsilon > 0$ is a small learning rate constant, and $\mathcal{F}$ and $\mathcal{H}$ are half-rectified non-decreasing functions.

Thus, *whenever a neuron is active, its input excitatory connections from active neurons tend to become slightly stronger, while its input excitatory connections from inactive neurons tend to become slightly weaker.* As discussed for Equation 5.1, the weight values in Equation 5.2 remain bounded.

The EXIN excitatory synaptic plasticity rule is an instar competitive learning rule. When used in conjunction with strong lateral inhibition, it causes model cortical neurons to become selective for a specific pattern of input activations (Marshall, 1995a).

Stability of EXIN networks

Like other competitive learning rules, the EXIN rules do not produce absolutely stable synaptic weights. The stability of the network depends on the input environment. If the input distribution changes for a sufficiently long time, the weights change to encode the new statistics. Such instability, reflecting the statistics of the input environment is

advantageous at lower-levels of cortical processing; e.g., the cortex can reorganize after cortical or peripheral damage.

The learning rates in competitive learning networks must be kept small enough to allow approximate stability in a statistically stationary input environment, yet large enough to allow plasticity in response to the statistical changes posed by perturbations such as scotomas. Stability in competitive learning networks and the various learning parameters are discussed in Appendix C, Section C.1.2.

Explanation of dynamic RF changes based on the EXIN rules

The maximum extent of a Layer 2 neuron's RF is limited by the axonal arborization spread of the Layer 1 neurons from which it receives afferent excitation. In addition, a Layer 2 neuron receives lateral inhibition from neurons with which it is frequently co-excited. Neurons in Layer 2 can be consistently co-excited if they share inputs from common Layer 1 neurons. Because of inhibition, it is possible that a Layer 2 neuron (p,q) does not become active in response to some active Layer 1 neuron (i,j), even though $Z^{+}_{ij,pq} > 0$.

The role of the EXIN afferent excitatory and lateral inhibitory synaptic plasticity rules in producing RF changes during scotoma conditioning are studied independently.

Role of EXIN lateral inhibitory synaptic plasticity. Consider the EXIN network with the afferent excitatory synaptic plasticity rule disabled and the lateral inhibitory synaptic plasticity rule enabled. When the network is exposed to scotoma stimuli with a sufficiently large scotoma, there exists a cortical scotoma region in Layer 2. During scotoma conditioning, neurons outside the cortical scotoma region are active and those inside the cortical scotoma region are not. Let neuron (p,q) be outside and neuron (r,s) be inside the initial cortical scotoma region (Figure 5.3a). Assume that after conditioning with normal stimuli, $Z^{-}_{pq,rs}$ and $Z^{-}_{rs,pq}$ are not zero, because neurons (p,q) and (r,s) share common afferent inputs. If for a given stimulus, neuron (p,q) is active, then according to the EXIN inhibitory synaptic plasticity rule, $Z^{-}_{pq,rs}$ weakens (Figure 5.3b). However, $Z^{-}_{rs,pq}$ is unchanged, since x_{rs} is zero. Thus, lateral inhibitory weights to neuron (r,s) from active neurons outside the cortical scotoma region weaken, but lateral inhibitory weights from neuron (r,s) are unaffected. The net effect, from the point of view of neuron (r,s), is

that its afferent excitatory input weights remain unchanged and its input lateral inhibitory weights from neurons outside the cortical scotoma region weaken (if nonzero before the conditioning). If the RF of neuron (r, s) is measured then, it will be more responsive to positions in its old RF and will be responsive to some new positions too (Figure 5.3b), thus producing RF expansion. The simulation results are presented in Section 5.3.1.

When the network is again conditioned with normal stimuli, the asymmetric lateral inhibitory weights between the neurons inside and outside the cortical scotoma region regain symmetry. Thus, the RFs of neurons in the cortical scotoma are restored.

Role of EXIN afferent excitatory synaptic plasticity. Now consider the EXIN network with the lateral inhibitory synaptic plasticity rule disabled and the afferent excitatory synaptic plasticity rule enabled. Neurons close to the edge of the cortical scotoma but outside it show some interesting changes (e.g., neuron (p, q) in Figure 5.3c). Because these neurons are near the cortical scotoma edge, the region of their RF inside the scotoma is not stimulated. Thus, because of the EXIN excitatory synaptic plasticity rule, afferent excitatory connections from Layer 1 neurons in the scotoma region to this neuron become weaker. Hence its RF shrinks, and the center of its RF shifts outward. During RF measurement after scotoma conditioning, these neurons (e.g., (p, q)) respond only weakly to stimuli in the scotoma region and hence exert less inhibition on neurons that were inactive during conditioning (e.g., (r, s)). Thus, the neurons that were inactive during the conditioning show increased responsiveness and RF expansion. This explanation for RF expansion during scotoma conditioning was proposed by Sirosh et al. (1996). The RF expansion causes the RF centers to shift away from the scotoma center (Section 5.3.2).

When the EXIN network with only afferent excitatory synaptic plasticity enabled is conditioned again using normal stimuli, the neurons do not recover their original RFs. The neurons whose afferent excitatory pathways from the scotoma region were weakened are weakly actived by stimulation of the region that was occluded during artificial scotoma conditioning, during the subsequent whole-field stimulation. On the other hand, the neurons whose initial RF was inside the scotoma region during artificial scotoma conditioning are more responsive to positions inside the scotoma during whole-field stimulation, following artificial scotoma conditioning. Thus, during whole-field stimulation following artificial

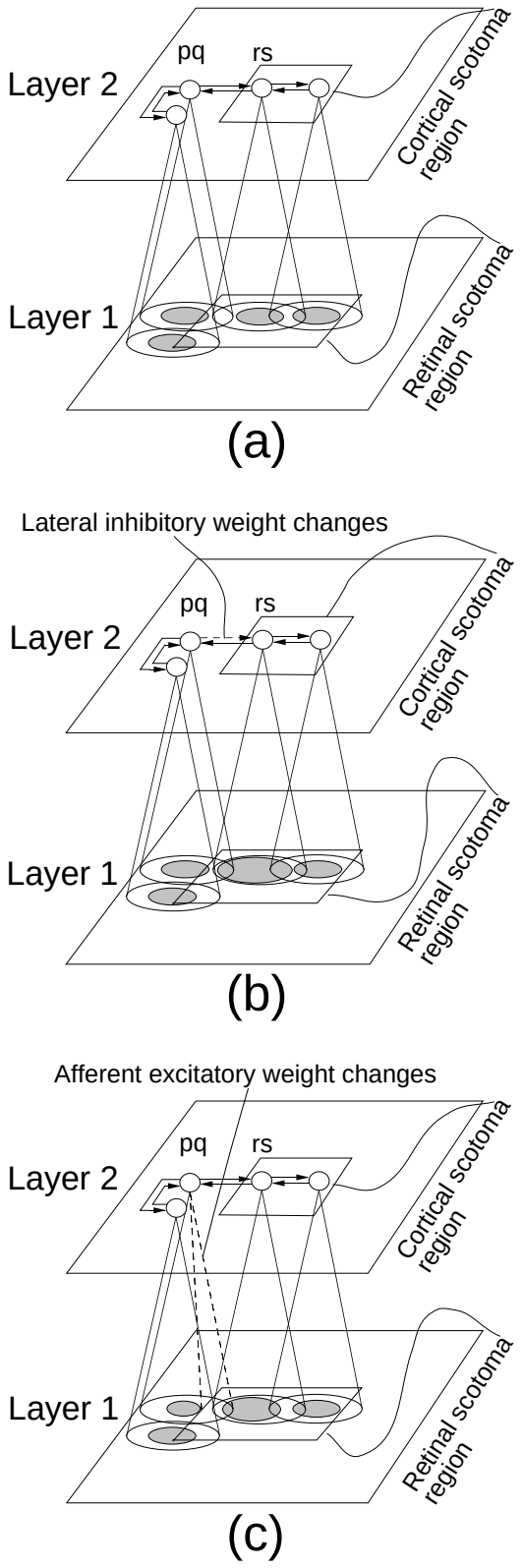

Figure 5.3: Legend on next page.

Figure 5.3: **The effects of scotoma conditioning on the EXIN model.** Figure on previous page. The unfilled ellipses represent the afferent connectivity pattern from Layer 1 to Layer 2 neurons. The shaded ellipses represent the RFs of Layer 2 neurons. The parallelogram within Layer 1 represents the scotoma region, and the parallelogram within Layer 2 represents the cortical scotoma region before scotoma conditioning. (a) The network state before scotoma conditioning. Neuron (r, s) is in the cortical scotoma region because its RF is within the scotoma region; neuron (p, q) is outside the cortical scotoma region. (b) The network state after scotoma conditioning with only lateral inhibitory synaptic plasticity enabled. After scotoma conditioning, lateral inhibitory connections between neurons in the cortical scotoma and lateral inhibitory connections between neurons outside the cortical scotoma do not change. However, lateral inhibitory connections from neurons outside the cortical scotoma (e.g., (p, q)) to neurons inside the cortical scotoma (e.g., (r, s)) weaken (dashed line). The decrease in inhibition received by neuron (r, s) results in expansion of its RF. (c) The network state after scotoma conditioning with only afferent excitatory synaptic plasticity enabled. After scotoma conditioning, afferent connections to neurons in the cortical scotoma do not change. However, afferent connections from locations inside the scotoma to neurons outside the cortical scotoma (e.g., (p, q)) weaken (dashed line). Neurons inside the cortical scotoma (e.g., (r, s)) receive less inhibition from neuron (p, q) when locations inside the scotoma are stimulated. Thus, neuron (r, s) shows new responsiveness to these locations, and its RF size thus increases.

scotoma conditioning, the neurons whose initial RF was inside the scotoma region strengthen afferent excitatory pathways from positions inside the scotoma region to which they are more responsive and exert greater inhibition on neurons whose initial RF straddled the scotoma boundary. The neurons whose RF straddled the scotoma boundary further weaken afferent excitatory pathways from positions inside the scotoma region to which they have become less responsive after artificial scotoma conditioning, as their responsiveness to positions inside the scotoma region is further suppressed. With strong fixed lateral inhibitory pathways weights, the lateral inhibition between neurons suppresses the activation of the neurons whose RF size was decreased (because of weakening of pathways from the scotoma during scotoma conditioning) when inputs are presented at positions inside the scotoma. According to the EXIN afferent excitatory synaptic plasticity rule, afferent pathway weights change only when postsynaptic neurons are active. Thus, the weak afferent connections from the scotoma region to the neurons whose RF size was decreased are not strengthened, and the RFs of these neurons do not shift back to their original positions (Section 5.3.2).

In the EXIN network (with either lateral inhibitory or afferent excitatory synaptic plasticity alone), in response to scotoma stimuli, all neurons that show RF expansion belong to the set of neurons that were inside the initial cortical scotoma. Thus, after scotoma conditioning, the EXIN network with both lateral inhibitory and afferent excitatory synaptic plasticity will produce RF expansion in neurons that were inside the initial cortical scotoma.

The activation equation

The activation level x_{pq} of each Layer 2 neuron is governed by a shunting equation (Grossberg, 1972) based on the Hodgkin (Hodgkin, 1964) model:

$$\frac{d}{dt}x_{pq} \;=\; -Ax_{pq} \;+\; \beta(B - x_{pq})E_{pq} \;-\; \gamma(C + x_{pq})I_{pq}, \tag{5.3}$$

where A, B, C, β, and γ are constants, and E_{pq} and I_{pq} represent respectively the neuron's total afferent excitatory and lateral inhibitory input signals. Because Equation 5.3 is a shunting equation, if $x_{pq}(0) \in [-C, B]$ then $x_{pq}(t) \in [-C, B]$ for all time $t \geq 0$ (Cohen & Grossberg, 1983). Thus, activation levels are forced to remain within a bounded range, between $-C$ and B. The total input excitation E_{pq} is defined as

$$E_{pq} = \left(\sum_{ij}[x_{ij}]Z^{+}_{ij,pq}\right)^2, \tag{5.4}$$

and the total input inhibition I_{pq} is given by

$$I_{pq} = \sum_{rs}[x_{rs}]Z^{-}_{rs,pq}, \tag{5.5}$$

where $[a] \equiv \max(a, 0)$. Parameters β and γ, respectively, control the effectiveness of the excitation and inhibition received by a Layer 2 neuron. The squaring in Equation 5.4 sharpens the RF profile of the Layer 2 neurons; squaring enhances excitation to Layer 2 neurons when $\sum_{rs}[x_{rs}]Z^{-}_{rs,pq} > 1$ and suppresses excitation to Layer 2 neurons when $\sum_{rs}[x_{rs}]Z^{-}_{rs,pq} < 1$.

Stability of the shunting equation: Cohen-Grossberg theorem

The shunting equation (Equation 5.3) with $Z^{-}_{rs,pq} = Z^{-}_{pq,rs} \geq 0$, belongs to a class of competitive dynamical systems that are absolutely stable; i.e., the system has fixed points

for any choice of parameters (Cohen & Grossberg, 1983). The neuronal activations in such a system are guaranteed to reach stable equilibrium values for all synaptic weight values with the restriction.

However, it is not known whether the shunting equation remains absolutely stable even when $Z^{-}_{rs,pq} \neq Z^{-}_{pq,rs} \geq 0$ for some pairs of neurons. The symmetry of reciprocal pairs of lateral inhibitory weights is not guaranteed by the EXIN lateral inhibitory synaptic plasticity rule. During normal stimulation, the lateral inhibitory weights are approximately symmetric (Marshall, 1995a). They become asymmetric between neurons across the scotoma boundary during scotoma conditioning. Nevertheless, simulations empirically show the stability of the EXIN network (Section C.1.1).

The initial weights

In the EXIN simulations, the initial afferent excitatory weight from Layer 1 neuron (i, j) to Layer 2 neuron (p, q) is given by

$$Z^{+}_{ij,pq}(0) = \left[\Psi \times \exp\left(\frac{-(x^2 + y^2)}{\sigma^2_{\mathbf{ff}}} \right), \Gamma_{\mathbf{ff}} \right], \tag{5.6}$$

where

$$[a, b] \equiv \begin{cases} a & \text{if } a > b, \\ 0 & \text{otherwise,} \end{cases} \tag{5.7}$$

$x, y \in \{-15, \cdots, 14\}$, $p = (((i+15)+x) \bmod 30) - 15$, and $q = (((j+15)+y) \bmod 30) - 15$. The indices i, j, p, and q are in $\{-15, \cdots, 14\}$. The indices i, j, p, and q and the distances x and y are related by the above equations because the model cortical and thalamic neurons are arranged in a wrapped-around two-dimensional grid. The parameters Ψ, $\sigma_{\mathbf{ff}}$, and $\Gamma_{\mathbf{ff}}$ are positive constants.

The initial lateral inhibitory weights between Layer 2 neurons (p, q) and (r, s), where $p \neq r$ or $q \neq s$, are set as follows. Let

$$X_{pq,rs} = \sum_{ij} \min(Z^{+}_{ij,pq}, Z^{+}_{ij,rs}) \tag{5.8}$$

and

$$W^{-}_{pq,rs}(0) = W^{-}_{rs,pq}(0) = [X_{pq,rs}, \Gamma_{\mathbf{i}}], \tag{5.9}$$

where $\Gamma_{\mathbf{i}}$ is a constant. Then

$$Z^{-}_{pq,rs}(0) = Z^{-}_{rs,pq}(0) = \frac{\Omega \times W^{-}_{ps,rs}}{\max\limits_{ab,cd \in \text{Layer 2}} W^{-}_{ab,cd}}, \tag{5.10}$$

where Ω is a constant. Equation 5.10 assigns inhibitory weights between two distinct Layer 2 neurons in proportion to the amount of overlap in the RFs of the two neurons.

The initial weight values of the pathways were chosen according to Equations 5.6–5.10, instead of completely random weights, to speed the convergence of weight values during subsequent whole field stimulation and to ensure RF topography, thereby avoiding RF shifts and RF size changes caused by RF scatter that may be present when the initial weights are chosen randomly. The networks produced after the whole field stimulation were used for scotoma conditioning simulations.

Neurons do not directly inhibit themselves in the EXIN network; that is, $Z^{-}_{pq,pq}$ is zero or nonexistent, and $\frac{d}{dt} Z^{-}_{pq,pq} = 0$.

Lateral excitatory pathways are omitted in this model; all $Z^{+}_{pq,rs}$ are fixed at zero. This is a simplification based on the assumption that the net effect of the lateral excitatory and inhibitory pathways on excitatory neurons is inhibitory. Partial support for setting $Z^{+}_{pq,rs}$ to zero comes from the lack of disynaptic excitatory postsynaptic potential due to stimulation of thalamocortical afferents during intracellular recordings in simple neurons of the cat visual cortex (Ferster, 1989) and in layer 5 neurons of adult mice (Gil & Amitai, 1996). Although lateral excitatory pathways exist in the cortex, Weliky et al. (1996) and Gil and Amitai (1996) showed that at high stimulation strengths the long-range horizontal pathways exert overall inhibition on pyramidal neurons. This issue is discussed further in Section 5.5.7.

5.2.6 The LISSOM model

The LISSOM model (Sirosh & Miikkulainen, 1994ab, 1995, 1997; Sirosh et al., 1996) uses afferent excitatory, lateral excitatory, and lateral inhibitory synaptic plasticity rules. All three rules are instar rules based on weight normalization. The LISSOM rules produce use-dependent weight changes and thus produce changes in RF properties during artificial scotoma conditioning and lesions.

The LISSOM synaptic plasticity rules

The most significant differences between the LISSOM model and the EXIN model are that LISSOM uses an instar, rather than outstar, inhibitory synaptic plasticity rule, and that LISSOM has used lateral excitatory pathways, in addition to lateral inhibitory and afferent excitatory pathways.

In the LISSOM model (Figure 5.4), intracortical interactions are mediated by both lateral excitatory and lateral inhibitory pathways. The weights of both lateral excitatory and lateral inhibitory pathways change according to an instar Hebbian synaptic plasticity rule. This rule keeps the sum of the squares of the synaptic weights of the excitatory connections constant, and likewise for the inhibitory connections. After the activations of Layer 2 neurons have stabilized, the weights are modified according to

$$Z_{ab,cd}(t+1) = \frac{Z_{ab,cd}(t) + \xi x_{ab} x_{cd}}{\left(\sum_{ef} \left(Z_{ef,cd}(t) + \xi x_{ef} x_{cd}\right)^2\right)^{\frac{1}{2}}} \tag{5.11}$$

(Sirosh & Miikkulainen, 1994b), where the constant ξ controls the rate of learning. The LISSOM rules are "instar" (Grossberg, 1972) rules because weight change in pathways to a target neuron is enabled only if the target neuron is active.

Sirosh et al. (1996) used Equation 5.11 for the afferent excitatory synaptic plasticity. They used sum normalization $\left(\sum_{ef} \left(Z_{ef,cd}(t) + \xi x_{ef} x_{cd}\right)\right)$ for the lateral excitatory and lateral inhibitory synaptic plasticity rules, instead of length normalization as in this chapter. Qualitatively, both length and sum normalization have the same effects. Length normalization causes the lateral excitatory and lateral inhibitory weight values to be larger than does sum normalization. In the simulations, length normalization produced larger RF size changes than did sum normalization.

For the afferent excitatory synaptic plasticity rule, *ab* and *ef* refer to Layer 1 neurons, and *cd* refers to Layer 2 neurons, $\xi = \xi_{\mathbf{ff}}$. For the lateral excitatory and lateral inhibitory synaptic plasticity rules, *ab*, *cd*, and *ef* refer to Layer 2 neurons. The parameter ξ is set to $\xi_{\mathbf{e}}$ and $\xi_{\mathbf{i}}$ for the lateral excitatory and lateral inhibitory synaptic plasticity rules, respectively. The weights remain bounded because of the weight normalizations.

In response to normal stimuli, LISSOM's learning rules cause the lateral inhibitory

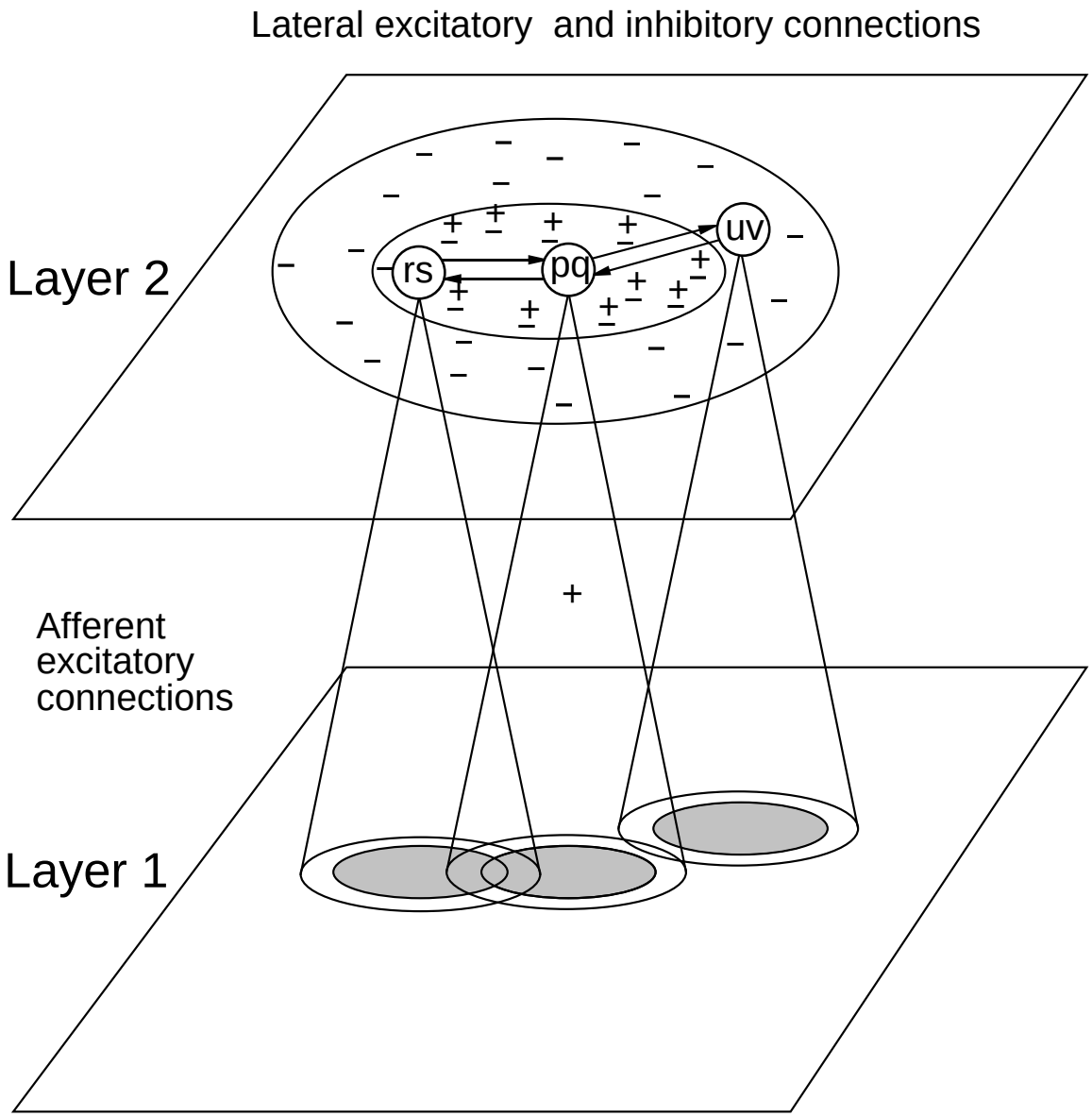

Figure 5.4: **Network architecture for the LISSOM model and the inhibition-dominant adaptation model.**
The connections from Layer 1 to Layer 2 are excitatory. There are lateral inhibitory and excitatory connections between Layer 2 neuron (p, q) and Layer 2 neurons within the inner ellipse (e.g., (r, s)). Neuron (p, q) also sends both inhibitory and excitatory connections to itself. The lateral connections between neuron (p, q) and Layer 2 neurons (e.g., (u, v)) outside the inner ellipse and inside the outer ellipse are inhibitory. The unfilled ellipses in Layer 1 represent the afferent connectivity pattern from Layer 1 to Layer 2 neurons. The shaded ellipses represent the RFs of Layer 2 neurons.

and lateral excitatory weights between pairs of Layer 2 neurons to remain approximately symmetric. In addition, the lateral inhibitory and excitatory weights become approximately proportional to the amount of coactivation between neuron pairs. The learning rules maintain the initial topographically arranged RFs (Sirosh & Miikkulainen, 1997).

Stability of LISSOM networks

The LISSOM learning rules are competitive learning rules. Therefore, the stability of LISSOM networks depends on the input environment and the learning rates (Sirosh & Miikkulainen, 1994b). This issues of network stability and choice of the various parameters in the current simulations are discussed in Appendix C, Section C.2.

Explanation of dynamic RF changes based on LISSOM rules

The effect of each of the three LISSOM synaptic plasticity rules is considered separately. The overall behavior of the LISSOM model depends on the relative learning rates of the three rules.

Role of LISSOM lateral inhibitory synaptic plasticity. Consider the LISSOM network with only the lateral inhibitory synaptic plasticity rule enabled. Let neuron (p, q) be outside and neuron (r, s) be inside the cortical scotoma region. Assume that after conditioning with normal stimuli, $Z^-_{pq,rs}$ and $Z^-_{rs,pq}$ are not zero, because neurons (p, q) and (r, s) share some common afferent inputs, and that they are approximately equal. According to the LISSOM lateral inhibitory synaptic plasticity rule, $Z^-_{pq,rs}$ does not change, because x_{rs} is 0. However, $Z^-_{rs,pq}$ decreases if some other neuron (u, v) is active, because the weights are normalized. In addition, the normalization causes the lateral inhibitory weights from active neurons (e.g, neurons (u, v) and (p, q)) to neuron (p, q) to become slightly stronger. In the LISSOM model, Layer 2 neurons send lateral excitatory and inhibitory pathways to themselves. Thus, because of the lateral inhibitory synaptic plasticity, neurons outside the cortical scotoma region receive a reduced overall amount of inhibition from neurons within the cortical scotoma. This causes neurons like (p, q) that are outside the cortical scotoma region to exhibit increased responsiveness, a RF expansion, and a slight inward RF shift toward the scotoma edge. The RF expansion of neuron (p, q) is asymmetric because it

receives reduced inhibition only when the input is in the scotoma region. For neurons in the overall excitatory zone of neuron (p, q) (e.g., (u, v) and (r, s)), the increased responsiveness of neuron (p, q) may result in increased responsiveness, a RF expansion, and a slight inward RF shift toward the scotoma edge. The increased responsiveness of (p, q) results in increased inhibition to neurons in the overall inhibitory zone of neuron (p, q) (e.g., (c, d) and (a, b)) (Figure 5.5b), when input locations inside the scotoma are stimulated. Because of the asymmetric RF profile, neurons whose initial RF center is inside the scotoma and in the overall inhibitory zone of neuron (p, q) (e.g., (a, b)) would show decreased responsiveness, RF contraction, and a small inward RF shift away from the scotoma edge (Figure 5.5b). The simulation results are in Section 5.3.1.

Role of LISSOM lateral excitatory synaptic plasticity. When only the LISSOM lateral excitatory synaptic plasticity rule is enabled, $Z^+_{pq,rs}$ does not change, $Z^+_{rs,pq}$ decreases, and the lateral excitatory weights from active neurons (e.g, neurons (u, v) and (p, q)) to neuron (p, q) become slightly stronger (in the LISSOM network neurons receive lateral excitatory pathways from itself), for the same reasons described in the previous paragraph (Figure 5.5c). Thus, neurons outside the cortical scotoma region receive a reduced amount of lateral excitation from neurons in the cortical scotoma. This results in reduced responsiveness, decreased RF size, and an outward RF shift, away from the scotoma edge, for neurons like (p, q) that are outside the cortical scotoma region. For neurons in the overall excitatory zone of neuron (p, q) (e.g., (u, v) and (r, s)), the decreased responsiveness of neuron (p, q) may result in decreased responsiveness, a RF contraction, and a slight outward RF shift away from the scotoma edge. For neurons in the overall inhibitory zone of neuron (p, q) (e.g., (c, d) and (a, b)), the decreased responsiveness of (p, q) results in reduced inhibition. Active neurons during scotoma conditioning receive weakened lateral excitatory signals from neurons inside the cortical scotoma. These asymmetric lateral excitatory weight changes lead to a decrease in RF size and an outward RF shift away from the scotoma in neurons whose initial RF center is close to the scotoma boundary (e.g., (p, q)). They also lead to an increase in RF size and an outward RF shift away from the scotoma center in neurons (e.g., (a, b)) whose initial RF is inside and close to the scotoma boundary (Figure 5.5c). The simulation results are shown in Section 5.3.3.

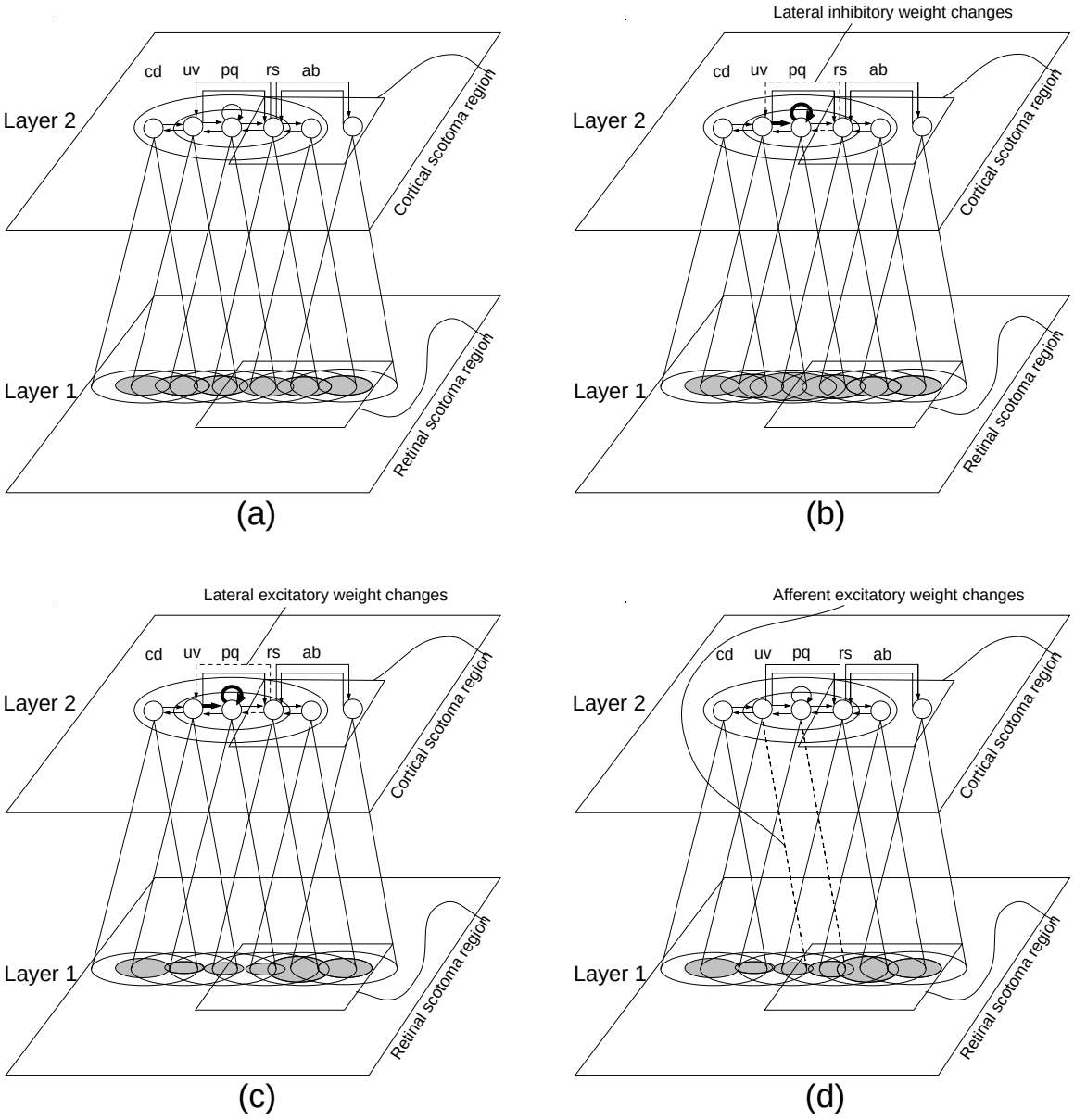

Figure 5.5: Legend on next page.

Figure 5.5: **The effects of scotoma conditioning on the LISSOM model.** Figure on previous page. The unfilled ellipses in Layer 1 represent the afferent connectivity pattern from Layer 1 to Layer 2 neurons. The shaded ellipses represent the RFs of Layer 2 neurons. The parallelogram within Layer 1 represents the scotoma region, and the parallelogram within Layer 2 represents the cortical scotoma region before scotoma conditioning. (a) The network state before scotoma conditioning. Neurons (r, s) and (a, b) are inside the cortical scotoma region because their RFs are within the scotoma region. Neurons (p, q), (u, v), and (c, d) are outside the cortical scotoma region. There are excitatory and inhibitory connections between neuron (p, q) and neurons in the small ellipse (e.g., (u, v) and (r, s)). The connections between neuron (p, q) and the neurons outside the small ellipse and inside the large ellipse are inhibitory. (b) The network state after scotoma conditioning with only instar lateral inhibitory synaptic plasticity enabled. The dashed lines represent a decrease in the connection weights and the thick lines represent an increase in the connection weights. (c) The network state after scotoma conditioning with only instar lateral excitatory synaptic plasticity enabled. (d) The network state after scotoma conditioning with only afferent excitatory synaptic plasticity enabled.

Role of LISSOM afferent excitatory synaptic plasticity. In the LISSOM network with only afferent excitatory synaptic plasticity enabled, the synaptic plasticity causes changes in the afferent connectivity of neurons close to the edge of the cortical scotoma region (Figure 5.5d). These neurons (e.g., (u, v) and (p, q)) have part of their input in Layer 1 within the scotoma. Thus, according to the afferent excitatory synaptic plasticity rule, when these neurons are activated, the weights from neurons within the scotoma become weaker, and weights from Layer 1 neurons outside the scotoma become stronger. This causes the RFs of Layer 2 neurons (e.g., (u, v) and (p, q)) close to the initial cortical scotoma edge to shrink and shift away from the scotoma center. In addition, these neurons respond weakly to stimulation at positions in the scotoma region and exert less inhibition on neurons (e.g., (a, b)) that were inactive during conditioning. Thus, the neurons that were inactive during the conditioning show increased responsiveness and RF expansion away from the scotoma center (Sirosh et al., 1996). The RF expansion causes the RF centers to shift away from the scotoma center (Figure 5.5d). The simulation results are in Section 5.3.2.

The overall effect on responsiveness, RF size, and RF position depends on the relative strengths and sizes of afferent excitation, lateral excitation, and lateral inhibition. It also depends on the learning rates of the three types of connections. In the LISSOM

model, the effects of inhibitory synaptic plasticity are in conflict with the effects of afferent and lateral excitatory synaptic plasticity. The RF expansion occurs in neurons *outside the cortical scotoma* if the relative strength and learning rate of lateral inhibitory weights are greater than those of the lateral and afferent excitatory weights. The RF expansion occurs in neurons *inside the cortical scotoma* if the relative strength and learning rate of lateral excitatory or afferent excitatory weights are greater than those of the lateral inhibitory weights. After artificial scotoma conditioning, the LISSOM rules produce RF expansion on one side of the scotoma boundary and RF contraction on the other side.

When the LISSOM networks (with plasticity in only one of the three types of pathways) are again conditioned with normal stimuli, the RFs of all affected neurons are restored.

The activation equation

In the LISSOM simulations, the Layer 2 neuron activations are determined iteratively by

$$x_{pq}(t+1) \;=\; S\left(\gamma_{\mathbf{ff}} \sum_{ij} Z^{+}_{ij,pq} x_{ij}(t) + \gamma_{\mathbf{e}} \sum_{rs} Z^{+}_{rs,pq} x_{rs}(t) - \gamma_{\mathbf{i}} \sum_{rs} Z^{-}_{rs,pq} x_{rs}(t)\right) \qquad (5.12)$$

where

$$S(a) \;=\; \frac{1}{1+\exp\left(-\left[a\right]\right)} - 0.5 \qquad (5.13)$$

(Sirosh & Miikkulainen, 1994b), and $[x] = \max(0, x)$. The constants $\gamma_{\mathbf{ff}}$, $\gamma_{\mathbf{e}}$ and $\gamma_{\mathbf{i}}$ are scaling factors on the excitatory and inhibitory weights and determine the strength of afferent and lateral interactions. The activations are bounded because of the sigmoid function S.

Stability of LISSOM activation equation

The LISSOM activation equation can quickly equilibrate (Sirosh & Miikkulainen, 1994b). Equation 5.12 approached a fixed point during the various input conditioning regimes for the parameters that are used in this chapter (Appendix C, Section C.2.1).

The initial weights

In simulations using the LISSOM model, the connection weights were computed as follows. Let

$$Y_{ab,cd} = \left[\exp\left(\frac{-(m^2+n^2)}{\sigma^2} \right), \Gamma \right], \tag{5.14}$$

where $a, b, c, d, m, n \in \{-15, \ldots, 14\}$, $c = (((a + 15) + m) \bmod 30) - 15$, and $d = (((b + 15) + n) \bmod 30) - 15$. The relationship between the indices a, b, c, and d and the distances m and n is such that the model cortical and thalamic neurons are arranged in a wrapped-around two-dimensional grid. The paramters σ and Γ are positive constants, and the notation $[.,.]$ is defined by Equation 5.7. Then

$$Z_{ab,cd}(0) = \frac{Y_{ab,cd}}{\left(\sum_{ef} Y_{ef,cd}^2 \right)^{\frac{1}{2}}} \tag{5.15}$$

is the initial weight of the connection pathway from neuron (a, b) to neuron (c, d).

For afferent weights, ab and ef refer to Layer 1 neurons, cd refers to Layer 2 neurons, $\sigma = \sigma_{\mathbf{ff}}$, and $\Gamma = \Gamma_{\mathbf{ff}}$. For lateral excitatory and lateral inhibitory weights, ab, cd, and ef refer to Layer 2 neurons. For lateral excitatory weights, $\sigma = \sigma_{\mathbf{e}}$ and $\Gamma = \Gamma_{\mathbf{e}}$, and for inhibitory weights, $\sigma = \sigma_{\mathbf{i}}$ and $\Gamma = \Gamma_{\mathbf{i}}$.

The initial weights were chosen to speed the simulations; in all simulations, these weight values were overridden by new values during an initial phase of whole-field stimulation.

5.2.7 The inhibition-dominant adaptation model

Xing and Gerstein (1994) described four models of dynamic RFs and argued in favor of an inhibition-dominant network with neural adaptation, or habituation. A neuron's ability to fire decreases/increases after a period of activity/inactivity, without any synaptic changes. In an inhibition-dominant adaptation network, the strength of the lateral inhibitory connections is greater than that of lateral excitatory connections, and all the weights are fixed.

Xing and Gerstein used a spiking neuron model. They modeled adaptation by modifying the action potential threshold, which depended on the number of spikes of a

neuron in the recent past. Thus, if a neuron spikes frequently, its action potential threshold increases, thereby making it spike less vigorously, even though the same input is present. On the other hand, if a neuron has not been activated for a long time, then it becomes highly responsive to inputs in its RF.

The adaptation equation

In the present simulations the spiking neuron model is not used. Instead, the output of a Layer 2 neuron (p, q) is modeled as $[x_{pq} - T_{pq}]$, where x_{pq} is controlled by a shunting equation (Grossberg, 1972):

$$\frac{d}{dt}x_{pq} \;=\; -Ax_{pq} \;+\; (B - x_{pq})E_{pq} \;-\; \gamma(C + x_{pq})I_{pq}, \tag{5.16}$$

with

$$E_{pq} \;=\; \beta_{\mathbf{ff}} \sum_{i,j \in \text{Layer 1}} [x_{ij}]Z^{+}_{ij,pq} \;+\; \beta_{\mathbf{e}} \sum_{r,s \in \text{Layer 2}} [x_{rs} - T_{rs}]Z^{+}_{rs,pq}, \tag{5.17}$$

$$I_{pq} \;=\; \sum_{(r,s) \in \text{Layer 2}} [x_{rs} - T_{rs}]Z^{-}_{rs,pq}, \tag{5.18}$$

and $[a] \equiv \max(a, 0)$. The positive constants $\beta_{\mathbf{ff}}$ and $\beta_{\mathbf{e}}$ control the effectiveness of afferent excitation and lateral excitation, respectively. The variable T_{pq} represents the adaptive firing threshold of neuron (p, q). After the activation of Layer 2 neurons has reached equilibrium, the adaptation parameter T_{pq} is modified according to

$$\frac{d}{dt}T_{pq} \;=\; \rho\left(-\eta T_{pq} + (\tau - T_{pq})\left[x_{pq} - T_{pq}\right]\right), \tag{5.19}$$

where ρ, η, τ are positive constants. The constant ρ controls the rate of change in T_{pq}. The constants η and τ determine the maximum value of T_{pq}, and the relative rates of increase and decrease in T_{pq}, respectively. As η increases the maximum value of T_{pq} decreases and the rate of decrease in T_{pq} when $[x_{rs} - T_{rs}] = 0$ increases, and as τ increases the maximum value of T_{pq} increases and the rate of increase in T_{pq} increases. According to Equation 5.19, if $T_{pq}(0) \geq 0$, then $T_{pq}(t) \geq 0$ for all $t \geq 0$. The threshold T_{pq} increases if neuron (p, q) was active in its recent past and decreases if (p, q) was not very active.

The spiking model was not implemented here because Xing and Gerstein (1994) did not provide complete implementation details of their model. Even though the model

described by Equations 5.16–5.19 differs from the spiking model used by Xing and Gerstein in their simulations, it captures the essential characteristics of their inhibition-dominant adaptation model: the simulation results based on Equations 5.16–5.19 replicate their results.

In the inhibition-dominant adaptation network, the lateral inhibitory and lateral excitatory pathway weights are symmetric. Extensive simulations show that the system defined by Equation 5.16 may be absolutely stable (Cohen & Grossberg, 1983). Simulations presented in this chapter show that the network equilibrates. The adaptation levels of the neurons reach stable fixed points with sufficient training. The initial pathway weights are set according to Equations 5.14 and 5.15.

Explanation of dynamic RF changes based on adaptation

After the network receives normal stimulation for a sufficiently long time, every Layer 2 neuron becomes adapted by approximately the same amount. In response to the scotoma stimuli, the neurons outside the cortical scotoma region are activated, thereby keeping them habituated. However, the inactive neurons whose RF is inside the scotoma become dishabituated. Dishabituation of neurons with RF inside the scotoma produces increased responsiveness and RF expansion. The increased responsiveness increases inhibition to neurons whose RF is outside the scotoma. Thus, the RF size of the neurons whose RF is occluded by the scotoma region increases, and the RF size of some neurons whose RF is just outside the scotoma decreases. As scotoma conditioning proceeds, some neurons in the initial cortical scotoma may recover functionality. As in the EXIN model, all neurons that show RF expansion are those whose RF lies within the scotoma (Figure 5.6).

If the network is exposed to normal stimuli again, the RF of the neurons that were in the cortical scotoma region is restored. The simulation results are in Section 5.3.1.

The above explanation is different from the one given by Xing and Gerstein (1994). In their simulations, they measured the initial RFs *before* any conditioning by the normal stimuli. Then they conditioned the network using scotoma stimuli. In this case, the neurons in the cortical scotoma region are not affected, and those outside the cortical scotoma adapt. The adaptation of the neurons outside the cortical scotoma causes them to be less

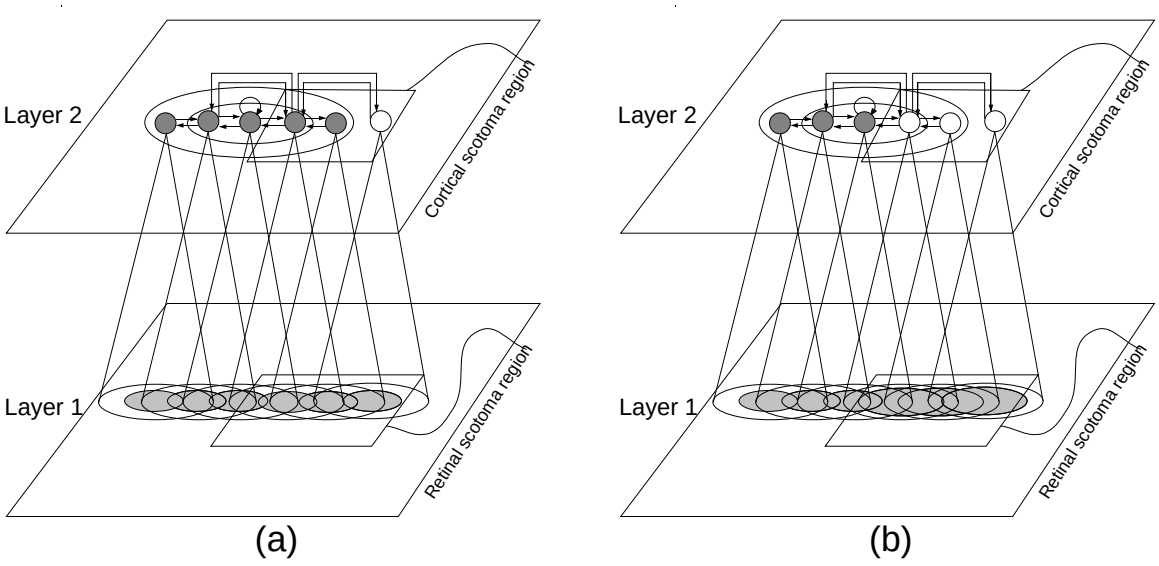

Figure 5.6: **The effects of scotoma conditioning on the inhibition-dominant adaptation model.**
The unfilled ellipses represent the afferent connectivity pattern from Layer 1 to Layer 2 neurons. The shaded ellipses represent the RFs of Layer 2 neurons. The parallelogram within Layer 1 represents the scotoma region, and the parallelogram within Layer 2 represents the cortical scotoma region before scotoma conditioning. (a) The network state before scotoma conditioning. All Layer 2 neurons have almost the same adaptation level (shaded circles). Thus, all Layer 2 neurons have almost the same RF size. (b) The network state after scotoma conditioning. The neurons inside the cortical scotoma are dishabituated (white circles) and hence are highly responsive to input stimulation. The neurons inside the cortical scotoma inhibit neurons outside the cortical scotoma and in turn receive weaker inhibition. Thus, neurons within the cortical scotoma show RF expansion.

responsive, and hence they exert less inhibition on neurons in the cortical scotoma. As a result, the size of the RF of the neurons in the scotoma region increases (see Section 5.3.1). The conditioning procedure used by Xing and Gerstein differs from that used by Pettet and Gilbert (1992). In the experiments of Pettet and Gilbert, the original RF was determined after a period of random stimulation within and outside the field.

In the inhibition-dominant adaptation model used in simulations presented in this chapter, if the T_{pq} values had not equilibrated during normal stimuli presentations, then they would increase for neurons outside the cortical scotoma and would decrease for those in the cortical scotoma. This situation would also produce expansion of the RF of neurons

in the cortical scotoma.

5.2.8 The adaptation model with no lateral interaction

In this variant of the adaptation model, there are no lateral excitatory or lateral inhibitory pathways. The neurons adapt according to Equation 5.19. In the simulations, the activation level of Layer 2 neuron (p,q) is $[x_{pq} - T_{pq}]$, where x_{pq} is controlled by Equation 5.16. With no lateral interactions, Equation 5.16 can be solved analytically (Appendix C, Section C.3.1). The afferent excitatory weights were the same as for the inhibition-dominant network.

Explanation of dynamic RF changes based on adaptation

In the adaptation network with no lateral interactions, all the neurons are adapted equally after normal stimulation. During scotoma conditioning, neurons with initial RFs in the scotoma region dishabituate due to inactivity. As the adaptation level in neurons within the cortical scotoma decreases, the effective RF size of these neurons increases. Neurons outside the cortical scotoma remain adapted because of activation by the input stimuli. During normal stimulation following scotoma conditioning, the previously inactive neurons are activated; hence they become adapted, and their RF size contracts. In the absence of lateral interactions, the RFs remain symmetric, and there are no shifts in RF position during scotoma conditioning. Simulation results are in Section 5.3.1.

5.2.9 The excitation-dominant adaptation model

In an excitation-dominant adaptation network, the strength of the lateral excitatory connections is greater than that of lateral inhibitory connections. In this model, the neurons adapt according to Equation 5.19. The output of Layer 2 neuron (p,q) is $[x_{pq} - T_{pq}]$, where x_{pq} is controlled by Equation 5.16. The initial connection weights are set according to Equation 5.15. In the simulations, the activation equation equilibrated (Appendix C, Section C.3.1).

Explanation of dynamic RF changes based on adaptation

In the excitation-dominant adaptation network, all the neurons are adapted equally after normal stimulation. During scotoma conditioning, neurons with initial RF in the scotoma region become less adapted, because of inactivity. The neurons close to the center of the cortical scotoma become least adapted and hence most responsive. In addition, because of lateral excitation, the neighboring neurons excite one another. Thus, neurons within the cortical scotoma show RF expansion. Since neurons receive more lateral excitation from neurons within the cortical scotoma, the RFs of the neurons shift toward the center of the scotoma. Neurons outside the cortical scotoma remain adapted because of activation by the input stimuli. During normal stimulation following scotoma conditioning, the previously inactive neurons are activated; hence they become adapted, and their RF size contracts. Simulation results are in Section 5.3.1.

5.3 Simulation results: Scotoma stimuli

The simulation results are organized to emphasize the effects of the different rules for RF changes after artificial scotoma conditioning and retinal lesions. The different synaptic plasticity rules in the EXIN and the LISSOM model serve different purposes during self-organization of various cortical properties. The analyses of the effects of each rule individually during artificial scotoma conditioning and retinal lesions elucidates the unique properties of the rules. Furthermore, the dynamic RF changes produced by the full EXIN and the full LISSOM model during artificial scotoma conditioning depend on the relative learning rates of the different synaptic plasticity rules, and thus the effects produced by one rule can mask the effects produced by the others.

In Section 5.3.1, the EXIN network with *only* lateral inhibitory synaptic plasticity enabled, the LISSOM network with *only* lateral inhibitory synaptic plasticity enabled, the inhibition-dominant adaptation network, the adaptation network with no lateral interaction, the excitation-dominant adaptation network, and the inhibition-dominant adaptation network with no prior normal stimulation are simulated during scotoma conditioning. These results are compared to experimental data. In Section 5.3.2, the effects of synaptic plasticity

in afferent excitatory pathways alone in the EXIN and LISSOM networks during scotoma conditioning are presented, and the effects of lateral excitatory synaptic plasticity alone during scotoma conditioning are presented in Section 5.3.3 using the LISSOM network. To further distinguish the effects of the various rules for cortical plasticity, a novel experiment is presented in Section 5.4.

5.3.1 Comparison of outstar/instar lateral inhibitory synaptic plasticity rules and neuronal adaptation

The following simulations highlight the opposite effects of instar and outstar lateral inhibitory synaptic plasticity rules.

Dynamic RF expansion and contraction

To induce robust expansion and contraction of RF size, Pettet and Gilbert (1992) presented the artificial scotoma conditioning stimuli for several minutes. Because quantitative mapping took several minutes, the exact time course of the observed changes was not determined. To minimize the effect of the RF measurement process on the RF size, Pettet and Gilbert (1992) alternated conditioning stimuli and RF mapping. Pettet and Gilbert (1992) reported that the RF expansion after artificial scotoma conditioning was always accompanied by an increased responsiveness from the region of the original RF. However, the spontaneous firing of the neuron in the absence of visual stimuli did not change.

In the simulations, the synaptic plasticity rules and the adaptation rules were turned-off so that the RF sizes are not affected by RF measurements. Figure 5.7 compares the RF sizes of Layer 2 neurons that show maximal RF expansion after scotoma conditioning. Neurons with maximal RF expansion are shown to emphasize the asymmetry in the RF profile after artificial scotoma conditioning in the models. The RF expands in the EXIN network with only lateral inhibitory synaptic plasticity enabled (Figure 5.7d) and in the inhibition-dominant adaptation network (Figure 5.7f) after scotoma conditioning, in neurons whose initial RF is inside the scotoma. In the LISSOM network with only lateral inhibitory synaptic plasticity enabled, the initial RF of the neuron that showed maximal

RF expansion after scotoma conditioning was located outside the scotoma (Figure 5.7e). Re-conditioning with normal stimuli resulted in RF restoration in all the three models, as shown in Figures 5.7g–i. The simulations illustrate the qualitative behavior of the models. The absolute RF size and the absolute RF size change in the three networks are parameter dependent, and can be matched better with some parameter adjustments. Therefore, the differences in the RF size and the absolute RF size change of model neurons in the models are not significant.

Pettet and Gilbert (1992) claimed that the expansion elicited by the artificial scotoma never exceeded the boundaries of the scotoma. However, the neurons that they studied had initial RFs in the center of the artificial scotoma, and the size of the scotoma was about three times the diameter of the initial RF. Darian-Smith and Gilbert (1995) showed rapid recovery of responsiveness in neurons whose RF was inside the cortical scotoma, following bilateral retinal lesions. This indicates that the RF of some neurons in the original cortical scotoma crossed the retinal scotoma boundary. The EXIN network with lateral inhibitory synaptic plasticity alone, the LISSOM network with only lateral inhibitory synaptic plasticity enabled, and the inhibition-dominant adaptation model produced RF expansions that cross the scotoma boundaries (Figure 5.7).

The RF expansions in the three simulations are accompanied by increased responsiveness of the corresponding Layer 2 neurons. Figures 5.8a–c compare the responsiveness of the neurons whose RFs are shown in Figure 5.7, before and after conditioning with scotoma stimuli in the three models. Note that after scotoma conditioning, the RF profile of some neurons in these models is asymmetric. The asymmetric RF shape is caused by asymmetric changes of the weights in the EXIN and LISSOM simulations and by asymmetric changes in adaptation level of the neurons in the inhibition-dominant adaptation network. The asymmetry in the RF profile produced by the EXIN and the inhibition-dominant adaptation networks is consistent with observations made by Das and Gilbert (1995b), that neurons were more responsive to locations outside the scotoma than to those inside, following artificial scotoma conditioning. DeAngelis et al. (1995) did not observe asymmetry in the RF of recorded neurons whose RF was inside the scotoma during scotoma conditioning; this may have happened because

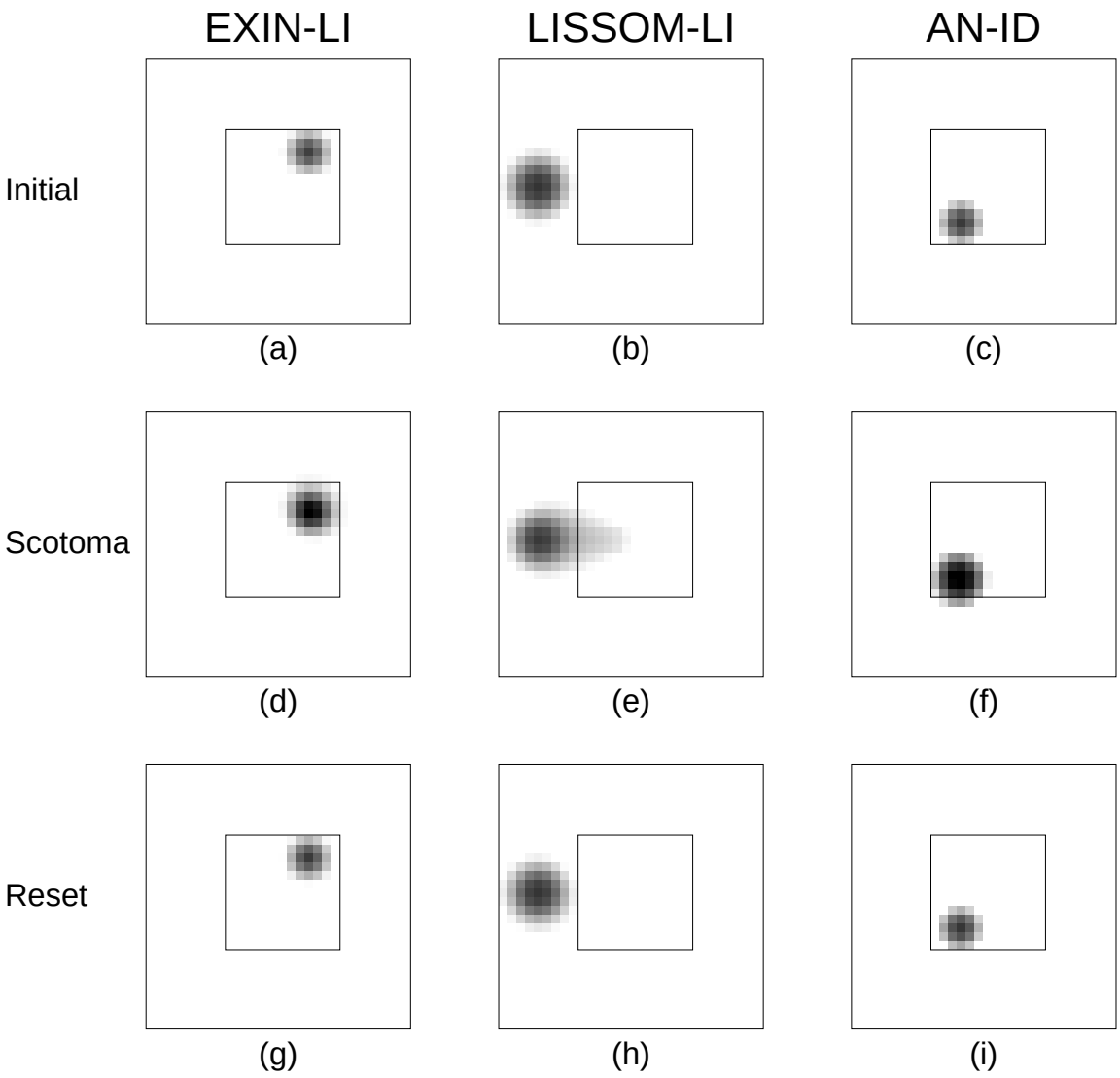

Figure 5.7: Legend on next page.

Figure 5.7: **Simulation results: RF expansion and contraction.**
Figure on previous page. The RFs of Layer 2 neurons that showed maximal expansion, in the EXIN network with only lateral inhibitory synaptic plasticity enabled (a,d,g), the LISSOM network with only lateral inhibitory synaptic plasticity enabled (b,e,h), and the inhibition-dominant adaptation network (c,f,i) are shown. The inner square indicates the extent of the scotoma. The responsiveness of the neurons to the test stimuli is proportional to the gray level. Panels (a,b,c) show the initial RF, (d,e,f) show the RF after scotoma conditioning using a 13×13 square scotoma centered at $(0, 0)$, and (g,h,i) show the RF after re-conditioning using normal stimuli. Panels (d,e,f) show expansion, and (g,h,i) show that the RF is restored by re-conditioning with normal stimuli. In the EXIN network with only lateral inhibitory synaptic plasticity enabled and in the inhibition-dominant adaptation network, the center of the RF is within the scotoma (d,f). In contrast, in the LISSOM network with only lateral inhibitory synaptic plasticity enabled the center of the RF is outside the scotoma (e). Furthermore, the RFs shown in panels (a,c), which are within the scotoma, cross the scotoma boundary after artificial scotoma conditioning, as shown in panels (d,f). The RF in panel (b), which is outside the scotoma, crosses the scotoma boundary after artificial scotoma conditioning, as shown in panel (e).

the RF of the recorded neurons in their experiments was in the center of the scotoma. In the simulations, asymmetric RFs were observed in neurons close to the scotoma boundary (Figure 5.8) but not in neurons at the scotoma center.

Spontaneous cortical activations were not incorporated in the EXIN and LISSOM simulations. However, synaptic plasticity during scotoma conditioning does not affect spontaneous activations in the absence of visual stimulation. Cortical spontaneous activity in the absence of any visual stimuli is close to zero (Movshon et al., 1978). This weak activity would have negligible effect on the spontaneous activation of other neurons, even if synapses between them were modified. Thus, spontaneous activity in the absence of visual stimuli would be almost unchanged if scotoma conditioning resulted in synaptic plasticity. Xing and Gerstein (1994) did not simulate the effect of adaptation on the spontaneous activation levels of Layer 2 neurons. However, they assumed that the spontaneous activation level is independent of adaptation.

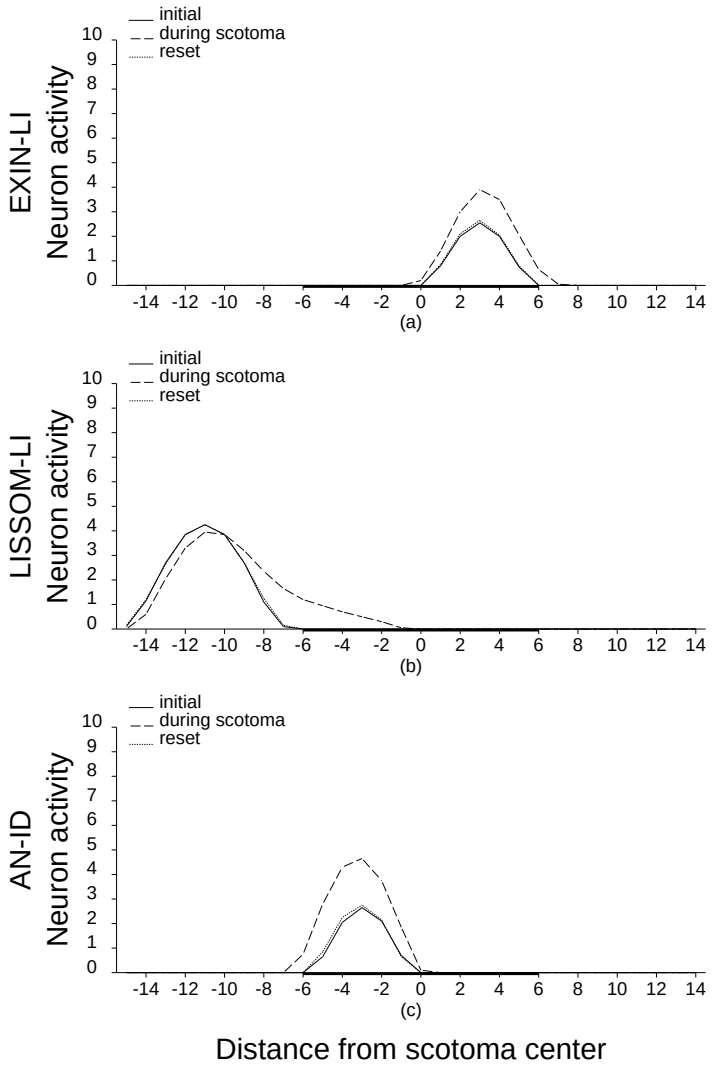

Figure 5.8: **Simulation results: The iceberg effect.**
Layer 2 neuron responsiveness before scotoma conditioning (solid line), after scotoma conditioning (dashed line), and after re-conditioning with normal stimuli (dotted line) are shown. Neuron activations in the EXIN network with only lateral inhibitory synaptic plasticity enabled (a), the LISSOM network with only lateral inhibitory synaptic plasticity enabled (b), and the inhibition-dominant adaptation network (c), are shown as a function of one-dimensional input positions across Layer 1 passing through the scotoma center. The responsiveness is for the neurons in Figure 5.7. The responsiveness is computed by summing the response of the Layer 2 neuron to test stimuli along the y axis at each x axis position. The neuron position is represented relative to the x coordinate of the scotoma center. The scotoma is a square of size 13×13. The thick line segment on the abscissa represents the scotoma region.

RF size as a function of position

Pettet and Gilbert (1992) showed RF expansion of cortical neurons whose initial RF was within the artificial scotoma, after conditioning with artificial scotoma stimuli. Darian-Smith and Gilbert (1995) reported that between five minutes and one hour after bilateral retinal lesions, cortical neurons located close to or just inside the cortical scotoma boundary showed a striking increase in RF size.

Figures 5.9a–c show the RF size before and after scotoma stimuli conditioning as a function of the position of the initial RF center, for the three models. For the EXIN network with only lateral inhibitory synaptic plasticity enabled, Figure 5.9a, and the inhibition-dominant adaptation model, Figure 5.9c, the most prominent RF expansions occur for Layer 2 neurons with initial RF centers close to and inside the scotoma edge. However, for the LISSOM network with only lateral inhibitory synaptic plasticity enabled, Figure 5.9b, the most prominent RF expansions occur for Layer 2 neurons with initial RF centers close to and *outside* the scotoma edge.

RF size profile as a function of scotoma size

In the three simulations, neurons whose initial RF was close to the scotoma boundary showed the maximal expansion. This is clearly visible in the bimodal peaks in Figure 5.9. In the EXIN network with lateral inhibitory synaptic plasticity alone and the inhibition-dominant adaptation model, the peaks occur for neurons with initial RF inside the scotoma region; in the LISSOM network with only lateral inhibitory synaptic plasticity enabled, the peaks occur for neurons with initial RF outside the scotoma region.

The three simulations suggest the prediction that as the scotoma size is reduced, the peaks will move closer. This prediction is illustrated by results shown in Figure 5.10. Figure 5.10 shows the RF size of a cross section of Layer 2 neurons after scotoma conditioning with a scotoma of size 9×9. The EXIN model with only lateral inhibitory synaptic plasticity enabled produced a unimodal function (Figure 5.10a). In the LISSOM model with only lateral inhibitory synaptic plasticity enabled and the inhibition-dominant adaptation model, the peaks are closer in Figures 5.10b–c than in Figures 5.9b–c.

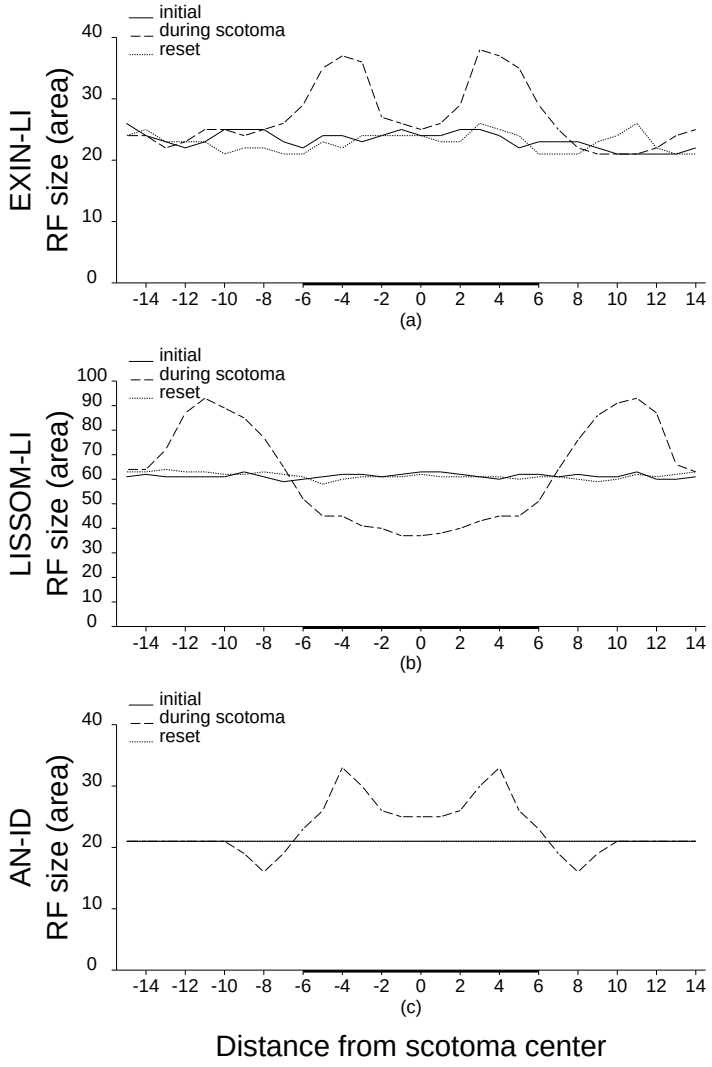

Figure 5.9: **Simulation results: RF size as a function of position.** The RF area before scotoma conditioning (solid line), after scotoma conditioning (dashed line), and after re-conditioning with normal stimuli (dotted line) in the EXIN network with only lateral inhibitory synaptic plasticity enabled (a), the LISSOM network with only lateral inhibitory synaptic plasticity enabled (b), and the inhibition-dominant adaptation network (c), are shown as a function of the position of the initial RF center of Layer 2 neurons relative to the scotoma center $(0, 0)$. The RF area shown is for a one-dimensional cross-section through Layer 2: neurons $(0, -15)$–$(0, 14)$. In panel (c) the dotted curve overlaps with the solid curve. The RF area of a Layer 2 neuron is the number of locations at which the test stimulus evokes a response in the Layer 2 neuron. See Figure 5.8 for simulation details and conventions.

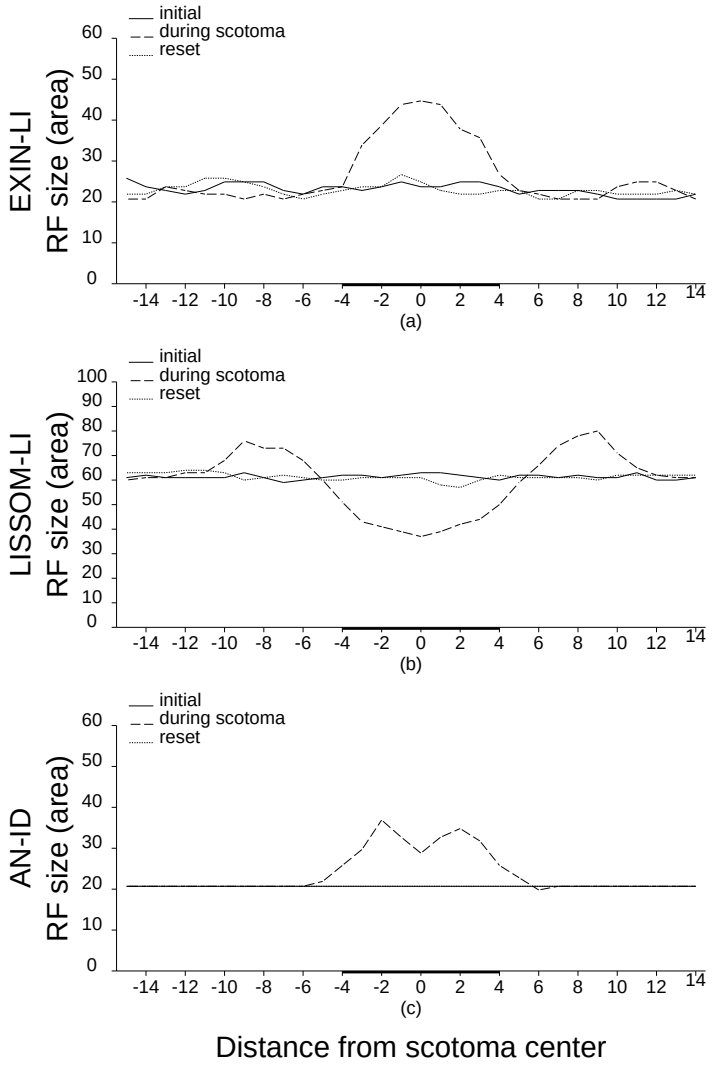

Figure 5.10: **Simulation results: Changes in RF after scotoma conditioning with a smaller scotoma.**
The RF area before scotoma conditioning (solid line), after scotoma conditioning (dashed line), and after re-conditioning with normal stimuli (dotted line) in the EXIN network with only lateral inhibitory synaptic plasticity enabled (a), the LISSOM network with only lateral inhibitory synaptic plasticity enabled (b), and the inhibition-dominant adaptation network (c), are shown as a function of the position of the initial RF center of Layer 2 neurons relative to the scotoma center $(0,0)$. The scotoma is a square of size 9×9 centered at $(0,0)$. In panel (c) the dotted curve overlaps with the solid curve. See Figure 5.9 for the definition of RF size. The RF area shown is for a one-dimensional cross-section through Layer 2: neurons $(0,-15)$–$(0,14)$. The thick line segment on the abscissa represents the scotoma region.

Recovery of neurons in the cortical scotoma

After bilateral retinal lesions, function returned over time to the cortex in a roughly concentric inward direction (Darian-Smith & Gilbert, 1995).

The EXIN network with only lateral inhibitory synaptic plasticity enabled exhibited this property during scotoma conditioning. According to the EXIN inhibitory synaptic plasticity rule, lateral inhibitory pathways to inactive or weakly active Layer 2 neurons with RF centers inside the scotoma weaken. The neurons closest to the edge of the cortical scotoma have relatively strong afferent inputs from locations outside the scotoma. Thus, these neuron respond first to inputs outside the scotoma. These newly responsive neurons in turn weaken inhibition to neurons farther inside the cortical scotoma. This behavior is illustrated in Figure 5.11a.

The LISSOM lateral inhibitory synaptic plasticity rule alone did not produce recovery in Layer 2 neurons in an concentric inward direction during scotoma conditioning. Contrary to the experimental data, the LISSOM lateral inhibitory rule caused loss of functionality in an concentric inward direction. According to the LISSOM lateral inhibitory synaptic plasticity rule, during scotoma conditioning Layer 2 neurons outside and close to the cortical scotoma edge show an increase in their responsiveness and RF size because of a decrease in the inhibitory weights from neurons inside the cortical scotoma. This increase in responsiveness results in increased inhibition to functional Layer 2 neurons very close to the scotoma boundary, and consequently, these lose responsiveness to locations outside the scotoma (Figure 5.11b).

In the inhibition-dominant adaptation model, during scotoma conditioning, adaptation of Layer 2 neurons in the cortical scotoma decreases, which lets neurons closest to the cortical scotoma edge recover responsiveness first (Figure 5.11c).

RF shifts

Figures 5.12a–c display the shift in RF center after conditioning with scotoma stimuli as a function of the position of the initial RF center of each Layer 2 neuron. The EXIN network with only lateral inhibitory synaptic plasticity enabled, Figure 5.12a, and the

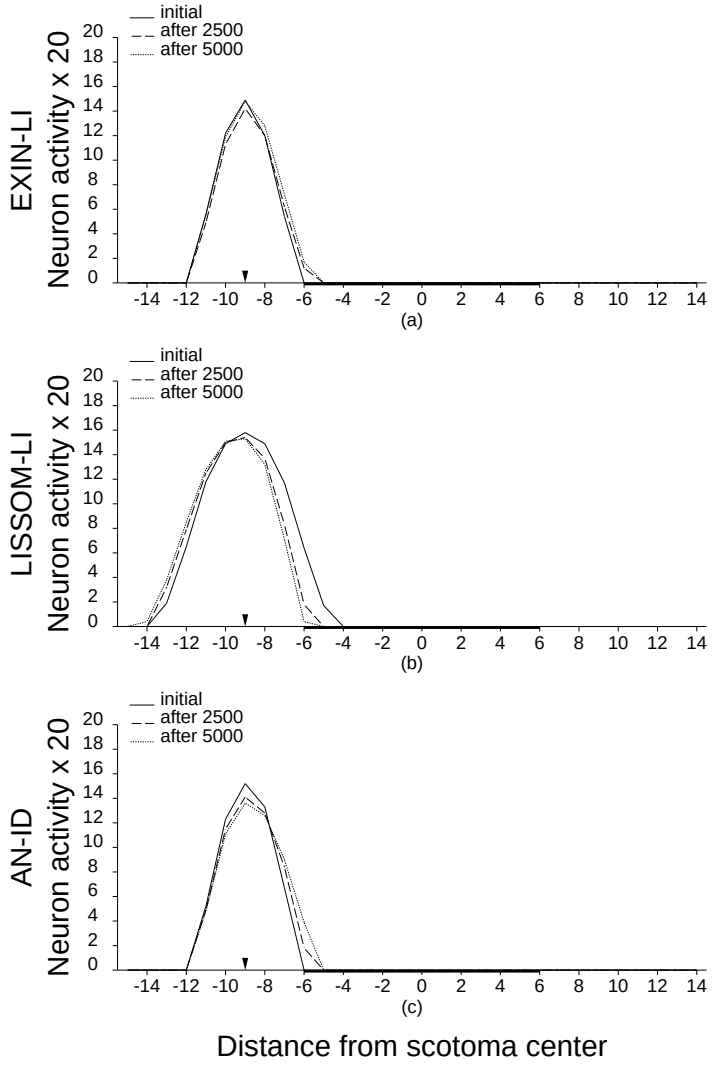

Figure 5.11: **Simulation results: Recovery of responsiveness of Layer 2 neurons.** The figures show the activation pattern in Layer 2 in response to input outside the scotoma before scotoma conditioning (solid line), after 2500 steps of scotoma conditioning (dashed line), and after 5000 steps of scotoma conditioning (dotted line) in the EXIN network with only lateral inhibitory synaptic plasticity enabled (a), the LISSOM network with only lateral inhibitory synaptic plasticity enabled (b), and the inhibition-dominant adaptation network (c). The abscissa represents the distance of initial RF center of Layer 2 neurons from the scotoma center. The input is a test stimulus centered at Layer 1 neuron $(0, -9)$. Panels (a) and (c) show recovery of neurons in a concentric inward direction. In panel (b) responsiveness is lost in a concentric inward direction. See Figure 5.8 for simulation details and conventions.

inhibition-dominant adaptation model, Figure 5.12c, exhibit consistent outward shifts in the RF center of Layer 2 neurons, and the maximal shifts occur for neurons with RF center close to the scotoma edge, consistent with the centrifugal RF displacements found within 1 hour after retinal lesions (Darian-Smith & Gilbert, 1995). In contrast, the LISSOM network with only lateral inhibitory synaptic plasticity enabled, Figure 5.12b, displays consistent shifts toward the scotoma center.

Effect of blank stimuli on RF

In the simulations with only lateral inhibitory synaptic plasticity (EXIN or LISSOM lateral inhibitory rule), the changes in RFs are the consequence of synaptic strength modifications that depend on neuronal activation. When the network is presented with a blank display, no Layer 2 neuron is activated, and hence no RF change occurs, consistent with the absence of changes observed in RFs during periods of no visual stimulation (Pettet & Gilbert, 1992).

In the inhibition-dominant adaptation model, the RF changes are due to differences in the adaptation thresholds of Layer 2 neurons whose initial RF is within and outside the scotoma region. In the inhibition-dominant adaptation model the adaptation threshold is a function of neuronal activation within a time interval. Blank stimuli do not activate Layer 2 neurons, and this causes the adaptation thresholds of all Layer 2 neurons to become approximately equal. The neurons whose RF is outside the scotoma region show RF expansion. The RF size increases because of the decrease in the threshold (Figure 5.13). In Figure 5.13a, the neurons inactive during scotoma conditioning are not fully dishabituated; therefore, during presentation of blank stimuli, these neurons too show RF expansion.

In Figure 5.13b, after a longer period of scotoma conditioning, some of the neurons are almost fully dishabituated, especially the neuron with initial RF center at position 0. During presentation of blank stimuli, changes in inhibition caused by dishabituation of the neurons whose initial RF center is outside the scotoma become dominant. Thus, during presentation of blank stimuli, as neurons whose RF is outside the scotoma rapidly become more responsive, and they exert more inhibition on neurons whose RF is inside the

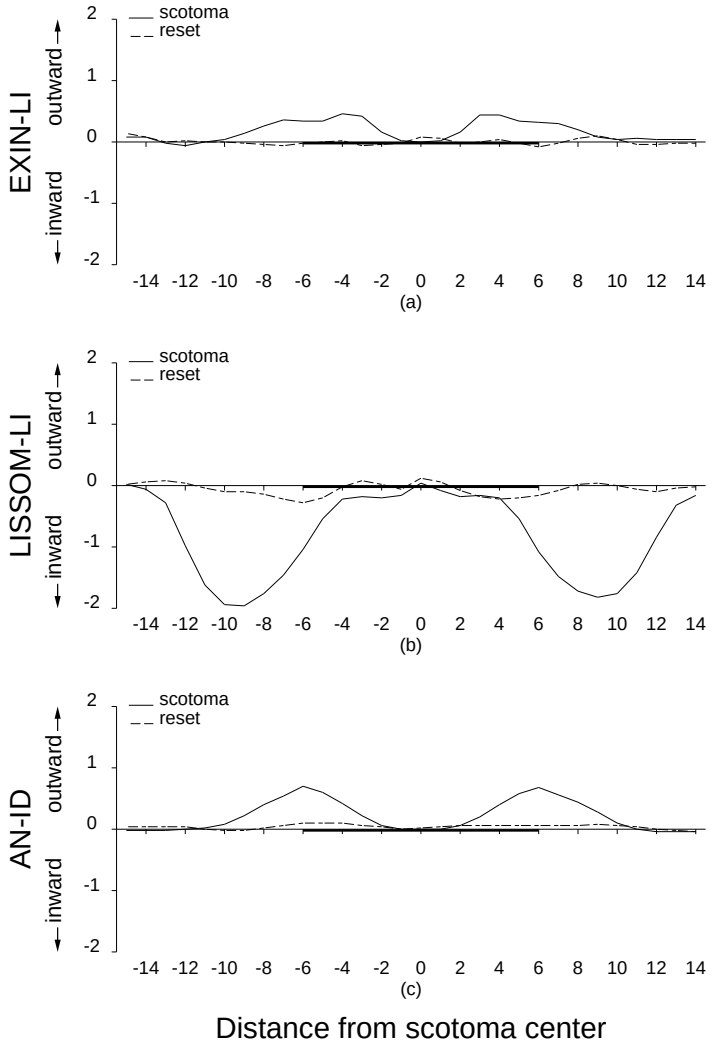

Figure 5.12: **RF shift as function of position.**
Shift in RF center after scotoma conditioning (solid line) and after re-conditioning with normal stimuli (dashed line) with respect to the initial RF centers is shown as a function of distance of the initial RF center of Layer 2 neurons from the scotoma center for the EXIN network with only lateral inhibitory synaptic plasticity enabled (a), the LISSOM network with only lateral inhibitory synaptic plasticity enabled (b), and the inhibition-dominant adaptation network (c). The RF shift shown is for a one-dimensional cross-section through Layer 2: neurons $(0,-15)$–$(0,14)$. Positive and negative shifts represent a shift away from and toward the center of the scotoma, respectively. The RF center of a Layer 2 neuron is the center of moment of the neuron's responsiveness to input at different positions within its RF. See Figure 5.8 for simulation details and conventions.

scotoma. This results in a slight RF contraction for neurons whose RF is inside the scotoma (Figure 5.13b).

Other adaptation models

Xing and Gerstein (1994) measured the initial RFs *before* conditioning with normal stimuli. Then they conditioned the network using scotoma stimuli. In this case, the neurons in the cortical scotoma region were not affected, and those outside the cortical scotoma adapted. Adaptation of the neurons outside the cortical scotoma decreases their responsiveness; hence they exert less inhibition on neurons in the cortical scotoma. As a result, the RFs of the neurons in the scotoma region increased in size and showed other changes consistent with experimental data (Figures 5.14–5.17a). However, presenting blank stimuli to the model would result in a decrease in adaptation of all neurons. Thus, the RFs would be restored to their pre-scotoma sizes.

Figures 5.14b–c show changes in RF size following artificial scotoma conditioning in an adaptation network with no lateral interaction and in an adaptation network with dominant lateral excitation, respectively. The two networks produce RF expansion in inactive neurons after scotoma conditioning, and they produce RF contraction during normal stimulation following scotoma conditioning.

However, in the adaptation network with no lateral interactions, RF profiles after scotoma conditioning are symmetric (Figure 5.15b), and the RF position of the neurons do not change (Figure 5.16b). In the adaptation network with dominant lateral excitation, the RF profile shows asymmetry, but the neurons are more responsive to locations within the occluded region during scotoma conditioning (Figure 5.15c); this manifests itself as RF shifts toward the center of the scotoma (Figure 5.16c). These effects are inconsistent with the observations of Darian-Smith and Gilbert (1995) and Das and Gilbert (1995b).

Figures 5.17b–c show that in these adaptation networks, responsiveness returns to neurons within the cortical scotoma in a concentric inward direction.

Because the adaptation level in these adaptation models depends on neuronal activation, the RF size of neurons in these models changes in the absence of input stimulation.

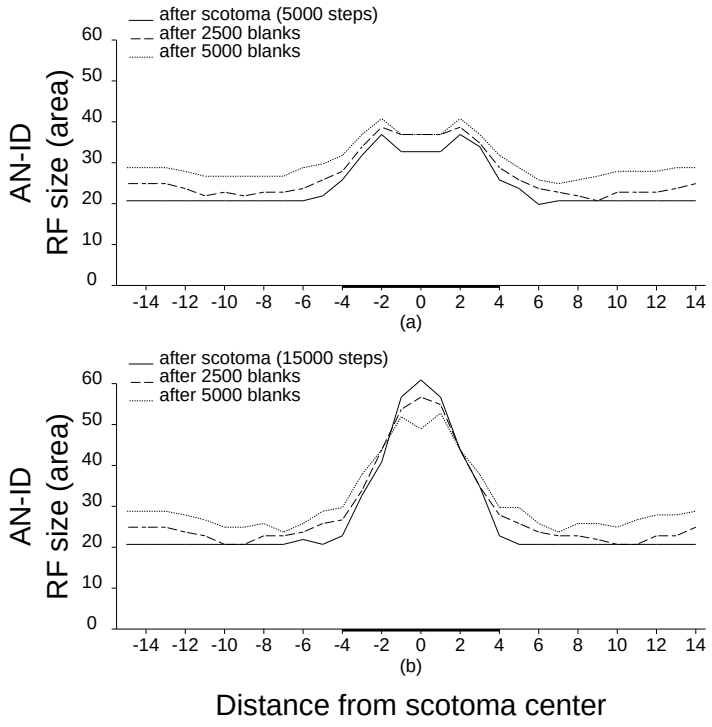

Figure 5.13: **Simulation results: Blank screen causes RF changes in the inhibition-dominant adaptation model.**
The RF area after scotoma conditioning (solid line), after 2500 steps of conditioning with blank stimuli (dashed line), and after 5000 steps of conditioning with blank stimuli (dotted line) in the inhibition-dominant adaptation network after 5000 steps of scotoma conditioning (a), and after 15000 steps of scotoma conditioning (b), are shown as a function of the position of the initial RF center of Layer 2 neurons relative to the scotoma center $(0,0)$. In (a) the neurons in the cortical scotoma were not fully dishabituated and therefore show RF expansion during no visual stimulation. In (b) prolonged inactivity in neurons in the cortical scotoma causes them to become almost fully dishabituated. With no visual stimulation, the neurons outside the cortical scotoma are dishabituated and they exert stronger inhibition on neurons inside the cortical scotoma. Thus, neurons outside the cortical scotoma show RF expansion, and neurons inside the cortical scotoma, which were highly dishabituated, show RF contraction. See Figure 5.10 for simulation details and conventions.

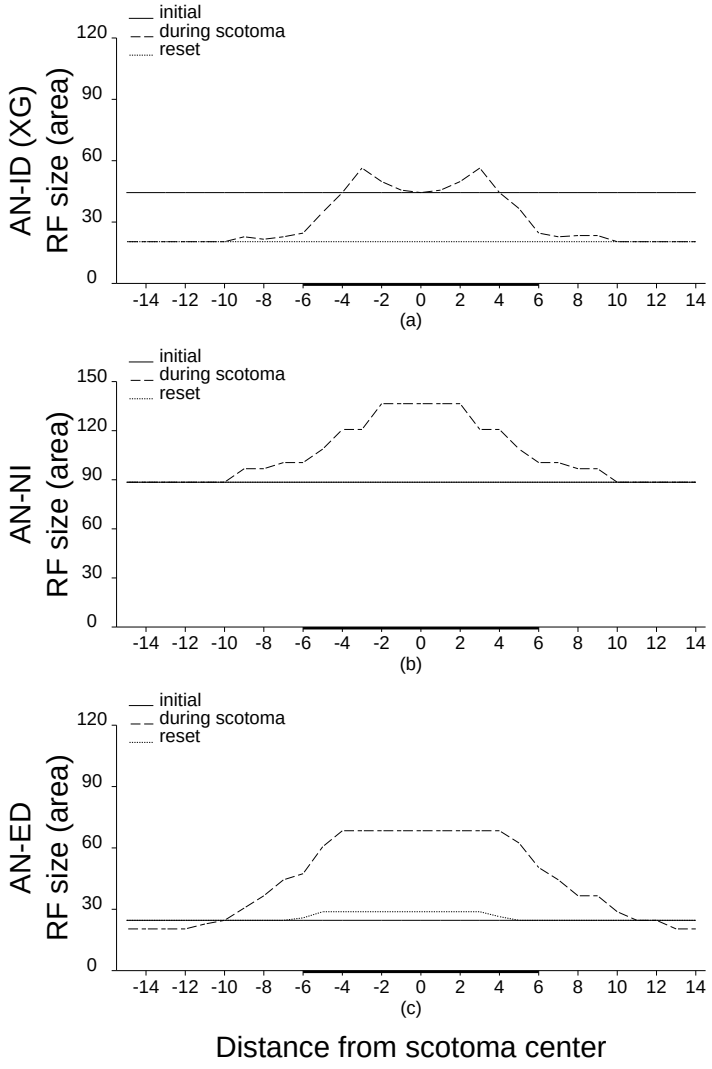

Figure 5.14: **Simulation results: RF size changes in other adaptation models.** The RF area before scotoma conditioning (solid line), after scotoma conditioning (dashed line), and after re-conditioning with normal stimuli (dotted line) in the inhibition-dominant adaptation network without prior normal stimulation (a), the adaptation network without lateral connections (b), and the excitation-dominant adaptation network (c), are shown as a function of the position of the initial RF center of Layer 2 neurons relative to the scotoma center $(0, 0)$. In panel (b) the dotted curve overlaps with the solid curve. See Figure 5.9 for simulation details and conventions.

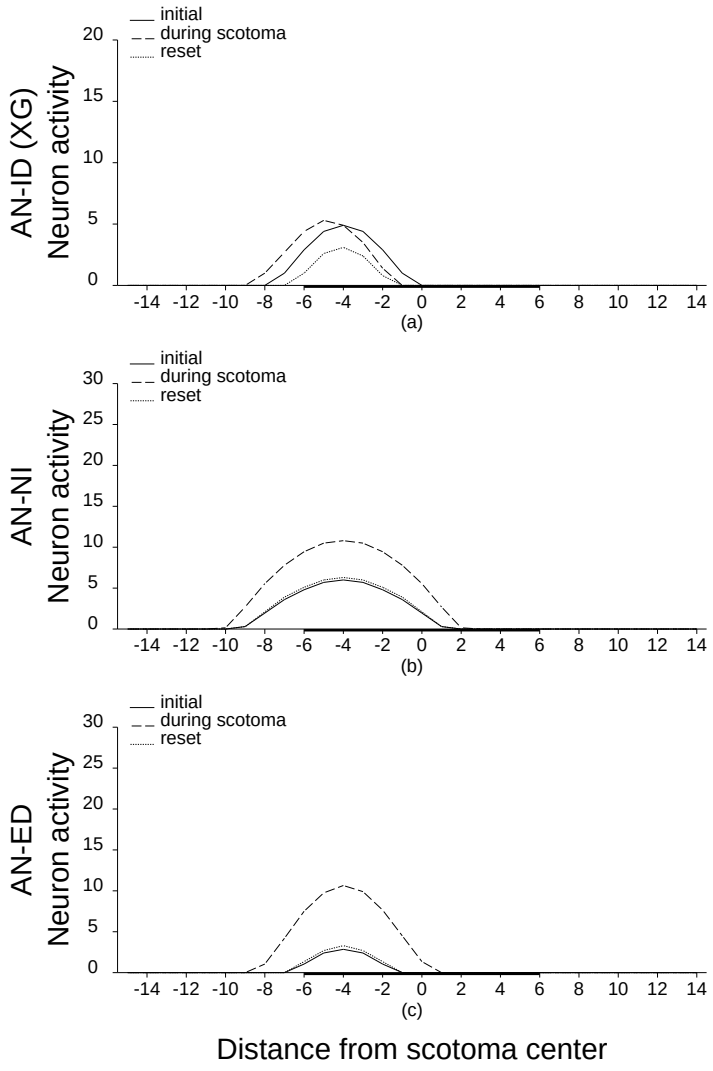

Figure 5.15: **Simulation results: The iceberg effect in other adaptation models.** Layer 2 neuron responsiveness before scotoma conditioning (solid line), after scotoma conditioning (dashed line), and after re-conditioning with normal stimuli (dotted line) in the inhibition-dominant adaptation network without prior normal stimulation (a), the adaptation network without lateral connections (b), and the excitation-dominant adaptation network (c), are shown as a function of one-dimensional input positions across Layer 1 passing through the scotoma center. See Figure 5.8 for simulation details and conventions.

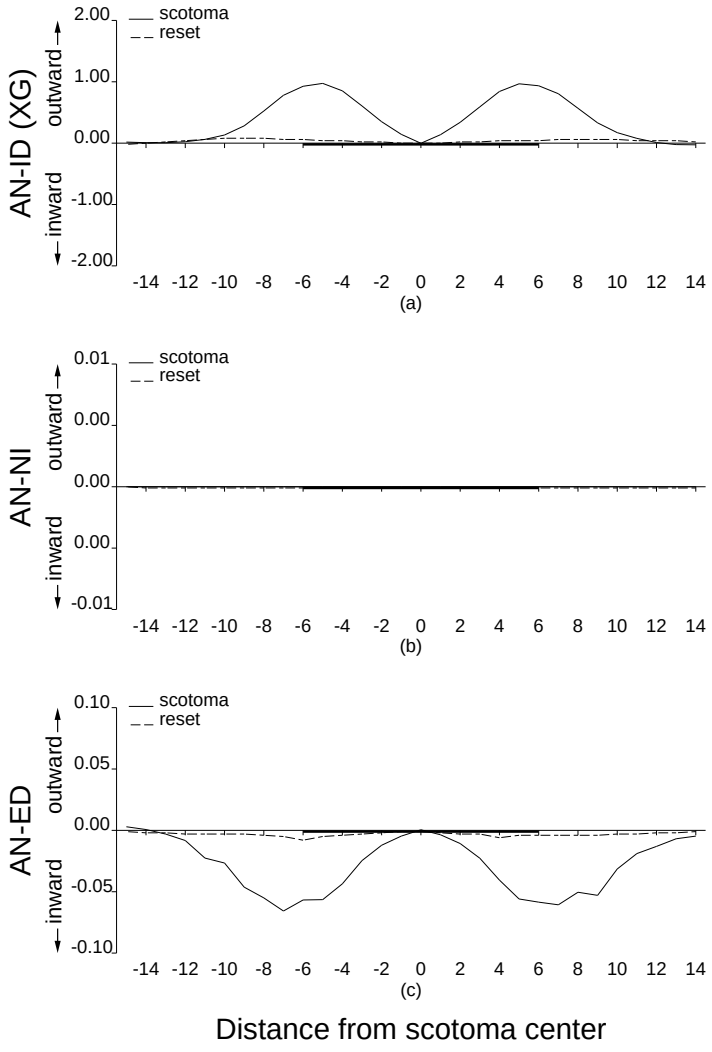

Figure 5.16: **Simulation results: RF shifts in other adaptation models.** Shift in RF center after scotoma conditioning (solid line) and after re-conditioning with normal stimuli (dashed line) with respect to the initial RF centers is shown as a function of distance of the initial RF center of Layer 2 neurons from the scotoma center for the inhibition-dominant adaptation network without prior normal stimulation (a), the adaptation network without lateral connections (b), and the excitation-dominant adaptation network (c). In panel (b) the solid and the dashed curves overlap with the abscissa. See Figure 5.12 for simulation details and conventions.

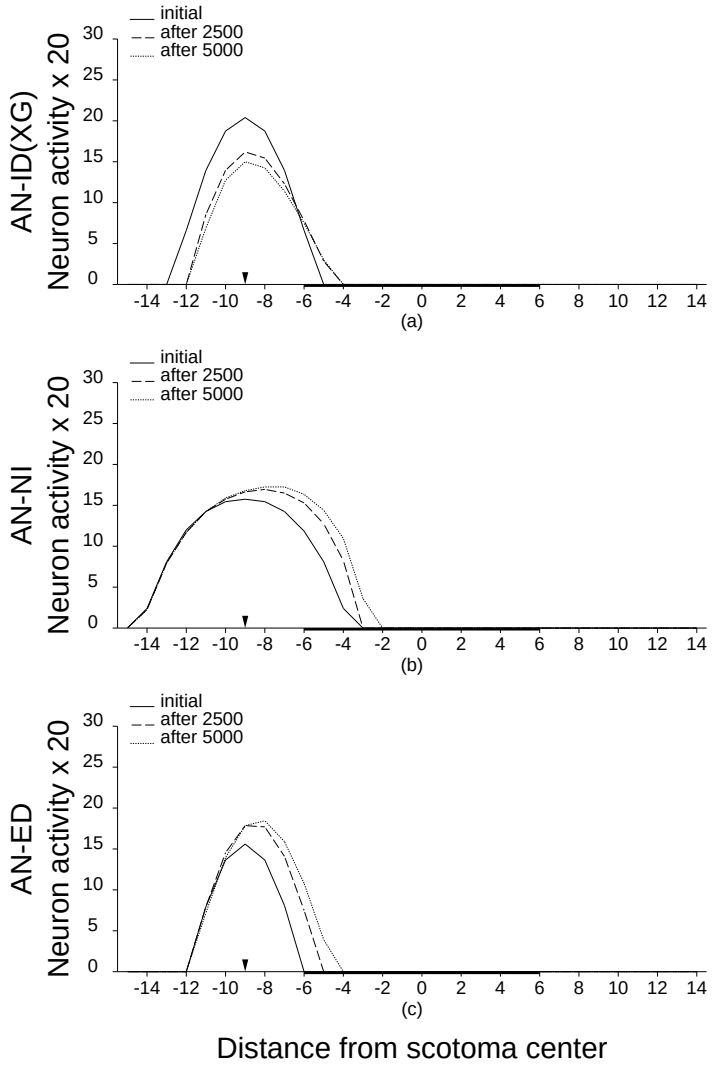

Figure 5.17: **Simulation results: Recovery of responsiveness in other adaptation models.**
The figures show the activation pattern in Layer 2 in response to input outside the scotoma before scotoma conditioning (solid line), after 2500 steps of scotoma conditioning (dashed line), and after 5000 steps of scotoma conditioning (dotted line) in the inhibition-dominant adaptation network without prior normal stimulation (a), the adaptation network without lateral connections (b), and the excitation-dominant adaptation network (c). The input is a test stimulus centered at Layer 1 neuron $(0, -9)$. See Figure 5.11 for simulation details and conventions.

Conclusions

From the simulations presented in this section, it is clear that the LISSOM instar lateral inhibitory synaptic plasticity rule is insufficient to model the effects of artificial scotoma conditioning and retinal lesions. However, the EXIN outstar lateral inhibitory synaptic plasticity rule is sufficient to model these effects.

Xing and Gerstein's (1994) inhibition-dominant adaptation network failed only in modeling the effects of presentation of blank stimuli after scotoma conditioning. In Section 5.4, a novel experiment is suggested to determine the role of neuronal adaptation in producing dynamic RF changes that persist over a long periods (about 15 minutes). Cortical neurons are maximally adapted within tens of seconds, and neurons recover their responsiveness over a period of tens of seconds (Hammond et al., 1986, 1989). Psychophysical experiments on humans using artificial scotoma conditioning produces shifts in position judgments consistent with the RF expansion hypothesis (Kapadia et al., 1994). These changes occurred over a period of 1-2 seconds, however, and would be consistent with the inhibition-dominant adaptation model.

Thus, we conclude that during scotoma conditioning, effects of neuronal adaptation occur over a period of tens of seconds; however, the persistent effects produced over a period of 15 minutes to hours may be caused by a long-term process, e.g., long-term synaptic plasticity. The RF changes observed over a period of months, however, may involve sprouting and establishment of new connections (Darian-Smith & Gilbert, 1994). The issue of time-scales is further discussed in Section 5.5.4.

The adaptation models without lateral interaction and with dominant lateral excitation produced RF expansion in neurons whose RFs were within the scotoma region. However, they produced RF shifts inconsistent with experimental data.

Sirosh et al. (1996) explained RF changes during scotoma conditioning using the LISSOM afferent excitatory synaptic plasticity. However, in their simulations the LISSOM lateral excitatory and lateral inhibitory synaptic plasticity rules were also enabled. To study the effects of afferent excitatory synaptic plasticity alone during scotoma conditioning, the next section (Section 5.3.2), presents simulations on the EXIN and LISSOM networks with

their respective afferent excitatory synaptic plasticity rules.

5.3.2 Role of afferent excitatory synaptic plasticity

In this section, the effects of scotoma conditioning on the EXIN and LISSOM networks with only afferent excitatory synaptic plasticity enabled are presented. Both the EXIN and LISSOM afferent excitatory synaptic plasticity rules are instar rules. One difference between the two networks is the presence of short-range lateral excitatory connections in the LISSOM network.

RF size as a function of position

Figures 5.18a–b show the RF size before and after scotoma conditioning as a function of the position of the initial RF center, for the EXIN and the LISSOM networks with only afferent excitatory synaptic plasticity enabled. For the EXIN network with only afferent excitatory synaptic plasticity enabled, small RF expansions occurred for Layer 2 neurons whose initial RF center is close to and inside the scotoma edge, and Layer 2 neurons whose initial RF center is close to and outside the scotoma boundary showed larger RF contraction (Figure 5.18a). Similarly, the LISSOM network with only afferent excitatory synaptic plasticity enabled produced RF expansion in neurons whose initial RF is inside the scotoma and produced RF contraction in neurons close to the scotoma boundary (Figure 5.18b).

The EXIN and the LISSOM networks with only afferent excitatory synaptic plasticity enabled produced RF expansion in neurons whose initial RF center is inside the scotoma, consistent with the results of Pettet and Gilbert (1992).

The LISSOM network with afferent excitatory synaptic plasticity alone showed larger RF expansion than the EXIN network with only afferent excitatory synaptic plasticity enabled because of the short-range lateral excitatory connections in the LISSOM network. In the LISSOM network, the neurons whose responsiveness increased (because of decreased inhibition through weakening of afferent pathways converging on other neurons) elevated the responsiveness of their neighbors via lateral excitatory connections, thereby producing large RF expansions. In Figure 5.18b, the curve showing RF size after scotoma conditioning

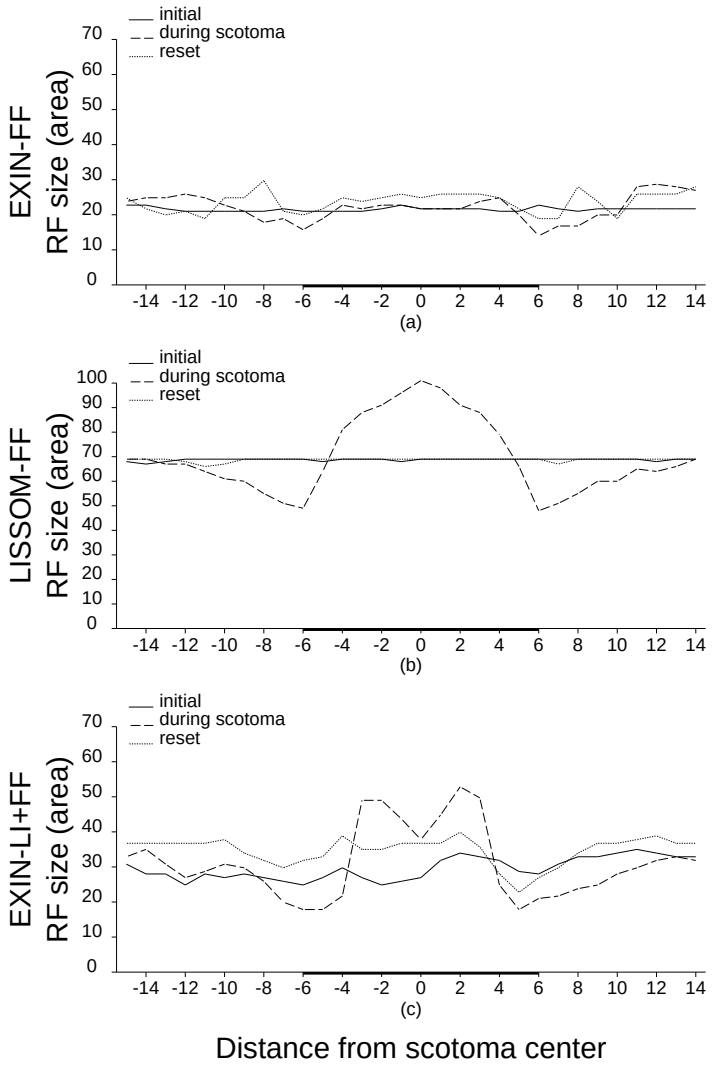

Figure 5.18: **Simulation results: RF size changes caused by afferent excitatory plasticity.**
The RF area before scotoma conditioning (solid line), after scotoma conditioning (dashed line), and after re-conditioning with normal stimuli (dotted line) in the EXIN network with only afferent excitatory synaptic plasticity enabled (a), the LISSOM network with only afferent excitatory synaptic plasticity enabled (b), and the EXIN network with afferent excitatory and lateral inhibitory synaptic plasticity (c), are shown as a function of the position of the RF center of Layer 2 neurons relative to the scotoma center $(0,0)$. See Figure 5.9 for conventions and simulation details.

is unimodal. The curve would become bimodal when the scotoma size is increased. In the LISSOM network, the weight of the lateral excitatory and inhibitory pathway decreases as the distance between the source and target neurons increases. Thus, as the scotoma size is increased, the effects of lateral pathways between neurons whose RFs are close to the scotoma boundary and neurons whose RFs are close to the center of the scotoma decrease, and therefore the amount of RF expansion in neurons whose RFs are close to the scotoma center will be less than the amount of RF expansion in neurons whose RFs are inside the scotoma, but closer to the scotoma boundary than the scotoma center. Thus, the RF size curve after scotoma conditioning becomes bimodal.

Figure 5.19 shows the RF profile of a neuron that exhibited RF expansion and another that exhibited RF contraction in the two simulations. After scotoma conditioning, the RF profile of some neurons in these networks was asymmetric, consistent with observations of Das and Gilbert (1995b). The asymmetric RF shape is caused by asymmetric changes in weights in the two networks.

In Figure 5.18a, neurons far away from the scotoma showed RF expansion. In the EXIN network with only afferent excitatory synaptic plasticity enabled, during scotoma conditioning neurons initially in the cortical scotoma strengthened their afferent connections from locations outside the scotoma. Thus, neurons surrounding the cortical scotoma received more inhibition when locations outside the scotoma were stimulated, and suppression of responsiveness of these neurons resulted in a slight increase in responsiveness of neurons farther away from the scotoma (Figure 5.20).

Recovery of neurons in the cortical scotoma

The EXIN and the LISSOM networks with only afferent excitatory synaptic plasticity enabled exhibited new responsiveness to stimuli outside the scotoma in neurons whose initial RF is inside the scotoma, during scotoma conditioning (Figure 5.21). This is consistent with the finding that after bilateral retinal lesions, function returned over time to the cortex in a roughly concentric inward direction (Darian-Smith & Gilbert, 1995).

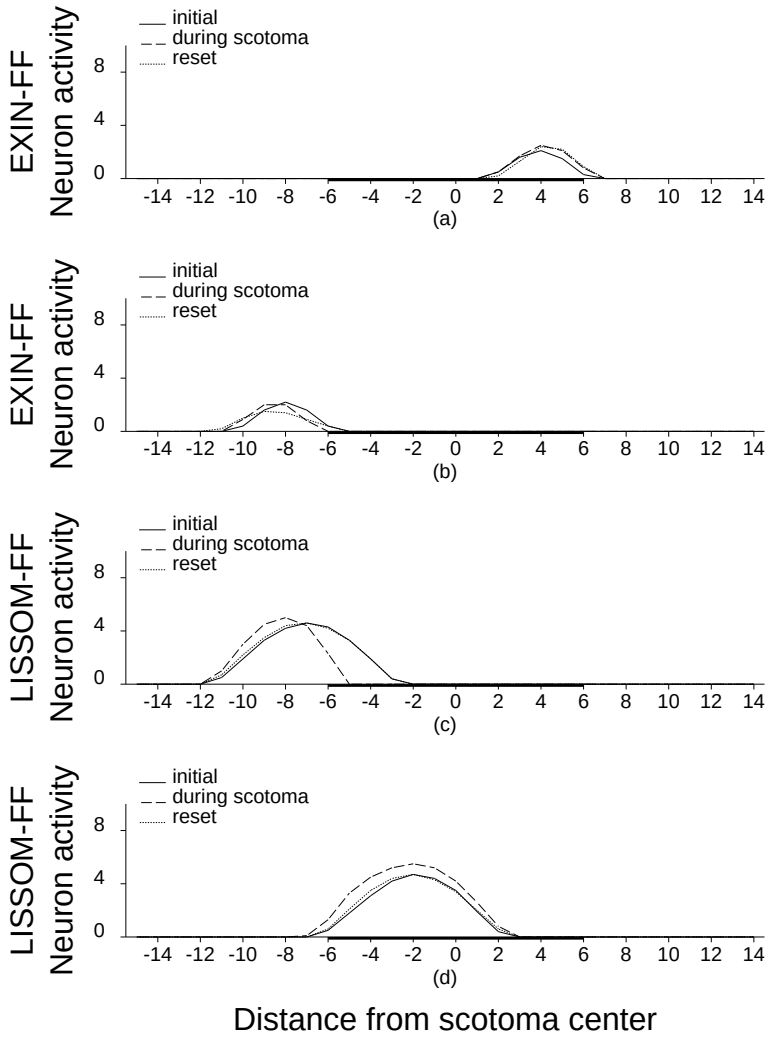

Figure 5.19: **Simulation results: RF profiles of neurons that show expansion or contraction.**

Layer 2 neuron RF profiles before scotoma conditioning (solid line), after scotoma conditioning (dashed line), and after re-conditioning with normal stimuli (dotted line) in the EXIN network with only afferent excitatory synaptic plasticity enabled (a,b), and the LISSOM network with only afferent excitatory synaptic plasticity enabled (c,d), as a function of a one-dimensional input positions across Layer 1 passing through the scotoma center. In (a) and (c), the neurons show RF expansion, and in (b) and (d), the neurons show RF contraction. See Figure 5.8 for simulation details and conventions. The thick line on the abscissa represents the scotoma region. In (a) and (c), the neurons showed RF expansion, and in (b) and (d) the neurons showed RF contraction.

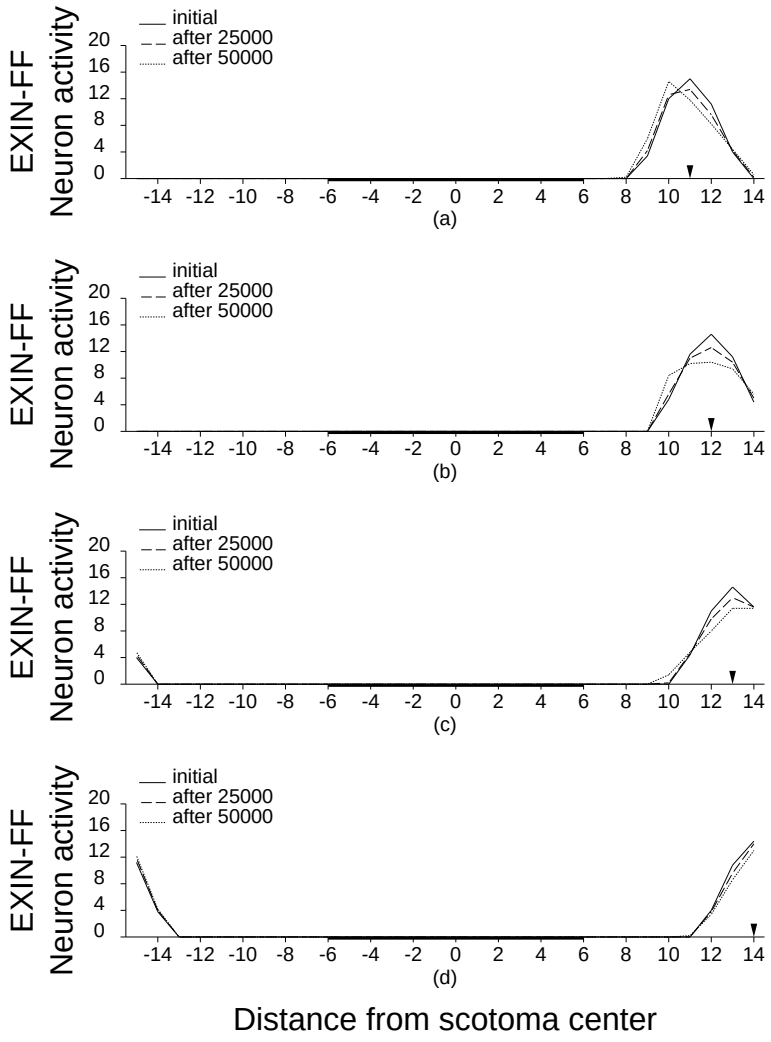

Figure 5.20: **Simulation results: Activation profiles in response to inputs at locations away from the scotoma.**
The figure shows activation of a one-dimensional cross-section of Layer 2 neurons: $(0,-15)$–$(0,14)$, in response to input stimulation at $(0,11)$ (a), $(0,12)$ (b), $(0,13)$ (c), and $(0,14)$ (d) in the EXIN network with only afferent excitatory synaptic plasticity enabled. The activation level of the neurons was scaled by a factor of 20. See Figure 5.11 for conventions and simulation details.

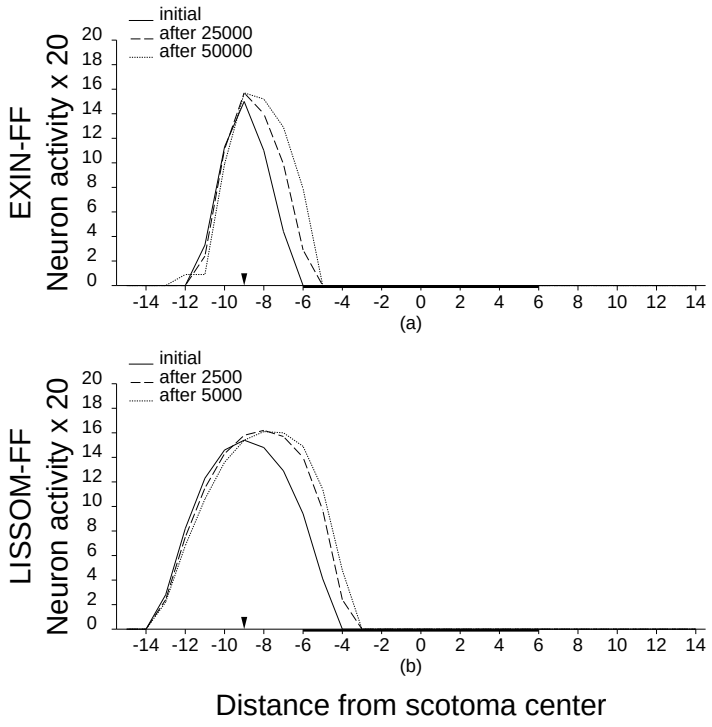

Figure 5.21: **Simulation results: Recovery of responsiveness of Layer 2 neurons caused by afferent excitatory plasticity.**
The figures show the activation pattern in Layer 2 in response to input outside the scotoma before scotoma conditioning (solid line), after 2500 steps of scotoma conditioning (dashed line), and after 5000 steps of scotoma conditioning (dotted line) in the EXIN network with only afferent excitatory synaptic plasticity enabled (a) and the LISSOM network with only afferent excitatory synaptic plasticity enabled (b). See Figure 5.11 for conventions and simulation details.

RF shifts

Figures 5.22a–b display the shift in RF center after conditioning with scotoma stimuli as a function of the position of the initial RF center of each Layer 2 neuron. The EXIN and LISSOM networks with only afferent excitatory synaptic plasticity enabled, Figures 5.22a–b, exhibited consistent outward shifts in the RF center of Layer 2 neurons. The maximal shifts occurred for neurons whose RF center was close to the scotoma edge. These results are consistent with the consistent small centrifugal RF shift away from the lesion center, between five minutes and one hour after the retinal lesions, observed by Darian-Smith and Gilbert (1995). In the two networks, neurons whose initial RF center was inside the scotoma showed outward shift because of the asymmetric RF expansion (Figure 5.19), and neurons whose initial RF overlapped the scotoma boundary showed an outward shift because of RF contraction (Figure 5.19).

During normal stimulation following scotoma conditioning, the EXIN network with only afferent excitatory synaptic plasticity enabled did not recover (Figure 5.22a). This effect was caused by strong lateral inhibition, which prevented the neurons whose RF size decreased (because of weakening of pathways from the scotoma during scotoma conditioning) from becoming strongly active to inputs at positions inside the scotoma. The weak afferent connections were thus prevented from becoming strong. In the LISSOM network with afferent excitatory synaptic plasticity alone, the short-range lateral excitatory connections helped neurons with weak afferent connections from the scotoma region to become more active, and hence to strengthen the weak afferent pathways (Figure 5.22b).

To ensure that the lack of recovery in the EXIN simulation was not caused by insufficient training, the simulation was run for much longer time (dotted line in Figure 5.22a). In fact, additional training shifted the RFs of neurons farther away from their original positions. The dotted line in Figure 5.22a is jagged, implying that the RF positions of some neurons shifted toward the scotoma center and the RF positions of neighboring neurons shifted away from the scotoma center. This behavior is the consequence of the strong lateral inhibitory interactions between the neurons. Because of strong lateral inhibition, when a neuron's responsiveness increases it suppresses the activation

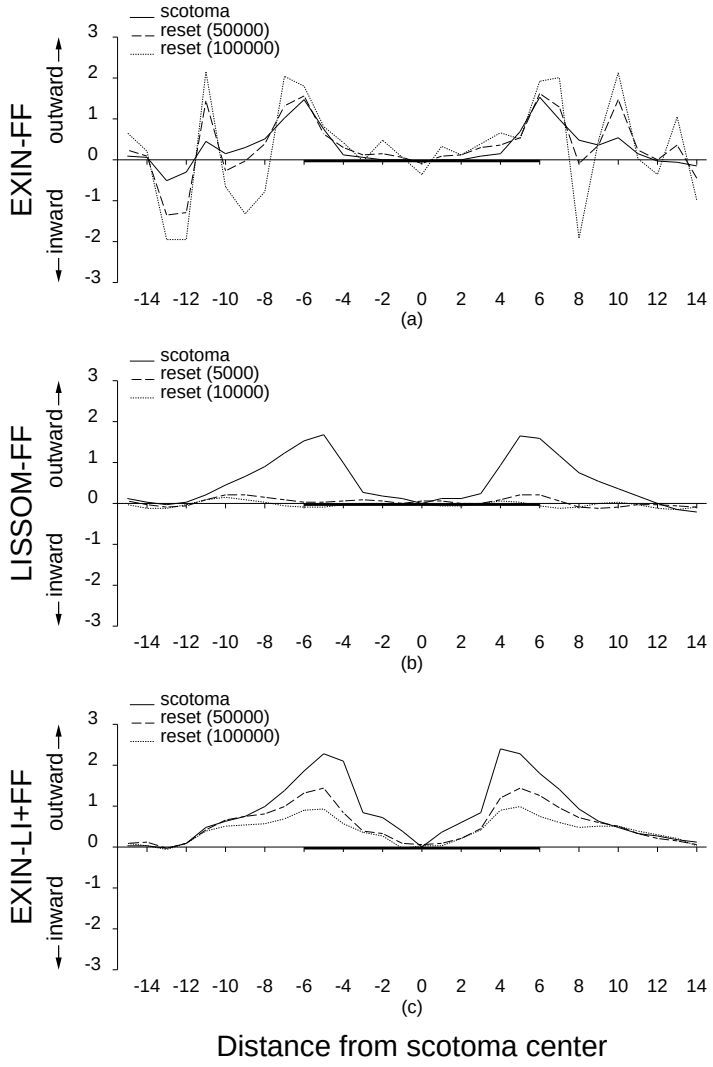

Figure 5.22: **Simulation results: RF shifts caused by afferent excitatory plasticity.** Shift in RF center after scotoma conditioning (solid line), after re-conditioning with normal stimuli for 50,000 steps (dashed line), and after re-conditioning with normal stimuli for 100,000 steps (dotted line) with respect to the initial RF centers is shown as a function of distance of the initial RF center of Layer 2 neurons from the scotoma center for the EXIN network with only afferent excitatory synaptic plasticity enabled (a), the LISSOM network with only afferent excitatory synaptic plasticity enabled (b), and the EXIN network with both afferent excitatory and lateral inhibitory synaptic plasticity (c). See Figure 5.12 for conventions and simulation details.

of neighboring neurons, and thus neurons farther away from the neighbor neurons receive less inhibition. This alternation of increased inhibition and decreased inhibition causes RF shifts in opposite directions in neighboring neurons.

However, with both the afferent excitatory and the lateral inhibitory synaptic plasticity enabled, the neurons in the EXIN network tended to recover their original RF properties (size, position, shape, and responsiveness) during normal stimulation following scotoma conditioning. During normal stimulation following scotoma conditioning, lateral inhibitory connection weights to the weakly active neurons decreased, and lateral inhibitory connection weights to strongly neurons increased. This led to an attraction effect on neurons with weakened afferent connections from the scotoma region and a repulsive effect on neurons with strengthened afferent connections from outside the scotoma region, resulting in a shift in RF centers toward their original locations (Figure 5.22c) and restoration of the original RF sizes (Figure 5.18c). During the normal stimulation following scotoma conditioning, the EXIN network with only lateral inhibitory synaptic plasticity rule completely recovered the original RF properties, but the EXIN network with only afferent excitatory synaptic plasticity enabled did not recover the original RF properties. Thus, in the full EXIN network, the amount of recovery of RF properties during normal stimulation following scotoma conditioning will depend on which rule produces the dominant effects.

Effect of blank stimuli on RFs

In the EXIN and LISSOM networks with afferent excitatory synaptic plasticity alone, a blank input display causes the Layer 2 neurons to be inactive, and therefore afferent excitatory pathway weights and cortical RFs do not change.

Conclusions

The EXIN and the LISSOM networks with only afferent excitatory synaptic plasticity enabled produced RF expansion consistent with experimental effects of artificial scotoma conditioning and bilateral retinal lesions. The EXIN network with only afferent excitatory synaptic plasticity enabled did not recover during normal stimulation following scotoma conditioning. However, the full EXIN network with both afferent excitatory and

lateral inhibitory synaptic plasticity enabled, did recover. In both the EXIN and the LISSOM networks with only afferent excitatory synaptic plasticity enabled, RF contraction in neurons whose initial RF overlapped the scotoma edge was observed during scotoma conditioning.

5.3.3 Role of lateral excitatory synaptic plasticity

In this section, the effects of the LISSOM instar lateral excitatory synaptic plasticity rule alone during scotoma conditioning are presented.

These simulations demonstrate that in a network with short-range lateral dominant excitatory connections and long-range lateral dominant inhibitory connections, an instar rule to modify the short-range lateral excitatory connections during scotoma conditioning produces RF expansion in neurons whose initial RF center is inside the scotoma.

RF size as a function of position

Figure 5.23a shows the RF size before and after scotoma stimuli conditioning as a function of the position of the initial RF center. In the LISSOM network with only instar lateral excitatory synaptic plasticity enabled, Figure 5.23a, RF expansions occurred for Layer 2 neurons whose initial RF center is inside the scotoma edge. In addition, neurons whose initial RF center is close to and outside the scotoma boundary showed RF contraction. These effects are similar to those observed in the EXIN and the LISSOM networks with only afferent excitatory synaptic plasticity enabled (Section 5.3.2).

In the LISSOM network with instar lateral excitatory synaptic plasticity alone, during scotoma conditioning the lateral excitatory pathways from the neurons just inside the cortical scotoma to those just outside weaken. Thus, in the LISSOM network with only instar lateral excitatory synaptic plasticity enabled, neurons whose RF is close to and outside the scotoma become less responsive to stimulation within and close to the scotoma boundary. This causes RF contraction in neurons whose initial RF is close to and outside the scotoma. Furthermore, because of the decreased responsiveness of these neurons to stimulation within and close to the scotoma boundary, they exert less inhibition on neurons whose initial RF is inside and away from the scotoma boundary, resulting in RF expansion.

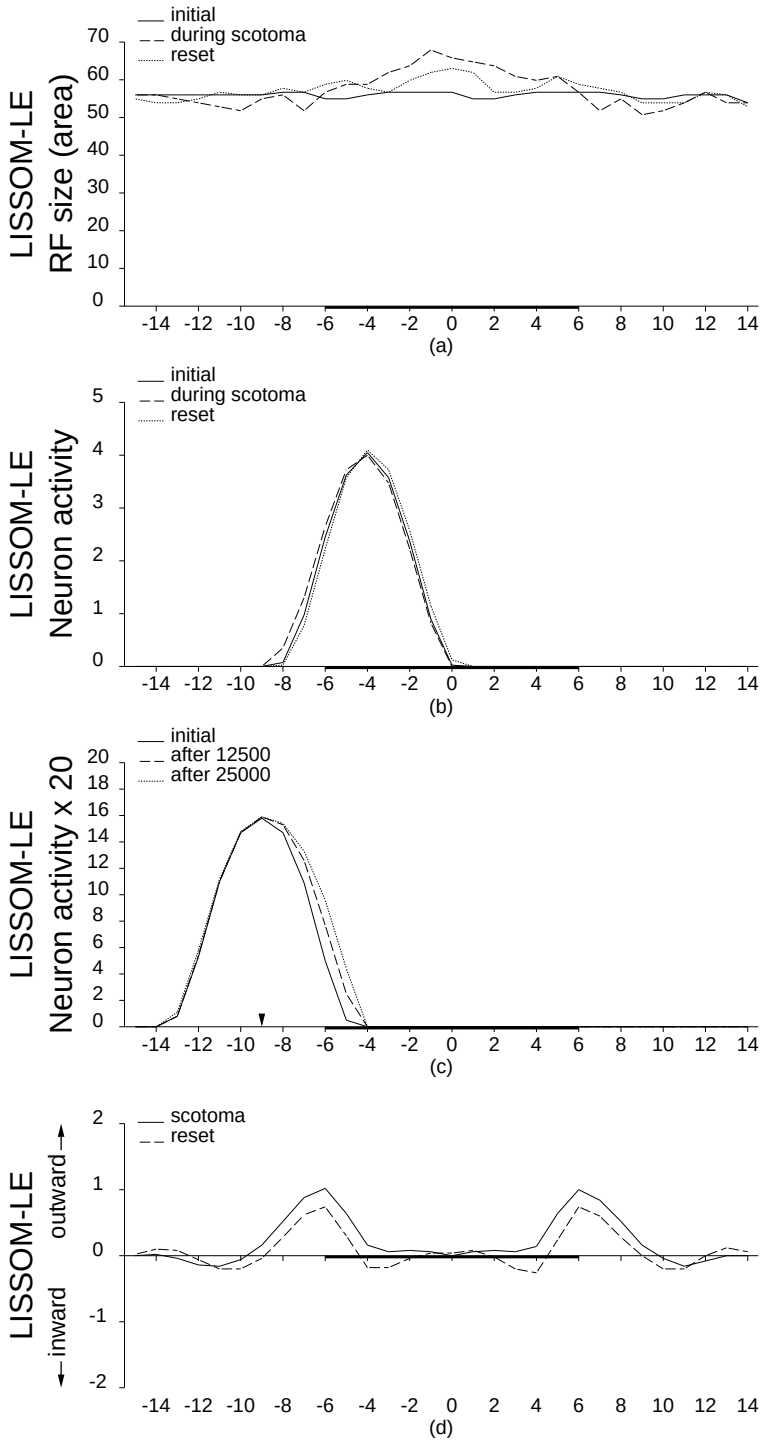

Figure 5.23: Legend on next page.

Figure 5.23: **Simulation results: RF changes in the LISSOM network with only lateral excitatory plasticity enabled.**
Figure on previous page. (a) The RF area before scotoma conditioning (solid line), after scotoma conditioning (dashed line), and after re-conditioning with normal stimuli (dotted line), is shown as a function of the position of the initial RF center of Layer 2 neurons relative to the scotoma center $(0, 0)$. See Figure 5.9 for conventions and simulation details. (b) Layer 2 neuron responsiveness before scotoma conditioning (solid line), after scotoma conditioning (dashed line), and after re-conditioning with normal stimuli (dotted line), are shown as a function of one-dimensional input positions across Layer 1 passing through the scotoma center. See Figure 5.8 for conventions and simulation details. (c) The activation pattern in Layer 2 in response to input outside the scotoma before scotoma conditioning (solid line), after 2,500 steps of scotoma conditioning (dashed line), and after 5,000 steps of scotoma conditioning (dotted line). The input is a test stimulus centered at Layer 1 neuron $(0, -9)$. (d) Shift in RF center after scotoma conditioning (solid line) and after re-conditioning with normal stimuli (dashed line) with respect to the initial RF centers is shown as a function of distance of Layer 2 neurons from the scotoma center. See Figure 5.12 for conventions and simulation details.

In Figure 5.23b, the neuron became more responsive to locations away from the scotoma center, consistent with the results of Das and Gilbert (1995b). Normal stimulation following scotoma conditioning restored the RF size in the LISSOM network with instar excitatory synaptic plasticity alone (Figure 5.23).

Recovery of neurons in the cortical scotoma

The LISSOM network with instar lateral excitatory synaptic plasticity alone exhibited new responsiveness to stimuli outside the scotoma in neurons whose initial RF is inside the scotoma, during scotoma conditioning (Figure 5.23c).

RF shifts

Figure 5.23d displays the shift in RF center after conditioning with scotoma stimuli as a function of the initial RF center position of Layer 2 neurons. The LISSOM network with only instar lateral excitatory synaptic plasticity enabled exhibits consistent outward shifts (Figure 5.23d).

In the LISSOM network with only instar lateral excitatory synaptic plasticity

enabled, neurons whose initial RF center is inside the scotoma showed outward shift because of asymmetric RF expansion (Figure 5.23b), and neurons whose initial RF overlapped the scotoma boundary showed outward shift because of RF contraction.

Effect of blank stimuli on RF

In the LISSOM network with only lateral excitatory synaptic plasticity enabled, when no input stimulation is present, Layer 2 neurons are inactive, and therefore lateral excitatory pathway weights and cortical RFs do not change.

Conclusions

The LISSOM network with instar lateral excitatory synaptic plasticity alone produces many effects consistent with the experimental effects of artificial scotoma conditioning and bilateral retinal lesions. The LISSOM network with only instar lateral excitatory synaptic plasticity enabled produces RF contraction in neurons whose initial RF is just outside the scotoma during scotoma conditioning. Instar lateral excitatory synaptic plasticity in a network with short-range lateral excitatory connections and long-range inhibitory connections thus models dynamic RF changes during artificial scotoma conditioning.

In the LISSOM network, if the outstar lateral excitatory synaptic plasticity rule is used instead of the LISSOM instar lateral excitatory synaptic plasticity rule, then after scotoma conditioning the network may produce RF expansion in neurons outside the cortical scotoma and may produce RF shifts toward the scotoma center. These may happen during scotoma conditioning because an outstar lateral excitatory synaptic plasticity rule weakens lateral excitatory pathways *from active neurons to inactive neurons*, whereas an instar lateral excitatory synaptic plasticity rule weakens lateral excitatory pathways *from inactive neurons to active neurons*.

5.4 Simulation results: Complementary scotoma stimuli

The EXIN network (with afferent excitatory synaptic plasticity or lateral inhibitory synaptic plasticity alone), the LISSOM network (with afferent excitatory synaptic plasticity or instar lateral excitatory synaptic plasticity alone), and the inhibition-dominant adaptation model explain many important features of the artificial scotoma experiment (Pettet & Gilbert, 1992) and the experiment on the short-term effects of the bilateral retinal lesion (Darian-Smith & Gilbert, 1995). However, the inhibition-dominant adaptation model differs from other models in its behavior after blank screen conditioning (Section 5.3.1). The EXIN network with instar afferent excitatory synaptic plasticity alone and the LISSOM network with instar afferent or instar lateral excitatory synaptic plasticity alone produce RF contraction during scotoma conditioning, in neurons whose initial RF overlaps the scotoma boundary.

To further distinguish between the EXIN synaptic plasticity rules, the LISSOM synaptic plasticity rules, and the adaptation rule, a "complementary scotoma" stimulation experiment is proposed. In this conditioning paradigm, after the initial conditioning with normal stimuli, the network is presented with stimuli that have two alternating, complementary scotoma regions. That is, for any stimulus, the scotoma is a hemifield or its complementary hemifield. The duration of presentation, inter-trial interval, and duration before testing after conditioning should be varied to control for the ubiquitous neuronal adaptation in the cortex. The duration of presentation of each hemifield should short (e.g., 1–10 seconds).

5.4.1 RF changes because of synaptic plasticity

In the EXIN network with only lateral inhibitory synaptic plasticity enabled, neurons whose RF is near the common boundary of the complementary scotoma regions show maximal increase in RF size. The expansion is due to the decrease in the lateral inhibitory weights between layer 2 neurons whose RFs are inside and outside the common boundary of the complementary scotoma regions. The decrease occurs because these neurons are never coactivated during complementary scotoma conditioning.

Figure 5.24a shows the results of a complementary scotoma simulation, plotting Layer 2 RF size as a function of position of the initial RF center. The RF expansion was accompanied by an increase in responsiveness of the corresponding Layer 2 neurons.

Figure 5.24b shows Layer 2 RF size as a function of position of the initial RF center, after the LISSOM network with only lateral inhibitory synaptic plasticity enabled was presented with complementary scotoma stimuli. The behavior of the LISSOM network with only lateral inhibitory synaptic plasticity enabled was similar to that of the EXIN network with only lateral inhibitory synaptic plasticity enabled for this conditioning. Layer 2 neurons in the LISSOM network, with RFs inside and outside the common boundary of the complementary scotoma regions, were never coactivated. This resulted in a decrease in the strength of lateral inhibitory connections between these neurons. Thus, RFs near the boundary increased in size.

Figure 5.25a shows Layer 2 RF size as a function of position of the initial RF center after the EXIN network with only afferent excitatory synaptic plasticity enabled was presented with complementary scotoma stimuli. The neurons whose initial RF overlapped the complementary scotoma boundary showed RF contraction, as these neurons received weakened afferent pathways from positions close to the complementary scotoma boundary. Complementary scotoma conditioning of the LISSOM network with only afferent excitatory synaptic plasticity enabled produced the same effects (Figure 5.25b).

The LISSOM network with instar lateral excitatory synaptic plasticity alone produced RF contraction in neurons whose initial RF straddled the complementary scotoma boundary. This happens because anti-correlated activity in neurons whose initial RF center lay on opposite sides of the complementary scotoma boundary results in weakening of mutual lateral excitatory connections, leading to RF contraction (Figure 5.25c).

In the EXIN and the LISSOM networks with only lateral inhibitory synaptic plasticity enabled, the RFs of neurons across the complementary scotoma boundary shifted *toward* each other (Figure 5.26). However, in the EXIN network with only afferent excitatory plasticity enabled and in the LISSOM network with either afferent excitatory or lateral excitatory plasticity enabled, the RFs of neurons across the complementary scotoma boundary shifted *away* from each other (Figure 5.27). In the LISSOM network with lateral

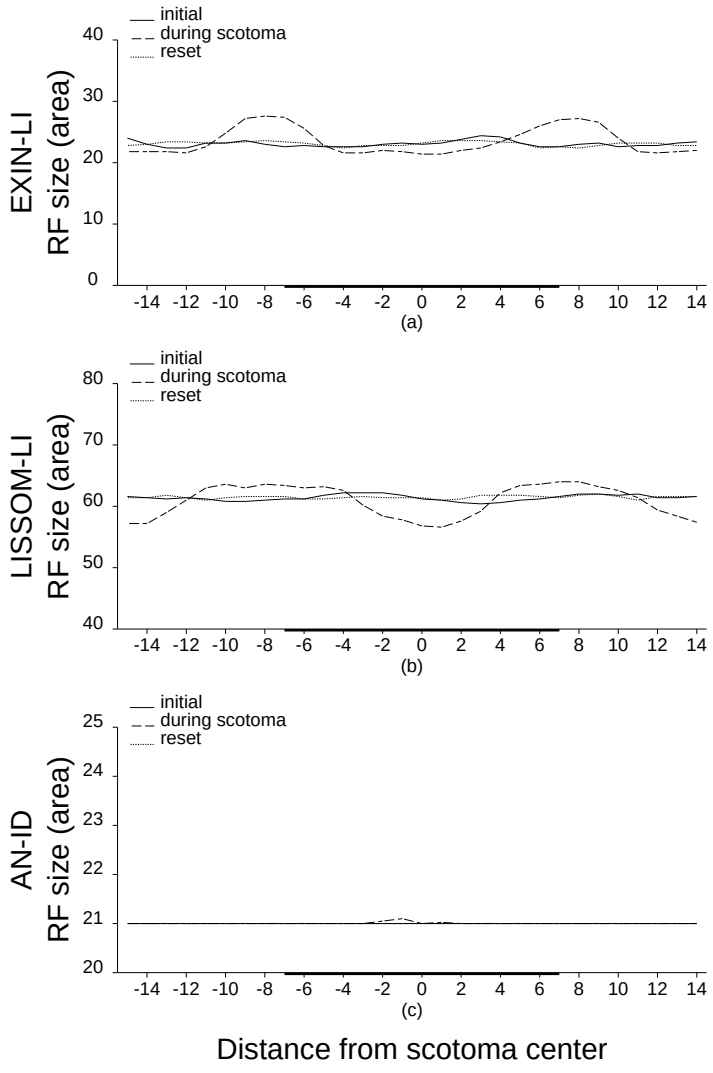

Figure 5.24: **Simulation results: Average RF size changes after complementary scotoma conditioning.**
The average RF area before complementary scotoma conditioning (solid line), after complementary scotoma conditioning (dashed line), and after re-conditioning with normal stimuli (dotted line) in the EXIN network with only lateral inhibitory synaptic plasticity enabled (a), the LISSOM network with only lateral inhibitory synaptic plasticity enabled (b), and the inhibition-dominant adaptation network (c), are shown as a function of the position of the initial RF center of Layer 2 neurons relative to the scotoma center. The scotoma is a hemifield of size 15×30. The average RF area shown at each position is the mean over the RF area of neurons with same x coordinate. The RF area of a Layer 2 neuron is defined as the number of locations at which the test stimulus evokes a response in the Layer 2 neuron. In panel (c) the dotted curve overlaps with the solid curve. The thick line segment on the abscissa represents the scotoma region.

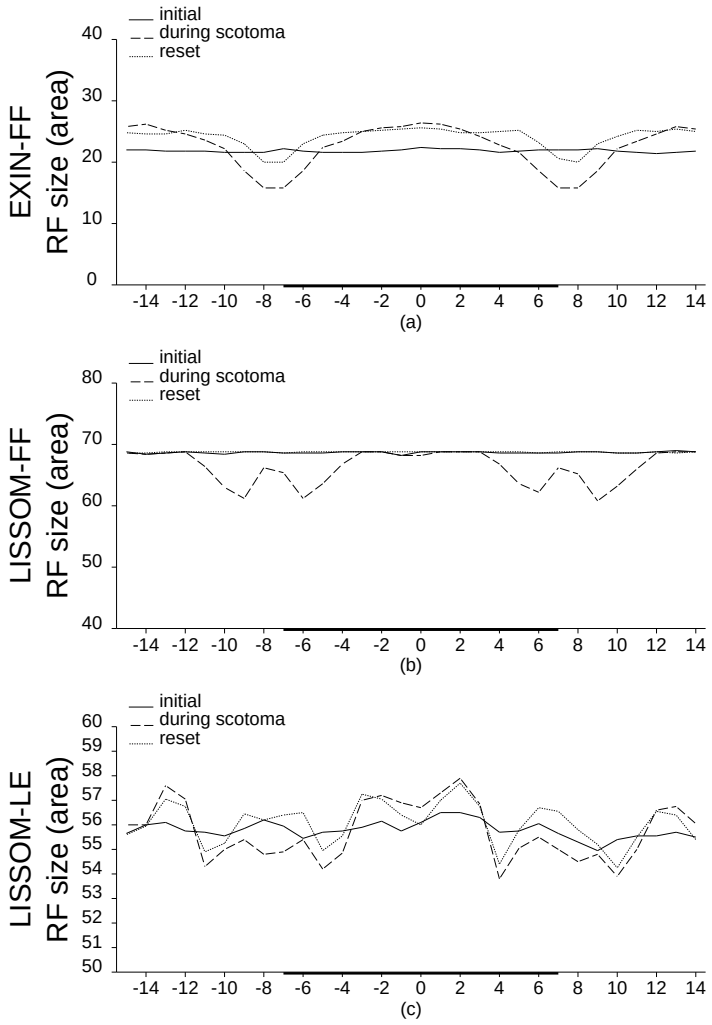

Figure 5.25: **Simulation results: Average RF size changes after complementary scotoma conditioning.**
The average RF area before complementary scotoma conditioning (solid line), after complementary scotoma conditioning (dashed line), and after re-conditioning with normal stimuli (dotted line) in the EXIN network with only afferent excitatory synaptic plasticity enabled (a), the LISSOM network with only afferent excitatory synaptic plasticity enabled (b), and the LISSOM network with only instar lateral excitatory synaptic plasticity enabled (c), are shown as a function of the position of the initial RF center of Layer 2 neurons relative to the scotoma center. See Figure 5.24 for conventions and simulation details.

excitatory plasticity alone, smaller RF shifts in neurons far from the cortical complementary scotoma boundary were due to reduced inhibition to these neurons from neurons close to the cortical complementary scotoma boundary.

5.4.2 RF changes because of neuronal adaptation

During complementary scotoma conditioning, Layer 2 neurons are activated alternately because of the alternate complementary input stimulations. Thus, Layer 2 neurons become less adapted compared to the adaptation level after the initial whole field stimulation.

In the computer simulations of complementary scotoma conditioning of the inhibition-dominant network, Layer 2 neurons whose initial RF straddles the complementary scotoma boundary were more adapted than neurons whose initial RF is away from the complementary scotoma boundary. But the Layer 2 RF size as a function of the initial RF center position was almost flat (Figure 5.24c). Note that the RF size of a Layer 2 neuron was defined as the number of input positions at which stimulation drives the neuron's activation above a threshold. The difference in adaptation level among the neurons was not large enough to produce significant change in RF size. The small differences in the adaptation level of Layer 2 neurons after complementary scotoma conditioning was manifested as small RF shifts (Figure 5.26c). Because neurons whose RF center was close to the complementary scotoma boundary were more adapted than the other neurons, they exerted less lateral inhibition on neurons whose initial RF center was away from the complementary scotoma boundary, and the RF center of neurons whose RF center was on either side of the complementary scotoma boundary shifted toward each other. If neurons whose RF center was close to the complementary scotoma boundary were less adapted than the other neurons, then they would have maximal RF size, and they would exert more lateral inhibition on neurons whose initial RF center was away from the complementary scotoma boundary; thus the RF centers of neurons whose RF centers were on either side of the complementary scotoma boundary would shift away from each other.

In the simulation of complementary scotoma conditioning of the adaptation network with no lateral interaction, Layer 2 neurons whose RF center was close to the

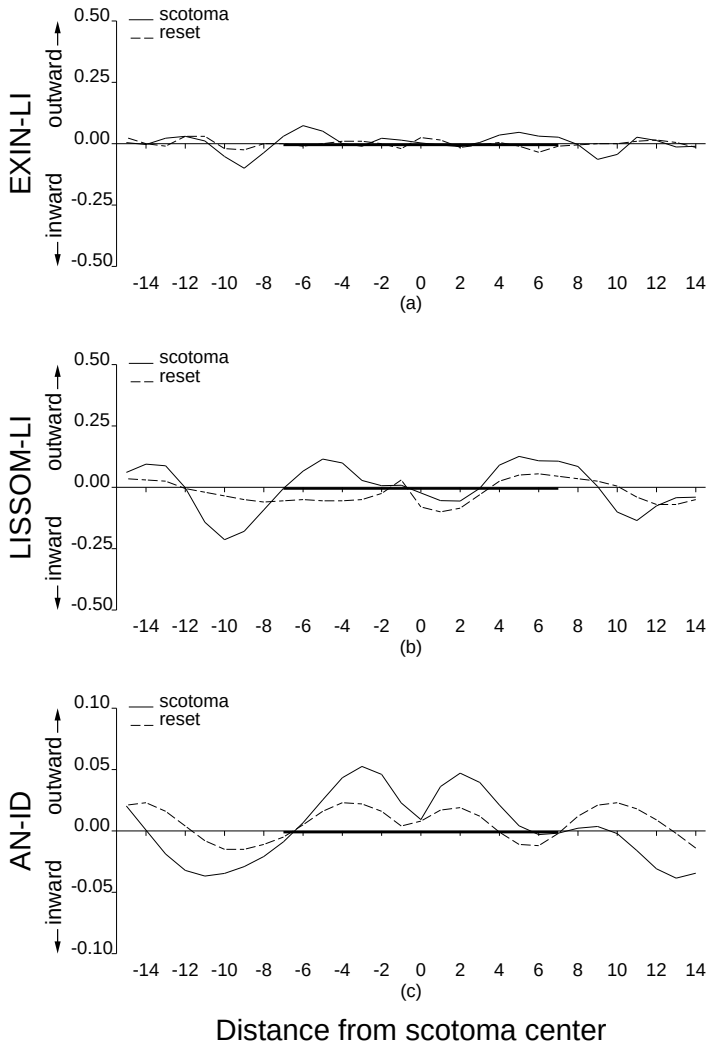

Figure 5.26: **Simulation results: Average RF shifts after complementary scotoma conditioning.**

The average shift in the RF center after complementary scotoma conditioning (solid line) and after re-conditioning with normal stimuli (dashed line) with respect to the initial RF centers is shown as a function of distance of the initial RF center of Layer 2 neurons from the scotoma center for the EXIN network with only lateral inhibitory synaptic plasticity enabled (a), the LISSOM network with only lateral excitatory synaptic plasticity enabled (b), and the adaptation network (c). The average RF shift shown at each position is the mean over the shift in RF center of neurons with same x coordinate. Positive and negative shifts represent a shift away from and toward the center of the scotoma, respectively. The RF center of a Layer 2 neuron is the center of moment of the neuron's responsiveness to input at different positions within its RF. See Figure 5.24 for simulation details and conventions.

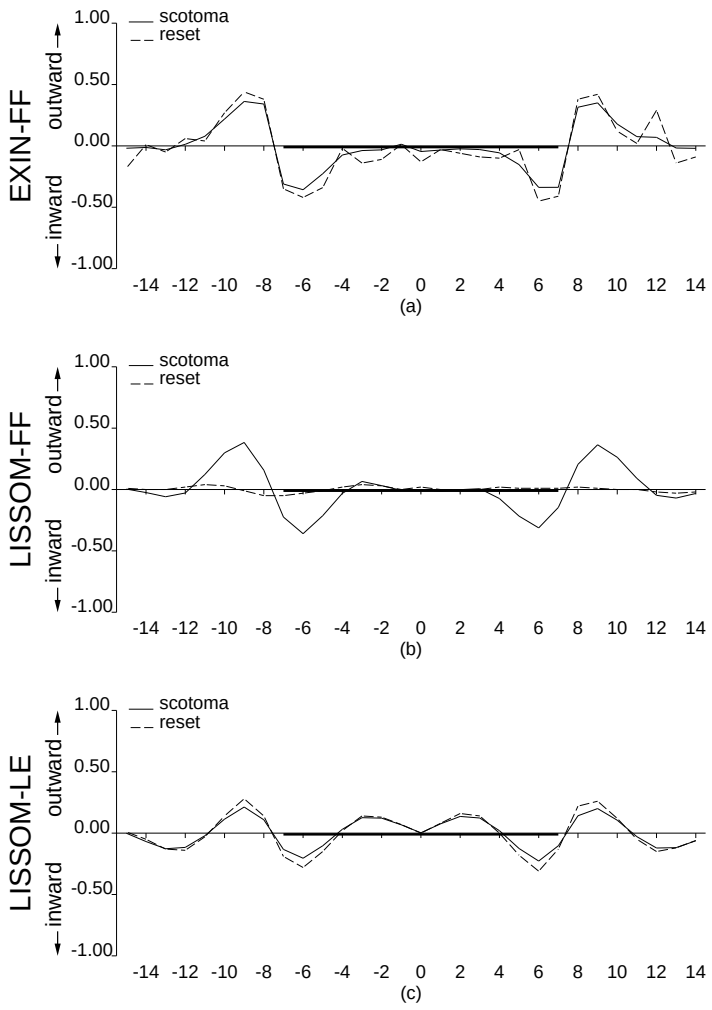

Figure 5.27: **Simulation results: Average RF shifts after complementary scotoma conditioning.**

The average shift in the RF center after complementary scotoma conditioning (solid line) and after re-conditioning with normal stimuli (dashed line) with respect to the initial RF centers is shown as a function of distance of the initial RF center of Layer 2 neurons from the scotoma center for the EXIN network with only afferent excitatory synaptic plasticity enabled (a), the LISSOM network with only afferent excitatory synaptic plasticity enabled (b), and and the LISSOM network with only instar lateral excitatory synaptic plasticity enabled (c). See Figure 5.26 for conventions.

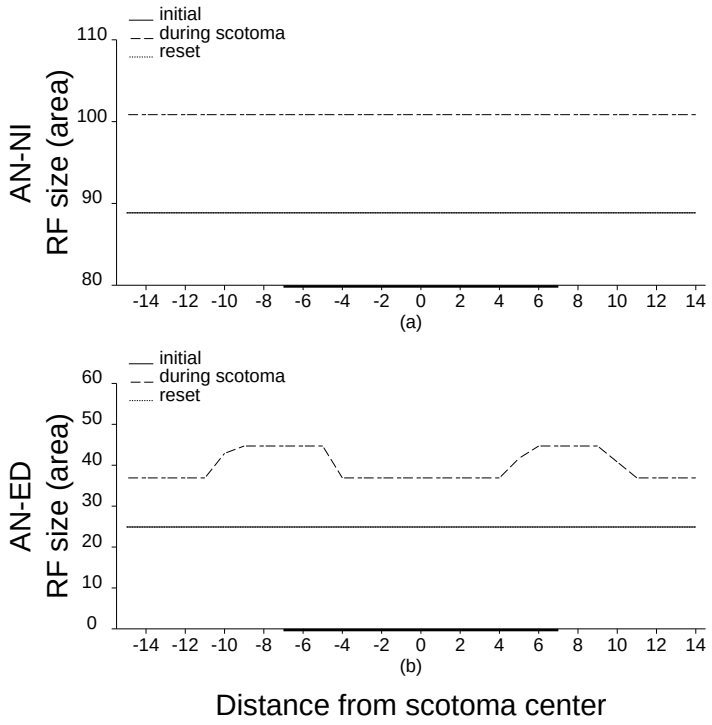

Figure 5.28: **Simulation results: Average RF size changes after complementary scotoma conditioning.**
The average RF area before complementary scotoma conditioning (solid line), after complementary scotoma conditioning (dashed line), and after re-conditioning with normal stimuli (dotted line) in the adaptation network with no lateral interaction (a), and in the excitation-dominant adaptation network (b), are shown as a function of the position of the initial RF center of Layer 2 neurons relative to the scotoma center. In panels (a,b) the dotted curve overlaps with the solid curve. See Figure 5.24 for conventions and simulation details.

complementary scotoma boundary were more adapted than other neurons. Thus, they may have a smaller RF than neurons whose initial RF center was away from the complementary scotoma boundary. As in the simulation of the inhibition-dominant adaptation model, the RF sizes of Layer 2 neurons were almost the same (Figure 5.28a). No RF shifts occurred because there are no lateral interactions (Figure 5.29a). If Layer 2 neurons whose RF center was close to the complementary scotoma were less adapted than other neurons, they would have larger RFs than other neurons, and again there would not be any RF shifts.

In the simulation of complementary scotoma conditioning of the

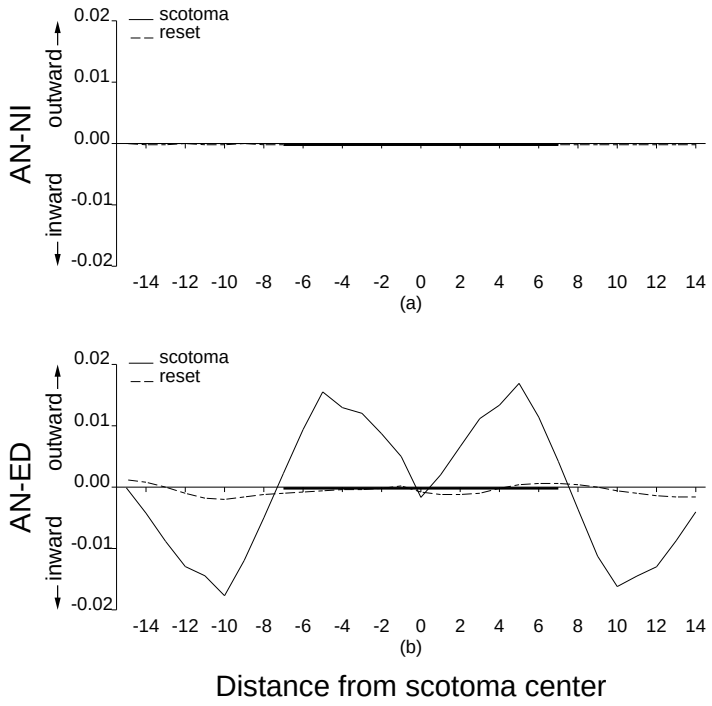

Figure 5.29: **Simulation results: Average RF shifts after complementary scotoma conditioning.**
The average shift in the RF center after complementary scotoma conditioning (solid line) and after re-conditioning with normal stimuli (dashed line) with respect to the initial RF centers is shown as a function of distance of the initial RF center of Layer 2 neurons from the scotoma center for the adaptation network with no lateral interaction (a) and for the excitation-dominant adaptation network (b). In panel (a) the solid and dashed curves overlap with the abscissa because there were no RF shifts. See Figure 5.26 for conventions.

excitation-dominant adaptation, Layer 2 neurons whose RF center was close to the complementary scotoma boundary were less adapted than other neurons. Thus, they had larger RFs than neurons whose initial RF center was away from the complementary scotoma boundary (Figure 5.28b). Because neurons whose RF center was close to the complementary scotoma boundary were less adapted than the other neurons, they exerted more lateral excitation on neurons whose initial RF center was away from the complementary scotoma boundary, and the RF centers of neurons whose RF centers were on either side of the complementary scotoma boundary shifted toward each other (Figure 5.29b). If neurons

whose RF center was close to the complementary scotoma boundary were more adapted than the other neurons, then they would have smaller RFs than other neurons, and they would exert less lateral excitation on neurons whose initial RF center was away from the complementary scotoma boundary; thus, the RF centers of neurons whose RF centers were on either side of the complementary scotoma boundary would shift away from each other.

Effects of network interactions on neuronal adaptation

In the adaptation networks, the complementary scotoma stimulation activates Layer 2 neurons with close to equal probability. The adaptation levels of Layer 2 neurons in the adaptation networks are not necessarily equal for the following reasons. (1) Neurons whose initial RF straddles the complementary scotoma boundary are activated slightly more often (although possibly at a lower intensity), and therefore these neurons may become slightly more adapted than other neurons. (2) Neurons whose RF center is close to the center of a hemifield have a large number of their afferent excitatory pathways excited when that hemifield is stimulated, whereas neurons whose RF center is close to the complementary scotoma boundary have only a small number of their afferent excitatory pathways excited. Thus, neurons whose RF center is close to the center of a hemifield are likely to be more strongly activated and therefore more adapted than neurons whose RF center is close to the complementary scotoma boundary. (3) The difference in the amount of afferent excitation received by the Layer 2 neurons is further accentuated by the adaptation threshold. If Layer 2 neurons have large thresholds, neurons receiving larger afferent excitation are more likely to be activated and hence be more adapted. (4) In the inhibition-dominant adaptation network, neurons whose RF center is close to the complementary scotoma boundary receive less lateral inhibition than neurons whose RF center is close to the center of a hemifield, thus making neurons whose RF center is close to the complementary scotoma boundary likely to respond strongly and become more adapted. On the other hand, in the excitation-dominant adaptation network, neurons whose RF center is close to the complementary scotoma boundary receive less lateral excitation than neurons whose RF center is close to the center of a hemifield, thus making them respond weakly and become less adapted. The eventual distribution of adaptation levels will be determined by the more dominant factors.

5.4.3 Recovery of RF properties

Normal stimulation following complementary scotoma conditioning caused restoration of the original RF size and position in the EXIN and LISSOM networks with only lateral inhibitory synaptic plasticity enabled, in all the adaptation networks, and in the LISSOM network with only afferent synaptic plasticity enabled (Figures 5.24–5.29).

The EXIN network with only afferent excitatory synaptic plasticity enabled (Figures 5.25a and 5.27a) did not recover its original RF properties. The LISSOM network with only lateral excitatory synaptic plasticity enabled (Figures 5.25c and 5.27c) also did not recover some of its original RF properties, because as the lateral excitatory pathways weaken, effective inhibition between neurons increases, and increased lateral inhibition makes Layer 2 neurons less coactive.

5.4.4 Conclusions

Complementary scotoma conditioning revealed differences in the behaviors of the various models. Thus, a neurobiological experiment using complementary scotoma conditioning could discriminate between the different models based on their predictions. The predictions of the different models are described below.

After complementary scotoma conditioning, the EXIN and the LISSOM network, with only their respective lateral inhibitory synaptic plasticity rules enabled, predict that cortical neurons whose initial RF centers were close to the complementary scotoma boundary would have larger RFs than neurons whose initial RF centers were far from the complementary scotoma boundary, and the initial RFs on opposite sides of the complementary scotoma boundary would shift toward each other, whereas the LISSOM network with only lateral excitatory synaptic plasticity and the EXIN and the LISSOM network with only afferent excitatory synaptic plasticity predict that neurons whose initial RF centers were close to the complementary scotoma boundary would have smaller RFs than neurons whose initial RF centers were far from the complementary scotoma boundary, and the initial RFs on opposite sides of the complementary scotoma boundary would shift away from each other.

After complementary scotoma conditioning, the adaptation network with no lateral interaction predicts that RFs of neurons whose initial RF centers were close to the complementary scotoma boundary would be smaller than, equal to, or greater than the RFs of other neurons, but no RF shifts would occur because the afferent weights were symmetric.

The inhibition-dominant adaptation network network predict that, complementary scotoma conditioning would (1) cause the RFs of neurons whose initial RF centers were close to the scotoma boundary to be smaller than the RFs of other neurons and cause the RFs on opposite sides of the complementary scotoma boundary to shift toward each other, or (2) cause the RFs of neurons whose initial RF centers were close to the scotoma boundary to be larger than the RFs of other neurons, and cause the RFs on opposite sides of the complementary scotoma boundary to shift away from each other. In the excitation-dominant network, however, when the RFs of neurons whose initial RF centers were close to the scotoma boundary are smaller (larger) than the RFs of other neurons, the RFs across the complementary scotoma boundary shift away from (shift toward) each other. The specific effects will depend on the conditions discussed in Section 5.4.2.

It is possible that the rates of change in the effective lateral excitation and the effective lateral inhibition may differ at short and long ranges. This can be probed by scotoma and complementary scotoma conditioning. For example, if at short ranges effective lateral excitation decreases faster than lateral inhibition, then scotoma conditioning should produce RF contraction in neurons whose initial RF center is close to the scotoma boundary and RF expansion in neurons whose initial RF is inside and far from the scotoma boundary.

5.5 Discussion

The effects of the EXIN rules, the LISSOM rules, and the adaptation rule in response to artificial scotoma stimuli have been compared. The experimental data and the simulation predictions are summarized in Table 5.1. The entries in boldface indicate where the models are in agreement with experimental data.

The EXIN network with outstar lateral inhibitory synaptic plasticity alone

Measurement	Exp'tal Data	EXIN Outstar Lateral Inh. Learning alone	EXIN Instar Afferent Exc. Learning alone	LISSOM Instar Lateral Inh. Learning alone	LISSOM Instar Lateral Exc. Learning alone	LISSOM Instar Afferent Exc. Learning alone	AN with no lateral inter-actions	AN Exc. Dom.	AN Inh. Dom.
RF expansion inside the scotoma	Yes	**Yes**	**Yes**	No	**Yes**	**Yes**	**Yes**	**Yes**	**Yes**
Asymmetric RF profile after scotoma conditioning	Yes	**Yes**	**Yes**	**Yes**	**Yes**	**Yes**	No	**Yes**	**Yes**
Asymmetric RF more responsive to locations away from scotoma center	Yes	**Yes**	**Yes**	No	**Yes**	**Yes**	No	No	**Yes**
Maximal RF expansion just inside the cortical scotoma boundary	Yes	**Yes**	**Yes**	No	**Yes**	**Yes**	No	No	**Yes**
Function returns in concentric inward direction	Yes	**Yes**	**Yes**	No	**Yes**	**Yes**	**Yes**	**Yes**	**Yes**
Retinal lesion produces small centrifugal RF shifts	Yes	**Yes**	**Yes**	No	**Yes**	**Yes**	No	No	**Yes**
Blank display changes RF size	No	**No**	**No**	**No**	**No**	**No**	Yes	Yes	Yes
Complem. scotoma cond. produces peak expansion near scotoma boundary	??	Yes	No	Yes	No	No	No/Yes	No/Yes	No/Yes
Complem. scotoma cond. shifts RFs across and close to the scotoma boundary toward each other	??	Yes	No	Yes	No	No	No/No	No/Yes	Yes/No

Table 5.1: **Comparison of models of dynamic RF changes**

produced the following effects, corresponding closely to the reported neurophysiology. During scotoma/normal conditioning, the EXIN model with only outstar lateral inhibitory synaptic plasticity enabled produced

- centrifugal expansion of RFs that were initially *inside* the scotoma region;
- the greatest expansion for RFs closest to the scotoma boundary;
- RF expansion that exceeded the boundaries of the scotoma for RFs close to the scotoma boundary;

- increased response from the area of the initial RF (DeAngelis et al., 1994, 1995), without changes in spontaneous activation in the absence of visual stimulation (Pettet & Gilbert, 1992);
- asymmetric RF profiles in neurons with initial RF close to the scotoma boundary (Das & Gilbert, 1995b);
- RF contraction to original size during subsequent normal stimulation; and
- no RF changes in the absence of stimulation.

During complementary scotoma conditioning the EXIN network with only outstar lateral inhibitory synaptic plasticity enabled showed

- maximal RF size for neurons whose initial RF was on *either* side of the scotoma boundary; and
- a shift in RF of neurons whose initial RFs were close the scotoma boundary *toward* each other.

The EXIN model with only afferent excitatory synaptic plasticity enabled produced the following effects, different from those produced by the EXIN model with only lateral inhibitory synaptic plasticity enabled:

- neurons affected by scotoma conditioning *did not* recover their original RF size and RF position; and
- complementary scotoma conditioning caused RF *contraction* and minimal RF size in neurons whose initial RF was on either side of the scotoma boundary; and
- complementary scotoma conditioning shifted the RFs of neurons whose initial RFs were close to the scotoma boundary *away* from each other.

The other effects were the same as those produced by the EXIN model with only lateral inhibitory synaptic plasticity enabled (see Table 5.1).

The effects of scotoma conditioning and complementary scotoma conditioning the full EXIN network (with the afferent excitatory and the lateral inhibitory synaptic

plasticity rules enabled) will depend on the relative rate of learning in the two rules. The effects obtained by disabling one of the two rules are at the ends of a continuum of effects produced by the EXIN rules. Because the two EXIN rules produce many common effects after scotoma conditioning (see Table 5.1), the full EXIN network too produces these effects. Unlike the EXIN network with only afferent excitatory synaptic plasticity, the full network can recover the original RFs during normal conditioning following scotoma conditioning. Thus, the full EXIN network produces effects consistent with neurophysiological data on artificial scotoma conditioning. However, during complementary scotoma conditioning the two EXIN rules produce opposite effects (Table 5.1), and thus the overall effects produced by the full EXIN network will depend on the relative magnitudes of changes produced by the two rules.

The LISSOM network with only instar lateral inhibitory synaptic plasticity enabled produced the following effect inconsistent with neurophysiological data. In response to normal/scotoma conditioning, the network showed

- expansion of RFs that were initially *outside* the scotoma and close to the scotoma boundary.

The LISSOM network with afferent excitatory synaptic plasticity alone or instar lateral excitatory synaptic plasticity alone produced RF expansion in neurons whose initial RF was inside the scotoma during scotoma conditioning and produced effects similar to those produced by the EXIN network with only outstar lateral inhibitory synaptic plasticity enabled during scotoma conditioning. However, during complementary scotoma conditioning, the LISSOM network with instar afferent excitatory synaptic plasticity alone or instar lateral excitatory synaptic plasticity alone produced

- RF *contraction* and minimal RF size in neurons whose initial RF was on either side of the scotoma boundary; and
- shifts in RF of neurons whose initial RFs were close the scotoma boundary, *away* each other.

As in the full EXIN network, the effects produced by the full LISSOM network after scotoma conditioning and complementary scotoma conditioning will depend on the

relative magnitudes of changes produced by the three rules in the LISSOM model. The important observation is that, after scotoma or complementary conditioning, many of the effects produced by the LISSOM lateral inhibitory synaptic plasticity rule are in conflict with those produced by the LISSOM afferent and lateral excitatory synaptic plasticity rules (see Table 5.1).

The inhibition-dominant adaptation model produced several effects (Xing & Gerstein, 1994) consistent with neurophysiological data. However, the inhibition-dominant adaptation network produced the following effect inconsistent with neurophysiological data:

- changes in RF size in the absence of stimulation.

The adaptation network with no lateral interaction and the excitation-dominant adaptation network produced RF expansion in neurons in the cortical scotoma. However, the RF size in these networks changed in the absence of stimulation, inconsistent with experimental data. In the adaptation network with no lateral interaction, the RFs remained symmetric, and RF positions did not change following scotoma conditioning. In the excitation-dominant adaptation network, the RFs shifted toward the scotoma center. These results are inconsistent with neurophysiological data.

After complementary scotoma conditioning the adaptation networks, the RFs of neurons whose initial RF centers were close to the complementary scotoma boundary may be smaller or larger than the RFs of other neurons; the RF size is parameter dependent. In the adaptation network with no lateral interaction no RF shifts occurred. In the inhibition-dominant adaptation network, when the RFs of neurons whose initial RF centers were close to the complementary scotoma boundary were larger than the RFs of other neurons, then the RFs on opposite sides of the boundary shifted away from each other, but when the RFs of neurons whose initial RF centers were close to the complementary scotoma boundary were smaller than the RFs of other neurons, then the RFs on opposite sides of the boundary shifted toward each other. In the excitation-dominant adaptation network, the relationship between the relative RF size and RF shift are opposite to that in the inhibition-dominant adaptation network.

The role of afferent excitatory synaptic plasticity rule in producing fast (on the

order of minutes or hours) RF changes in adult animals may be very limited or non-existent. Restricted retinal lesion in cats produced RF changes in neurons in layers 3 and 4 of area 17 within hours *only* if the non-lesioned eye was *closed* (Chino et al., 1992). This result is contrary to the prediction of a model with only a fast *instar* afferent excitatory synaptic plasticity rule (e.g., the EXIN and the LISSOM afferent excitatory synaptic plasticity rules), because active neurons would weaken their connections from the lesioned region, regardless of whether the other eye is open or closed, to produce changes in RF properties. Furthermore, changes in ocular dominance, which are presumed to be caused by changes in thalamocortical afferents (Clothiaux et al., 1991; Miller et al., 1989), cannot be induced in adult animals by visual deprivation. However, dynamic RF changes because of afferent excitatory plasticity would be consistent with the results of Chino et al. (1992) *if the afferent excitatory plasticity occurs in pathways originating from a binocular layer*. With the unlesioned eye open, there will be no scotoma in the binocular layer, and hence afferent excitatory pathways from the binocular layer will not change. But, Chino et al. (1992) observed no change in RF of neurons in layer 4 of cat area 17 (which may receive monocular thalamocortical inputs) when the unlesioned eye was open. In the EXIN network with outstar lateral inhibitory synaptic plasticity alone, the LISSOM networks with instar lateral excitatory or instar lateral inhibitory synaptic plasticity alone, and the adaptation networks, with the unlesioned eye open there is no cortical scotoma; all binocular neurons in the networks are active during the conditioning and therefore the lateral weights in the EXIN or the LISSOM networks and the adaptation level in the inhibition-dominant adaptation network would remain almost unchanged. However, there might be some small changes in RF properties because some cortical neurons are binocularly activated while others are monocularly activated by the unlesioned eye.

Instar lateral excitatory synaptic plasticity alone in the LISSOM network decreases lateral excitatory connection weights from neurons inside the cortical scotoma to those outside the cortical scotoma. This directly reduced the RF size of neurons whose initial RF center is close to and outside the scotoma (Figure 5.23) and indirectly leads to RF expansion in neurons whose initial RF is inside the scotoma (Figure 5.23). In the EXIN model with lateral inhibitory synaptic plasticity alone, scotoma conditioning leads to

weakening of the lateral inhibitory connections from neurons outside the cortical scotoma to those inside. This directly leads to RF expansion in neurons inside the cortical scotoma. The increased responsiveness of neurons inside the cortical scotoma then lets those neurons exert more inhibition on neurons outside the cortical scotoma, leading indirectly to RF contraction of neurons outside the cortical scotoma (Figures 5.7 and 5.10). Thus, these two models produce qualitatively similar results during scotoma conditioning; the results are closest to the experimental data on artificial scotoma conditioning and retinal lesions. However, as shown in Section 5.4, they exhibit different RF changes during complementary scotoma conditioning.

Grajski and Merzenich (1990) proposed a model with plasticity in afferent excitatory, feedback excitatory, lateral excitatory, and lateral inhibitory pathways, for RF changes following repetitive peripheral stimulation of a restricted skin region. Their plasticity rule is a covariance rule with normalization; pathway strength is weakened if either the source or the target neuron is inactive. Such a rule would produce roughly symmetric RF changes across the cortical scotoma boundary even during scotoma conditioning, contrary to the experimental data and contrary to the EXIN and LISSOM rules.

5.5.1 Models based on the EXIN and the LISSOM rules

Several visual functions and visual cortical properties have been modeled by the EXIN and the LISSOM rules.

The EXIN afferent excitatory and lateral inhibitory synaptic plasticity rules together have been used to model visual disparity selectivity (Marshall, 1990c), visual motion selectivity and grouping (Marshall, 1990a), visual inertia (Hubbard & Marshall, 1994), visual motion integration in the aperture problem (Marshall, 1990a), visual length selectivity and end-stopping (Marshall, 1990b), visual depth perception from occlusion events (Marshall & Alley, 1993; Marshall et al., 1996a), visual depth from motion parallax (Marshall, 1989), visual motion smearing (Martin & Marshall, 1993), visual orientation selectivity (Marshall, 1990d), and visual stereomatching (Marshall et al., 1996b).

The LISSOM rules have been used to model development of topographic RFs (Sirosh & Miikkulainen, 1994b, 1997), visual orientation tuning and orientation

columns (Sirosh et al., 1996), ocular dominance columns (Sirosh & Miikkulainen, 1995, Sirosh et al., 1996), RF changes after cortical lesions (Sirosh & Miikkulainen, 1994a), and tilt aftereffects (Bednar & Miikkulainen, 1997).

Although, the EXIN and the LISSOM rules model some visual functions and cortical properties, they produce different effects after artificial scotoma conditioning. Thus, the analyses of the effects of the various synaptic plasticity rules during artificial scotoma conditioning provides a basis for determining the rules for cortical plasticity.

5.5.2 Transient response bias in RF measurements

The changes in RFs produced by the EXIN and the LISSOM rules persist after cessation of the conditioning stimuli. However, several results show that some dynamic RF changes produced by artificial scotoma conditioning are transient. For example, some RF changes occurred within seconds of the conditioning, and recovery time was also on the order of seconds, in the absence of stimulation (DeAngelis et al., 1995; Kapadia et al., 1994). These transient changes in RF can be modeled by the Xing and Gerstein (1994) inhibition-dominant adaptation model, operating at a fast time-scale (1–10 seconds). Adaptation could also be added to the EXIN and the LISSOM models to describe the transient RF changes. The transient RF affects appear to be a separate phenomenon from the RF dynamics that operate at a slower time scale (5–15 minutes).

5.5.3 Effect of orientation on RF dynamics

Pettet and Gilbert (1992) studied the effects of conditioning a neuron by presenting the artificial scotoma against a background of moving bars oriented orthogonally to the preferred orientation of the neuron (cross-orientation artificial scotoma). For a few neurons (3 out of 15), they found an expansion with iso-orientation conditioning stimuli and did not find an expansion with the orthogonal pattern. In these cases, the orthogonal pattern actually reduced the RF size and responsiveness of the neuron.

The EXIN rules predict that cross-orientation artificial scotoma conditioning of a neuron would produce less expansion than would iso-orientation artificial scotoma conditioning. Lateral inhibition between neurons becomes roughly proportional to the

amount of overlap in their RFs, using the EXIN rules (Marshall, 1990bcd; 1992ab; 1995a). The EXIN model predicts strong iso-orientation inhibition and weak ortho-orientation inhibition (Marshall, 1990d) consistent with the results of Ferster (1989). During cross-orientation artificial scotoma conditioning, the decrease in lateral inhibition to the test neuron will be small because according to the EXIN rules, the ortho-orientation inhibition is small. In addition, the EXIN rules can model the shrinkage after cross-orientation artificial scotoma conditioning observed by Pettet and Gilbert (1992). The cross-orientation scotoma conditioning causes neurons with the near-orthogonal preferred orientation within the cortical scotoma to become more responsive and to exert more inhibition on the recorded neuron. Further simulations are needed to demonstrate this prediction.

Gilbert and Wiesel (1990) found short term modifications in the orientation specificity of neurons, in response to contextual stimuli placed outside a neuron's RF. Presentation of differently oriented bars in the surround of a neuron's RF caused the neuron's tuning curve to shift. In some cases, the change persisted even after the removal of the surround stimuli. The most effective way of restoring the neuron's original orientation tuning was to stimulate the surround with lines of varying orientation, for a period of about 10 mins. This persistent effect may be produced by changes in the lateral inhibitory weights between neurons with different orientation specificity. An explanation of this effect based on synaptic changes may explain development of connection patterns that can produce the various kinds of contextual effects (Badcock & Westheimer, 1985; Butler & Westheimer, 1978; Westheimer, 1986, 1989; Westheimer & McKee, 1977; Westheimer et al., 1976).

5.5.4 Long-term effects of retinal lesions on RF properties

Darian-Smith and Gilbert (1995) found that about 5 minutes after bilateral retinal lesions neurons in the cortical scotoma became responsive to visual stimuli outside the lesioned regions. However, the neurons that acquired responsiveness to locations outside the lesioned retina were less responsive and more sluggish in their response compared to neurons in the normal cortex. The sluggish response of neurons in the recovered area of the cortical scotoma in the primary visual cortex may arise because these neurons receive

afferent excitation via weak connections, which can activate these neurons because of the reduced lateral inhibition they receive, as a consequence of the EXIN lateral inhibitory synaptic plasticity rule, the EXIN or the LISSOM afferent excitatory synaptic plasticity rule, or the LISSOM lateral excitatory synaptic plasticity rule. It is also possible that the cortical recovery is aided by long-range lateral excitation or by feedback connections from other cortical layers (Darian-Smith & Gilbert, 1994, 1995), in addition to the changes in lateral inhibition in the primary visual cortex. Cortical scotoma in deeper layers can modify RF properties of neurons in the deeper layers, and these changes can affect RF properties in lower cortical layers via feedback pathways. Within the EXIN learning framework, feedback connections have been used in the representation of oblique and transparent surfaces defined by stereo disparity (Marshall & Kalarickal, 1995; Marshall et al., 1996b) and in motion grouping (Schmitt & Marshall, 1995, 1996).

The cortical reorganization occurring over a period of weeks and months following retinal lesions may also involve the sprouting and establishment of new connections – either synaptogenesis along existing fibers or the physical extension of axonal/dendritic terminals in addition to synaptogenesis (Darian-Smith & Gilbert, 1994).

Even after several months after the retinal lesions, a small region of the cortex remained unresponsive to visual stimulation in the unlesioned retinal regions. Darian-Smith and Gilbert (1995) invoke physical limits on the extent of changes in the horizontal connections to explain the existence of the persistent deprived cortical region.

5.5.5 Role of lateral excitatory pathways in RF properties

The LISSOM network has been used to model self-organization of topographic RF organization and ocular dominance columns and the effects of cortical lesions (Sirosh & Miikkulainen, 1994ab, 1995, 1997). In the LISSOM network, topographically ordered RFs develop if the initial afferent connections are ordered in overlapping patches and the synaptic weights are random (Sirosh & Miikkulainen, 1997). This possibility suggests that undeveloped cortex with input afferents ordered in overlapping connections but with random synaptic weights can develop into topographically organized cortex.

The EXIN network described in this chapter does not have lateral excitatory

connections. Lateral excitatory connections with signal transmission latencies have been used in conjunction with the EXIN rules to model several aspects of visual motion perception (Hubbard & Marshall, 1994; Marshall, 1989, 1990a, 1991, 1995b; Marshall & Alley, 1993; Martin & Marshall, 1993). The EXIN lateral connectivity pattern can be viewed of as a limiting case of the LISSOM connectivity pattern, when the lateral excitatory zone of a Layer 2 neuron contains only itself. Smaller lateral excitatory zones lead to smaller regions of topographic ordering. Like the LISSOM network, the EXIN network could show local topographic ordering if it had lateral excitatory connection pathways.

5.5.6 Significance of the EXIN lateral inhibitory plasticity rule

In the EXIN model, strong lateral inhibitory pathways develop between neurons that are consistently coactivated. Neurons can be consistently coactivated if they receive excitatory afferents from many common input neurons. Thus, in the EXIN model, cortical neurons that share inputs have strong lateral inhibitory pathways between them. This is consistent with experimental results suggesting that a neuron receives the strongest inhibition when its stimuli are most similar to the preferred stimuli of the neuron (Blakemore & Tobin, 1972; DeAngelis et al., 1992; Ferster, 1989).

The EXIN lateral inhibitory plasticity rule has several desirable functional properties. The inhibitory synaptic plasticity rule leads to improved stimulus discrimination, sparse and distributed coding, and exclusive allocation (Marshall, 1995a; Marshall & Gupta, 1997). The EXIN synaptic plasticity rules have been used to model the development of disparity selectivity (Marshall, 1990c), motion selectivity and grouping (Marshall, 1990a, 1995b; Schmitt & Marshall, 1995), orientation selectivity (Marshall, 1990d), and length selectivity and end-stopping (Marshall, 1990b).

Note that the EXIN lateral inhibitory plasticity rule (Equation 5.1) is an asymmetric rule; lateral inhibitory pathways from active neurons to inactive weaken, however, lateral inhibitory pathways from inactive neurons to other neurons *do not* change. This asymmetry makes it possible to produce RF expansion in the inactive neurons in response to artificial scotoma conditioning and retinal lesions, without necessarily producing RF expansion in neurons that are activated. The EXIN lateral inhibitory synaptic plasticity

rule directly reduces inhibition to neurons inactivated by peripheral scotomas or lesions, thus making them more likely to respond to some visual stimuli. The EXIN lateral inhibitory synaptic plasticity rule enhances the efficiency of a neural network's representation of perceptual patterns, by recruiting unused and under-used neurons to represent input patterns (Marshall, 1995a; Marshall & Gupta, 1998). In comparison, the LISSOM lateral inhibitory synaptic plasticity rule weakens lateral inhibitory pathways *from inactive neurons to active neurons*, thereby tending to make the active neurons more strongly active and to suppress the inactive neurons more strongly. In the LISSOM model, neurons that are inactive or very weakly active because of a peripheral scotoma or because of weak afferent excitatory pathways can become more responsive to some specific visual feature only *indirectly* via weakening of either afferent excitatory pathways to other active neurons or lateral excitatory pathways to other active neurons.

Thalamocortical afferent arbors can spread over a large cortical area; thalamocortical afferents from the lateral geniculate nucleus can extend over a region up to 3 mm in cat primary visual cortex (Humphrey et al., 1985). Gilbert & Wiesel (1983) observed thalamocortical arbors that extended 2 mm in layer 4 of primary visual cortex of cats. Interlaminar excitatory pathways in the primary visual cortex of cats spread over a few millimeters (Gilbert & Wiesel, 1983). Thus, large overlap in the afferent excitatory inputs to model neurons in the simulations is reasonable.

In animal cortex, lateral pathways spread over large distances. Axonal arbors of GABAergic large basket neurons extend up to 1.5 mm in cortex and terminate on the soma of pyramidal neurons in small patches of cortex (Somogyi et al., 1983; Somogyi & Martin, 1985). Based on the anatomical structure of the axonal arbors of basket neurons, these neurons appear to have the greatest effect on neurons with orientation selectivity similar to their own; however, they may affect neurons with other orientations and other RF positions (Martin, 1988). Long-range inhibitory influences in cortex may also be subserved by the long-range horizontal pathways that extend 2–8 mm in primary visual cortex of cat (Gilbert & Wiesel, 1983, 1989). The long-range horizontal pathways have an excitatory effect at low stimulation strength and have an inhibitory effect at high stimulation strength (Gil & Amitai, 1996; Weliky et al., 1995). Furthermore, the excitatory and

inhibitory effects of the long-range horizontal connections are concentrated on neurons with similar orientation selectivity to that of the source neuron (Weliky et al., 1995). Combined measurement of spiking point-spread using extracellular recording and optical point-spread in cat primary visual cortex showed that the spiking point-spread accounts for only 5% of the optical point-spread; the remainder of the optical point-spread was largely caused by inhibition (Das & Gilbert, 1995a). The optical point-spread had a diameter between 3.2 and 5.2 mm and showed greatest magnitude for cortical neurons with similar stimulus orientation preference to that of the spiking neurons.

These data are consistent with the suggestion that cortical neurons with common inputs, and hence similar properties, should have relatively strong lateral inhibitory pathways between them, for improved stimulus discrimination (e.g., orientation selectivity, disparity selectivity, length selectivity, spatial frequency selectivity, motion direction selectivity) and sparse distributed coding. Thus, lateral inhibitory plasticity may play an active and important role in the development of cortical function. An alternative is to hardwire lateral inhibitory pathway weights as a function of cortical distance. However, the strength of lateral inhibitory pathways in primary visual cortex is not uniform, but depends on topographical organization of RF properties such as orientation selectivity (Weliky et al., 1995).

5.5.7 Neurophysiological realization of the EXIN lateral inhibitory plasticity rule

The EXIN model is a functional model that describes modifications in the effective synaptic weights, including modifications in effective lateral inhibitory weights. *In vivo*, intracortical inhibition is mediated by inhibitory interneurons, which receive excitation from excitatory neurons in addition to afferent input (Douglas & Martin, 1991; Somogyi, 1989).

Neurophysiologically, the EXIN lateral inhibitory synaptic plasticity rule could be realized in a disynaptic circuit containing a lateral excitatory horizontal connection (either short- or long-range) and an inhibitory interneuron, either by modifying the excitatory weights from the excitatory neuron or by changing the inhibitory weight from the inhibitory neuron (Darian-Smith & Gilbert, 1994, 1995; Das & Gilbert, 1995ab; Gilbert et al., 1996;

Hirsch & Gilbert, 1993). The axonal arbors of many inhibitory neurons (e.g., clutch, basket, chandelier) terminate mainly on excitatory neurons (Somogyi, 1989; Somogyi & Martin, 1985), and axonal arbors of most excitatory neurons terminate on other excitatory neurons (McGuire et al., 1991; Somogyi, 1989; Somogyi & Martin, 1985). During development, lateral pathways in the primary visual cortex are initially widespread, and then develop into clustered patches (Katz & Callaway, 1992; Dalva & Katz, 1994). The development of the lateral connectivity depends on external input (Katz & Callaway, 1992). The axonal arbors of inhibitory large basket neurons are also clustered (Somogyi & Martin, 1985) and may develop from initially widespread pathways during development, suggesting that there is synaptic plasticity in these connections. Stimulation of the long-range horizontal excitatory pathways produce excitatory and inhibitory effects on excitatory neurons (Gil & Amitai, 1996; Weliky et al., 1995). Thus, changing the efficacy of lateral inhibitory pathways or the lateral excitatory pathways to inhibitory neurons will change effective inhibition to cortical neurons. Hirsch & Gilbert (1993) have suggested that long-term depression could be a decrease in the strength of excitatory connections or an increase in the strength of inhibitory connections. If the synapses of the long-range excitatory connections to both excitatory and inhibitory neurons change, then to be consistent with the EXIN inhibitory rule, the synapses onto inhibitory neurons should change faster than the synapses onto excitatory neurons, so that the overall effect is a change in lateral inhibition.

Plasticity in inhibitory synapses would be more likely to produce large RF changes than plasticity in excitatory synapses on inhibitory interneurons. The axonal arbors of many inhibitory neurons (e.g., clutch, basket, chandelier) terminate mainly on excitatory neurons (Somogyi, 1989; Somogyi & Martin, 1985), and axonal arbors of most excitatory neurons terminate on other excitatory neurons (McGuire et al., 1991; Somogyi, 1989; Somogyi & Martin, 1985). Thalamocortical stimulation produces a monosynaptic EPSP and a disynaptic IPSP in primary visual cortical neurons, but disynaptic EPSPs are rarely produced (Gil & Amitai, 1996; Ferster, 1989). Neurons receive disynaptic IPSPs because of thalamocortical excitation at all stimulation intensities that evoke early EPSPs (Gil & Amitai, 1996). Weak stimulation of the long-range horizontal excitatory pathways produces excitatory effects on excitatory neurons, but strong stimulation leads to inhibition

of excitatory neurons (Gil & Amitai, 1996; Weliky et al., 1995); this implies that inhibitory interneurons are inactive or very weakly active during weak stimulation of the long-range horizontal excitatory pathways. The above data suggest that the inhibition received by excitatory neurons from inhibitory interneurons tends to be stronger than the lateral excitation received by the excitatory neurons. Thus, changing the efficacy of lateral inhibitory pathways directly (using the EXIN lateral inhibitory synaptic plasticity rule) may affect RF properties more drastically than changing lateral excitatory pathways to inhibitory neurons or lateral excitatory pathways to excitatory neurons (e.g., using the LISSOM lateral excitatory synaptic plasticity rule).

5.5.8 Conclusions

The major conclusions of this chapter are:

1. the subtle distinction between instar and outstar rules produces a dramatic difference in neural behavior and plasticity;

2. the outstar EXIN lateral inhibitory and the instar LISSOM lateral excitatory synaptic plasticity rules are sufficient to produce effects consistent with neurophysiological data on RF changes after artificial scotoma conditioning and retinal lesions in adult animals;

3. the instar LISSOM lateral inhibitory synaptic plasticity rule produces effects contrary to experimental data;

4. the adaptation networks do not produce stable RF changes after scotoma conditioning; and

5. synaptic plasticity in afferent excitatory pathways does not contribute to RF changes after artificial scotoma conditioning and retinal lesions.

Chapter 6

Rearrangement of receptive field topography after intracortical and peripheral stimulation: The role of plasticity in inhibitory pathways

Abstract

Intracortical microstimulation (ICMS) of a single site in the somatosensory cortex of rats and monkeys for 2–6 hours produces a large increase in the number of neurons responsive to the skin region corresponding to the ICMS-site receptive field (RF), with very little effect on the position and size of the ICMS-site RF, and the response evoked at the ICMS site by tactile stimulation (Recanzone et al., 1992b). Large changes in RF topography are observed following several weeks of repetitive stimulation of a restricted skin region in monkeys (Jenkins et al., 1990; Recanzone et al., 1992acde). Repetitive stimulation of a localized skin region in monkeys produced by training the monkeys in a tactile frequency discrimination task improves their performance (Recanzone et al., 1992a). It has been suggested that these changes in RF topography are caused by competitive

learning in excitatory pathways (Grajski & Merzenich, 1990; Jenkins et al., 1990; Recanzone et al., 1992abcde). ICMS almost simultaneously excites excitatory and inhibitory terminals and excitatory and inhibitory cortical neurons within a few microns of the stimulating electrode. Thus, this chapter investigates the implications of the possibility that lateral inhibitory pathways too may undergo synaptic plasticity during ICMS. Lateral inhibitory pathways may also undergo synaptic plasticity in adult animals during peripheral conditioning. The "EXIN" (afferent excitatory and lateral inhibitory) synaptic plasticity rules (Marshall, 1995a) are used to model RF changes after ICMS and peripheral stimulation. The EXIN model produces RF topographical changes similar to those observed experimentally. The possible role of inhibitory synaptic plasticity in cortical reorganization is studied by simulating ICMS with only lateral inhibitory synaptic plasticity. The model also produces an increase in the number of neurons responsive to the skin region represented by the ICMS-site RF. In the EXIN model lateral inhibitory pathway plasticity is sufficient to model RF changes and increase in position discrimination after peripheral stimulation. Several novel and testable predictions are made based on the EXIN model. It is also suggested that lateral inhibitory synaptic plasticity may be a general principle of cortical organization and reorganization.

6.1 Introduction

6.1.1 Cortical plasticity in adult animals

Cortical receptive field (RF) properties undergo substantial change in adult animals following deviations from a normal sensory input distribution. RF size, position, shape, and sensitivity of primary visual cortical neurons are modified by artificial scotoma conditioning (Das & Gilbert, 1995ab; DeAngelis et al., 1995; Pettet & Gilbert, 1992; Volchan & Gilbert, 1994); changes in RF topography occur within minutes to hours following retinal lesions, and these changes continue to occur over a period of months (Chino et al., 1992; Darian-Smith & Gilbert, 1994, 1995). In human behavior, artificial scotoma conditioning for a few seconds modifies position judgments (Kapadia et al., 1994). Primary somatosensory cortical RF topography in adult animals is rearranged by two

to six hours of low intensity intracortical microstimulation (Recanzone et al., 1992b). Peripheral stimulation of a localized skin region in adult owl monkeys increased the cortical representation (the cortical region responsive to stimulation at a particular skin region) of the stimulated skin region and decreased the RF size of the neurons sensitive to the stimulated region (Jenkins et al., 1990). The cortical representation of a skin region can be quantified by the size of the cortical region containing neurons responsive to the skin region. Because cortical layers have uniform neuron density, the area of a cortical region responsive to a skin region will be proportional to the number of neurons responsive to the skin region. Adult owl monkeys performed better in a tactile frequency discrimination task with training over a period of several weeks (Recanzone et al., 1992a). The training produced substantial changes in the cortical representation of the stimulated skin region (Recanzone et al., 1992cde).

In these experiments, some neurons were differentially activated by repetitive peripheral stimulation of the same sensory region or by intracortical microstimulation. These experiments reveal how the cortex adaptively reorganizes in adult animals following a lesion, scotoma, or changes in input stimulation pattern. The neurophysiological data on ICMS and peripheral stimulation place further constraints on plausible common mechanisms for dynamic RF changes following artificial scotoma conditioning, retinal lesions, ICMS, and repetitive peripheral stimulation.

This chapter presents and tests a neural network model, using the "EXIN" synaptic plasticity rules (Marshall, 1995a), which exhibit RF changes similar to those in somatosensory cortex following intracortical microstimulation and peripheral stimulation of restricted skin region. The model also produces an increase in discrimination between stimuli presented at the conditioning site and nearby positions after peripheral conditioning. The EXIN model uses a lateral inhibitory synaptic plasticity rule, which is crucial in producing the results of the various experiments, as well as an afferent excitatory synaptic plasticity rule. Several predictions are made based on the EXIN model.

6.1.2 Receptive field topography changes after intracortical microstimulation

Intracortical microstimulation (ICMS) of a single site in layers 3–4 of primary somatosensory cortex of rats and monkeys produced reorganization of RF topography over a large region of the cortex (Recanzone et al., 1992b). ICMS involves stimulating a single cortical site by delivering current pulses using a microelectrode. ICMS almost simultaneously excites nearly all excitatory and inhibitory terminals and excitatory and inhibitory cortical neurons within a few microns of the stimulating electrode. The strength of excitation of cortical neurons, the afferent excitatory pathways, and the lateral inhibitory pathways is maximum at the ICMS site and decreases with distance from the ICMS site (Recanzone et al., 1992b). In addition, some of the excitatory and inhibitory terminals receive secondary, ortho- and antidromic excitation. However, not all ortho- and antidromically excited excitatory afferents succeed in driving their target neurons above threshold (Recanzone et al., 1992b). Recanzone et al. (1992b) mapped the tactile RFs of cortical neurons surrounding the stimulation site before and after low intensity ICMS.

ICMS of the cortex for 2–6 hours produced a large (2-fold to over 20-fold) increase in the cortical representation of the skin region represented by the ICMS-site RF (Recanzone et al., 1992b). In addition, the RFs of neurons surrounding the stimulation site overlapped the ICMS-site RF to a greater extent following ICMS.

ICMS did not affect the location and the size of the ICMS-site RF or the response evoked at the ICMS site by tactile stimulation. However, RFs of cortical neurons *surrounding* the ICMS site shifted and/or expanded to produce greater overlap with the ICMS site RFs. In some cases, the RF of cortical neurons was "substituted" for part of the ICMS-site RF; i.e., neurons gained sensitivity to part of the ICMS-site RF area and lost sensitivity to parts of their original RF. RF shifts both toward and away from the ICMS-site RF were observed.

6.1.3 Receptive field topography changes after peripheral stimulation

Jenkins et al. (1990) mapped primary somatosensory cortical RF topography in adult owl monkeys before and after several weeks of repetitive stimulation of a restricted skin region. In this experiment, peripheral stimulation increased the cortical representation of the stimulated region, and the RF size of the neurons responsive to the stimulated region was much smaller than normal.

Recanzone et al. (1992acde) determined behavioral and somatosensory cortical RF changes following three to twenty weeks of training adult owl monkeys on a tactile frequency discrimination task. The monkeys' performance on the task progressively improved (Recanzone et al., 1992a). RF measurements after training showed that the cortical representation of the stimulated skin increased significantly, the RF of neurons responsive to the stimulated region expanded, and the overlap in the RFs of neurons sensitive to the stimulated region increased (Recanzone et al., 1992c). Measurement of the temporal response properties revealed that after tactile frequency discrimination training, stimulation of the trained skin region produced larger-amplitude response, the response peaked earlier, and the response was sharper (Recanzone et al., 1992e). The tactile frequency discrimination training also produced emergence of responsiveness to touch in area 3a of the adult owl monkeys (Recanzone et al., 1992d). Furthermore, stimulating a restricted skin region while the monkeys attended to auditory stimuli (passive stimulation) produced similar, though smaller, changes in cortical RF topography.

6.1.4 Previously suggested mechanisms

The above experiments have been taken as evidence for plasticity in excitatory and inhibitory synapses to cortical neurons based on activity-dependent coactivation of presynaptic and postsynaptic elements (Jenkins et al., 1990; Recanzone et al., 1992abcde). Activity dependent synaptic plasticity rules have been used in modeling the reorganization of retinotectal maps (Willshaw & von der Malsburg, 1976), the development of ocular dominance columns in the visual cortex and changes in ocular dominance columns following various deprivation conditioning in young animals (Clothiaux et al., 1991; Miller et al., 1989;

Sirosh & Miikkulainen, 1994b), and the development of orientation maps in visual cortex (Linsker, 1986c; von der Malsburg, 1973; Sirosh et al., 1996). However, the interactions of plasticity in inhibitory and excitatory synapses in producing the effects of ICMS and localized peripheral stimulation has not been previously studied.

Previous explanations for RF changes after ICMS

The following possible mechanisms have been suggested to contribute to RF changes after ICMS.

Changes in RF topography at subcortical sites could occur through feedback pathways from the cortex or via anterograde stimulation of the thalamocortical afferents during ICMS (Recanzone et al., 1992b).

Nearly simultaneous activation of a small cortical region and a subset of pathways terminating in this region, during ICMS and during stimulation of a restricted skin region, could alter cortical RFs based on competitive synaptic plasticity rules (Jenkins et al., 1990; Recanzone et al., 1992abcde).

Synchronous activation of neurons could strengthen interconnections between neighboring neurons that belong to cooperative neuron groups (von der Malsburg & Singer, 1988; Merzenich, 1987; Pearson et al., 1987). Strengthening intrinsic lateral excitatory pathways further coordinates the activation of the neurons and can recruit nearby neurons to create a larger functional group of neurons that respond to a common skin region (Recanzone et al., 1992b). This mechanism alone, however, does not explain why the ICMS-site RF does not change after ICMS. As more and more neurons develop stronger lateral excitatory pathways with ICMS-site neurons, the ICMS-site neurons should become responsive to parts of the RFs of other neurons, and hence the ICMS-site RF should expand.

Previous explanations for RF changes after peripheral stimulation

Grajski and Merzenich (1990) modeled the increase in the number of neurons sensitive to a restricted skin region and the concomitant decrease in the RF size of these neurons observed by Jenkins et al. (1990), after repetitive stimulation of the restricted skin region. The model had afferent excitatory, feedback excitatory, lateral

excitatory, and lateral inhibitory pathways. All these pathways were modified using a single competitive rule based on neuronal activation, passive decay, and normalization (Grajski & Merzenich, 1990). Jenkins et al. (1990) used a rotating disk with grooves which moved across a skin region. To explain the decrement in RF size, it was assumed that the peripheral stimulation in Jenkins et al. (1990) produced several small skin areas in which sensory nerves were synchronously activated and the stimulation of the sensory nerves responsive to different skin areas were not correlated (Recanzone et al., 1992d). Thus, the small skin areas of synchronous inputs compete with one another to according to a Hebbian afferent excitatory rule to produce contraction in the RF of the cortical neurons (Recanzone et al., 1992d). Grajski and Merzenich (1990) repeatedly stimulated a *small* input region. The competitive learning in afferent excitatory pathways led to strengthening of a small number of afferents activated simultaneously by the small peripheral stimulation and to weakening of inactive afferent excitatory pathways; RF contraction was thus produced. Furthermore, during training the stimulation site was more frequently stimulated than the surrounding regions. This caused more neurons to become sensitive to the stimulation site via the competitive learning in afferent excitatory pathways (Grajski & Merzenich, 1990; Recanzone et al., 1992d).

To model the increase in the RF size of neurons responsive to the repetitively stimulated skin region as observed by Recanzone et al. (1992d), it was assumed that the stimulation procedure, which was restricted to a fixed skin region, synchronously activated a large number of afferent pathways from the stimulated skin region. Because the afferent pathways receive synchronous stimulation, they all form stronger synaptic connections with active cortical neurons. Thereby expanding the RFs of the active neurons (Recanzone et al., 1992d).

Grajski and Merzenich (1990) also showed that RF contraction and increase in cortical representation of the stimulated skin region was also produced in their model in the absence of lateral excitatory and feedback excitatory pathways or with plasticity only in excitatory pathways. In their model, lateral excitatory synaptic plasticity was needed to model long-term effects of digit amputation.

After repetitive peripheral stimulation of a restricted skin region, in addition to

an increase in the number of cortical neurons responsive to the stimulated skin region (Jenkins et al., 1990; Recanzone et al., 1992d), the RF of cortical neurons shifted towards the stimulated skin region and the RF size of neurons initially responsive to the peripheral stimulation site increased (Recanzone et al., 1992d) or decreased (Jenkins et al., 1990). Furthermore, RF of neurons surrounding the cortical representation of the stimulated skin region expanded, but the general excitability of these neurons did not change (Recanzone et al., 1992e). Models based on increase in excitability of neurons because of withdrawal of tonic inhibition or increase in excitatory cholinergic input can produce increase in cortical representation of the stimulated skin region and RF expansion. Recanzone et al. (1992d) discounted this possibility on the grounds that decrease in increased excitability alone (1) would not produce RF shifts; (2) would cause changes in the general excitability of affected neurons; and (3) cannot produce RF contraction. These effects are inconsistent with experimental data.

6.1.5 EXIN model of RF changes

The model uses the EXIN (excitatory+inhibitory) synaptic plasticity rules (Marshall, 1995a), to describe the effects of ICMS and peripheral stimulation. A novel feature of the EXIN model is the role of lateral inhibitory synaptic plasticity rule.

The EXIN lateral inhibitory synaptic plasticity to model dynamic RF changes produced by artificial scotoma conditioning and retinal lesions (Kalarickal & Marshall, 1996b, 1997b; Marshall & Kalarickal, 1997). The EXIN rules have been used to model development of disparity selectivity (Marshall, 1990c), motion selectivity and grouping (Marshall, 1990a, 1995b; Schmitt & Marshall, 1995), orientation selectivity (Marshall, 1990d), and length selectivity and end-stopping (Marshall, 1990b). A neural model of stereomatching that allows slanted surfaces and transparently overlaid surfaces to be represented has been proposed based on analysis of the EXIN synaptic plasticity rules (Marshall et al., 1996b). The EXIN rules produce networks with stimulus discrimination, sparse and distributed coding, and exclusive allocation properties (Marshall, 1995a; Marshall & Gupta, 1998).

6.1.6 Significance and contributions of the chapter

The EXIN model of the effects of ICMS and repetitive peripheral stimulation

1. reproduces the neurophysiological data qualitatively (Sections 6.3.1, 6.3.3, and 6.3.4);
2. emphasizes the role of a lateral inhibitory rule in producing RF changes in neurons over a large cortical region (Section 6.3.2);
3. demonstrates substantial rearrangement of RF topography with plasticity only in lateral inhibitory pathways (Section 6.3.4);
4. produces increased cortical representation of a repetitively stimulated peripheral region with either RF expansion or contraction in neurons responsive to the stimulated region (Section 6.3.4);
5. increases discrimination between the peripheral conditioning site and other nearby positions following repetitive stimulation of a fixed conditioning site (section 6.3.5); and
6. suggests novel and testable predictions (Section 6.4.5).

6.2 Methods

This section describes the network architecture and the simulation procedures.

The neural architecture used for computational simulations is a two-layered network with afferent excitatory and lateral inhibitory pathways (Figure 6.1). The two layers may correspond to parts of subcortical and cortical layers or two cortical layers. In the chapter, Layer 2 is referred to as the model cortical layer and Layer 1 as the model thalamic layer. In this neural architecture, the changes in RF topography following ICMS or peripheral stimulation can be produced by changes in the afferent excitatory or lateral inhibitory pathway weights.

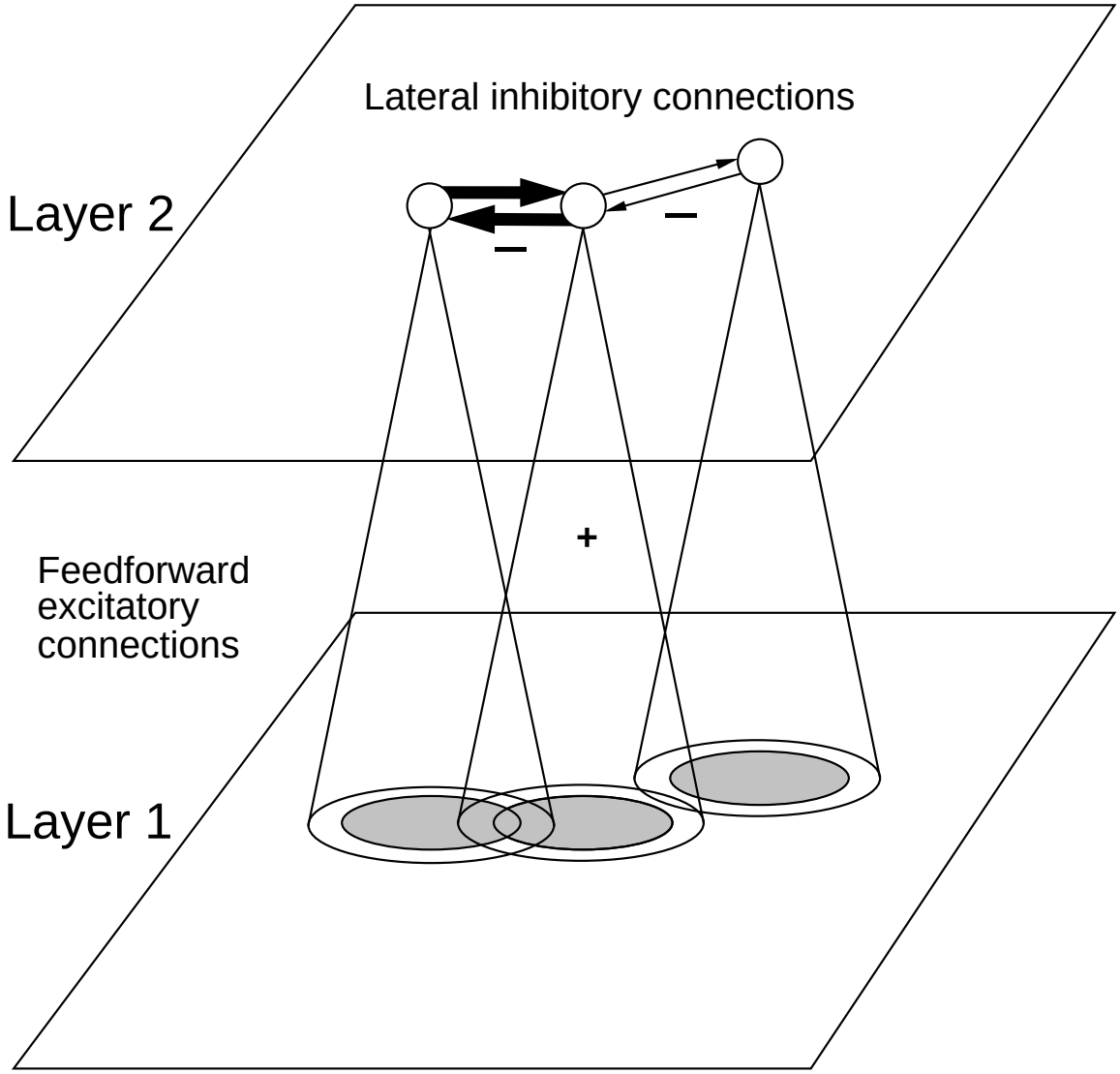

Figure 6.1: **Network architecture of the EXIN model.**
The pathways from Layer 1 to Layer 2 are excitatory (+). The lateral pathways within Layer 2 are inhibitory (−). The unshaded ellipses represent the region of Layer 1 projecting afferent excitatory pathways to Layer 2 neurons. The shaded ellipses represent the RFs of Layer 2 neurons. The weights of lateral inhibitory pathways are approximately proportional to the correlation in the activation of the neurons, which in turn depends on the amount of overlap in the afferent excitatory pathway connectivity patterns of Layer 2 neurons. Weights of lateral inhibitory pathways are indicated by the width of the arrows.

6.2.1 Model architecture

In the computer simulations, Layer 1 and Layer 2 each have a 30×30 grid array of neurons. The indices (i,j) and (k,l) are consistently used to refer to Layer 1 neurons, and (p,q), (r,s), and (u,v) refer to Layer 2 neurons, where $i,j,k,l,p,q,r,s,u,v \in \{-15,\ldots,14\}$. These indices also represent the topographic spatial coordinates of the neurons within their layers.

The weight of the afferent excitatory connection pathway from a Layer 1 neuron (i,j) to a Layer 2 neuron (p,q) at time t is denoted by $Z^{+}_{ij,pq}(t)$. The weight of the lateral inhibitory pathway from Layer 2 neuron (p,q) to Layer 2 neuron (r,s) is represented by $Z^{-}_{pq,rs}(t)$ (Figure 6.1). These pathway weight values may represent the effect of a monosynaptic connection or the total effect of a polysynaptic chain of connections (see Section 6.4.6).

The activation levels (mean spike rate) over time of Layer 1 neuron (i,j) and Layer 2 neuron (p,q) are represented by $x_{ij}(t)$ and $x_{pq}(t)$, respectively.

6.2.2 Model stimulation procedures

Model intracortical microstimulation

ICMS was modeled by

1. directly activating model cortical neurons close to the ICMS site and

2. activating nearby model thalamocortical excitatory and lateral inhibitory pathways.

The direct excitation received by model cortical neuron (p,q) is

$$E^{(\mathrm{d})}_{pq} \;=\; \varphi_0 \exp\left(-\frac{x^2+y^2}{\sigma_1}\right), \tag{6.1}$$

where $x,y \in \{-15,\cdots,14\}$, $p = (((p_0+15)+x) \bmod 30) - 15$, and $q = (((q_0+15)+y) \bmod 30) - 15$. The indices $p_0,q_0,p,q \in \{-15,\cdots,14\}$. The indices p_0,q_0,p, and q and the distances x and y are related such that the model cortical neurons are arranged in a wrapped-around two-dimensional grid. The position (p_0,q_0) is the ICMS site and φ_0 is a positive constant. The parameter φ_0 determines the magnitude of direct excitation to

model cortical neurons and the parameter σ_1 controls the spread of direct excitation to cortical neurons.

Let $y^+_{ij,pq}$ be the presynaptic activation at the terminal of the afferent from model thalamic neuron (i,j) to model cortical neuron (p,q) that is due to ICMS (a combination of direct activation and anti/orthodromic activation of thalamocortical afferents). Then

$$y^+_{ij,pq} = \left(\phi_1 + \varphi_1 \exp\left(-\frac{x^2+y^2}{\sigma_2}\right)\right) \times \exp\left(-\frac{x'^2+y'^2}{\sigma_3}\right), \tag{6.2}$$

where $x, y, x', y' \in \{-15, \cdots, 14\}$, $i = (((i_0 + 15) + x) \bmod 30) - 15$, $j = (((j_0 + 15) + y) \bmod 30) - 15$, $p = (((p_0 + 15) + x') \bmod 30) - 15$, and $q = (((q_0 + 15) + y') \bmod 30) - 15$. The position (p_0, q_0) is the ICMS site, and (i_0, j_0) is the position of the model thalamic neuron projecting the strongest afferent excitatory pathway to model cortical neuron at (p_0, q_0). The parameters φ_1 and σ_2 determine the magnitude and the width, respectively, of the Gaussian distribution of excitation to afferent excitatory terminals as a function of the distance between the thalamocortical pathway from which the excitatory terminals originate and the thalamocortical pathway most responsive to the ICMS-site RF. The parameter ϕ_1 specifies a tonic excitation to afferent excitatory terminals. The second term in Equation 6.2 scales the excitation to the afferent excitatory terminals according a Gaussian function of the distance between the ICMS site and the position of the cortical neuron at which the afferent terminal terminates, and the spread of the Gaussian function is determined by σ_3.

Let $y^-_{pq,rs}$ be the presynaptic activation at the terminal of the lateral inhibitory pathway from model cortical neuron (p,q) to model cortical neuron (r,s) due to ICMS (a combination of direct activation and anti/orthodromic activation of inhibitory pathways and inhibitory neurons). Then

$$y^-_{pq,rs} = \left(\phi_2 + \varphi_2 \exp\left(-\frac{x^2+y^2}{\sigma_4}\right)\right) \times \exp\left(-\frac{x'^2+y'^2}{\sigma_5}\right), \tag{6.3}$$

where $x, y, x', y' \in \{-15, \cdots, 14\}$, $p = (((p_0 + 15) + x) \bmod 30) - 15$, $q = (((q_0 + 15) + y) \bmod 30) - 15$, $r = (((p_0 + 15) + x') \bmod 30) - 15$, and $s = (((q_0 + 15) + y') \bmod 30) - 15$. The position (p_0, q_0) is the ICMS site. The first term in Equation 6.3 is additively composed of tonic excitation ϕ_2 and a Gaussian function of the distance between ICMS site and the cortical position of the neuron from which the lateral inhibitory terminal originates; the

magnitude and the width of the Gaussian function is given by φ_2 and σ_4, respectively. The second term in Equation 6.3 scales the excitation to the lateral inhibitory terminals according a Gaussian function of the distance between the ICMS site and the position of the cortical neuron at which the lateral inhibitory terminal terminates, and the spread of the Gaussian function is determined by σ_5.

Equation 6.1 specifies that the direct excitation of the model cortical neurons due to model ICMS decreases according to a Gaussian function with distance from the ICMS site. Equation 6.2 specifies that the afferent excitatory terminals that branch from thalamocortical pathways close to the stimulation site are more active; in Figure 6.2 the excitatory terminal from model thalamic neuron (i,j) to model cortical neuron (p,q) is more strongly activated than those arising from neuron (k,l), whose thalamocortical pathway is farther from the ICMS site. Furthermore, afferent excitatory terminals branching *from* the same thalamocortical pathway are less excited with increasing distance from the ICMS site. These assumptions of the model ICMS are illustrated in Figure 6.2 by the orientation and the thickness of the crescents attached to the circles representing the model cortical neurons. A similar activation distribution is applied to the lateral inhibitory pathways (Equation 6.3).

This distribution of excitation to the presynaptic excitatory and inhibitory terminals was chosen based on the assumption that ortho- and antidromic excitation of the pathways combine to increase presynaptic excitation of the excitatory and inhibitory synapses. Thus, a presynaptic terminal originating from pathways close to the ICMS site would be more active than a terminal originating from distant pathways. Likewise, and a presynaptic terminal on a model cortical neuron close to the ICMS site would be more active than a terminal on a model cortical neuron far from the ICMS site, even though these two terminals originate from a common pathway. This assumption may be reasonable at weak stimulation strengths; at very high stimulation strengths all the presynaptic terminals converging onto a postsynaptic neuron could be close to saturation because of the strong direct excitation from the stimulation electrode, and thus the antidromic excitation may not have any significant effect at the ICMS site.

The spread of $E_{pq}^{(\mathrm{d})}$ is small. However, $y_{ij,pq}^{+}$ and $y_{pq,rs}^{-}$ spread over large distances. Although the presynaptic excitatory terminal activation spreads over large distances, most

of them are initially ineffective in driving model cortical neurons because of inhibition.

The way that the excitation of excitatory and inhibitory pathways are combined to obtain postsynaptic neuronal activation is described in Section 6.2.5 (Equations 6.8, 6.9, and 6.10). The parameters used in the simulations are presented in Appendix D.

Model peripheral stimulation

In the simulations requiring peripheral stimulation, the model thalamic neurons were directly activated. To apply local peripheral stimulation at location (i, j), model thalamic neurons were assigned activation levels according to a scaled Gaussian kernel K centered at (i, j). The kernel K is defined in Appendix D, Section D.5.

6.2.3 Simulation procedure

The network was initially assigned excitatory and lateral inhibitory weights according to Equations 6.13–6.17 in Section 6.2.5. The initial weights are such that the initial RFs of the model cortical neurons were topographically arranged and of the same size. With such a choice of the initial weights, the RF topography was maintained during a training phase (Appendix D, Section D.2).

The network was trained with whole-field stimuli. The training stimuli were obtained as follows. First, two-dimensional 30×30 images were convolved with a Gaussian kernel, K, with wraparound. The input stimulus at each position in the images could be 0 or 1. The input at each position took value 1 with probability Ξ. After convolution, the resultant image was normalized by the maximum value in the image. The normalization is done so that the peak value in the training inputs was 1. The resultant images from the normalization stage were the inputs to Layer 1.

Model ICMS and peripheral stimulation were applied on the network obtained after a training phase. To simulate ICMS, $E_{pq}^{(\mathrm{d})}$, $y_{ij,pq}^{+}$, and $y_{pq,rs}^{-}$ were held constant. However, the effect of the presynaptic activation of the excitatory and inhibitory terminals on the postsynaptic neuron changes as the excitatory and inhibitory pathways undergo synaptic plasticity. To simulate peripheral stimulation, the model thalamic activations were fixed.

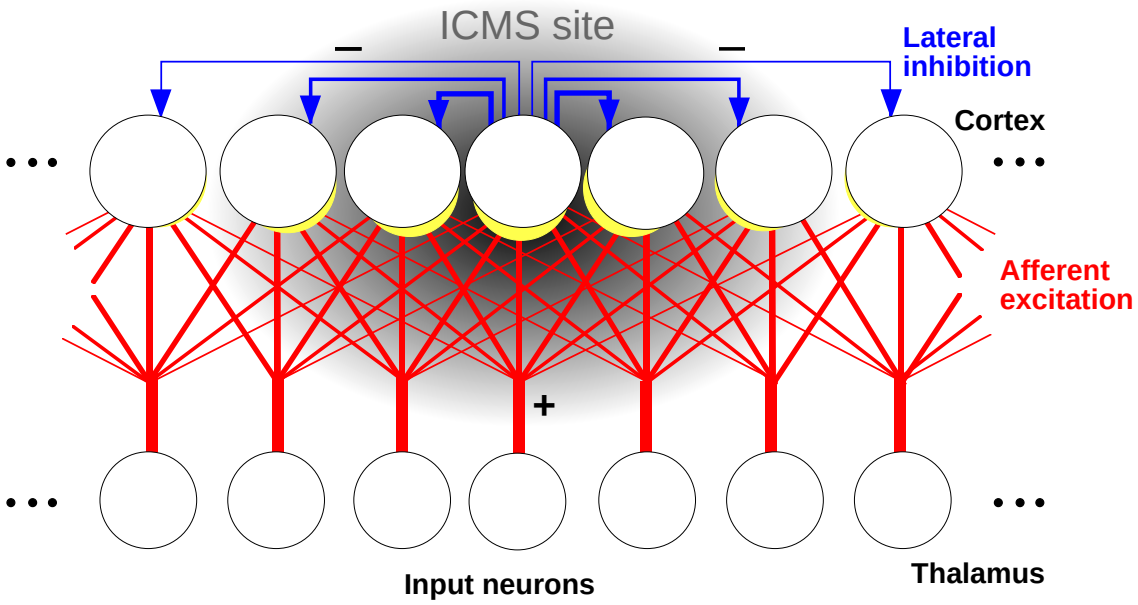

Figure 6.2: **Intracortical microstimulation of model cortical layer.** The figure illustrates the model ICMS. The gradient of shading represents the spread and relative strength of ICMS in the model cortical layer. The model cortical neurons are directly excited (shown by the pluses within the circles representing the cortical neurons). The strength of direct excitation (number of pluses) of the model cortical neurons decreases with distance from the ICMS site. The distribution of excitation of the presynaptic excitatory terminals onto a model cortical neuron is depicted by the orientation and the thickness of the crescents. The presynaptic inhibitory terminals are excited by distribution similar to the afferent excitatory terminals. See text for details and the assumptions about ICMS.

6.2.4 RF measurements

The RF was mapped using single-point stimulation, blurred with the Gaussian kernel K, at all input positions (i, j). The RF of a Layer 2 neuron (p, q) is defined as the collection of positions (i, j) at which the test input causes the activation level x_{pq} to exceed a threshold Θ.

In the ICMS experiments (Recanzone et al., 1992a), cortical neural responses were measured using extracellular recording techniques. Because several neurons may contribute to the extracellular potentials, the RF measured at the ICMS site was the composite RF

of neurons close to the ICMS site. In the simulations, however, the ICMS-site RF was the RF of a single model cortical neuron at the model ICMS site.

In the simulations, the RF center of a model cortical neuron was determined by the centroid of the RF. The centroid was calculated by weighting the RF positions by the response evoked in the neuron. Shifts in the RF of a model cortical neurons was determined by changes in the RF center of the neuron.

6.2.5 The EXIN model

This section describes the EXIN network (Marshall, 1995a). The EXIN network relies on synaptic modifications to explain dynamic RFs. In the following subsections the equations governing synaptic plasticity, the activation equation, and the initial connectivity pattern are presented.

The EXIN model combines an instar afferent excitatory and an outstar lateral inhibitory synaptic plasticity rule. The EXIN (excitatory + inhibitory) synaptic plasticity rules cause the weights to change as a function of the input environment so that different neurons become selective for different input patterns and every input pattern is represented (Marshall, 1995a). During ICMS and peripheral stimulation, a small number of neurons are activated. The EXIN rules change the weights so that the inactive neurons become responsive to input patterns in the new environment, thereby causing changes in RFs.

The EXIN lateral inhibitory synaptic plasticity rule

The lateral inhibitory weights, $Z^{-}_{pq,rs}$, are modified according to the anti-Hebbian outstar rule

$$\frac{d}{dt} Z^{-}_{pq,rs} \;=\; \delta \, \mathcal{G}(x_{pq}) \left(-Z^{-}_{pq,rs} + \mathcal{Q}(x_{rs}) \right) \tag{6.4}$$

(Marshall, 1995a), where $\delta > 0$ is a small learning rate constant, and $\mathcal{G}$ and $\mathcal{Q}$ are half-rectified non-decreasing functions.

Thus, *whenever a neuron is active, its output inhibitory pathways to other active neurons tend to become slightly stronger (i.e., more inhibitory), while its output inhibitory pathways to inactive neurons tend to become slightly weaker.* Layer 2 neuronal activations

remain within $[-C, B]$ according to a shunting equation (Equation 6.8) based on the Hodgkin model (Hodgkin, 1964); this causes the weight values to be bounded as well, because according to Equation 6.4, $Z^-_{pq,rs}(t) \in [0, \mathcal{Q}(B)]$ for $t \geq 0$, if $Z^-_{pq,rs}(0) \in [0, \mathcal{Q}(B)]$ (Grossberg, 1982). The weight change in Equation 6.4 approaches zero as $Z^-_{pq,rs}$ approaches $\mathcal{Q}(x_{rs})$, the weight change is positive when $Z^-_{pq,rs} < \mathcal{Q}(x_{rs})$, and the weight change is negative when $Z^-_{pq,rs} > \mathcal{Q}(x_{rs})$. If $\mathcal{Q}(x_{rs}) = 0$, then the weight change approaches zero as $Z_{pq,rs}$ approaches zero.

In an outstar synaptic plasticity rule (Grossberg, 1972), *pre*synaptic activity "enables" the plasticity at a synapse; when the plasticity is enabled, the weight tends to become proportional to the postsynaptic activity. In an instar synaptic plasticity rule, *post*synaptic activity enables the plasticity; when the plasticity is enabled, the weight tends to become proportional to the presynaptic activity. Thus, to make Equation 6.4 into an instar rule, x_{pq} and x_{rs} would be interchanged.

An effect of the EXIN inhibitory synaptic plasticity rule is that if two neurons are frequently coactivated, then the lateral inhibitory weights between them become strong. If two neurons are only rarely coactivated, then their reciprocal lateral inhibitory weights become weak. Strong lateral inhibition between two neurons tends to make them less likely to be coactivated, causing the two to become selective to different inputs according to the excitatory synaptic plasticity rule (Equation 6.6). Thus, when the network is exposed to normal stimuli, the lateral inhibitory weights and the excitatory afferent weights are modified so that each neuron becomes selective to different inputs and the RFs of all Layer 2 neurons cover the input space (Marshall, 1995a; Marshall & Gupta, 1998). This leads to improved discrimination and sparse coding (Marshall, 1995a).

In Equation 6.4, the term $\mathcal{G}(x_{pq})$ represents the presynaptic activation, and the term $\mathcal{Q}(x_{rs})$ represents the postsynaptic activation. During ICMS the presynaptic terminals are activated directly by ICMS, even though the presynaptic neurons may be inactive. In this case, $\mathcal{G}(x_{pq})$ is replaced by presynaptic activation caused by a combination of direct excitation by ICMS and activation of the presynaptic neuron, i.e.,

$$\frac{d}{dt} Z^-_{pq,rs} \;=\; \delta \;\left(\mathcal{G}(x_{pq}) + y^-_{pq,rs}\right)\left(-Z^-_{pq,rs} + \mathcal{Q}(x_{rs})\right). \tag{6.5}$$

The EXIN afferent excitatory synaptic plasticity rule

The afferent excitatory weight changes are governed by a variant of a Hebbian synaptic plasticity rule. The rule can be expressed (Grossberg, 1982; Marshall, 1995a) as

$$\frac{d}{dt}Z^{+}_{ij,pq} \;=\; \epsilon\, \mathcal{F}(x_{pq}) \left(-Z^{+}_{ij,pq} + \mathcal{H}(x_{ij})\right), \tag{6.6}$$

where $\epsilon > 0$ is a small learning rate constant, and $\mathcal{F}$ and $\mathcal{H}$ are half-rectified non-decreasing functions.

Thus, *whenever a neuron is active, its afferent excitatory pathways from active neurons become slightly stronger, while its afferent excitatory pathways from inactive neurons become slightly weaker.* Layer 2 neuronal activations remain within $[-C, B]$ according to a shunting equation (Equation 6.8), and Layer 1 neuronal activations are within $[0, 1]$ in all the simulations (Appendix D). This causes the afferent weight values to be bounded because according to Equation 6.6, $Z^{+}_{ij,pq}(t) \in [0, \mathcal{H}(1)]$ for $t \geq 0$, if $Z^{+}_{ij,pq}(0) \in [0, \mathcal{H}(1)]$.

The EXIN excitatory synaptic plasticity rule is a competitive learning rule. Because of the inhibition, it causes each modeled cortical neuron to become selective for a specific pattern of input activations (Grossberg, 1982; Marshall, 1995a).

In Equation 6.6, the term $\mathcal{H}(x_{ij})$ represents the amount of presynaptic activation reaching the synapse, and the term $\mathcal{F}(x_{pq})$ represents the amount of postsynaptic activation at the synapse. During ICMS the presynaptic afferent excitatory terminals are activated directly by ICMS, even though the presynaptic model thalamic neuron is inactive. In this case, $\mathcal{H}(x_{pq})$ is replaced by the presynaptic activation, $y^{+}_{ij,pq}$ (see Equation 6.2), i.e.,

$$\frac{d}{dt}Z^{+}_{ij,pq} \;=\; \epsilon\, \mathcal{F}(x_{pq}) \left(-Z^{+}_{ij,pq} + y^{+}_{ij,pq}\right). \tag{6.7}$$

The activation equation

The activation level x_{pq} of each Layer 2 neuron is governed by a shunting equation (Grossberg, 1972) based on the Hodgkin model (Hodgkin, 1964):

$$\frac{d}{dt}x_{pq} \;=\; -Ax_{pq} \;+\; \beta(B - x_{pq})E_{pq} \;-\; \gamma(C + x_{pq})I_{pq}, \tag{6.8}$$

where A, B, C, β, and γ are positive constants, and E_{pq} and I_{pq} represent respectively the neuron's total afferent excitatory and lateral inhibitory input signals. The first term in Equation 6.8 is the passive decay term which decreases activation of model neurons after removal of excitation. The excitatory and inhibitory contributions to the activation of model cortical neurons are given by the second and the third terms, respectively. The factors $(B - x_{pq})$ and $(C + x_{pq})$ "shunts" the input excitation E_{pq} and the input inhibition I_{pq}, respectively, i.e., the contribution of input excitation and of input inhibition goes to zero as activation approaches B and C, respectively. Because Equation 6.8 is a shunting equation, if $x_{pq}(0) \in [-C, B]$ then $x_{pq}(t) \in [-C, B]$ for all time $t \geq 0$ (Cohen & Grossberg, 1983). Thus, activation levels are driven to remain within a bounded range, between $-C$ and B. Parameters β and γ, respectively, control the effectiveness of excitation and inhibition received by a model cortical neuron.

Excitation and inhibition during ICMS. During ICMS the total input excitation E_{pq} was modeled as

$$E_{pq} = \left(\sum_{ij} y^{+}_{ij,pq} Z^{+}_{ij,pq} \right)^2 + E^{(\mathrm{d})}_{pq}, \tag{6.9}$$

and the total input inhibition I_{pq} was given by

$$I_{pq} = \sum_{rs} \left([x_{rs}] + y^{-}_{rs,pq} \right) Z^{-}_{rs,pq}, \tag{6.10}$$

where $[a] \equiv \max(a, 0)$. The total input excitation received by model cortical neurons was a combination of the excitation received because of stimulation of excitatory synapses, given by the first term in Equation 6.9, and direct excitation because of ICMS, the second term in Equation 6.9. The input excitation via the excitatory synapses was modeled by weighting the presynaptic stimulation, $y^{+}_{ij,pq}$, by the excitatory synaptic weight, $Z^{+}_{ij,pq}$. In the model, cortical neurons received inhibition because of stimulation of lateral inhibitory synapses. The total inhibition to a model cortical neuron was obtained by the sum of the product of presynaptic stimulation and lateral inhibitory synaptic weight over all the lateral inhibitory terminals onto a cortical neuron. The presynaptic stimulation of lateral inhibitory pathways during ICMS was obtained by adding the activation of lateral inhibitory source neurons and excitation because of ICMS.

Excitation and inhibition during peripheral stimulation and RF measurement. During peripheral conditioning and RF measurement, the total input excitation E_{pq} was

$$E_{pq} = \left(\sum_{ij} x_{ij} Z^{+}_{ij,pq} \right)^2 , \tag{6.11}$$

and the total input inhibition I_{pq} was given by

$$I_{pq} = \sum_{rs} [x_{rs}] Z^{-}_{rs,pq}, \tag{6.12}$$

where $[a] \equiv \max(a, 0)$. During peripheral stimulation, the model cortical neurons received excitation and inhibition via excitatory and inhibitory synapses, respectively. Thus, input excitation and input inhibition was obtained by some function of the sum of the product of presynaptic excitation and the synaptic weight.

Stability of the shunting equation: Cohen-Grossberg theorem. The shunting equation (Equation 6.8) with $Z^{-}_{rs,pq} = Z^{-}_{pq,rs} \geq 0$, belongs to a class of competitive dynamical systems that are absolutely stable; i.e., the system has fixed points (stable equilibrium states) for any choice of parameters (Cohen & Grossberg, 1983). The neuronal activations in such a system are guaranteed to reach stable equilibrium values for all synaptic weight values, with the restriction that $Z^{-}_{rs,pq} = Z^{-}_{pq,rs} \geq 0$ for all pairs of neurons.

However, it is not known whether the shunting equation remains absolutely stable even when $Z^{-}_{rs,pq} \neq Z^{-}_{pq,rs} \geq 0$ for some pairs of neurons. The symmetry of reciprocal pairs of lateral inhibitory weights is not guaranteed by the EXIN lateral inhibitory synaptic plasticity rule. During normal stimulation, the lateral inhibitory weights are approximately symmetric (Marshall, 1995a). They become asymmetric between active and inactive neurons during ICMS and repetitive local peripheral conditioning. Nevertheless, simulations have empirically shown the stability of the activation equation in the EXIN network (Appendix D, Section D.1).

The initial weights

A patch of neurons in the primary somatosensory cortex, arranged in a 30×30 grid of spatial positions, was simulated. The position of each neuron's RF corresponded to the neuron's position in the grid. Adjacent RFs initially had more than 50% spatial overlap.

In the EXIN simulations, the initial afferent excitatory weight from model thalamic neuron (i,j) to model cortical neuron (p,q) was given by the truncated Gaussian function

$$Z^{+}_{ij,pq} \;=\; \left[\exp\left(\frac{-(x^2+y^2)}{\sigma^2_{\mathbf{ff}}}\right), \Gamma_{\mathbf{ff}}\right], \tag{6.13}$$

where

$$[a,b] \equiv \begin{cases} a & \text{if } a > b, \\ 0 & \text{otherwise,} \end{cases} \tag{6.14}$$

$x, y \in \{-15, \cdots, 14\}$, $p = (((i+15)+x) \bmod 30) - 15$, $q = (((j+15)+y) \bmod 30) - 15$, and $\sigma_{\mathbf{ff}}$ and $\Gamma_{\mathbf{ff}}$ are positive constants. The indices $i, j, p,$ and q are in the set $\{-15, \cdots, 14\}$. The relationship between the indices $i, j, p,$ and q and the distances x and y is such that the model cortical and thalamic neurons are arranged in a two-dimensional grid which was wrapped around.

The initial lateral inhibitory weights between model cortical neurons (p,q) and (r,s), where $p \neq r$ or $q \neq s$, are set as follows. Let

$$X_{pq,rs} \;=\; \sum_{ij} \min(Z^{+}_{ij,pq}, Z^{+}_{ij,rs}) \tag{6.15}$$

and

$$W^{-}_{pq,rs} = W^{-}_{rs,pq} = [X_{pq,rs}, \Gamma_{\mathbf{i}}], \tag{6.16}$$

where $\Gamma_{\mathbf{i}}$ is a constant. Then

$$Z^{-}_{pq,rs} \;=\; Z^{-}_{rs,pq} \;=\; \frac{\mu W^{-}_{ps,rs}}{\max\limits_{ab,cd \,\in\, \text{layer 2}} W^{-}_{ab,cd}}. \tag{6.17}$$

Neurons do not directly inhibit themselves in the EXIN network; that is, $Z^{-}_{pq,pq}$ is zero and $\frac{d}{dt} Z^{-}_{pq,pq} = 0$. Equation 6.17 assigns inhibitory weights between two distinct Layer 2 neurons in proportion to the amount of overlap in the RFs of the two neurons. Equation 6.15 computes a measure of the amount of overlap in the afferent excitatory pathways to two model cortical neurons. The measure is the sum of the lesser of the afferent excitatory weights to the two model cortical neurons from common input neurons. According to Equation 6.16, the measure of the amount of overlap in afferent excitatory pathways is set to zero if it is below a threshold, $\Gamma_{\mathbf{i}}$. Finally, the initial lateral inhibitory

synaptic weights are set after normalizing $W^{-}_{pq,rs}$ according to Equation 6.17 such that the maximum lateral inhibitory synaptic weight is 1.

The initial weight values of the connections were chosen to speed the convergence of weight values during the simulated training phase and to preserve RF topography, thereby avoiding RF shifts and RF size changes caused by RF scatter that would have been present if the initial weights were chosen randomly. The network produced after the training phase was used for simulated ICMS and peripheral conditioning.

Lateral excitatory pathways were omitted in this model. This is a simplification based on the assumption that the net effect of the lateral excitatory and inhibitory pathways on excitatory neurons is inhibitory. Partial support for setting $Z^{+}_{pq,rs}$ to zero comes from the lack of disynaptic excitatory postsynaptic potentials (EPSPs) caused by stimulation of thalamocortical afferents during intracellular recordings in simple neurons of the cat visual cortex (Ferster, 1989), and in layer 5 neurons of adult mice (Gil & Amitai, 1996), even though lateral excitatory pathways exist in the cortex. Stimulation of thalamocortical afferents and lateral excitatory pathways produce monosynaptic EPSPs in cortical neurons (Gil & Amitai, 1996; Hirsch & Gilbert, 1993). Therefore, if lateral excitatory pathways in the cortex were strong, then stimulation of thalamocortical pathways should produce strong disynaptic EPSPs via the lateral excitatory pathways. Weliky et al. (1995) and Gil and Amitai (1996) showed that strong stimulation of the long-range horizontal pathways exerts overall inhibition on pyramidal neurons. Weak stimulation of lateral excitatory pathways produces predominant excitation in cortical neurons presumably because the inhibitory neurons, which have high activation thresholds, are not activated by weak stimulation (Weliky et al., 1995). Sections 6.4.3 and 6.4.6 describe the possible role of lateral excitatory pathways and feedback excitatory pathways in producing RF changes after ICMS and repetitive local peripheral conditioning.

6.3 Simulation results

In all the simulations except the one in Section 6.3.3, the network with topographically arranged RFs after a training phase was used. In Section 6.3.3, a network

with RF scatter was used. Section 6.3.1 presents the results of modeling ICMS on a network with topographically arranged RFs. The role of some of the parameters in the model are explored in Section 6.3.2, and the effects of RF scatter are demonstrated in Section 6.3.3. Section 6.3.4 shows the effects of peripheral stimulation in the model. The parameters used in the simulations are in Appendix D.

6.3.1 The effects of ICMS on the model

In this simulation, the network was conditioned using all the inputs to the neurons during ICMS – direct excitation to the postsynaptic neurons, and excitation of excitatory and inhibitory presynaptic terminals, as explained in Section 6.2.2. Both afferent excitatory synaptic plasticity (Equation 6.7) and lateral inhibitory synaptic plasticity (Equation 6.5) were simulated.

The spatial distributions of presynaptic excitation and inhibition are shown in Figure 6.3. The ICMS site was at the center of the squares representing the model cortical surface. The activation levels of model cortical layer neurons are shown in Figures 6.3c and 6.5.

Increase in the cortical representation of the ICMS-site RF

Recanzone et al. (1992b) observed a large increase in the cortical area representing the skin region corresponding to the pre-ICMS ICMS-site RF after ICMS. Before ICMS only the ICMS-site RF had $\geq 85\%$ RF overlap with the ICMS-site RF. After ICMS the cortical region containing neurons with $\geq 85\%$ RF overlap with the pre-ICMS ICMS-site RF increased in area.

Qualitatively similar results were obtained in the simulation. Figure 6.4 shows the number of model cortical neurons whose RF overlaps the pre-ICMS ICMS-site RF, before and after ICMS. After ICMS, there was a large increase in the number of neurons whose RFs have $> 0 - 25\%$ and $> 75 - 100\%$ overlap with the ICMS-site RF. In the simulation, the neurons whose RFs have $> 75 - 100\%$ overlap with the pre-ICMS ICMS-site RF were very close to the ICMS site, and these neurons were active during ICMS (Figures 6.5 and 6.11). The neurons whose RFs have $> 0 - 25\%$ overlap with the pre-ICMS ICMS-site RF were

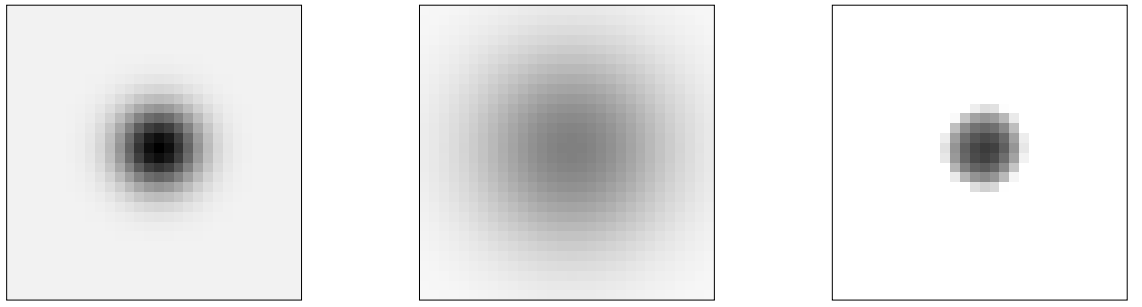

Figure 6.3: **Spatial distribution of presynaptic excitation and postsynaptic activation.**
(a) The distribution of presynaptic excitation of afferent excitatory pathways to the ICMS-site neuron $(0, 0)$. Other model cortical neurons receive a fraction of the presynaptic afferent excitation received by the ICMS-site neuron, scaled according to distance. The scaling factor is a Gaussian centered at the ICMS site (see Section 6.2.2). (b) The distribution of presynaptic excitation of lateral inhibitory pathways to the ICMS-site neuron $(0, 0)$. Other model cortical neurons receive a fraction of the presynaptic excitation of lateral inhibitory pathways received by the ICMS-site neuron. The scaling factor is a Gaussian centered at the ICMS site. (c) Initial postsynaptic activation of model cortical neurons in response to ICMS.

farther from the ICMS site and were inactive during ICMS (Figures 6.5 and 6.11).

RF expansion, contraction, and substitution

Figure 6.6 shows examples of neurons that exhibited RF expansion, RF contraction, and RF substitution.

The neuron $(0, -7)$ in Figure 6.6 was inactive during the early stages of ICMS (Figure 6.5). As a consequence of the EXIN lateral inhibitory synaptic plasticity, active lateral inhibitory pathways to neuron $(0, -7)$ weakened (Figure 6.7), and the afferent excitatory pathways to neuron $(0, -7)$ did not change much (Figure 6.7). Thus, its RF size increased to overlap more with the pre-ICMS ICMS-site RF (see Section 6.4.1).

The neuron $(0, -4)$ in Figure 6.6 was weakly active during ICMS (Figure 6.5) and was close to inactive neurons. The distribution of the presynaptic excitation received by

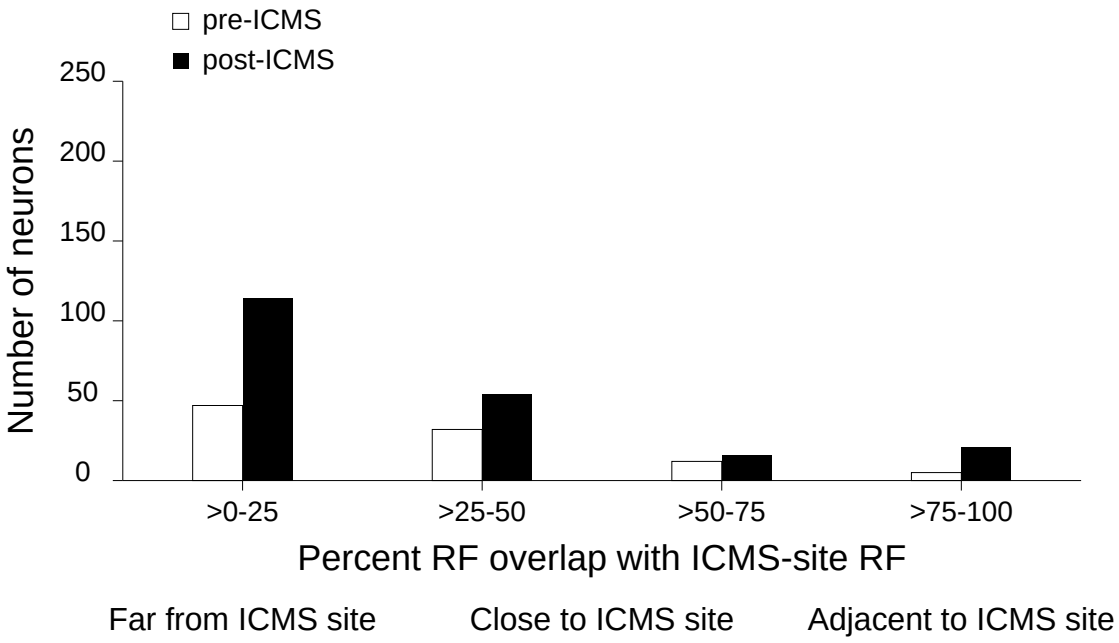

Figure 6.4: **Changes in RF overlap with the ICMS-site RF.**
The figure shows the number of the model cortical neurons with RF overlapping with the pre-ICMS ICMS-site RF before and after ICMS. The percentage of overlap is computed with respect to the pre-ICMS RF size of the ICMS-site neuron.

neuron $(0, -4)$ shows that the neuron receives stronger presynaptic excitation from afferents selective to positions close to the ICMS-site RF center. The EXIN afferent excitatory synaptic plasticity rule strengthened the strongly excited synapses with afferents selective to positions close to the ICMS-site RF center and weakened the weakly excited synapses (Figure 6.7). This resulted in a shift of the neuron's RF position toward the pre-ICMS ICMS-site RF and an increase in RF overlap with the pre-ICMS ICMS-site RF. The neuron weakened its previously strong synapses, and this contributed to a decrease in its RF size. Thus, a part of the pre-ICMS ICMS-site RF has been substituted for neuron $(0, -4)$'s former RF.

The change in RF of neuron $(0, -1)$ in Figure 6.6 illustrates another example of RF substitution. This neuron, being very close to the ICMS site, was active during ICMS (Figure 6.5). Neuron $(0, -1)$ received presynaptic stimulation similar to that received by the

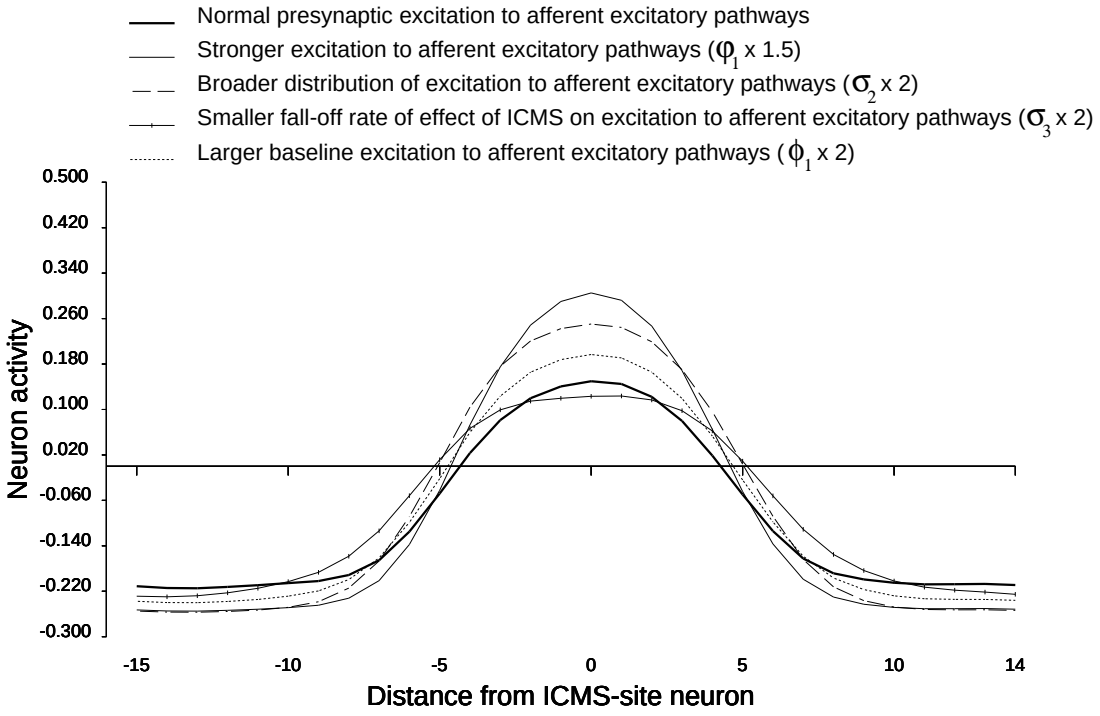

Figure 6.5: **Changes in activation level of neurons caused by changes in the distribution of presynaptic excitation to afferent excitatory pathways.**
The activation levels of a cross-section of model cortical layer neurons through the ICMS site, neurons $(0,-15)$–$(0,14)$, in the initial stage of ICMS (when ICMS was first applied and synaptic weights were not yet changed) as parameter values in Equation 2 are varied. The parameters values in Equations 1, 2, and 3 were the same as those used in the simulations presented in Section 6.3.1 (see Appendix D, Section D.4.1). The normal presynaptic excitation to afferent excitatory pathways was produced using the values of parameters in Equation 2 that were used in the ICMS simulation in Section 6.3.1. For stronger excitation to afferent excitatory pathways the value of φ_1 in Section 6.3.1 was multiplied by 1.5; for broader distribution of excitation to afferent excitatory pathways the value of σ_2 in Section 6.3.1 was multiplied by 2; for smaller fall-off rate of the effect of ICMS on excitation to afferent excitatory pathways the value of σ_3 in Section 6.3.1 was multiplied by 2; and for larger baseline excitation to afferent excitatory pathways the value of ϕ_1 in Section 6.3.1 was multiplied by 2.

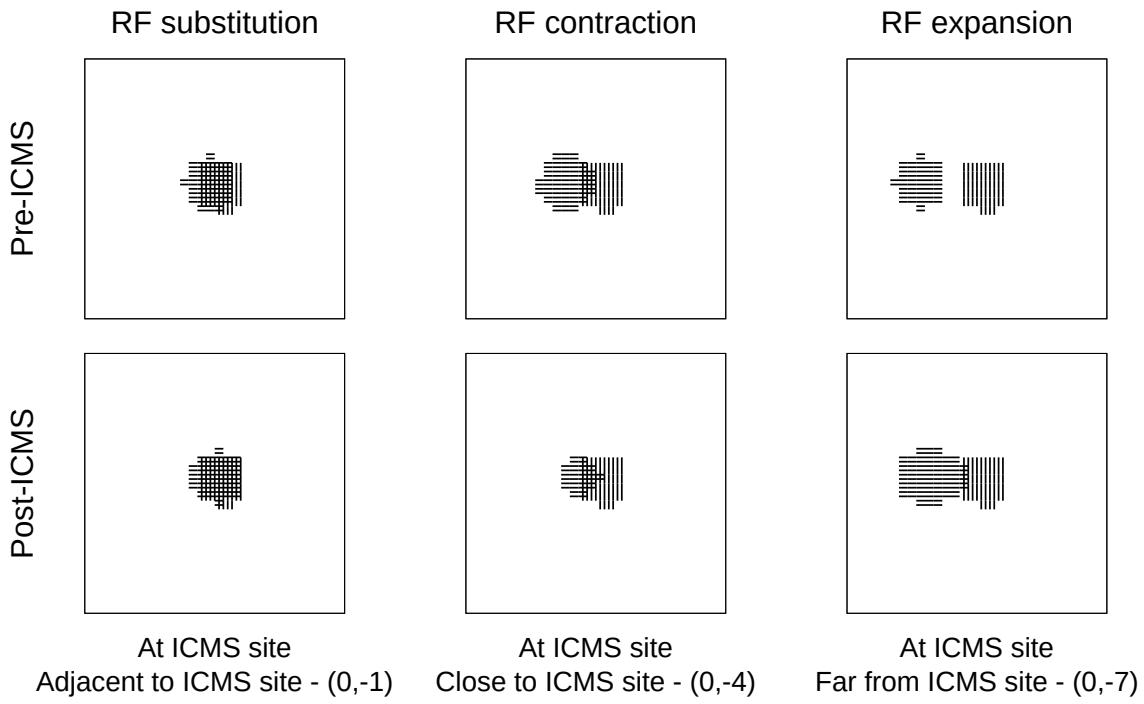

Figure 6.6: **Pre- and post-ICMS RFs.**
Examples of RF substitution, RF contraction, and RF expansion are shown. The RF drawn with vertical lines represents the pre-ICMS ICMS-site RF, and the RFs drawn with horizontal lines represent another RF at other model cortical sites.

ICMS-site neuron $(0,0)$. Thus, according to the EXIN afferent excitatory synaptic plasticity rule, neuron $(0,-1)$ developed strong synapses with afferents selective to the ICMS-site RF center and weakened its synapses with afferents selective to positions away from the ICMS-site RF center (Figure 6.7). Thus, neurons $(0,-1)$ and $(0,0)$ have very similar distributions of synaptic strength with the afferent terminals (Figure 6.7). This caused the RF of neuron $(0,-1)$ to shift toward the pre-ICMS ICMS-site RF. The direct stimulation of lateral inhibitory pathways during ICMS caused the neurons closest to the ICMS-site to be weakly active. Thus, neuron $(0,-1)$ did not develop strong lateral inhibitory pathways with neuron $(0,0)$ (Figure 6.7). Thus, the RF size of neuron $(0,0)$ did not contract (Figure 6.8), and the RF of neuron $(0,-1)$ became almost identical to the pre-ICMS RF of neuron $(0,0)$.

In this simulation, the presynaptic activation levels of the afferents were chosen

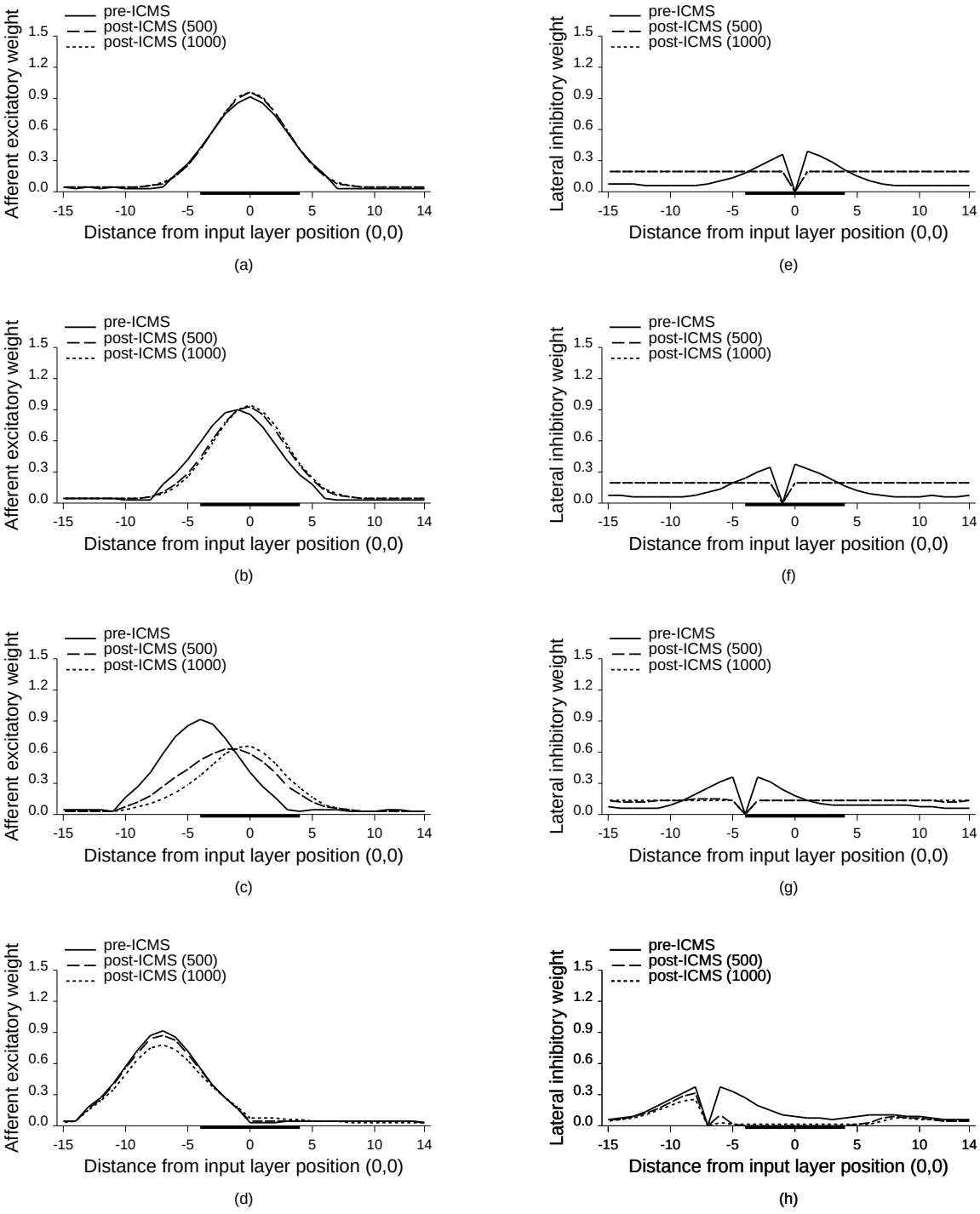

Figure 6.7: Legend on next page.

Figure 6.7: **Pre- and post-ICMS afferent excitatory and lateral inhibitory synaptic weights.**
Figure on previous page. The figure shows weights of afferent excitatory pathways (left column) and lateral inhibitory pathways (right column) to different model cortical neurons – neuron $(0, 0)$ in (a) and (e), neuron $(0, -1)$ in (b) and (f), neuron $(0, -4)$ in (c) and (g), and neuron $(0, -7)$ in (d) and (h) – before ICMS, after 500 ICMS presentations, and after 1000 ICMS presentations. In the EXIN network model, cortical neurons did not inhibit themselves; i.e., the lateral inhibitory pathway from a neuron to itself was zero. Thus, the distribution of the weights of lateral inhibitory pathways to a neuron has a dip. The thick line segment on the abscissa represents the neurons that were active during the initial stage of ICMS.

so that the synaptic strength of the afferents to the ICMS-site neuron remained almost unchanged (Figure 6.7). In Section 6.3.2 the effects of varying the presynaptic excitation to afferent excitatory pathways are presented.

In the model, the RFs of the model cortical neurons were topographically arranged, and all the neurons had almost identical RF sizes. In the cortex, however, the RF positions are not strictly topographically arranged at a finer level of detail, and RF sizes show large variations even among neighboring cortical neurons (Favorov & Kelly, 1996; Hubel & Wiesel, 1962; Recanzone et al., 1992b). In the model, if the neuron close to the ICMS site had a RF larger than the pre-ICMS ICMS-site RF size, it will receive stronger presynaptic excitation from afferents selective to positions close to the ICMS-site RF center than from afferents selective to positions far from the ICMS-site RF center. In this case, the RF size of the neuron will decrease to become almost identical to the pre-ICMS ICMS-site RF. If a neuron close to the ICMS site had a RF smaller than the pre-ICMS ICMS-site RF size, it will form strong synapses with afferents selective to positions close to the ICMS-site RF center, and its RF size could increase because the lateral inhibition between the neurons close to the ICMS site is weakened. In Section 6.3.3, ICMS is simulated in a network with RF scatter.

Changes in RF size

Figure 6.8a shows the RF size before and after ICMS as a function of the position of the initial RF center. It is clear from the figure that after ICMS

1. the ICMS-site RF size increased by a very small amount;

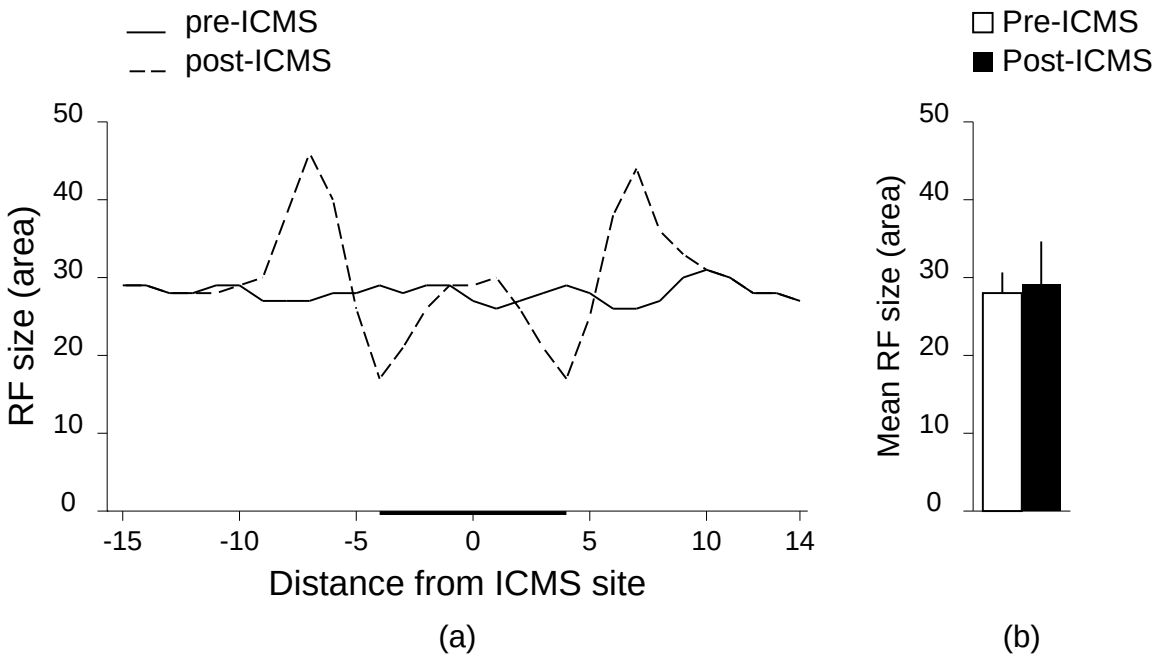

Figure 6.8: **Changes in RF size.**
(a) The figure shows the RF area of neurons in a cross-section of model cortical layer passing through the ICMS site before and after ICMS. The thick line segment on the abscissa represents the neurons active during the initial phase of ICMS. (b) The figure shows the mean RF area of model neurons before (white bar) and after (black bar) ICMS. The vertical line on the bars represent the standard deviation.

2. the RF size of neurons closest to the ICMS site underwent very little change;

3. the RF size of the neurons 2–4 units of distance away from the ICMS site showed a decrease in their RF size. These neurons were active during ICMS; and

4. neurons 6–10 units of distance away from the ICMS site showed an increase in their RF size. These neurons were inactive during ICMS.

Thus, in the model, changes in RF size varied systematically with distance from the ICMS site.

Recanzone et al. (1992b) reported that after ICMS the mean RF size showed a slight increase. Figure 6.8b shows the pre- and post-ICMS mean RF sizes of the model neurons.

Changes in neuronal responsiveness

Figure 6.9a shows the RF profile of the ICMS-site neuron, and Figure 6.9b shows the maximal responsiveness of a one-dimensional cross-section of model cortical neurons through the ICMS site, before and after ICMS. In the simulation, responsiveness of the neuron at the ICMS site showed very little change. This is consistent with results of Recanzone et al. (1992b). In addition, maximal responsiveness of distal neurons increased. The distal neurons were inactive for most of the ICMS duration and therefore, the lateral inhibitory pathways to these neurons weakened (especially the strongly excited lateral inhibitory pathways from neurons close to the ICMS site), and the afferent excitatory pathways to these neurons changed very little (e.g., neuron $(0, -7)$ in Figure 6.7). In contrast, maximal responsiveness of neurons surrounding the ICMS site decreased. Because the strength of excitation to the presynaptic afferent excitatory terminals decreases as distance from the ICMS site increases, neurons close to the ICMS site, which were active during ICMS, have weaker afferent excitatory pathways after ICMS (e.g., neuron $(0, -4)$ in Figure 6.7).

Changes in RF position

In the ICMS experiment, the RF of neurons close to the ICMS site shifted after ICMS toward the ICMS-site RF. However at cortical sites away from the ICMS site, some RFs shifted toward the ICMS-site RF and others shifted away from the ICMS-site RF at random (Recanzone et al., 1992b).

In the model with topographically arranged RFs, the RF of most neurons shifted toward the ICMS-site RF (Figure 6.10). Small RF shifts away from the ICMS-site RF in the RF of model neurons were seen in some neurons far from the ICMS site (Figure 6.30).

Spatial distribution of the affected cortical region

In the ICMS experiment, the cortical region affected by ICMS extended asymmetrically around the ICMS site for several hundred microns. In addition, there were sharp discontinuities at some locations between a region in which the RF of neurons

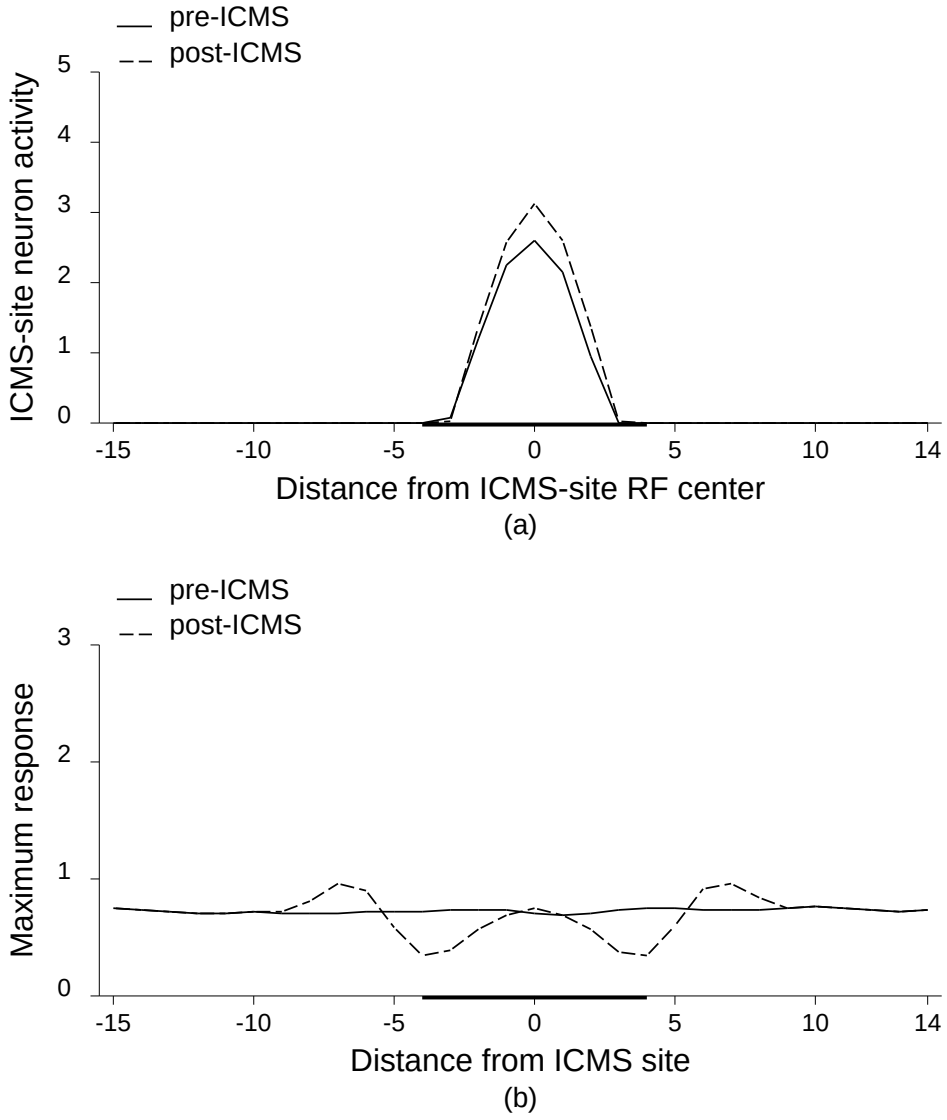

Figure 6.9: **Changes in neuronal responsiveness after ICMS.**
(a) One-dimensional RF profile of ICMS-site neuron. The RF profile was obtained by adding the neuron's response to input at positions along the y axis. (b) The maximal responsiveness of neurons in a cross-section of the model cortical layer passing through the ICMS site, neurons $(0, -15)$–$(0, 14)$, before and after ICMS. The thick line segment on the abscissa represents the neurons active during the initial stage of ICMS.

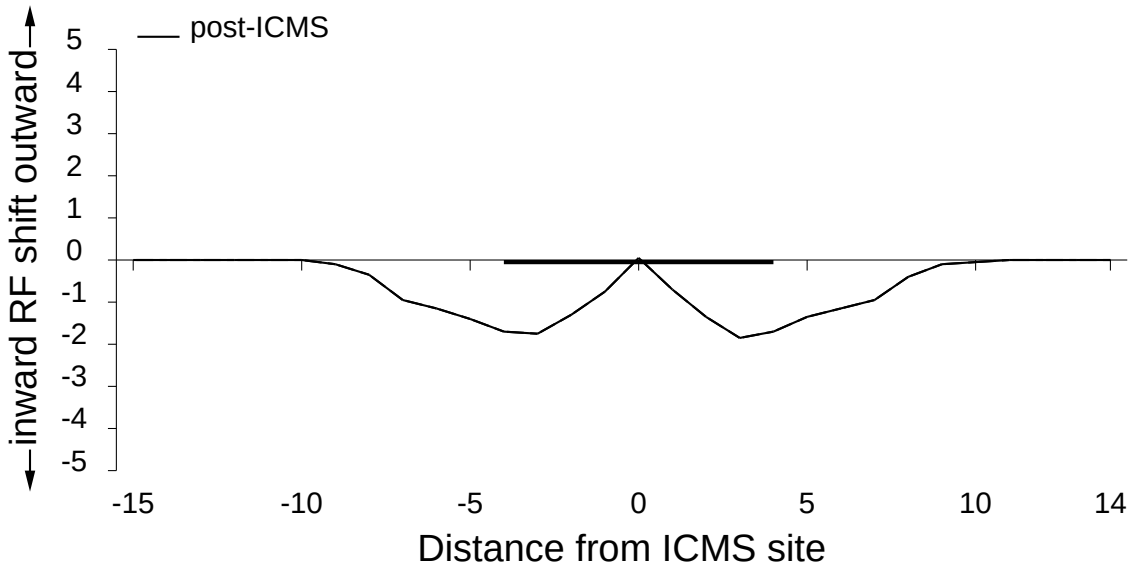

Figure 6.10: **RF shift after ICMS.**
The figure shows the RF shift of neurons in a cross-section of the model cortical layer passing through the ICMS site after ICMS, neurons $(0, -15)$–$(0, 14)$. The thick line segment on the abscissa represents the neurons active during the initial phase of ICMS.

overlapped with the pre-ICMS ICMS-site RF and an adjacent region in which the RF of neurons did not overlap with the pre-ICMS ICMS-site RF (Recanzone et al., 1992b).

A lack of systematic variation in the amount of overlap of the RF of neurons surrounding the ICMS site and the ICMS-site RF may have occurred because the pre- and post-stimulation recordings were not necessarily from exactly the same neurons (Recanzone et al., 1992b). However, the neurons recorded at the same site before and after ICMS were within 10–20 microns from each other (Recanzone et al., 1992b). The observed asymmetries in the distribution of RF changes over the cortical space may be due to variations in the anatomical spread of arborizations of the thalamocortical afferents and/or the cortical axons and dendrites (Recanzone et al., 1992b).

Figure 6.11 shows the amount of RF shift and the amount of overlap of the RF of model cortical neurons with the pre-ICMS ICMS-site RF after ICMS. In the simulation, RF changes extended symmetrically over a large distance, and there were no sharp discontinuities between regions containing neurons whose RF overlaps with the

pre-ICMS ICMS-site RF and adjacent regions with neurons whose RF does not overlap with the pre-ICMS ICMS-site RF.

In the simulation, all model cortical neurons had similar afferent and lateral connectivity profiles. In addition, the lateral inhibitory pathways were almost symmetrical. The uniformity in the connectivity patterns of the neurons is responsible for the systematic RF changes observed in this simulation. A more random connectivity pattern across model cortical neurons results in less systematic RF changes during ICMS (Section 6.3.3).

Temporal effects of ICMS

The cortical representation of the ICMS-site RF continues to increase with progressively longer stimulation duration, and the effects of ICMS persist after cessation of ICMS (Recanzone et al., 1992b). In the simulation, additional conditioning led to an increase in the overlap of the RF of model cortical neurons with the ICMS-site RF at farther distances (Figures 6.12 and 6.14). In the absence of any stimulation, the effects of ICMS persisted in the model: synaptic plasticity in the model requires neuronal activation (Equations 6.4 and 6.6).

In the simulation, the lateral inhibitory synaptic plasticity rate was faster than the afferent excitatory synaptic plasticity rate (Appendix D, Section D.4.1). Thus, during the early stages of ICMS, RF changes were mainly caused by changes in the lateral inhibitory weights, and during the later stages, RF changes were mainly caused by the afferent excitatory synaptic plasticity. At an early stage (after 250 ICMS steps), there was a large increase in the number of neurons whose RF has 0-25% overlap with the pre-ICMS ICMS-site RF (Figure 6.12a). Since the ICMS causes model cortical neurons to be weakly active, the faster lateral inhibitory synaptic plasticity caused weakening of lateral inhibitory pathways to neurons close to the ICMS site, thereby resulting in a small increase in neuronal responsiveness in the neurons close to the ICMS site (Figure 6.13).

As ICMS proceeded (after 1000 ICMS steps), the afferent excitatory synaptic plasticity strengthened the afferent pathways from the the pre-ICMS ICMS-site RF to the active neurons near the ICMS site, thereby increasing the amount of overlap (Figure 6.12a). As more and more model cortical neurons became responsive to the

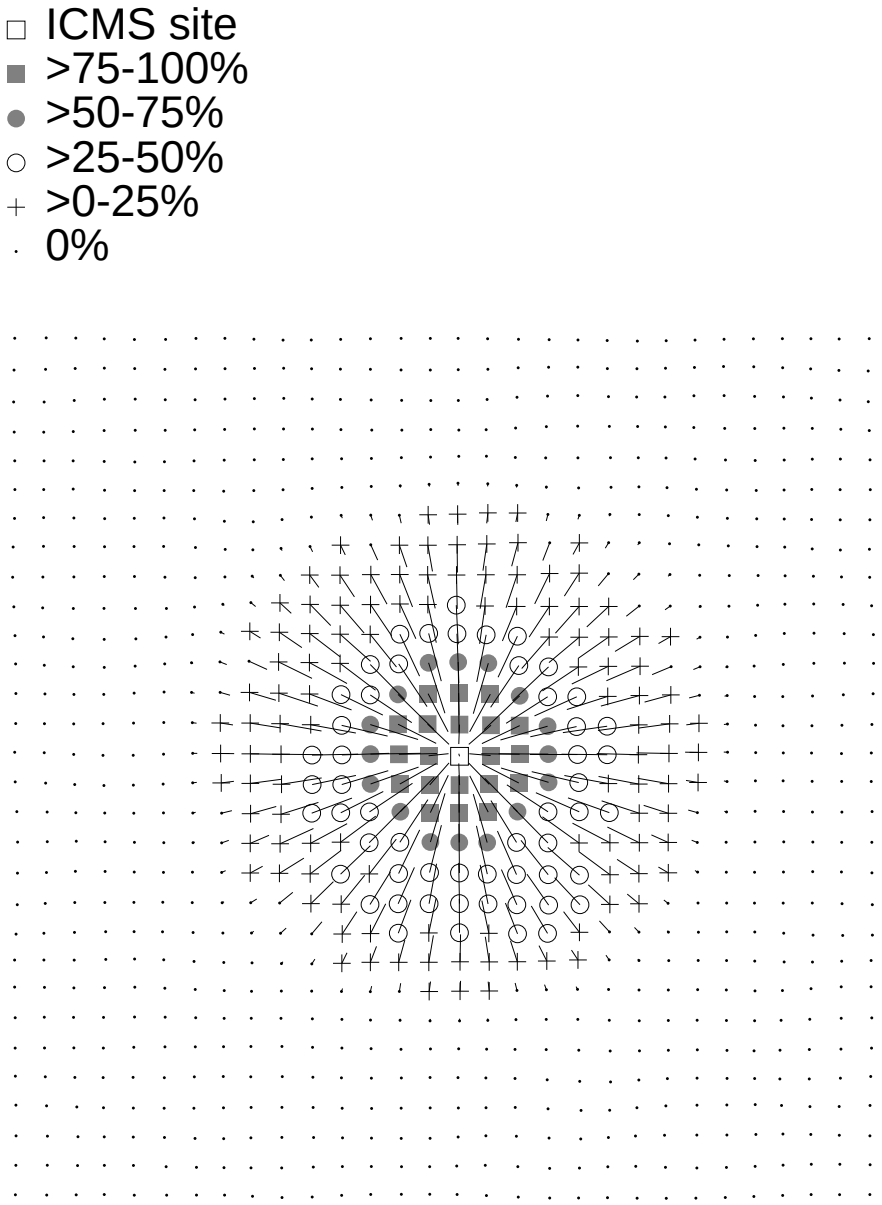

Figure 6.11: **Spatial distribution of changes in model cortical RF topography.** The positions of the centroids of the RF of model cortical neurons before ICMS are presented by the position of the center of the symbols. The lines code the shift of the centroid of the RF of the model cortical neurons after ICMS. The length of the lines represent the amount of shift, and the orientation of the lines represent the direction of shift. The symbols code the amount by which the RF of the model cortical neurons overlap with the pre-ICMS ICMS-site RF.

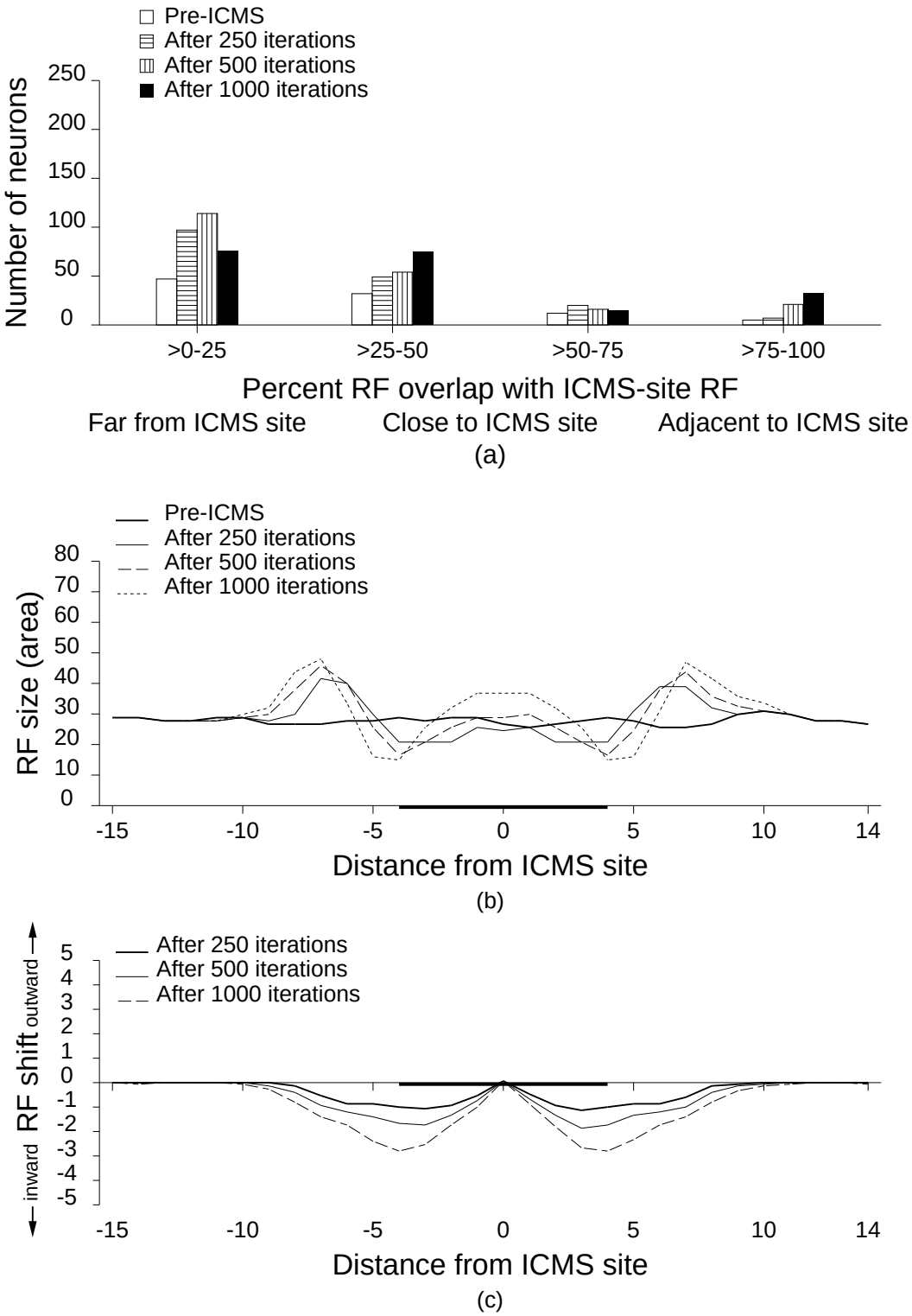

Figure 6.12: Legend on next page.

Figure 6.12: **Temporal changes in RF topography and RF size during ICMS.** Figure on previous page. (a) The number of model cortical neurons whose RF overlaps the pre-ICMS ICMS-site RF before and after ICMS. (b) RF area of neurons in a cross-section of the model cortical layer passing through the ICMS site, neurons $(0,-15)$–$(0,14)$, before and after ICMS. (c) RF shift of neurons in a cross-section of the model cortical layer passing through the ICMS site after ICMS, neurons $(0,-15)$–$(0,14)$. The line segment parallel to the abscissa represents the neurons that were active during the initial stage of ICMS.

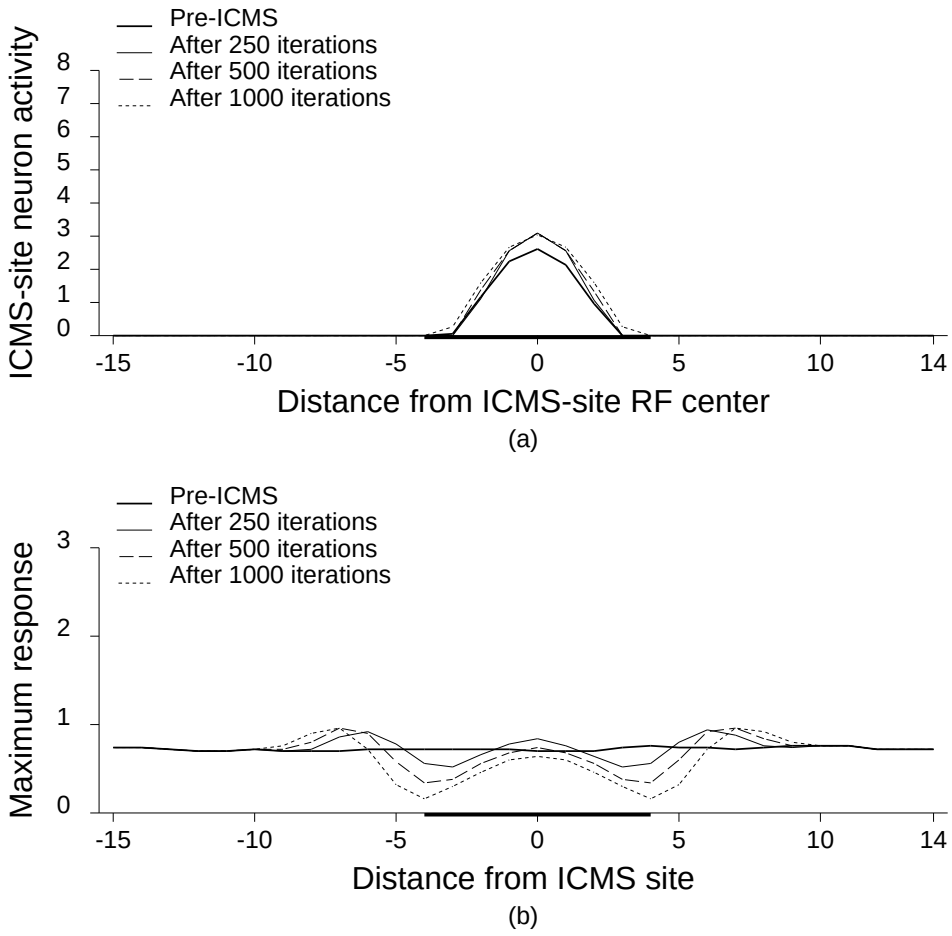

Figure 6.13: **Temporal effects of ICMS on responsiveness.** (a) One-dimensional RF profile of ICMS-site neuron. (b) The maximal responsiveness of neurons in a cross-section of the model cortical layer passing through the ICMS site, neurons $(0,-15)$–$(0,14)$, at different stages of ICMS. See Figure 6.9 for conventions.

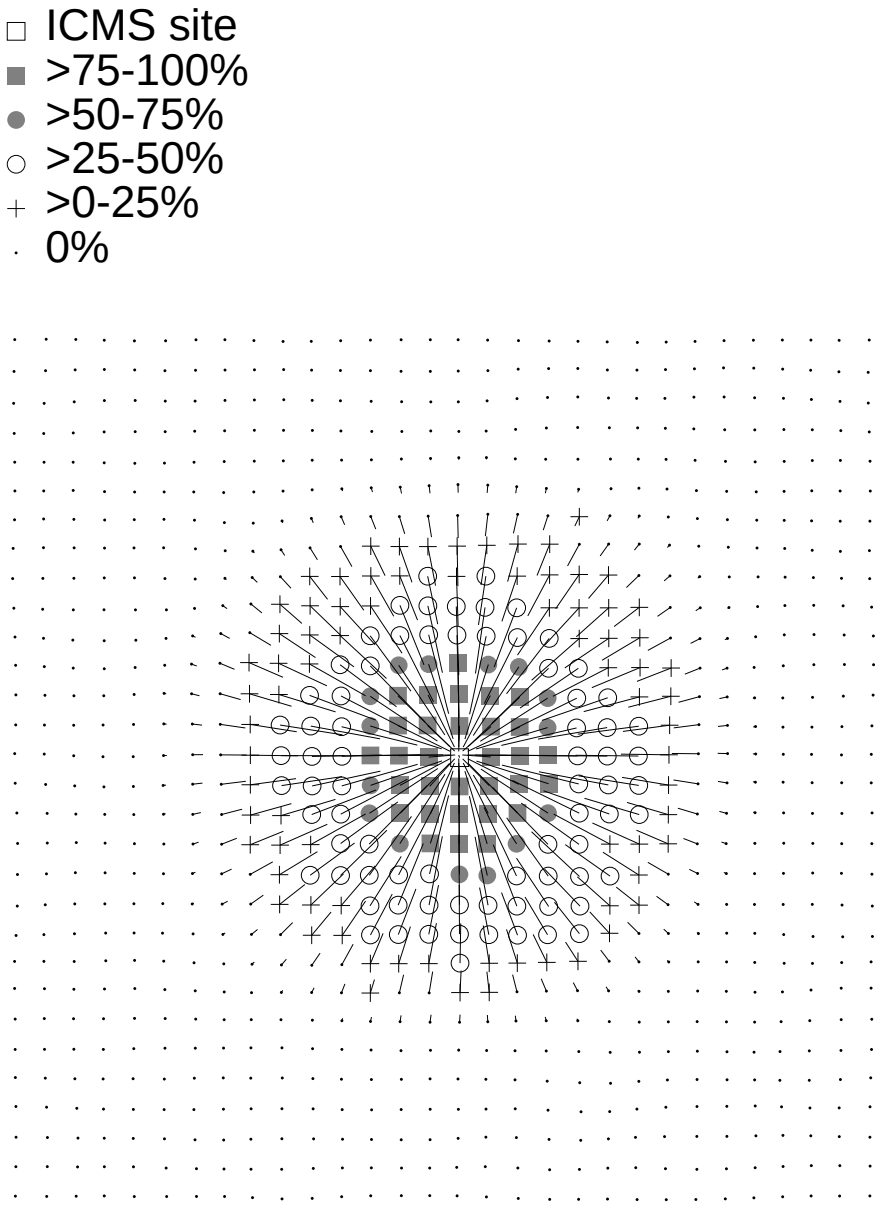

Figure 6.14: **RF changes with additional ICMS.**
Changes in RF topography of model cortical neurons after 1000 steps of ICMS. See Figure 6.11 for conventions.

same locations, their responsiveness to test stimuli decreased (Figure 6.13b). The afferent excitatory pathway weights to the ICMS-site neuron remained almost unchanged (Figure 6.7), and neurons surrounding the ICMS site strengthened synapses with afferent excitatory pathways from the the pre-ICMS ICMS-site RF (e.g., neurons (0,-1) and (0,-4) in Figure 6.7), and these neurons therefore had overlapping RFs. Because some neurons, e.g., neuron $(0, -4)$ in Figure 6.7, weakened afferent pathways from which they had the strongest synapses, neurons close to the ICMS site became responsive to positions farther from the pre-ICMS ICMS-site RF. Thus, the RF of neurons close to the ICMS site expanded (Figures 6.12b and 6.13a). Furthermore, as the amount of overlap of the RF of neurons close to the ICMS site with the pre-ICMS ICMS-site RF increased, the responsiveness of neurons close to the ICMS site decreased (Figure 6.13b).

The amount of shift in the RF of model cortical neurons toward the pre-ICMS ICMS-site RF increased with the number of ICMS time steps (Figure 6.12c).

6.3.2 The effects of model ICMS parameters

This section illustrates the role of some of the parameters in the model, especially the specific effects of the afferent excitatory synaptic plasticity, the lateral inhibitory synaptic plasticity, and the distribution of presynaptic excitation to the afferent excitatory and lateral inhibitory pathways.

Role of afferent excitatory synaptic plasticity

To determine the effects of synaptic plasticity in afferent excitatory pathways, ICMS was performed with the lateral inhibitory synaptic plasticity disabled. With only afferent excitatory synaptic plasticity, active neurons strengthened their synapses with strongly active afferents and weaken their synapses with weakly active afferents. Thus, the RF of these neurons shifted toward the ICMS-site RF (Figure 6.16c), and there was an increase in number of neurons responsive to the pre-ICMS ICMS-site RF (Figures 6.16a and 6.17).

In the absence of lateral inhibitory synaptic plasticity, as more active neurons strengthened synapses with afferents selective to the ICMS-site RF, the ICMS-site neuron

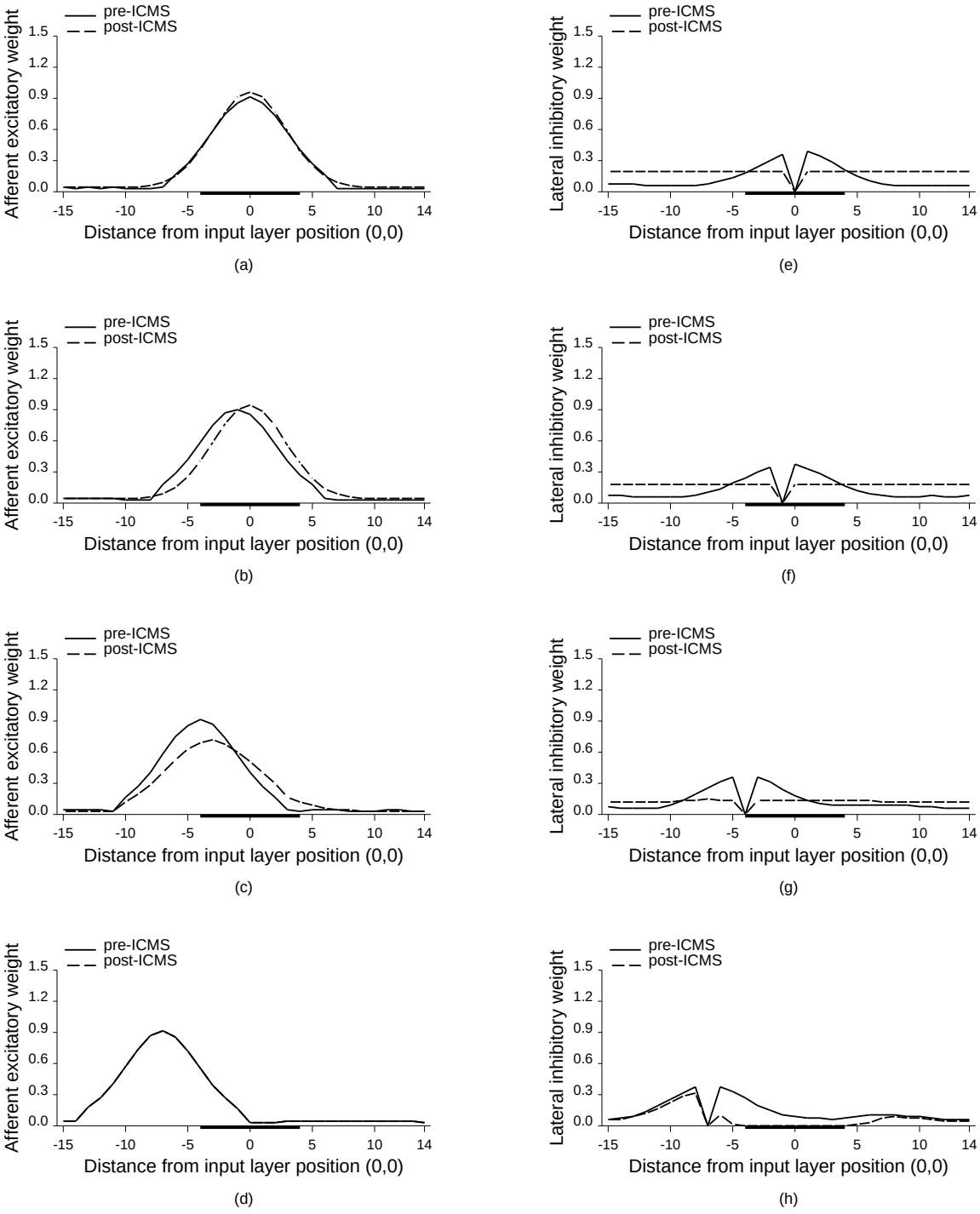

Figure 6.15: Legend on next page.

Figure 6.15: **Changes pathway weights in ICMS simulations with afferent excitatory or lateral inhibitory synaptic plasticity disabled.**
Figure on previous page. Weights of afferent excitatory pathways in the ICMS simulation with lateral inhibitory synaptic plasticity disabled (left column), and weights of lateral inhibitory pathways in the ICMS simulation with afferent excitatory synaptic plasticity disabled (right column) to different model cortical neurons are shown before ICMS and after 500 ICMS presentations. (a,e) neuron $(0,0)$, (b,f) neuron $(0,-1)$, (c,g) neuron $(0,-4)$, and (d,h) neuron $(0,-7)$. See Figure 6.7 for conventions.

received more inhibition when the ICMS-site RF was stimulated. This led to a decrease in responsiveness of the ICMS-site neuron and neurons close to the stimulation site (Figure 6.18b). Because some neurons, e.g., neuron $(0,-4)$ in Figure 6.15, weakened afferent pathways from which they had the strongest synapses, neurons close to the ICMS site became responsive to positions farther from the pre-ICMS ICMS-site RF. Thus, the RF of neurons close to the ICMS site expanded (Figures 6.16b and 6.18a).

Role of lateral inhibitory synaptic plasticity

With only lateral inhibitory synaptic plasticity, model ICMS resulted in weakening of lateral inhibitory pathways to neurons close to the ICMS site, which were weakly active (Figure 6.15). This led to an increase in responsiveness (Figure 6.18b) and RF size of model cortical neurons close to the ICMS site (Figures 6.16b and 6.18a). Because lateral inhibitory pathways from neurons close to the ICMS site to inactive/weakly active neurons weakened more than lateral inhibitory pathways from neurons far from the ICMS site to inactive/weakly active neurons (Figure 6.15; see Section 6.4.1), the RF of neurons far from the ICMS site showed a small shift toward the ICMS-site RF (Figure 6.16c).

Comparison of the effects of afferent excitatory and lateral inhibitory synaptic plasticity

The afferent excitatory synaptic plasticity and the lateral inhibitory synaptic plasticity produce complementary effects during ICMS. With both plasticity rules, the increase in the number of neurons inhibiting the ICMS-site neuron when the ICMS-site RF is stimulated caused by the afferent excitatory synaptic plasticity is balanced by the decrease

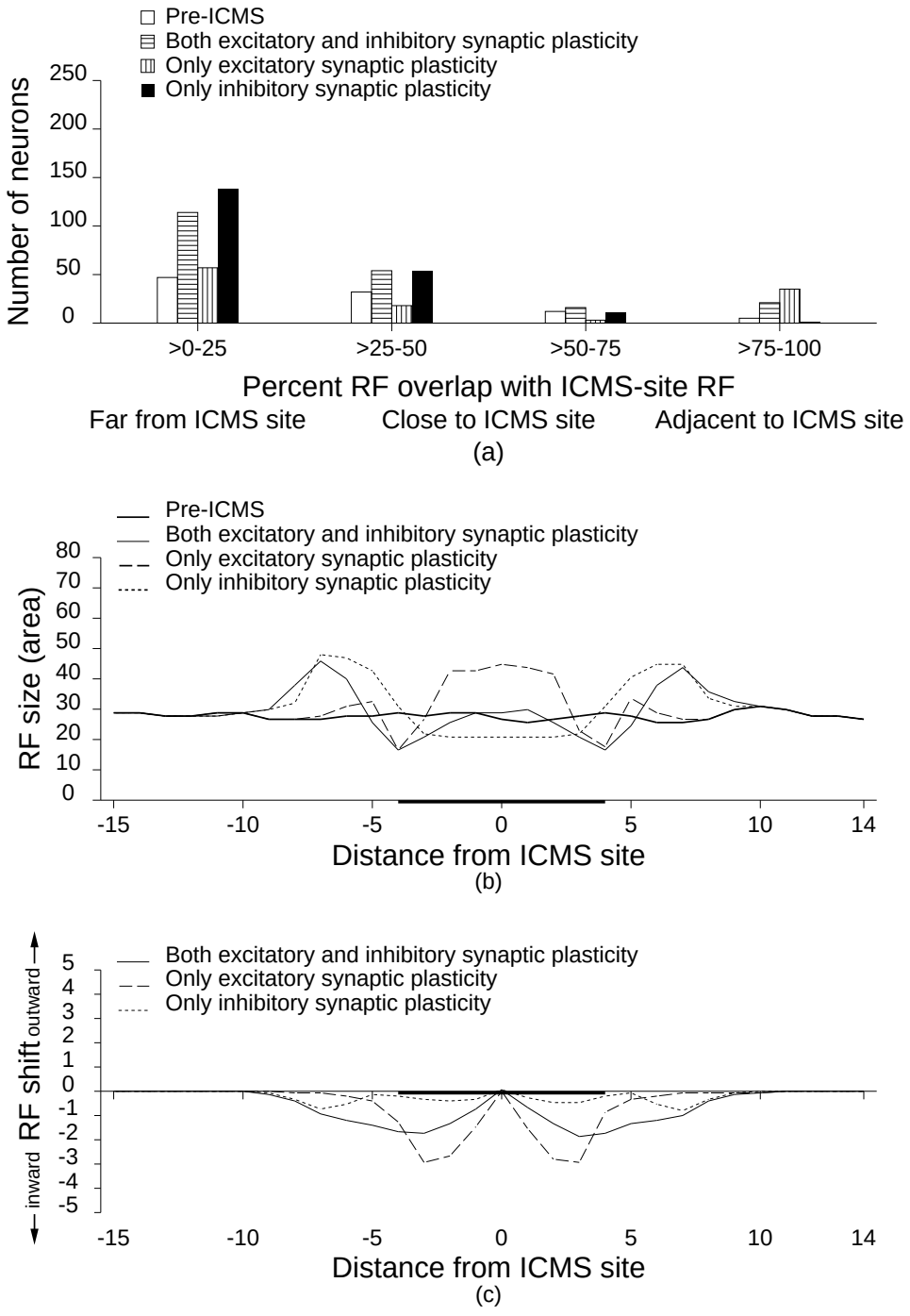

Figure 6.16: **Role of afferent excitatory and lateral inhibitory plasticity in producing RF changes.**
In these simulations either the afferent excitatory or the lateral inhibitory synaptic plasticity rule was disabled during ICMS. See Figure 6.12 for conventions.

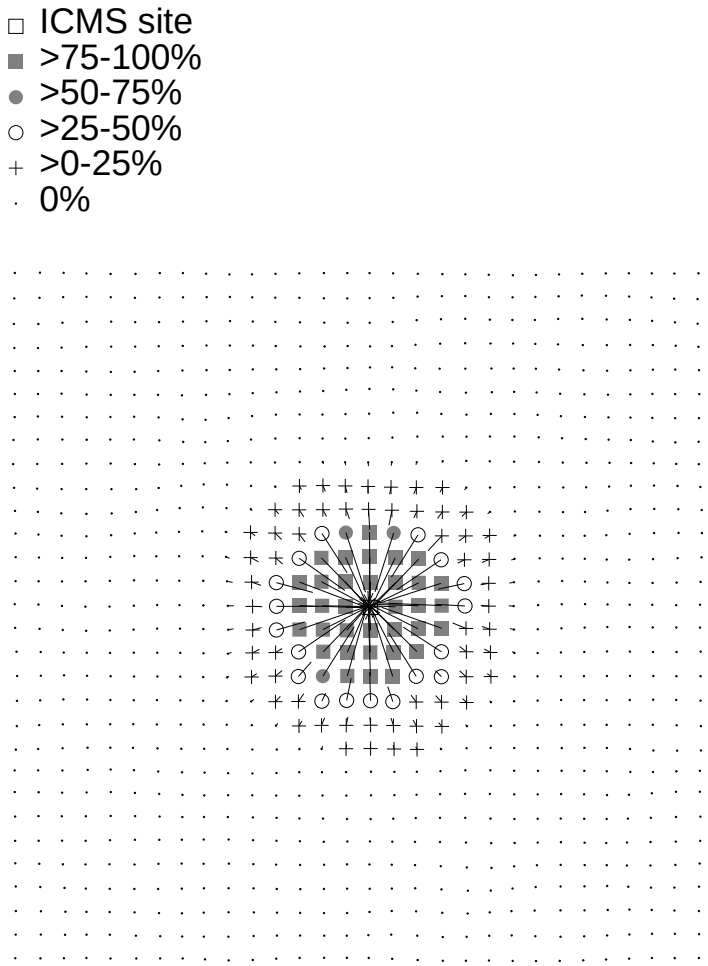

Figure 6.17: **Changes in model cortical RF topography with only afferent excitatory plasticity.**
Only afferent excitatory plasticity was enabled during model ICMS. See Figure 6.11 for conventions.

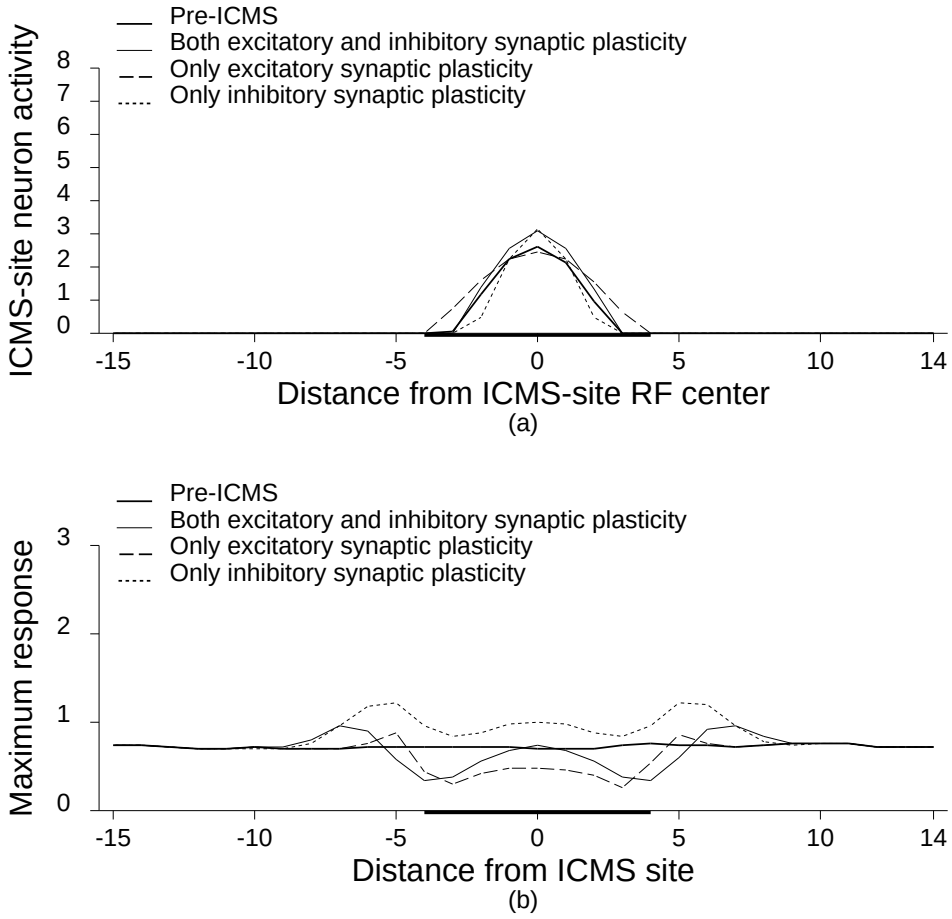

Figure 6.18: **Effect of afferent excitatory plasticity and lateral inhibitory plasticity on responsiveness.**
See Figure 6.9 for conventions.

in the strength of the lateral inhibitory pathways to the ICMS-site neuron. Furthermore,

- afferent excitatory synaptic plasticity increases the number of neurons whose RFs have more than 75% overlap with the ICMS-site RF, and these neurons are close to the ICMS site (Figures 6.16b and 6.17), whereas lateral inhibitory synaptic plasticity mainly increases the number of neurons whose RFs have $>$ 0–25% overlap with the ICMS-site RF, and these neurons are far from the ICMS site (Figures 6.16a and 6.19);
- afferent excitatory synaptic plasticity alone produces RF expansion in neurons close to the ICMS site and RF contraction in surrounding neurons, whereas lateral inhibitory synaptic plasticity alone produces RF contraction in neurons close to the ICMS site and RF expansion in surrounding neurons (Figures 6.16b and 6.18a);
- afferent excitatory synaptic plasticity alone produces large RF shifts toward the ICMS-site RF in neurons close to the ICMS site, whereas lateral inhibitory synaptic plasticity alone produces comparatively larger RF shifts toward the ICMS-site RF in neurons far from the ICMS site (Figure 6.16c); and
- afferent excitatory synaptic plasticity reduces responsiveness of neurons close to the ICMS site; lateral inhibitory synaptic plasticity increases responsiveness of neurons close to the ICMS site (Figure 6.18b).

Effects of distribution of presynaptic stimulation of afferent excitatory pathways

In the simulation in Section 6.3.1, a decrease in responsiveness of the ICMS-site neuron caused by afferent excitatory synaptic plasticity was balanced by the effects of lateral inhibitory synaptic plasticity. Another possibility for balancing for the decrease in responsiveness of the ICMS-site neuron is to increase the strength of the afferent excitatory synapses. According to the EXIN afferent excitatory synaptic plasticity rule, the afferent excitatory synaptic strength equilibrates at a value proportional to the presynaptic activation. Thus, increasing the strength of presynaptic activation strengthens the afferent pathways to the ICMS-site neuron.

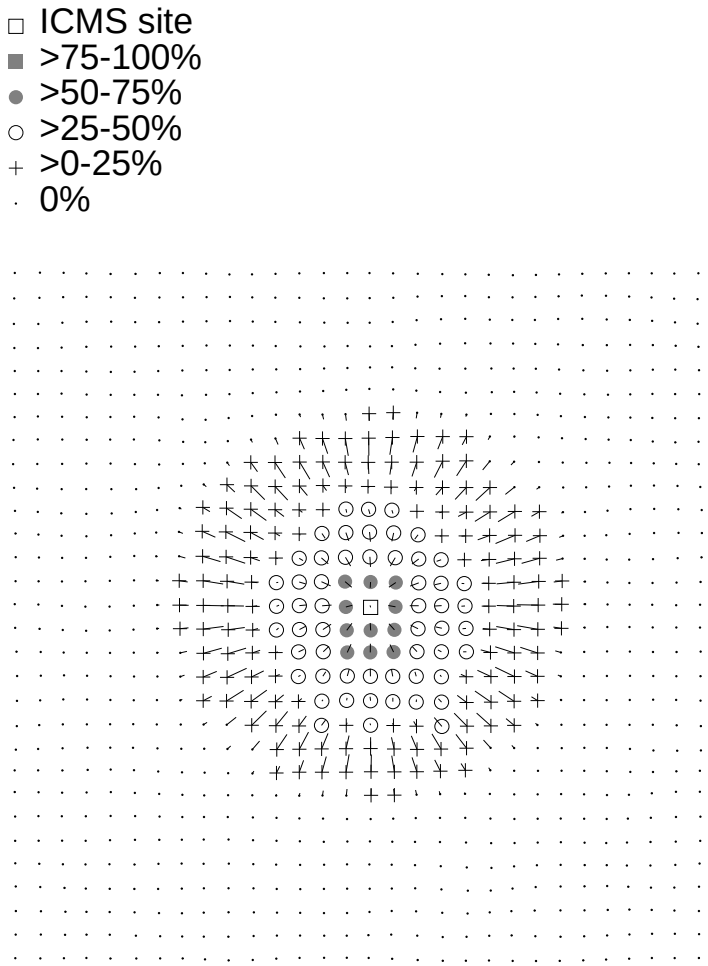

Figure 6.19: **Changes in model cortical RF topography with only lateral inhibitory plasticity.**
Afferent excitatory synaptic plasticity was disabled during model ICMS. See Figure 6.11 for conventions.

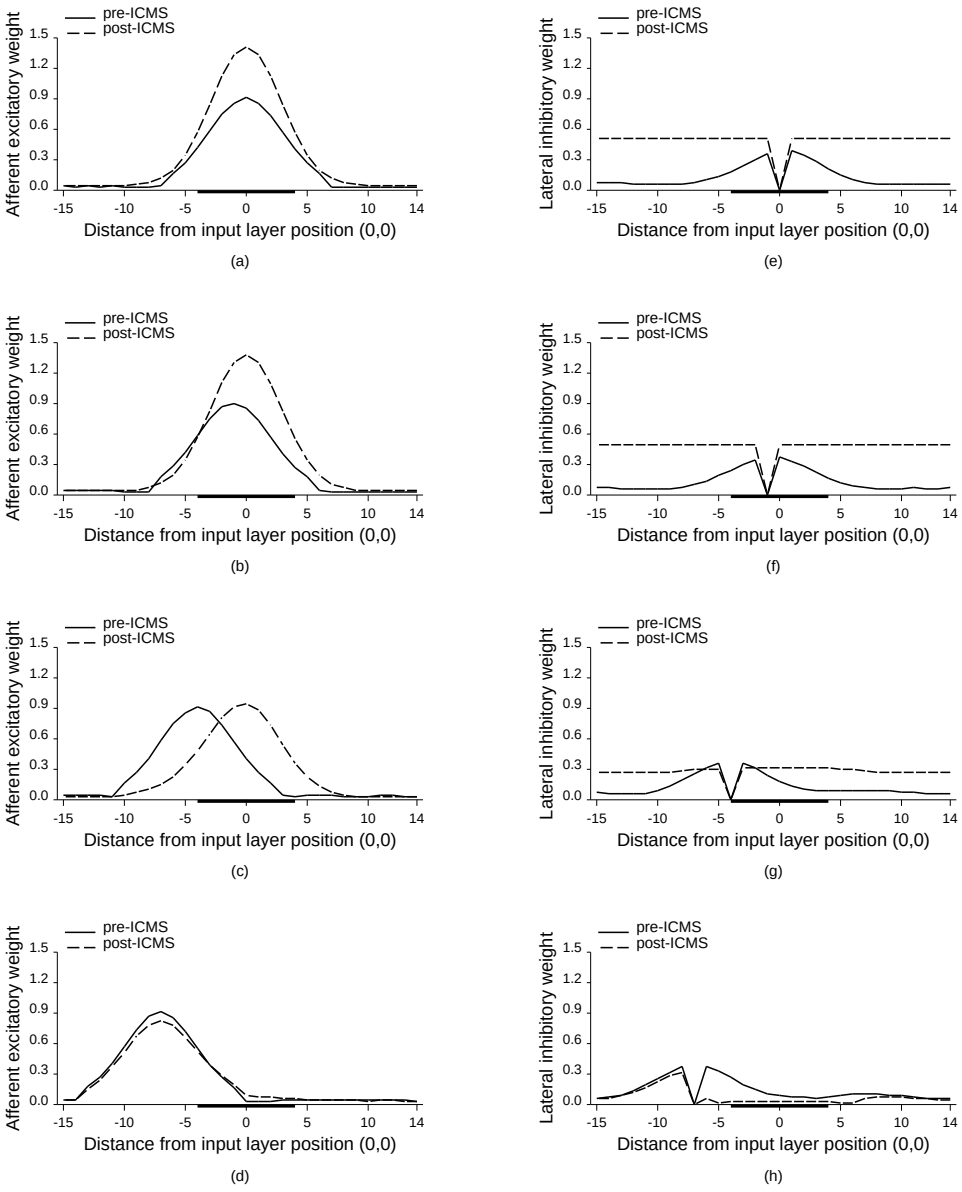

Figure 6.20: **Synaptic plasticity in the simulation manipulating the magnitude of presynaptic excitation to afferent excitatory synapses produced by ICMS.** Weights of afferent excitatory pathways (left column) and lateral inhibitory pathways (right column) to different model cortical neurons – neuron $(0,0)$ in (a) and (e), neuron $(0,-1)$ in (b) and (f), neuron $(0,-4)$ in (c) and (g), and neuron $(0,-7)$ in (d) and (h) – are shown before ICMS and after 500 ICMS presentations. In this simulation, the value of the parameter φ_1 in Equation 2 was 1.5 times the value used in Section 6.3.1. The other parameters controlling the model ICMS were the same as those used in Section 6.3.1. See Figure 6.7 for conventions.

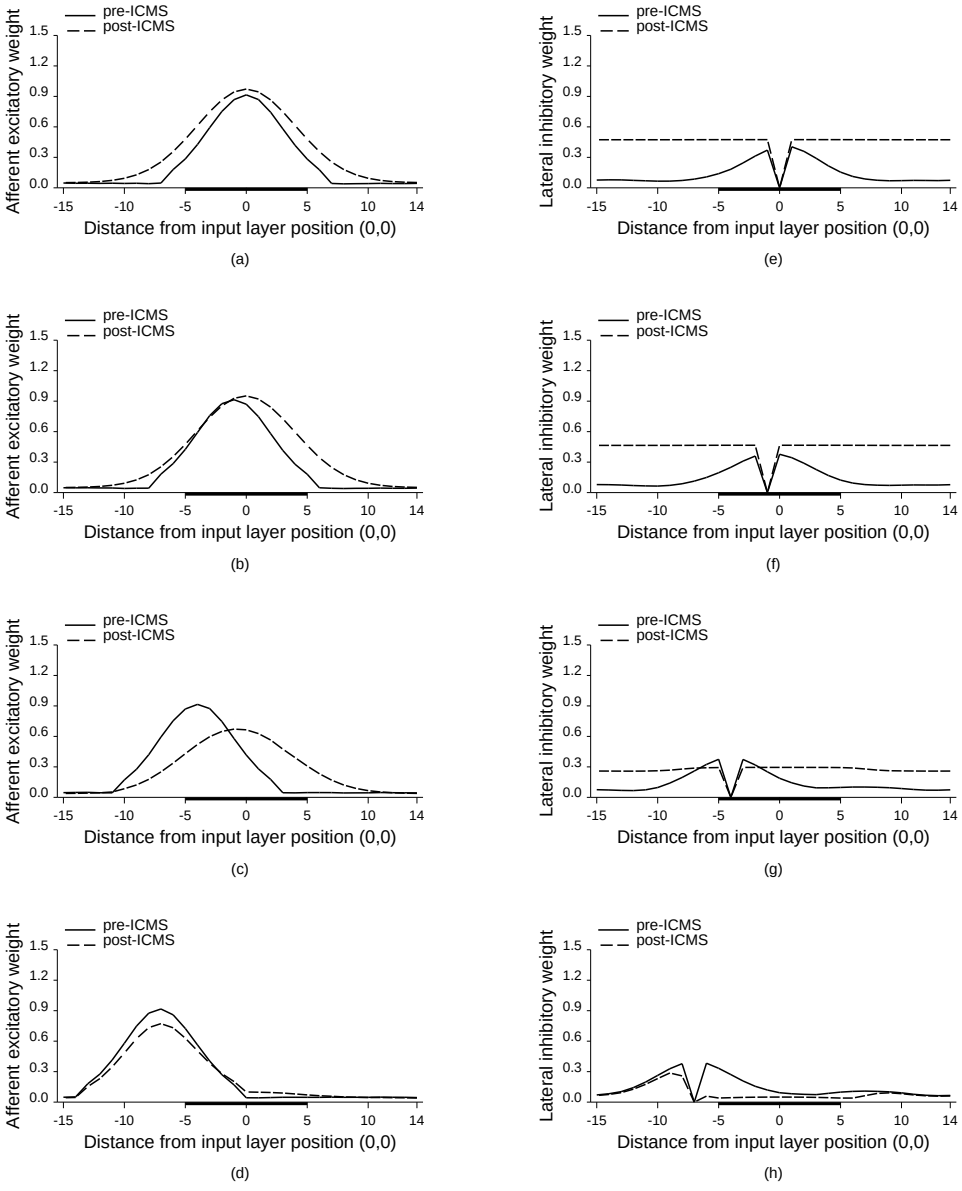

Figure 6.21: **Synaptic plasticity in the simulation manipulating the distribution of presynaptic excitation to afferent excitatory synapses produced by ICMS.** Weights of afferent excitatory pathways (left column) and lateral inhibitory pathways (right column) to different model cortical neurons – neuron $(0,0)$ in (a) and (e), neuron $(0,-1)$ in (b) and (f), neuron $(0,-4)$ in (c) and (g), and neuron $(0,-7)$ in (d) and (h) – are shown before ICMS and after 500 ICMS presentations. In this simulation, the value of the parameter σ_2 in Equation 2 was twice the value used in Section 6.3.1. The other parameters controlling the model ICMS were the same as those used in Section 6.3.1. See Figure 6.7 for conventions.

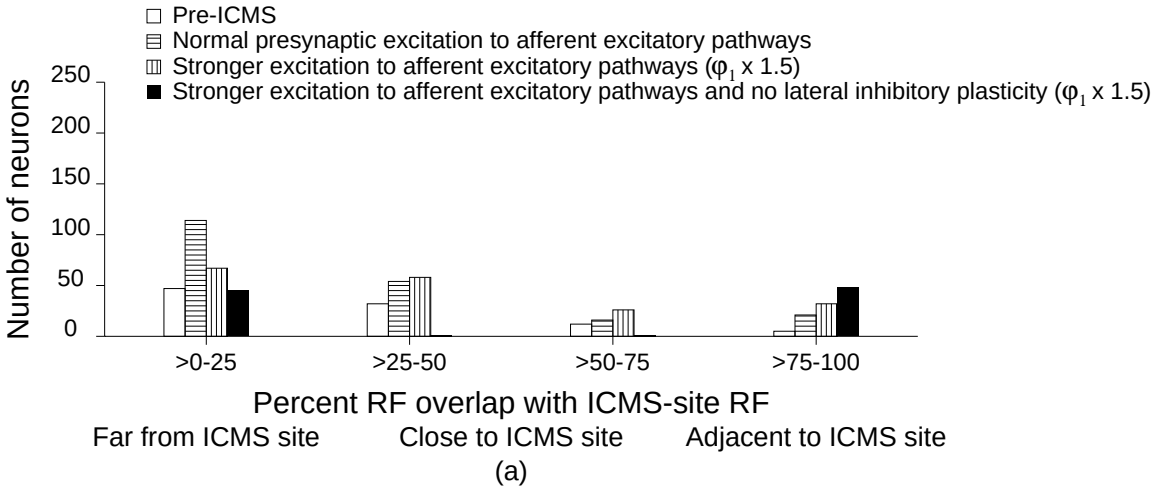

(a)

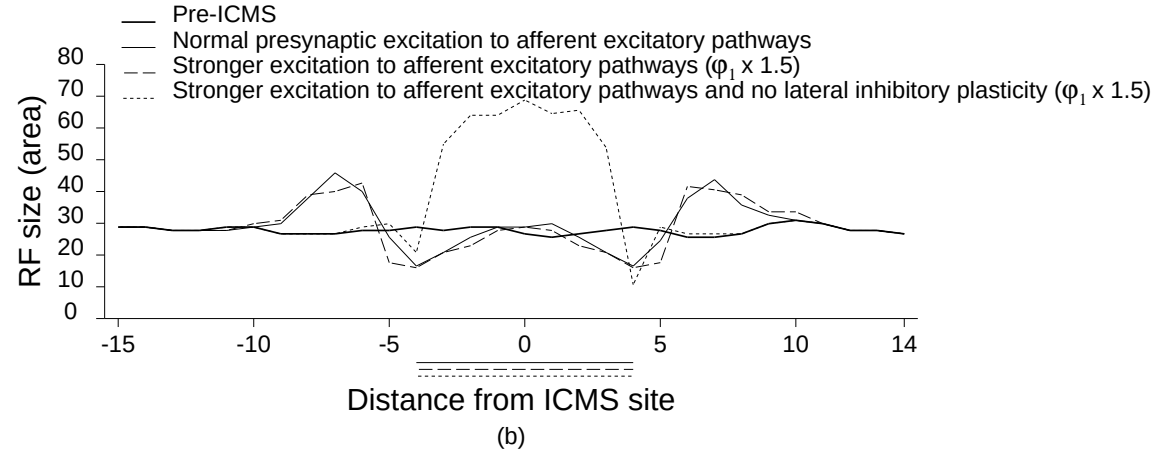

(b)

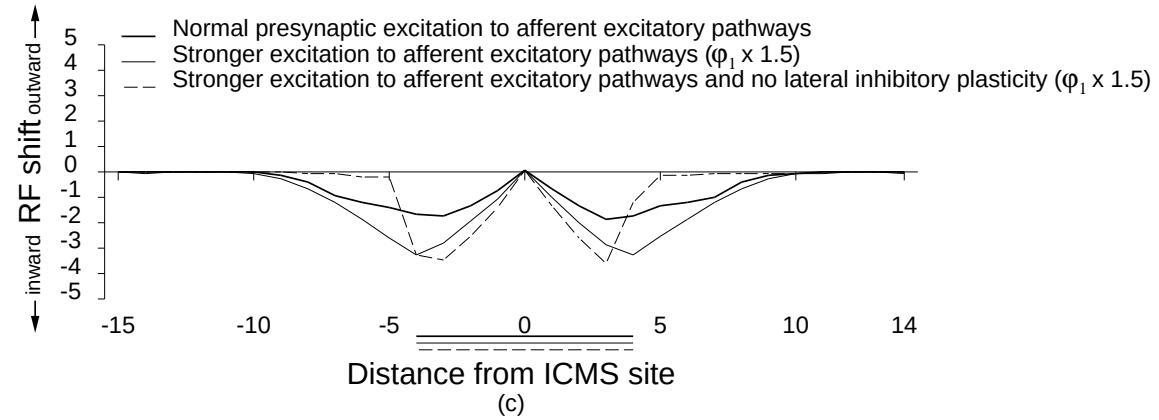

(c)

Figure 6.22: Legend on next page.

Figure 6.22: **Effects of the strength of presynaptic excitation of afferent excitatory pathways on model RF size and position.**
Figure on previous page. Some of the effects of varying presynaptic excitation strength of the afferent excitatory pathways during ICMS are shown. The values of the parameters in Equation 2 are given in Figure 6.5. (a) The number of model cortical neurons with RF overlapping the pre-ICMS ICMS-site RF before and after ICMS. (b) RF area of neurons $(0,-15)$–$(0,14)$, before and after ICMS. (c) RF shift of neurons in a cross-section of the model cortex passing through the ICMS site after ICMS, neurons $(0,-15)$–$(0,14)$. The line segments parallel to the abscissa represent the neurons that were active during the initial ICMS step as the ICMS parameters were varied.

When ICMS was simulated in the EXIN network with stronger stimulation of the afferent excitatory pathways (i.e., φ_1 in Equation 6.2 was increased) and with the lateral inhibitory synaptic plasticity disabled, there was a large increase in the RF size of neurons close to the ICMS site (Figures 6.22b and 6.23a), and the responsiveness of the ICMS-site neuron was almost equal to the pre-ICMS ICMS-site neuronal responsiveness (Figure 6.23b). With a smaller value for φ_1, the responsiveness of the ICMS-site neuron in the EXIN network with the lateral inhibitory synaptic plasticity disabled was smaller (Figure 6.18b).

When the ICMS was simulated with both afferent excitatory and lateral inhibitory synaptic plasticity and with a larger φ_1, the neuronal responsiveness of the ICMS-site neuron decreased (Figure 6.23b) but its RF size remained close to the pre-ICMS size (Figure 6.22b). Stronger stimulation of the afferent excitatory pathways during ICMS caused neurons close to the ICMS site to be more strongly activated (Figure 6.5), which led to strengthening of lateral inhibitory pathways to these neurons and to a decrease in neuronal responsiveness of these neurons. Since the presynaptic activation level of the afferent excitatory pathways to the ICMS-site neuron was larger, the afferent excitatory synaptic plasticity rule caused these pathways to strengthen (Figure 6.20). In this simulation, the effects of stronger afferent excitatory and lateral inhibitory pathways to the ICMS-site neuron combined to produce no change in the size of the ICMS-site RF after ICMS (Figures 6.22b and 6.23a). When φ_1 in Equation 6.2 was increased, the EXIN model produced an increase in the overlap of the RF of model cortical neurons with the pre-ICMS ICMS-site RF (Figure 6.22a) and in RF shifts toward the pre-ICMS ICMS-site RF (Figure 6.22c).

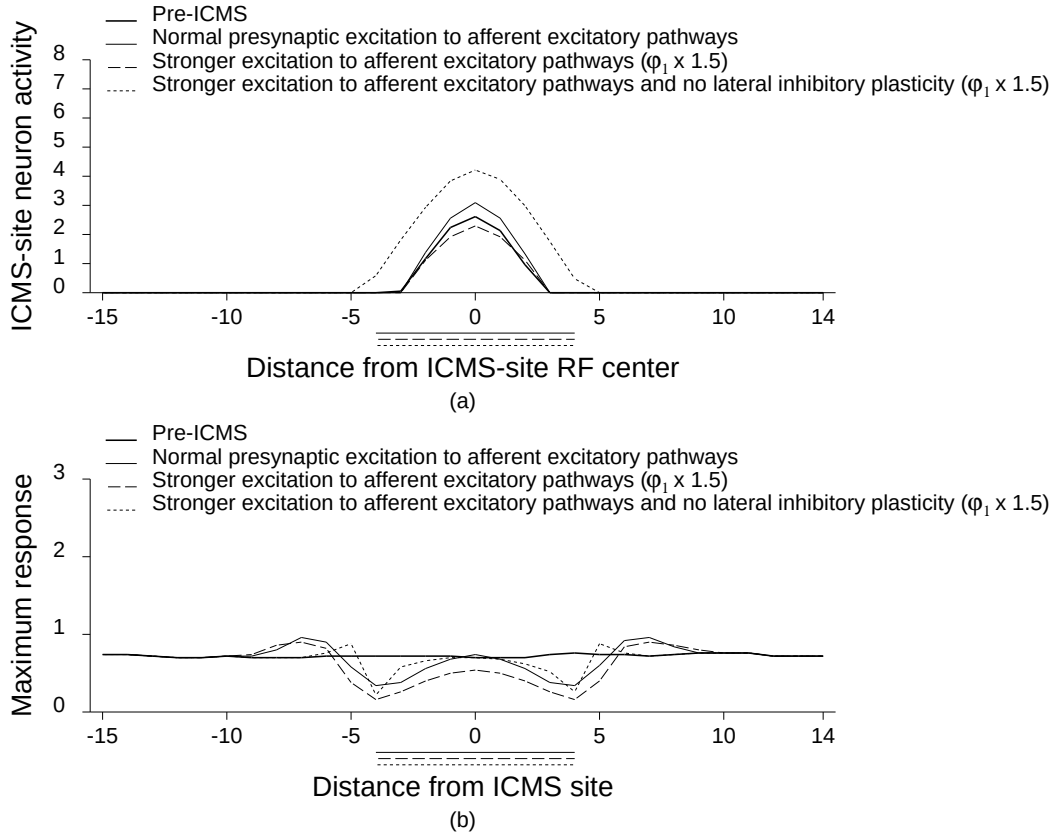

Figure 6.23: **Effects of excitation strength of the presynaptic afferent excitatory pathways on model responsiveness.**
Some of the effects of varying presynaptic excitation strength of the afferent excitatory pathways during ICMS are shown. The values of the parameters in Equation 2 are given in Figure 6.5. (a) One-dimensional RF profile of ICMS-site neuron. The RF profile was obtained by adding the neuron's response to input at positions along the y axis. (b) The maximal responsiveness of neurons in a cross-section of model cortical layer passing through the ICMS site, neurons $(0, -15)$–$(0, 14)$, before and after ICMS. The line segments parallel to the abscissa represent the neurons that were active during the initial ICMS step as the ICMS parameters were varied.

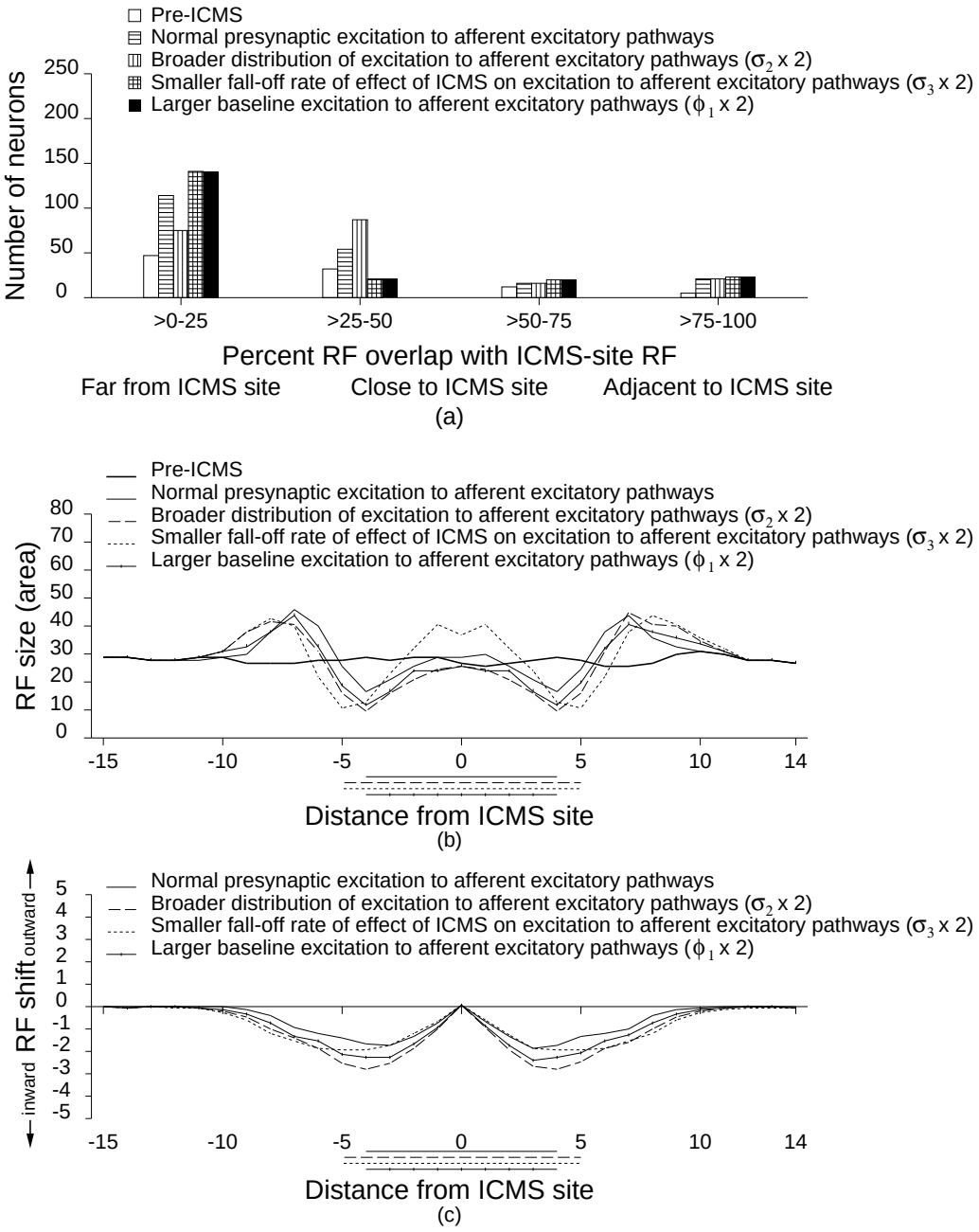

Figure 6.24: **Effects of presynaptic stimulation distribution to the afferent excitatory pathways on model RF properties.**
Some of the effects of varying the presynaptic stimulation distribution to the afferent excitatory pathways during ICMS are shown. The values of the parameters in Equation 2 are given in Figure 6.5. See Figure 6.22 for conventions. In this figure, the line segments parallel to the abscissa are of different lengths because as the ICMS parameters were varied the distribution of active model cortical neurons was different (see Figure 6.5).

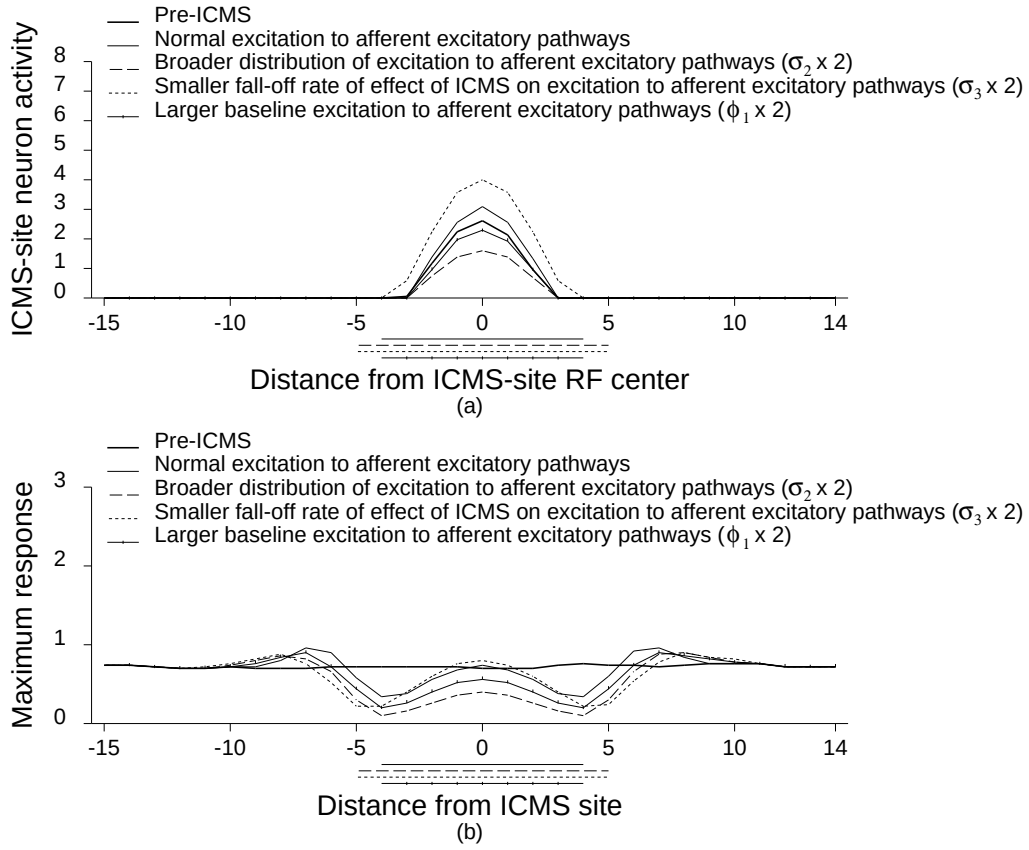

Figure 6.25: **Effects of presynaptic stimulation distribution to the afferent excitatory pathways on model responsiveness.**

Some of the effects of varying the presynaptic stimulation distribution to the afferent excitatory pathways during ICMS are shown. The values of the parameters in Equation 2 are given in Figure 6.5. See Figure 6.23 for conventions. In this figure, the line segments parallel to the abscissa are of different lengths because as the ICMS parameters were varied the distribution of active model cortical neurons was different (see Figure 6.5).

Figures 6.24 and 6.25 show the effects of varying other parameters in Equation 6.2 (ϕ_1, σ_2, and σ_3). As these parameters are varied, the EXIN synaptic plasticity rules produce an increase in the number of neurons whose RF has more than 75% overlap with the pre-ICMS ICMS-site RF (Figure 6.24a), a contraction of the RF of neurons close to the ICMS site, an expansion of the RF of neurons far from the ICMS site expands (Figure 6.24b), a shift in the RF of model cortical neurons towards the pre-ICMS ICMS-site RF (Figure 6.24c), a decrease in the responsiveness of neurons close to the ICMS site, and an increase in the responsiveness of neurons far from the ICMS site (Figure 6.25b). This shows that the proposed model is quite robust in producing changes in RF properties following ICMS similar to those observed experimentally. However, as these parameters are varied, the RF size of the ICMS-site neuron and the ICMS-site neuronal responsiveness to test stimuli change (Figures 6.24b and 6.25b).

The changes in ICMS-site neuronal responsiveness to test stimuli are correlated with the activation level of the ICMS-site neuron in the initial stage of ICMS. In general, as the activation level of the ICMS-site neuron in the initial stage of ICMS increases, the RF size of the ICMS-site neuron and the ICMS-site neuronal responsiveness to test stimuli after ICMS decrease (Figures 6.5, 6.24b, and 6.25ab). As the activation level of the ICMS-site neuron in the initial stage of ICMS increases, the lateral inhibitory pathways to the ICMS-site neuron strengthen, according to the EXIN lateral inhibitory synaptic plasticity rule, thereby reducing the ICMS-site neuron's RF size and responsiveness to the test input.

The relationship between the activation level of the ICMS-site neuron in the initial stage of ICMS and the various parameters in Equation 6.2 is as follows. As the baseline stimulation strength of the afferent excitatory pathways (ϕ_1 in Equation 6.2) is increased, excitation to the ICMS-site neuron increases (Equation 6.9), and therefore the activation of the neuron increases (Figure 6.5). The activation of the ICMS-site neuron increases (Figure 6.5) as the distribution of the stimulation strength of the afferent excitatory pathways to the model cortical neurons is broadened (i.e., σ_2 in Equation 6.2 is increased) because increasing σ_2 increases afferent excitation to the ICMS-site neuron (Equation 6.9). The activation of neurons close to the ICMS site decreases (Figure 6.5) as the fall-off rate

of the strength of the ICMS to the afferent excitatory pathways is reduced (i.e., σ_3 in Equation 6.2 is increased), because excitation to the ICMS-site neuron remains the same but the excitation to neurons surrounding the ICMS site increases, which in turn increases the activation of the surrounding neurons. As the activation of the surrounding neurons increases they exert greater inhibition on the ICMS-site neuron, leading to a decrease in the activation of the ICMS-site neuron.

Figures 6.27 and 6.28 show the effects of varying the parameters in Equation 6.1. Increasing φ_0 in Equation 6.1 increases excitation to the ICMS-site neuron and increases the activation of the ICMS-site neuron in the initial stage of ICMS (Figure 6.26). Increasing σ_1 in Equation 6.1 increases excitation to neurons surrounding the ICMS-site neuron and decreases the activation level of the ICMS-site neuron in the initial stage of ICMS (Figure 6.26). ICMS with the larger φ_0 decreased the ICMS-site RF size (Figures 6.27b and 6.28a) and decreased ICMS-site neuronal responsiveness to test stimuli (Figure 6.28b). ICMS with the larger σ_1 increased ICMS-site RF size (Figures 6.27b and 6.28a) and increased ICMS-site neuronal responsiveness to test stimuli (Figure 6.28b). Changes in RF properties of other model cortical neurons were similar to those presented in Section 6.3.1.

Effects of distribution of presynaptic stimulation of lateral inhibitory pathways

Figures 6.30–6.33 show the effects of varying the parameters in Equation 6.3 (ϕ_2, φ_2, σ_4, and σ_5). As these parameters are increased, the EXIN synaptic plasticity rules produce an increase in the number of neurons whose RF has a large overlap with the pre-ICMS ICMS-site RF (Figures 6.30a and 6.32a), a contraction of the RF of neurons close to the ICMS site and an expansion of the RF of neurons far from the ICMS site (Figures 6.30b and 6.32b), a shift of the RF of model cortical neurons towards the pre-ICMS ICMS-site RF (Figures 6.30c and 6.32c), a decrease in responsiveness of neurons close to the ICMS site, and an increase in responsiveness of neurons far from the ICMS site (Figures 6.31b and 6.33b). Thus, the proposed model is quite robust in producing changes in RF properties following ICMS similar to those observed experimentally. However, as these parameters are varied, the RF size of the ICMS-site neuron and the ICMS-site neuronal

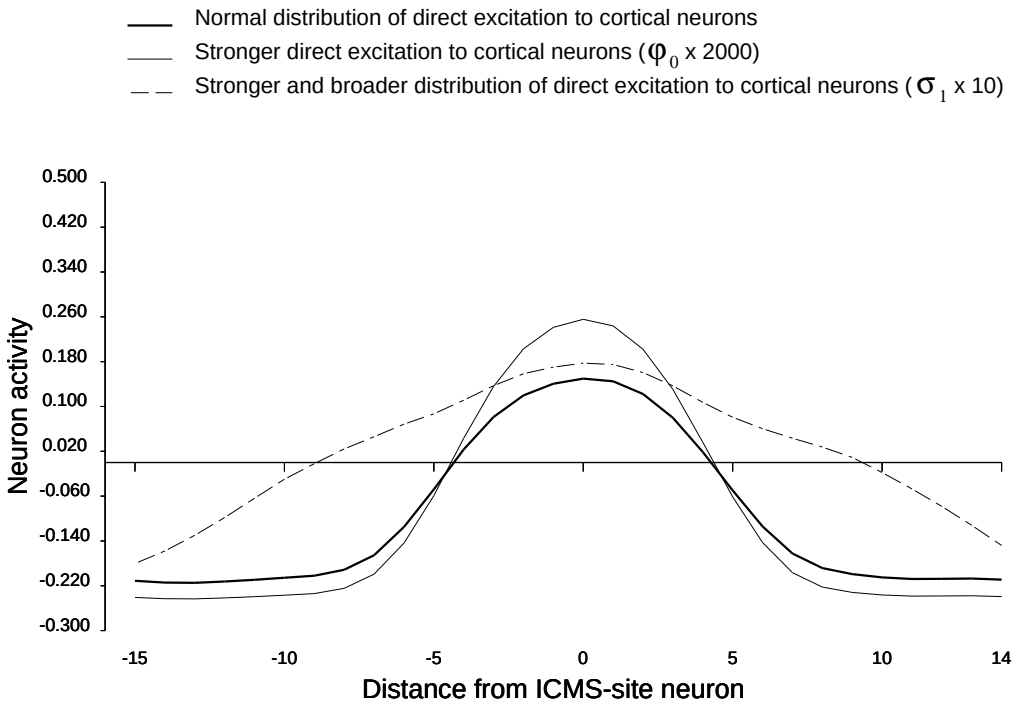

Figure 6.26: **Changes in activation of model neurons caused by changes in the distribution of direct excitation to the neurons.**
The activations of a cross-section of model cortical layer neurons through the ICMS site, neurons $(0,-15)$–$(0,14)$, in the initial stage of ICMS, as parameter values in Equation 1 are varied, are shown. The parameter values in Equations 2 and 3 were the same as those used in the simulations presented in Section 6.3.1 (see Appendix D, Section D.4.1). For the normal distribution of direct excitation to model cortical neurons, the values of parameters in Equation 1 were the same as those used in Section 6.3.1. For stronger direct excitation to cortical neurons, the value of φ_0 in Section 6.3.1 was multiplied by 2000, and for broader distribution of direct excitation to cortical neurons, the value of σ_1 in Section 6.3.1 was multiplied by 10.

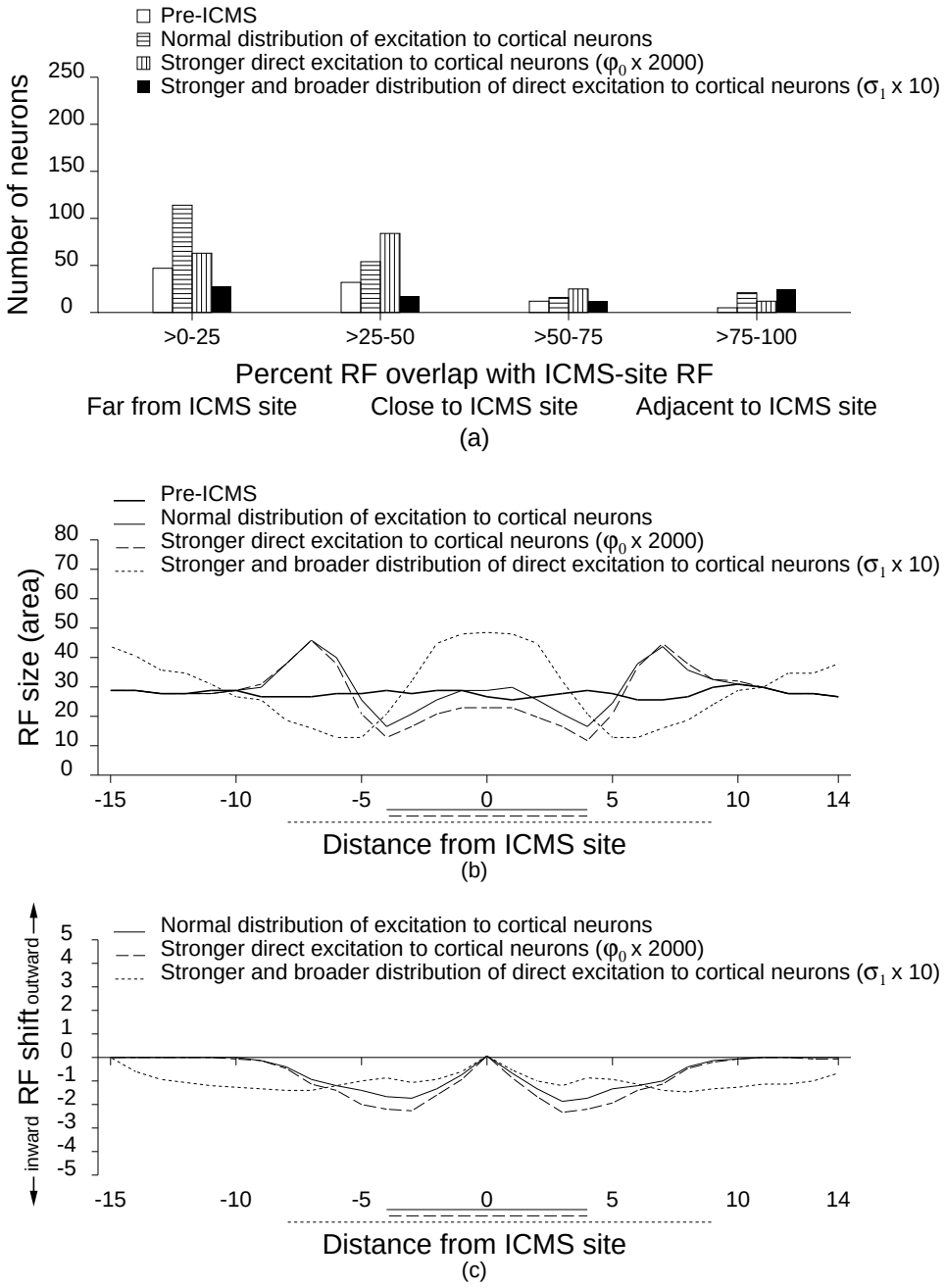

Figure 6.27: **Effects of distribution of direct stimulation to the model cortical neurons on RF properties.**

Some of the effects of varying the parameters controlling direct excitation to the model cortical neurons during ICMS are shown. The values of the parameters in Equation 1 are give in Figure 6.26. See Figure 6.22 for conventions.

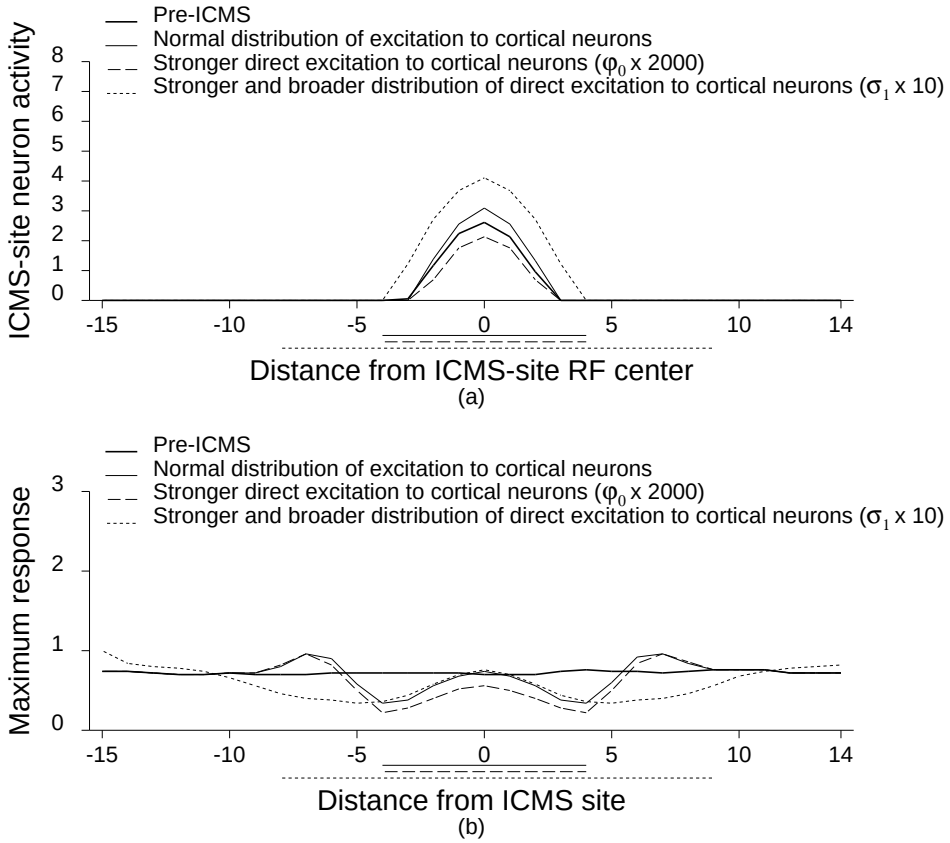

Figure 6.28: **Effects of distribution of direct stimulation to the model cortical neurons on responsiveness.**

Some of the effects of varying the parameters controlling direct excitation to the model cortical neurons during ICMS are shown. The values of the parameters in Equation 1 are give in Figure 6.26. See Figure 6.23 for conventions.

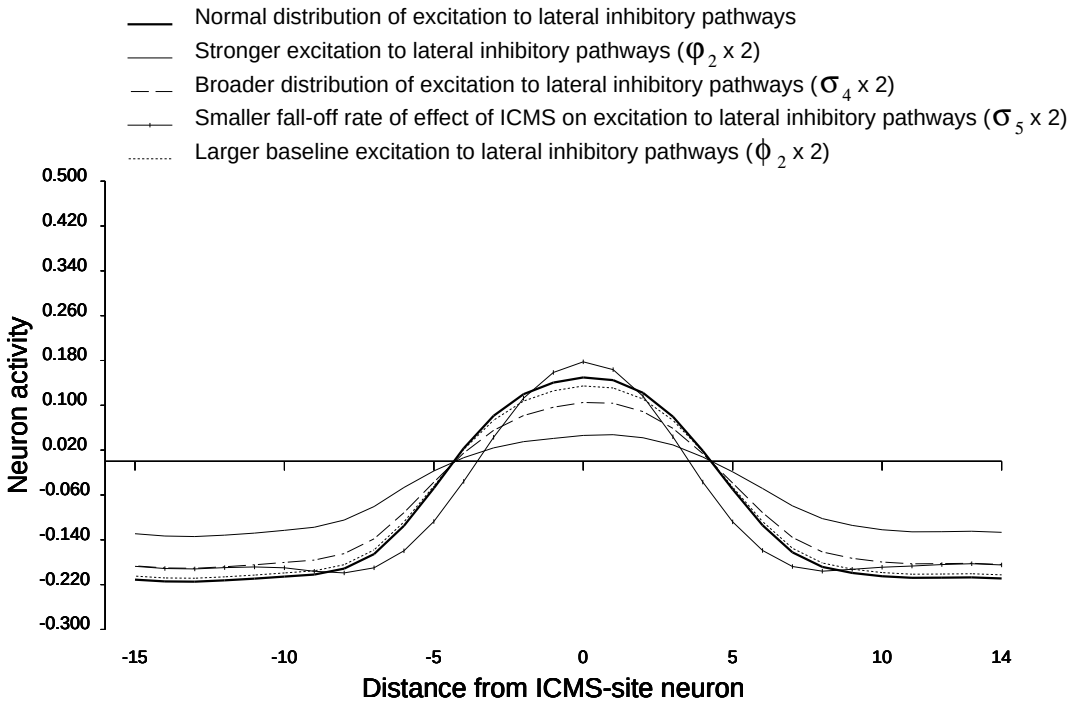

Figure 6.29: **Changes in activation of model neurons caused by changes in the distribution of presynaptic excitation to lateral inhibitory pathways.**
The activation of a cross-section of model cortical layer neurons through the ICMS site, i.e., neurons $(0, -15)$–$(0, 14)$, in the initial stage of ICMS, as parameter values in Equation 3 are varied, are shown. The parameter values in Equations 1 and 2 were the same as those used in the simulations presented in Section 6.3.1 (see Appendix D, Section D.4.1). For the normal distribution of excitation to lateral inhibitory pathways, the parameters in Equation 3 were assigned the values used in the ICMS simulation in Section 6.3.1. For stronger excitation to the lateral inhibitory pathways, the value of φ_2 in Section 6.3.1 was multiplied by a factor of 2; for broader distribution of excitation to the lateral inhibitory pathways, the value of σ_4 used in Section 6.3.1 was multiplied 2; for a smaller fall-off rate of the effect of ICMS on excitation to the lateral inhibitory pathways, the value of σ_5 in Section 6.3.1 was multiplied by 2; and for a larger baseline excitation to the lateral inhibitory pathways, the value of ϕ_2 used in Section 6.3.1 was multiplied by 2.

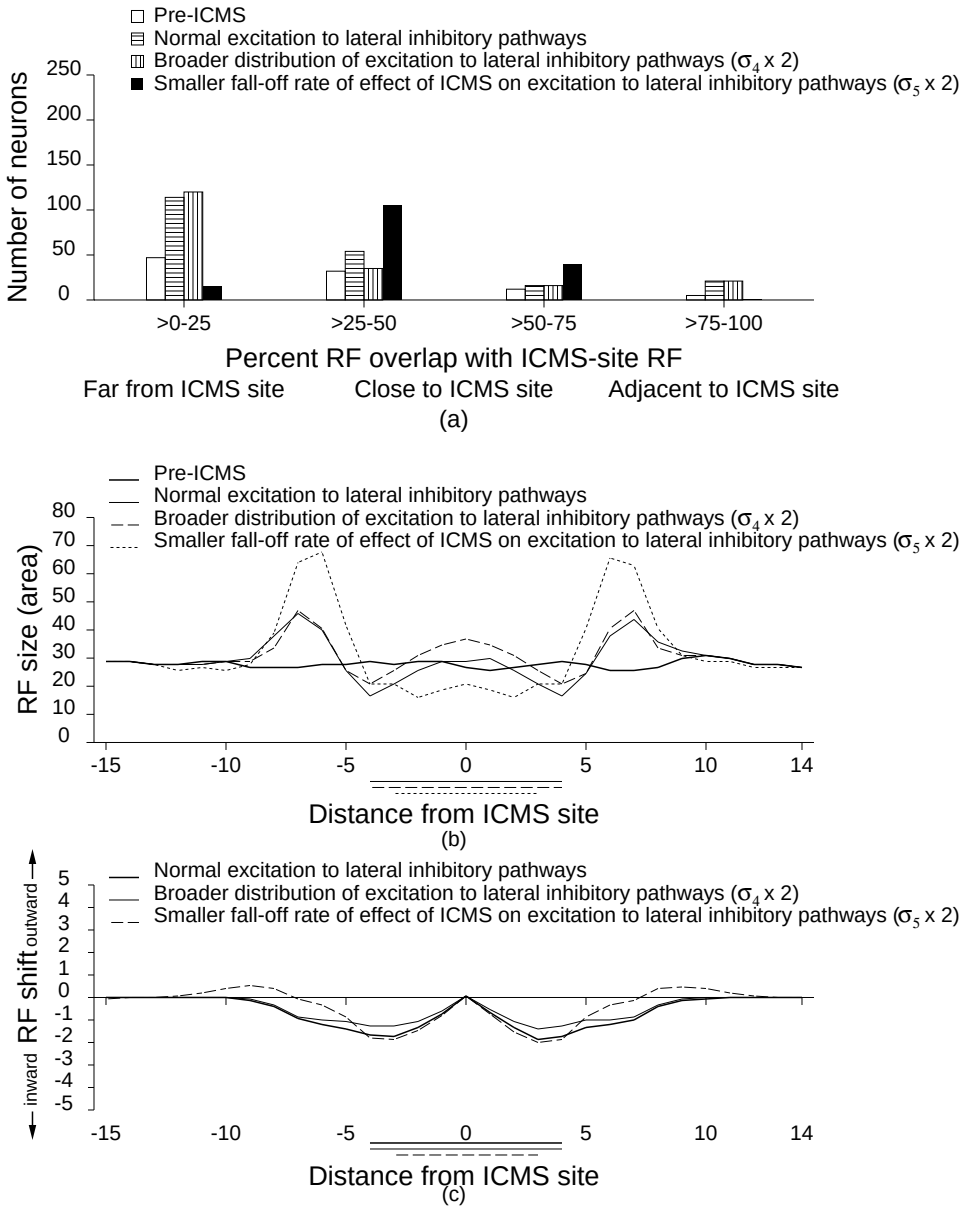

Figure 6.30: **Effects of distribution of presynaptic stimulation of lateral inhibitory pathways during ICMS on model RF topography and RF size.**
Some of the effects of varying the parameters controlling the distribution of presynaptic stimulation of lateral inhibitory pathways during ICMS are shown. The parameter values used in these simulations are given in Figure 6.29. See Figure 6.22 for conventions.

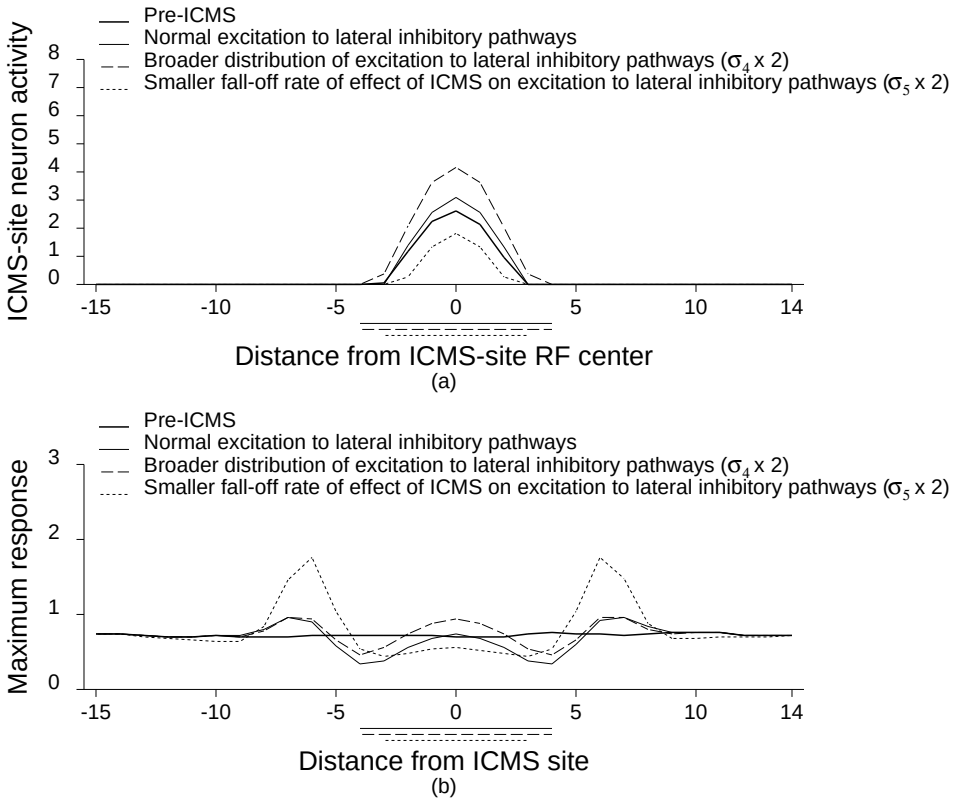

Figure 6.31: **Effects of distribution of presynaptic stimulation of lateral inhibitory pathways during ICMS on model responsiveness.**
The parameter values used in these simulations are given in Figure 6.29. See Figure 6.23 for conventions.

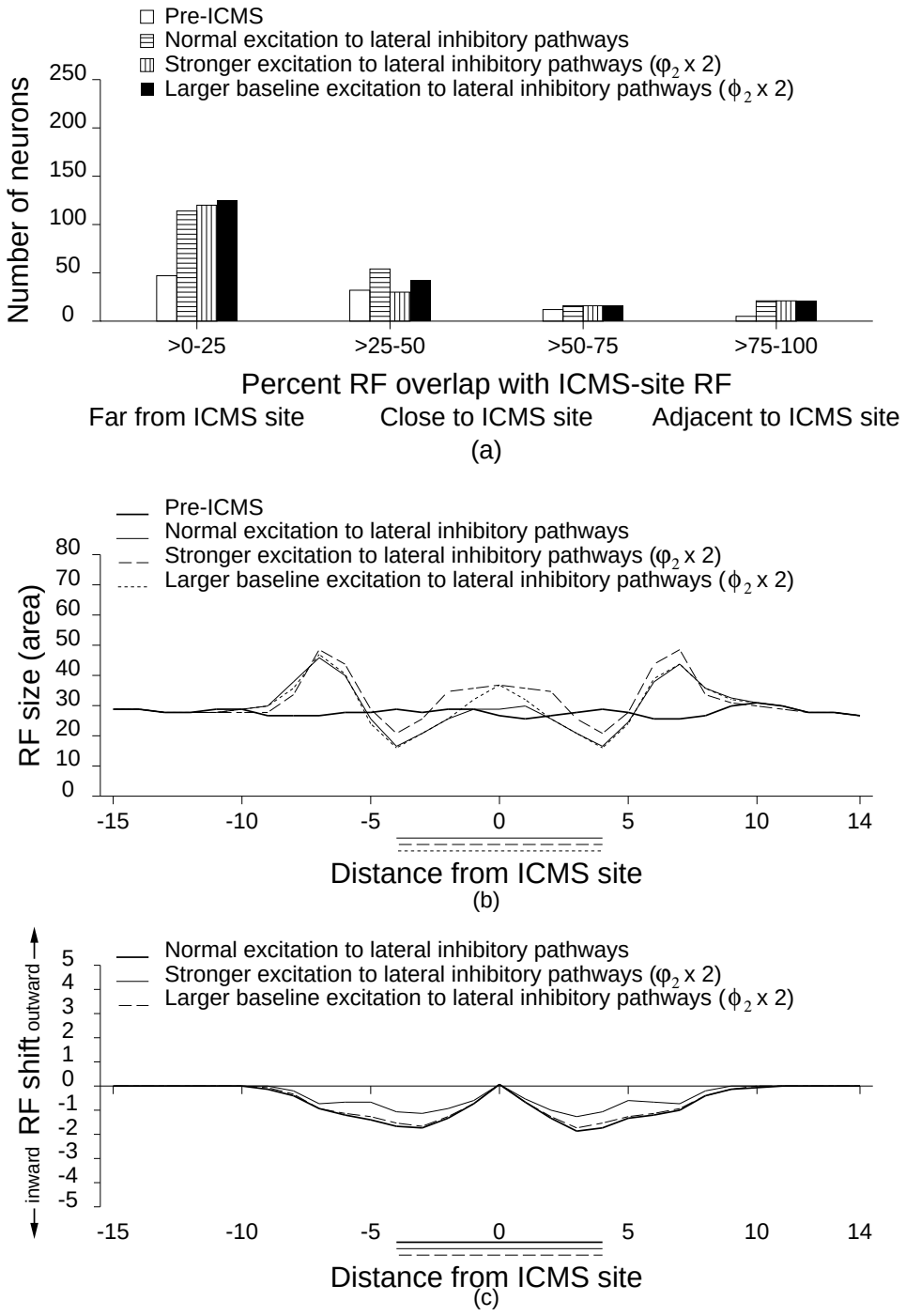

Figure 6.32: **Effects of distribution of presynaptic stimulation of lateral inhibitory pathways during ICMS on model RF topography and RF size.**
The parameter values used in these simulations are given in Figure 6.29. See Figure 6.22 for conventions.

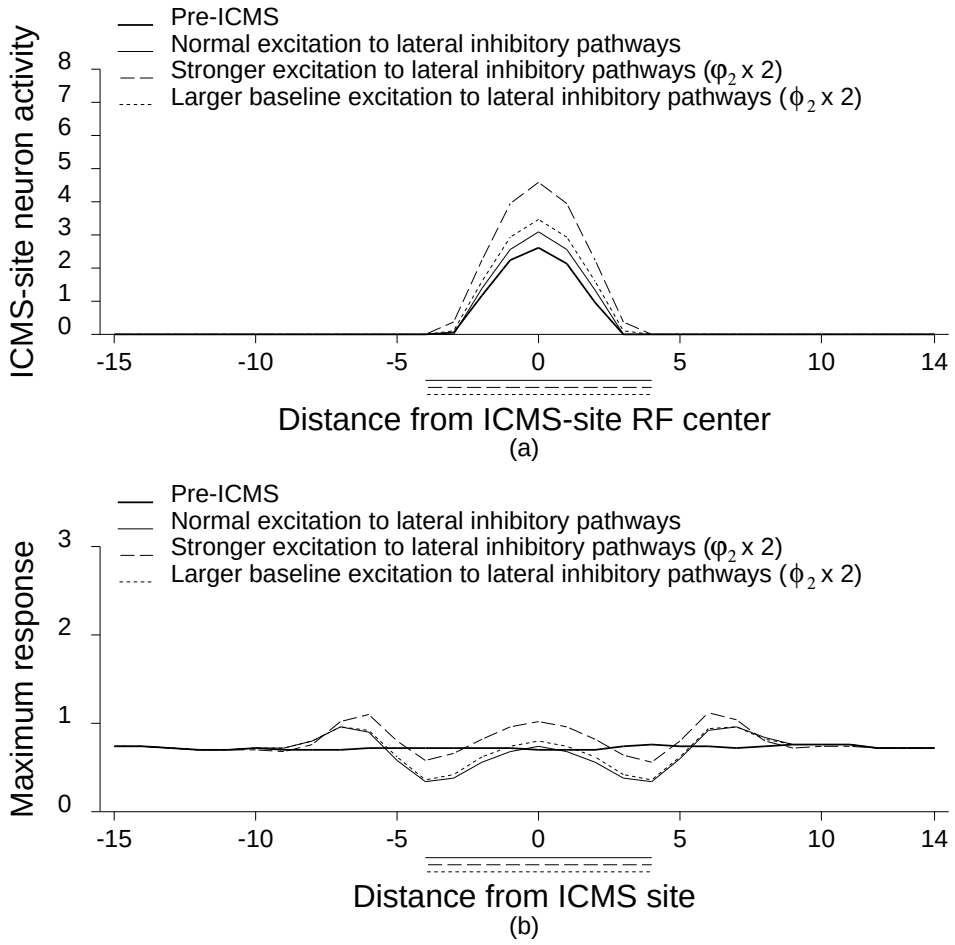

Figure 6.33: **Effects of distribution of presynaptic stimulation of lateral inhibitory pathways during ICMS on model responsiveness.**
The parameter values used in these simulations are given in Figure 6.29. See Figure 6.23 for conventions.

responsiveness to test stimuli change (Figures 6.30b and 6.32b).

Changes in the parameters controlling the strength and distribution of stimulation of the lateral inhibitory pathways directly affect the activation level of the model cortical neurons. As the activation of the ICMS-site neuron in the initial stage of ICMS increases, the RF size of the ICMS-site neuron and the ICMS-site neuronal responsiveness to test stimuli after ICMS decrease (Figures 6.29, 6.30 – 6.33). As activation of the ICMS-site neuron in the initial stage of ICMS increases, the lateral inhibitory pathways to the ICMS-site neuron strengthen according to the EXIN lateral inhibitory synaptic plasticity rule, thereby reducing the ICMS-site neuron's RF size and responsiveness to the test input.

The relationship between the activation of the ICMS-site neuron in the initial stage of ICMS and the various parameters in Equation 6.3 are as follows. The activation of the ICMS-site neuron decreases (Figure 6.29) as the distribution of the stimulation strength of the lateral inhibitory pathways to the model cortical neurons is broadened (i.e., σ_4 in Equation 6.3 is increased) because increasing σ_4 increases the effect of lateral inhibition to the ICMS-site neuron (Equation 6.10). The activation of neurons close to the ICMS site increases (Figure 6.29) as the fall-off rate of the strength of the ICMS on inhibitory pathways is reduced (i.e., σ_5 in Equation 6.3 is increased), because inhibition to the ICMS-site neuron caused by stimulation of the lateral inhibitory pathways remains constant but the inhibition to neurons surrounding the ICMS site caused by stimulation of the lateral inhibitory pathways increases, thereby decreasing the activation of the surrounding neurons. As the activation of the surrounding neurons decreases, they exert less inhibition on the ICMS-site neuron, leading to an increase in the activation of the ICMS-site neuron. As the stimulation strength of the lateral inhibitory pathways increases (i.e., φ_2 in Equation 6.3 is increased) or as the baseline stimulation strength of the lateral inhibitory pathways increases (i.e., ϕ_2 in Equation 6.3 is increased), inhibition to the ICMS-site neuron increases (Equation 6.10), and therefore the activation of the ICMS-site neuron decreases (Figure 6.29).

When σ_5 in Equation 6.3 was increased, the increased inhibition to neurons far from the ICMS site kept those neurons inactive during ICMS, and according to the EXIN lateral inhibitory synaptic plasticity rule the lateral inhibitory pathways to those inactive neurons weakened. The weakening of the lateral inhibitory pathways to the distant

neurons, which were inactive during ICMS, made these neurons highly responsive to test stimuli (Figure 6.31b). Such high responsiveness of these neurons resulted in large inhibition to the surrounding neurons farther away from the ICMS site, and their RF shifted away from the pre-ICMS ICMS site RF (Figure 6.30c).

6.3.3 The effects of RF scatter during ICMS

In the earlier simulations, the RFs of the model cortical neurons were topographically arranged. In this simulation, ICMS was performed in a network with initial RF scatter and non-uniform RF sizes (Figure 6.34). The parameters used were the same as those used in the simulation presented in Section 6.3.1. The procedure for producing the network with RF scatter is described in Appendix D, Section D.2.

With RF scatter in the initial RF topography, the model reproduced all the qualitative aspects of the effects of ICMS (Figures 6.35–6.37). In particular, the model produced sharp discontinuities at some positions where a region containing neurons whose RFs overlap the ICMS-site RF abuts another in which the RFs of the neurons do not overlap the ICMS-site RF (Figure 6.35).

In this simulation, the RF size, position, and responsiveness of the ICMS-site neuron changed (Figures 6.36–6.37). This happened because the most strongly activated model thalamocortical afferents during ICMS were not the thalamocortical afferents that had the strongest synapses with the ICMS-site neuron.

6.3.4 The effects of peripheral stimulation

The effects of repetitive peripheral stimulation of a restricted skin region were modeled using lateral inhibitory plasticity and varying peripheral stimulation strength (see Section 6.4.1). The results of Jenkins et al. (1990) were modeled by assuming that strong peripheral stimulation was used (Figure 6.38a), producing strong activation in the cortical neurons (Figure 6.38b). The changes in RF topography reported by Recanzone et al. (1992b) were modeled by weak peripheral stimulation (Figure 6.38cd).

Jenkins et al. (1990) simulated fingers of monkeys using a rotating disk with wedge-shaped indentations. The monkeys were required to keep their fingers in contact

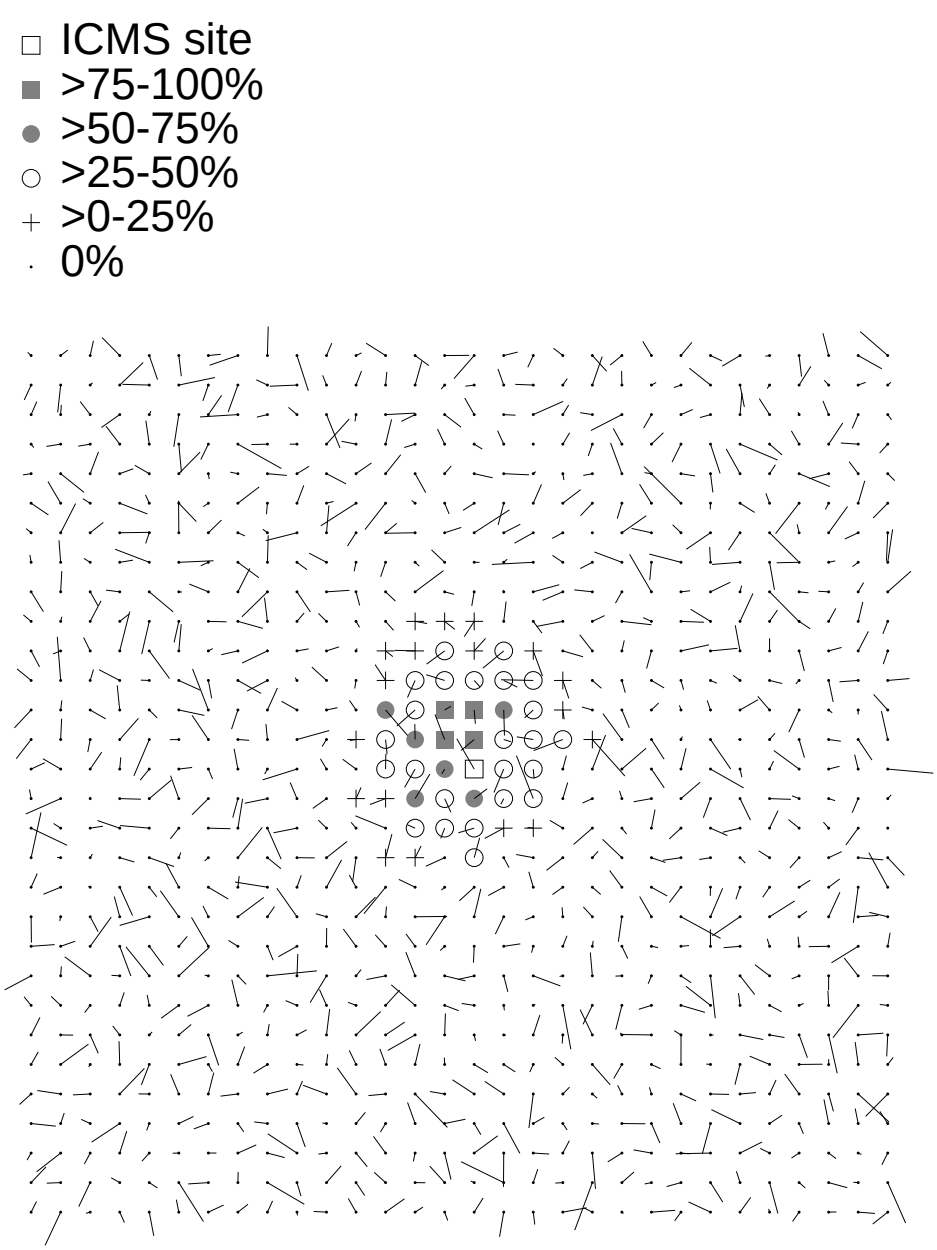

Figure 6.34: **Initial model cortical RF topography in the scatter simulation.** The figure shows scatter in the model cortical RFs after a training phase. The center of the symbols in the legend represent the expected position of the center of the RF of model cortical neurons based on topographically arranged RFs. The line segments represent the shift in the center of the RF of the model cortical neurons away from the expected RF center.

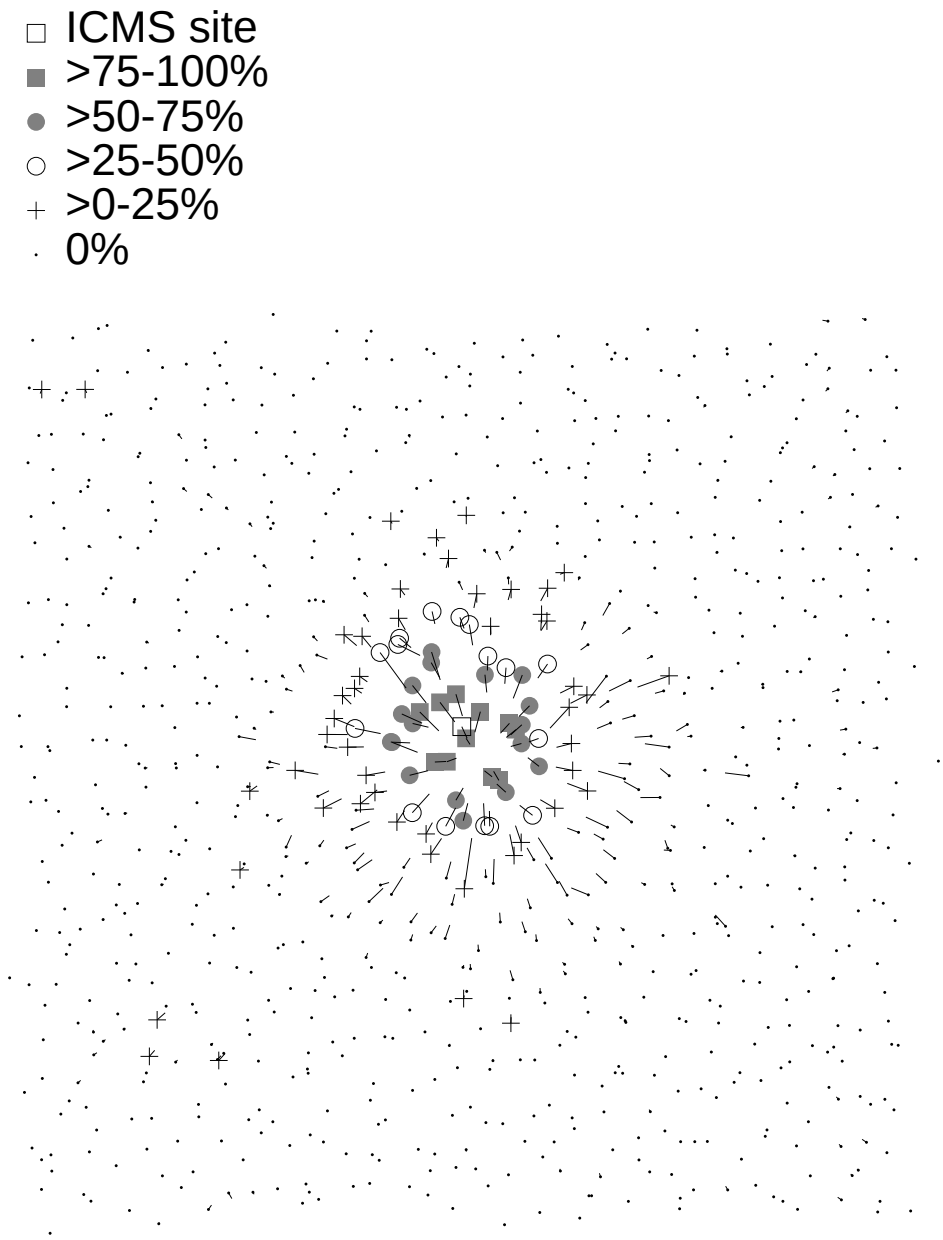

Figure 6.35: **Changes in RF topography after ICMS in a network with RF scatter.** Model ICMS was applied in a network whose initial RFs were not topographically arranged. See Figure 6.11 for conventions.

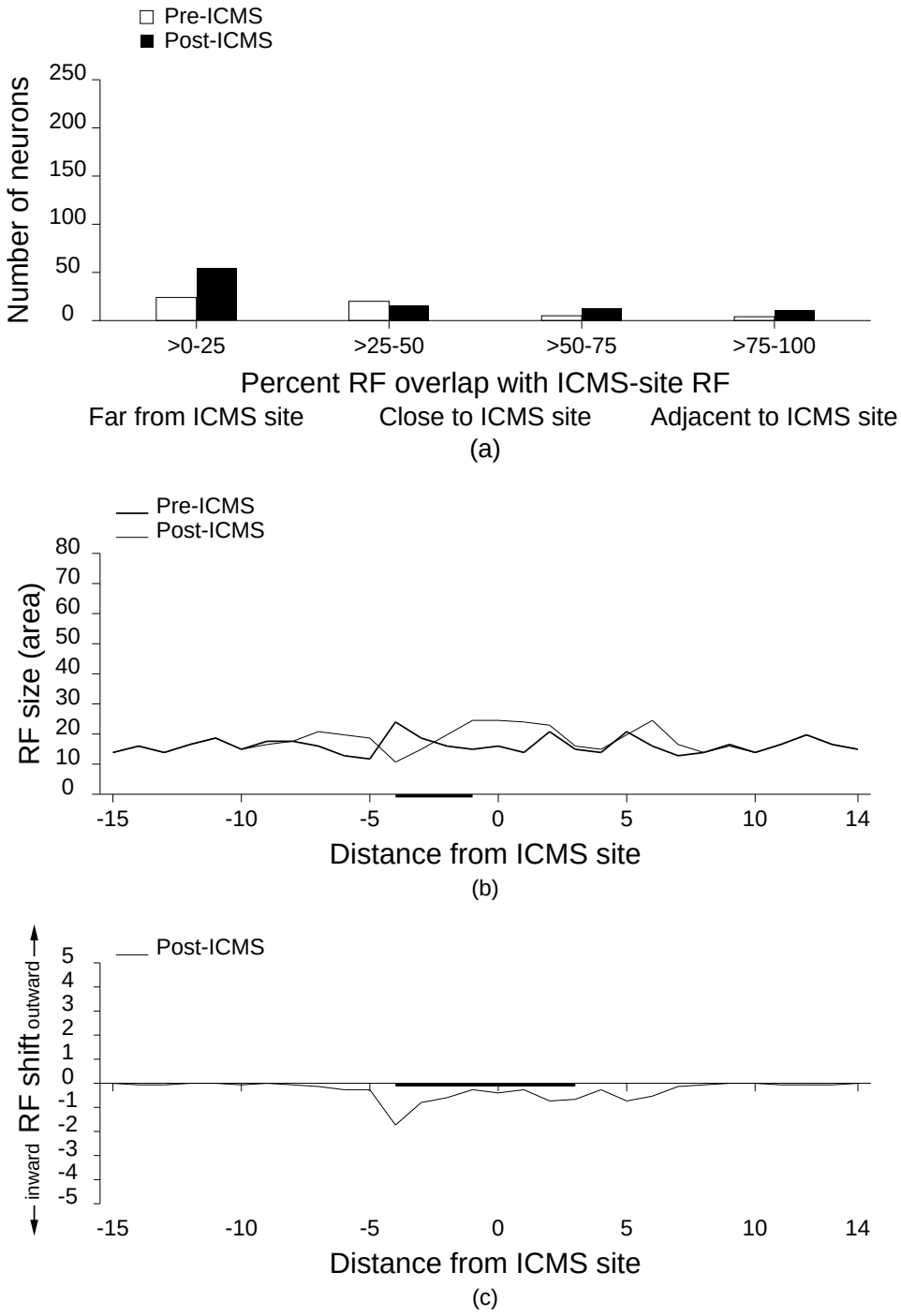

Figure 6.36: **Changes in RF properties in a model network with RF scatter.** Model ICMS was applied in a network with RF scatter. The model ICMS parameters were the same as those used in the simulation in Section 6.3.1. The ICMS was presented 500 times. See Figure 6.12 for conventions.

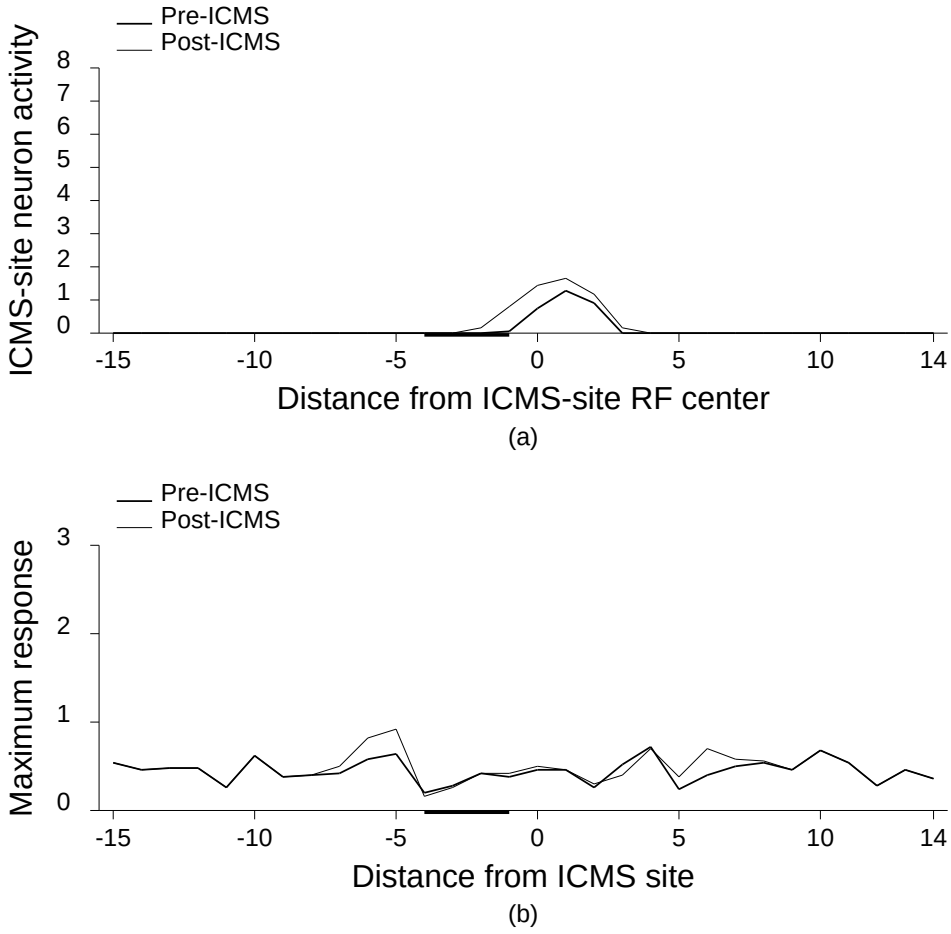

Figure 6.37: **Changes in responsiveness in a model network with RF scatter.** The model ICMS parameters were the same as those used in the simulation in Section 6.3.1. See Figure 6.9 for conventions.

with the rotating disk. Because of the grooves on the disk it was difficult to maintain contact with the disk. Initially, the monkeys pressed their fingers to the disk very strongly causing their hands to be dragged by the rotating disk. Gradually, they learned to control the contact pressure to maintain contact with the rotating disk. Thus, the rotating disk may have stimulated a large skin region. Furthermore, mechanoreceptors are much more strongly activated by moving surfaces than flat stationary surfaces, and a larger proportion of cutaneous mechanoreceptors are activated by moving ridged surfaces than flat stationary surfaces (Jenkins et al., 1990). On the other hand, Recanzone et al. (1990acde) used a tactile probe with a 2 mm diameter and a rounded tip. The probe was vibrated sinusoidally at a fixed frequency. The stimulation was applied to a fixed skin region and was applied with a constant small force of about 6–10 gram weight. The area of the tactile probe used by Recanzone et al. (1992acde) was smaller than the RF size of the somatosensory cortical neurons. Thus, the stimulation procedure employed by Jenkins et al. (1990) could have strongly stimulated a large skin region than the procedure used by Recanzone et al. (1992acde).

When the input was a strong local stimulation, model cortical neurons were strongly activated (Figure 6.38b). During conditioning, the lateral inhibitory pathways between the strongly active neurons strengthened, and lateral inhibitory pathways from active neurons to inactive neurons weakened. This caused a decrease in the RF size of the neurons activated by the conditioning input and an increase in the number of neurons responsive to the conditioning input (Figures 6.40–6.42). These results are qualitatively similar to those reported by Jenkins et al. (1990).

When the input was a weak local stimulation, model cortical neurons were weakly activated (Figure 6.38d). During conditioning, the lateral inhibitory pathways between the weakly active neurons weakened, and the lateral inhibitory pathways from active neurons to inactive neurons also weakened. This caused an increase in the RF size of the neurons activated by the conditioning input and an increase in the number of neurons responsive to the conditioning input (Figures 6.40–6.42). These results are qualitatively similar to those reported by Recanzone et al. (1992b).

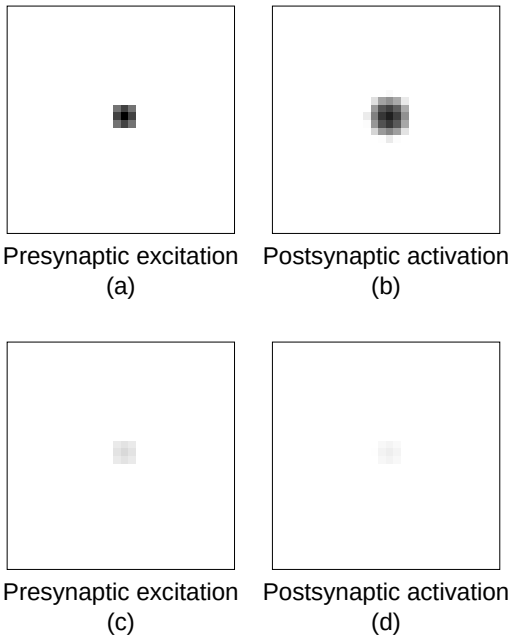

Figure 6.38: **Spatial distribution of presynaptic excitation and postsynaptic activation in model during peripheral stimulation.**
(a) Strong local peripheral stimulation distribution centered at $(0,0)$. (b) Initial postsynaptic activation of model cortical neurons caused by strong peripheral stimulation. (c) Weak local peripheral stimulation distribution centered at $(0,0)$. The weak local peripheral stimulation was 0.15 times the one used in (a). (d) Initial postsynaptic activation of model cortical neurons caused by weak peripheral stimulation.

6.3.5 Changes in stimulus discrimination after peripheral stimulation

Monkeys improved their performance in a tactile frequency discrimination task after training (Recanzone et al., 1992a). The improvement occurred gradually over several weeks (3–20) of training. The task involved discriminating a stimulus with 20 Hz stimulation frequency (the standard stimulus) from stimuli with more than 20 Hz stimulation frequency (the comparison stimuli). During training the standard stimulus was presented more frequently than the others. The standard stimulus was presented in every trial followed by a brief pause. After the pause, 1 to 5 stimuli were presented, of which one had stimulation frequency greater than 20 Hz. The monkey was required to maintain contact while the standard stimulus was presented, but was conditioned to break contact with the stimulus

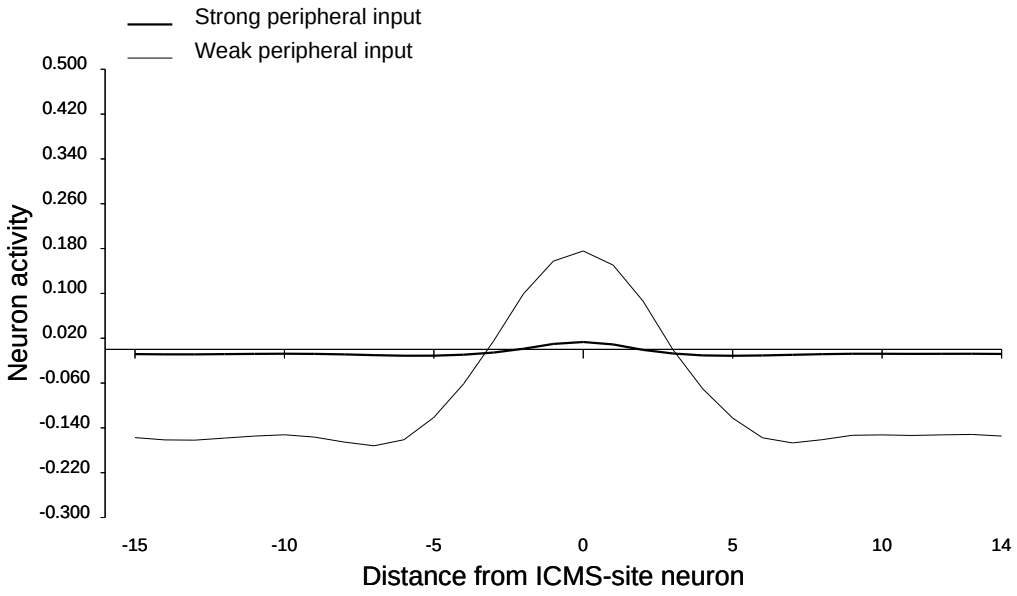

Figure 6.39: **Changes in activation of model neurons caused by variations in peripheral stimulation strength.**
The activation of a cross-section of the model cortical layer neurons, neurons $(0,-15)$–$(0,14)$, in the initial stage of peripheral conditioning, is shown as the strength of the peripheral stimulus is varied. Strong local peripheral stimulation was the Gaussian K (Appendix D, Section D.5) centered at $(0,0)$. Weak local peripheral stimulation was $0.15 \times K$.

if its stimulation frequency was greater than 20 Hz. The probability of occurrence of the comparison stimuli was small (≈ 0.388).

In the simulations, tactile frequency selectivity was not incorporated. Therefore, instead of tactile frequency discrimination, the stimulus position discrimination of the model was analyzed. The frequency of tactile stimulation can be encoded by distribution of activity in input fibers innervating mechanoreceptors. Mechanoreceptors in the skin have different temporal properties. The rapidly adapting (RA) mechanoreceptors respond selectively to high-frequency tactile stimulation and the slowly adapting (SA) mechanoreceptors convey information about constant pressure applied to skin. Thus, the frequency of tactile stimulation at a particular location is encoded in the distribution of activity in the fibers innervating the RA and SA receptors. Furthermore, the fibers from RA and SA mechanoreceptors terminate in adjacent positions in the somatosensory cortex. Thus,

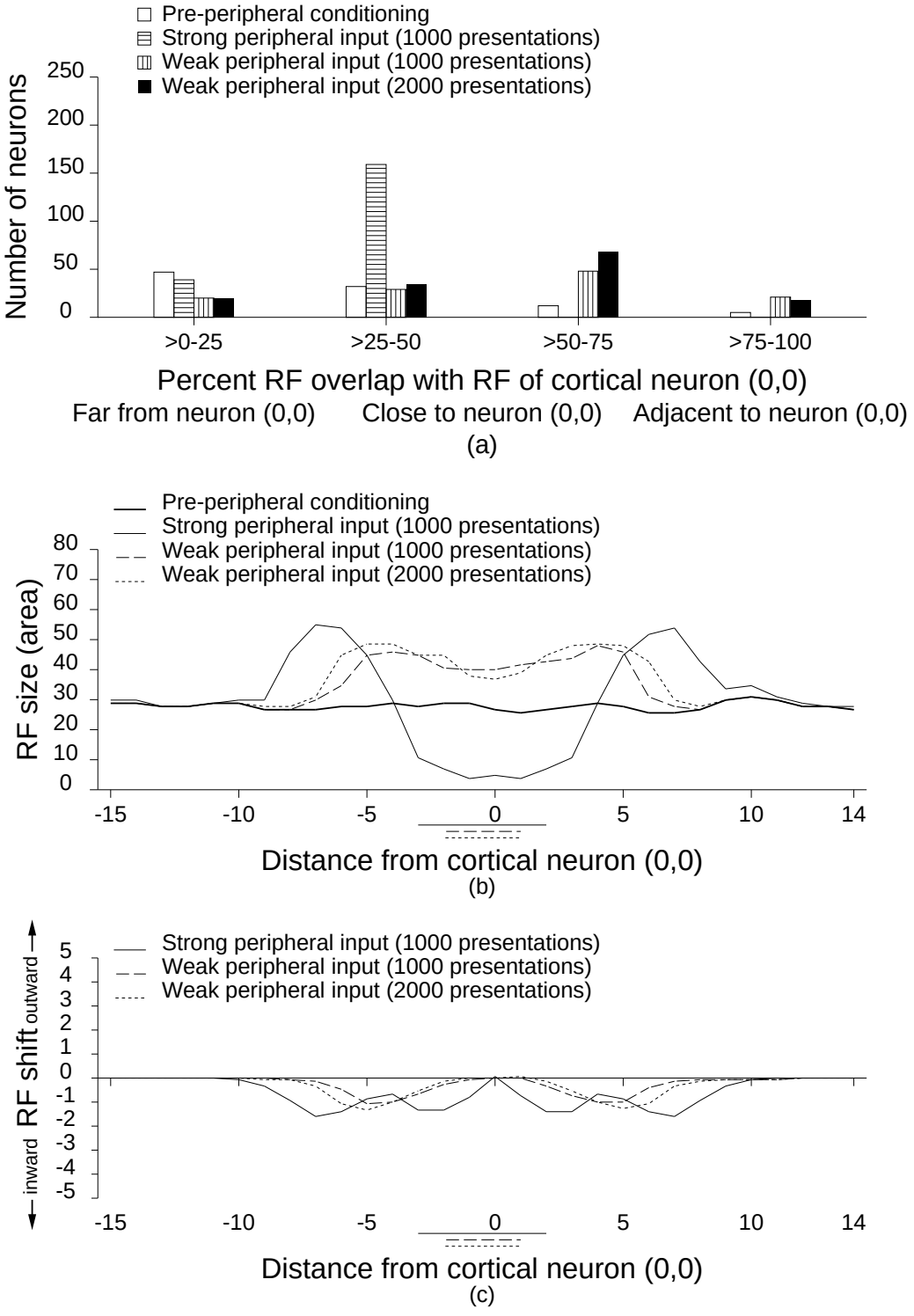

Figure 6.40: Legend on next page.

Figure 6.40: **Changes in model RF properties caused by peripheral stimulation.** Figure on previous page. In this simulation, the peripheral stimulation was centered at Layer 1 position $(0,0)$. Before conditioning the conditioning stimuli evoked the highest activation in Layer 2 neuron $(0,0)$. The stimulus used for measurement of RF properties was also used as the strong peripheral stimulus. The weak peripheral stimulus was 0.15 times the stimulus used for measurement of RF properties. See Figure 6.12 for conventions. The line segments parallel to the abscissa represent the neurons that were active during the initial stage of the two peripheral conditioning simulations.

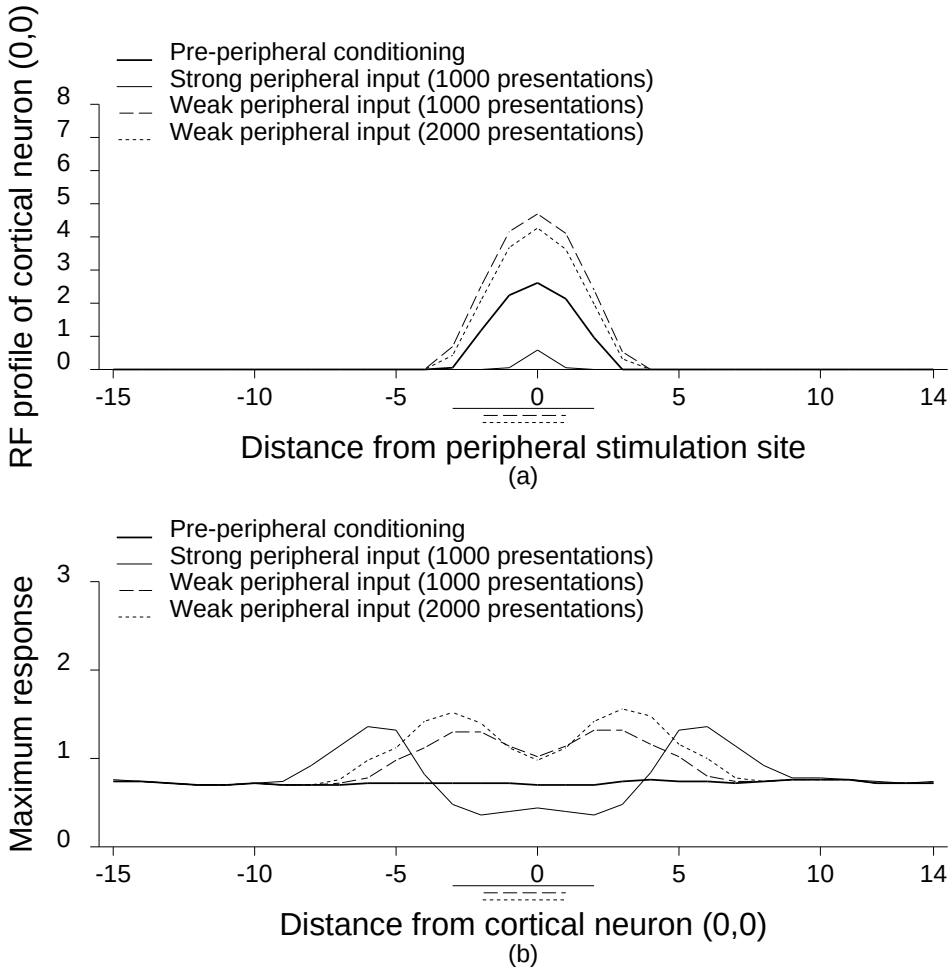

Figure 6.41: **Changes in model neuron responsiveness caused by peripheral stimulation.**
Simulation details are presented in Figure 6.40. See Figure 6.9 for conventions. The line segments parallel to the abscissa represent the neurons that were active during the initial stage of the two peripheral conditioning simulations.

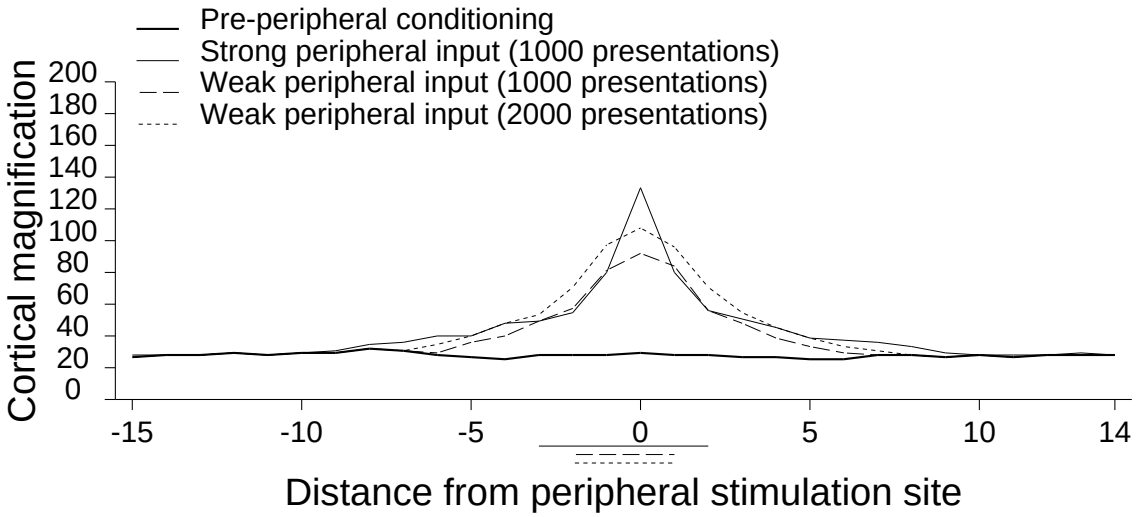

Figure 6.42: **Changes in model cortical magnification caused by peripheral stimulation.**
See Figure 6.40 for simulation details. Cortical magnification was computed as the number of neurons responsive to the test stimulus at each input location. The figure shows the cortical magnification of a cross-section of the input layer through the peripheral stimulation site, input positions from $(0, -15)$ to $(0, 14)$, before and after peripheral conditioning. The line segments parallel to the abscissa represent the neurons that were active during the initial stage of the two peripheral conditioning simulations.

changes in the frequency of a tactile stimulation changes the input distribution to adjacent neurons in the somatosensory cortex. This is similar to varying the position of the input in the model.

In the simulations, a conditioning stimulus was presented at a single position in the input layer. The peripheral stimulation used in the simulations is an abstraction of the stimulation procedure used in Recanzone et al. (1992a) because the conditioning stimulation was presented at only one position. Peripheral comparison stimuli were presented at other locations during the discrimination test phase, during which synaptic plasticity in the model was disabled.

Changes in position discrimination were modeled by lateral inhibitory synaptic plasticity. Figure 6.43 shows that discrimination between the conditioned input position and other test positions close to the conditioning site increased after training. The parameters

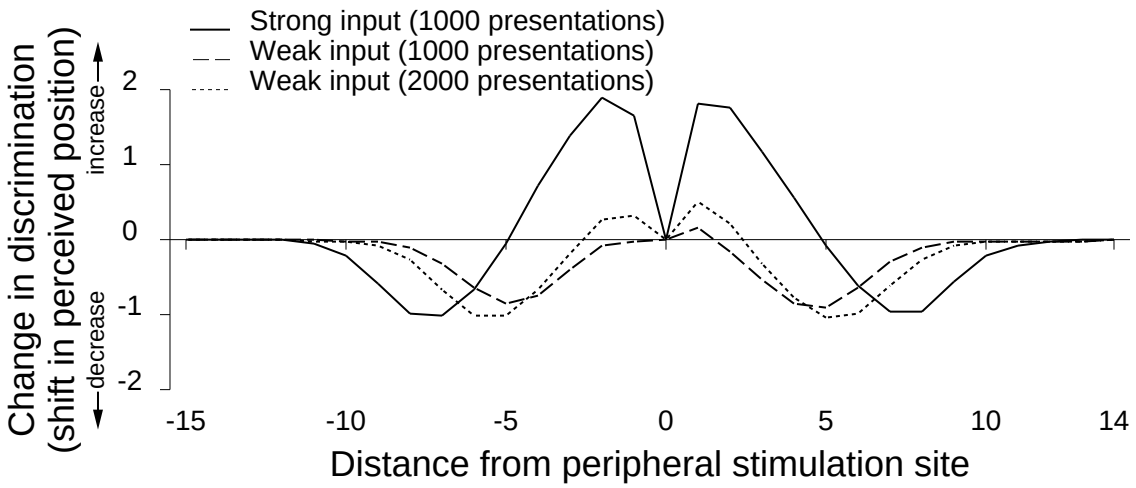

Figure 6.43: **Changes in position discrimination after peripheral stimulation.** Each model cortical neuron was assumed to code a particular position which was the centroid of its RF. The centroid was computed by weighting each input position by the response of the cortical neuron to test stimulus at that position. The position of the test stimulus was interpreted from cortical activation produced by input stimulation by determining the centroid of the distribution of cortical activity in the input space; the centroid was computed by weighting the preferred position of each model cortical neuron by its activation in response to the test stimulus. As the amount of overlap in the distributions of cortical activation produced by inputs at different positions decreases, i.e., distance between the centroids of cortical activation distributions increases, the chances of making errors in distinguishing the two positions because of noise in the neuronal activations decrease. Thus, position discrimination increases. In the simulations, the change in discrimination was computed as the difference between the "perceived" position of the test stimuli after conditioning and the "perceived" position of the test stimuli before conditioning. Increase in discrimination represents a shift in the "perceived" position away from the conditioning site; decrease represents a shift towards the conditioning site.

used in these simulations were the same as those used in the previous section (Section 6.3.4). The increase in position discrimination was obtained after stimulating the standard input position with strong and weak stimuli. The position discrimination was determined using the stimulus that was used to map the RF of the model cortical neurons. In the model, increase in position discrimination occurred with increase or decrease in the RF size and responsiveness of model cortical neurons initially responsive to conditioning stimulation at the conditioning site (Figures 6.40 and 6.41).

In the simulations, position discrimination between the conditioning site and input positions close to the conditioning site increases because model cortical neurons selective for positions surrounding the conditioning site become more responsive to positions close to the conditioning site *relative* to the responsiveness of neurons which were highly responsive to stimulation at the conditioning site. Therefore, test stimulation at positions close to conditioning site activates neurons whose initial RFs were farther from the conditioning site more strongly relative to the neurons whose RFs were closer to the conditioning site. This causes the "perceived" test stimulus position to shift farther away from the actual test stimulation site. Thus, even a small shift in the position of the test stimulus from the conditioning site causes a large difference in the "perceived" position of the test stimulus.

In the simulations, input positions at which position discrimination increased were surrounded by positions at which position discrimination decreased (Figure 6.43). Test stimulation at positions where position discrimination decreased caused model cortical neurons responding to the test stimulus and closer to the cortical neurons selective for the conditioning site to be more active than the neurons responding to the test stimulus and farther from the neurons selective for the conditioning site. This occured because the EXIN lateral inhibitory synaptic plasticity rule caused a large weakening in lateral inhibitory pathways from the active neurons to weakly active/inactive neurons whose RFs overlap with the RFs of the active neurons, i.e., neurons close to the neurons selective for the conditioning site. According to the EXIN lateral inhibitory synaptic plasticity rule, plasticity is enabled only when the presynaptic neuron is active, and the strength of lateral inhibitory synaptic weights becomes proportional to the amount of overlap in the RFs of neurons (Marshall, 1995a). Thus, during peripheral stimulation the lateral

inhibitory pathways from the active neurons to weakly active/inactive neurons weaken, and maximal weakening occurs in lateral inhibitory pathways from the active neurons to weakly active/inactive neurons whose RFs have large overlap with the the RFs of the active neurons. Lateral inhibitory pathways to neurons whose RFs have little overlap with the RFs of the active neurons are very weak and therefore undergo very little change.

Gilbert and Wiesel (1990) showed that the perception of oriented test bars was repelled from a standard oriented bar; i.e., the discrimination between the test and the standard orientation increased, if one of the followed occurred: (1) reduction in the responsiveness of neurons selective for the standard orientation, (2) shift in the peak of the orientation tuning of model neurons towards the standard orientation, (3) broadening of orientation tunings of neurons different from the one selective for the standard orientation, or (4) sharpening of the orientation tuning of neurons selective for the standard orientation. In addition, the discrimination between the test and the standard orientation decreased if (1) responsiveness of neurons selective for orientations different from the standard orientation was reduced relative to the responsiveness of neurons selective for the standard orientation or (2) the peak of the orientation tuning of model neurons shifted away from the standard orientation.

In the case of peripheral conditioning with the strong input, increase in position discrimination occurred because of (1) decrease in responsiveness and RF size of neurons selective for the conditioning site (Figures 6.40 and 6.41), (2) RF expansion of neurons surrounding the neurons selective for the conditioning site (Figure 6.40), or (3) shift in the RF of neurons surrounding the neurons selective for the conditioning site towards the conditioning site (Figure 6.40).

In the case of peripheral conditioning with weak input, an increase in position discrimination occurred because of (1) RF expansion of neurons surrounding the neurons selective for the conditioning site (Figures 6.40) and (2) shift in the RF of neurons surrounding the neurons selective for the conditioning site towards the conditioning site (Figure 6.40). The increase in discrimination between the conditioning site and nearby positions produced after conditioning with the weak stimulus was small because the RF size and responsiveness of neurons selective for the conditioning site increased

(Figures 6.40 and 6.41), thereby reducing discrimination (Gilbert & Wiesel, 1990). It is clear from Figure 6.43 that the increase in position discrimination increased with training.

Thus, the EXIN lateral inhibitory synaptic plasticity rule can improve discrimination of test tactile stimulation frequency from the training tactile stimulation frequency. Furthermore, the model predicts that tactile stimulation frequencies far from the training frequency will be perceived to be closer to the training frequency.

6.4 Discussion

Computer simulations of the EXIN network with afferent excitatory and lateral inhibitory synaptic plasticity have qualitatively reproduced aspects of changes in somatosensory cortical RFs in adult animals following ICMS and repetitive stimulation of localized skin region. To closely model RF changes after ICMS, especially the lack of RF changes at the ICMS site, it was assumed that ICMS excites afferent terminals branching from afferent pathways close to the ICMS site more strongly than those arising from afferent pathways far from the ICMS site (Section 6.2.2). To model the effects of restricted peripheral stimulation, the EXIN lateral inhibitory synaptic plasticity rule was sufficient (Section 6.3.4). The EXIN network that had topographically arranged initial RFs exhibited the following RF changes after ICMS, consistent with experimental data:

- a large increase in the number of neurons responsive to the pre-ICMS ICMS-site RF;
- almost no change in RF size and responsiveness of the ICMS-site neuron;
- substitution of the ICMS-site RF for the former RF of surrounding neurons;
- RF expansion in some neurons and contraction in others; and
- RF shift towards the ICMS-site RF in neurons close to the ICMS site and RF shift away from the ICMS-site RF in neurons far from the ICMS site.

However, to model discontinuous cortical representation of the ICMS-site RF, RF scatter in the initial RF topography was introduced (Section 6.3.3).

The EXIN network with lateral inhibitory plasticity alone modeled some of the RF changes caused by peripheral stimulation. With weak peripheral stimulation, the model produced an increased cortical representation of the stimulated input region and expanded the RF of model cortical neurons responsive to the stimulated input region, consistent with the results of Recanzone et al. (1992d). Increased cortical representation of the stimulated skin region with decreased RF size of the neurons representing the skin region following peripheral stimulation (Jenkins et al., 1990) was modeled by presenting strong peripheral stimulation to the model. Furthermore, in the model, peripheral stimulation with weak and strong stimuli improved the discrimination between a stimulus placed at the conditioning site and a stimulus placed at positions close to the conditioning site.

The RF changes after peripheral stimulation have previously been explained by afferent excitatory plasticity (Grajski & Merzenich, 1990; Recanzone et al., 1992d). Some experiments to determine the relative possible influence of afferent excitatory and lateral inhibitory plasticity on RF changes during ICMS and peripheral stimulation are suggested in Section 6.4.5.

Several weeks of training monkeys in a frequency discrimination task affected somatosensory cortical area 3a (Recanzone et al., 1992c). Neurons in area 3a usually do not respond to the stimulation of skin surface, but these neurons respond specifically to pressure on muscles, to muscle stretching, or to movement of the joints – "deep inputs" (Powell & Mountcastle, 1959). Frequency discrimination training resulted in the emergence of responsiveness to stimulation of the skin surface in area 3a neurons and loss of responsiveness to parts of the neurons' deep input RF (Recanzone et al., 1992c). The emergence of new responsiveness to tactile stimulation can be explained by weakening of lateral inhibitory pathways in area 3a, thereby making the neurons responsive to previously subthreshold tactile stimulation (Kang et al., 1985; Iwamura et al., 1993). In fact, several experiments have shown emergence of new responsive zones in neurons after cortical infusion of GABA antagonists (e.g., Lane et al., 1997; Sillito et al., 1981). But withdrawal of inhibition cannot explain the concomitant loss of responsiveness to deep inputs with the emergence of responsiveness to tactile inputs, because withdrawal of inhibition would make neurons in area 3a more responsive both to deep inputs and to tactile inputs.

The above objection is not applicable to the EXIN lateral inhibitory synaptic plasticity rule. Because of the asymmetry of the EXIN lateral inhibitory rule, it is possible that some area 3a neurons become less responsive to deep inputs. The explanation based on the EXIN lateral inhibitory synaptic plasticity rule is as follows. As neurons in area 3a with slight sensitivity to tactile input are weakly activated during peripheral training, lateral inhibitory pathways into the neuron from other weakly active neurons weaken, thereby making the neurons more responsive to tactile stimulation. Lateral inhibitory pathways to inactive area 3a neurons from active neurons weaken, but the lateral inhibitory pathways from inactive to other neurons do not change. Thus, neurons that were insensitive to tactile stimulation become highly responsive to deep inputs. This results in more inhibition to neurons that were weakly active during conditioning with tactile stimulation, when deep inputs are stimulated, thereby reducing the responsiveness of neurons that were weakly active during tactile stimulation to deep inputs. Thus, neurons that were weakly active during tactile stimulation become more responsive to tactile stimulation and less responsive to deep input stimulation.

6.4.1 Explanation of the RF changes during ICMS and peripheral stimulation

These subsections describe how the model exhibits changes in RF properties.

Explanation of the effects of ICMS

In the EXIN network, the synaptic plasticity rules depend on the locally available pre- and post-synaptic activations and the weight at synaptic junctions. Therefore, during ICMS, afferent excitatory synaptic plasticity occurs even though model thalamic neurons are not activated, and lateral inhibitory synaptic plasticity is enabled when the presynaptic inhibitory pathway terminal is excited from ICMS or from presynaptic activated.

During ICMS the following synaptic modifications occur in the EXIN model.

1. The EXIN inhibitory synaptic plasticity rule weakens the active lateral inhibitory

pathways to inactive or very weakly active neurons. This weakening of inhibitory weights to the initially inactive/weakly active neurons allows these neurons to respond to the excitation they receive via anti- and orthodromically activated excitatory afferents. According to the EXIN afferent excitatory synaptic plasticity rule, afferent excitatory pathway weights to inactive neurons do not change. The decreased inhibition to inactive or very weakly active neurons, combined with the lack of change in afferent excitatory pathway weights to inactive or very weakly active neurons, causes an expansion in RF size of these neurons, an increase in their responsiveness, and an increase in the amount of overlap of their RF with the pre-ICMS ICMS-site RF. During ICMS the lateral inhibitory pathways from neurons close to the ICMS site are more strongly activated by ICMS than lateral inhibitory pathways from neurons far from the ICMS site (Section 6.2.2). Also, synaptic plasticity in the lateral inhibitory pathways from neurons close to the ICMS site is enabled because of activation of neurons close to the ICMS site (Equation 6.5). Since the rate of change in the lateral inhibitory weights is controlled by presynaptic activation in the outstar lateral inhibitory synaptic plasticity rule (Equation 6.5), the lateral inhibitory pathways from neurons close to the ICMS site weaken more than the lateral inhibitory pathways from neurons far from the ICMS site. This asymmetry causes the RF of the inactive/weakly active neurons to shift *toward* the ICMS-site RF.

2. According to the EXIN afferent excitatory synaptic plasticity rule, the active cortical neurons during ICMS strengthen excitatory synapses from the strongly active afferents at the ICMS site or the branches of the afferents at the ICMS site and weaken excitatory synapses from weakly active and inactive afferents. During ICMS the RF of the active neurons shift to overlap with the ICMS-site RF, as these neurons strengthen synapses from thalamocortical afferents sensitive to the ICMS-site RF and weaken synapses from thalamocortical afferent that previously strongly excited the neuron. Neurons closest to the ICMS site eventually have a RF almost identical to the ICMS-site RF. These changes produce RF substitution (Recanzone et al., 1992b). If an active neuron weakens most of its initial strong afferent excitatory pathways, its

RF size contracts.

3. In response to the relatively weak activation of neurons close to the ICMS site during ICMS, the lateral inhibitory synaptic plasticity rule causes the lateral inhibitory weights between the active neurons close to the ICMS site to weaken. This weakening of the lateral inhibitory weights to the ICMS-site model cortical neuron balances the increased inhibition caused by increased responsiveness of neurons close to the ICMS site to stimulation of the ICMS-site RF, because of strengthening of afferent excitatory pathways from the ICMS-site RF to the neurons close to the ICMS site according to the afferent excitatory synaptic plasticity rule. This keeps the RF size and responsiveness of the ICMS-site neuron roughly constant.

The EXIN rules, thus exhibit RF substitution, RF expansion, RF contraction, and RF shift similar to those observed by Recanzone et al. (1992b).

Explanation of the effects of peripheral stimulation

In the EXIN network, RF changes in adult animals after peripheral stimulation were modeled with only the EXIN lateral inhibitory synaptic plasticity rule in this chapter.

After repeated stimulation of a restricted skin region, the number of neurons responsive to the stimulated region increased substantially (Jenkins et al., 1990; Recanzone et al., 1992d). Jenkins et al. (1990) reported contraction in RF size of neurons sensitive to the stimulated region. However, Recanzone et al. (1992d) observed RF expansion of neurons coding the stimulated skin region. These apparently contradictory results of Jenkins et al. (1990) and Recanzone et al. (1992d) are modeled using the EXIN lateral inhibitory synaptic plasticity rule, by considering the following cases. These also serve as predictions of the EXIN model.

1. Strong peripheral stimulation. Because of strong peripheral stimulation, the model cortical neurons are strongly activated. According to the EXIN lateral inhibitory synaptic plasticity rule, the inhibitory pathways between strongly activated neurons strengthen. At the same time, the lateral inhibitory pathways from active neurons to inactive neurons weaken. Thus, weakened inhibition to inactive neurons during

stimulation enables these neurons to respond to input at the conditioned region. Hence, the number of neurons responsive to the stimulated region increases. Because the neurons that were activated during conditioning develop stronger inhibitory pathways between one another, their RF size contracts. Thus, strong peripheral stimulation produces RF changes similar to those observed by Jenkins et al. (1990).

2. Weak peripheral stimulation. Weak peripheral stimulation produces low activation of the model cortical neurons. According to the EXIN lateral inhibitory synaptic plasticity rule, the inhibitory pathways between weakly activated neurons weaken. At the same time, the lateral inhibitory pathways from active neurons to inactive neurons weaken. Thus, weakened inhibition to inactive neurons during stimulation enables these neurons to respond to input at the conditioned region. Hence, the number of neurons responsive to the stimulated region increases. Because the neurons that were activated during conditioning have weakened inhibitory pathways between one another, their RF size increases. Thus, weak peripheral stimulation produces RF changes similar to those reported by Recanzone et al. (1992d).

6.4.2 Stability of EXIN networks

Like other competitive learning rules, the EXIN rules do not produce absolutely stable synaptic weights. The stability of the network depends on the input environment. If the input distribution changes for sufficiently long time, the weights change to encode the new statistics. Such instability, reflecting the statistics of the input environment is advantageous at the lower levels of cortical processing; e.g., the cortex can reorganize after cortical or peripheral damage.

The learning rates in competitive learning networks must be kept small enough to allow approximate stability in a statistically stationary input environment, yet large enough to allow plasticity in response to the statistical changes posed by perturbations such as scotomas. Empirically, the EXIN synaptic plasticity rules produce stable fixed points in a stationary input environment, if the rate of learning is sufficiently small (Marshall, 1995a).

6.4.3 Assumptions of the model

Distribution of presynaptic terminal activation during ICMS

To model the effects of ICMS, it was assumed that the thalamocortical afferents terminating on a model cortical neuron were not equally excited. Instead, thalamocortical excitatory afferent terminals that branched from thalamocortical pathways close to the ICMS site were more strongly excited than excitatory afferent terminals from thalamocortical pathways far from the ICMS site (Section 6.2.2). With this assumption it was easy to ensure that the RF properties at the ICMS site did not change after ICMS.

If it were assumed that all presynaptic terminals onto a model cortical neuron are equally stimulated and that the stimulation strength of the presynaptic terminals decreases with increasing distance from the ICMS site, then the EXIN synaptic plasticity rules would eventually expand the ICMS-site RF. According to Equation 6.7, the afferent excitatory pathway weights become proportional to presynaptic excitation. Thus, all afferent excitatory pathway weights to an active model cortical neuron during ICMS would become equal, and the afferent excitatory pathways to the ICMS-site neuron would be the strongest. Furthermore, all the lateral inhibitory pathway weights to model cortical neuron activated by ICMS would become equal. However, activated lateral inhibitory pathways to inactive neurons would weaken; these neurons would thus be highly responsive to input stimulation and would exert strong inhibition on the ICMS-site neuron. Thus, theICMS-site neuron may respond to stimulation of a large number of input positions but not all input locations from which the ICMS-site neuron receives afferent pathways. But, at some intermediate stage during ICMS, when most afferent excitatory pathways from input locations far from the ICMS-site RF center to the ICMS-site neuron are still weak, the ICMS-site RF size may not change much.

Afferent excitatory and lateral inhibitory plasticity during ICMS

To reproduce the effects of ICMS, the model assumed plasticity in afferent excitatory and lateral inhibitory pathways. Synaptic plasticity in excitatory and inhibitory pathways have been observed experimentally. Intracortical stimulation in adult animals

produces synaptic long-term potentiation and long-term depression (Kirkwood et al., 1993). Simultaneous intracellular recording of pairs of CA3 pyramidal neurons in guinea pig hippocampal slices has revealed a significant reduction in recurrent inhibition 12–20 minutes after repetitive stimulation of afferent pathways (Miles & Wong, 1987). In neocortical cultures, the strength of lateral inhibition was decreased by lowering the activation of the neurons (Rutherford et al., 1997). In adult primary visual cortex, monocular deprivation weakens lateral inhibitory interactions in the monocularly deprived cortical regions (Kasamatsu et al., 1998b).

No afferent excitatory plasticity during peripheral stimulation in adult animals

The effects of restricted repetitive peripheral stimulation were modeled using only the EXIN lateral inhibitory rule. This was done for two reasons.

First, the role of afferent excitatory plasticity in producing RF changes in adult animals during peripheral stimulation may be limited, or plasticity in afferent pathways may be very slow. Restricted retinal lesions in cats produced RF changes in neurons in layers 3 and 4 of area 17 within hours *only* if the non-lesioned eye was *closed* (Chino et al., 1992). This result is contrary to the prediction of a model with a Hebbian afferent excitatory plasticity rule, which would cause active neurons to weaken their thalamocortical pathways from the lesioned region, regardless of whether the other eye is open or closed. Furthermore, Darian-Smith and Gilbert (1995) did not observe anatomical reorganization of the thalamocortical afferent distribution several months after bilateral retinal lesions in adult cats. But, Darian-Smith and Gilbert (1994) observed axonal sprouting in existing long-range excitatory pathway terminals inside the inactive cortical region several months after bilateral retinal lesions in adult cats. Kirkwood et al. (1993) showed that synaptic plasticity is very easily produced in excitatory pathways to neurons in layer 2/3 of the primary visual cortex of adult animals when the conditioning is applied in layer 4, but synaptic plasticity is not produced or produced very infrequently when the conditioning is applied in the layer 6-white matter border without any pharmacological treatments to reduce inhibition. Thus, it appears that synaptic plasticity in afferent excitatory pathways to neurons in layer 2/3 can be produced by intracortical stimulation

but not by stimulation of geniculocortical pathways.

Second, the RF changes have been previously modeled by plasticity in afferent excitatory pathways (Grajski & Merzenich, 1990; Recanzone et al., 1992d). Plasticity in lateral inhibitory pathways is an alternative to model these RF changes. Furthermore, the model based on lateral inhibitory plasticity makes predictions distinct from those of the model based on plasticity in afferent excitatory pathways (see Section 6.4.5).

Absence of lateral excitatory and feedback excitatory pathways in the simulations

The simulations did not incorporate lateral excitatory and feedback excitatory pathways. In the cortex axonal arbors from pyramidal neurons make excitatory synapses with neurons close to (near the dendritic field) and far from (> 0.5 mm) the source neuron (Gilbert & Wiesel, 1983, 1989; McGuire et al., 1991). These horizontal excitatory pathways have approximately 80% of their synapses with excitatory neurons; the rest are made onto inhibitory neurons (McGuire et al., 1991). In addition, thalamocortical afferents also terminate on GABAergic neurons (Somogyi, 1989). Thus, stimulation of thalamocortical afferents or lateral excitatory pathways produces a mixture of excitatory and inhibitory postsynaptic potentials. However, intracellular recordings did not reveal any disynaptic excitatory postsynaptic potentials (EPSPs) when thalamocortical afferents were stimulated in layer 4 simple neurons in cat primary visual cortex (Ferster, 1989), or in layer 5 pyramidal neurons in the barrel area of neocortex in adult mice (Gil & Amitai, 1996). Thalamocortical afferent stimulation produced disynaptic inhibitory postsynaptic potentials (IPSPs) and polysynaptic EPSPs. Thus, the effects of the short-range excitatory pathways are rendered ineffective by strong local inhibition. The polysynaptic EPSPs may be caused by the long-range excitatory pathways or feedback excitatory pathways from other layers or cortical areas (Gil & Amitai, 1996; Hirsch & Gilbert, 1993).

The lateral excitatory and feedback excitatory pathways were not included in the simulations to keep the simulations relatively simple. Furthermore, based on physiological data, lateral excitatory and feedback excitatory pathways appear to contribute mainly to polysynaptic EPSPs (Gil & Amitai, 1996; Hirsch & Gilbert, 1993) and have mainly

subthreshold effects in normal cortex. A decrease in lateral inhibition can cause the lateral excitatory pathways to have suprathreshold effects (Das & Gilbert, 1995a; Gilbert & Wiesel, 1989, 1990; Gilbert et al., 1996). Thus, incorporating lateral excitatory/feedback pathways in the model can produce even larger changes in RF properties after ICMS and localized peripheral stimulation. Because lateral excitatory and feedback excitatory pathways contribute to polysynaptic EPSPs in response to thalamocortical stimulation (Hirsch & Gilbert, 1993; Gil & Amitai, 1996), synaptic plasticity in these pathways may produce changes in the late responses of cortical neurons after stimulation of their RF.

6.4.4 Significance of lateral inhibitory plasticity

In the model, lateral inhibitory pathways are present between model cortical neurons separated by large distances. Changes in these pathways, therefore, affected the RF of model cortical neurons over a large area of the model cortical layer (Section 6.3.2). Furthermore, the lateral inhibitory synaptic plasticity rule balanced the effects of the afferent excitatory synaptic plasticity to ensure that the RF properties at the ICMS site were unaffected (Section 6.3.2).

In the EXIN model, strong lateral inhibitory pathways develop between neurons that are consistently coactivated. Neurons can be consistently coactivated if they receive excitatory afferents from many common input neurons. Thus, in the EXIN network, model cortical neurons that share inputs have strong lateral inhibitory pathways between them. This is consistent with experimental results suggesting that neurons receive the strongest inhibition when stimulated with their preferred stimuli. (Blakemore & Tobin, 1972; DeAngelis et al., 1992; Ferster, 1989).

In addition to the usefulness of lateral inhibitory plasticity in modeling the effects of ICMS and peripheral stimulation, the EXIN lateral inhibitory plasticity rule has several desirable properties. The inhibitory synaptic plasticity rule leads to improved stimulus discrimination, sparse distributed coding, and exclusive allocation (Marshall, 1995a; Marshall & Gupta, 1998). In addition, the EXIN inhibitory plasticity rule has been used to model development of disparity selectivity (Marshall, 1990c), motion selectivity and grouping (Marshall, 1990a, 1995b; Schmitt & Marshall, 1995), orientation selectivity

(Marshall, 1990d), and length selectivity and end-stopping (Marshall, 1990b).

The EXIN lateral inhibitory plasticity rule (Equation 6.4) is an asymmetric rule; lateral inhibitory pathways from active neurons to inactive neurons weaken; however, lateral inhibitory pathways from inactive neurons to other neurons *do not* change. This asymmetry makes it possible to produce RF expansion in the inactive neurons during ICMS or peripheral stimulation, without necessarily producing RF expansion in neurons activated by ICMS or peripheral stimulation. The EXIN lateral inhibitory synaptic plasticity rule directly reduces inhibition to neurons inactivated by peripheral scotomas or lesions, thus making the inactive neurons more likely to respond to some visual stimuli. The EXIN lateral inhibitory synaptic plasticity rule enhances the efficiency of a neural network's representation of perceptual patterns, by recruiting unused and under-used neurons to represent input data (Marshall, 1995a; Marshall & Gupta, 1998).

Thalamocortical afferent arbors can spread over a large cortical area; thalamocortical afferents from the lateral geniculate nucleus can extend over a region up to 3 mm in cat primary visual cortex (Humphrey et al., 1985). Gilbert & Wiesel (1983) observed thalamocortical arbors that extended 2 mm in layer 4 of primary visual cortex of cats. Interlaminar excitatory pathways in the primary visual cortex of cats spread over a few millimeters (Gilbert & Wiesel, 1983). Thalamocortical arbors to the somatosensory cortex in monkeys can extend over a range of 1.2–2 mm (Garraghty et al., 1989; Garraghty & Sur, 1990; Juliano & Whitsel, 1987; Mayner & Kaas, 1986). Thus, a large overlap in the afferent excitatory inputs to model neurons is reasonable.

In animal cortex, lateral pathways spread over large distances. Axonal arbors of GABAergic large basket neurons extend up to 1.5 mm in cortex and terminate on the soma of pyramidal neurons in small patches of cortex (Somogyi et al., 1983; Somogyi & Martin, 1985). Based on the anatomical structure of the axonal arbors of basket neurons, these neurons appear to have the greatest effect on neurons with orientation selectivity similar to their own; however, they may also affect neurons with other orientations and other RF positions (Martin, 1988). Long-range inhibitory influences in cortex may also be subserved by the long-range horizontal pathways that extend 2–8 mm in primary visual cortex of cat (Gilbert & Wiesel, 1983; 1989). The long-range horizontal pathways have an

excitatory effect at low stimulation strength and have an inhibitory effect at high stimulation strength (Gil & Amitai, 1996; Weliky et al., 1995). Furthermore, the excitatory and inhibitory effects of the long-range horizontal pathways are concentrated on neurons with similar orientation selectivity to that of the source neuron (Weliky et al., 1995). Combined measurement of spiking point-spread using extracellular recording and optical point-spread in cat primary visual cortex showed that the spiking point-spread accounts for only 5% of the optical point-spread; the remainder of the optical point-spread was caused largely by inhibition (Das & Gilbert, 1995a). The optical point-spread had a diameter between 3.2 and 5.2 mm and showed greatest magnitude for cortical neurons with similar stimulus orientation preference to that of the spiking neurons.

These data are consistent with the suggestion that cortical neurons with common inputs, and hence similar properties, should have relatively strong lateral inhibitory pathways between them, for improved stimulus discrimination (e.g., orientation selectivity, disparity selectivity, length selectivity, spatial frequency selectivity, motion direction selectivity), and sparse distributed coding. Thus, lateral inhibitory plasticity may play an active and important role in the development of cortical function.

6.4.5 Model predictions

Based on the mechanism of the EXIN synaptic plasticity rules, the following experimental suggestions and EXIN model predictions are made.

ICMS and peripheral stimulation with an NMDA receptor antagonist

NMDA receptor antagonists block synaptic plasticity in excitatory synapses in cortex (Bear et al., 1990; Dudek & Bear, 1992; Kirkwood et al., 1993). Furthermore, NMDA receptor antagonists may not abolish neuronal activation caused by peripheral or cortical stimulation (although neuronal activation levels are lowered) at concentrations sufficient to block NMDA receptors (Bear et al., 1990).

With the *assumption* that lateral inhibitory pathway plasticity is not blocked by NMDA receptor antagonists and afferent excitatory plasticity is blocked by NMDA receptor antagonists, it is predicted that ICMS or localized peripheral stimulation during cortical

infusion of NMDA receptor antagonists will produce increased cortical representation of the ICMS-site RF or the localized peripheral stimulation site (Sections 6.3.2 and 6.3.4). According to the EXIN outstar lateral inhibitory synaptic plasticity rule, presynaptic activation is required to enable plasticity in lateral inhibitory pathways. Therefore, the concentration of NMDA receptor antagonists should be such that cortical activation is not suppressed but plasticity in afferent excitatory pathways is blocked. RF measurements should be made after sufficient duration for the effects of NMDA receptor antagonists to wash out. As a control, EPSPs to a few neurons before and after conditioning should be measured to determine whether any plasticity in the afferent excitatory pathways occurred.

Measurement of changes in EPSPs and IPSPs following ICMS and peripheral stimulation

Based on the EXIN model of ICMS, it is predicted that

1. IPSPs to neurons far from the ICMS site (which were inactive during the initial stages of ICMS and whose RF is affected by ICMS) caused by peripheral stimulation of the ICMS-site RF or cortical stimulation at the ICMS site decrease after ICMS, because of weakening of lateral inhibitory pathways to these neurons from neurons close to the ICMS site (Figure 6.7).

2. Neurons close to the ICMS site whose RF was substituted for part of the ICMS-site RF receive reduced early EPSPs from peripheral stimulation of those parts of the neuron's initial RF that are ineffective in activating the neuron after ICMS, because of weakening of the afferent excitatory pathways (Figure 6.7).

After peripheral stimulation, it is predicted that

1. IPSPs to neurons inactive during localized peripheral stimulation and whose RF is changed after peripheral stimulation decrease because of peripheral stimulation of the conditioning peripheral site. Also, these inactive neurons receive reduced IPSPs from cortical stimulation of cortical sites that were active during the conditioning phase. These effects are predicted because the EXIN lateral inhibitory synaptic plasticity rule

weakens lateral inhibitory pathways from active neurons to inactive or very weakly active neurons.

2. IPSPs to neurons sensitive to the localized stimulation site increase as the stimulation strength during the conditioning phase is increased. This is accompanied by reduced responsiveness and RF contraction in these neurons. These effects are predicted because the EXIN lateral inhibitory synaptic plasticity rule strengthens lateral inhibitory pathways between strongly activated neurons.

Peripheral stimulation with varying strength

The EXIN lateral inhibitory plasticity rule suggests that RF changes in somatosensory cortex after repetitive peripheral stimulation in the same skin region of adult animals depend on the strength of stimulation (Section 6.3.4). It is predicted that for a stimulated skin region of a particular size, the change in somomatosensory cortical neuronal RF size will vary from expansion to contraction as the stimulation strength is increased (Section 6.3.4). Because lateral inhibitory plasticity in the model requires neuronal activation (Equation 6.4), no RF change occurs in the absence of peripheral stimulation or at very weak peripheral stimulation strength. As peripheral stimulation strength is increased there is some value at which no RF change occurs; stimulation strength less than this causes RF expansion, and stimulation strength greater than this causes RF contraction. In Equation 6.4, neuronal activation affects the rate of change; hence, more RF changes are expected as stimulation strength is increased.

In a model relying on afferent excitatory plasticity, RF size after repetitive peripheral stimulation depends on the size of the stimulated region; RF size increases if a large skin region is stimulated, and RF size decreases if a small skin region is stimulated. According to the EXIN lateral inhibitory plasticity rule the RF size after repetitive peripheral stimulation may not be a monotonic function of the size of the stimulated region because the activation level of cortical neurons may not be a monotonic function of size of the stimulated region – the neuron may be end-stopped or have side-inhibition. However, if the size of the stimulated region is small and the stimulation strength is small, a model

relying on afferent excitatory plasticity predicts a contraction in the RF size of weakly active neurons, whereas the EXIN lateral inhibitory plasticity rule predicts expansion in the RF size of weakly active neurons.

6.4.6 Neurophysiological realization of the EXIN synaptic plasticity rules

The EXIN model is a *functional* model that describes the modifications in the *effective* excitation and inhibition through synaptic weight changes. *In vivo*, intracortical inhibition to excitatory neurons is mediated by inhibitory neurons, which receive lateral excitation from excitatory neurons in addition to afferent input (Martin, 1988; McGuire et al., 1991; Somogyi, 1989; Somogyi & Martin, 1985). In addition, inhibitory neurons have inhibitory synapses with other inhibitory neurons (Somogyi, 1989; Somogyi & Martin, 1985).

Neurophysiologically, the EXIN lateral inhibitory synaptic rule could be realized directly by plasticity in the GABAergic synapses onto excitatory neurons or indirectly by plasticity in lateral excitatory horizontal pathways (both short- and long-range) terminating on inhibitory neurons (Darian-Smith & Gilbert, 1994, 1995; Das & Gilbert, 1995ab; Gilbert et al., 1996; Hirsch & Gilbert, 1993). The axonal arbors of many inhibitory neurons (e.g., clutch, basket, chandelier) terminate mainly on excitatory neurons (Somogyi, 1989; Somogyi & Martin, 1985), and axonal arbors of most excitatory neurons terminate on other excitatory neurons (McGuire et al., 1991; Somogyi, 1989; Somogyi & Martin, 1985). Stimulation of the long-range horizontal excitatory pathways produces both excitatory and inhibitory effects on excitatory neurons (Gil & Amitai, 1996; Weliky et al., 1995). Thus, changing the efficacy of lateral inhibitory pathways or the lateral excitatory pathways to inhibitory neurons will change effective inhibition to cortical neurons.

The double bouquet inhibitory neurons have a majority of their axonal arbors terminating on other inhibitory neurons (Somogyi & Martin, 1985). The axonal terminals of these neurons have mainly radial spread (Somogyi & Martin, 1985). Thus, these neurons may not contribute much to producing RF changes in neurons over a large cortical area. However, plasticity in axonal arbors of these neurons may affect the RF of ICMS-site neurons.

It might at first appear that weakening inhibitory synapses to an excitatory neuron is equivalent to increasing lateral excitatory synapses to the same neuron. However, these possibilities can produce different network behaviors. Consider the following two cases – (1) lateral excitatory synapses to excitatory neurons are fixed and lateral inhibitory synapses to cortical neurons or lateral excitatory synapses to inhibitory neurons are modifiable, and (2) lateral inhibitory synapses to cortical neurons are fixed and lateral excitatory synapses to excitatory neurons alone are modifiable. With the additional assumption that both excitatory and inhibitory pathways are strengthened if the neurons are strongly coactivated and weakened if the neurons are weakly coactivated or uncorrelated or anti-correlated, in case (1) strong coactivation causes decorrelation of activation of cortical neurons because of strengthening lateral inhibitory pathways or strengthening of lateral excitatory pathways to inhibitory neurons, but in case (2) strong coactivation causes stronger correlation between cortical neurons because of strengthening of lateral excitatory pathways to excitatory neurons. Thus, with plasticity only in lateral excitatory pathways to excitatory neurons, lateral excitatory pathways should be weakened if two neurons are strongly correlated (Rubner & Schulten, 1990), in order have the same overall effect as in case (1). Case (2) is similar to the mechanism suggested for RF changes based on cooperative neuron groups (Section 6.1.4). When neurons are weakly activated by peripheral stimulation, the mechanism in case (1) produces RF expansion from reduced lateral inhibition, and the mechanism in case (2) produces RF contraction from reduced lateral excitation. Strong neuronal activation causes RF contraction in case (1) and RF expansion in case (2). In adult animal cortex, lateral excitatory pathways to excitatory and inhibitory neurons and lateral inhibitory pathways to excitatory and inhibitory neurons may undergo synaptic plasticity. Therefore, the overall effect of synaptic plasticity in these pathways will depend on the rate of plasticity on these pathways and the relative contribution of these pathways to RF properties.

No conclusive evidence exists on the role of changes in the excitatory and inhibitory pathway strength in producing cortical plasticity. Intracellular measurements of EPSPs and IPSPs in excitatory and inhibitory neurons are required to provide more conclusive evidence on the site of cortical plasticity in adult animals during various types of conditioning.

Chapter 7

Conclusions and future work

The objectives of this dissertation were to model cortical plasticity in early postnatal development and in adulthood and to analyze the role of lateral inhibitory synaptic plasticity in developmental and adult cortical plasticity. Previous models of cortical development and cortical plasticity (Linsker, 1986abc; Miller et al., 1989, von der Malsburg, 1973; Kohonen, 1987; Willshaw & von der Malsburg, 1976) used synaptic plasticity in the afferent excitatory pathways to model development of cortical maps and neuronal stimulus feature selectivity. Grossberg (1982) used afferent excitatory and feedback excitatory synaptic plasticity to model development of stable neural codes. Synaptic plasticity in afferent excitatory and lateral excitatory pathways has been used to model cortical organization of model neuronal groups with common receptive field properties (Favorov & Kelly, 1994; von der Malsburg & Singer, 1988; Merzenich, 1987; Pearson et al., 1987). In the above models, lateral inhibitory synaptic pathway weights were set according to a predefined function.

It has been recognized that receptive field changes can occur because of modifications in excitatory and inhibitory inputs to cortical neurons (Merzenich, 1987). Grajski and Merzenich (1990) modeled the changes in receptive field topography after repetitive localized peripheral stimulation using a model with synaptic plasticity in afferent excitatory, lateral excitatory, and lateral inhibitory pathways. All these pathways were modified using a single competitive rule based on neuronal activation, passive decay, and

normalization (Grajski & Merzenich, 1990). However, none of the above models analyzed the possible role of lateral inhibitory synaptic plasticity in the development of cortical properties and functions and in adult cortical plasticity.

Several recent models (e.g., Hubbard & Marshall, 1994; Marshall, 1989, 1990abcd, 1995ab; Marshall & Alley, 1993; Marshall et al., 1996a; Martin & Marshall, 1993; Schmitt & Marshall, 1995, 1996; Sirosh et al., 1996; Sirosh & Miikkulainen, 1997) have emphasized the role of lateral excitatory and lateral inhibitory synaptic plasticity in the development of cortical maps, neuronal feature selectivity, and cortical functions. Marshall and Gupta (1998) showed that an instar afferent excitatory and an outstar lateral inhibitory synaptic plasticity rule (the EXIN rules) lead to the development of neural codes with low redundancy, high discrimination, and sparse distributed coding. Marshall et al. (1996b) showed that a neural network with anisotropic lateral inhibitory pathways, whose strength was proportional to the amount of overlap in the receptive fields of binocular neurons, could represent stereo transparency and assign unique disparities to each visual feature in the two eyes.

Lateral excitatory synaptic plasticity in cortex has been examined experimentally (e.g., Darian-Smith & Gilbert, 1994; Frégnac et al., 1994; Hirsch & Gilbert, 1991; Kirkwood & Bear, 1994; Kirkwood et al., 1993). However, lateral inhibitory synaptic plasticity and its role in cortical development and cortical plasticity has received very little attention experimentally (e.g., Kasamatsu et al, 1998b; Rutherford et al., 1997).

In this dissertation, results based on several experimental paradigms to study the neural basis of cortical development and cortical plasticity, e.g., long-term synaptic plasticity, "classical" rearing conditioning, retinal lesions, artificial scotoma conditioning, repetitive localized peripheral stimulation, and intracortical microstimulation, were modeled using the EXIN rules. In addition, the predictions of the EXIN rules and some other synaptic plasticity rules from literature, e.g., the BCM rule (Bear et al., 1987; Bienenstock et al., 1982; Clothiaux et al., 1991) and the LISSOM synaptic plasticity rules (Sirosh et al., 1996), were analyzed and compared with experimental data, and novel predictions were made. It was shown that the outstar lateral inhibitory synaptic plasticity rule

1. along with the instar afferent excitatory plasticity rule leads to the development

of model neurons with high position selectivity and binocularity; without the development of strong lateral inhibitory pathways, model cortical neurons become monocular and have have weak position selectivity;

2. develops lateral inhibitory pathways that can produce ocular dominance changes even when plasticity in afferent excitatory pathways are pharmacologically blocked;

3. is sufficient to model dynamic receptive field changes after retinal lesions and artificial scotoma conditioning;

4. is sufficient to model changes in receptive field topography and stimulus feature discrimination after repetitive localized peripheral stimulation; and

5. along with the instar afferent excitatory synaptic plasticity rule produces cortical plasticity after intracortical microstimulation.

Repetitive localized peripheral stimulation produced by tactile frequency discrimination training in monkeys produced widespread changes in the receptive field properties of somatosensory cortical neurons (Recanzone et al., 1992cde). The training also improved the monkeys' performance (Recanzone et al., 1992a). In Chapter 6, it was shown that repetitive localized peripheral stimulation produced receptive field changes in the model cortical neurons similar to those observed experimentally. In addition, the conditioning improved the model's discrimination of test stimuli from the training stimuli. The model was based on lateral inhibitory synaptic plasticity. Thus, it is suggested that lateral inhibitory synaptic plasticity may play an important role in perceptual learning. Several novel and testable experiments are suggested to test the predictions of the model.

The main results in the chapters of this dissertation are summarized in Section 7.1, and some open questions related to cortical development and adult cortical plasticity are discussed in Section 7.2.

7.1 Summary

In Chapter 2, long-term potentiation (LTP) and long-term depression (LTD) were modeled using the instar and the outstar excitatory synaptic plasticity rules. The instar

and the outstar excitatory synaptic plasticity rules were compared with the BCM rule (Bear et al., 1987; Bienenstock et al., 1982; Clothiaux et al., 1991). Furthermore, the properties of the outstar lateral inhibitory synaptic plasticity rule were analyzed. It was shown that the instar and the outstar excitatory synaptic plasticity rules model most experimental data on excitatory synaptic plasticity and that the BCM rule is inconsistent with some experimental results.

In Chapter 3, shifts of ocular dominance during postnatal classical rearing conditioning (Blakemore & Van Blakemore, 1974; Buisseret et al., 1982; Freeman & Olson, 1982; Hubel & Wiesel, 1965, 1970) were modeled using the EXIN rules. The afferent excitatory synaptic plasticity was primarily responsible for ocular dominance plasticity. However, the lateral inhibitory interactions produced some secondary changes in ocular dominance. In the model, lateral inhibitory synaptic plasticity was important in the development of binocular neurons and high input feature selectivity. Weak lateral inhibitory pathways during normal rearing caused model cortical neurons to become monocular and weakly selective.

The effects of cortical infusion of pharmacological agents APV (an NMDA receptor antagonist) and muscimol (a GABA agonist) were modeled in Chapter 4. The self-organized network obtained after normal rearing conditioning using the EXIN rules in Chapter 3 was used for the simulations in this chapter. It was shown that the network produced the effects of cortical infusion of APV in adult animals during normal binocular vision. Experimentally, cortical infusion of APV decreases binocularity and responsiveness of primary cortical neurons (Kasamatsu et al., 1997, 1998a). In addition, the effects of cortical infusion of APV or muscimol during monocular deprivation in animals in their critical period were modeled. A reverse ocular dominance shift was observed after monocular deprivation with cortical infusion of APV (Bear et al., 1990) and muscimol (Reiter & Stryker, 1988). The model in Chapter 4 is based on lateral inhibitory interactions. In the model, it was assumed (consistent with experimental data on long-term synaptic plasticity) that excitatory synaptic plasticity is blocked by infusion of high concentrations of APV and muscimol. On the other hand, previous models (e.g., Bear et al., 1990; Clothiaux et al., 1991; Miller et al., 1989) were based on plasticity in afferent excitatory pathways from the open

eye to the cortical region treated with APV or muscimol, inconsistent with experimental data on long-term synaptic plasticity.

In Chapter 5, dynamic changes in the size, shape, and position of neuronal receptive fields in response to artificial scotoma conditioning (Pettet & Gilbert, 1992; DeAngelis et al., 1994) and retinal lesions (Chino et al., 1992; Darian-Smith & Gilbert, 1995) were modeled using the EXIN synaptic plasticity rules. The effects produced by the EXIN rules were compared with a model based on neuronal adaptation (Xing & Gerstein, 1994) and another based on the LISSOM plasticity rules (Sirosh et al., 1996). The analyses showed that the outstar lateral inhibitory synaptic plasticity rule in the EXIN network or the LISSOM lateral excitatory synaptic plasticity rule in the LISSOM network are sufficient to model the experimental data on artificial scotoma conditioning and retinal lesions. A novel *complementary scotoma* conditioning experiment, in which stimulation of scotoma and non-scotoma regions are alternated repeatedly, was proposed to test the predictions of the EXIN outstar lateral inhibitory and the LISSOM lateral excitatory synaptic plasticity rules. In addition, this chapter emphasized the drastic effects produced by the subtle distinction between instar and outstar synaptic plasticity rules.

In Chapter 6, the changes in the size and position of neuronal receptive fields in response to intracortical microstimulation (Recanzone et al., 1992b) and repetitive peripheral stimulation of a localized region (Jenkins et al., 1990; Recanzone et al., 1992cde) were simulated based on the EXIN synaptic plasticity rules. It was shown that the EXIN outstar lateral inhibitory synaptic plasticity rule can produce increase in cortical magnification of the peripheral stimulation site and increase in discrimination of stimuli from the conditioning stimuli along with expansion or contraction in the receptive field size of the neurons initially responsive to the stimulated region.

7.2 Future work

The simulations in this dissertation demonstrated that the EXIN synaptic plasticity rules produce effects consistent with many neurobiological data on cortical

development and adult cortical plasticity. However, several important cortical phenomena were not modeled in this dissertation. Some of these are discussed in this section.

7.2.1 Development of topographic cortical maps

In Chapters 3 and 4, changes in ocular dominance, responsiveness, and positional selectivity of model cortical neurons during normal rearing and visual deprivation conditioning were modeled using the EXIN rules. The simulations in Chapters 3 and 4, however, ignored the spatial topography of ocular dominance and orientation columns. To provide a stronger support for the claim that the EXIN rules may be part of a set of fundamental rules for cortical development and adult cortical plasticity, the development of ocular dominance and orientation columns in networks using the EXIN rules needs to be studied.

The primary visual cortex is topographically arranged, i.e., in general, neurons with similar stimulus feature selectivities are located close to each other in the cortex. Because primary visual cortical neurons are selective for several different stimulus features, cortical maps can be constructed with respect to each stimulus feature, e.g., the ocular dominance map, the orientation map, and the spatial frequency map (Hübener et al., 1997). Direction of motion and orientation maps have been constructed in cat area 18 (Shmuel & Grinvald, 1996), and orientation maps of subjective contours in adult cat areas 17 and 18 have been determined (Sheth et al., 1996)

The organization of the maps of ocular dominance and orientation selectivity are related (Blasdel, 1992ab; Obermayer & Blasdel, 1993; Obermayer et al., 1992). The ocular dominance and orientation maps have the following general features: (1) linear zones in which orientation preference changes linearly with distance; (2) singularities at which orientation preference changes by 180° along a closed path; (3) fractures across which orientation preferences change rapidly; (4) saddle point regions with respect to orientation preference; (5) singularities and saddle points that usually occur in the center of the ocular dominance columns; and (6) iso-orientation lines that tend to intersect the ocular dominance borders at 90°. Furthermore, the cortical maps display global disorder; i.e., the properties of the maps do not repeat periodically over the cortical surface.

The development of the orientation and ocular dominance maps and their relationships have been simulated by several models (Erwin et al., 1995; Grossberg & Olsen, 1994). Many of the models have the following common characteristics (Erwin et al.,1995; Grossberg & Olsen, 1994) – noise inputs, a spatial band-pass filter, and competitive weight normalization. These models have a tendency to correlate binocularity and orientation specificity – the binocular neurons tend to have much greater orientation specificity than monocular neurons (Erwin et al., 1995). However, experimentally monocular neurons too can be highly orientation specific (Bonhoeffer & Grinvald, 1991). In these models, the lateral interactions between model neurons have no modular specificity; i.e., there is no preferential lateral interaction between neurons with similar orientation preference and ocular dominance, as observed experimentally (Bosking et al., 1997; Gilbert & Wiesel, 1989). Furthermore, the lateral long-range pathways in the visual cortex undergo development during the early postnatal stages, and their development is susceptible to changes in visual environment (Dalva & Katz, 1994; Katz & Callaway, 1992; Löwel & Singer, 1992).

The LISSOM network (Sirosh & Miikkulainen, 1997) used synaptic plasticity in afferent excitatory and lateral pathways to model the self-organization of ocular dominance and orientation maps. They showed that synaptic plasticity in lateral pathways can model the correlation between the distribution of lateral pathway connectivity with respect to stimulus feature selectivity of model neurons.

Many models of orientation selectivity rely on lateral inhibition to produce high orientation selectivity (Marshall, 1990bd; Sirosh et al., 1996; Somers et al., 1995). Experimentally, blockade of inhibition causes decrease in orientation selectivity (Sillito, 1975, 1977, 1979; Sillito et al., 1980). Cortical neurons are also selective for disparity (Barlow et al., 1967; Blakemore et al., 1972; DeAngelis et al., 1991; Ohzawa et al., 1990; Pettigrew et al., 1968; Nikara et al., 1968). Several studies have shown that disparity selectivity and stereopsis develop postnatally in normal binocular visual environments (Chino et al., 1997; O'Dell & Boothe, 1997; Held et al., 1980). The presence of disparity in the input affects the ocular dominance of model neurons (Chapter 3). Thus, the analysis of the relationship between orientation maps and the organization and development of lateral

inhibition and of the effects of disparity on the relationship between orientation and ocular dominance maps can be interesting research projects.

Some interesting research questions on cortical maps are

1. Can lateral inhibitory synaptic plasticity with afferent excitatory synaptic plasticity produce orientation and ocular dominance maps in which monocular neurons too have high orientation specificity?

2. How do orientation specific lateral pathway connections develop?

3. Does the strength of lateral inhibitory pathways vary across orientation map features such as singularities, linear zones, fracture, saddle points?

4. What is the relationship between ocular dominance, orientation preference, and disparity preference maps?

5. How is the modeled development of orientation and ocular dominance maps affected by the introduction of disparity in the training inputs?

7.2.2 Neural basis of perceptual learning

The analysis and modeling of perceptual learning using the EXIN rules would be an interesting future project.

In humans, training improves performance of several perceptual tasks such as orientation perception (Fiorentini & Berardi, 1980), vernier acuity (Fahle & Edelman, 1993), and texture discrimination (Karni & Sagi, 1991). These improvements are very specific, as they are observed mainly in tests involving the training stimulus features, e.g., orientation, position, etc. In monkeys, training in a tactile frequency discrimination task led to a gradual improvement in the task over a period of several weeks (Recanzone et al., 1992a).

In Chapter 6, it was shown that repeated stimulation of a small region in a network with outstar lateral inhibitory synaptic plasticity improved discrimination of the stimulated region from other surrounding positions. It was also suggested that the outstar lateral inhibitory synaptic plasticity rule may produce perceptual learning. Thus, investigation

of the possible role of the outstar inhibitory synaptic plasticity rule in perceptual learning would be interesting.

7.2.3 Changes in information content of self-organizing networks after changes in input environment

It has been suggested that, the brain adapts in order to maximize its information content (Atick & Redlich, 1990). Although the information theoretic approach to brain adaptation does not directly suggest possible rules for brain adaptation, it can be used to constrain possible rules for brain plasticity.

Thus, the various synaptic plasticity rules proposed by self-organizing models of cortical development and cortical plasticity can be analyzed in terms of the changes in information content they produce in the neural models following artificial scotoma conditioning, complementary scotoma conditioning, repeated localized peripheral stimulation, intracortical microstimulation, and classical rearing conditioning.

7.2.4 Self-organization of stereopsis

In humans and monkeys stereopsis develops postnatally (O'Dell & Boothe, 1997; Held et al., 1980). Therefore, self-organizing models are useful for understanding the neural basis of stereopsis and its development. An understanding of the self-organizing process of stereopsis may possibly help in the induction of normal development of stereopsis in strabismic children.

Marshall et al. (1996) proposed a hardwired model, the exclusive grouping (EG) network, for stereomatching that performed better than previous stereomatching models. Previous stereomatching algorithms cannot simultaneously represent transparently overlaid surfaces (Frisby & Pollard, 1991; Marr & Poggio, 1976), cannot directly represent surfaces of arbitrary orientation (Marr & Poggio, 1976; Qian & Sejnowski, 1989), or cannot assign unique disparity values to features (Prazdny, 1985).

In the EG network, monocular neurons project excitatory pathways to binocular neurons at appropriate disparities, binocular neurons project excitatory pathways to appropriately tuned "surface patch" neurons, and the surface patch neurons project

reciprocal excitatory pathways to the binocular neurons. Anisotropic intralayer inhibitory pathways project between neurons with overlapping receptive fields. The network was tested with simulated stereo image pairs depicting a variety of oblique and transparently overlaid surfaces. For all the surfaces, the EG network

1. assigns disparity matches and surface patch representations based on global surface coherence and uniqueness;

2. permits coactivation of neurons representing multiple disparities at the same image location, unlike the Marr & Poggio (1976) algorithm;

3. represents oblique slanted and tilted surfaces directly, rather than approximating them with a series of frontoparallel steps;

4. assigns disparities to a cloud of points at random depths, like human observers, and unlike Prazdny's (1985) method; and

5. causes globally consistent matches to override greedy local matches.

The EG network constitutes a general solution for resolving conflicts in grouping and transparency representation.

Thus, an interesting research problem would be to model the self-organization of the EG network. Previously, the EXIN rules have been used to model the self-organization of disparity selective neurons (Marshall, 1990c).

7.2.5 Binocular rivalry

Stereomatching and binocular rivalry are related in the sense that binocular rivalry ensues when stereomatching is not possible, e.g., when very different input stimuli such as orthogonally oriented gratings are presented dichoptically to corresponding locations in the two eyes. In binocular rivalry, the disparate stimuli presented to the two eyes are alternately perceived over time. There is considerable debate on whether binocular rivalry and stereopsis are parallel, independent processes (Blake, 1989; Blake & O'Shea, 1988; Wolfe, 1986, 1988).

None of the current models (e.g, Blake, 1989; Grossberg, 1987; Lehky, 1988; Lehky & Blake, 1991; Matsuoka, 1984) is successful in explaining binocular rivalry. Most models assume ortho-orientation inhibition (Blake, 1989; Grossberg & Marshall, 1989; Lehky & Blake, 1991). However, ortho-orientation inhibition has not been observed in intracellular recordings (Ferster, 1986, 1989). Some models have rivalry occurring at a monocular stage (Blake, 1989; Lehky & Blake, 1991; Matsuoka, 1984). However, binocular rivalry has not been observed at any monocular stage of visual processing (Lehky & Maunsell, 1996; Leopold & Logothetis, 1996). Experimental evidence suggests that stereopsis precedes binocular rivalry and that binocular rivalry ensues when stereopsis fails (Blake, 1989; Wolfe, 1986, 1988). Recently, Kalarickal and Marshall (1998a) modeled most of the temporal and stochastic properties of binocular rivalry (Blake et al., 1971; Leopold & Logothetis, 1996; Levelt, 1965; Mueller & Blake, 1989); but this model does explain how the rivalry alternations are set up nor does it incorporate the interactions between stereopsis and binocular rivalry. Furthermore, the relationship between self-organization of stereopsis and binocular rivalry has not been previously studied. Shimojo & Nakayama (1990, 1994) have psychophysically studied the relationship between stereopsis and binocular rivalry. Blake et al. (1991) have demonstrated that stereopsis and binocular rivalry can coexist under certain conditions.

The EXIN synaptic plasticity rules predict that lateral inhibition will become the strongest between neurons with similar stimulus feature selectivities, e.g., similar orientations at a given spatial position (Marshall, 1990bcd, 1995a). But binocular rivalry is induced when orthogonal gratings are dichoptically presented, and stereopsis ensues when the dichoptically presented gratings are of similar orientations. In addition, high contrast orthogonal gratings presented to the same eye at corresponding locations do not produce alternations in the perception of the gratings. However, at low contrasts, alternations in the perception of orthogonal gratings presented to the same eye do occur (Breese, 1899, 1909; Campbell & Howell, 1972); this is called *monocular rivalry*.

Thus, important research questions on binocular rivalry in the context of self-organization and the EXIN rules are:

1. How is binocular rivalry initiated at a binocular stage between neurons selective for

the rivalrous stimuli in a network with iso-orientation inhibitionΓ

2. Monocular orientation-selective neurons inhibit each other; so why is monocular rivalry not initiated by high contrast disparate stimuli, while binocular rivalry can be initiated by high contrast disparate stimuliΓ

3. What rules of self-organization of lateral inhibitory pathways between neurons with different ocular dominance and orientation selectivity can produce networks that exhibit binocular and monocular rivalryΓ

4. Why is binocular rivalry not produced in half-occluded regions in stereopsisΓ

5. Can stereopsis and binocular rivalry self-organize within the same network using common self-organizing rulesΓ

Answers to the above questions will advance our understanding of the decision mechanisms in the brain. When the input stimuli in the two eyes are incompatible, the visual system has to decide between the differing signals coming through the two eyes. The binocular rivalry phenomenon shares several properties with the alternations in bistable percepts, e.g., bistable perceptions of the Necker cube. Thus, an understanding of the binocular rivalry mechanism may shed light on how the brain interprets natural scenes that contain ambiguities.

Appendix A

Parameters used in the simulations of Chapter 2

The notation $[a]$ is defined to mean $\max(0, a)$. The notation $\lfloor a \rfloor$ is defined to mean the largest integer less than or equal to a.

The activation equation (Equation 2.1) was numerically integrated using the Euler method with a time step of 0.04, and the activation levels of all the neurons were initially set to zero. The network was close to an equilibrium state by time = 40 (the maximal change in activation level was less than 10^{-4}).

At equilibrium $\frac{d}{dt}x_j = 0$, and the activation levels of Layer 2 neurons are given by

$$x_j = \frac{\beta B E_j - \gamma C I_j}{A + \beta E_j + \gamma I_j} \tag{A.1}$$

Since, Equation 2.1 is a shunting equation, $x_j(t) \in [-C, B]$ if $x_j(0) \in [-C, B]$, $t \geq 0$ (Cohen & Grossberg, 1983). Thus, B is the maximum activation level and $-C$ is the minimum activation level of Layer 2 neurons. The constant A determines the passive decay rate.

In the activation equation, if $\beta = 0$ or $B = 0$, the activation level will converge to zero (Figures A.1cd and A.2ab), and if $\gamma = 0$, the neurons do not receive inhibition from other neurons and therefore $x_j = \frac{\beta B E_j}{A + \beta E_j}$ (Figure A.2cd).

If $A \to \infty$, then $A \gg (\beta E_j + \gamma I_j)$ and $A \gg (\beta B E_j - \gamma C I_j)$ in Equation A.1. Thus,

$x_j(\infty) \approx 0$. Figure A.1a shows that increasing A causes the activation level of neuron a to moves closer to 0.

Increasing β is equivalent to increasing the input strength. As β is increased, the activation levels of neurons receiving excitation increases, but the activation level is bounded by B. This property of the shunting equation is shown in Figure A.2ab. As γ is increased, the activation level of neurons decrease and the response profile becomes narrower. At very large values of γ, the network behaves in a winner-take-all manner (Figure A.2cd).

Increasing B increases the maximal activation level of the neurons (Figure A.1cd). And increasing C causes the activation level of neurons to decrease, and lowers the lower bound for the activation level (Figure A.1ef). For very large values of C, the network behaves in a winner-take-all manner.

Figure A.2ef shows the effects of introducing non-linearity in input excitation and input inhibition to the neurons.

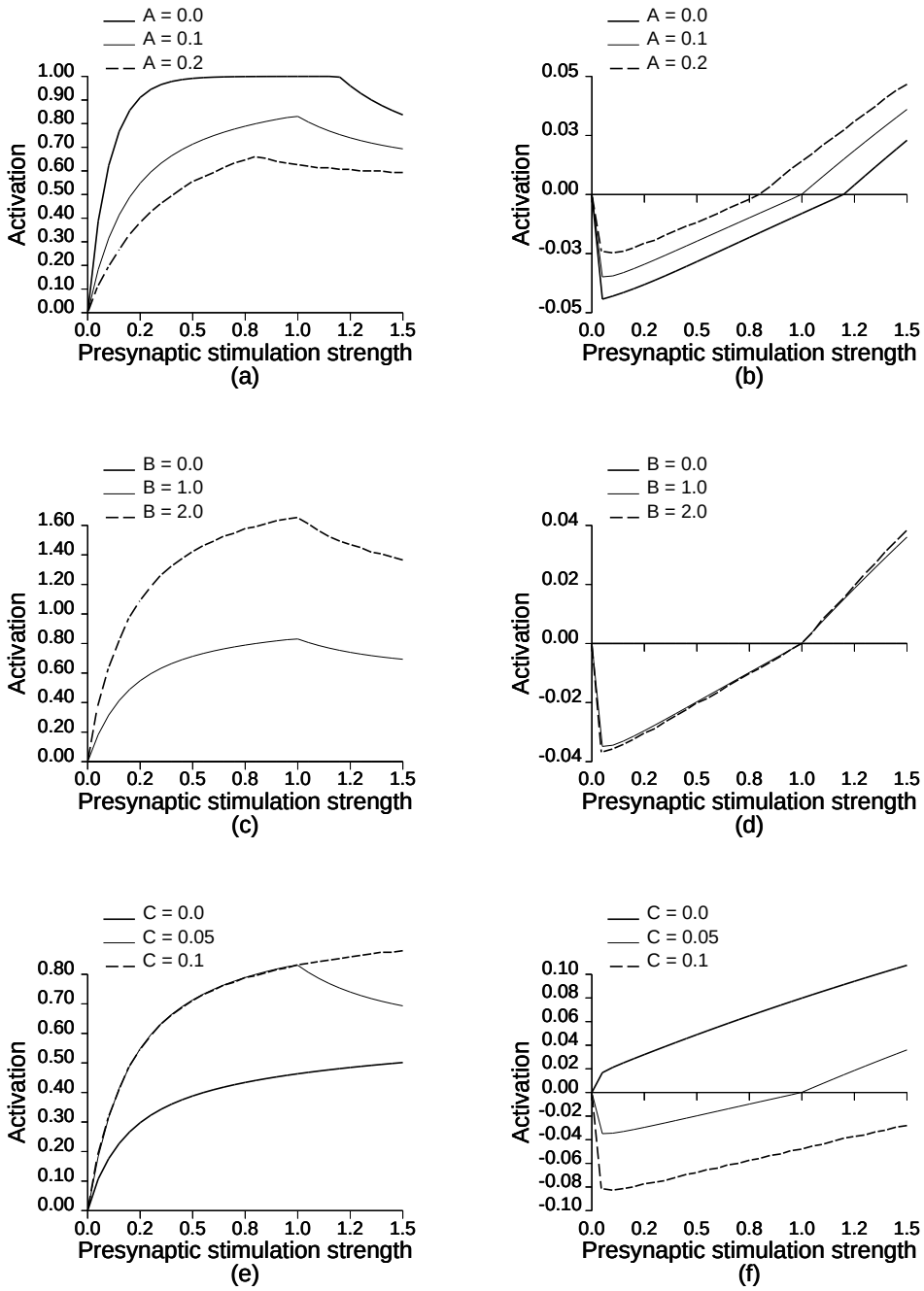

Figure A.1: Legend on next page.

Figure A.1: **The effects of parameters A, B, and C on the activation equation.** Figure on previous page. The initial network synaptic weights are given in Figure 2.8. The activation level of neuron a (left panels) and neuron b (right panels) was determined using Equation 2.1. The activation level of the input neuron a was varied from 0 to 1.5. In panels (a) and (b) $A \in \{0.0,\ 0.1,\ 0.2\}$, $B = 1.0$, $C = 0.05$, $\beta = 1.0$, and $\gamma = 15$. In panels (c) and (d) $A = 0.1$, $B \in \{0.0,\ 1.0,\ 2.0\}$, $C = 0.05$, $\beta = 1.0$, and $\gamma = 15$. In panels (e) and (f) $A = 0.1$, $B = 1.0$, $C \in \{0.0,\ 0.05,\ 0.1\}$, $\beta = 1.0$, and $\gamma = 15$. When $B = 0$, the activation of neurons a and b is 0.

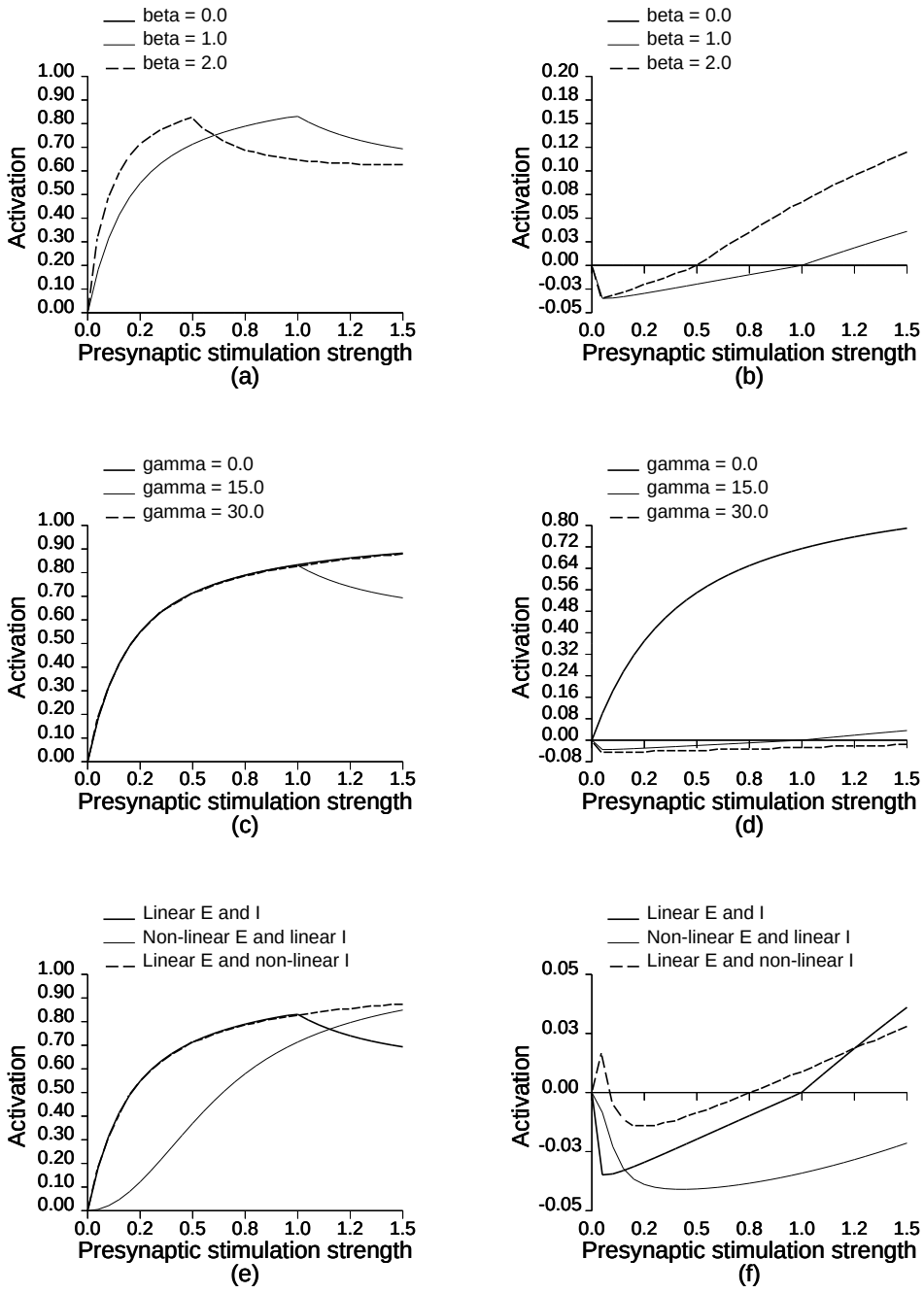

Figure A.2: Legend on next page.

Figure A.2: **The effects of varying β, γ, input excitation function, and input inhibition function on the activation equation.**
Figure on previous page. The initial network synaptic weights are given in Figure 2.8. The activation level of neuron a (left panels) and neuron b (right panels) was determined using Equation 2.1. The activation level of the input neuron a was varied from 0 to 1.5. In panels (a) and (b) $A = 0.1$, $B = 1.0$, $C = 0.05$, $\beta \in \{0.0,\ 1.0,\ 2.0\}$, and $\gamma = 15$. In panels (c) and (d) $A = 0.1$, $B = 1.0$, $C = 0.05$, $\beta = 1.0$, and $\gamma \in \{0,\ 15,\ 30\}$. In panels (e) and (f) $A = 0.1$, $B = 1.0$, $C = 0.05$, $\beta = 1.0$, and $\gamma = 15$. The label "Linear E and I" refers to using Equations 2.2 and 2.3 in Equation 2.1. The label "Non-linear E and linear I" refers to using Equations 2.3 in Equation 2.1, but Equation 2.2 was replaced by $E_j = \left(\sum_i [x_i] W_{ij}^{+}\right)^2$, and the "Linear E and non-linear I" refers to using Equations 2.2 in Equation 2.1, but Equation 2.3 was replaced by $I_j = \sum_k [x_k]^2 W_{kj}^{-}$. When $\beta = 0$, the activation of neurons a and b is 0.

Appendix B

Parameters used in the simulations of Chapters 3 and 4

The parameter values used in the simulations are presented in the following sections. The notation $[a]$ is defined to mean $\max(0, a)$. The notation $\lfloor a \rfloor$ is defined to mean the largest integer less than or equal to a.

B.1 Activation equation parameters

The parameters used for computing the activations were $A = 0.1$, $B = 1.0$, $C = 0.05$, $\beta = 0.1$, and $\gamma = 10$. The activation equation for Layer 2 neurons was numerically integrated using the Euler method with a time step of 0.013, and the activation levels of all the neurons were initially set to zero. The network was close to an equilibrium state by time = 27 (the maximal change in activation level was less than 10^{-6}).

During conditioning, the synaptic weight values were updated every 200 time steps. Weights were not changed during RF measurement.

B.2 Initial network

The initial network weights were set to have a coarse receptive field topography; nearby neurons were assigned overlapping afferent excitatory inputs. The model cortical

layer and the model left and right eye selective input layers had a 1-D ring arrangement.

Let model cortical neurons be refered to by the index $j \in \{0, \cdots, 41\}$, and left and right eye selective model input neurons be indexed by l and r, respectively. Then,

$$Z^+_{lj} = 0.56 \left(\exp\left(-\frac{((\lfloor i \rfloor + p) - i)^2}{1.22} \right) + 0.2\mathbf{R}_{lj} \right), \tag{B.1}$$

and

$$Z^+_{rj} = 0.56 \left(\exp\left(-\frac{((\lfloor i \rfloor + p) - i)^2}{1.22} \right) + 0.2\mathbf{R}_{rj} \right), \tag{B.2}$$

where $i = (\lfloor j/3 \rfloor)/2$, $p \in \{-3, -2, -1, 0, 1, 2, 3\}$, and $l, r = (\lfloor i \rfloor + p) \bmod 4$, and $\mathbf{R}_{lj}$ and $\mathbf{R}_{rj}$ are uniformly distributed independent random variables in $[0, 1)$.

The initial lateral inhibitory weights were assigned based on the amount of overlap in afferent pathways to the model cortical neurons. Lateral inhibitory weights between model cortical neurons j and k, where $j, k \in \{0, \cdots, 41\}$, were computed as follows. Let $j \neq k$ and

$$W^-_{jk} = W^-_{kj} = \sum_{l\,=\,0}^{6} \min\left(Z^+_{lj}, Z^+_{lk}\right) + \sum_{r\,=\,0}^{6} \min\left(Z^+_{rj}, Z^+_{rk}\right). \tag{B.3}$$

Then

$$Z^-_{jk} = Z^-_{kj} = \frac{0.05 W^-_{jk}}{\max\limits_{a,b \,\in\, \text{Model cortical layer}} W^-_{ab}}. \tag{B.4}$$

The lateral inhibitory pathway weights Z^-_{jj} were always fixed at 0.

After assigning the initial weights, the network was trained using binocular stimuli (Section B.3), and the resulting network was used for the various "classical" rearing and model pharmacological manipulations.

B.3 Training and test stimuli

During NR, the training stimuli were binocular inputs with a range of disparities, and some noise. The input to an eye was a 1-D truncated Gaussian centered at real-valued positions in the corresponding model input layer. The model left and right eye selective input neurons were placed at integer positions $\{0, \cdots, 6\}$. The inputs were wrapped around a 1-D ring topology. When monocular input was at position $x \in [0, 7)$, input layer neuron

$p \in \{0, \cdots, 6\}$ in that eye was assigned activation level

$$x_p = \exp\left(-1.2\left((q + \lfloor x \rfloor) - x\right)^2\right) + (0.01 - 0.02\mathbf{R}_p) \tag{B.5}$$

where $q \in \{-3, -2, -1, 0, 1, 2, 3\}$, $p = (\lfloor x \rfloor + q) \bmod 4$, and $\mathbf{R}_p$ is a uniformly distributed independent random variable in $[0, 1)$. The noise added to the left and right eyes was independent. If $x_p < 0.31$, it was set to 0. The disparities used were $\{-2,\ -4/3,\ -2/3,\ 0,\ 2/3,\ 4/3,\ 2\}$.

The 1-D truncated Gaussian input without any noise was used to map the monocular left and right eye RF of the model cortical neurons.

B.4 Normal rearing procedure

During normal rearing, a binocular input with randomly chosen disparity d at a randomly chosen cyclopean position $x \in [0, 7)$ was presented, where $d \in \{-2,\ -4/3,\ -2/3,\ 0,\ 2/3,\ 4/3,\ 2\}$. The disparity and cyclopean position were picked with a uniform probability distribution. A binocular input with disparity d at cyclopean position x had left eye input at $x - d/2$ and right eye input at $x + d/2$.

The network was trained with 1,500,000 presentations of binocular inputs. After 1,500,000 input presentations, the network weights and model cortical neuronal RFs were stable. The stability of the network was evaluated by measuring the Euclidean distance between the network weight vectors at intervals of 5000 input presentations. After 1,500,000 presentations of binocular inputs, the distance between the network weight vectors had reached an asymptote. With an additional 150,000 binocular input presentations, the mean distance between the afferent excitatory weight vectors after every 5000 input presentations (d_e) was was $5.009 \times 10^{-2} \pm 1.029 \times 10^{-2}$, the mean distance between the lateral inhibitory weight vectors after every 5000 input presentations (d_i) was $5.422 \times 10^{-2} \pm 1.180 \times 10^{-2}$, and the mean distance between the response vector of the neurons to monocular inputs after every 5000 input presentations (d_r) was $1.225 \times 10^{-2} \pm 1.629 \times 10^{-3}$. The Euclidean distance between weight vectors and the response vector between the network before and after the additional 150,000 binocular input presentations were: $D_e = 1.531 \times 10^{-1}$ for

afferent excitatory weights, $D_i = 8.637 \times 10^{-2}$ for lateral inhibitory weights, and $D_r = 2.958 \times 10^{-2}$ for the monocular responses. Because $D_e/d_e = 3.046 \ll (150,000/5000) = 30$, $D_i/d_i = 1.593 \ll 30$, and $D_r/d_r = 2.415 \ll 30$, the network appears to be very stable.

B.5 Classical rearing manipulations

To model MD, the right eye selective model input neurons were stimulated using the truncated 1-D Gaussian inputs, and the left eye selective model input neuron l was activated by zero mean noise, $(0.01 - 0.02\mathbf{R}_l)$, where $\mathbf{R}_l \in [0, 1)$ is a uniformly distributed independent random variable. The network was trained with 75,000 monocular inputs.

After 75,000 presentations of monocular inputs to the right eye, the left eye alone was stimulated by 50,000 presentations of monocular inputs to simulate RS. The left eye selective model input neurons were stimulated using the truncated 1-D Gaussian inputs, and the right eye selective model input neuron r was activated by zero mean noise, $(0.01 - 0.02\mathbf{R}_r)$, where $\mathbf{R}_r \in [0, 1)$ is a uniformly distributed independent random variable.

To model ST, the right eye selective model input neurons or the left eye selective model input neurons were stimulated using the truncated 1-D Gaussian inputs, and the unstimulated eye selective model input neuron m was activated by zero mean noise, $(0.01 - 0.02\mathbf{R}_m)$, where $\mathbf{R}_m \in [0, 1)$ is a uniformly distributed independent random variable. The network was trained with 500,000 strabismic inputs.

During BD, left eye and right eye selective model input neurons were activated by zero mean noise. Left eye selective model input input neuron l was activated by $(0.01 - 0.02\mathbf{R}_l)$, and right eye selective model input neuron r was activated by $(0.01 - 0.02\mathbf{R}_l)$, where $\mathbf{R}_l, \mathbf{R}_r \in [0, 1)$ are uniformly distributed independent random variables. The network was trained with 5,000,000 input presentations.

Following MD, ST, and BD, the network was trained with 500,000 presentations of binocular inputs used for normal rearing, to model RE.

B.6 Parameters for synaptic plasticity rules

The parameters used in the EXIN lateral inhibitory plasticity rule were $\delta = 0.00505$, $\mathcal{G}(x_i) = [([x_i])^2 + N_1]$, and $\mathcal{Q}(x_j) = \min(0.2, 3[x_j])$. The parameters used in the EXIN afferent excitatory plasticity rule were $\epsilon = 0.0025$, $\mathcal{F}(x_j) = [([x_j])^2 + N_2]$, and $\mathcal{H}(x_i) = [x_i]$.

N_1 and N_2 were zero-mean noise, where $\mathbf{N}_i = (0.0001 - 0.0002\mathbf{R}_i)$, where $i \in \{1, 2\}$, and $\mathbf{R}_i \in [0, 1)$ is a uniformly distributed independent random variable. Noise in the model input and cortical neurons was important in modeling the effects of chronic binocular deprivation (see Chapter 3, Section 3.3.5).

B.7 Parameters for aspecific action of pharmacological infusion

In these simulations, all the model cortical neurons were pharmacologically treated. APV strength was varied by using $\omega = 0.6$ and 0.2 in Equation 4.6, and muscimol strength was varied by using $\Im = 0.05$ and 0.1 in Equation 4.7 to obtain the simulation results presented in Figures 4.3 and 4.5, respectively.

For the results in Figure 4.4, lateral inhibitory learning alone was enabled ($\epsilon = 0$), and $\omega = 0.6$ was used in Equation 4.6. For the results in Figure 4.6, $\Im = 0.05$ was used in Equation 4.7 with lateral inhibitory and afferent excitatory plasticity using the parameters in Section B.6. The network was trained with 500,000 binocular input presentations.

B.8 Effects of pharmacological infusion

To model MD with pharmacological infusion, the right eye selective model input neurons were stimulated using the truncated 1-D Gaussian inputs, and the left eye selective model input neuron l was activated by zero mean noise, $(0.01 - 0.02\mathbf{R}_l)$, where $\mathbf{R}_l \in [0, 1)$ is a uniformly distributed independent random variable, and model cortical neurons $\{12, \cdots, 30\}$ were treated with an equal concentration of model APV or muscimol. OD after MD was measured at a residual APV or muscimol concentration of half the strength of the APV or

muscimol used during MD, or with no residual APV or muscimol. The network was trained with 75,000 monocular inputs.

To model NR with pharmacological infusion, binocular inputs were used to train the network with all model cortical neurons equally affected by the pharmacological infusion. The network was trained with 5,000,000 binocular inputs.

B.8.1 APV infusion

To study the effects of the amount of afferent excitatory plasticity and APV concentration during MD, ω was assigned values 0.9, 0.8, and 0.7, and the afferent excitatory plasticity rate ϵ was multiplied by a factor of 0, 0.35, and 0.70 (Figure 4.11) in afferent excitatory pathways to the APV-treated neurons.

To determine the role of cortical responsiveness on RF width and responsiveness after NR with APV, ω was varied through 1, 0.325, and 0.1, and the afferent excitatory plasticity rate in pathways to the model APV-affected neurons was zero. All the model cortical neurons were affected by model APV (Figure 4.13).

B.8.2 Muscimol infusion

To study the effects of the amount of lateral inhibitory plasticity and muscimol concentration during MD, $\Im$ was assigned the values 0.05, 0.1, and 0.2, and the afferent excitatory plasticity rate ϵ was not changed (Figure 4.12). The lateral inhibitory plasticity rate δ was multiplied by a factor of $0, 0.5, 1.0$ in lateral inhibitory pathways to neurons affected by muscimol.

To determine the role of cortical responsiveness on RF width and responsiveness after NR with muscimol, $\Im$ was varied through 0, 0.2, and 0.4. The lateral inhibitory and afferent excitatory plasticity rules used the parameters in Section B.6 (Figure 4.13).

Appendix C

Parameters used in the simulations of Chapter 5

The parameter values used to simulate the three models were chosen as follows. The notation $[a]$ is defined to mean $\max(0, a)$.

C.1 Parameters for the EXIN model simulations

The following parameters were used in all the EXIN simulations. To compute the initial weights, $\sigma_{\mathbf{ff}} = 1.41$, $\Psi = 0.2$, $\Gamma_{\mathbf{ff}} = 0.01$, $\Omega = 0.45$, and $\Gamma_{\mathbf{i}} = 0$ were used.

The parameters used for computing the activations were $A = 0.2$, $B = 2$, $C = 0.3$, $\beta = 0.1$, and $\gamma = 0.2$. The activation equation for Layer 2 neurons were numerically integrated using the Euler method with a time step of 0.2. The initial activation level of all the neurons was zero. The simulations were stopped at time = 110. At time = 110, the network was close to an equilibrium state by time = 110; the maximal change in Layer 2 neuronal activation at that point was less than 10^{-5}.

In the simulation, the weights were modified after the Layer 2 activations reached equilibrium on each input presentation. To compute the lateral inhibitory weight changes, parameters $\delta = 0.2$, $\mathcal{G}(a) = [a]$, and $\mathcal{Q}(a) = 3[a]$ were used. To compute the afferent excitatory weight changes, $\epsilon = 0.0016$, $\mathcal{F}(a) = [a]$, and $\mathcal{H}(a) = 0.4[a]$ were used. When the

afferent excitatory synaptic plasticity was enabled, the initially zero afferent weights are not changed. This was done to speedup convergence of the afferent weights.

C.1.1 Parameters for the activation equation

The parameters of the activation equation were chosen so that the network gave a distributed activation response to an input, instead of a winner-take-all response.

At equilibrium, $\frac{d}{dt}x_{pq} = 0$ and the activation levels of Layer 2 neurons are given by

$$x_{pq} = \frac{\beta B E_{pq} - \gamma C I_{pq}}{A + \beta E_{pq} + \gamma I_{pq}} \tag{C.1}$$

Because Equation 5.3 is a shunting equation, $x_{pq}(t) \in [-C, B]$ if $x_{pq}(0) \in [-C, B]$, for all $t \geq 0$ (Cohen & Grossberg, 1983). Thus, B is the maximum activation level and $-C$ is the minimum activation level of Layer 2 neurons. The constant A determines the passive decay rate.

Increasing β is equivalent to increasing the input strength. As β is increased, the activation levels of neurons receiving large excitation increase and the activation levels of neurons receiving zero or very weak excitation are suppressed. This property of the shunting equation is shown in Figure C.1a. Note that as β is increased (by a factor of 21), the Layer 2 activation profile expands very little. The activation level of neurons receiving strong excitation increases, and the activation level of neurons receiving very weak or zero excitation is further suppressed. As γ is increased, the activation levels of neurons first decrease and the response profile becomes narrower. At very large values of γ, the network behaves in a winner-take-all manner (Figure C.1b).

Increasing B is similar to increasing β. This property of the shunting equation is shown in Figure C.1c. Increasing C causes the Layer 2 activation profile to shift downwards. This property of the shunting equation is shown in Figure C.1d. At very large values of C, the network behaves in a winner-take-all manner.

The parameters were chosen so that none of the terms in the shunting equation (Equation 5.3) dominates the others. With such a choice, changes in the weights resulted in significant changes in RF size, shape, and responsiveness. The desirable dynamic

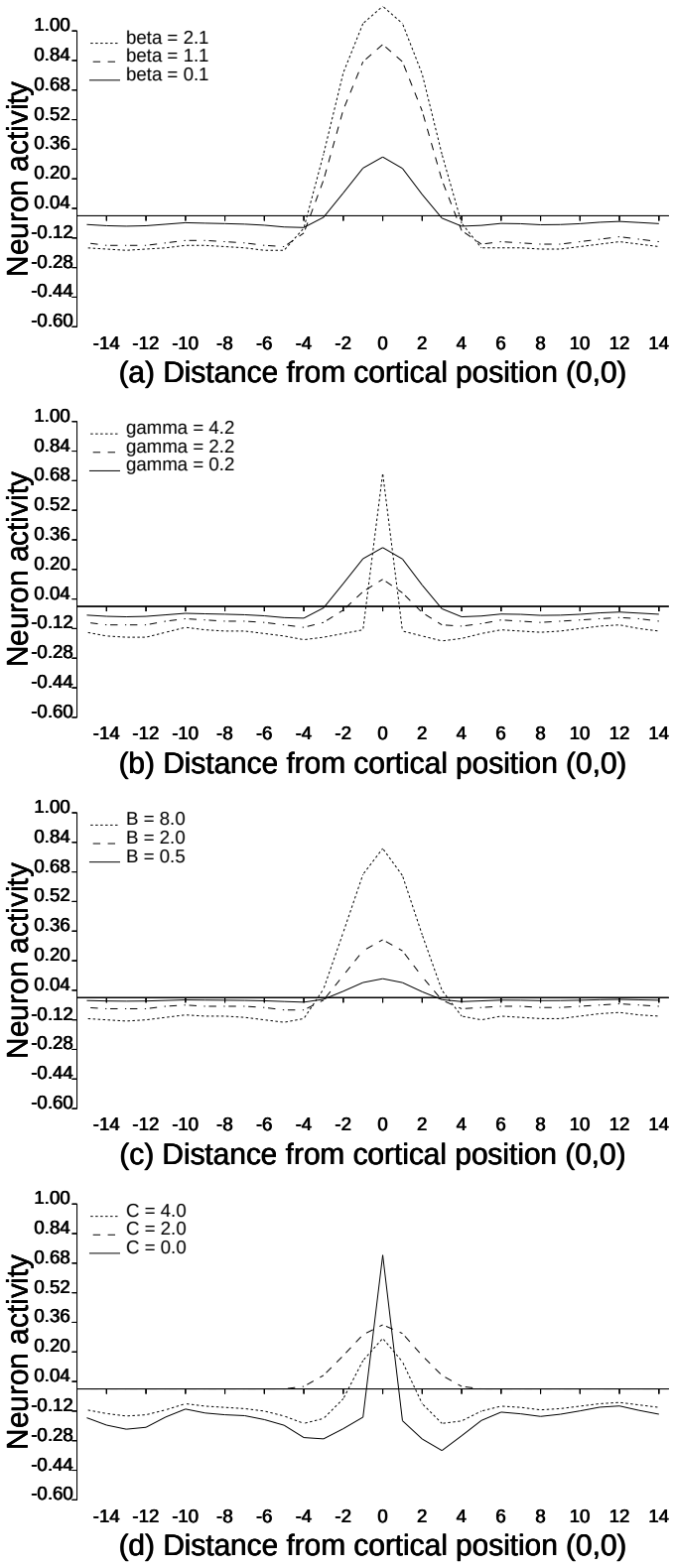

Figure C.1: Legend on next page.

Figure C.1: **Behavior of the EXIN network as a function of activation equation parameters.**
Figure on previous page. The equilibrium activation level of a one-dimensional cross-section of Layer 2: neurons $(0,-15)$–$(0,14)$, in response to input at $(0,0)$. The EXIN network used was obtained after training with 25,000 normal inputs with only lateral inhibitory synaptic plasticity enabled. The network reached a stable state by time 110. (a) The parameter β in Equation 3 is varied by a factor of 21, yet the width of the response curve increases by only a small amount. (b) When the parameter γ in Equation 3 is increased from 0.2 to 4.2, the network exhibits winner-take-all behavior. (c) The parameter B in Equation 3 is varied by a factor of 16, yet the width of the response curve increases by only a small amount. (d) When the parameter C in Equation 3 is set to 4, the network exhibits winner-take-all behavior. When C is zero, the neurons have non-negative activation levels.

RF changes can be obtained for a wide range of choices for the parameters in the shunting equation, as long as no term dominates the others.

The stability of the activation equation was established empirically. The activation equation was computed using the Euler method. Care was taken to ensure that the step size and the number of steps resulted in convergence and that there were no oscillations. Figure C.2 shows the activation as a function of time of 30 Layer 2 neurons in response to input at $(0,0)$.

Figures C.3b–c show that the activation equation converged during the training phase. During the training phase, the sum over all the Layer 2 neurons of the absolute change in activation level, at each step of the Euler method, is averaged over training input presentation at intervals of 100 input presentations.

Figures C.3b–c demonstrate the convergence of the shunting equation during the training phase using normal stimuli and scotoma stimuli, respectively, in the EXIN network with only lateral inhibitory synaptic plasticity enabled. The activation equation also converged to a fixed point during the other types of conditioning; the maximal change in Layer 2 neuronal activation was less than 10^{-5}.

C.1.2 Parameters for the learning equations

The rates of weight change in the EXIN synaptic plasticity rules were chosen so that spurious correlations do not produce large changes in the connection weights;

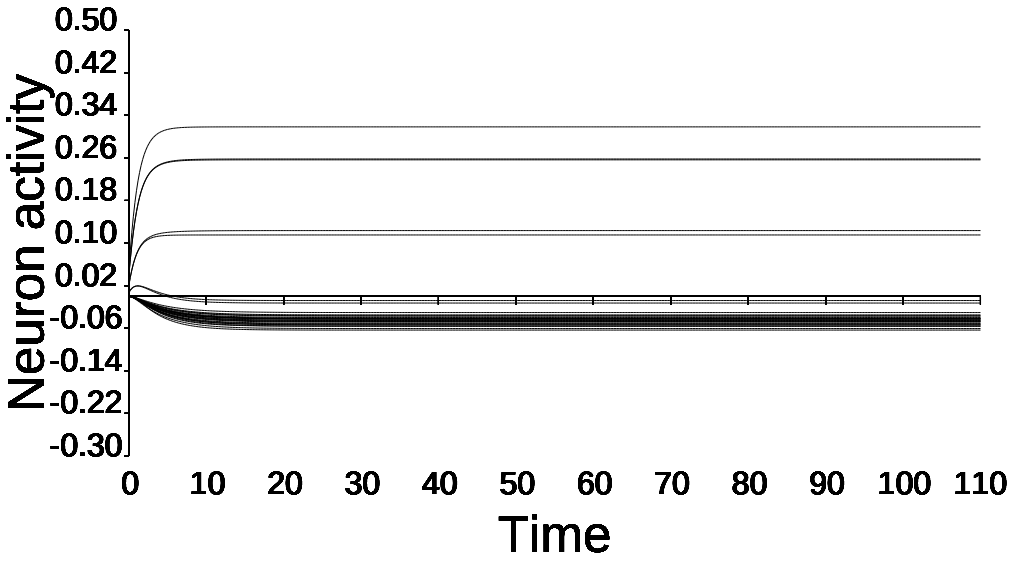

Figure C.2: **Activation curves in the EXIN network after whole-field stimulation.** The activation level of a one-dimensional cross-section of Layer 2: neurons $(0, -15)$–$(0, 14)$, in response to input at $(0, 0)$ in the EXIN network after training with 25,000 normal inputs with only lateral inhibitory synaptic plasticity enabled. The network equilibrates by time 110. Note that some neurons that were active during the initial stages are eventually suppressed.

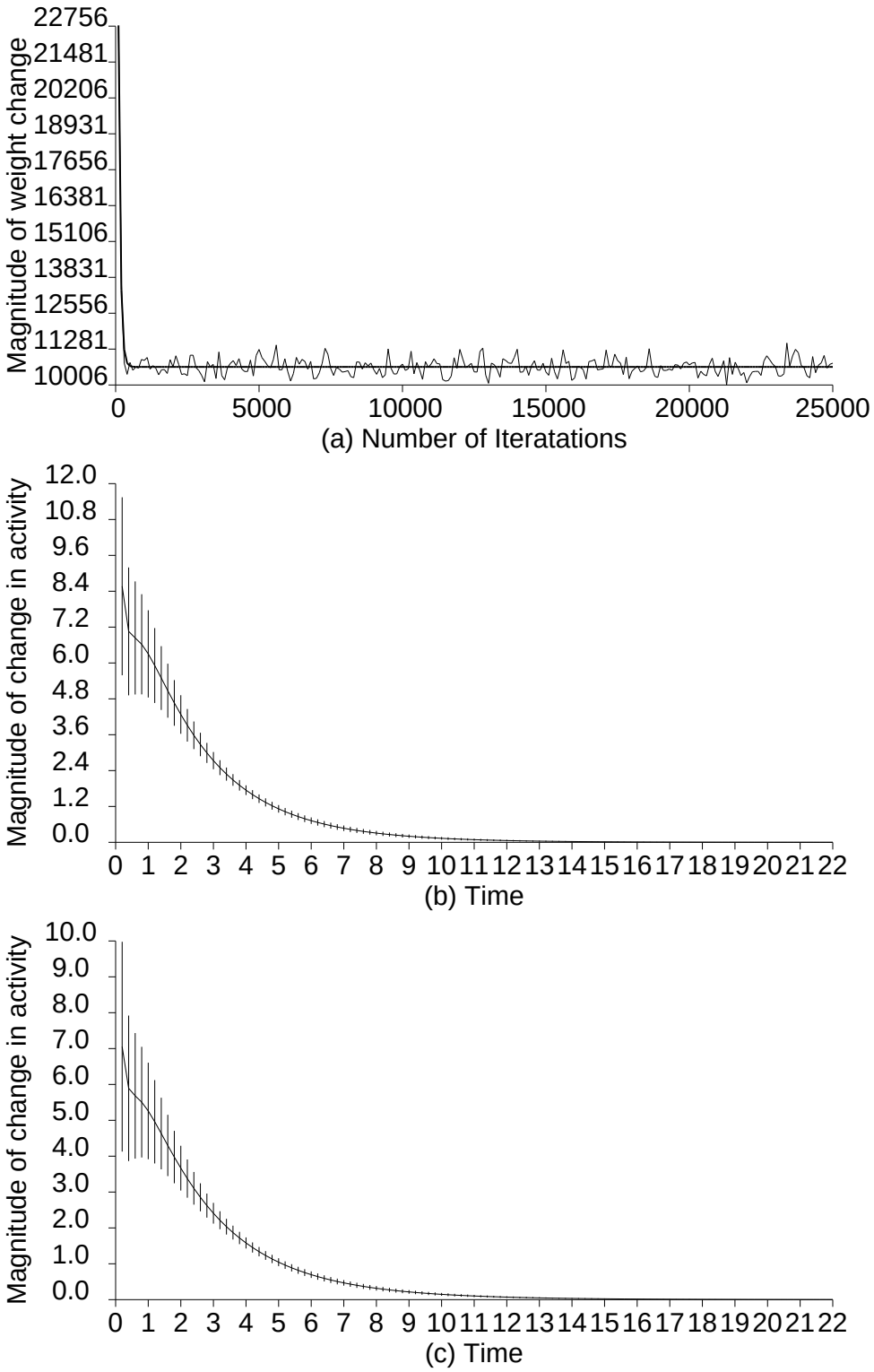

Figure C.3: Legend on next page.

Figure C.3: **Stability of the EXIN network with lateral inhibitory synaptic plasticity alone.**
Figure on previous page. The jagged line in panel (a) shows the total change in the lateral inhibitory pathway weights in the EXIN network, after 100 presentations of normal stimuli, over the course of 25,000 normal input presentations. The total change is obtained by summing the magnitude of the weight changes at intervals of 100 input presentations, over all the lateral inhibitory pathways. The smooth line in panel (a) is the nonlinear least squares fit of the data using the Marquardt-Levenberg algorithm. The non-linear function is $a \times \exp(-b \times \text{iteration number}) + c$. The best fit parameters are $a = 53864.9 \pm 5665.23$, $b = 1.490 \pm 0.098$, and $c = 10648.6 \pm 18.26$. The sum over all Layer 2 neurons, of the magnitude of change in the activation level at each step in the Euler method for solving the activation equation (Equation 3), is averaged over input presentations at intervals of 100 during normal conditioning (b), and during scotoma conditioning (c). The vertical lines in (b,c) represent the standard deviation.

only consistent correlations over several input presentations produce significant changes in connection weights. Figure C.3a plots the sum of the absolute weight change in all lateral inhibitory pathways after every 100 training input presentations, in the EXIN network with only lateral inhibitory synaptic plasticity enabled during normal conditioning.

During the normal conditioning phase, the EXIN network simulations with lateral inhibitory plasticity alone, with afferent excitatory plasticity alone, and with both lateral inhibitory and afferent excitatory plasticity were trained until the sum of the absolute weight change in plastic pathways after every 100 input presentations reached an asymptote.

The Euclidean distance between the network weight vector before and after an additional $10,000$ training steps (D), was compared with the average Euclidean distance between the network weight vectors at successive intervals of 100 training steps (d). With lateral inhibitory synaptic plasticity alone $D = 24.599667$, $d = 15.691748 \pm 0.251141$ ($D/d = 1.568$), with afferent excitatory synaptic plasticity alone $D = 0.451494$ and $d = 0.050187 \pm 0.000005$ ($D/d = 8.996$), and with both synaptic plasticity rules $D = 0.699971$ and $d = 0.052240 \pm 0.000005$ ($D/d = 13.399$) for the afferent excitatory weights and $D = 19.516132$ and $d = 12.193612 \pm 0.194959$ ($D/d = 1.601$) for the lateral inhibitory weights. In all cases $D/d \ll 10,000/100 = 100$, suggesting that the networks are close to an equilibrium point.

C.2 Parameters for the LISSOM simulations

To compute the initial weights in the LISSOM simulations $\sigma_{\mathbf{ff}} = 1$, $\sigma_{\mathbf{e}} = 1.41$, $\sigma_{\mathbf{i}} = 2.36$, $\Gamma_{\mathbf{ff}} = 0.01$, $\Gamma_{\mathbf{e}} = 0.1$, and $\Gamma_{\mathbf{i}} = 0.001$ were used.

The parameters used for computing the activations were $\gamma_{\mathbf{ff}} = 0.8$, $\gamma_{\mathbf{e}} = 1.8$, and $\gamma_{\mathbf{i}} = 1.3$. During training and testing LISSOM with only afferent excitatory, lateral excitatory, or lateral inhibitory synaptic plasticity enabled, the activation equation was close to an equilibrium state by 30 iterations. The initial value of the activation level was zero for all neurons.

The weights were modified after the Layer 2 activations reached equilibrium on each input presentation. To compute the weight changes, parameters $\xi_{\mathbf{ff}} = 0.01$, $\xi_{\mathbf{e}} = 0.0005$, and $\xi_{\mathbf{i}} = 0.01$ were used. The weights, which were initially set to zero, were not changed. Without this restriction, normalization would cause all the weights to become very small.

C.2.1 Parameters for the activation equation

The parameters of the activation equation were chosen so that the network gave a distributed activation response to its inputs. The LISSOM activation equation rapidly converges (Sirosh & Miikkulainen, 1994b). The parameters were chosen so that none of the terms in the LISSOM activation equation (Equation 5.14) dominated the others. In all the LISSOM simulations, the maximal change in Layer 2 neuronal activation was less than 10^{-5} when the activation equation computation was stopped.

C.2.2 Parameters for the learning equations

The rates of weight change in the LISSOM synaptic plasticity rules were chosen so that changes in the connection weights because of spurious correlations gets averaged over a large number of input presentations.

In the initial normal conditioning phase, the networks were trained until the amount of weight change reached an asymptote (the criterion is the same as for the EXIN simulations).

With an additional 10,000 normal training inputs, $D = 0.219775$, $d = 0.017082 \pm 0.000001$ ($D/d = 12.866$) with only lateral inhibitory synaptic plasticity enabled, $D = 2.256291$ and $d = 0.620959 \pm 0.000422$ ($D/d = 3.634$) with only lateral excitatory synaptic plasticity enabled, and $D = 3.065377$ and $d = 0.795790 \pm 0.000873$ ($D/d = 3.852$) with only afferent excitatory synaptic plasticity enabled. $D/d \ll 100$, suggesting that the networks are close to an equilibrium state.

C.3 Parameters for the adaptation model simulations

To compute the initial weights in the inhibition-dominant adaptation model, parameters $\sigma_{\mathbf{ff}} = 2.13$, $\sigma_{\mathbf{e}} = 1.19$, $\sigma_{\mathbf{i}} = 3.53$, $\Gamma_{\mathbf{ff}} = 0.01$, $\Gamma_{\mathbf{e}} = 0.1$, and $\Gamma_{\mathbf{i}} = 0.001$ were used.

In the adaptation model with no lateral interaction, the lateral excitatory and lateral inhibitory weights were set to zero. The excitation-dominant adaptation model had the same weights as the inhibition-dominant adaptation model. The initial adaptation level was 0.

In the inhibition-dominant adaptation model, the parameters used for computing the activations were $A = 0.2$, $B = 2$, $C = 0.3$, $\beta_{\mathbf{ff}} = 1$, $\beta_{\mathbf{e}} = 0.1$, and $\gamma = 8$. The activation equations for Layer 2 neurons were numerically integrated using the Euler method with a time step of 1/75. The network was very close to an equilibrium state by time = 15; the maximal change in Layer 2 neuronal activation was less than 10^{-5}.

In the adaptation model with no lateral interaction, the activation equation was solved analytically. With no lateral interactions, the activation equation equilibrates when

$$x_{pq} = \frac{BE_{pq}}{A + E_{pq}}, \tag{C.2}$$

where $E_{pq} = \beta_{\mathbf{ff}} \Sigma_{(i,j) \in \text{Layer } 1} [x_{ij}] Z^{+}_{ij,pq}$, $A = 0.2$, $B = 2$, and $\beta_{\mathbf{ff}} = 1$.

In the excitation-dominant adaptation model, $A = 0.2$, $B = 2$, $C = 0.3$, $\beta_{\mathbf{ff}} = 0.1$, $\beta_{\mathbf{e}} = 0.01$, and $\gamma = 0$. The activation equations for Layer 2 neurons were numerically integrated using the Euler method with a time step of 1/75. The network reached an equilibrium state by time = 15.

In all three adaptation models, the initial activation level of all neurons was zero. The adaptation threshold parameters were modified after the Layer 2 activations reached equilibrium on each input presentation. To compute the changes in the adaptation threshold, $\rho = 0.0004$, $\eta = 0.3$, and $\tau = 15$ were used in the inhibition-dominant adaptation model. In the adaptation model without lateral interaction and the excitation-dominant adaptation model, $\rho = 0.0004$, $\eta = 0.3$, and $\tau = 2$ were used.

C.3.1 Parameters for the activation equation

The shunting equation (Equation 5.16) was used in the adaptation models. However, the activation equation in the adaptation models differs from the activation equation in the EXIN model in two respects: (1) the presence of lateral excitation in the adaptation model; (2) the threshold in computing lateral excitation and lateral inhibition. The parameters of the activation equation were chosen so that the network gave a distributed response to its inputs.

The activation equation in the adaptation model behaved similarly to the activation equation in the EXIN model. To make the model inhibition-dominant (excitation-dominant) the constant β_e was chosen to be much smaller (larger) than the constant γ. As neurons are habituated they propagate less lateral excitation and lateral inhibition.

In all the adaptation model simulations, the maximal change in Layer 2 neuronal activation was less than 10^{-6} when the activation equation computation was stopped. The adaptation model with no lateral interaction had a unique fixed point (Equation C.2).

C.3.2 Parameters for the adaptation equation

The rate of the adaptation equation was chosen so that the adaptation level of neurons depended on neuronal activation over a large number of input presentations. In the initial normal conditioning phase, the networks were trained until the amount of weight change reached an asymptote (the criterion is the same as for the EXIN simulations).

With an additional 10,000 normal training inputs, $D = 0.229360$, $d = 0.088466 \pm 0.000293$ ($D/d = 2.593$) in the network with no lateral interaction, $D = 0.113066$

and $d = 0.032176 \pm 0.000004$ ($D/d = 3.514$) in the inhibition dominant network, and $D = 0.131278$ and $d = 0.026841 \pm 0.000017$ ($D/d = 4.891$) in the excitation dominant network. In the all these networks $D/d \ll 100$, suggesting that the networks are close to an equilibrium point.

C.4 Parameters for generating the inputs for the simulations

In generating the input patterns for training, the kernel K was

$$K = \begin{bmatrix} 0.55 & 0.74 & 0.55 \\ 0.74 & 1.00 & 0.74 \\ 0.55 & 0.74 & 0.55 \end{bmatrix}.$$

The probability, Φ, that the input at each position is 1 was 0.02.

C.5 Parameters for RF measurements

The threshold Θ used for RF measurements was chosen as follows. The activation level of Layer 2 neurons was scaled relative to 1.25 times the maximal response of Layer 2 neuron to test stimuli, in the network obtained after the initial whole-field stimulation. In all the simulations, $\Theta = 0.01$.

C.6 Conditioning procedure

After setting the initial weights in the models, the equilibrium state of the weights or the adaptation levels with respect to the inputs used in the simulations was obtained by training the networks with 25,000 presentations of normal stimuli, except for the EXIN network with afferent synaptic plasticity, and the EXIN network with afferent and lateral inhibitory synaptic plasticity, which were trained with 50,000 presentations of normal stimuli, and the LISSOM network with only lateral excitatory synaptic plasticity, which was trained with 75,000 presentations of normal stimuli. For scotoma and complementary scotoma conditioning and for reversing the effects of scotoma and complementary scotoma

conditioning, 5000 presentations of the appropriate stimulus were used, except for the EXIN network with afferent synaptic plasticity and the EXIN network with afferent and lateral inhibitory synaptic plasticity, which were trained with 50,000 input presentations, and the LISSOM network with only lateral excitatory synaptic plasticity, which was trained with 25,000 input presentations. In complementary scotoma conditioning, the complementary scotoma stimuli were alternated.

Appendix D

Parameters used in the simulations of Chapter 6

The parameter values used in the simulations are presented in the following sections. The notation $[a]$ is defined to mean $\max(0, a)$, and the notation $\lfloor a \rfloor$ is defined to mean the largest integer less than or equal to a. In all the simulations, the weights were modified after the Layer 2 activations were close to equilibrium on each input presentation.

D.1 Parameters for the activation equation

The parameters used for computing the activations were $A = 0.2$, $B = 2.0$, $C = 0.3$, $\beta = 0.01$, and $\gamma = 1.3$. The activation equations for Layer 2 neurons were numerically integrated using the Euler method with a time step of $1/1200$, and the activations of all the neurons were initially set to zero. The network was close to an equilibrium state by time = 14.

The parameters of the activation equation were chosen so that the network gave a distributed activation response to an input, instead of a winner-take-all response.

Because Equation 6.8 is a shunting equation, $x_{pq}(t) \in [-C, B]$ if $x_{pq}(0) \in [-C, B]$, $t \geq 0$ (Cohen & Grossberg, 1983). Thus, B is the maximum activation level and $-C$ is the minimum activation level of Layer 2 neurons. The constant A determines the passive decay

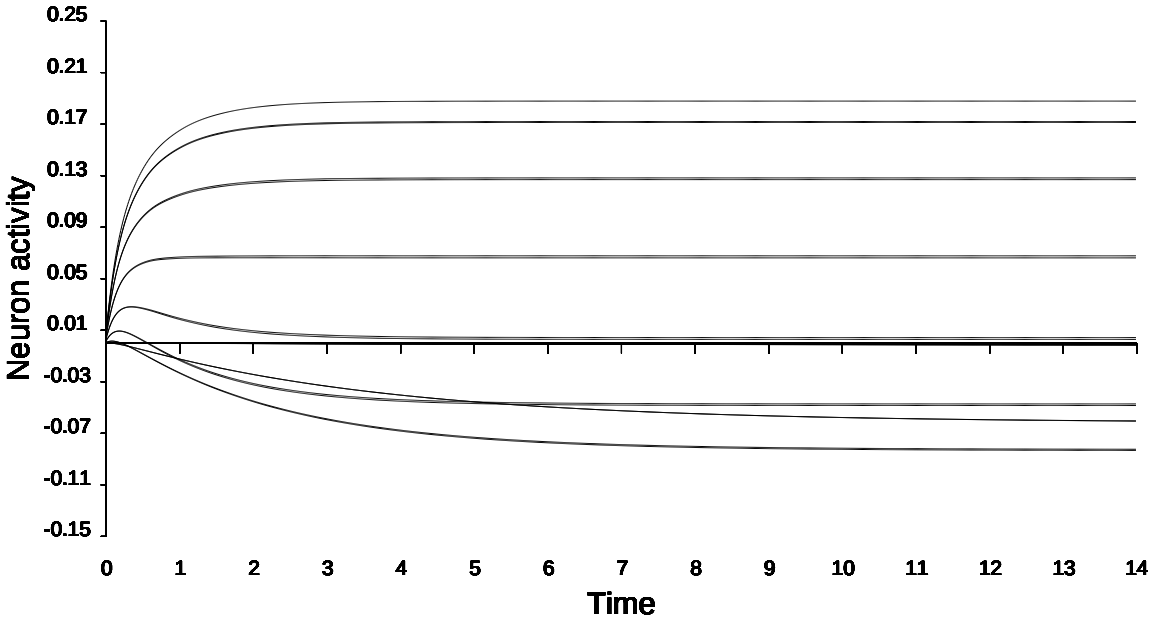

Figure D.1: **Activation curves in the EXIN network after ICMS.** The activation of a one-dimensional cross-section of Layer 2, neurons $(0,-15)$–$(0,14)$, in response to a test input at $(0,0)$ in the EXIN network after 500 ICMS presentations using the parameters of the simulation in Section 6.3.1. After ICMS the lateral inhibitory weights were not symmetric (Figure 6.5). The network equilibrated by time 14. Some neurons that were active during the initial stage were eventually suppressed.

rate. The effects of the parameters on neuronal activation are described in Appendix C.

The stability of the activation equation was established empirically. The activation equation was computed using the Euler method. Care was taken to ensure that the step size and the number of steps resulted in convergence, and that there were no oscillations (Figure D.1). The activation equation was close to a stable fixed point during the various ICMS and peripheral stimulation simulations; the maximal change in activation level of Layer 2 neurons was less than 5×10^{-5} when the Euler method was terminated.

D.2 Parameters for initial synaptic strength values

To obtain topographically arranged RFs, the parameters in Equations 6.13 and 6.17 were set to the following values: $\sigma_{\mathbf{ff}} = \sqrt{20}$, $\Gamma_{\mathbf{ff}} = 0.1$, $\mu = 0.45$,

and $\Gamma_{\mathbf{i}} = 0.0$.

To obtain nontopographically arranged RFs, Equation 6.13 was replaced by

$$Z^{+}_{ij,pq} = \left[(0.25 + 0.75\Phi_{ij,pq}) \exp\left(\frac{-(x'^2 + y'^2)}{\sigma^2_{\mathbf{ff}}} \right), \Gamma_{\mathbf{ff}} \right], \tag{D.1}$$

where

$$[a, b] \equiv \begin{cases} a & \text{if } a > b, \\ 0 & \text{otherwise,} \end{cases} \tag{D.2}$$

$x' = x + (\lfloor 7\Psi_{1,pq} \rfloor - 3)$, $y' = y + (\lfloor 7\Psi_{2,pq} \rfloor - 3)$, $x, y \in \{-15, \cdots, 14\}$, $p = (((i + 15) + x) \bmod 30) - 15$, and $q = (((j + 15) + y) \bmod 30) - 15$. The variables $\Phi_{ij,pq}$, $\Psi_{1,pq}$, and $\Psi_{2,pq}$ are independent uniformly distributed random variable in $[0, 1)$. The lateral inhibitory weights were computed using Equation 6.17. The parameter values were $\sigma_{\mathbf{ff}} = \sqrt{20}$, $\Gamma_{\mathbf{ff}} = 0.1$, $\mu = 0.45$, and $\Gamma_{\mathbf{i}} = 0.0$. The indices i, j, p, and q range from -15 to 14. The above equations relating the indices i, j, p, and q and the distances x and y were used because the model cortical and thalamic neurons were arranged in a two-dimensional grid which was wrapped around.

After setting the weight values of the afferent excitatory and lateral inhibitory pathways, the network underwent a training phase using whole-field stimulation.

D.3 Parameters for the initial training phase

After the initial weights in the network were set, the network was trained with 5,000 presentations of whole-field stimuli. The probability, Ξ, that the input at each position is 1 was 0.0033. The resultant network was used for ICMS simulations.

During the whole-field training phase, to compute the lateral inhibitory weight changes, Equation 6.4 with $\delta = 0.2$, $\mathcal{G}(a) = [a]$, and $\mathcal{Q}(a) = 3.0 \times [a]$ was used, and to compute the afferent excitatory weight changes, Equation 6.6 with $\epsilon = 0.04$, $\mathcal{F}(a) = [a]$, and $\mathcal{H}(a) = 2.5 \times [a]$ was used. The excitation and inhibition in this simulation were combined using Equations 6.11–6.12. The same equations were used during the training phase of the network with nontopographically arranged RFs. The rates of weight change in the learning rules were chosen so that spurious correlations did not significantly change the connection weights.

D.4 Parameters for ICMS simulations

The network obtained after the initial training phase (Section D.3) was used for ICMS simulations.

D.4.1 ICMS simulations in Section 6.3.1

This simulation was performed on the network with topographically arranged RFs. The lateral inhibitory weight changes were governed by Equation 6.5 with $\delta = 0.2$, $G(a) = [a]$, and $Q(a) = 3.0 \times [a]$, and afferent excitatory weights changed according to Equation 6.7 with $\epsilon = 0.04$, $F(a) = [a]$, and $H(a) = 2.5 \times [a]$.

The model ICMS was simulated using Equations 6.1–6.3 in Section 6.2.2 with $(p_0, q_0) = (0,0)$, $(i_0, j_0) = (0,0)$, $\varphi_0 = 0.04$, $\sigma_1 = 10$, $\phi_1 = 0.02$, $\varphi_1 = 0.37$, $\sigma_2 = 16.67$, $\sigma_3 = 50$, $\phi_2 = 0.0037$, $\varphi_2 = 0.0686$, $\sigma_4 = 100$, and $\sigma_5 = 12.5$. The excitation and inhibition during ICMS were combined using Equations 6.9–6.10. Model ICMS was presented 500 times. To determine the temporal effects of ICMS the network was trained with an additional 500 presentations of ICMS.

D.4.2 ICMS simulations in Section 6.3.2

In all the simulations in this section, ICMS was presented 500 times. To determine the role of afferent excitatory synaptic plasticity in producing RF changes after ICMS, lateral inhibitory synaptic plasticity was disabled. To analyze the effects produced by lateral inhibitory synaptic plasticity rule, afferent excitatory synaptic plasticity was disabled. In these two simulations, other parameters were the same as in Section 6.3.1 (see the previous subsection).

To determine the effects of the strength and distribution of direct excitation to model cortical neurons and excitation to afferent excitatory synaptic terminals because of ICMS, the parameters in Equation 6.1 and Equation 6.2 were varied. The values of parameters in Equation 6.1 were changed as follows. The value of φ_0 was independently changed from 0.04 to 80, and the value of φ_0 and σ_1 were simultaneously changed from 0.04 to 80 and 10 to 100, respectively. The other parameter values were the same as in

Section 6.3.1 (see the previous subsection).

The values of parameters in Equation 6.2 were changed independently. The other parameter values were the same as in Section 6.3.1 (see the previous subsection). The value of ϕ_1 was changed from 0.02 to 0.04, φ_1 was changed from 0.37 to 0.555, σ_2 was changed from 16.67 to 33.34, and σ_3 was changed from 50 to 100.

To analyze the effects of the strength and distribution of excitation to lateral inhibitory pathways induced by ICMS, the parameters in Equation 6.3 were independently varied. The other parameter values were the same as in Section 6.3.1 (see the previous subsection). The value of ϕ_2 was changed from 0.0037 to 0.0074, φ_2 was changed from 0.0686 to 0.1372, σ_4 was changed from 100 to 200, and σ_5 was changed from 12.5 to 25.

D.4.3 ICMS simulations in Section 6.3.3

This simulation was performed on the network obtained after an initial training phase (Section D.3) on a network with nontopographically arranged RFs (Section D.2). The values for the parameters in Equations 6.1–6.3 were the same as those in Section 6.3.1. The ICMS was presented 500 times.

D.5 Parameters for peripheral stimulation simulations

The network obtained after the initial training phase (Section D.3) was used for ICMS simulations. During peripheral stimulation only lateral inhibitory learning was enabled. To compute the lateral inhibitory weight changes, Equation 6.4 with $\delta = 0.2$, $\mathcal{G}(a) = [a]$, and $\mathcal{Q}(a) = 3.0 \times [a]$ was used. These parameter values are the same as in the lateral inhibitory synaptic plasticity rule during the initial training phase (Section D.3). The total excitation and inhibition to the model cortical neurons were computed using Equations 6.11–6.12.

To simulate strong localized peripheral stimulation a truncated Gaussian convolution kernel K was centered at Layer 1 location $(0, 0)$. To simulate weak localized peripheral stimulation, K was scaled by a multiplicative factor of 0.15. The peripheral

stimulation was presented 1000 times. The kernel K was

$$K = \begin{bmatrix} 0.55 & 0.74 & 0.55 \\ 0.74 & 1.00 & 0.74 \\ 0.55 & 0.74 & 0.55 \end{bmatrix}.$$

D.6 Parameters for RF measurements

The RF was mapped using single-point stimulation, blurred with the kernel K, at all input positions (i, j). The activation of model cortical neurons was scaled relative to the maximal activation of model cortical neurons in response to the RF test input, K, over all the input locations. The RF of a Layer 2 neuron (p, q) was defined as the collection of positions (i, j) at which the test input caused the scaled activation of model cortical neurons to exceed a threshold $\Theta = 0.01$.

Bibliography

[1] Abraham, W.C. & Goddard, G.V. (1983) Asymmetric relationships between homosynaptic long-term potentiation and heterosynaptic long-term depression. *Nature*, **305**, 717–719.

[2] Ahmed, B.A., Anderson, J.C., Douglas, R.J., Martin, K.A.C., & Nelson, J.C. (1994) Polyneuronal innervation of spiny stellate neurons in cat visual cortex. *The Journal of Comparative Neurology*, **341**, 39–49.

[3] Andersen, P., Sundberg, S.H., Sveen, O., & Wigström, H. (1977) Specific long-lasting potentiation of synaptic transmission in hippocampal slices. *Nature*, **266**, 736–737.

[4] Artola, A., Bröcher, S., & Singer, W. (1990) Different voltage-dependent threshold for inducing long-term depression and long-term potentiation in slices of rat visual cortex. *Nature*, **347**, 69–72.

[5] Artola, A. & Singer, W. (1987) Long-term potentiation and NMDA receptors in rat visual cortex. *Nature*, **330**, 649–652.

[6] Atick, J. & Redlich, A. (1990) Toward a theory of early visual processing. *Neural Computation*, **2**, 308–320.

[7] Badcock, D.R. & Westheimer, G. (1985) Spatial location and hyperacuity: The center-surround localization function has two substrates. *Vision Research*, **25**, 1259–1269.

[8] Baloch, A.A. & Grossberg, S. (1997) A neural model of high-level motion processing: Line motion and formotion dynamics. *Vision Research*, **37 (21)**, 3037–3059.

[9] Barlow, H.B., Blakemore, C., & Pettigrew, J.D. (1967) The neural mechanism of binocular depth discrimination. *Journal of Physiology*, **193**, 327–342.

[10] Barrionuevo, G. & Brown, T.H. (1983) Associative long-term potentiation in hippocampal slices. *Proceedings of the National Academy of Sciences of the USA*, **80**, 7347–7351.

[11] Bear, M.F., Cooper, L.N., & Ebner, F.F. (1987) The physiological basis of a theory for synapse modification. *Science*, **237**, 42–48.

[12] Bear, M.F., Kleinschmidt, A., Gu, Q., & Singer, W. (1990) Disruption of experience-dependent synaptic modifications in striate cortex by infusion of an NMDA receptor antagonist. *The Journal of Neuroscience*, **10(3)**, 909–925.

[13] Bear, M.F., Press, W.A., & Connors, B.W. (1992) Long-term potentiation in slices of kitten visual cortex and the effects of NMDA receptor blockade. *Journal of Neurophysiology*, **67(4)**, 841–851.

[14] Bednar, J.A. & Miikkulainen, R. (1997) A neural network model of visual tilt aftereffect. In *Proceedings of the 19th Annual Conference of the Cognitive Science Society*, 37–42. Hillsdale, NJ: Erlbaum.

[15] Benevento, L.A., Creutzfeldt, O.D., & Kuhnt, U. (1972) Significance of intracortical inhibition in the visual cortex. *Nature*, **238**, 124–126.

[16] Bienenstock, E.L., Cooper, L.N., & Munro, P.W. (1982) Theory for the development of neuron selectivity: Orientation specificity and binocular interaction in visual cortex. *The Journal of Neuroscience*, **2**, 32–48.

[17] Blake, R. (1989) A neural theory of binocular rivalry. *Psychological Review*, **96**, 145–167.

[18] Blake, R., Fox, R., & McIntyre, C. (1971) Stochastic properties of stabilized-imaged binocular rivalry alternations. *Journal of Experimental Psychology*, **88**, 327–332.

[19] Blake, R. & O'Shea, R.P. (1988) "Abnormal fusion" of stereopsis and binocular rivalry. *Psychological Review*, **95**, 151–154.

[20] Blake, R., Yang, Y., & Wilson, H.R. (1991) On the coexistence of stereopsis and binocular rivalry. *Vision Research*, **31**, 1191–1203.

[21] Blakemore, C., Carpenter, R.H.S., & Georgeson, M.A. (1970) Lateral inhibition between orientation detectors in the human visual system. *Nature*, **228**, 37–39.

[22] Blakemore, C., Fiorentini, A., & Maffei, L. (1972) A second neural mechanism of binocular depth discrimination. *Journal of Physiology*, **226**, 725–749.

[23] Blakemore, C. & Nachmias, J. (1971) The orientation specificity of two visual after-effects. *Journal of Physiology*, **213**, 157–174.

[24] Blakemore, C. & Tobin, E.A. (1972) Lateral inhibition between orientation detectors in the cat's visual cortex. *Experimental Brain Research*, **15**, 439–440.

[25] Blakemore, C. & Van Sluyters, R.C. (1974) Reversal of the physiological effects of monocular deprivation in kittens: Further evidence for a sensitive period. *Journal of Physiology*, **237**, 195–216.

[26] Blakemore, C. & Van Sluyters, R.C. (1975) Innate and environmental factors in the development of the kitten's visual cortex. *Journal of Physiology*, **248**, 663–716.

[27] Blasdel, G.G. (1992a) Differential imaging of ocular dominance and orientation selectivity in monkey striate cortex. *The Journal of Neuroscience*, **12**, 3115–3138.

[28] Blasdel, G.G. (1992b) Orientation selectivity, preference and continuity in monkey striate cortex. *The Journal of Neuroscience*, **12**, 3139–3161.

[29] Blasdel, G.G., Lund, J.S., & Fitzpatrick, D. (1985) Intrinsic connections of macaque striate cortex: Axonal projections of cells outside lamina 4C. *The Journal of Neuroscience*, **5**, 3350–3369.

[30] Blasdel, G.G., Obermayer, K., & Kiorpes, L. (1995) Organization of ocular dominance and orientation columns in the striate cortex of neonatal macaque monkeys. *Visual Neuroscience*, **12**, 589–603.

[31] Blasdel, G.G. & Salama, G. (1986) Voltage sensitive dyes reveal a modular organization in monkey striate cortex. *Nature*, **321**, 579–585.

[32] Bonds, A.B. & DeBruyn, E.J. (1985) Inhibition and spatial selectivity in the visual cortex: The cooperative neuronal network revisited. In *Models of the Visual Cortex*, D. Rose & V.G. Dobson (eds.), 292–299. New York: John Wiley & Sons.

[33] Bonhoeffer, T. & Grinvald, A. (1991) Iso-orientation domains in cat visual cortex are arranged in pinwheel-like patterns. *Nature*, **353**, 429–431.

[34] Bosking, W.H., Zhang, Y, Schofield, B., & Fitzpatrick, D. (1997) Orientation selectivity and the arrangement of horizontal connections in tree shrew striate cortex. *The Journal of Neuroscience*, **17(6)**, 2112–2127.

[35] Breese, B.B. (1899) On inhibition. *Psychological Review*, **3(11)**.

[36] Breese, B.B. (1909) Binocular rivalry. *Psychological Review*, **16**, 410–415.

[37] Brown, T.H. & Chattarji, S. (1995) Hebbian synaptic plasticity. In *The Handbook of Brain Theory and Neural Networks*, M.A. Arbib (ed.), 454–459. Cambridge, MA: MIT Press.

[38] Brown, T.H., Kairiss, E.W., & Keenan, C.L. (1990) Hebbian synapses: Biophysical mechanisms and algorithms. *Annual Review of Neuroscience*, **13**, 475–511.

[39] Buisseret, P., Gary-Bobo, E., & Imbert, M. (1982) Plasticity in the kitten's visual cortex: Effects of the suppression of visual experience upon the orientational properties of visual cortical cells. *Developmental Brain Research*, **4**, 417–426.

[40] Butler, T. & Westheimer, G. (1978) Interference with stereoscopic acuity: Spatial, temporal, and disparity tuning. *Vision Research*, **18**, 1387–1392.

[41] Callaway, E.M. & Katz, L.C. (1990) Emergence and refinement of clustered horizontal connections in cat striate cortex. *The Journal of Neuroscience*, **10**, 1134–1153.

[42] Campbell, F.W. & Howell, E.R. (1972) Monocular alternation: A method for the investigation of pattern vision. *Journal of Physiology*, **225**, 19–21.

[43] Carew, T.J., Hawkins, R.D., Abrams, T.W., & Kandel, E.R. (1984) A test of Hebb's postulate at identified synapses which mediate classical conditioning in *Aplysia*. *The Journal of Neuroscience*, **4**, 1217–1224.

[44] Carpenter, G. & Grossberg, S. (1987) A massively parallel architecture for a self-organizing neural pattern recognition machine. *Computer Vision, Graphics, and Image Processing*, **37**, 54–115.

[45] Chapman, B. & Stone, L.S. (1996) Turning a blind eye to cortical receptive fields. *Neuron*, **16**, 9–12.

[46] Chapman, B., Stryker, M.P., & Bonhoeffer, T. (1996) Development of orientation preference maps in ferret primary visual cortex. *The Journal of Neuroscience*, **16**, 6443–6453.

[47] Chino, Y.M., Kaas, J.H., Smith III, E.L., Langston, A.L., & Cheng, H. (1992) Rapid reorganization of cortical maps in adult cats following restricted deafferentation in retina. *Vision Research*, **32(5)**, 789–796.

[48] Chino, Y., Smith, E., Hatta, S., & Cheng, H. (1997) Postnatal development of binocular disparity sensitivity in neurons of the primate visual cortex. *The Journal of Neuroscience*, **17**, 1–12.

[49] Clothiaux, E.E., Cooper, L.N., & Bear, M.F. (1991) Synaptic plasticity in visual cortex: Comparison of theory with experiment. *Journal of Physiology*, **66**, 1785–1804.

[50] Cohen, M.A. & Grossberg, S. (1983) Absolute stability of global pattern formation and parallel memory storage by competitive neural networks. *IEEE Transactions on Systems, Man, and Cybernetics*, **13(5)**, 815–826.

[51] Crepel, J., Hemart, N., Jaillard, D., & Daniel, H. (1995) Long-term depression in the cerebellum. In *The Handbook of Brain Theory and Neural Networks*, M.A. Arbib (ed.), 560–563. Cambridge, MA: MIT Press.

[52] Crist, R.E., Kapadia, M.K., Westheimer, G., & Gilbert, C.D. (1997) Perceptual learning of spatial localization: Specificity for orientation, position, and context. *Journal of Neurophysiology*, **78(6)**, 2889–2894.

[53] Cynader, M. (1983) Prolonged sensitivity to monocular deprivation in dark-reared cats: Effects of age and visual exposure. *Developmental Brain Research*, **8**, 155–164.

[54] Dalva, M.B. & Katz, L.C. (1994) Rearrangements of synaptic connections in visual cortex revealed by laser photostimulation. *Science*, **265**, 255–258.

[55] Darian-Smith, C. & Gilbert, C.D. (1994) Axonal sprouting accompanies functional reorganization in adult cat striate cortex. *Nature*, **368**, 737–740.

[56] Darian-Smith, C. & Gilbert, C.D. (1995) Topographic reorganization in the striate cortex of the adult cat and monkey is cortically mediated. *The Journal of Neuroscience*, **15(3)**, 1631–1647.

[57] Das, A. (1997) Plasticity in adult sensory cortex: A review. *Network: Computation in Neural Systems*, **8**, R33–R76.

[58] Das, A. & Gilbert, C.D. (1995a) Long-range horizontal connections and their role in cortical reorganization revealed by optical recording of cat primary visual cortex. *Nature*, **375**, 780–784.

[59] Das, A. & Gilbert, C.D. (1995b) Receptive field expansion in adult visual cortex is linked to dynamic changes in strength of cortical connections. *Journal of Neurophysiology*, **74(2)**, 779–792.

[60] DeAngelis, G.C., Anzai, A., Ohzawa, I., & Freeman, R.D. (1992) Organization of suppression in receptive fields of neurons in cat visual cortex. *Journal of Neurophysiology*, **68(1)**, 144–163.

[61] DeAngelis, G.C., Anzai, A., Ohzawa, I., & Freeman, R.D. (1995) Receptive field structure in the visual cortex: Does selective stimulation induce plasticityΓ *Proceedings of the National Academy of Sciences of the USA*, **92**, 9682–9686.

[62] DeAngelis, G.C., Ohzawa, I., Anzai, A., & Freeman, R.D. (1994) Does an artificial scotoma induce plasticity of receptive field structure for neurons in the visual cortexΓ *Investigative Ophthalmology & Visual Science*, **35(4)**, 1468.

[63] DeAngelis, G.C., Ohzawa, I., & Freeman, R.D. (1991) Depth is encoded in the visual cortex by a specialized receptive field structure. *Nature*, **352**, 156–159.

[64] Debanne, D., Gähwiler, B.H., & Thompson, S.M. (1997) Bidirectional associative plasticity of unitary CA3-CA1 EPSPs in the rat hippocampus *in vitro*. *Journal of Neurophysiology*, **77**, 2851–2855.

[65] O'Dell, C. & Boothe, R.G. (1997) The development of stereoacuity in infant rhesus monkeys. *Vision Research*, **37**, 2675–2684.

[66] DeSieno, D. (1988) Adding a conscience to competitive learning. In *IEEE 1st International Conference on Neural Networks, Volume 1*, M. Caudill & C. Butler (eds.), 117–124. San Diego: IEEE.

[67] Dews, P.B. & Wiesel, T.N. (1970) Consequences of monocular deprivation on visual behavior in kittens. *Journal of Physiology*, **206**, 437–455.

[68] Douglas, R.J. & Martin, K.A.C. (1991) A functional microcircuit for cat visual cortex. *Journal of Physiology*, **440**, 735–769.

[69] Dudek, S.M. & Bear, M.F. (1992) Homosynaptic long-term depression in area CA1 of hippocampus and the effects on NMDA receptor blockade. *Proceedings of the National Academy of Sciences of the USA*, **89**, 4363–4367.

[70] Einstein, G., Davis, T.L., & Sterling, P. (1987) Pattern of lateral geniculate synapses on neuron somata in layer IV of the cat striate cortex. *The Journal of Comparative Neurology*, **260**, 76–86.

[71] Engel, A.K., König, P., & Singer, W. (1991) Direct physiological evidence for scene segmentation by temporal coding. *Proceedings of the National Academy of Sciences of the USA*, **88**, 9136–9140.

[72] Erwin, E., Obermayer, K., & Schulten, K. (1995) Models of orientation and ocular dominance columns in the visual cortex: A critical comparison. *Neural Computation*, **7**, 425–468.

[73] Fahle, M. (1997) Specificity of learning curvature, orientation, and vernier discriminations. *Vision Research*, **37(14)**, 1885–1895.

[74] Fahle, M. & Edelman, S. (1993) Long-term learning in vernier acuity: Effects of stimulus orientation, range and of feedback. *Vision Research*, **33**, 397–412.

[75] Fahle, M., Edelman, S., & Poggio, T. (1995) Fast perceptual learning in hyperacuity. *Vision Research*, **35**, 3003–3013.

[76] Felleman, D.J. & Van Essen, D.C. (1991) Distributed hierarchical processing in the primate cerebral cortex. *Cerebral Cortex*, **1**, 1–47.

[77] Favorov, O.V. & Kelly, D.G. (1994a) Minicolumnar organization within somatosensory cortical segregates: I. Development of afferent connections. *Cerebral Cortex*, **4(4)**, 408–427.

[78] Favorov, O.V. & Kelly, D.G. (1994b) Minicolumnar organization within somatosensory cortical segregates: II. Emergent functional properties. *Cerebral Cortex*, **4(4)**, 428–442.

[79] Favorov, O.V. & Kelly, D.G. (1996) Local receptive field diversity within cortical neuronal populations. In *Somesthesis and the Neurobiology of the Somatosensory Cortex*, O. Franzén, R. Johansson, & L. Terenius (eds.), 395–408. Basel, Switzerland: Birkhäuser Verlag.

[80] Ferster, D.L. (1986) Orientation selectivity of synaptic potentials in neurons of cat primary visual cortex. *The Journal of Neuroscience*, **6(5)**, 1284–1301.

[81] Ferster, D.L. (1989) The synaptic inputs to simple cells of the cat visual cortex. In *Proceedings of the Retina Research Foundation, Volume 2: Neural Mechanisms of Visual Perception*, D.M. Lam & C.D. Gilbert (eds.), 63–85. Texas: Portfolio.

[82] Fiorentini, A. & Berardi, N. (1980) Perceptual learning is specific for orientation and spatial frequency. *Nature*, **287**, 43–44.

[83] Fitzpatrick, D., Lund, J.S., & Blasdel, G.G. (1985) Intrinsic connections of macaque striate cortex: Afferent and efferent connections of lamina 4C. *The Journal of Neuroscience*, **5**, 3329–3349.

[84] Fox, K. & Daw, N.W. (1993) Do NMDA receptors have a critical function in visual cortical plasticityΓ *Trends in Neurosciences*, **16(3)**, 116–122.

[85] Freeman, R.D., Mallach, R., & Hartley, S. (1981) Responsitivity of normal kitten striate cortex deteriorates after brief binocular deprivation. *Journal of Neurophysiology*, **45**, 1074–1084.

[86] Freeman, R.D. & Olson, C. (1982) Brief periods of monocular deprivation in kittens: Effects of delay prior to physiological study. *Journal of Neurophysiology*, **47**, 139–150.

[87] Frégnac, Y., Burke, J.P., Smith, D., & Friedlander, M.J. (1994) Temporal covariance of pre- and postsynaptic activity regulates functional connectivity in the visual cortex. *Journal of Neurophysiology*, **71(4)**, 1403–1421.

[88] Frégnac, Y. & Imbert, M. (1978) Early development of visual cortical cells in normal and dark-reared kittens: Relationship between orientation selectivity and ocular dominance. *Journal of Physiology*, **278**, 27–44.

[89] Frègnac, Y. & Imbert, M. (1984) Development of neuronal selectivity in primary visual cortex of cat. *Physiological Review*, **64**, 325–434.

[90] Frégnac, Y., Shulz, D., Thorpe, S., & Bienenstock, E. (1988) A cellular analogue of visual cortical plasticity. *Nature*, **333**, 367–370.

[91] Frisby, J.P. & Pollard, S.B. (1991) Computational issues in solving the stereo correspondence problem. In *Computational Models of Visual Processing*, M.S. Landy & J.A. Movshon (eds.), 331–358. Cambridge, MA: MIT Press.

[92] Garraghty, P.E., Pons, T.P., Sur, M., & Kaas, J.H. (1989) The arbors of axons terminating in middle cortical layers of somatosensory area 3b in owl monkeys. *Somatosensory and Motor Research*, **6**, 401–411.

[93] Garraghty, P.E. & Sur, M. (1990) Morphology of single intracellularly stained axons terminating in area 3b of macaque monkeys. *The Journal of Comparative Neurology*, **294**, 583–593.

[94] Gil, Z. & Amitai, Y. (1996) Spatial integration and cortical dynamics. *The Journal of Neuroscience*, **16(20)**, 6567–6578.

[95] Gilbert, C.D. (1996) Plasticity in visual perception and physiology. *Current Opinion in Neurobiology*, **6(2)**, 269–274.

[96] Gilbert, C.D. (1998) Adult cortical dynamics. *Physiological Review*, **78(2)**, 467–485.

[97] Gilbert, C.D., Das, A., Ito, M., Kapadia, M., & Westheimer, G. (1996) Spatial integration and cortical dynamics. *Proceedings of the National Academy of Sciences of the USA*, **93**, 615–622.

[98] Gilbert, C.D., Hirsch, J.A., & Wiesel, T.N. (1990) Lateral interactions in visual cortex. In *Cold Spring Harbor Symposia on Quantitative Biology*, **55**, 663–677. Cold Spring Harbor, NY: Cold Spring Harbor Laboratory Press.

[99] Gilbert, C.D. & Wiesel, T.N. (1979) Morphology and intracortical projections of functionally characterised neurones in the cat visual cortex. *Nature*, **280**, 120–125.

[100] Gilbert, C.D. & Wiesel, T.N. (1983) Clustered intrinsic connections in cat visual cortex. *The Journal of Neuroscience*, **3(5)**, 1116–1133.

[101] Gilbert, C.D. & Wiesel, T.N. (1989) Columnar specificity of intrinsic horizontal and corticocortical connections in cat visual cortex. *The Journal of Neuroscience*, **9(7)**, 2432–2442.

[102] Gilbert, C.D. & Wiesel, T.N. (1990) The influence of contextual stimuli on the orientation selectivity of cells in primary visual cortex of the cat. *Vision Research*, **30**, 11, 1689–1701.

[103] Gilchrist, A.L. (1994) *Lightness, Brightness, and Transparency*. Hillsdale, NJ: Erlbaum.

[104] Goda, Y. & Stevens, C.F. (1996) Long-term depression properties in a simple system. *Neuron*, **16**, 103–111.

[105] Gove, A., Grossberg, S., & Mingolla, E. (1995) Brightness perception, illusory contours, and corticogeniculate feedback. *Visual Neuroscience*, **12**, 1027–1052.

[106] Grajski, K.A. & Merzenich, M.M. (1990) Hebb-type dynamics is sufficient to account for the inverse magnification rule in cortical somatotopy. *Neural Computation*, **2**, 71–84.

[107] Gray, C.M. & Singer, W. (1989) Stimulus-specific neuronal oscillations in orientation columns of cat visual cortex. *Proceedings of the National Academy of Sciences of the USA*, **86**, 1698–1702.

[108] Gray, C.M., König, P., Engel, A.K., & Singer, W. (1989) Oscillatory responses in cat visual cortex exhibit inter-column synchronization which reflects global stimulus properties. *Nature*, **338**, 334–337.

[109] Grossberg, S. (1972) Neural expectation: Cerebellar and retinal analogs of cells fired by learnable or unlearned pattern classes. *Kybernetik*, **10**, 49–57.

[110] Grossberg, S. (1976a) On the development of feature detectors in the visual cortex with applications to learning and reaction-diffusion systems. *Biological Cybernetics*, **21**, 145–159.

[111] Grossberg, S. (1976b) Adaptive pattern classification and universal recoding: I. Parallel development and coding of neural feature detectors. *Biological Cybernetics*, **23**, 121–134.

[112] Grossberg, S. (1976c) Adaptive pattern classification and universal recoding: II. Feedback, expectation, olfaction, and illusions. *Biological Cybernetics*, **23**, 187–202.

[113] Grossberg, S. (1978) A theory of human memory: Self-organization and performance of sensory-motor codes, maps, and plans. In *Progress in Theoretical Biology, Volume 5*, R. Rosen & F. Snell (eds.). New York: Academic Press.

[114] Grossberg, S. (1980) How does brain build a cognitive codeΓ *Psychological Review*, **89**, 529–572.

[115] Grossberg, S. (1982) *Studies of Mind and Brain: Neural Principles of Learning, Perception, Development, Cognition, and Motor Control*. Boston, MA: Reidel Press.

[116] Grossberg, S. (1985) The adaptive self-organization of serial order in behavior: Speech, language, and motor control. In *Pattern Recognition by Humans and Machines, Volume 1: Speech Perception*, E.C. Schwab & H.C. Nusbaum (eds.). New York: Academic Press.

[117] Grossberg, S. (1987) Cortical dynamics of three-dimensional form, color and brightness perception: 2. Binocular rivalry. *Perception & Psychophysics*, **41**, 117–158.

[118] Grossberg, S., Boardman, I., & Cohen, M.A. (1997a) Neural dynamics of variable-rate speech categorization. *Journal of Experimental Psychology: Human Perception and Performance*, **23**, 418–503.

[119] Grossberg, S. & Marshall, J.A. (1989) Stereo boundary fusion by cortical complex cells: A system of maps, filters, and feedback networks for multiplexing distributed data. *Neural Networks*, **2**, 29–51.

[120] Grossberg, S. & Merrill, J.W.L. (1996) The hippocampus and cerebellum in adaptively timed learning, recognition, and movement. *Journal of Cognitive Neuroscience*, **8**, 257–277.

[121] Grossberg, S. & Mingolla, E. (1985a) Neural dynamics of form perception: Boundary completion, illusory figures, and neon color spreading. *Psychological Review*, **92**, 173–211.

[122] Grossberg, S. & Mingolla, E. (1985b) Neural dynamics of form perception: Textures, boundaries, and emergent and segmentations. *Perception and Psychophysics*, **38**, 141–171.

[123] Grossberg, S., Mingolla, E., & Ross, W.D. (1994) A neural theory of attentive visual search: Interactions of boundary, surface, spatial, and object representations. *Psychological Review*, **101(3)**, 470–489.

[124] Grossberg, S., Mingolla, E., & Ross, W.D. (1997b) Visual brain and visual perception: How does the cortex do perceptual groupingΓ *Trends in Neurosciences*, **20(3)**, 106–111.

[125] Grossberg, S. & Olson, S.J. (1994) Rules for the cortical map of ocular dominance and orientation columns. *Neural Networks*, **7**, 883–894.

[126] Grossberg, S. & Rudd, M.E. (1992) Cortical dynamics of visual motion perception: Short-range and long-range apparent motion. *Psychological Review*, **99(1)**, 78–121.

[127] Grunewald, A. & Grossberg, S. (1997) Self-organization of binocular disparity tuning by reciprocal corticogeniculate interactions. In press, *Journal of Cognitive Neuroscience*.

[128] Hammond, P., Mouat, G.S., & Smith, A.T. (1986) Motion after-effects in cat striate cortex elicited by moving textures. *Vision Research*, **26(7)**, 1055–1060.

[129] Hammond, P., Pomfrett, C.J.D., & Ahmed, B. (1989) Neural motion after-effects in the cat's striate cortex: Orientation selectivity. *Vision Research*, **29(12)**, 1671–1683.

[130] Held, R., Birch, E, & Gwiazda, J. (1980) Stereoacuity of human infants. *Proceedings of the National Academy of Sciences of the USA*, **77**, 5572–5574.

[131] Hendry, S.H.C., Fuchs, J., deBlas, A.J., & Jones, E.G. (1990) Distribution and plasticity of immunocytochemically localized $GABA_A$ receptors in adult monkey visual cortex. *The Journal of Neuroscience*, **10**, 2438–2450.

[132] Herzog, M.H. & Fahle, M. (1995) A recurrent model for learning a hyperacuity task. *Perception*, **24**, S84.

[133] Hess, G. & Donoghue, J.P. (1994) The influence of prior synaptic activity on the induction of long-term potentiation. *Journal of Neurophysiology*, **71(6)**, 2543–2547.

[134] Heynen, A.J., Abraham, W.C., & Bear, M.F. (1996) Bidirectional modification of CA1 synapses in the adult hippocampus *in vivo*. *Nature*, **381**, 163–166.

[135] Hirsch, J. & Gilbert, C.D. (1991) Synaptic physiology of horizontal connections in the cat's visual cortex. *The Journal of Neuroscience*, **11**, 1800–1809.

[136] Hirsch, J.A. & Gilbert, C.D. (1993) Long-term changes in synaptic strength along specific intrinsic pathways in the cat visual cortex. *Journal of Physiology*, **461**, 247–262.

[137] Hodgkin, A.L. (1964) *The Conduction of the Nervous Impulse*. Liverpool, England: Liverpool University Press.

[138] Huang, Y.Y., Colino, A., Selig, D.K., & Malenka, R.C. (1992) The influence of prior synaptic activity on the induction of long-term potentiation. *Science*, **225**, 730–733.

[139] Hubbard, R.S. & Marshall, J.A. (1994) Self-organizing neural network model of the visual inertia phenomenon in motion perception. Technical Report 94–001, University of North Carolina at Chapel Hill, Department of Computer Science, 26 pp.

[140] Hubel, D.H. & Wiesel, T.N. (1962) Receptive fields, binocular interaction, and functional architecture in the cat's visual cortex. *Journal of Physiology*, **160**, 106–154.

[141] Hubel, D.H. & Wiesel, T.N. (1963) Receptive fields of cells in striate cortex of very young, visually inexperienced kittens. *Journal of Neurophysiology*, **26**, 994–1002.

[142] Hubel, D.H. & Wiesel, T.N. (1965) Binocular interaction in striate cortex of kitten reared with artificial squint. *Journal of Neurophysiology*, **28**, 1041–1059.

[143] Hubel, D.H. & Wiesel, T.N. (1970) The period of susceptibility to the physiological effects of unilateral eye closure in kittens. *Journal of Physiology*, **206**, 419–436.

[144] Hubel, D.H. & Wiesel, T.N. (1972) Laminar and columnar distribution of geniculo-cortical fibers in the macaque monkey. *The Journal of Comparative Neurology*, **146**, 421–450.

[145] Hubel, D.H., Wiesel, T.N., & LeVay, S. (1977) Plasticity of ocular dominance columns in monkey striate cortex. *Philosophical Transactions of the Royal Society* (London), **278**, 377–409.

[146] Hübener, M, Shoham, D., Grinvald, A., & Bonhoeffer, T. (1997) Spatial relationships among three columnar systems in cat area 17. *The Journal of Neuroscience*, **17(23)**, 9270–9284.

[147] Humphrey, A.L., Sur, M., Ulrich, D.J., & Sherman, S.M. (1985) Receptive fields, binocular interaction, and functional architecture in the cat's visual cortex. *The Journal of Comparative Neurology*, **233**, 159–189.

[148] Intrator, N. (1992) Feature extraction using an unsupervised neural network. *Neural Computation*, **4**, 98–107.

[149] Intrator, N. & Cooper, L.N. (1992) Objective function formulation of the BCM theory of visual cortical plasticity: Statistical connections, stability conditions. *Neural Networks*, **5**, 3–17.

[150] Intrator, N. & Cooper, L.N. (1995) BCM theory of visual cortical plasticity. In *The Handbook of Brain Theory and Neural Networks*, M.A. Arbib (ed.), 153–157. Cambridge, MA: MIT Press.

[151] Iwamura, Y., Tanaka, M., Sakamoto, M., & Hikosaka, O. (1983) Functional subdivisions representing different finger regions in area 3 of the first somatosensory cortex of conscious monkey. *Experimental Brain Research*, **51**, 315–326.

[152] Jenkins, W.M., Merzenich, M.M., Ochs, M.T., Allard, T., & Guíc-Robles, E. (1990) Functional reorganization of primary somatosensory cortex in adult owl monkey after behaviorally controlled tactile stimulation. *Journal of Neurophysiology*, **63(1)**, 82–104.

[153] Johansson, G. (1950) *Configurations in Event Perception*. Stockholm, Sweden: Almqvist & Wiksell.

[154] Juliano, S.L. & Whitsel, B.L. (1987) A combined 2-deoxyglucose and neurophysiological study of primate somatosensory cortex. *The Journal of Comparative Neurology*, **263**, 514–525.

[155] Kang, R., Herman, D., MacGillis, M., & Zarzecki, P. (1985) Convergence of sensory inputs in somatosensory cortex: Interactions from separate afferent sources. *Experimental Brain Research*, **57**, 271–278.

[156] Kalarickal, G.J. & Marshall, J.A. (1996a) Dynamic receptive fields in visual cortex: Adaptive neural model and predictions. *Investigative Ophthalmology & Visual Science*, **37(3)**, 483.

[157] Kalarickal, G.J. & Marshall, J.A. (1996b) Dynamic cortical receptive field changes: Neuronal adaptation or connection plasticityΓ *Society for Neuroscience Abstracts*, **22**, 1613.

[158] Kalarickal, G.J. & Marshall, J.A. (1996c) Synaptic plasticity: Comparison of EXIN and BCM learning rules. *Journal of Mathematical Psychology*, **40(4)**, 355.

[159] Kalarickal, G.J. & Marshall, J.A. (1997a) The role of feedforward excitatory and lateral inhibitory learning in visual classical rearing. *Investigative Ophthalmology & Visual Science*, **38(4)**, 360.

[160] Kalarickal, G.J. & Marshall, J.A. (1997b) Receptive field dynamics in visual cortex: Models based on synaptic plasticity and neuronal adaptation. Technical Report 97-029, Department of Computer Science, University of North Carolina at Chapel Hill.

[161] Kalarickal, G.J. & Marshall, J.A. (1998a) Modeling temporal and stochastic properties of binocular rivalry. *Investigative Ophthalmology & Visual Science*, **39(4)**, 862.

[162] Kalarickal, G.J. & Marshall, J.A. (1998b) Modeling dynamic receptive field changes produced by intracortical microstimulation. In press, *Computational Neuroscience: Trends in Research, 1998*, J.M. Bower (ed.).

[163] Kano, M., Lino, K., & Kano, M. (1991) Functional reorganization of adult cat somatosensory cortex is dependent on NMDA receptors. *NeuroReport*, **2**, 77–80.

[164] Kano, M., Rexhausen, U., Dreessen, J., & Konnerth, A. (1996) Synaptic excitation produces a long-lasting rebound potentiation of inhibitory synaptic signals in cerebellar Purkinje cells. *Nature*, **356**, 601–604.

[165] Kapadia, M.K., Gilbert, C.D., & Westheimer, G. (1994) A quantitative measure for short-term cortical plasticity in human vision. *The Journal of Neuroscience*, **14(1)**, 451–457.

[166] Kapadia, M.K., Ito, M., Gilbert, C.D., & Westheimer, G. (1995) Improvement in visual sensitivity by changes in local context: Parallel studies in human observers and in V1 of alert monkeys. *Neuron*, **15**, 843–856.

[167] Karni, A. & Sagi, D. (1991) Where practice makes perfect in texture discrimination: Evidence for primary visual cortex plasticity. *Proceedings of the National Academy of Sciences of the USA*, **88**, 4966–4970.

[168] Kasamatsu, T., Imamura, K., & Mataga, N. (1997) Abnormal response properties in APV-infused, otherwise normal visual cortex of adult cats. *Investigative Ophthalmology & Visual Science*, **38(4)**, 106.

[169] Kasamatsu, T., Imamura, K., Mataga, N., Hartveit, E., Heggelund, U., & Heggelund, P. (1998a) Roles of N-methyl-D-aspartate receptors in ocular dominance plasticity in developing visual cortex: Re-evaluation. *Neuroscience*, **82(3)**, 687–700.

[170] Kasamatsu, T., Kitano, M., Sutter, E.E., & Norcia, A.M. (1998b) Lack of lateral inhibitory interactions in visual cortex of monocularly deprived cats. *Vision Research*, **38**, 1–12.

[171] Katz, L.C. & Callaway, E.M. (1992) Development of local circuits in mammalian visual cortex. *Annual Review of Neuroscience*, **15**, 31–56.

[172] Kelso, S.R. & Brown, T.H. (1986) Differential conditioning of associative synaptic enhancement in hippocampal brain slices. *Science*, **232**, 85–87.

[173] Kirkwood, A. & Bear, M.F. (1994) Homosynaptic long-term depression in the visual cortex. *The Journal of Neuroscience*, **14(5)**, 3404–3412.

[174] Kirkwood, A., Dudek, S.M., Gold, J.T., Aizenman, C.D., & Bear, M.F. (1993) Common forms of synaptic plasticity in hippocampus and neocortex *in vitro*. *Science*, **260**, 1518–1521.

[175] Kobayashi, K., Manabe, T., & Takahashi, T. (1996) Presynaptic long-term depression at the hippocampal mossy fiber–CA3 synapse. *Science*, **273**, 648–650.

[176] Kohonen, T. (1987) *Self-Organization and Associative Memory.* New York: Springer-Verlag.

[177] Kohonen, T. (1988) The "neural" phonetic typewriter. *Computer*, **21**, 11-22.

[178] König, P., Engel, A., & Singer, W. (1995) Relation between oscillatory activity and long-range synchronization in cat visual cortex. *Proceedings of the National Academy of Sciences of the USA*, **92**, 290–294.

[179] Land, E.H. (1986) Recent advances in retinex theory. *Vision Research*, **26**, 7–21.

[180] Lane, R.D., Killackey, H.P, & Rhoades, R.W. (1997) Blockade of GABAergic inhibition reveals reordered cortical somatotopic maps in rats that sustained neonatal forelimb removal. *Journal of Neurophysiology*, **77**, 2723–2735.

[181] Law, C.C. & Cooper, L.N. (1994) Formation of receptive fields in realistic visual environments according to the BCM theory. *Proceedings of the National Academy of Sciences of the USA*, **91**, 7797–7801.

[182] Lehky, S.R. (1988) An astable multivibrator model of binocular rivalry. *Perception*, **17**, 215–228.

[183] Lehky, S.R. & Blake, R. (1991) Organization of binocular pathways: Modeling and data related to rivalry. *Neural Computation*, **3**, 44–53.

[184] Lehky, S.R. & Maunsell, J.H.R. (1996) No binocular rivalry in the LGN of alert macaque monkeys. *Vision Research*, **36**, 1225–1234.

[185] Leopold, D.A. & Logothetis, N.K. (1996) Activity changes in early visual cortex reflect monkeys' percepts during binocular rivalry. *Nature*, **379**, 549–553.

[186] LeVay, S., Wiesel, T.N., & Hubel, D.H. (1980) The development of ocular dominance columns in normal and visually deprived monkeys. *The Journal of Comparative Neurology*, **191**, 1–51.

[187] Levelt, W.J.M. (1965) *On Binocular Rivalry*. Soesterberg, The Netherlands: Institute for Perception RVO-TNO.

[188] Levy, W.B. (1985) Associative changes at the synapse: LTP in the hippocampus. In *Synaptic Modification, Neuron Selectivity, and Nervous System Organization*, W.B. Levy, J.A. Anderson, & S. Lehmkuhle (eds.), 5–33. Hillsdale, NJ: Erlbaum.

[189] Levy, W.B. & Burger, B. (1987) Electrophysiological observations which help describe an associative synaptic modification rule. In *IEEE 1st International Conference on Neural Networks, Volume 4*, M. Caudill & C. Butler (eds.), 11–15. San Diego: IEEE.

[190] Levy, W.B. & Desmond, N.L. (1985) The rules of elemental synaptic plasticity. In *Synaptic Modification, Neuron Selectivity, and Nervous System Organization*, W.B. Levy, J.A. Anderson, & S. Lehmkuhle (eds.), 105–121. Hillsdale, NJ: Erlbaum.

[191] Levy, W.B. & Steward, O. (1979) Synapses as associative memory elements in the hippocampal formation. *Brain Research*, **175**, 233–245.

[192] Levy, W.B. & Steward, O. (1983) Temporal contiguity requirements for long-term associative potentiation/depression in the hippocampus. *Neuroscience*, **8**, 791–797.

[193] Linsker, R. (1986a) From basic network principles to neural architecture: Emergence of spatial opponent cells. *Proceedings of the National Academy of Sciences of the USA*, **83**, 7508–7512.

[194] Linsker, R. (1986b) From basic network principles to neural architecture: Emergence of orientation selective cells. *Proceedings of the National Academy of Sciences of the USA*, **83**, 8390–8394.

[195] Linsker, R. (1986c) From basic network principles to neural architecture: Emergence of orientation columns. *Proceedings of the National Academy of Sciences of the USA*, **83**, 8779–8783.

[196] Linsker, R. (1988) Self-organization in a perceptual network. *Computer*, **21**, 105–117.

[197] Logothetis, N.K. & Schall, J.D. (1990) Binocular motion rivalry in macaque monkeys: Eye dominance and tracking eye movements. *Vision Research*, **30**, 1409–1419.

[198] Löwel, S. & Singer, W. (1992) Selection of intrinsic horizontal connections in the visual cortex by correlated neuronal activity. *Science*, **255**, 209–212.

[199] Lynch, G.S., Dunwiddie, T., & Gribkoff, V. (1977) Heterosynaptic depression: A postsynaptic correlate of long-term potentiation. *Nature*, **266**, 737–739.

[200] Maffei, L. & Fiorentini, A. (1973) The visual cortex as a spatial frequency analyzer. *Vision Research*, **13**, 1255–1267.

[201] Malinow, R. & Tsien, R.W. (1990) Presynaptic enhancement shown by whole-cell recordings of long-term potentiation in hippocampal slices. *Nature*, **346**, 177–180.

[202] Marr, D. & Poggio, T. (1976) Cooperative computation of stereo disparity. *Science*, **194**, 283–287.

[203] von der Malsburg, C. (1973) Self-organization of orientation sensitive cells in the striate cortex. *Kybernetik*, **14**, 85–100.

[204] von der Malsburg, C. & Singer, W. (1988) Principles of cortical network organization. *Neurobiology of Neocortex*, T.P. Rakic & W. Singer (eds.), 69–99. New York: John Wiley & Sons.

[205] Marshall, J.A. (1989) Self-organizing neural network architectures for computing visual depth from motion parallax. In *Proceedings of the International Joint Conference on Neural Networks*, Washington DC, **II**, 227–234.

[206] Marshall, J.A. (1990a) Self-organizing neural networks for perception of visual motion. *Neural Networks*, **3**, 45–74.

[207] Marshall, J.A. (1990b) Development of length-selectivity in hypercomplex-type cells. *Investigative Ophthalmology & Visual Science*, **31(4)**, 397.

[208] Marshall, J.A. (1990c) A self-organizing neural network for computing stereo disparity and transparency. *Technical Digest, Optical Society of America Annual Meeting*, 268.

[209] Marshall, J.A. (1990d) Adaptive neural methods for multiplexing oriented edges. In *Intelligent Robots and Computer Vision IX: Neural, Biological, and 3-D Methods*, D.P. Casasent (ed.), Proceedings of the SPIE, **1382**, Boston, MA, 282–291.

[210] Marshall, J.A. (1991) Challenges of vision theory: Self-organization of neural mechanisms for stable steering of object-grouping data in visual motion perception. In *Stochastic and Neural Methods in Signal Processing, Image Processing, and Computer Vision*, S.-S. Chen (ed.), Proceedings of the SPIE, **1569**, San Diego, CA, 200–215.

[211] Marshall, J.A. (1992a) Development of perceptual context-sensitivity in unsupervised neural networks: Parsing, grouping, and segmentation. In *Proceedings of the International Joint Conference on Neural Networks*, **III**, Baltimore, MD, 315–320.

[212] Marshall, J.A. (1992b) Unsupervised learning of contextual constraints in neural networks for simultaneous visual processing of multiple objects. In *Neural and Stochastic Methods in Image and Signal Processing*, S.-S. Chen (ed.), Proceedings of the SPIE, **1766**, San Diego, CA, 84–93.

[213] Marshall, J.A. (1995a) Adaptive perceptual pattern recognition by self-organizing neural networks: Context, uncertainty, multiplicity, and scale. *Neural Networks*, **8**, 335–362.

[214] Marshall, J.A. (1995b) Visual motion perception: Self-organization. In *The Handbook of Brain Theory and Neural Networks*, M.A. Arbib (ed.), 589–591. Cambridge, MA: MIT Press.

[215] Marshall, J.A. & Alley, R.K. (1993) A self-organizing neural network that learns to detect and represent visual depth from occlusion events. In *Proceedings of the AAAI Fall Symposium on Machine Learning and Computer Vision*, K. Bowyer & L. Hall (eds.), 70–74.

[216] Marshall, J.A., Alley, R.K., & Hubbard, R.S. (1996a) Learning to predict visibility and invisibility from occlusion events. In *Advances in Neural Information Processing Systems*, **8**, D.S. Touretzky, M.C. Mozer, & M.E. Hasselmo (eds.), 816–822. Cambridge, MA: MIT Press.

[217] Marshall, J.A. & Gupta,V.S. (1998) Generalization and exclusive allocation of credit in unsupervised category learning. *Network: Computation in Neural Systems*, **9**, 279–302.

[218] Marshall, J.A. & Kalarickal, G.J. (1995) A neural circuit for stereomatching of transparent and oblique surfaces. *Investigative Ophthalmology & Visual Science*, **36(4)**, 366.

[219] Marshall, J.A. & Kalarickal, G.J. (1997) Modeling dynamic receptive field changes in primary visual cortex using inhibitory learning. In *Computational Neuroscience: Trends in Research, 1997*, J.M. Bower (ed.), 395–401. New York: Plenum Press.

[220] Marshall, J.A., Kalarickal, G.J., & Graves, E.B. (1996b) Neural model of visual stereomatching: Slant, transparency, and clouds. *Network: Computation in Neural Systems*, **7**, 635–669.

[221] Marshall, J.A., Schmitt, C.P., Kalarickal, G.J., & Alley, R.K. (1998) Neural model of transfer-of-binding in visual relative motion perception. In press, *Computational Neuroscience '98*, J.M. Bower (ed.).

[222] Martin, K.A.C. (1988) From single cells to simple circuits in the cerebral cortex. *Quarterly Journal of Experimental Physiology*, **73**, 637–702.

[223] Martin, K.E. & Marshall, J.A. (1993) Unsmearing visual motion: Development of long-range horizontal intrinsic connections. In *Advances in Neural Information Processing Systems Networks*, **5**, S.J. Hanson, J.D. Cowan, & C.L. Giles (eds.), 417–424. San Mateo, CA: Morgan Kaufmann Publishers.

[224] Matsuoka, M. (1984) The dynamic model of binocular rivalry. *Biological Cybernetics*, **49**, 201–208.

[225] Maunsell, J.H.R. & Van Essen, D.C. (1983) The connections of the middle temporal visual area (MT) and their relationship to a cortical hierarchy in the macaque monkey. *The Journal of Neuroscience*, **3(12)**, 2563–2586.

[226] Mayner, L. & Kaas, J.H. (1986) Thalamic projections from electrophysiologically defined sites of body surface representations in areas 3b and 1 of somatosensory cortex of cebus monkeys. *Somatosensory and Motor Research*, **4**, 13–29.

[227] Mayo, T.H., Gilinsky, A.S., & Jochnowitz, A. (1968) Visual masking and tilt aftereffects as a function of tilt and angular separation between test and adaptation patterns. *Proceedings of the 76th Annual Convention, American Psychological Association*, **3**, 97–98.

[228] McGuire, B.A., Gilbert, C.D., Rivlin, P.K., & Wiesel, T.N. (1991) Targets of horizontal connections in macaque primary visual cortex. *The Journal of Comparative Neurology*, **305**, 370–392.

[229] McMahon, L.L. & Kauer, J.A. (1997) Hippocampal interneurons express a novel form of synaptic plasticity. *Neuron*, **18**, 295–305.

[230] Merzenich, M.M. (1987) Dynamic neocortical processes and the origins of higher brain functions. In *The Neural and Molecular Bases of Learning*, J.-P. Changeux & M. Konishi (eds.), 337–358. New York: John Wiley & Sons.

[231] Miles, R. & Wong, R.K.S. (1987) Latent synaptic pathways revealed after tetanic stimulation in the hippocampus. *Nature*, **329**, 724–726.

[232] Miller, K.D., Keller, J.B., & Stryker, M.P. (1989) Ocular dominance column development: Analysis and simulation. *Science*, **245**, 605–615.

[233] Mioche, L., & Singer, W. (1989) Chronic recordings from single sites of kitten striate cortex during experience-dependent modifications of receptive field properties. *Journal of Neurophysiology*, **62**, 185–197.

[234] Movshon, J.A. & Lennie, P. (1979) Pattern-selective adaptation in visual cortical neurones. *Nature*, **278**, 850–852.

[235] Movshon, J.A., Thompson, I.D., & Tolhurst, D.J. (1978) Spatial summation in the receptive fields of simple cells in the cat's striate cortex. *Journal of Physiology*, **283**, 53–77.

[236] Mueller, T.J. & Blake, R. (1989) A fresh look at the temporal dynamics of binocular rivalry. *Biological Cybernetics*, **61**, 223–232.

[237] Mulkey, R.M. & Malenka, R.C. (1992) Mechanisms underlying induction of homosynaptic long-term depression in area CA1 of the hippocampus. *Neuron*, **9**, 967–975.

[238] Nelson, S., Toth, L.J., Sheth, B., & Sur, M. (1994) Orientation selectivity of cortical neurons during intracellular blockade of inhibition. *Science*, **265**, 774–777.

[239] Nigrin, A. (1993) *Neural Networks for Pattern Recognition*. Cambridge, MA: MIT Press.

[240] Nikara, T., Bishop, P.O., & Pettigrew, J.D. (1968) Analysis of retinal correspondence by studying receptive fields of binocular single units in cat striate cortex. *Experimental Brain Research*, **6**, 353–372.

[241] Obermayer, K. & Blasdel, G.G. (1993) Geometry of orientation and ocular dominance columns in monkey striate cortex. *The Journal of Neuroscience*, **13(10)**, 4114–4129.

[242] Obermayer, K., Blasdel, G.G., & Schulten, K. (1992) Statistical-mechanical analysis of self-organization and pattern formation during the development of visual maps. *Physical Review A*, **45(10)**, 7568–7589.

[243] Ohzawa, I., DeAngelis, G.C., & Freeman, R.D. (1990) Stereoscopic depth discrimination in the visual cortex: Neurons ideally suited as disparity detectors. *Science*, **249**, 1037–1041.

[244] Pavlov, I. (1927) *Conditioned reflexes*. London: Oxford University Press.

[245] Pearson, J.C., Finkel, L.H., & Edelman, G.M. (1987) Plasticity in the organization of adult cerebral cortical maps: A computer simulation based on neuronal group selection. *The Journal of Neuroscience*, **7(12)**, 4209–4223.

[246] Peters, A. & Payne, B.R. (1993) Numerical relationships between geniculocortical afferents and pyramidal cell modules in cat primary visual cortex. *Cerebral Cortex*, **3**, 69–78.

[247] Petersen, R. & Taylor, J. (1997) Short-term cortical reorganisation in a lateral inhibitory neural network. In *Computational Neuroscience: Trends in Research, 1997*, J.M. Bower (ed.), 449–453. New York: Plenum Press.

[248] Pettet, M.W. & Gilbert, C.D. (1992) Dynamic changes in receptive-field size in cat primary visual cortex. *Proceedings of the National Academy of Sciences of the USA*, **89(7)**, 8366–8370.

[249] Pettigrew, J.D., Nikara, T., & Bishop, P.O. (1968) Binocular interaction on single units in cat striate cortex: Simultaneous stimulation by single moving slit with receptive fields in correspondence. *Experimental Brain Research*, **6**, 392–410.

[250] Poggio, T., Fahle, M., & Edelman, S. (1992) Fast perceptual learning in visual hyperacuity. *Science*, **256**, 1018–1021.

[251] Powell, T.P.S. & Mountcastle, V.B. (1959) The cytoarchitecture of the postcentral gyrus of the monkey *Macaca mulatta*. *Johns Hopkins Hospital Bulletin*, **105**, 108–131.

[252] Prazdny, K. (1985) Detection of binocular disparities. *Biological Cybernetics*, **52**, 93–99.

[253] Qian, N. & Sejnowski, T.J. (1989) Learning to solve random-dot stereograms of dense and transparent surfaces with recurrent backpropagation. In *Proceedings of the 1988 Connectionist Models Summer School*, D. Touretzky, G. Hinton, & T. Sejnowski (eds.), 435–443. San Mateo, CA: Morgan Kaufmann Publishers,

[254] Rauschecker, J. & Singer, W. (1979) Changes in the circuitry of the kitten's visual cortex are fated by postsynaptic activity. *Nature*, **280**, 58–60.

[255] Recanzone, G.H., Jenkins, W.M., Hradek, G.T., & Merzenich, M.M. (1992a) Progressive improvement in discriminative abilities in adult owl monkeys performing a tactile frequency discrimination task. *Journal of Neurophysiology*, **67(5)**, 1015–1030.

[256] Recanzone, G.H., Merzenich, M.M., & Dinse, H.R. (1992b) Expansion of the cortical representation of a specific skin field in primary somatosensory cortex by intracortical microstimulation. *Cerebral Cortex*, **2**, 181–196.

[257] Recanzone, G.H., Merzenich, M.M., & Jenkins, W.M. (1992c) Frequency discrimination training engaging a restricted skin surface results in an emergence of a cutaneous response zone in cortical area 3a. *Journal of Neurophysiology*, **67(5)**, 1057–1070.

[258] Recanzone, G.H., Merzenich, M.M., Jenkins, W.M., Grajski, K.A., & Dinse, H.R. (1992d) Topographic reorganization of the hand representation in cortical area 3b of owl monkeys trained in a frequency-discrimination task. *Journal of Neurophysiology*, **67(5)**, 1031–1056.

[259] Recanzone, G.H., Merzenich, M.M., & Schreiner, C.E. (1992e) Changes in the distributed temporal response properties of SI cortical neurons reflect improvements in performance on a temporally based tactile discrimination task. *Journal of Neurophysiology*, **67(5)**, 1071–1091.

[260] Reiter, H.O. & Stryker, M.P. (1988) Neural plasticity without postsynaptic action potentials: Less-active inputs become dominant when kitten visual cortical cells are pharmacologically inhibited. *Proceedings of the National Academy of Sciences of the USA*, **85**, 3623–3627.

[261] Rescorla, R.A. & Wagner, A.R. (1972) A theory of Pavlovian conditioning: Variations in the effectiveness of reinforcement and non-reinforcement. In *Classical Conditioning II: Current Research and Theory*, A.H. Black & W.F. Prokasy (eds.), 64–99. New York: Appleton-Century-Crofts.

[262] Rockland, K.S. & Lund, J.S. (1983) Intrinsic laminar lattice connections in primate visual cortex. *The Journal of Comparative Neurology*, **216**, 303–318.

[263] Rose, D. & Blakemore, C.B. (1974) Effects of bicuculline on functions of inhibition in visual cortex. *Nature*, **249**, 375–377.

[264] Rubner, J. & Schulten, K. (1990) Development of feature detectors by self-organization: A network model. *Biological Cybernetics*, **62**, 193–199.

[265] Rumelhart, D.E. & McClelland, J.L. (1986) *Parallel Distributed Processing: Explorations in the Microstructure of Cognition, Volumes 1 & 2.* Cambridge, MA: MIT Press.

[266] Rutherford, L.C., DeWan, A., Lauer, H.M., & Turrigiano, G.G. (1997) Brain-derived neurotrophic factor mediates the activity-dependent regulation of inhibition in neocortical culture. *The Journal of Neuroscience*, **17(12)**, 4527–4535.

[267] Schmajuk, N.A. (1997) *Animal Learning and Cognition: A Neural Network Approach*. New York, NY: Cambridge University Press.

[268] Schmitt, C.P. & Marshall, J.A. (1995) Development of a neural circuit for motion grouping and disambiguation. *Investigative Ophthalmology & Visual Science*, **36(4)**, 377.

[269] Schmitt, C.P. & Marshall, J.A. (1996) Effects of coherence and context on visual motion grouping: A self-organizing neural model. *Investigative Ophthalmology & Visual Science*, **37(4)**, 483.

[270] Sekuler, R. & Blake, R. (1994) *Perception*, 3rd (ed.). New York: McGraw-Hill.

[271] Sengpiel, F., Sen, A., & Blakemore, C. (1997) Characteristics of surround inhibition in cat area 17. *Experimental Brain Research*, **116**, 216–228.

[272] Sejnowski, T.J. (1977a) Statistical constraints on synaptic plasticity. *Journal of Theoretical Biology*, **69**, 385–389.

[273] Sejnowski, T.J. (1977b) Storing covariance with nonlinearly interacting neurons. *Journal of Mathematical Biology*, **4**, 303–321.

[274] Sejnowski, T.J. & Stanton, P.K. (1990) Covariance storage in the hippocampus. In *An Introduction to Neural and Electronic Networks*, S.F. Zornetzer, J.L. Davis, & C. Lau (eds.), 365–377. San Diego: Academic Press.

[275] Sejnowski, T.J., Chattarji, S., & Stanton, P.K. (1990) Homosynaptic long-term depression in hippocampus and neocortex. *Seminars in the Neurosciences*, **2**, 355–363.

[276] Sheth, B.R., Sharma, J., Rao, S.C., & Sur, M. (1996) Orientation maps of subjective contours in visual cortex. *Science*, **274**, 2110–2115.

[277] Shimojo, S. & Nakayama, K. (1990) Real world occlusion constraints and binocular rivalry. *Vision Research*, **30**, 69–80.

[278] Shimojo, S. & Nakayama, K. (1994) Interocularly unpaired zones escape local binocular matching. *Vision Research*, **34**, 1875–1881.

[279] Shmuel, A. & Grinvald, A. (1996) Functional organization for direction of motion and its relationship to orientation maps in cat area 18. *The Journal of Neuroscience*, **16(21)**, 6945–6964.

[280] Shouval, H., Intrator, N., Law, C.C., & Cooper, L.N. (1996) Effect of binocular cortical misalignment on ocular dominance and orientation selectivity. *Neural Computation*, **15(8)**, 1021–1040.

[281] Sik, A., Penttonen, M., Ylinen, A., & Buzsaki, G. (1995) Hippocampal CA1 interneurons: An *in vivo* intracellular labeling study. *The Journal of Neuroscience*, **15**, 6651–6665.

[282] Sillito, A.M. (1975) The contribution of inhibitory mechanisms to the receptive field properties of neurones in the striate cortex of the cat. *Journal of Physiology*, **250**, 305–329.

[283] Sillito, A.M. (1977) Inhibitory processes underlying the directional specificity of simple, complex and hypercomplex cells in the cat's visual cortex. *Journal of Physiology*, **271**, 699–720.

[284] Sillito, A.M. (1979) Inhibitory mechanisms influencing complex cell orientation selectivity and their modification at high resting discharge levels. *Journal of Physiology*, **289**, 33–53.

[285] Sillito, A.M., Jones, H.E., Gerstein, G.L., & West, D.C. (1994) Feature-linked synchronization of thalamic relay cell firing induced by feedback from the visual cortex. *Nature*, **369**, 479–482.

[286] Sillito, A.M., Kemp, J.A., Milson, J.A., & Berardi, N. (1980) A re-evaluation of the mechanisms underlying simple cell orientation selectivity. *Brain Research*, **194**, 517–520.

[287] Sillito, A.M., Kemp, J.A., & Blakemore, C. (1981) The role of GABAergic inhibition in the cortical effects of monocular deprivation. *Nature*, **291**, 318–320.

[288] Sillito, A.M. & Versiani, V. (1977) The contribution of excitatory and inhibitory inputs to the length preference of hypercomplex cells in layers II and III of the cat's striate cortex. *Journal of Physiology*, **273**, 775–790.

[289] Sirosh, J. & Miikkulainen, R. (1994a) Modeling cortical plasticity based on adapting lateral interaction. In *The Neurobiology of Computation: Proceedings of the Third Annual Computational and Neural Systems Conference*, J.M. Bower (ed.), 305–310. Boston, MA: Kluwer Academic Publishers.

[290] Sirosh, J. & Miikkulainen, R. (1994b) Cooperative self-organization of afferent and lateral connections in cortical maps. *Biological Cybernetics*, **71**, 66–78.

[291] Sirosh, J. & Miikkulainen, R. (1995) Ocular dominance and patterned lateral connections in a self-organizing model of the primary visual cortex. In *Advances in Neural Information Processing Systems*, **7**, G. Tesauro, D.S. Touretzky, & T.K. Leen (eds.), 109–116. Cambridge, MA: MIT Press.

[292] Sirosh, J. & Miikkulainen, R. (1997) Topographic receptive fields and patterned lateral interaction in a self-organizing model of the primary visual cortex. *Neural Computation*, **9**, 577–594.

[293] Sirosh, J., Miikkulainen, R., & Bednar, J.A. (1996) Self-organization of orientation maps, lateral connections, and dynamic receptive fields in the primary visual cortex. In *Lateral Interactions in the Cortex: Structure and Function*, J. Sirosh, R. Miikkulainen, & Y. Choe (eds.), UTCS Neural Networks Research Group, Austin, TX, 1996. Electronic book, ISBN 0-9647060-0-8, http://www.cs.utexas.edu/users/nn/web-pubs/htmlbook96.

[294] Somers, D.C., Nelson, S.B., & Sur, M. (1995) An emergent model of orientation selectivity in cat visual cortical simple cells. *The Journal of Neuroscience*, **15(8)**, 5448–5465.

[295] Somers, D.C., Todorov, E.V., Siapas, A.G., Toth, L.J., Kim, D-S., & Sur, M. (1998) A local circuit approach to understanding integration of long-range inputs in primary visual cortex. *Cerebral Cortex*, **8(3)**, 204–217.

[296] Somers, D.C., Toth, L.J., Todorov, E.V., Rao, S.C., Kim, D-S., Siapas, A.G., & Sur, M. (1996) Variable gain control in local cortical circuitry supports context-dependent modulation by long-range connections. In *Lateral Interactions in the Cortex: Structure and Function*, J. Sirosh, R. Miikkulainen, & Y. Choe (eds.), UTCS Neural Networks Research Group, Austin, TX, 1996. Electronic book, ISBN 0-9647060-0-8, http://www.cs.utexas.edu/users/nn/web-pubs/htmlbook96.

[297] Somogyi, P. (1989) Synaptic organization of GABAergic neurons and $GABA_A$ receptors in the lateral geniculate nucleus and visual cortex. In *Proceedings of the Retina Research Foundation, Volume 2: Neural Mechanisms of Visual Perception*, D.M. Lam & C.D. Gilbert (eds.), 35–62. Woodlands, TX: Portfolio.

[298] Somogyi, P., Kisvárday, Z.F., Martin, K.A.C., & Whitteridge, D. (1983). Synaptic connections of morphologically identified and physiologically characterized large basket cells in the striate cortex of cat. *Neuroscience*, **10**, 261–294.

[299] Somogyi, P. & Martin, K.A.C. (1985) Cortical circuitry underlying inhibitory processes in cat area 17. In *Models of the Visual Cortex*, D. Rose & V.G. Dobson (eds.), 514–523. New York: John Wiley & Sons.

[300] Stanton, P.K. & Sejnowski, T.J. (1989) Associative long-term depression in the hippocampus induced by Hebbian covariance. *Nature*, **339**, 215–218.

[301] Sur, M., Pallas, S.L., & Roe, A.W. (1990) Cross-modality plasticity in cortical development: Differentiation and specification of sensory neocortex. *Trends in Neurosciences*, **13(6)**, 227–233.

[302] Todorov, E.V., Siapas, A.G., Somers, D.C., & Nelson, S.B. (1997) Modeling visual cortical contrast adaptation effects. In *Computational Neuroscience: Trends in Research, 1997*, J.M. Bower (ed.), 525–531. New York: Plenum Press.

[303] Toth, L.J., Kim, D-S., Rao, S.C., & Sur, M. (1997) Integration of local inputs in visual cortex. *Cerebral Cortex*, **7**, 703–710.

[304] Toth, L.J., Rao, S.C., Kim, D-S., Somers, D., & Sur, M. (1996) Subthreshold facilitation and suppression in primary visual cortex revealed by intrinsic signal imaging. *Proceedings of the National Academy of Sciences of the USA*, **93**, 9869–9874.

[305] Ts'o, D., Gilbert, C.D., & Wiesel, T.N. (1986) Relationships between horizontal connections and functional architecture in cat striate cortex as revealed by cross-correlation analysis. *The Journal of Neuroscience*, **6**, 1160–1170.

[306] Varela, J.A., Sen, K., Gibson, J., Fost, J., Abbott, L.F., & Nelson, S.B. (1997) A quantitative description of short-term plasticity at excitatory synapses in layer 2/3 of rat primary visual cortex. *The Journal of Neuroscience*, **17(20)**, 7926–7940.

[307] Varela, F.J. & Singer, W. (1987) Neuronal dynamics in the visual corticothalamic pathway revealed through binocular rivalry. *Experimental Brain Research*, **66**, 10–20.

[308] Vidyasagar, T.R. & Urbas, J.V. (1982) Biases to oriented moving lines in cat LGN and the role of the visual cortical areas 17 and 18. *Experimental Brain Research*, **46**, 157–169.

[309] Volchan, E. & Gilbert, C.D. (1995) Interocular transfer of receptive field expansion in cat visual cortex. *Vision Research*, **35**, 1–6.

[310] Weliky, M., Kandler, K., Fitzpatrick, D., & Katz, L.C. (1995) Patterns of excitation and inhibition evoked by horizontal connections in visual cortex share a common relationship to orientation columns. *Neuron*, **15**, 541–552.

[311] Weliky, M. & Katz, L.C. (1997) Disruption of orientation tuning in visual cortex by artificially correlated neuronal activity. *Nature*, **386**, 680–685.

[312] Westheimer, G. (1986) Spatial interaction in the domain of disparity signals in human stereoscopic vision. *Journal of Physiology*, **370**, 619–629.

[313] Westheimer, G. (1989) Line orientation considered as a separate psychophysical domain. In *Proceedings of the Retina Research Foundation, Volume 2: Neural Mechanisms of Visual Perception*, D.M. Lam & C.D. Gilbert (eds.), 237–246. Woodlands, TX: Portfolio.

[314] Westheimer, G. & McKee, S.P. (1977) Spatial configurations for visual hyperacuity. *Vision Research*, **17**, 941–949.

[315] Westheimer, G., Shimamura, K., & McKee, S.P. (1976) Interference with line orientation sensitivity. *Journal of the Optical Society of America A*, **66**, 332–338.

[316] Wiesel, T.N. (1982) Postnatal development of the visual cortex and the influence of environment. *Nature*, **299**, 583–591.

[317] Wiesel, T.N. & Hubel, D.H. (1963) Single-cell responses in striate cortex of kittens deprived of vision in one eye. *Journal of Neurophysiology*, **26**, 1003–1017.

[318] Wiesel, T.N. & Hubel, D.H. (1965) Comparison of the effects of unilateral and bilateral eye closure on cortical unit responses in kittens. *Journal of Neurophysiology*, **28**, 1029–1040.

[319] Wiesel, T.N. & Hubel, D. (1974) Ordered arrangement of orientation columns in monkeys lacking visual experience. *The Journal of Comparative Neurology*, **158**, 307–318.

[320] Wigström, H. & Gustafsson, B. (1983) Facilitated induction of hippocampal long-lasting potentiation during blockade of inhibition. *Nature*, **301**, 603–604.

[321] Willshaw, D.J. & von der Malsburg, C. (1976) How patterned neural connections can be set up by self-organization. *Proceedings of the Royal Society of London, Series B*, **194**, 431–445.

[322] Wolfe, J.M. (1986) Stereopsis and binocular rivalry. *Psychological Review*, **93**, 269–282.

[323] Wolfe, J.M. (1988) Parallel ideas about stereopsis and binocular rivalry: A reply to Blake and O'Shea (1988). *Psychological Review*, **95**, 155–158.

[324] Xing, J. & Gerstein, G.L. (1994) Simulation of dynamic receptive fields in primary visual cortex. *Vision Research*, **34**, 1901–1911.

[325] Yang, X.-D., Connors, J.A., & Faber, D.S. (1994) Weak excitation and simultaneous inhibition induce long-term depression in hippocampal CA1 neurons. *Journal of Neurophysiology*, **71(4)**, 1586–1590.

[326] Yang, X.-D. & Faber, D.S. (1991) Initial synaptic efficacy influences induction and expression of long-term changes in transmission. *Proceedings of the National Academy of Sciences of the USA*, **88**, 4299–4303.